

Lecture Notes in Civil Engineering

Chih-Huang Weng *Editor*

Proceedings of The 5th International Conference on Advances in Civil and Ecological Engineering Research

Proceedings of ACEER2023

 Springer

Series Editors

Marco di Prisco, *Politecnico di Milano, Milano, Italy*

Sheng-Hong Chen, *School of Water Resources and Hydropower Engineering, Wuhan University, Wuhan, China*

Ioannis Vayas, *Institute of Steel Structures, National Technical University of Athens, Athens, Greece*

Sanjay Kumar Shukla, *School of Engineering, Edith Cowan University, Joondalup, WA, Australia*

Anuj Sharma, *Iowa State University, Ames, IA, USA*

Nagesh Kumar, *Department of Civil Engineering, Indian Institute of Science Bangalore, Bengaluru, Karnataka, India*

Chien Ming Wang, *School of Civil Engineering, The University of Queensland, Brisbane, QLD, Australia*

Zhen-Dong Cui, *China University of Mining and Technology, Xuzhou, China*

Lecture Notes in Civil Engineering (LNCE) publishes the latest developments in Civil Engineering—quickly, informally and in top quality. Though original research reported in proceedings and post-proceedings represents the core of LNCE, edited volumes of exceptionally high quality and interest may also be considered for publication. Volumes published in LNCE embrace all aspects and subfields of, as well as new challenges in, Civil Engineering. Topics in the series include:

- Construction and Structural Mechanics
- Building Materials
- Concrete, Steel and Timber Structures
- Geotechnical Engineering
- Earthquake Engineering
- Coastal Engineering
- Ocean and Offshore Engineering; Ships and Floating Structures
- Hydraulics, Hydrology and Water Resources Engineering
- Environmental Engineering and Sustainability
- Structural Health and Monitoring
- Surveying and Geographical Information Systems
- Indoor Environments
- Transportation and Traffic
- Risk Analysis
- Safety and Security

To submit a proposal or request further information, please contact the appropriate Springer Editor:

- Pierpaolo Riva at pierpaolo.riva@springer.com (Europe and Americas);
- Swati Meherishi at swati.meherishi@springer.com (Asia—except China, Australia, and New Zealand);
- Wayne Hu at wayne.hu@springer.com (China).


All books in the series now indexed by Scopus and EI Compendex database!

Chih-Huang Weng
Editor

Proceedings of The 5th International Conference on Advances in Civil and Ecological Engineering Research

Proceedings of ACEER2023

Editor

Chih-Huang Weng 

Department of Civil Engineering

I-Shou University

Kaohsiung, Taiwan

ISSN 2366-2557

ISSN 2366-2565 (electronic)

Lecture Notes in Civil Engineering

ISBN 978-981-99-5715-6

ISBN 978-981-99-5716-3 (eBook)

<https://doi.org/10.1007/978-981-99-5716-3>

© The Editor(s) (if applicable) and The Author(s), under exclusive license
to Springer Nature Singapore Pte Ltd. 2024

This work is subject to copyright. All rights are solely and exclusively licensed by the Publisher, whether the whole or part of the material is concerned, specifically the rights of translation, reprinting, reuse of illustrations, recitation, broadcasting, reproduction on microfilms or in any other physical way, and transmission or information storage and retrieval, electronic adaptation, computer software, or by similar or dissimilar methodology now known or hereafter developed.

The use of general descriptive names, registered names, trademarks, service marks, etc. in this publication does not imply, even in the absence of a specific statement, that such names are exempt from the relevant protective laws and regulations and therefore free for general use.

The publisher, the authors, and the editors are safe to assume that the advice and information in this book are believed to be true and accurate at the date of publication. Neither the publisher nor the authors or the editors give a warranty, expressed or implied, with respect to the material contained herein or for any errors or omissions that may have been made. The publisher remains neutral with regard to jurisdictional claims in published maps and institutional affiliations.

This Springer imprint is published by the registered company Springer Nature Singapore Pte Ltd.

The registered company address is: 152 Beach Road, #21-01/04 Gateway East, Singapore 189721, Singapore

Preface

The 5th International Conference on Advances in Civil and Ecological Engineering Research (ACEER 2023) is held in a hybrid offline mode in Macau, China, and online via Microsoft Teams from July 4–7, 2023. It aims to provide a platform for scientists, researchers, scholars, and engineers worldwide to present their latest research results and development activities in Civil, Environmental, and Ecological Engineering. The conference will also provide an opportunity for the participants to exchange new ideas and application experiences face-to-face, establish business or research relations, and find global partners for future collaboration.

With the success of the past four ACEER conferences, 80 submissions have been received and 33 of them have been accepted after an intense and strict peer review. The acceptance is about 41%.

On behalf of the ACEER 2023 organizing committee, we sincerely thank all the keynote and invited speakers, authors, and listeners who have participated in this event. Meanwhile, thanks to the international reviewers and the members of the program committee who have taken their valuable time to review the manuscripts and give comments and suggestions, which help authors improve the quality of the manuscripts.

Chih-Huang Weng

Organization

The 5th International Conference on Advances in Civil and Ecological Engineering Research (ACEER 2023)

Technical Program Committee Chair

Chih-Huang Weng Distinguished Professor, Department of Civil Engineering, I-Shou University, Taiwan

Technical Program Committee

Ali Al-Balhawi	Department of Civil Engineering, College of Engineering, Mustansiriyah University, Iraq
Ehsan Dadkhah	Department of Civil and Environment Engineering, University of Tabriz, Iran
Marco Guerrieri	Department of Civil, Environmental and Mechanical Engineering, University of Trento, Italy
Malek Hassanpour	Department of Environmental Science, Osmania University, India
Xiuhong Li	State Key Laboratory of Remote Sensing Science, College of Global Change and Earth System Science, Beijing Normal University, China
Pavlo Maruschak	Department of Industrial Automation, Ternopil Ivan Puluj National Technical University, Ukraine
Yap Soon Poh	Department of Civil Engineering, Faculty of Engineering, Universiti Malaya, Malaysia
Anoop Kumar Shukla	Manipal School of Architecture and Planning, Manipal Academy of Higher Education, India
H. Sally Xie	Department of Technology, Illinois State University, USA

Contents

Construction and Structural Engineering

Research on the Application of EPC in China's Prefabricated Building Market: A Case Study of Shenzhen	3
<i>Songyang Li, Hang Ma, Huan Liu, and Jiayin Zhou</i>	
Safety Factors in the Use and Formation of Intelligent Economic Systems of Construction Enterprises: Definition and Assessment Features	14
<i>Bieliatynskiy Andrii, Kostyantyn Mamonov, Vasyl Goi, Inna Khrystych, and Lyudmyla Kovalenko</i>	
Architecture and Techniques of Environmental Control of Climatic Colonies in Italy and Abruzzo	33
<i>Eleonora Laurini, Patrizia Montuori, and John D. Murphy Jr.</i>	
Method for the Design of Local Temporary Buildings to Ensure the Sustainable Development of the Liquid Society	52
<i>Stefania De Gregorio and Pierluigi De Berardinis</i>	
Monitoring of Bridges Damage Based on the System Transfer Function Maps from Sensors Datasets	71
<i>Dangui Guo, Weixing Hong, and Wael A. Altabey</i>	
Bridges Damage Assessment Techniques Improvement Through Machine Learning Algorithm	82
<i>Liping Zhou, Weixing Hong, and Wael A. Altabey</i>	
Numerical and Theoretical Study on Shear Capacity of Segmental Joints in UHPC-RC Composite Beam Bridge	93
<i>Yun Shen and Jianluan Li</i>	
Study on the Influence of Temperature Rise on the Stress Change of Prefabricated Cantilever Composite Subgrade (PCCS)	102
<i>Xiaoxiang Cao, Liang Yin, Cheng Peng, Zhigang Wu, and Shengwei Yang</i>	
Construction Technology of Tunnel Lining Vault Embedded Pipe Timely Grouting	112
<i>Dongshan Zhang and Bin Yang</i>	

Numerical Study on Performance of Single-Keyed Dry Joint of Ultra-High Performance Concrete (UHPC) Under Combined Shear and Torsion Load 122
Zening Xu, Yun Shen, and Jing Yan

First Master-Permanentization Solution for Telecommunication Tower 131
Hastining Bagyo Astuti, Rosadi Makhdor, Detriana Margita Sari, and Soekhata Setiawan

Environmental Monitoring and Risk Assessment

Impacts of Tibetan Plateau Vortex Activities on the Ecological Environment in the Yellow River Basin 143
Shuhua Yu, Jun Peng, and Wenliang Gao

Assessment of Wind Energy Resources in Fujian Sea Areas Based on WRF Model 156
Dawei Ji, Lianjie Guo, Na Wang, Feifei Jiang, Yingzhi Cao, and Hong Deng

Case Analysis of a Squall Line Process in Beijing Area in 2021 167
Jianjun Geng and Lei Lei

Research on Ecological Environment Impacts Assessment During the Construction Period of Railway Projects 178
Jieyu Zhang, Yitong Yin, Xiuhong Li, Yanrong Lu, and Yuying Zhang

Analysis of the Spatial Changes and Influencing Factors of Landscape Patterns Along the Fujian-Guangdong Interconnection 189
Jianxun Zhang, Guowei Chen, and Chang Lu

Impact of Electric Power Grid Projects on Bird Diversity and the Suggestion of Bird Conservative Technology 201
Chang Lu, Xi Li, Ying Deng, Jian Wang, Huaizhou Zheng, and Mingfeng Zhang

Methodology for Monitoring the Ecological Environment of Railway Construction 213
Jieyu Zhang, Yuying Zhang, Xiuhong Li, Yanrong Lu, and Yitong Yin

Analysis and Suggestions on Agricultural Non-Point Source Pollution-Yongchuan District, Chongqing as an Example 223
Yanrong Lu, Rongjin Yang, Zhang Le, Meiyang Sun, and Xiuhong Li

Role of Rare Taxa in the Structure and Function of Soil Fungal Community 234
Jianfei Guan

Hydraulics, Hydrology and Water Resources Engineering

Experimental Study on Flow Capacity of a Typical Side Weir 245
Xiaowei Han, Haifeng Zhang, Nan Yi, and Guanglei Gao

The Sustainable Development Model of Rural Domestic Sewage
 Treatment in China 256
Xinying Fan, Xiaotao Gao, Ming Cai, Hao Ma, Jian Fu, and Zhengwei Li

Comparative Study on Real-Time Economic Operation Algorithm
 of Three Gorges Hydropower Station 266
*Kui Huang, Zhenyu Mu, Xuanyu Shi, Xueshan Ai, Jiajun Guo,
 and Jie Ding*

Flood Forecast and Control for Urban Rivers Using LSTM Neural-Network ... 278
Lars-Eric Ertlmeier, Zhenyu Yang, and Benjamin Refsgaard

Spatial Variation of Agricultural Drought Vulnerability in Eastern
 Agricultural Zone of Qinghai Province, China 296
Youwen Zhang, Xueqin Cao, and Rentian Shu

Geotechnical Engineering

A Review on Application of Soft Computing Techniques in Geotechnical
 Engineering 313
T. V. Nagaraju, Mantena Sireesha, B. M. Sunil, and Shaik Subhan Alisha

Study on Enhanced Oil Recovery Technology of Tight Reservoir Modified
 in Highly Deviated Well: A Case Study of the L183 Area in the Huaqing
 Oilfield Ordos Basin, China 323
*Ce Wang, Xizhu Zhu, Tianhao Jiang, Libiao Li, Fangxin Song,
 Ping Zheng, and Jiuli Gu*

Suitability Evaluation of Subsurface Space Development and Utilization
 in Langfang North Three Counties, Hebei Province 336
*Dong Du, Xinliang Guo, Yaonan Bai, Chuanming Ma, Hongwei Liu,
 Jinjie Miao, and Jing Zhang*

Spatial Distribution, Influencing Factors and Suitability Evaluation
 of Rural Tourism - An Example from Guizhou, China 347
Yan Xiang, Junwei Zhao, and Yanlin Hou

Coastal Engineering and Fluid Mechanics

Coastline Change Monitoring by Remote Sensing in Coastal Zone
of Bohai Bay in China 363
Hualiang Xie, Jie Han, Huaiyuan Li, Shuhua Zuo, and Zhiyuan Han

The Progress and Management Suggestions for the Renovation
and Restoration of Sea Area and Coastal Zone 372
*Dawei Ji, Jian Zhang, Shiyue Fan, Yuanjun Wang, Yingzhi Cao,
and Hong Deng*

Building an Economic Argumentation Model for Vessel Train 384
Fangfang Jiao, Wendi Liu, and Jingjing Lin

Numerical Investigation of Turbulence Models for Swirling Nitrogen/Air 398
*Aoshuang Ding, Nenghui Wang, Zaixing Yang, Wenqing Mei, Lin Chen,
Congyang Xiao, Hai Wu, and Siyang Yi*

Author Index 411



About the Editor

Distinguished Professor Chih-Huang Weng is the Chairman of the Department of Civil Engineering at I-Shou University, Taiwan. He also served as vice president of North Kaohsiung Community University, Taiwan. He received his MS and Ph.D. degrees in 1990 and 1994, respectively, from the Department of Civil Engineering of The University of Delaware, USA. He is serving as the Associate Editor of *Environmental Geochemistry and Health* (Springer) and on the Editorial Board Panel Member of *Coloration Technology* (Wiley). He has also served as a Guest Editor of SCI journals, such as *Agricultural Water Management* (Elsevier) and *Environmental Science and Pollution Research* (Springer). He has also organized and chaired several international conferences. His main research interests focus on using advanced oxidation processes and adsorption to treat wastewater and bacteria inactivation, groundwater modeling, and application of electrokinetic technologies to soil remediation/sludge treatment/activated carbon regeneration.

Construction and Structural Engineering



Research on the Application of EPC in China's Prefabricated Building Market: A Case Study of Shenzhen

Songyang Li^{1,2} , Hang Ma¹, Huan Liu², and Jiayin Zhou³  

¹ Harbin Institute of Technology, Shenzhen 518055, China

s2255506@ed.ac.uk

² China Construction Science and Technology Group Co., Ltd., Shenzhen 518118, China

³ Tianjin University, Tianjin 300072, China

mmszhou@foxmail.com

Abstract. The EPC has experienced rapid development in China over the past 10 years, having completed several experimental projects and entered the promotion phase. Notably, the development of EPC in Shenzhen has been particularly outstanding. This study has compiled and analyzed the overall situation of promoting EPC engineering general contracting in Shenzhen's prefabricated building industry. A total of 85 prefabricated building projects involving the largest prefabricated construction company in Shenzhen were selected, and their construction area, prefabrication rate, and other indicators were analyzed. For one thing, a comparison was made with the overall distribution of prefabricated building projects in Shenzhen. For another thing, a comparison was made based on the time and regional distribution. Furthermore, rational thinking was applied to analyze the development of Shenzhen's prefabricated building market, and reference suggestions were provided for the industry's development through discussion.

Keywords: EPC · Prefabricated Building · Shenzhen · Construction Industry

1 Introduction

EPC stands for “Engineering, Procurement, and Construction,” which refers to a project delivery method in which a single contractor or team is responsible for the entire project life cycle, from design and procurement to construction and commissioning [1]. In the early 21st century, China set clear goals, tasks, and measures to the modernization of the housing industry. Facing the continuous expansion of the construction industry's industrial scale, people's higher demands for building quality, energy conservation, and environmental protection, and the objective fact that the demographic dividend was gradually fading, the construction industry must transform and upgrade. In 2016, the Central Committee of the Communist Party of China and the State Council of the People's Republic of China issued several opinions on further strengthening urban planning and construction management, proposing for the first time the explicit requirement to “develop new construction methods, vigorously promote prefabricated buildings, and

strive to make prefabricated buildings account for 30% of new construction within about 10 years”. According to information released by the Ministry of Industry and Information Technology of the People’s Republic of China and the China Prefabricated Building and Construction Industry Association, the scale of the Chinese EPC prefabricated building market was estimated to reach around 2.4 trillion RMB yuan by the end of 2021, with a year-on-year growth rate of approximately 40%, higher than that of the entire construction market [2].

Shenzhen has become one of the largest EPC markets in China and has taken a proactive approach to promote EPC development. The city has released several policy documents, including the “*Guiding Rules for EPC Project Contracting and Tendering (Trial Implementation)*” and the “*Notice on Further Standardizing EPC Project Contracting Activities*”, which have clarified the requirements, bidding conditions, pricing models, and preparatory work for EPC project contracting [3]. Shenzhen has also explicitly promoted the use of the EPC general contracting construction model in government investment projects for prefabricated building development in light of the “*Special Plan for the Development of Prefabricated Buildings in Shenzhen (2018–2020)*” [4, 5]. In addition, the “*Notice on Implementing Relevant Work for Prefabricated Building Projects*” and the “*Shenzhen Prefabricated Building Evaluation Rules*” have included the EPC management model as a scoring item, encouraging construction units with EPC management capabilities and experience, as well as large enterprises with full industry chain capabilities in design, production, and construction, to independently or jointly develop EPC business and play a leading role in demonstration projects [6–8]. As of 2022, Shenzhen accounted for over 20% of the national EPC market share, indicating its strong leadership in the EPC industry in China [9].

2 Study Area and Data Sources

2.1 Study Area

The study area of this research is Shenzhen, a rapidly developing city located in the Guangdong Province of China and the middle of the Guangdong-Hong Kong-Macau Greater Bay Area (Fig. 1). With a population of over 13 million and a land area of 2,342 square kilometers, Shenzhen is one of the largest cities in China [10]. It has made significant strides in developing prefabricated buildings and has become China’s largest market for the EPC construction mode. The city has implemented various policies and regulations to promote the use of EPC in the construction industry, including the “*Guiding Rules for EPC Project Contracting and Tendering (Trial Implementation)*” and the “*Notice on Further Standardizing EPC Project Contracting Activities*” [11]. Therefore, this study will focus on the application of EPC mode in the prefabricated building market in Shenzhen and analyze the key factors that have contributed to the success of EPC in the city.

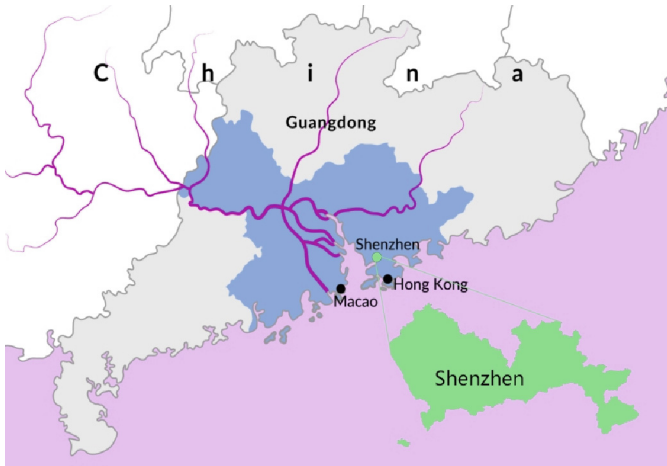


Fig. 1. Study Area.

2.2 Data Sources

The data for this study were obtained from the reports published by the Housing and Construction Bureau of Shenzhen and Company A, the largest state-owned enterprise with the qualification of undertaking prefabricated building projects in Shenzhen. A total of 85 recent projects were selected in chronological order for statistical analysis. Important information, such as project name, location, construction area, maximum unit building area, maximum single-beam span, maximum unit building height, the maximum number of floors per unit, maximum size of beam components, whether the project included prefabrication rate, whether it was a general contracting project, and its start and completion time were collected. Part of the information is shown in Table 1.

3 Result

3.1 Overall Allocation of EPC Projects in Shenzhen

As of May 2022, a total of 447 prefabricated building projects were adopted in Shenzhen. Among them, as shown in Fig. 2, 98 projects utilized the full-process engineering consultation or prefabricated building single-process consultation services, accounting for 22%; 44 projects were managed under the EPC model, accounting for 9.8%.

Regarding investment, there were 38 government-funded projects, accounting for 86%, and 6 social investment projects, accounting for 14%.

Regarding project types, there were 29 residential building projects, accounting for 66%; 14 public building projects, accounting for 32%; and 1 factory project, accounting for 2%.

Regarding venture types, there were 33 EPC projects under joint ventures, accounting for 75%, and 11 non-joint venture EPC projects, accounting for 25%.

Table 1. Information of Prefabricated Building Projects.

Location	Max building area per unit (m ²)	Max span of a single beam (m)	Max height of a single building (m)	Max number of floors for a single building	Max size of beam components (mm × mm)	Assembly rate	EPC (Yes/No)
Yunnan	3352.70	8.40	14.00	4	300*900	77.00%	√
Chongqing	4011.84	10.90	19.15	6	350*1200	51.11%	√
Guizhou	26536.42	9.00	32.10	6	400*850	45.13%	√
Guizhou	5000.00	6.00	5.30	1	250*700	—	×
Shenzhen	23191.62	10.20	78.30	23	2250*300	55.10%	×
Guizhou	23864.60	10.00	33.00	8	800*890	30.00%	√
Chongqing	24623.22	3.60	98.60	34	200*600	—	×
Guangdong	66897.79	116.00	146.30	32	500*800	45.60%	√
Guizhou	10865.34	8.40	78.35	26	500*1200	—	×
Guangdong	12850.00	11.60	78.40	25	400*1700	60.60%	√
Guangdong	4677.00	18.60	49.80	12	600*1500	56.00%	√
Shenzhen	11100.39	10.70	97.80	16	400*1100	45.76%	×
Beijing	2819.00	7.70	4.20	1	110*170	95.00%	√
Shenzhen	4250.11	17.00	23.95	6	900*1500	40.00%	×
Guizhou	58933.04	11.00	23.70	6	600*1300	70.60%	√
Guizhou	58933.04	11.00	23.70	6	600*1300	70.00%	√
Guizhou	8492.00	27.30	29.30	4	600*600	—	√
Shenzhen	4250.12	17.00	23.95	6	900*1500	40.00%	×
Chongqing	46383.66	10.40	82.10	19	300*2600	20.00%	×
Guizhou	28116.06	9.60	35.00	6	450*900	60.00%	√
Beijing	3276.24	6.10	13.50	3	450*200	92.00%	√
Chongqing	28341.00	24.00	39.80	9	380*620	70.00%	√
Chongqing	14278.83	8.10	23.80	8	600*800	50.00%	×
Chongqing	14278.83	8.10	23.80	8	600*800	50.00%	√
Chongqing	17020.28	8.00	49.00	13	300*800	76.30%	√
Chongqing	28341.00	24.00	39.80	9	380*620	70.00%	√
Shenzhen	9388.68	9.00	10.02	2	800*300	—	×
Shenzhen	13476.00	6.60	97.90	32	300*800	—	√
Shenzhen	48415.00	48.80	37.20	8	1200*1500	56.40%	×

(continued)

Table 1. (continued)

Location	Max building area per unit (m ²)	Max span of a single beam (m)	Max height of a single building (m)	Max number of floors for a single building	Max size of beam components (mm × mm)	Assembly rate	EPC (Yes/No)
Shenzhen	6687.92	8.55	12.00	3	400*200	—	×
Shenzhen	65100.00	8.40	91.05	25	400*770	67.90%	√
Guangdong	13677.00	26.30	30.75	4	800*1800	91.00%	×
Shenzhen	60000.00	13.00	196.50	42	700*2800	80.60%	√
Guizhou	58081.07	8.90	23.30	3	500*1300	68.30%	√
Guizhou	58081.07	8.90	23.30	3	500*1300	52.50%	√
Guizhou	59309.44	7.15	16.95	4	400*430	82.00%	√
Guangdong	14196.01	8.00	95.55	31	500*1200	30.00%	√
Guizhou	20698.00	8.90	19.20	4	350*850	61.30%	√
Guizhou	7740.59	7.90	88.50	27	1200*1800	—	×
Guizhou	58081.07	9.00	23.30	7	500*600	77.80%	√
Guizhou	21363.37	8.40	42.75	10	500*900	77.00%	×
Guizhou	59309.44	7.15	16.95	4	400*430	82.00%	√
Shenzhen	30000.00	10.80	11.00	21	300*1150	—	√
Shenzhen	2400.00	5.37	14.50	3	0.3*0.66	—	√
Shenzhen	15730.35	7.00	96.00	32	200*700	—	×
Shenzhen	19266.59	8.00	76.75	25	300*1760	70.00%	√
Heibei	18569.00	17.80	16.80	3	650*900	70.00%	√
Shenzhen	77835.42	12.00	134.60	40	2300*2000	56.67%	√
Sichuan	16020.23	10.20	20.80	4	400*2250	30.00%	×
Guizhou	20808.60	8.30	87.23	26	200*2800	—	×
Shenzhen	40381.47	21.10	49.95	14	700*1000	77.62%	√
Shenzhen	38228.53	27.00	38.95	6	700*1500	30.00%	×
Shenzhen	78000.00	29.00	152.10	34	600*1400	82.22%	√
Shenzhen	88953.96	17.60	196.90	43	700*1500	74.50%	√
Sichuan	23080.00	7.20	62.80	16	200*2200	70.00%	√
Guangdong	45651.00	24.00	40.70	12	400*800	90.00%	√
Shenzhen	44349.93	10.40	141.60	46	1000*2000	62.81%	√
Shenzhen	15669.24	7.00	96.15	32	300*700	—	√

(continued)

Table 1. (continued)

Location	Max building area per unit (m ²)	Max span of a single beam (m)	Max height of a single building (m)	Max number of floors for a single building	Max size of beam components (mm × mm)	Assembly rate	EPC (Yes/No)
Shenzhen	38758.99	13.00	82.80	13	700*1800	76.60%	√
Shenzhen	114169.50	19.60	147.90	40	1000*600	76.50%	√
Shenzhen	38753.52	11.90	82.80	13	550*2350	75.70%	√
Shenzhen	99163.03	12.00	97.20	22	450*3300	75.10%	√
Guanxing	25095.64	11.00	85.70	27	300*2000	20.00%	√
Shenzhen	21740.30	19.75	64.20	16	600*1400	66.40%	√
Guangdong	44844.24	10.20	149.90	52	600*1200	76.48%	√
Shenzhen	12430.63	23.00	48.00	11	600*1600	—	×
Gansu	30074.83	8.45	97.43	33	8450*400	—	√
Guangdong	498.72	13.60	75.20	25	300*1600	53.10%	√
Shenzhen	35050.00	19.80	23.70	6	600*1400	—	√
Sichuan	8028.92	9.10	78.15	24	650*1200	30.00%	×
Sichuan	8028.92	8.20	78.15	24	600*1200	—	×
Sichuan	24902.67	8.50	78.15	24	400*2500	30.00%	×
Shenzhen	25601.00	40.00	59.95	15	800*1500	62.80%	√
Sichuan	28803.52	9.00	54.00	18	300*2300	50.40%	×
Shenzhen	12945.79	9.00	24.40	7	350*1200	69.00%	√
Shenzhen	39143.00	9.00	42.00	11	450*1250	76.80%	√
Hainan	8063.73	10.79	36.80	12	550*900	51.00%	√
Sichuan	12785.00	8.20	27.90	6	7220*300	62.00%	√
Chongqing	1676.00	7.95	22.50	4	600*1000	—	×
Sichuan	8862.00	8.20	33.00	11	400*1300	20.00%	×
Sichuan	8517.64	16.20	33.00	11	600*1800	20.00%	×
Sichuan	9305.00	7.80	15.15	3	450*1800	68.53%	×
Sichuan	11204.98	6.10	75.55	25	400*2350	30.00%	√
Sichuan	28803.52	9.00	54.00	18	300*2300	50.40%	×
Sichuan	24737.45	9.76	23.95	5	350*700	—	×

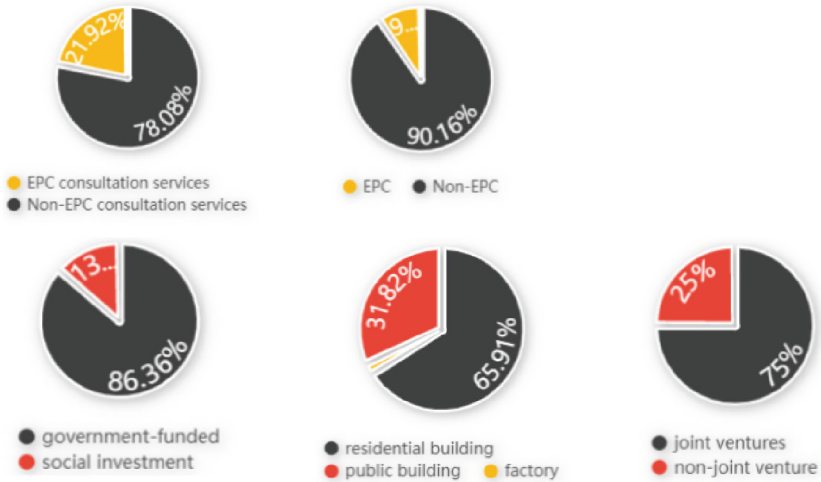


Fig. 2. The Proportion of Various Types of Projects.

Although Shenzhen is at the forefront of the prefabricated building industry in China, the adoption rate of EPC mode is still relatively low, representing 1/10 of the total. Most of the 102 EPC projects were government-funded projects and joint venture EPC projects, particularly talent housing, school, and emergency engineering construction projects. For instance, Shenzhen Talent Housing Group invited bids for 59 projects. In addition, modular kindergartens, primary schools, and middle schools in various districts of Shenzhen were also constructed under the EPC mode. Since the outbreak of COVID-19 in 2020, the construction of the Third People's Hospital of Shenzhen (Emergency Hospital), the supporting constructions of Beijing University Hospital on Beidaihe Island, and the Hong Kong Infection Control Centre all adopted the EPC mode, which significantly shortened the construction period and met social demand more efficiently [12].

3.2 EPC Projects Participated by Company A

Among the 85 prefabricated projects sampled in Company A, as shown in Table 2, 55 EPC projects accounted for 64.7% of the total. The projects were mainly located in southern provinces of China, including 31 projects in Shenzhen, accounting for 36.5% and ranking first, besides, there were 17 projects in Guizhou, 13 in Sichuan, 9 in Chongqing, and 8 in other areas of Guangdong province, as well as 1–2 projects in Beijing, Hebei, Hainan, and other regions. Comparing the proportion of EPC projects in different regions shows that the proportion in Shenzhen is similar to the overall sample average, at 67.7%, while Sichuan has the lowest proportion of EPC projects, at only 23.1%.

Table 2. Geographical Location Distribution of the 85 Prefabricated Projects.

Location	Shenzhen	Guizhou	Sichuan	Chongqing	Guangdong	Beijing
Projects	31	17	13	9	8	2
EPC Projects	21	12	3	5	7	1
EPC Rate	67.7%	70.1%	23.1%	55%	87.5%	50%
Location	Beijing	Yunnan	Guangxi	Gansu	Heibei	Hainan
Projects	2	1	1	1	1	1
EPC Projects	1	1	1	1	1	1
EPC Rate	50%	100%	100%	100%	100%	100%

In addition, it is shown in Table 3 that the assembly rate of the projects ranged from 20% to 92%, with an average of 59.8%. The project with the highest assembly rate was a residential project in Beijing Yizhuang, and the assembly rate of residential projects was generally higher than that of public buildings. The average building area per unit was approximately 28,000 square meters, and the average number of floors was 15.75, indicating that residential and commercial office buildings are still the major markets for prefabricated construction. In addition, medical and educational projects such as the constructions and supporting constructions of Guizhou Provincial People's Hospital and Guizhou Provincial Maternal and Child Health Hospital, as well as the expansion and renovation project of Shenzhen Yaohua Experimental School, accounted for 1/3 of the projects, highlighting the flexibility of the entire management cycle.

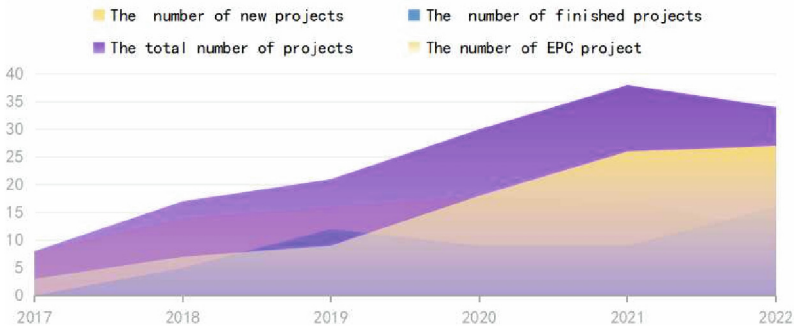
Table 3. Prefabricated building quantity distribution.

	Maximum building area per unit (m ²)	Maximum span of a single beam (m)	Maximum height of a single building unit (m)	Maximum number of floors for a single building unit	Assembly rate
Average	28296.72528	13.75907059	57.88505882	15.75294118	59.9%
Maximum	114169.5	116	196.9	52	92%
Minimum	498.72	3.6	4.2	1	20%

By comparing the start time and termination time of these projects (Table 4), the study finds that the proportion of EPC projects has gradually increased in recent years. In 2017, EPC projects accounted for only 37.5% of the total (Fig. 3), while in 2022, this proportion increased to 79.4%. This trend indicates that the EPC model is becoming more and more popular in the market.

Table 4. Timeline of the Sample Projects.

Year	The number of new projects	The number of finished projects	The total number of projects	The number of EPC projects	Rate
2017	8	0	8	3	37.50%
2018	14	5	17	7	41.18%
2019	16	12	21	9	42.86%
2020	18	9	30	18	60.00%
2021	17	9	38	26	68.42%
2022	15	19	34	27	79.41%

**Fig. 3.** Year-to-year Comparison of Item Categories from 2017–2022.

4 Conclusion

This study provides valuable insights into the application of EPC in China's prefabricated building market, with a focus on Shenzhen. The research finds that the EPC mode has been widely promoted in Shenzhen and has contributed significantly to the development of the prefabricated building industry. It means that EPC contracting has become an increasingly popular model in the prefabricated building market in Shenzhen. Out of the 85 projects analyzed, 60 were implemented using the EPC model, accounting for 70.6% of the total. This shows that the EPC model has been widely accepted and applied in the market. And the average assembly rate of prefabricated components was 66.1%, which was higher than the average assembly rate of prefabricated components in China's prefabricated building market. This shows that the EPC model has the potential to improve the efficiency of the construction process and the quality of the building.

In summary, the data analysis results of the study show that the EPC model has great potential and advantages in the prefabricated building market in Shenzhen, and its application has been widely accepted and promoted. However, there are also challenges and potential risks that need to be addressed to ensure the sustainable development of the EPC model in the market [13].

5 Discussion

In terms of proportion, Company A has participated in 31 EPC projects in Shenzhen, accounting for 70% of the total. However, not all regions in China have such large enterprises engaged in the prefabricated building industry like Shenzhen, which has matured in its development. This situation has resulted in a lack of attention to EPC general contracting in many other cities' engineering construction units. The lack of confidence in the ability of general contracting units and dependence on traditional interest chains by construction units has made them unwilling to adopt the design-construction integration and decoration-mechanical-electrical integration bidding mode actively [14]. Consequently, most prefabricated building projects still use the management model of owner contracting or segmented cutting, where all parties still need to have the goal of the overall interests of the project in mind. However, design products are challenging to manufactures to assemble on a large scale with high efficiency. Multiple links and specialties, such as design, production, construction, and operation, are difficult to coordinate effectively as well, not only putting forward challenges to fully leverage the advantages of prefabricated construction, but also going against the cost-effectiveness principle. In a word, this does not suit industrial production methods.

Apart from cultivating comprehensive enterprises, the Shenzhen government has formulated many targeted policies to highlight the leading and overall coordinating ability of EPC units. Recently, Shenzhen has successively issued policy documents that clearly state that construction units can relax the qualification management when setting bidding conditions and implement capability recognition and return to qualification management during project implementation phase. According to the different compositions of EPC units, the prefabricated building engineering general contracting market in Shenzhen has been subdivided into four categories: enterprises with a complete industrial chain, independent EPC; EPC consortium led by construction units; EPC consortium led by construction units; and EPC consortium led by design units [15]. Currently, the EPC consortium led by construction units is the most prevalent market in Shenzhen. Its advantages lie in the fact that construction units have long been deeply involved in the construction field, with strong labor control, procurement, and resource integration capabilities [16]. They can provide preliminary construction requirements such as pre-construction methodology, scheme selection, and construction measures to the design institutions, which contribute to promote the integration of design and construction. Ultimately, all of these analyses have put forward significant implications for China's EPC market development.


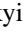




References

1. Navaratnam, S., Ngo, T., Gunawardena, T., Henderson, D.: Performance review of prefabricated building systems and future research in Australia. *Buildings* **9**(2), 38 (2019)
2. Weishu, Z., Beibei, Z., Yang, Y.: RETRACTED: Empirical study of comprehensive benefits for prefabricated buildings: a case study of Hefei city. *Int. J. Electr. Eng. Educ.* (2020). 002072092092846
3. Li, C.Z., et al.: A blockchain- and IoT-based smart product-service system for the sustainability of prefabricated housing construction. *J. Clean. Prod.* **286**, 125391 (2021)

4. Xia, M., Zhao, L., Zhao, L.: A comprehensive risk-assessment method for prefabricated buildings using EPC: a case study from China. *Sustainability* **14**(3), 1910 (2022)
5. Yuan, Z., Zhang, Z., Ni, G., Chen, C., Wang, W., Hong, J.: Cause analysis of hindering on-site lean construction for prefabricated buildings and corresponding organizational capability evaluation. *Adv. Civ. Eng.* **2020**, 1–16 (2020)
6. Fan, C., Binchao, D., Yin, Y.: Hierarchical structure and transfer mechanism to assess the scheduling-related risk in construction of prefabricated buildings: an integrated ISM-MICMAC approach. *Eng. Construct. Architect. Manag.* (3), 30–48 (2022). <https://doi.org/10.1108/ECAM-09-2021-0785>
7. Jin, Y., Zhang, J., Sun, L.: Safety risk assessment of prefabricated building construction based on bayesian network. *IOP Conf. Ser.: Earth Env. Sci.* **371**(3), 032052 (2019)
8. Jiang, L., Li, Z., Li, L., Gao, Y.: Constraints on the promotion of prefabricated construction in China. *Sustainability* **10**(7), 2516 (2018)
9. Wang, Z.L., Shen, H.C., Zuo, J.: Risks in prefabricated buildings in China: importance-performance analysis approach. *Sustainability* **11**(12), 3450 (2019)
10. Wang, T., Tang, W., Du, L., Duffield, C.F., Wei, Y.: Relationships among risk management, partnering, and contractor capability in international EPC project delivery. *J. Manag. Eng.* **32**(6), 04016017 (2016)
11. Wang, B., Geng, L., Dang, P., Zhang, L.: Developing a framework for dynamic organizational resilience analysis in prefabricated construction projects: a project life cycle perspective. *J. Constr. Eng. Manag.* **148**(10), 04022110 (2022)
12. Liu, K., Su, Y., Zhang, S.: Evaluating supplier management maturity in prefabricated construction project-survey analysis in China. *Sustainability* **10**(9), 3046 (2018)
13. Li, Z., Shen, G.Q., Xue, X.: Critical review of the research on the management of prefabricated construction. *Habitat Int.* **43**, 240–249 (2014)
14. Wang, Q., Gong, Z., Li, N., Liu, C.: Policy framework for prefabricated buildings in under-developed areas: enlightenment from the comparative analysis of three types of regions in China. *Buildings* **13**(1), 201 (2023)
15. Wang, J., Teng, Y., Chen, Z., Bai, J., Niu, Y., Duan, H.: Assessment of carbon emissions of building interior decoration and renovation waste disposal in the fast-growing Greater Bay Area, China. *Sci. Total Env.* **798**, 149158 (2021)
16. Jiang, W., Huang, Z., Peng, Y., Fang, Y., Cao, Y.: Factors affecting prefabricated construction promotion in China: a structural equation modeling approach. *PLoS ONE* **15**(1), e0227787 (2020)



Safety Factors in the Use and Formation of Intelligent Economic Systems of Construction Enterprises: Definition and Assessment Features

Bieliatynskiy Andrii¹  , Kostyantyn Mamonov² , Vasyl Goi³ ,
Inna Khrystych⁴ , and Lyudmyla Kovalenko⁵ 

¹ Department of Road and Bridge, School of Civil Engineering, North Minzu University, 204 Wenchang Road, Yinchuan 750021, NingXia, China
beljatynskij@mail.ru

² Department of Land Administration and Geoinformation Systems, O. M. Beketov National University of Urban Economy, Kharkiv, Ukraine

³ Department of Entrepreneurship and Business Administration, O. M. Beketov National University of Urban Economy, Kharkiv, Ukraine

⁴ Department of Criminological Research, Academician Stashis Scientific Research Institute for the Study of Crime Problems of the National Academy of Law Sciences, Kharkiv, Ukraine

⁵ Department of Higher Mathematics, O. M. Beketov National University of Urban Economy, Kharkiv, Ukraine

Abstract. The relevance and necessity of identifying safety factors for the use and formation of intelligent economic systems of construction companies is proven. The purpose of the study is to form a quantitative basis for the development and use of intelligent economic systems of construction companies, considering the influence of safety factors. As a result of studying the condition and development trends of the construction sector, it was determined that the construction sector is essential branch of the state's economy, which affects its development and ensures the functioning of other spheres of activity. It reflects trends and is an indicator of the evolution of the state's economy. The construction sector reacts more inertly to the changes taking place in the state, both in terms of development and the accumulation of negative phenomena. This especially applies to the development and implementation of intelligent economic systems. Proposed security factors for the use and formation of the intelligent economic system of building companies, the evaluation of which is based on the application of qualitative methods used for construction enterprises and regions. The presented indicators are determined by the level of national security, directions of use and formation of financial, economic and information security, features of stakeholder relations of construction enterprises. Safety indicators make it possible to build a quantitative basis for assessing the level of formation and use of an intelligent economic system for making informed management decisions. It has been established that the formation of information and analytical support for the implementation of security measures is mediocre, which indicates the need to implement directions for increasing their effectiveness.

Keywords: Intelligent Economic System · Construction Enterprises · Construction Sphere · Safety Factors · Integral Factor

1 Introduction

The formation of a modern system of management of construction enterprises requires a rethinking the approaches to the formation of directions for their development. Of particular importance is the use of innovative tools based on the use and formation of intelligent economic systems. An important element of the presented system is the safety component, which includes relevant factors.

In order to make informed management decisions, it is necessary to form a quantitative basis by evaluating the safety indicators of the use and formation of the intelligent economic system of construction enterprises. Along with this, in the construction sector, significant attention is not paid to ensuring the safety parameters of construction enterprises, an intelligent economic system has not been developed and is not applied. This inhibits their development, reduces the efficiency of functioning. An intelligent economic system has not been built at construction enterprises, which allows formation of a quantitative basis for making effective decisions on managing all types of resources. In the intellectual economic system, an important element is the security element, which consists of informational, resource, financial, economic, and physical elements. Unfortunately, only certain safety elements are used at construction enterprises, but a single safety system for the development of business entities has not been built.

The purpose of the study is to form a quantitative basis for the development and use of intelligent economic systems of construction enterprises, considering the influence of safety factors. Achieving the set goal is achieved by solving the following tasks:

Identification of safety factors affecting the use and formation of intelligent economic systems of construction enterprises.

Assessment of safety factors.

Determination of the integral safety indicator of the formation and use of intelligent economic systems of construction enterprises.

Thus, the research topic is relevant, and its development is important.

2 Materials and Methods

The features of the functioning of the construction sector are defined:

non-stationarity, temporary nature, non-homogeneous building production and the nature of the final product;

technological relationship of all operations included in the construction process;

instability of the ratio of construction and installation works in terms of their complexity and types during the month, which complicates the calculation of the numerical and vocational composition of workers;

participation of various organizations in the production of final building products;

role of climate and local conditions in construction works;

features of construction are due to a large variety of objects under construction [1].

It should be noted that during the studied period, undulating nature of changes in indicators of construction products is observed: in 2011–2014, the index decreased, and in 2015–2017, it increased. In subsequent years, the period of decline was replaced

by periods of growth. As a result of the research, ambiguous trends regarding changes in the index of building products for 2021 by region of Ukraine were determined. In general, there was an increase in the index of construction products compared to last year by 6.8% due to an increase in this indicator in the Ukrainian regions [2]. Similar trends characterized changes in the index of construction products for residential and non-residential buildings and engineering structures.

During the studied period, there was an increase in the volume of manufactured construction products by their types, in addition to the construction of ports, canals, dams, and other water structures. In 2021, the largest volume of manufactured construction products was observed in the Odesa, Vinnytsia, Dnipropetrovsk, and Kharkiv regions. Kirovohrad, Luhansk, Chernivtsi, Sumy, and Kherson regions were characterized by the lowest specific weight of the presented indicator. The total area of residential buildings at the start of construction in 2018–2021 generally decreased. This process took place due to the reduction of the total area of single-apartment houses and houses with two or more apartments. Only the total area of dormitories increased by 31% during the studied period [2]. The total area of residential buildings at the start of construction in 2021 by region was characterized by the largest values: Kyiv, Lviv, Dnipropetrovsk. The regions with the lowest values were: Kirovohrad, Luhansk, and Donetsk. It should be noted that the total area of non-residential buildings by types of construction products increased in 2018–2021. Only the total area of non-residential buildings decreased by 10% during the studied period [2].

During the studied period, there is an increase in the total number apartments in residential buildings at the beginning of construction by 2%, which occurred due to an increase in apartments in buildings with two or more apartments. This process of reducing the number of objects in single-apartment houses was slowed down. The largest number of apartments in residential buildings at the start of construction by type in the regions of Ukraine in 2021 was observed in the regions: Kyiv, Odesa, Dnipropetrovsk, and Kharkiv. Along with this, the low level of this indicator was characterized by: Luhansk, Donetsk, Kirovohrad regions [2].

Indices of capital investments by types of economic activity in 2021 indicate their growth throughout Ukraine. This was due to their increase in: agriculture, forestry and fisheries, industry, real estate transactions, activities in the field of administrative support services, health care and social assistance, arts, sports, entertainment and recreation, and other types of services. The reduction of the volume of capital investments during the investigated period occurred in the following areas: information and telecommunications, financial and insurance activities, public administration and defense; mandatory social insurance, education [2]. By region in the construction sector, there is a slowdown in the number of active economic entities, which corresponds to the general trend in Ukraine as a whole. In addition, it should be noted that the formation and functioning of economic entities is carried out according to the directions of construction: construction of buildings; organization of building construction; construction of residential and non-residential buildings; construction of buildings; construction of roads and railways; construction of roads and highways; construction of railways and metro; construction of bridges and tunnels; construction of communications; construction of pipelines; construction of power supply and telecommunications facilities; construction

of other buildings; construction of water structures; construction of other structures, not classified in other groups; specialized construction works; demolition and preparatory work at the construction site; exploratory drilling; electrical, plumbing and other construction and assembly works; construction completion works; plastering works; installation of carpentry; floor covering and wall cladding; painting and glazing; other construction completion works; other specialized construction works; roofing works; other specialized construction works, not classified in other groups.

As a result of the study, the increase in the turnover of personnel in Ukraine as a whole and in the construction sector, in particular, was determined. Moreover, this process took place for all types of construction activities. This testifies to the growing attention to the provision of working capital and the possibilities of its implementation in the production process. In addition, there are changes in focusing attention on the provision of working capital as an important element of the development of construction enterprises.

The dynamics of added value by production costs by types of construction activity is characterized by its growth both in Ukraine as a whole and in construction during the studied period. This was facilitated by the increase of this indicator by types of construction activity.

The dynamics of capital investments during the studied period in Ukraine as a whole was characterized by growth. A similar trend was observed by types of construction activity. Moreover, capital investments in tangible assets increased, along with the reduction of this indicator in intangible assets. In the largest part of types of construction activities, capital investments grew during the studied period. However, this process was hampered in the following areas: organization of construction of buildings; construction of railways and metro; construction of other buildings; demolition and preparatory work at the construction site.

Average number of employees in the equivalent of full employment, the number of hours worked by employees during the studied period decreased in Ukraine as a whole and in construction in particular. This was facilitated by a decrease in the presented indicators by types of construction activity: building; construction of residential and non-residential buildings; construction of structures; construction of bridges and tunnels; construction of other structures; construction of water facilities; construction of other structures not classified in other groups; specialized construction works; dismantling and preparatory work at the construction site; exploration drilling; electrical installation, plumbing and other construction and installation works; electric installation work; installation of water supply networks, heating and air conditioning systems; plastering works; installation of joinery; flooring and wall cladding; painting and glazing; other specialized construction works; roofing.

During the researched period, there is an increase in incomes performed under contract conditions for most types of construction activities. Only the construction of railways and the metro and exploratory drilling are characterized by a decrease in income. The presented trend shows the growth of income and opportunities of construction enterprises. Along with this, the processes are affected by factors related to the increase in prices, in particular, for construction materials, wage levels, inflationary processes that affect the formation of income from construction works.

The dynamics of profit before taxation shows the growth of its value over the studied period by regions in Ukraine as a whole and in construction in particular. This indicates an increase in the level of effectiveness of activities, including by types of construction activities. It should be noted that according to the presented indicators, there is a decrease in the level of information and analytical support, which negatively affects the ability to make informed management decisions and build an intelligent geospatial economy at construction enterprises.

The dynamics of non-current assets in Ukraine as a whole and in the construction sector in particular shows growth [2]. This indicates the strengthening of the production and economic potential and the increase of opportunities for the performance of production tasks. Along with this, for some types of construction activities and especially for medium and small enterprises, there is a decrease in the volume of non-current assets. This indicates a decrease in attention to the growth of the production and economic potential of the represented business entities and the increase in the level of monopolization of construction activities. It should be pointed out the decrease in information and analytical support regarding the dynamics of non-current assets, which affects the level of effectiveness of making informed management decisions.

It should be noted the growth of current assets in most types of construction activities. This testifies to the growing possibilities of construction enterprises to use the most mobile funds. However, a similar trend has been identified as with previous assets regarding the reduction of information and analytical support.

The dynamics of own capital during the investigated period indicates a reduction in its volume due to construction and outflow. This affects the financial stability of construction enterprises. Special attention is focused on the reduction of information and analytical support in the system of use and formation of own capital.

During the studied period, there is a reduction in the volume of long-term obligations and guarantees in construction, which does not correspond to the general trends in Ukraine [2]. This indicates an effort to reduce debt by types of construction activities, unsatisfactory conditions for long-term lending, a decrease in the ability of customers, instability of socio-economic conditions.

Along with this, there is an increase in current liabilities and collateral, which indicates an increase in opportunities for attracting short-term borrowed funds, as well as a slowdown in the processes of forming the financial stability of building enterprises.

It should be noted a decrease in the amount of liabilities for non-current assets and disposal groups and the net value of assets of a non-state pension fund by types of construction activities. In addition, it is necessary to note the low level of information and analytical support for these obligations, especially for specific types of construction activities.

In general, Ukraine and regions have the largest share of enterprises with positive financial results. The specific weight of a positive result for enterprises varies from 50% to 100%. This testifies to the effectiveness of business entities.

The practice of applying intelligent economic systems at construction enterprises is carried out along the lines of introducing artificial intelligence as an integral part of the fourth industrial revolution “Industry 4.0” [3].

The international experience of the development of artificial intelligence is determined by the creation of new platforms. The World Economic Forum has launched The Global AI Action Alliance, a new multi-stakeholder collaboration platform and project incubator designed to accelerate the adoption of inclusive, trusted and transparent artificial intelligence, bringing together more than 100 leading companies, governments, international organizations, non-profit organizations and scientists [4].

Identified artificial intelligence technologies used in the personnel management system: Resume Matcher (SAP); Skillaz; TalentTech Sever.AI; Hurma System; Veriato 360; Workday; Yva.ai 3.0 – Visier Announces Asset Acquisition; Isaak Status Today by Glickon; Cornerstone + EdCast; Degreed; Filtered Content Intelligence; WalkMe ActionBot; AIOps.

The presented artificial intelligence technologies are used to organize the recruitment of personnel, control their movement, provide training, form appropriate management decisions, and automate the processes of using labor resources.

The introduction and development of artificial intelligence in economic processes is connected with the development of the “Industry 4.0” system, which uses the Internet of Things (IoT), big data (BigData) and cyber-physical systems.

According to experts, the prospects for the development of artificial intelligence in Ukraine are important, but to a greater extent they are related to the areas of: autonomous control; biotechnology; face recognition; internet of things; trade; robotic systems.

As a result of studying, the methods and models of using artificial intelligence were determined: methods of finding solutions in the space of states; bidirectional search method; methods of uninformed or “blind” search (full search); methods of complete search; finding a solution when reducing tasks to subtasks; heuristic search methods; knowledge presentation models in artificial intelligence systems; proof methods; method of resolution in numerous predicates; models of fuzzy logic; production models of knowledge presentation; scenario approach; formation of expert systems; formation of neural networks.

At construction enterprises, separate elements of spatial support are used, but the directions and features of the application of geoinformation systems and technologies are insufficiently defined.

To ensure the safety of the development and use of an intelligent economic system at construction enterprises, information systems of the first generation are formed based on the formation of data and the construction of a mathematical model for a separate economic task. Second generation information systems are aimed at information management. Information systems of the third generation are defined by decision support.

Identified information economic systems and their application in international practices:

SCAN (large projects implemented in developing countries. Developed according to directions proposed by the UN);

BUSINESS (international trade, contracts, technology development and implementation, licensing activities);

HURFAX (market research, formation of results in the form of relevant documents);

PASCAL, SGBD (economic, financial and banking sector of France);

COMEXT (trade area of the European Union);
CISI (formation of databases to ensure the development of the spheres of economic activity of the European Union);
BRIL (scientific research activity);
WATS (assessment and analysis of directions and features of the economic activity of the American company);
PUNS (evaluation and management of activities of international companies);
ICOF, JORDAN, IML (evaluation and analysis of the activities of British companies);
BODAS, ESSOR, DETOFEL (commercial sphere, management system, distribution of property, formation and use of capital, use of personnel of French companies) [3].

A wide range of application of economic information systems has been established, but they solve only certain issues of the functioning of enterprises. There are no comprehensive economic systems for managing all types of resources, automation of the processes of their use and formation, taking into account the modern tools of artificial intelligence, spatial aspects of the activities of business entities, which is especially relevant in the construction sector. Therefore, the development of the intellectual economic system of construction enterprises proposed by the author will solve the actual issues aimed at the development of construction enterprises, using modern informational, analytical, economic, geospatial, security tools and tools of artificial intelligence.

There are no unified approaches to the definition of the intellectual economic system of construction enterprises in the existing scientific developments. It should be noted that the formation and use of the intelligent economic system of construction enterprises is influenced by relations with stakeholders [5–12].

Dovbysh, V. Tron, R. Kvasny, and L. Chernyak, N. Nylson, A. Horelyk, D. Goldberg focus on the functional directions for the formation and use of the intellectual economic system of enterprises [13–17].

The modern toolkit used for the formation and use of the intellectual economic system of building enterprises is presented in the works [18–21].

Thus, a theoretical basis and a platform for defining the intelligent economic system of construction enterprises have been formed, where the main attention is focused on the formation of a set of economic, informational, geospatial, and security components that allow building directions for making management decisions in the context of the development of construction enterprises.

To develop and implement sound management decisions regarding the formation and use of intelligent economic systems of construction enterprises, the selection and evaluation of safety factors is carried out. As a result of the study, the necessity of characterizing financial and economic security was determined. P. Nikiforov, V. Stolbov, T. Davidiuk point to the importance of financial and economic security [22–24].

In addition, in the context of the assessment of security indicators, the level of information security of construction enterprises is determined using the method of expert assessments:

Because of the study, the factors of the level of information security were determined, which are characterized by:

Principles of ensuring information security.

Interests reflected in the information sphere.

Real and potential threats to information security.
 Priorities of state policy in the field of information security.
 Stakeholders to ensure information security.
 Coordination and control over the activities of stakeholders that ensure information security.
 Level of personal data protection.
 The level of ensuring information protection in information, electronic communication and information and communication systems.
 Organizational areas of ensuring information protection.
 The level of interaction of stakeholders with the information protection service;
 Level of information society formation. An important indicator in the system of safety indicators is the level of safety of interaction between stakeholders of construction enterprises:
 Customers of construction products;
 Contractors;
 Social organizations;
 Suppliers of goods and material values;
 Project organizations;
 Internal and external audit organizations;
 Public organizations;
 Workers of construction enterprises;
 Owners;
 Top management;
 Managers of different levels.

The presented factor is determined on the basis of expert assessments for each construction enterprise. So, summarizing the above, the safety indicators of construction enterprises are highlighted (Table 1).

Table 1. Safety factors of the formation and use of the intellectual economic system of construction enterprises.

Indicators	Evaluation methods		Object of assessment
	Quantitative assessment methods	Qualitative evaluation methods	
The level of national security			
formation and implementation of the principles of ensuring national security	—	+	Regions
interaction of interested parties in the field of national security	—	+	Regions

(continued)

Table 1. (continued)

Indicators	Evaluation methods		Object of assessment
	Quantitative assessment methods	Qualitative evaluation methods	
The level of financial and economic security of construction enterprises			
ensuring interaction between interested parties in the field of financial and economic security	–	+	Construction enterprises
The level of implementation of measures for the formation and application of financial and economic security	–	+	Construction enterprises
prevention of threats and risks based on financial and economic security	–	+	Construction enterprises
The level of formation of information security of construction enterprises			
implementation of information security principles	–	+	Construction enterprises
ensuring the interests of construction enterprises in the field of information security	–	+	Construction enterprises
identification of real and potential threats to the information security of construction enterprises	–	+	Construction enterprises
ensuring the priorities of state policy in the field of information security	–	+	Construction enterprises
interaction of interested parties in the field of ensuring information security	–	+	Construction enterprises

(continued)

Table 1. (continued)

Indicators	Evaluation methods		Object of assessment
	Quantitative assessment methods	Qualitative evaluation methods	
protection of personal data	—	+	Construction enterprises
ensuring the protection of information in information, electronic communication and information and communication systems of construction enterprises	—	+	Construction enterprises
formation and implementation of organizational measures to ensure information security of construction enterprises	—	+	Construction enterprises
functioning of the information protection service of construction enterprises	—	+	Construction enterprises
information society formation	—	+	Regions
ensuring the interaction of stakeholders of construction enterprises			
Customers of construction products	—	+	Construction enterprises
Contractors	—	+	Construction enterprises
Social organizations	—	+	Construction enterprises
Suppliers of commodity values	—	+	Construction enterprises
Project organizations	—	+	Construction enterprises
Internal and external audit organizations	—	+	Construction enterprises

(continued)

Table 1. (continued)

Indicators	Evaluation methods		Object of assessment
	Quantitative assessment methods	Qualitative evaluation methods	
NGOs	–	+	Construction enterprises
Workers of construction enterprises	–	+	Construction enterprises
Owners of construction enterprises	–	+	Construction enterprises
Top management	–	+	Construction enterprises
Managers of different levels	–	+	Construction enterprises

The determination of the safety factors of the construction enterprise with regard to the formation and use of the intellectual economic system is carried out through the prism of local indicators.

At the intermediate level, directions for the formation and implementation of financial and economic security at the construction enterprise are carried out in relation to:

Ensuring interaction between interested parties in the field of financial and economic security.

Implementation of measures for the formation and application of financial and economic security.

Prevention of threats and risks based on financial and economic security (Tables 2 and 3).

Table 2. Expert survey results of builders' experts on the level of financial and economic security of construction enterprises, resp. Unit

Indicators	K_{311}	K_{312}	K_{313}
Experts			
E_1	6	5	6
E_2	6	6	5
E_3	6	5	5
E_4	6	7	6

(continued)

Table 2. (continued)

Indicators	K_{311}	K_{312}	K_{313}
E_5	5	6	5
E_6	6	5	5
E_7	5	7	5
E_8	6	5	6
E_9	6	5	5
E_{10}	5	7	5
E_{11}	6	6	5
E_{12}	5	6	6
Wed arithmetic	5,667	5,833	5,333
Wed geom	5,646	5,78	5,313

Table 3. The results of the statistical processing of the results of the expert survey, taking into account the weighting coefficients of expert builders of the level of financial and economic security of construction enterprises, resp. Unit

Indicators	K_{311}	K_{312}	K_{313}
Experts			
E_1	0,855	0,713	0,855
E_2	0,805	0,805	0,671
E_3	0,761	0,634	0,634
E_4	0,694	0,81	0,694
E_5	0,437	0,524	0,437
E_6	0,468	0,39	0,39
E_7	0,355	0,496	0,355
E_8	0,383	0,319	0,383
E_9	0,362	0,301	0,301
E_{10}	0,219	0,307	0,219
E_{11}	0,237	0,237	0,198
E_{12}	0,185	0,222	0,222
\sum_k^y	5,761	5,759	5,359

Expert survey results of builders' experts on the level of formation of information security of construction enterprises are presented in the Table 4.

Table 4. Expert survey results of builders' experts regarding the level of formation of information security of construction enterprises, resp. Unit

Indicators	K_{321}	K_{322}	K_{323}	K_{324}	K_{325}	K_{326}	K_{327}	K_{328}	K_{329}	K_{3210}
Experts										
E_1	5	5	6	5	6	5	6	6	4	5
E_2	6	5	6	5	5	6	5	5	6	5
E_3	4	6	5	6	5	6	5	5	5	6
E_4	6	5	5	6	6	5	6	6	5	5
E_5	6	5	5	5	5	4	5	5	5	6
E_6	6	7	6	5	6	5	5	6	4	6
E_7	5	6	6	5	6	5	5	6	6	5
E_8	6	6	5	6	5	5	6	5	4	5
E_9	6	5	6	6	7	6	5	6	5	6
E_{10}	6	5	6	6	6	6	6	6	5	5
E_{11}	5	5	6	7	6	6	6	6	6	5
E_{12}	6	6	6	4	6	6	4	6	5	6
Wed arithme-tic	5,583	5,5	5,667	5,5	5,75	5,417	5,333	5,667	5,0	5,417
Wed geom	5,542	5,464	5,646	5,446	5,719	5,376	5,295	5,646	4,949	5,395

At construction enterprises, the level of information security for the formation and use of an intelligent economic system is decreasing, which negatively affects the possibilities of applying innovative development tools (Table 5).

Table 5. The results of statistical processing of the expert survey taking into account the weighting coefficients of construction experts of the level of formation of information security of construction enterprises, resp. Unit

Indicators	K_{321}	K_{322}	K_{323}	K_{324}	K_{325}	K_{326}	K_{327}	K_{328}	K_{329}	K_{3210}
Experts										
E_1	0,713	0,713	0,855	0,713	0,855	0,713	0,855	0,855	0,57	0,713
E_2	0,805	0,671	0,805	0,671	0,671	0,805	0,671	0,671	0,805	0,671
E_3	0,507	0,761	0,634	0,761	0,634	0,761	0,634	0,634	0,634	0,761
E_4	0,694	0,579	0,579	0,694	0,694	0,579	0,694	0,694	0,579	0,579
E_5	0,524	0,437	0,437	0,437	0,437	0,35	0,437	0,437	0,437	0,524

(continued)

Table 5. (continued)

Indicators	K_{321}	K_{322}	K_{323}	K_{324}	K_{325}	K_{326}	K_{327}	K_{328}	K_{329}	K_{3210}
E_6	0,468	0,546	0,468	0,39	0,468	0,39	0,39	0,468	0,312	0,468
E_7	0,355	0,425	0,425	0,355	0,425	0,355	0,355	0,425	0,425	0,355
E_8	0,383	0,383	0,319	0,383	0,319	0,319	0,383	0,319	0,255	0,319
E_9	0,362	0,301	0,362	0,362	0,422	0,362	0,301	0,362	0,301	0,362
E_{10}	0,263	0,219	0,263	0,263	0,263	0,263	0,263	0,263	0,219	0,219
E_{11}	0,198	0,198	0,237	0,277	0,237	0,237	0,237	0,237	0,237	0,198
E_{12}	0,222	0,222	0,222	0,148	0,222	0,222	0,148	0,222	0,185	0,222
\sum_k^y	5,494	5,455	5,606	5,452	5,648	5,354	5,368	5,588	4,96	5,389

At the intermediate level, information-analytical support is determined by the interaction of stakeholders regarding the formation and use of the intellectual economic system of construction enterprises (Tables 6 and 7).

Table 6. The results of an expert survey of builders' experts regarding the level of ensuring the interaction of stakeholders of construction enterprises, resp. Unit

Indicators	K_{331}	K_{332}	K_{333}	K_{334}	K_{335}	K_{336}	K_{337}	K_{338}	K_{339}	K_{3310}	K_{3311}
Experts											
E_1	6	6	5	6	6	5	6	6	6	5	6
E_2	7	6	5	5	6	6	5	6	6	5	6
E_3	6	7	5	5	6	6	5	5	6	6	5
E_4	6	7	5	6	5	6	5	6	5	5	6
E_5	6	6	5	7	6	5	6	5	6	5	5
E_6	6	6	5	6	5	6	5	5	5	6	5
E_7	6	5	5	6	6	5	5	5	6	5	6
E_8	6	7	6	6	6	5	6	6	6	7	6
E_9	7	5	5	5	5	5	4	6	6	5	5
E_{10}	6	5	5	6	5	5	5	6	5	6	5
E_{11}	6	6	5	5	6	6	4	5	6	6	6
E_{12}	6	6	6	5	7	6	6	5	5	5	5
Wed arithmetic	6,167	6,0	5,167	5,667	5,75	5,5	5,167	5,5	5,667	5,5	5,5
Wed geom	6,156	5,958	5,154	5,633	5,719	5,477	5,119	5,477	5,646	5,464	5,477

Table 7. The results of the statistical processing of the expert survey, taking into account the weighting coefficients of expert builders of the level of ensuring the interaction of stakeholders of construction enterprises, resp. Unit

Indicators	K_{331}	K_{332}	K_{333}	K_{334}	K_{335}	K_{336}	K_{337}	K_{338}	K_{339}	K_{3310}	K_{3311}
Experts											
E_1	0,855	0,855	0,713	0,855	0,855	0,713	0,855	0,855	0,855	0,713	0,855
E_2	0,939	0,805	0,671	0,671	0,805	0,805	0,671	0,805	0,805	0,671	0,805
E_3	0,761	0,887	0,634	0,634	0,761	0,761	0,634	0,634	0,761	0,761	0,634
E_4	0,694	0,81	0,579	0,694	0,579	0,694	0,579	0,694	0,579	0,579	0,694
E_5	0,524	0,524	0,437	0,612	0,524	0,437	0,524	0,437	0,524	0,437	0,437
E_6	0,468	0,468	0,39	0,468	0,39	0,468	0,39	0,39	0,39	0,468	0,39
E_7	0,425	0,355	0,355	0,425	0,425	0,355	0,355	0,355	0,425	0,355	0,425
E_8	0,383	0,447	0,383	0,383	0,383	0,319	0,383	0,383	0,383	0,447	0,383
E_9	0,422	0,301	0,301	0,301	0,301	0,301	0,241	0,362	0,362	0,301	0,301
E_{10}	0,263	0,219	0,219	0,263	0,219	0,219	0,219	0,263	0,219	0,263	0,219
E_{11}	0,237	0,237	0,198	0,198	0,237	0,237	0,158	0,198	0,237	0,237	0,237
E_{12}	0,222	0,222	0,222	0,185	0,259	0,222	0,222	0,185	0,185	0,185	0,185
$\sum y_k$	6,194	6,131	5,101	5,69	5,739	5,531	5,231	5,56	5,725	5,416	5,567

Generalized indicators of safety factors for the use and formation of intelligent economic systems of construction enterprises are determined by the geometric mean of group local indicators of the i -th group:

$$K_i = \sqrt[n]{K_{ij}} \tag{1}$$

n – the number of local factors in the i -th group, resp. Unit.

The generalized economic indicators calculated according to model (1) are presented in the Table 8.

Table 8. Generalized indicators of safety factors for the formation and use of intelligent economic systems of construction enterprises.

Group indicators	Value
financial and economic security of construction enterprises,	5,623
formation of information security of construction enterprises	5,428
ensuring the interaction of stakeholders of construction enterprises	5,617

3 Result

The general indicator of safety factors in the formation and use of intelligent economic systems of building enterprises should be resistant to possible fluctuations in the values of individual group indicators. Based on statistical observations, the integral indicator of safety factors of the formation and use of intelligent economic systems of construction enterprises was calculated according to the Kolmogorov root mean square, which fully meets the requirements of stability:

$$I = \sqrt{\frac{1}{k} \sum_{i=1}^k K_i^2}, \quad (2)$$

k – safety factors of the formation and use of intelligent economic systems of construction enterprises.

The value of the complex indicator of the level of safety factors of the formation and use of intelligent economic systems of the construction enterprise calculated by (2) is equal to 5.557.

4 Conclusion

So, because of the study of the state and development trends of the construction sector, it was determined:

1. Construction industry is an important branch of the state economy, which affects its development and ensures the functioning of other spheres of activity. It reflects trends and is an indicator of the development of the state's economy. Construction industry reacts more inertly to the changes taking place in the state, both in terms of development and the accumulation of negative phenomena.
2. For the period until 2020, there is an increase in the main indicators of the construction sector. In particular, the production and economic potential is strengthened due to the growth of fixed assets, current assets, sources of financing. It should be noted that the value of equity is decreasing along with an increase in the level of current liabilities. This affects the level of financial stability of construction enterprises.
3. During the studied period, the majority of enterprises in the construction sector are profitable, which indicates positive financial performance and provides a shift in the development of construction business entities.
4. It should be pointed out the slowdown in the development of labor potential in the construction sector, which reduces the trends and level of development of construction enterprises. This especially applies to the development and implementation of intelligent economic systems.

Thus, safety factors for the use and formation of the intelligent economic system of construction enterprises are proposed, the assessment of which is based on the application of qualitative methods used for construction enterprises and regions. The presented indicators are determined by the level of national security, directions of formation and use of financial, economic and information security, features of interaction of construction

companies with stakeholders. Safety indicators make it possible to build a quantitative basis for assessing the level of formation and use of an intelligent economic system for making informed management decisions.

A quantitative basis for the development and implementation of safety directions for the formation and use of the intellectual economic system of construction enterprises has been formed by evaluating safety factors. It has been established that the formation of information and analytical support for the implementation of security measures is mediocre, which indicates the need to implement directions for increasing their effectiveness.

The formation of intelligent economic systems requires the solution of complex problematic issues related to:

transformation of the information security system and the use of modern information technologies;

Expanding the possibilities of using artificial intelligence tools;

Low level of personnel training regarding the development and application of intelligent economic systems;

Insufficient level of completeness of spatial information on the functioning of construction companies;

The Problem of the formation of economic and social factors for the development of intellectual economic systems;

Transformation of the organizational structure of construction enterprises in accordance with the directions of formation and use of intelligent economic systems;

Insufficient Level of determination of urban planning factors, considering the peculiarities of regulatory and legal support.

Based on the identified problematic issues, directions for further research are proposed:

Studying and determining the possibilities of applying artificial intelligence at construction enterprises;

Formation of educational programs for personnel training, taking into account directions and features of implementation and application of intelligent economic systems;

Determination of directions of organizational and instrumental transformation at building enterprises for the use of intelligent economic systems;

Research of spatial aspects regarding the activity of construction enterprises using geoinformation systems and technologies;

Study of economic factors as a system affecting the formation of intellectual economic systems of construction enterprises;

Determination of urban planning factors and their research in the system of formation of factors of intellectual economic systems;

Determination of growth points of relevant factors;

Development of an organizational and economic mechanism for the use and formation of intelligent economic systems of construction enterprises.

References

1. Construction as a branch of material production and its features. <https://cutt.ly/p2uuJzL>
2. Official website of the State Statistics Service of Ukraine. <https://ukrstat.gov.ua>
3. Androschuk, G.: Artificial intelligence: economy, intellectual property, threats. Economics of intellectual property. Theory Pract. Intellect. Property (2), 56–74 (2021)
4. Economic information systems in business. https://pidru4niki.com/1652020557064/ekonomika/ekonomichni_informatsiyeni_sistemi_biznesi
5. Hrytskov, E.V.: Steykkholderno-oriyentovany pidkhid do upravlinnya budivelnymy pidpryyemstvamy. Naukovo-vyrobnychyy zhurnal “Biznes-navihator”. Vypusk 3–1(46) (2018). http://business-navigator.ks.ua/journals/2018/46_1_2018/26.pdf
6. Mamonov, K.A.: Steykkholderna stratehiya vartisno-oriyentovanoho upravlinnya kapitalom brendu budivel'nykh korporatyvnykh pidpryyemstv: dys... d-ra ekon. nauk: 08.00.04/Kharkivs'ka natsional'na akademiya mis'koho hospodarstva. 557 p. (2013)
7. Mamonov, K.A., Nesterenko, S.G., Shterndok, E.S., Grek, M.A., Rudomakha, A.V.: Steykkholderno-integririvannyi podkhod k otsenke urovnya inzhenerno-infrastrukturnogo obespecheniya gorodov. Nauka i tekhnika. T. 17(2), 130–141 (2018)
8. Mamonov, K.A., Dymchenko, E.V., Grytskov, E.V., Velychko, V.A.: Integrated approach for assessing the level of stakeholder interaction on construction enterprises. In: European Proceedings of Social and Behavioural Sciences. EpSBS, pp. 1054–1063 (2021)
9. AA1000 Stakeholder Engagement Standard. https://www.accountability.org/wp-content/uploads/2016/10/AA1000SES_2015.pdf (2015)
10. Bendheim, C.L., Waddock, S.A., Graves, S.B.: Determining best practices in corporate-stakeholder relations using data envelopment analysis: an industry level study. Bus. Soc. 37(3), 306–338 (1998)
11. Borrini-Feyerabend, G., Brown, M.: Social actors and stakeholders. IUCN World Conservation, Social Policy Programme, Beyond Fences: Seeking Social Sustainability in Conservation, Section 4. Concept files. http://www.iucn.org/themes/spg/beyond_fences/bf_section4_1.html
12. D'Anselmi, P.: Values and Stakeholders in an Era of Social Responsibility. Free Press, New York (2011)
13. Dovbysh, A.S., Tron, V.A.: Predictive learning of the automated control system for the technological process of phosphoric acid production, vol. 2, pp. 85–91. Visnyk Sumy State University. Series: Technical sciences (2009)
14. Kvasny, R.: Artificial intelligence – an Internet resource. <http://neural.narod.ru/> (2001)
15. Nylson, N.: Ykysustvennyy yntellekt. Metody poyska resheniy: Per. s anh./Pod red. S.V. Fomya.–M.: Myr. 270 p. (1973)
16. Horelyk, A.L., Skrypky, V.A.: Metody raspoznavanyia.–M. Vysshaya, shkola. 232 p. (1989)
17. Goldberg, D.E.: Genetic Algorithms in Search, Optimisation and Machine Learning, 412 p. Addison – Wesley Publishing Company, Inc., USA (1989)
18. Mamonov, K., Nesterenko, S., Radzinskaya, Y., Dolia, O.: City lands investment attractiveness calculation. Geodesy Cartography 68(1), 211–223 (2019)
19. Mamonov, K.: Methodological approach to the integral assessment of the regional lands use territorial development. Geodesy Cartography 45(3), 110–115 (2019)
20. Mamonov, K.A., Wen, M.M., Liu, C., Du, J.: Measurement of coordinated and coupled development and evaluation of sustainable development for marine economic-ecological complex system. Hindawi Discrete Dyn. Nat. Soc. 2021, 2043635 (2021)
21. Mamonov, K., Bieliatynskyi, A., Wen, M.M., Liu, C., Dymchenko, E.: Formation of the intellectual systems for the territorial development of land administration in the coastal regions. J. Environ. Eng. Landsc. Manag. 30(3), 424–432 (2022)

22. Nikiforov, P.O., Kucherivska, S.S.: Sutnist i znachennya finansovoyi bezpeky strakhovoyi kompaniyi. *Finansy Ukrainy* **5**, 86–94 (2006)
23. Stolbov, V., Shapoval, H.: Osoblyvosti upravlinnya systemoyu finansovo-ekonomichnoi bezpeky budivel'nykh pidpryyemstv. *Komunalne hospodarstvo mist: Zb. nauk. prats. – Vyp. 111*, 103–107 (2019)
24. Davydyuk, T.: Finansovo-ekonomichna bezpeka chy finansova skladova ekonomichnoi bezpeky: epistemolohichnyy pidkhid. *Problemy teorii ta metodolohii bukhhalterskoho obliku, kontrolyu i analizu* **1(25)**, 39–52 (2013)



Architecture and Techniques of Environmental Control of Climatic Colonies in Italy and Abruzzo

Eleonora Laurini¹(✉), Patrizia Montuori¹, and John D. Murphy Jr.²

¹ Department of Civil, Architectural Construction and Environmental Engineering, Piazzale Ernesto Pontieri, Monteluco di Roio, University of L'Aquila, 67100 L'Aquila, AQ, Italy
{eleonora.laurini, patrizia.montuori}@univaq.it

² College of Engineering and Integrated Design, University of Texas at San Antonio, 1 Utsa Cir, San Antonio, TX 78249, USA
john.murphy@utsa.edu

Abstract. The climatic colonies are a new typology of buildings, an unprecedented synthesis of health and educational structures, promoted by the National Fascist Party for the care and training of young people with the aim of physically and mentally “shaping” the new Italian, from the very early childhood. The buildings are complex “sanitary machines”, using distribution and construction solutions based on studies and experience gained since the 19th century to make buildings for the healthy treatment of tuberculosis and lung diseases (hospices and sanatoriums). The contribution starts with a study of the architectural, typological and construction characteristics of colonies, located in both marine and mountain environments, and focuses attention, in particular, on two of those built in Abruzzo in the 1920s during the Fascist Fascist period. The original functioning of the two buildings will be investigated, as well as the effectiveness of the solutions adopted to achieve internal comfort and the building-environment relationship. This study is aided by computer simulations. These themes are fundamental for guiding the recovery of this type of existing structure, and also consider recent and continuing climate change to which the entire planet is subjected.

Keywords: Climatic Colonies · Comfort Indoor · Thermo-Hygro-metric

1 Introduction

1.1 Marine and Mountain Colonies in Italy and Abruzzo during the Fascist Period: Architecture, Typology and Environmental Control in Comparison

With law no. 2447 of 3 April 1926, the Opera Nazionale Balilla (ONB) was founded, which in 1937 was incorporated into the GIL, Gioventù Italiana del Littorio: with these institutions, the Fascist regime replaced the vast movement of local and philanthropic committees that in previous decades had promoted the creation of seaside hospices in Italy to treat lung diseases and tuberculosis with sea air [1–3], with a health and education strategy aimed at forging new Italians, making them healthy and loyal to the regime [4–6].

In this system, architecture takes on a central role, thanks to new architectural typologies conceived for this purpose, including the “climatic colonies”, buildings that are the result of an unprecedented synthesis between the health and prophylaxis function of 19th century hospices and sanatoriums and the scholastic and sporting functions.

Central to the regime’s social policy, especially since the 1930s, the colonies became a precious opportunity for Italian architects to experiment with a modern architectural language, using more rhetorical futuristic references to shapes that evoke biplanes, ships, submarines or symbols of the regime that stimulate the imagination of the young guests with their image; or using more rigorous applications of the formal logic of the modern movement.

According to the data provided by the regime in 1936, 3,128 colonies of all types had been set up, with a total of 568,681 children being cared for, compared with 99,256 in 1923 [3]. They were of various types: ‘permanent colonies’ for the prophylaxis and treatment of pathological cases, run by the Opera Nazionale Maternità e Infanzia (ONMI); ‘day colonies’, where destitute but basically healthy children spent the day in places close to urban centres; ‘temporary colonies’, where children spent holidays, usually at the seaside or in the mountains.

Per the data provided by the regime in 1936 [3] (see above), even with this dramatic increase in numbers, there was some confusion as late as the thirties about the typological classification of these buildings, denounced by the entry “Summer colonies” in the Treccani encyclopedia written by Arcangelo Ilvento [7] in which they are still flanked by marine and mountain hospices. Also, in the “Manual of the Architect” by Daniele Donghi [8] they are still included in the chapter dedicated to sanatoriums and distinct in mountain colonies, for anti-tuberculosis prevention, and scholastically conceived as outdoor schools particularities in marine localities without construction and assimilation to para-hospital buildings. The confusion is partially overcome only thanks to the architectural-typological classification of the marine, mountain and heliotherapeutic colonies, proposed in 1941 by Attilio Labò and Mario Podestà (1941), in which it is specified that “the theme resumes, in some way, the tradition of the Greek ‘gyms’; which, as we know, were not only a place for gymnastics” and “at the architectural level, the hygienic goal, with the impeccable healthiness of the rooms and with their equipment, is only a premise, an implicit preliminary [beginning]. The plant holds the hotel, the school, and the clinic at the same time”. The authors then proceed to identify four main organizational schemes, in particular, for the marine colonies: the “village”, with separate and sometimes communicating buildings; the ‘open plan’, with asymmetrical juxtapositions and interpenetration of volumes; the “tower” and the “monoblock”, with a single body built vertically or horizontally; to the latter type is added a fifth “hybrid”, the “contaminations”, with a vertical element inserted in a predominantly horizontal form.

The mountain colony, according to Labò and Podestà, is also typologically interpretable “as a compromise between the hotel and the house”, but in this case, the issue of orientation is more complex: according to the two authors, in fact, who deal only superficially with the environmental problem, while in the marine structures the only conditioning factor is “the scorching summer sun reflected by the sea”. In the mountains, dominant winds also come into play, which could depend or not on the primary

wind directions. Dramatic change in elevations/altitudes can also have great importance. Finally, from the architectural point of view, the reduced availability of surface and the binding presence of the vertical dimension in the mountain landscape, makes the use of recurring planimetric schemes and rationalist-type volumes less frequent: therefore, they observe “some architects will adapt with a planimetric inflection at the curve of an amphitheater of mountains, others will divide or break up their volumes, others will eventually resort to borrowing from rustic architecture language, with varying fortune”.

In reality, the more limited number of mountain colonies built during the Fascist period actually makes unrealistic cataloging them by typological schemes. The only observation in this regard is, precisely, the greater diffusion of a vernacular architectural language, which echoes the motifs of the chalet and mountain hut on different scales, using and exhibiting natural materials characteristic of Alpine building. Only a few examples, such as the Rinaldo Piaggio in S. Stefano d’Aveto, Genoa (1938) by Luigi Carlo Daneri or the IX Maggio, in Monteluco of Roio, L’Aquila (1934) by Ettore Rossi escape the judgment of architectural mediocrity of this type of colonies formulated by Labò and Podestà. In fact, the two designers both not only adopt a refined rationalist language, but also materials and design devices designed to favor the internal healthiness of buildings, maximizing or mitigating the effects of external environmental factors.

In the semi-arched monoblock of Daneri, in fact, the façades of the dormitories are oriented to the north and south, exploiting the bactericidal action of the sun with a solution typical of sanatoriums with the southern orientation, completely glazed to capture the sun’s rays. The opposite facades are almost completely blind except for small transom windows with roller shutters. Rossi, among the first experts in Italy in “monoblock” hospital construction, designed for the Ente Nazionale Assistenza Gente di Mare (ENAGM) a colony located on the hill overlooking L’Aquila, characterized by an elegant double-curved layout. The services are arranged in the center and divide the body into two wings, male and female, with the gyms on the first floor and the dormitories on the upper floors, inclined exactly 15 degrees from the central body and facing south-east so as to enjoy an optimal insulation during the day and also in the Winter, since the colony was also active from November to June. The corridors and services, instead, are arranged on the opposite side of the dormitories, also taking advantage of ventilation and direct lighting, avoiding the need to use forced ventilation and, indeed, guaranteeing a healthy transverse ventilation of the dormitories. Two stairwells particularly located also likely created a further “chimney effect” [7, 9] (Fig. 1).

Also one of the two marine colonies created in Abruzzo during the Fascist period, the Stella Maris in Montesilvano, Pescara (1937), was characterized by a monoblock scheme, but more volumetrically articulated. It was designed by the Roman architect Francesco Leoni for the “Federazione of Fasci di Combattimento di Rieti”. Its futuristic image of an aircraft, “ready to take flight”, in the signs of the Littorio¹ contrasts with the more canonical “village” system of the colony Rosa Maltoni Mussolini (1936) [10], built in Giulianova, Teramo, a project by Eng. Alberto Ricci for the “Istituto Nazionale Assistenza Magistrale (INAM) (Montuori 2019). The shape of the airplane is used by Leoni not only as a symbolic and evocative reference but for the rational organization of spaces and the internal environmental control: the central block, destined to the first floor of the refectory and to the helicoidal staircase that leads to the upper tower, in

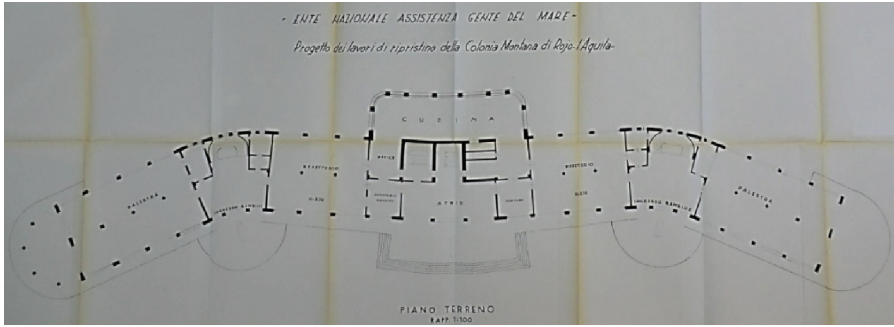


Fig. 1. Colony IX Maggio: plan of the ground floor of the building (Archive of Ispettorato Generale del Ministero delle Finanze, ENAGM)

fact, is conceived as a sort of ventilation tower of the building, with large windows facing east towards the sea, with guillotine openings and shutters, to control currents and radiation during the hottest hours; the dormitories, separated from the central tower by filter rooms with vestibules and toilets, are arranged in the wings of the biplane with a canonical east-west orientation, and equipped with windows on both sides to facilitate cross-ventilation of the rooms [9] (Fig. 2).

The colonies IX Maggio and Stella Maris, therefore, are, on one hand, a perfect demonstration of how this type of building was conceived in relation to the different environmental contexts to respond to precise hygienic parameters of sunshine, aeration and lighting. For example, the marine colonies were arranged mostly towards the south-east and somewhat parallel to the coast, to exploit not only the air movement triggered by the temperature difference of the opposite walls, but also the sea breeze. However, in the mountain colonies the environment was orientated mostly to the south, to take advantage of the sun's rays and heat as much as possible. On the other hand, these progressive designs over time show the ability of some of the designers to “bend” this technical approach to precise formal and architectural choices, created differing expressions of the modern language.

The changes introduced in the buildings after the loss of the original function and their transformation have often caused alterations not only in the architectural image of the buildings, but also in the original internal environmental control. The former colony IX May, for example, today still awaiting consolidation and restoration after being damaged by the earthquake in L'Aquila in 2009. It was functional until the outbreak of the Second World War, then transformed between the Forties and Fifties into a reception center for displaced persons and, since the 1960s, converted into the new headquarters of the Faculty of Engineering of the University of L'Aquila: in addition to the architectural image, therefore, the distribution and operation of the building has also been strongly modified, with the division of the dormitories and the occlusion of the two side staircases and with the insertion of elevators. Even the colony of Montesilvano, although never activated for the outbreak of war, has undergone several distribution alterations over the years. The last being to transform it into a dormitory for the students of the hotel

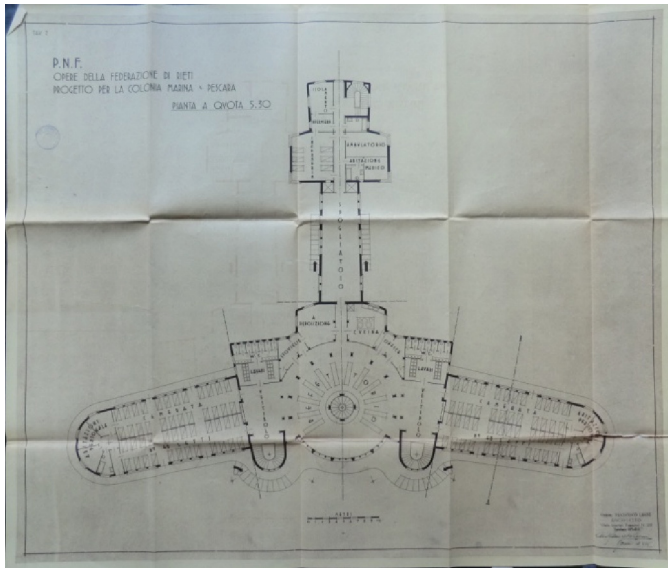


Fig. 2. Colony Stella Maris, Montesilvano (PE): Plan of the first floor of the building (Archivio Centrale dello Stato)

management school of Pescara, with the division of the dormitories to create the rooms and the closure of the arcades on the ground floor.

2 Materials and Methods

The historical analyses of the typology of the climatic colonies and, in particular, of the Stella Maris in Montesilvano (Pescara) and IX Maggio in Monteluco di Roio (L'Aquila), will be verified in quantitative terms, analyzing the original state of the two buildings, as well as in the years of respective numerous modifications and alterations (architectural and construction) in order to demonstrate the perfect functioning of the same as “thermal machines”, in particular, as it relates to natural ventilation and the natural cooling of the buildings [10]. This research does not include analyses of the heating, because it focuses on analysis during the summer season. They have been conducted, therefore, considering the buildings from an unoccupied passive perspective such as the orientation and the spatiality of the buildings, the number and position of the openings, the presence of specific similar architectural elements such as the towers of ventilation, with the aim of knowing the original potential of these structures from a thermohygrometric point of view [11, 12].

The thermohygrometric efficacy, in fact, is influenced by six factors: four about environmental nature (air temperature, average radiant temperature, relative humidity and air speed), and two related to users [activity (metabolism) (met) and clothing (clo)].

As the subject of this study, environmental performance is greatly influenced by the planimetric conformation and the distribution and construction solutions adopted in the buildings [13]. In fact, the intrinsic thermo-hygrometric behavior can be associated with

construction solutions, which favor the bioclimatic functioning of the structures (Masetti, 2009). Among these are the most ancient thermal machines built by man: the ventilation chimneys, inside which the air circulates according to differences in temperature and, above all, pressure between inside and outside, and between the different building floors which, even if minimal, increase with height and temperature differences. Moreover, each gas, if heated, expands proportionally to the increase of its absolute temperature, undergoing a decrease in the specific weight and tending to rise upwards. This phenomenon can be exploited to naturally ventilate the otherwise contained environment and obtain optimal climatic conditions. Also, in the climatic colonies it is possible to identify some architectural features that originally worked as ventilation towers, conceived also in relation to the specific exposure and site configuration, and that is assumed to be a key role in the buildings design.

2.1 The Stella Maris in Montesilvano (Pescara) and IX Maggio in Monteluco di Roio (L'Aquila) Colonies: Thermo-Hygrometric Analysis

The Stella Maris marine colony in Montesilvano (Pescara) and the IX Maggio colony in Monteluco di Roio (L'Aquila) are located in two areas of Abruzzo at the antipodes from both the climatic and the altimetric point of view. In both cases, the achievement of internal comfort has been evaluated through natural ventilation in the summer months (from 21 June to 21 September), during which time the buildings were both originally used, in order to check whether the buildings have been designed according to the altitude. As a result, simulation models have been created with the Designer Builder software, positioning the buildings in both the elevations (810 m asl – Monteluco di Roio- and 0 m asl- Montesilvano) and checking the results according to the thermal hygrometric conditions obtained. Even if the analyzes in naturally ventilated buildings are carried out with the adaptive method, it is possible to use the Fanger method in non-hot climate zones (as reported by Parisi E., Cap III Grosso, 2011). Both colonies are located in temperate climate zones and since the development of the research involves a comparison with the buildings redeveloped from the point of view of the envelope and the systems (including VMC), the examination of comfort levels has been carried out using the Fanger index method, considering an average value of air speed equal to 0.1 m/s and two parameters related to the activities carried out inside the buildings and the clothing type (1.00 met – sedentary activity- and 0.5 clo – light summer clothing). Moreover, in computer simulations the wind direction plays a fundamental role in both locations, for which the prevailing wind has been considered and compared to the data monitored during the year.

Design Builder, in fact, allows to study the movement of thermal masses and natural ventilation flows in accordance with the external weather conditions, to evaluate the masses of air exchanged between exterior and interior and in different areas of the model, through openings based on the wind speed and pressure differences [14, 15].

In the absence of reliable data on the materials originally used in the construction of the two buildings, modeling was performed on the basis of the information found in the archives. In the simulations, therefore, it was hypothesized that the presence of perimeter walls in solid brick (Stella Maris) or mixed bricks, in stones and bricks (IX Maggio), were practically equivalent for thermal inertia, without thermal insulation,

also non-insulated covers and wooden window frames with single, non-insulated and non-sealed glass [16, 17] (Fig. 3).

3 The Cases Study

3.1 Thermo-Hygrometric Simulations on the Behavior Colonies: Stella Colony

The Stella Maris colony is located near the sea coast in the municipality of Montesilvano, in the province of Pescara. As shown by the aerial view, the two “wings” of the building widen towards the coast and, as shown in the wind rose, the wind intensity, equal to 3 m/s, is strongly influenced by the presence of the sea and directed towards the North-East (Figs. 4 and 5).

The modelling, taking into account openings with windows, but above all the presence at the intersection of the two wings, of a tower, intended for the refectory and the spiral staircase leading to the terrace and the director’s accommodation, which extends over the entire height of the building. That staircase/tower acts as a ventilation chimney, creating internal air flows, generated by convective motions which allow a thermo-hygrometric ‘washing’ that favors internal well-being.

Applying qualitative considerations, the air flows that develop from the central tower, in fact, are also propagated in the “wings” and in the tail of the building, crossing all the rooms and ensuring comfort conditions throughout the building, as evidenced by the quality of flows (Fig. 6).

On the building model elaborated with the software (Fig. 7), a simulation in dynamic regime was then carried out in order to evaluate the interior comfort of the building during the warmer months, for which it is usually necessary to use mechanical ventilation or conditioning systems for users’ well-being. However, for this purpose, only natural ventilation was evaluated, facilitated by the presence of the central tower and the shape of the building.

The first simulation was elaborated positioning the building in its real location, in the municipality of Montesilvano (PE) and creating a linear graph with the performance of the comfort parameters during the summer months. The average data relative to the air temperature, the radiating temperature and the resulting relative humidity, were used to verify the comfort according to Fanger indices (PPD and PMV) (Fig. 7).

The curve of the Fanger indices shows that the simulation in the Montesilvano town had obtained verified results in terms of thermo-hygrometric comfort.

The same simulation was carried out by positioning the Stella Maris colony, in a mountainous area, at 810 m asl, in the locality of Montelucio di Roio (AQ).

Also in this case, as shown by the graphs obtained and the Fanger Indices curve, comfort is verified (Fig. 8), a sign of the building’s excellent functioning both in the climatic zone for which it was designed, so too in a completely different climate (Fig. 9).

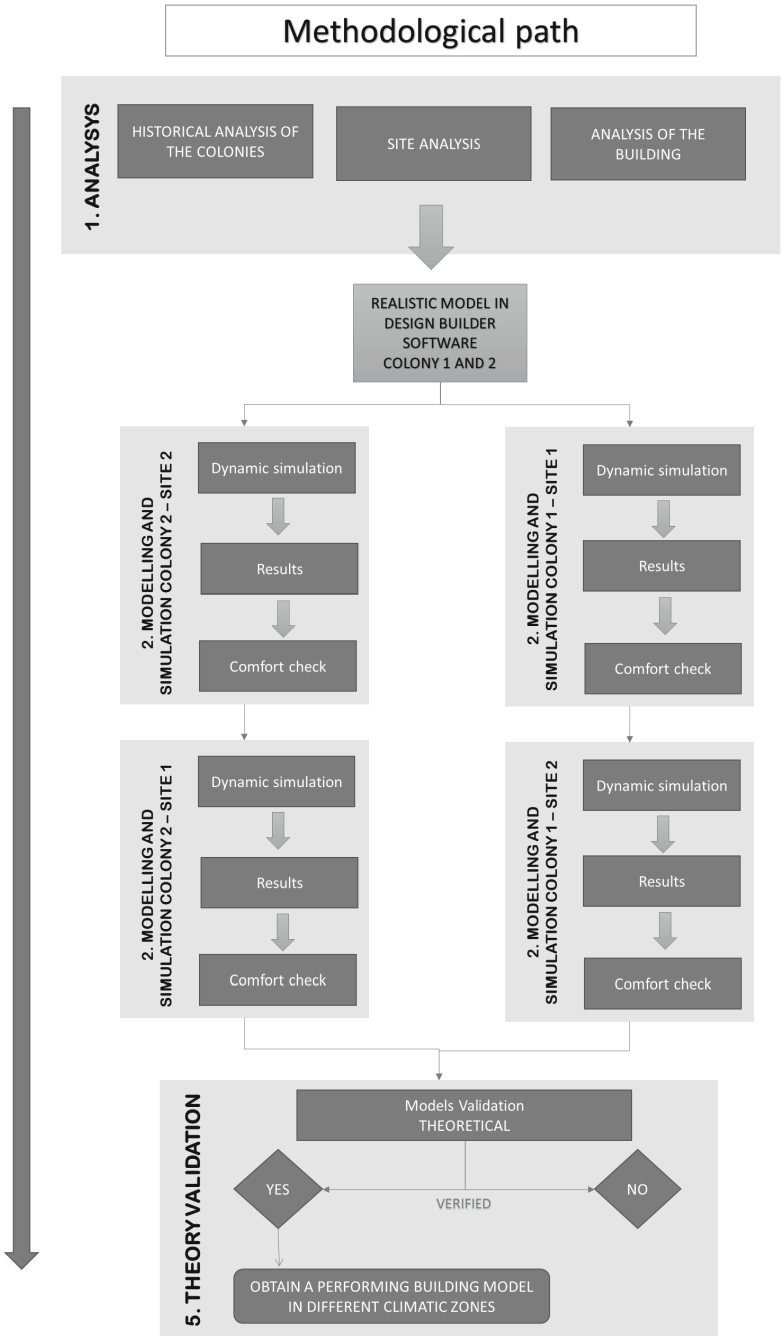


Fig. 3. Methodological path.



Fig. 4. (a) Google earth photo; (b) wind rose of the Montesilvano area (PE).



Fig. 5. Photo of Stella Maris building.

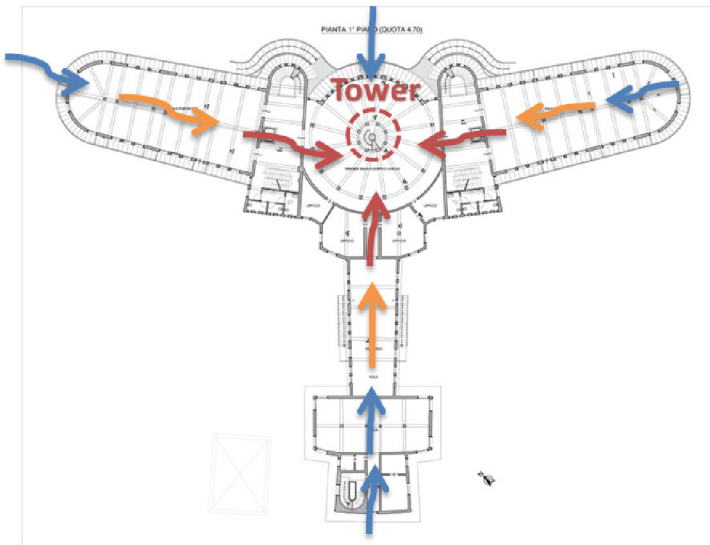


Fig. 6. Colony Stella Maris. Qualitative scheme of air flows: cold (blue); at intermediate temperatures (orange); hot (red). At the center the tower that serves as a ventilation chimney.

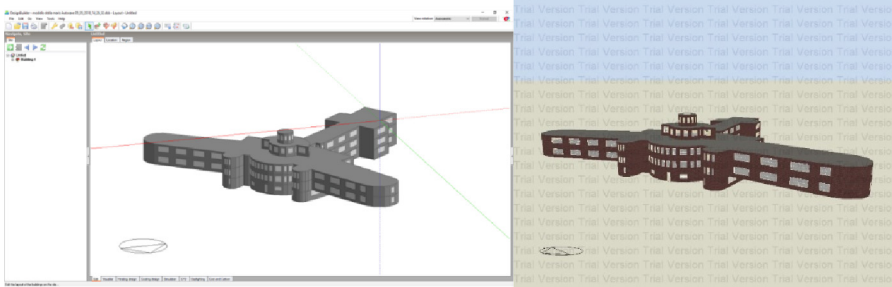


Fig. 7. Model of Stella Maris colony elaborated with Design Builder.

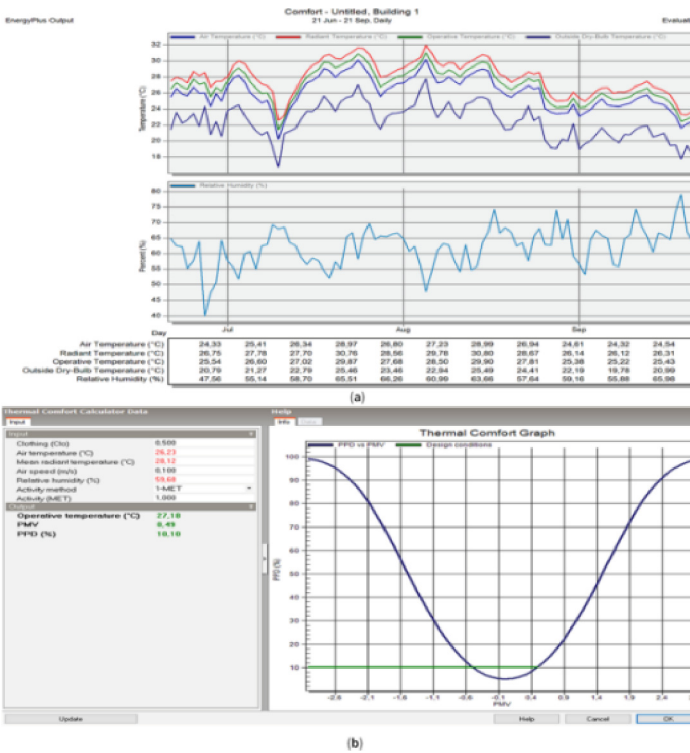
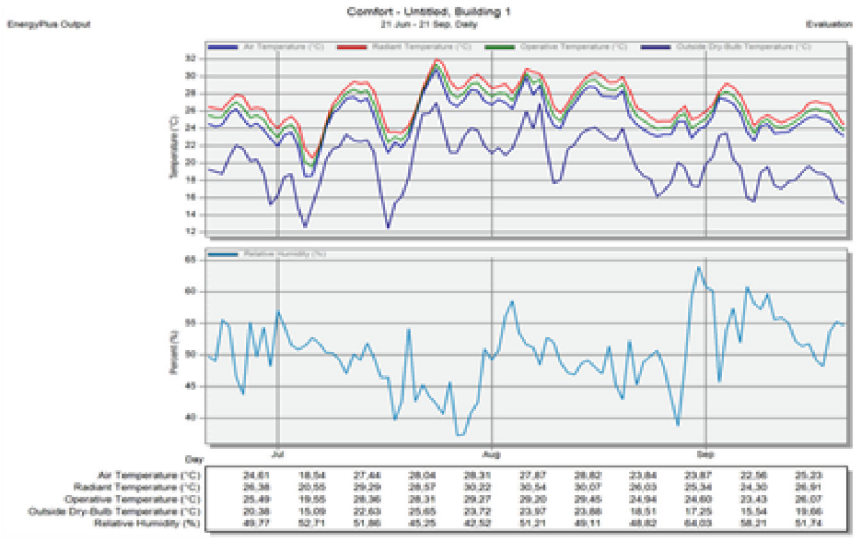
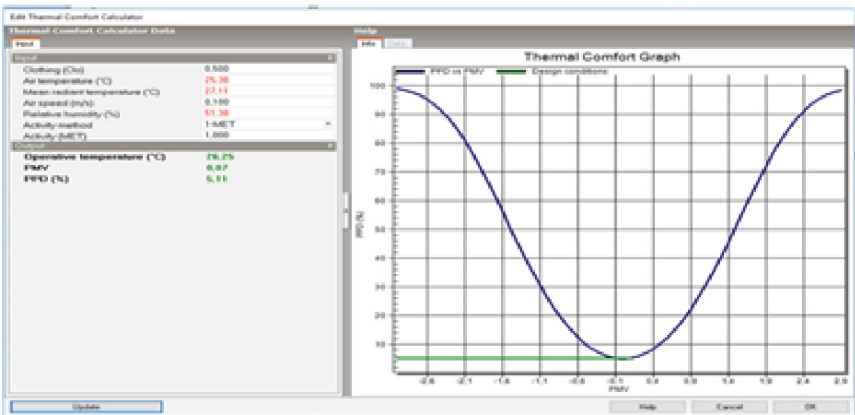


Fig. 8. Colony Stella Maris. Graphs of the trend of the comfort parameter curves (a) and verification graph of the Fanger indices (b) in the climatic zone of Montesilvano (PE). Graphs of the trend of the comfort parameter curves (a) and verification graph of the Fanger indices (b) in the climatic zone of Montelucio di Roio (AQ).



(a)



(b)

Fig. 9. Colony Stella Maris. Graphs of the trend of the comfort parameter curves (a) and verification graph of the Fanger indices (b) in the climatic zone of Montesilvano (PE). Graphs of the trend of the comfort parameter curves (a) and verification graph of the Fanger indices (b) in the climatic zone of Montelucio di Roio (AQ).

The IX Maggio colony is situated instead, at 810 m asl, on a hill in the locality of Montelucio di Roio, not far from the center of L’Aquila. Both the position and the planimetric characteristics of the L’Aquila building are, therefore, completely different from the one made in Montesilvano. In fact, if the open plan of the Stella Maris turned towards the sea coast in the North-East direction, in the case of the IX Maggio colony, the highlighted directionality is in the opposite direction (South-East) with a wind intensity equal to 2 m/s (Figs. 10 and 11).



Fig. 10. (a) Google earth photos; (b) wind rose of the locality Montelucio di Roio, L'Aquila.

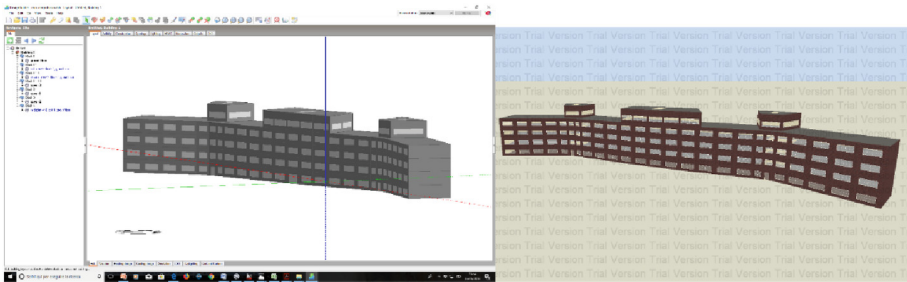


Fig. 11. Model of IX Maggio colony elaborated with Design Builder.

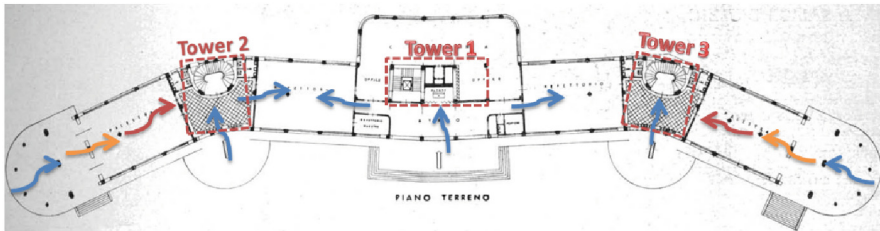


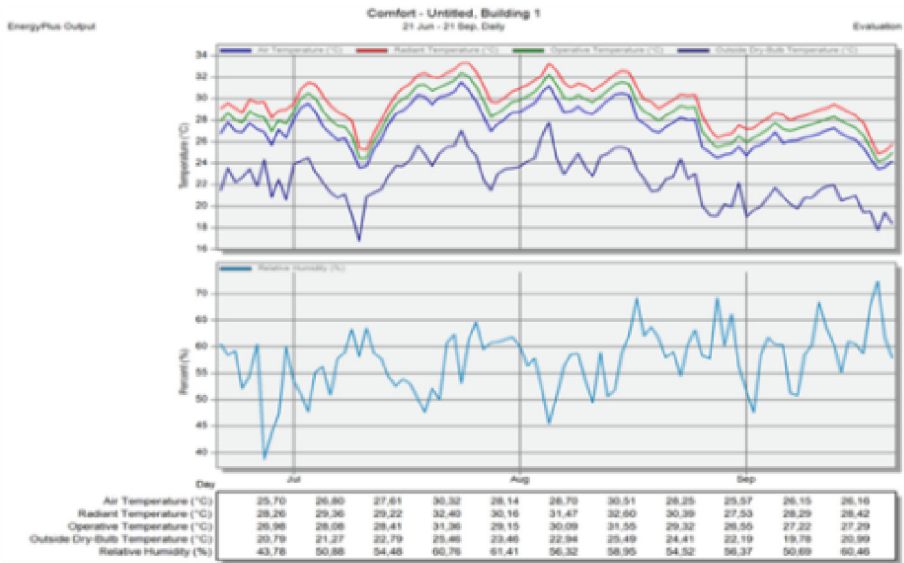
Fig. 12. Colony IX Maggio. Qualitative scheme of air flows: cold (blue); at intermediate temperatures (orange); hot (red). At the center and the sides the towers that act as ventilation chimneys.

The planimetric layout of the IX Maggio colony is much simpler than the Stella Maris plan: a single building with the ends slightly inclined towards the inside and three “towers” at full height, corresponding to the three entrances and staircases, a larger central one and two lateral ones, which act as ventilation chimneys. They create currents inside the building, which favor air exchange and natural ventilation (Fig. 12). Through the simulation under dynamic regime the graph relating to the progress of the internal comfort parameters has been reconstructed.

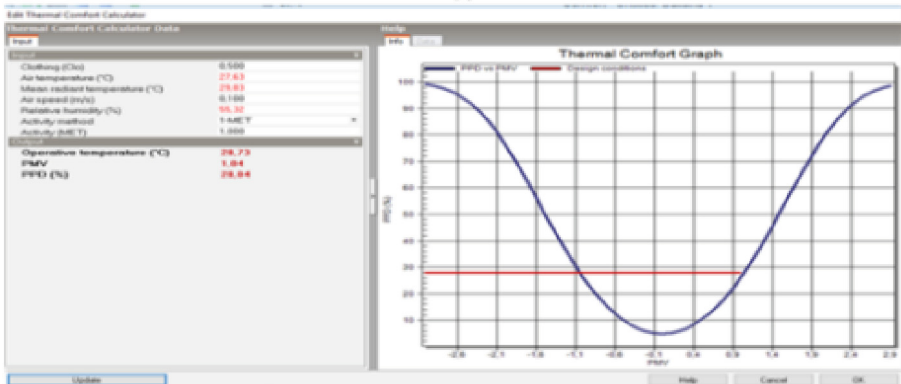
The average summer values of air temperature, radiant and relative humidity, were then used for the comfort check with the Fanger index method, which showed how the colony IX Maggio, in its real location, has an excellent thermo-hygrometric behavior during the summer months (Fig. 13).

It was then suggested to place the building in a different climatic context, positioning it, for example, on the Stella Maris site, with the aim of verifying whether its functioning as a thermal machine is effective even in a place with different temperatures and humidity.

In this case, the simulation gave a negative result, because in this different location, the IX May colony does not have the same internal comfort parameters (Fig. 14).

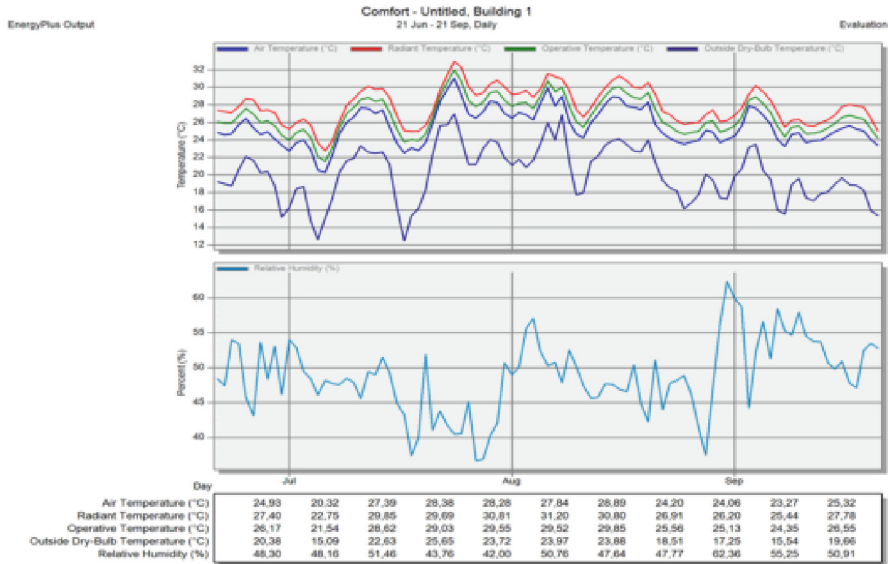


(a)

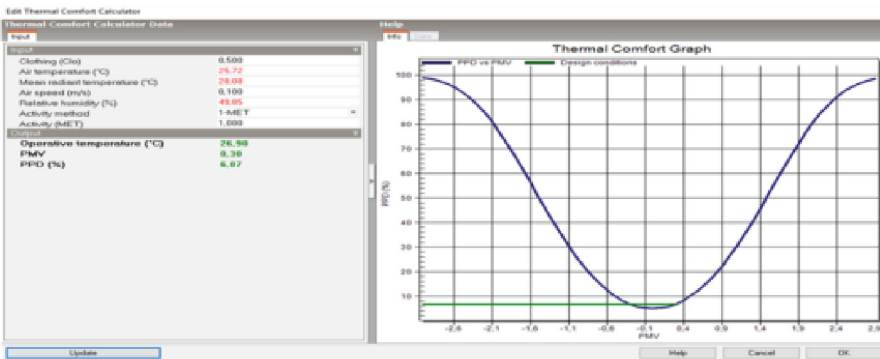


(b)

Fig. 13. Colony IX May. Graphs of the trend of the comfort parameter curves (a) and verification graph of the Fanger indices (b) in the climatic zone of Monteluco of Roio (AQ) and Montesilvano (PE).



(a)



(b)

Fig. 14. Colony IX May. Graphs of the trend of the comfort parameter curves (a) and verification graph of the Fanger indices (b) in the climatic zone of Montelucio of Roio (AQ) and Montesilvano (PE).

4 Discussion

4.1 Simulations Results on the Stella Maris and IX May Colonies: Comparisons

The results obtained from the computer simulations on the two buildings were traced back to the average summer values regarding the air temperature, radiant and relative humidity (Table 1). This enabled gathering unit data from its application to the psychrometric comfort maps (Fig. 15) with the aim of comparing the behavior of the two ‘thermal machines’.

Table 1. Average values of the parameters obtained by means of dynamic simulation, relating to the climatic zone of Montesilvano (PE) and to Montelucio di Roio, L'Aquila (AQ), for both the buildings under study.

Loc. Montelucio di Roio, L'Aquila (AQ) 21 July-21 Sept, Altitude 810slm, orientation SW, 2 m/s wind speed, 26 °C outdoor running mean outdoor temperature			
	Air Temperature (°C)	Mean radiant temperature (°C)	Relative Humidity (%)
IX Maggio	26	28	50
Stella Maris	25	27	51
Montesilvano (PE) 21 July-21 Sept, Altitude 0slm, orientation NE, 3m/s wind speed, 29 °C outdoor running mean outdoor temperature			
IX Maggio	28	30	55
Stella Maris	26	28	60

Analyzing the values individually, and considering the approximate values to zero decimal places, it is evident that the different data in the two structures relates to the relative humidity, while the air temperature and the mean radiant temperature vary slightly more than 1 °C.

In the IX May colony there are, in fact, values of relative humidity lower than the Stella Maris colony, which can be explained by the presence of three ventilation towers, rather than a single one as in the Montesilvano building. This triggers far more significant internal ventilation mechanisms, which lower the relative humidity through increased airflow.

Generally, historical buildings in which, among other things, there were fewer plant requirements than modern buildings, were designed in strict relation with the environment in which they were built, taking into account the climatic variables, the geographic, topographic and parametric parameters, and biological variables linked to users. On these bases, the pre-existing structures usually follow repetitive and constructive models of construction in the different climatic zones. The compact building design, for example, is an instrument to protect the building from both heat and cold, but is less suitable to favor air circulation. The first numerical analyzes in this research, to be confirmed following an energy analysis of the two buildings, shows that the mountain colony IX Maggio works very well in its place of origin, but not so in the marine environment, precisely because its single block shape, and with smaller glass surfaces, does not allow air to circulate as the planimetric distribution is less rigid, which is more advantageous in the Montesilvano building [18].

This conformation, however, made it suitable to be used also in the winter period, since the colony of Roio, unlike that of Montesilvano, was originally also utilized from November to June.

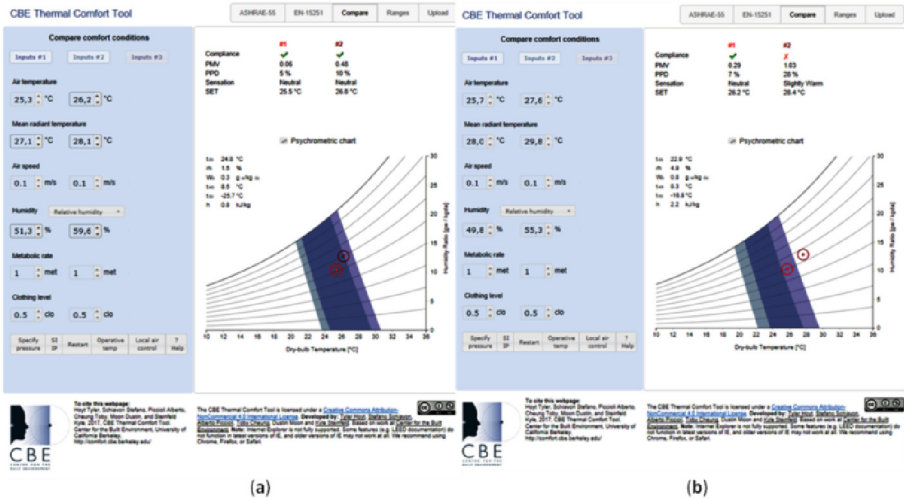


Fig. 15. Average values of the parameters obtained by means of dynamic simulation, relating to the climatic zone of Montesilvano (PE) and to Montelucio di Roio, L’Aquila (AQ), for both the buildings under study.

Both buildings, therefore, are designed in strict relation to the construction site, taking into account the outside temperatures, the optimal orientation with respect to the sun and the prevailing wind direction. This allowed designers to exploit the benefits of passive heating and cooling in obtaining an optimal interior comfort, as shown by the verification of the relative humidity levels that, in all the simulations on the two buildings, falls within the normative comfort parameters (range 40–60%).

Among other things, further aspects that could not be taken into account in the simulations, but which might certainly effect (presumably improve) the data produced, include but are not limited to, in the IX May colony, the presence of natural vegetation which guarantees shading and the regulation of the air circulation in the hottest periods, and defense from the wind in the cold periods. In addition, the external color of the two buildings likely create an effect related to heat gain and/or reflection. Originally the color of Stella Maris was, selected to maximize solar reflection, while a darker, probably other color, was implemented on the IX May colony to favor the fundamental thermal accumulation in a mountain environment with a colder climate.

It was important to compare the two buildings assuming the same climatic data, as starting from the same hypotheses. The comparable results highlight how each building of this typology is designed according to planimetric and altimetric conformations, but also internal building layout in order to implement the natural exchange of internal air with outside ambient air, maximizing the effects of comfort [19, 20].

5 Conclusion: Future Related Research: Climate Change Implications to Design Effectiveness

In a historical period of strong awareness of climate change, in view of the foreseeable increase in outside temperatures, existing buildings will see a significant increase in their consumption for cooling. In particular, in the long term, the increase in energy required to cover the summer demand, depending on the building type and the level of insulation of the buildings (construction period), may not be offset by the decrease in the corresponding winter energy requirement. This will lead to an increase in global primary energy consumption with a consequent increase in climate-changing gas emissions for the civil sector. The preliminary analyzes carried out to investigate the effectiveness of energy efficiency measures in tackling climate change, also highlight how in existing non-insulated buildings the priority of intervention will still be the thermal insulation of the building envelope. Meanwhile, in existing buildings already insulated the control of solar inputs will be primarily required. From these considerations the question can arise whether and how buildings similar to those studied in this research can adapt to the today's differing climatic conditions with respect to the original design time, and how to fulfill the greater request for internal comfort by using the shape of the building rather than mechanical elements with high energy consumption. Of course, there will be the consideration of combining the two systems.

As one considers four of the fundamental six thermo-hygrometric factors stated earlier related to climate (air temperature, average radiant temperature, relative humidity and air speed), there is scientific data (Montoya, 2019) that indicates climate change will affect all of these factors over time. Therefore, a separate analysis is needed to specifically determine at what level of change one would see through another modelling exercise a resultant comfort level drop below acceptable limits. Specifically, from a recent climate projection study for the city of San Antonio, Texas [20], at approximately the same latitude as southern Italy, *“by 2040 the average number of days with temperatures exceeding 38 °C could quadruple to more than 30 days per year, and by the end of the century we can expect to see 55–100 days with maximum temperatures above 38 °C. We will soon start to see summer nights where temperatures never drop below 27 °C, reaching a total of at least 10 of these nights by end of century.”* More specifically: Summer Maximum Temperature about +3 °C +5 °C; Hot Days (Maximum Temperature > 38 °C) +48 days +94 days; Warm Nights (Minimum Temperature > 27 °C) +10 nights +55 nights; Annual Precipitation –76 mm –101,6 mm.

While the correlation along similar latitude lines on the globe might be questionable (i.e. The relationship may not be that linear), this study does provide a strong study result that illustrates expected differentials. Intuitively we can say that further thinning of the ozone is expected to increase solar radiation which will also alter temperature differentials from both day vs night, and ambient air vs sea water which will consequently alter the convection rate which drives wind velocity both over sea and land. Primary wind patterns will be affected in velocity and possibly pattern direction due to environmental-geographical interactions. Wind inversion at the upslope of mountainous regions will change as driven by differing solar radiant gain on mountain massing and convection patterns thereon. With all these variables in flux, forecasting a combined accumulated effect is complex and beyond the scope of such proposed research. In that light, it is

suggested that a matrix of differing conditions be created which addresses “revised” a) wind direction, b) average wind velocity, c) ambient air temperature, d) relative velocity and e) radiant heat gain indication [21]. From there, calculations/modelling can be run for a set of changes in all variables that highlight “what if” scenarios in order to calculate at what level occupancy becomes uncomfortable, and therefore presumably calling for mechanical system intervention. Finally, by creating an matrix of geometric characteristics (and possibly a related multi variable algorithm), with particular regard to the arrangement of the openings according to the types of climatic conditions, it will be possible to obtain the best construction technique aimed at increasing the level of internal comfort. These systems should be as an “open systems” (for example with movable shading systems, or easily modifiable openings) in able to change configurations over time adapting to various climatic changes, to obtain a comfortable building over time [22–24].

Author Contributions. P.M. e E.L. designed the research and have defined the structure of the article. P.M. wrote Sect. 1 and conducted all historical analyzes; E.L. constructed the models, performed the simulations and wrote Sects. 2, 3 and 4; J. M. Jr wrote the Sect. 5 and provided overall translation editing.

Conflicts of Interest: The authors declare no conflict of interest.

References

1. Balducci, V., Bica, S.: *Architecture and Society of the Holiday Camps. History and Perspectives*, Timisoara (2007)
2. Bartoli, B.: *Raffrescamento Passivo degli Edifici, Progettare Edifici a Energia Quasi Zero*. Milanofiori, Assago
3. Campani, A., Ilvento, A., Mendes, G.: *1923 Lo stato attuale della lotta antitubercolare in Italia*. Editrice salute e igiene, Roma (2015)
4. Capomolla, R., Vittorini, R.: *Architecture and construction of children’s colonies in fascist italy. The Question of Environmental Control*, in A. Guida, A. Pagliuca (a cura di), *ColloquiATE 2016. Materials, architecture, Technology, Energy/Environment, Reuse (Interdisciplinary), Adaptability*, Gangemi, Roma (2016)
5. Ciranna, S., Montuori, P.: *Healthy and beautiful. italian colonies during the fascist period: two architectures between abruzzi’s mountain and sea*. In: *ArcHistoR architettura storia restauro – architecture history restoration*, VI, vol. 11, pp. 53–87 (2019)
6. Cutini, V.: *Le colonie climatiche in Italia. Genesi insediativa e architettonica, consistenza del patrimonio edilizio, problemi di conservazione e recupero*. In: Cutini, V., Pierini, R. (eds.) *Le Colonie marine della Toscana. La conoscenza, la valorizzazione, il recupero dell’architettura per la riqualificazione del territorio*. Edizioni Ets, Pisa, pp. 9–43 (1993)
7. Ilvento, A.: *Colonie Estive*. In *Enciclopedia Italiana Treccani* (1931)
8. Donghi, D.: *Manuale dell’Architetto*. UTET, Milano (1930)
9. Montuori, P.: *Al mare e ai monti contro il ‘mal sottile’. Tipologia, architettura e controllo ambientale dagli ospizi ottocenteschi alle colonie del ventennio fascista in Italia*. In: Ciranna, S., Lombardi, A., Montuori, P. (eds.) *La Storia incontra la scienza tra l’Abruzzo e il Texas: Architettura, Restauro e Controllo Ambientale del Costruito Storico*. Roma: Edizioni Quasar, pp. 65–78 (2019)
10. Kwan, S.E., Shaughnessy, R., Haverinen-Shaughnessy, U., Kwan, T.A., Peccia, J.: *The impact of ventilation rate on the fungal and bacterial ecology of home indoor air*. *Build. Environ.* **177**, 106800 (2020)

11. Huang, Z., Wu, Z., Yu, M., Dong, Y.: The measurement of natural ventilation in Huizhou traditional dwelling in summer. *Procedia Eng.* **2017**(205), 1439–1445 (2017)
12. Labò, M., Podestà, A.: Colonie marine, montane, elioterapiche. In: Casabella-Costruzioni, vol. XIV, pp. 167–168 (1941)
13. Grosso, M.: Il raffrescamento passivo degli edifici in zone a clima temperato, 3rd edn. Maggioli Editore, Santarcangelo di Romagna (RN) (2011)
14. Laurini, E., Taballione, A., Rotilio, M., De Berardinis, P.: Analysis and exploitation of the stack ventilation in the historic context of high architectural, environmental and landscape value. *Energy Procedia* **133**, 268–280 (2017)
15. Manzia, C.M.: Organizzazione e tecnica delle colonie estive. Pontificia Opera di Assistenza, Roma (1954)
16. Masetti, P., Amista, G.: La Ventilazione Comfort per gli Edifici ad Alte Prestazioni Energetico. Maggioli Editore, Santarcangelo di Romagna (2009)
17. Meadow, J.F., et al.: Indoor airborne bacterial communities are influenced by ventilation, occupancy, and outdoor air source. *Indoor Air* **2014**(24), 41–48 (2014)
18. De Santoli, L., Mariotti, M.: La Ventilazione naturale, il moto naturale dell'aria per il controllo delle condizioni ambientali. Dario Flaccovio Editore, Palermo (2011)
19. Montoya, A.: SA Climate Ready: a pathway for climate action & adaptation. In: https://digitalcommons.trinity.edu/cgi/viewcontent.cgi?article=1052&context=soc_anthro_faculty. Consulted in Nov 2019
20. Rome, Archivio Centrale dello Stato (ACS), Partito Nazionale Fascista, Servizi Vari, Serie II, b (1368)
21. Moosavi, L., Mahyuddin, N., Ab Ghafar, N., Ismail, M.A.: Thermal performance of atria: an overview of natural ventilation effective designs. *Renew. Sustain. Energy Rev.* **2014**(34), 654–670 (2014)
22. Laurini, E., Taballione, A., De Berardinis, P., Celi, A., Gentile, S.: Progettazione di Dispositivi per il Raffrescamento Passivo nei Contesti di alto Valore Architettonico. In: Aicarr Proceedings: Padova (2016)
23. Sachta, H., Lukiantchuki, M.: Windows size and the performance of natural ventilation. *Procedia Eng.* **2017**(196), 972–979 (2017)
24. Wall, A., de Martino, S.: Cities of Childhood. Italian Colonie of the 1930s. London (1988)



Method for the Design of Local Temporary Buildings to Ensure the Sustainable Development of the Liquid Society

Stefania De Gregorio^(✉) and Pierluigi De Berardinis

Department of Civil, Building and Environmental Engineering, University of L'Aquila,
67100 L'Aquila, Italy

{stefania.degregorio, pierluigi.deberardinis}@univaq.it

Abstract. “Liquid modernity” with its continuous and rapid change and the need to safeguard the environment, which is severely compromised by anthropogenic action, find an answer in local impermanence, that is, the art of designing and implementing man-made spaces conceived for a specific time, which arise from the peculiarities of the place, coexist in synergy with the local environment and return to it at the end of the time of use. A metabolism thought out at the design stage, in which the characteristics of compatible places are predefined for the “birth” and “death” of the building organism. The paper describes the method for the design and realization of local temporary building organisms, defining a three-stage process analysis of local potential, identification of requirements, design stage, guarantors of the compliance of the construction process with both the dynamic lifestyle of modern man and the sustainability of the intervention. The project is the result of analyses that start from the area allowing its promotion and sustainable development, and at the same time the environmental and economic cost of the building intervention is reduced. A benefit therefore for both the community and the individual, in a scalar and cyclical process guaranteeing that sustainable development capable of involving environmental, economic and social aspects. The methodology described is verified through a case study in the territory of L'Aquila (Italy): the design of a temporary building organism that can be used either to upgrade an existing building or in constrained or emergency contexts.

Keywords: Liquid Architecture · Local Temporariness · Reuse · Sustainable Development · Local Supply Chain

1 Introduction

Polish sociologist Zygmunt Bauman invites us to reflect on liquid postmodernity in which there is a belief that “change is the only permanent thing and uncertainty is the only certainty” [1, 2]. In the modern era everything was given as a solid situation, in the postmodern era everything is constantly changing and nothing has sharp and defined contours anymore, everything is precisely liquid. The human being for climate protection

needs spends more than half of his existence inside the anthropic space, a box that he himself has built around himself for shelter. But this box takes on a different value than in the past because nowadays human life is in an existing but unstable balance. It is the time when challenges such as environmental pollution, energy and economic crisis have to be faced. It is the time when one is a citizen of the world and goods cross the boundaries not only of continents, but even of the earth, becoming waste in space. These challenges impose responsiveness, movement, flexibility, imposing precisely a liquid approach in which one cannot stop to think, but must think while acting. The immutable, rigid, stable architecture, “daughter of the Colosseum” that has been the symbol of a safe place, of man’s ability to leave an imprint in natural space strong enough to endure over the centuries, nowadays turns into limitation, into impossibility to change with speed and to protect the human being despite constant changes, of architecture’s inability to be “enclosed in a suitcase.” Architecture that by its very nature brings back the concept of stability needs a rethinking, a deep reflection that starts from the historical reasons for the project and arrives at the future impacts of it. What is needed is an architecture that does not live in the present, but is capable of traversing time, leaning on the knowledge established in history to be capable of responding to the needs of the present, but above all capable of glimpsing and predicting the needs of the future.

The “liquid architecture” is the art of creating organized human spaces capable of evolving rapidly and easily to flow in parallel with the life course of human beings. Rapidity and ease of evolution are two of the foundational requirements of liquid architecture. Speed allows the space not to lag behind the changing life of the human being, allows it to “keep up.” Ease of evolution, being “ecofriendly” allows liquid architecture to be “an architecture for all.” The key to evolution is, in fact, in the sharing of knowledge. We are facing the speciation of architecture, that is, new environmental conditions that lead to change, to an evolution of architecture. But to do this, architecture should evolve with ease; it should be easy for the human user of the space to modify the space itself. This is a temporary architecture in which the succession of actions is so rapid that it is in motion, just like a fluid. This does not mean that “the fluid” cannot, depending on human needs, also remain stationary, but it does mean that it is designed to have the possibility of movement. In fact, liquid architecture is only seemingly at odds with the Vitruvian concept of *firmitas* [3]. The liquidity of architecture does not consist in the absence of static and material solidity, but it explicates the concept of solidity in a different form from traditional architecture. The latter links the concept of solidity to that of stability, liquid architecture on the other hand links the concept of *firmitas* to that of security. Architecture thus reinterprets *firmitas* in its own dynamism. The constant evolution of liquid architecture is expressed in the impermanence of the building organism, in which space changes in function, size and performance and which is capable of adapting to changing contexts.

Parallel to the needs of human beings, since the 1980s the planet has been facing the great challenge of environmental pollution, which, while on the one hand has been a consequence of industrial progress and globalization, on the other hand imposes in the immediate term a rethinking of lifestyle (daily habits, mobility, industrial system, economic processes), aimed at safeguarding the planet, acting in consideration of the limited resources therein. According to UNEP data [4], construction field contributes

more than 50% of global environmental pollution in terms of resource use, waste production, air and water pollution, and land consumption. Thus, a rethinking of human space aimed at directing the construction industry and all other sectors involved toward sustainability of the building process and related products is needed.

If liquid society imposes temporary spaces how can these spaces be designed and built sustainably? The temporariness of building is historically linked to the concept of “non-place” that is the possibility for humans to shelter and protect themselves in a variable territory. In the 1900s with the spread of the use of steel and in the 1970s with the advent of plastic, the temporary habitat becomes a tool to reach every place in the world and is linked to the concept of globalization [5].

Temporariness brings with it requirements such as reversibility and flexibility that help make the building organism sustainable. But this is not enough. Strategically, it is necessary to rethink temporariness from a local perspective [6], returning from a methodological point of view to the design and construction process typical of traditional temporary architecture, when the movement of the building organism was present, but limited to a territory (think of the yurt, igloo or tipi), architecture that uses local materials, whose construction systems are designed in a manner consistent with local resources and performance-related to the climate of a given territory) [7]. While traditionally local choices were dictated by the difficulty of global movement of people and goods, today local choice is a choice, a necessary choice as a function of the need for environmental preservation.

Therefore, to the concept of liquid architecture that is a response to human dynamism, it is necessary to associate the concept of local impermanence, i.e., the art of designing and realizing human spaces conceived for a specific time, which arise from the peculiarities of the place, coexist in synergy with the local environment and return to it at the end of the time of use. A metabolism thought out in the design phase. It is possible to draw a parallel between the metabolism of a living being and the metabolism of the building organism [8]. This means designing and implementing a building organism by planning the place where it will “be born” i.e., be assembled and “die” i.e., be disassembled. This does not mean that the building once constructed must necessarily remain in a particular place. In its “adult” life, that is, once it is structured, it may be assembled/disassembled or transported a given number of times (compatible with the durability of its components), but the beginning and end of life phases will have to be territorially well-defined. It is not a matter of specifically defining a place or territory, but it is a matter of defining the characteristics of that territory. For “born” and “die” all places consistent with the characteristics of the territory defined in the design phase are compatible. Moreover, to enable the building in its use phase to be able to respond to human dynamism, it is necessary to design the building system flexibly to ensure environmental comfort despite changing climatic conditions.

The literature review shows many studies related to the environmental comfort of temporary systems [9–11] to change of use that implies the search for variable comfort conditions [12], to constructive solutions that allow reversibility and ease of assembly [13, 14]. Innovative solutions, moreover, are those related to structural exoskeletons, which, while a reversible regeneration tool, have a significant impact of the materials

used [15]. There are also studies concerning the environmental impact of temporary systems used for exposures [16].

However, there are no studies present that illustrate how to design temporariness in a local dimension, breaking free from the concept of “globalization” and returning to the relationship with place.

The objective of the research illustrated in this paper is therefore to define how local temporariness is designed and constructed, what requirements it should meet, and what are its operational declinations.

2 Method

The design of local temporariness has two areas of operation: intervention on built heritage and intervention on virgin soil (in constrained or emergency contexts), which have a similar design and implementation process, subject to the specificities of each. The world’s built-up area from 2015 to 2020 has grown by 9.8% [17], considering that the land area is limited and in the future the population is expected to grow, it is necessary to safeguard the productive capacity of the soil. Therefore, as confirmed by the “Sustainable Cities and Communities” and “Life on Land” goals of Agenda 2030 [18], anthropogenic spaces should as much as possible be limited to the existing by providing through temporary building organisms for redevelopment or densification of the already existing built environment. In the case of intervention on the built environment, the complexity lies in the need to interface with the pre-existing and to customize the temporary building body based on the constraints and values of the already existing building [19]. Otherwise, in emergency or constrained contexts, it is possible to intervene through temporary systems such as to occupy the soil reversibly and without altering the natural habitat and its biodiversity.

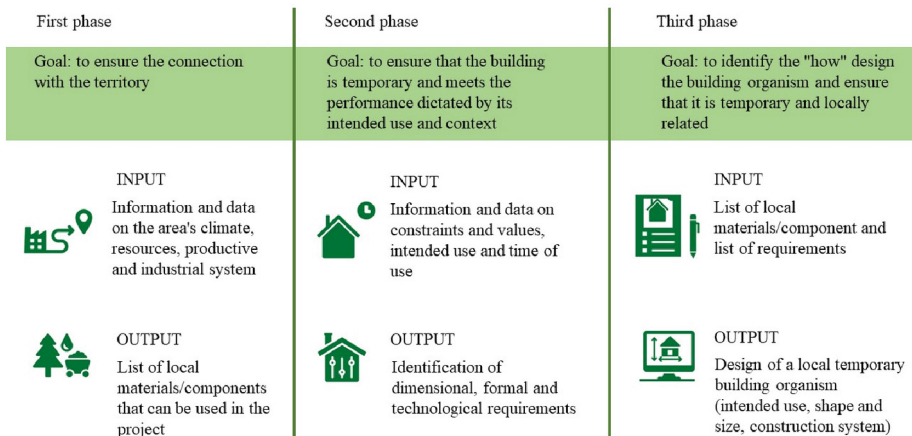


Fig. 1. The method and its phases.

In the case of intervention on virgin soil, the complexity stems from the need to design a building organism that is flexible and dynamic with respect to locations and climates

that may vary [20]. That is, the building must be able to be easily assembled/disassembled or transported pre-assembled a variable number of times during its life cycle. The method for the design and construction of the local temporary building consists of the following steps: the analysis of the potential of the territory, the identification of requirements, and the design of the local temporary building body (see Fig. 1). The link with the territory and the requirements that by their very nature identify temporariness become guarantors of the sustainability of the intervention and at the same time of the building's responsiveness to the dynamism of "liquid modernity."

2.1 Analysis of the Potential of the Territory

The first phase ensures the link with the territory and consists of identifying the context in which the building begins its life cycle and planning the context in which the building will end its life cycle. At this stage, the characteristics of the territory such as to condition the project in an identity form must be defined. Identifying the beginning-of-life context is less complex than identifying the end-of-life context, as it takes place in the present. Otherwise, the characteristics of the end-of-life context presuppose a projection into the future of the evolution of the building system and how it will vary according to the dynamic needs of users. It is therefore necessary to take as a temporal reference the durability that is assigned to the temporary building organism and with respect to it to make a forecasting action. For the identification of the characteristics of the spatial context of the beginning of life, the climatic peculiarities, the availability of resources and the related productive organization, both existing and potential, will have to be analyzed. In the case of intervention on the built environment the climatic peculiarities remain constant during the phase of use of the temporary system, otherwise in the case of building bodies insisting on virgin soil it is necessary to design the possibility of varying the building envelope with ease in order to ensure environmental comfort as external conditions change.

The local production system needs to be analyzed to identify:

- Building-related materials/components by defining for each product whether the raw materials are sustainable (from controlled and renewable resources) and whether they are derived from local supply chains. Consider, for example, the presence in the territory of the timber structural component manufacturing industry and the need for raw material supply, which can be from local forest resources if the territory is by orography and climate compatible with the species used for construction purposes, or the supply can be from other places other than the local surroundings, changing, however, the sustainability of the process not only from an environmental point of view, due to the incidence of transport and the positive contribution of vegetation, but also from an economic and social point of view through the linking of a part of the supply chain to a specific territory.
- Materials/components related to sectors other than construction, both primary products and by-products, which can also be used in construction. In the case of primary products, the same assessments described for materials/components related to construction must be made; in the case of secondary products, the impact related to the processing functional to their use in construction must be assessed.

Materials/components that can potentially be produced by the existing production system, using existing know-how and machinery to process available local resources in a quantity that can generate new local supply chains. This assessment is instrumental in identifying the potential of the area, but it is complex in that the time and economic resources required for the reconversion or new development of an industrial system must also be assessed. This is such an operation that promotes sustainable development but is sometimes, due to the number and timing of the process, functional for the enhancement of the territory but not compatible with the design and implementation of a single intervention. It finds meaning in a systemic and non-point approach to the definition of land resources.

An illustrative case of the valorization of waste products from the production system through industrial system know-how is the emergence of the sheep wool insulation industry in Sardinia (Italy). Sheep farming for milk production is historically rooted in this area. The wool from such sheep has been used for centuries to make mattresses and pillows as it is very durable. The presence of imported synthetic fabrics on the market has brought an end to this use of wool. The availability of sheep's wool, waste from the dairy sector, combined with a structured know-how of using this resource and the availability of wool processing machinery already present in the territory's industrial system, has led to the emergence of industries that make insulating building mats from sheep's wool, enhancing a waste from the territory [21–23].

In parallel, the analysis of traditional architecture allows us to identify resources that are historically linked to the area and define which among them are also potentially usable today. Among the resources, local waste materials must also be considered, the reuse of which is a sustainable operation [24, 25].

Such analyses allow us to identify a list of usable materials/components according to a hierarchy ranging from the most sustainable to the least sustainable, including in the assessment the occurrence in a local geographic surroundings of production system processing and the use of local materials.

For the identification of the territorial end-of-life context, the characteristics to which the territory must respond must be defined in order to favor sustainable end-of-life scenarios. In the intervention on the built environment and, therefore, in a predetermined location throughout the life cycle of the building organism, it is necessary to identify the reconditioning, recycling and disposal centers present and verify whether, with respect to the resources we have identified as a database for the project, there are productive possibilities (even potential ones) for re-introduction into the market at the end of life. Going back to the example already described, if there is a timber structural use component processing industry in the territory, I will have to check whether there is also a non-structural use building component processing industry in the same territory that can use as raw material structural components that no longer have sufficient characteristics to fulfill their primary function (think of wood decay). For example, it will be possible to check whether the chipboard wood processing industry is present. A compatibility check between the list of resources related to “early life” and the list of resources related to “end of life” will reduce the number of resources to those with a structured life course in the territory at both stages. In the case of predictive difficulty of the end-of-life context, it is possible to direct the choice toward materials/components derived from simple

production processes, which can be re-injected into the environment without the need for processing according to a Cradle to Cradle-like approach (such as unfired earth or hemp lime building systems) [24–26].

Otherwise, in the case of operating in constrained or emergent contexts on virgin soil, the possibility of using the building organism in different places during its life cycle is considered in the project. Therefore, the identification of the end-of-life spatial context is carried out methodologically in a similar way to what has already been illustrated in the case of intervention in the built environment, but from a temporal point of view it is carried out at the end of life, after the identification of the building's construction system. The place where the building organism will “die” will be chosen according to the peculiarities of the building system, identifying what are the characteristics of the territory such as to ensure the sustainability of this phase.

2.2 Identification of the Requirements of the Building Organism

The second phase ensures compliance with the temporariness of the intervention, consistency with the constraints and values of the pre-existence, and compliance with the performance dictated by the destination and time of use. It consists, therefore, in defining the requirements to which the building organism must respond. Proper requirement of temporariness is reversibility. In the case of intervention in the built environment, the system of connection between the intervening and pre-existing building organism and that of the building system must be reversible. In the case of intervention in virgin soil, reversibility of the ground connection is essential. The reversibility of the building system is not directly functional to the temporariness of the intervention-as temporary is also a building organism that can be moved without being disassembled-but it is functional to the sustainability of the intervention by allowing the end of life of each material/component to be released according to its residual performance and durability [27]. Flexibility (constructive, use and dimensional) [28, 29] also while not a prerequisite for temporariness becomes a functional requirement for meeting changing needs over the time of use of the building. When intervening in the built environment the size of the space is static, but the way in which it is used varies, which becomes dynamic; when intervening on virgin soil and in a variable context flexibility can be expressed in the possibility of varying the size of the space and the possibility of varying the stratigraphy of the building system in order to achieve performance consistent with the climate of the specific place.

The context in which one operates, whether it is a pre-existing building on which one intervenes or an area constrained by historical, landscape or urban planning value (as is the case in emergency situations), defines limits in terms of constraints and values, the identification and analysis of which makes it possible to identify the requirements to which the temporary building organism must respond. The identification of use (compatible and appropriate in the case of pre-existing and functional in the case of natural context) provides dimensional indications (minimum spaces, served spaces and servant spaces) [19–30]. Time of use, on the other hand, provides information regarding performance related to environmental comfort [11–31].

2.3 Design the Local Temporary Building Organism

The third phase is associated with the design phase, identifies the “how” we can realize the building organism from both a dimensional and technological point of view, and ensures that the building organism is temporary and locally related. The building system should be designed from the locally compatible materials/components (identified in the first phase) and the dimensional and performance requirements of the building (identified in the second phase). Into this moves the creative space of the designer, who has the option of using existing building systems or designing new building systems, enhancing local resources. The assessment of spatial compatibility is not only about material/technological aspects, but also about quantity, i.e., one has to assess whether a given resource has the technical characteristics to be used and whether it is present in a sufficient quantity to feed a production process at a local scale. The most complex part to manage are the facilities. In the project, strategically, the plant part can be concentrated in a functional block. This frees the vertical and horizontal closures of the building from the conditioning of the systems, simplifying the construction process both during assembly and disassembly. In the case of intervention on the building, the installations of the temporary building must relate to the installations of the pre-existence. Differently in the case of intervention in a constrained natural context or temporary use of an area having a different urban vocation, the installations must be made off-grid in order to facilitate the restoration of the situation prior to the construction of the temporary building body. The use of facilities that take advantage of clean energy sources increases the sustainability of the intervention.

3 Analysis

The described methodology is verified in its phases through a case study: the design of a temporary building organism aimed at the redevelopment of a pre-existing building and for use in constrained or emergency contexts in the territory of L’Aquila (Italy).

3.1 Analysis of the Territory of L’Aquila

The territory taken as a reference covers a radius of 50 km from the city of L’Aquila (Italy) [32]. The analysis of the productive sector produced the following results. The productive sectors in the territory of L’Aquila involve: building materials (15.9%), recovery and preparation for recycling (12.6%), chemicals and pharmaceuticals (10.9%), electronics and electrical equipment (10%), food and beverages (9.2%), manufacturing industries (7.8%), rubber and plastics (7.6%), ceramics and glass (7.3%), paper, papermaking and polygraphs (6.9%), metallurgy and metal products (6.4%), and followed by the other sectors with negligible percentages [33]. Except for the food sector and the building materials sector, no supply chains are found whose entire production process from raw material extraction to end-of-life is linked to the local area. In particular, the procurement of raw materials does not occur at a local scale. The building materials sector is tied to the territory exclusively for the extraction of aggregates and clays, a mining process that has a high environmental impact as it involves nonrenewable resources. Conversely, the

wood supply chain, a renewable resource, processes raw materials from abroad due to the absence in the territory of controlled supply chains for logging (see Fig. 2).

Analysis of traditional building systems shows the use of wood for making floors and roofs, and analysis of the territory confirms that potentially the current forest resources would be sufficient in quality and quantity for the creation of an entirely local supply chain [34]. Moreover, the food sector is strongly linked to sheep farming for both meat and milk production, the wool of which, parallel to what happened in Sardinia (see Sect. 2.1) is to date a waste product of the food industry. Given the know-how and quantitative availability of wool, it would be possible to trigger a new supply chain for building insulation.

The L'Aquila area also is a producer of straw, used in animal husbandry, which has such quality and quantity that it could also be used in construction to make insulated shells.

The series of earthquakes that struck Abruzzo, particularly the area of L'Aquila in April 2006, caused significant damage to buildings. To secure them during the reconstruction process, temporary systems made of steel and wood, such as shoring, tie rods, hoops, tubes-clamps systems, multidirectional systems, and systems in wood, were employed. However, the dismantling of these safety systems, after the restoration of the box-like behaviour of the buildings, generates a large amount of waste with no defined end-of-life scenarios, posing economic, environmental, and logistical challenges to the community. Selective demolitions have also resulted, mostly when working on historic buildings, in waste materials that can be reused such as roof tiles, solid and hollow bricks, and stones [35].

The supply of materials needed for reconstruction also produces another element of waste, relevant for quantity: the pallet. Nevertheless, these waste materials could potentially be transformed into resources, as they still possess residual performance with high potential for reuse. By implementing a new cycle of life for these materials, it is possible to reduce end-of-life burdens, fully utilize their embodied energy, lessen the environmental impact of production, and generate closed cycles of matter that mirror those found in nature.

3.2 Defining the Requirements of Local Temporariness

The territory of L'Aquila has a Mediterranean climate, considering the average values of the last 10 years, winter minimum temperatures (December–January) average 2.3 °C and summer maximum temperatures (July–August) average 21.6 °C. Precipitation is about 700 mm per year, with the least rainy month being July and the wettest month being November.

From an orographic point of view, the territory of L'Aquila stretches in a valley between the Ocre and Velino Mountains to the south and the Gran Sasso Massif to the north, a feature that produces a form of thermal inversion in winter, due to which temperatures fall below 0 °C at night. Similarly, in summer the humidity level is low and there is a temperature difference of 8 °C on average between day and night.

The prevailing wind direction in winter is from the southeast and northwest, and in summer it is from the southwest [36]. Therefore, the design of the temporary building body should ensure environmental comfort. In the design of the intervention on the

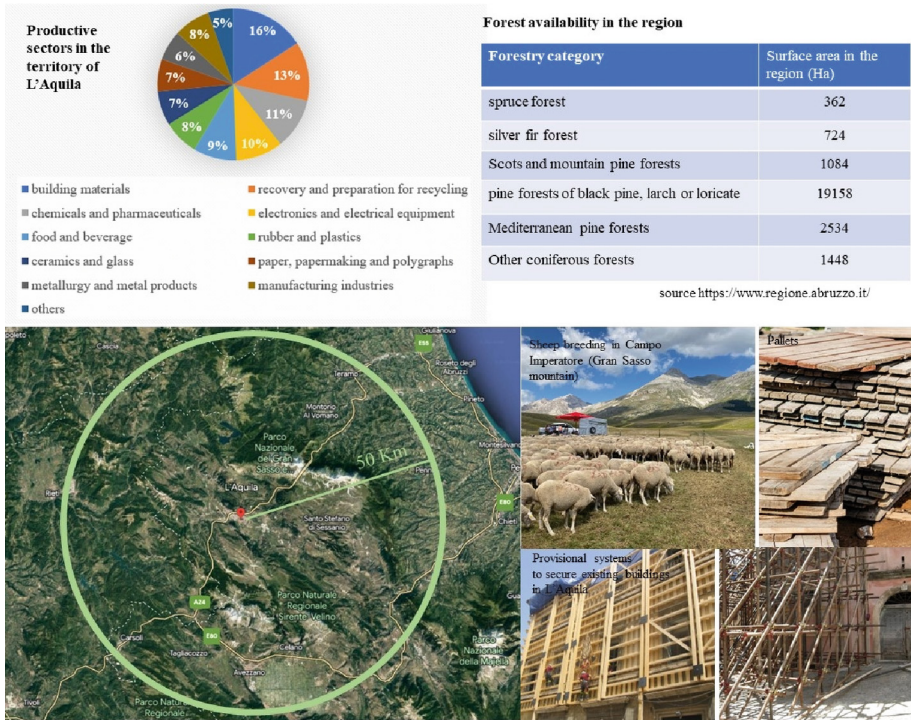


Fig. 2. Analysis of the territory of L'Aquila: productive sectors, forest availability, materials from agriculture and animal husbandry (straw and sheep wool) and materials from selective demolition and reconstruction sites (wood and steel beams, scaffolding, bricks, pallets).

built-up area, the orientation of the temporary module is dictated by the location of the pre-existence, otherwise in the case of intervention on virgin land, the orientation of the temporary organism can be variable compatibly with the uses of the various rooms, therefore the optimal orientation of the same is designed at the design stage. In built intervention, the orientation is a constraint dictated by the pre-existence, in virgin soil intervention it is a constraint defined by the designer with the positioning of the use spaces.

The designed temporary module has a high degree of flexibility that allows its variation in intended use, dimensional variation (as a multiple of a basic macro-module), and variation of the construction system in order to both achieve the comfort required by the specific intended use and interface with the pre-existence. In addition, the flexibility allows the load-bearing structure and systems of the pre-existence to be related to the load-bearing structure and systems of the temporary module. The intervention on the built environment concerns a densification of the built environment of a residential building located in the earthquake-damaged historic center of L'Aquila.

The earthquake caused the roof to collapse with the loss of a residential unit. The temporary module, therefore, can rest on the underlying uninjured slab, configuring itself as an addition at the top of the building, such as to restore the dwelling damaged by

the earthquake. The pre-existing building consists of a load-bearing masonry structure. Therefore, the size of the macro-module should be such that it rests on the load-bearing masonry of the pre-existing building, or alternatively, it will be necessary to provide an intermediate load-spreading structure such that the temporary module can bear on the load-bearing part of the pre-existing building. The integrated building system will have to be reversible and flexible. The ease of construction will have to be calibrated for implementation by skilled workers, as it is necessary to carry out interventions on the pre-existence while working at height.

The temporary module for constrained or emergency contexts, will have to relate to variable ground. A fundamental requirement is therefore the adaptability of the ground attachment by means of reversible point anchors capable of placing the module horizontal to the ground, which may have variable slopes. A further requirement is the ability to assemble/disassemble the module easily and quickly. Indeed, the assembly time must be consistent with the time of use, which in a constrained or emergency context is a seasonal time at most. The ease of construction also allows the possibility of using workers who are not necessarily specialists, also helping to reduce the assembly/disassembly time and the cost of the intervention. The reversibility of even partial construction system allows reducing the number of transports while moving the module. Flexibility allows the building organism to be modified according to the varying dimensional or performance requirements that depend on the intended use and geographical (and consequently climatic) variation. The territory of L'Aquila is in fact, very heterogeneous, and for example the same building organism could be used as a mountain shelter in the constrained context of the National Park, as an infopoint in an urban context or as emergency housing.

The plant engineering system of the temporary module for constrained/emergency contexts should be designed off-grid, otherwise in case of intervention on the built environment it has to interface with the systems of the pre-existence. Therefore, it will be convenient to concentrate the facilities and services (bathroom/kitchen block) in one block and are planned sustainable plant systems (rainwater recovery, photovoltaic panels, solar thermal panels).

4 Results

Among the resources identified in the first phase (see Sect. 3.1), waste materials from selective demolition of post-seismic reconstruction were chosen. In particular, the pallet and materials from the dismantling of the securing systems (wooden beams, steel IPEs, and steel scaffoldings consisting in pipes and joints).

The horizontal and vertical closures are made by means of EPAL pallets, and the load-bearing structure is made in the case of intervention on the built-up area with a wooden beam-and-pillar structure and in the case of intervention on virgin soil with in steel pipe-and-joint system. This difference arises from the difference in requirements highlighted in the second phase. In fact, the wooden beam-and-pillar system allows interfacing with the pre-existing load-bearing structure, and the pipe-and-joint system facilitates and speeds up construction operations in the case of intervention on virgin soil, not requiring specialized workers. In both projects the system is reversible and flexible, and the plant blocks are pre-assembled.

The design of the building temporary organism presents a high degree of flexibility of use and size, through the possibility of making modules with different functions and dimensions starting from a repeatable basic module, and constructive, through the possibility of varying the number of layers consistently with the place of use and intended use. The pallet becomes the element that dictates the modularity of the system and allows for dimensional and performance variation. The repetition of macro-modules based on the unity of the pallet allows the creation of spaces of different sizes (see Fig. 3).

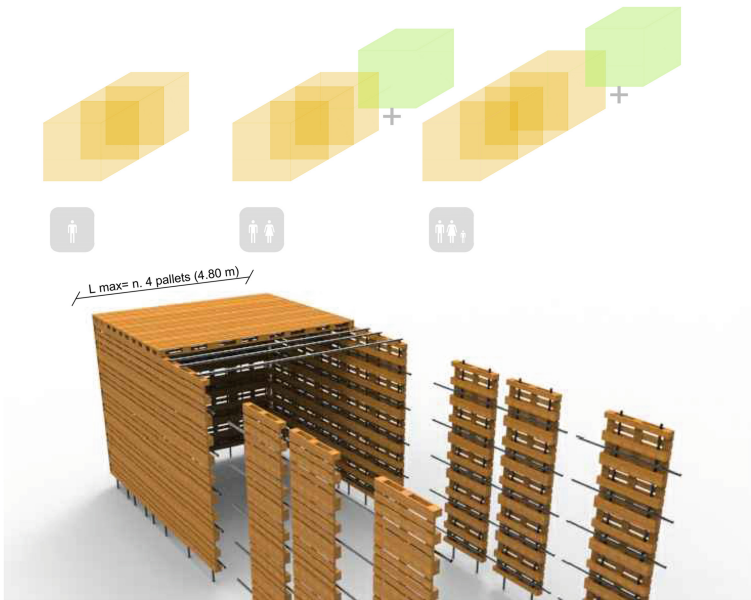


Fig. 3. Modularity of the system based on standard pallet size

Indeed, by leveraging the constructive, geometric, and dimensional configuration of the pallet, the load-bearing structure and technical installations can be housed within its hollow areas. Combining two pallets enables the use of the second layer's cavity for thermal insulation. The layers of the vertical and horizontal closures can be mixed and matched to achieve specific performance criteria and adapt to the variability of available materials (which can be reused) (see Fig. 4). Based on this fundamental setup, it's possible to design various vertical and horizontal closures, depending on the materials, environmental comfort needs, worker specialization (and available installation time), and the building's projected lifespan. Different vertical and horizontal closures can be designed based on the basic configuration, taking into account factors such as available materials, environmental comfort requirements, worker specialization, time available for mounting, and building usage.

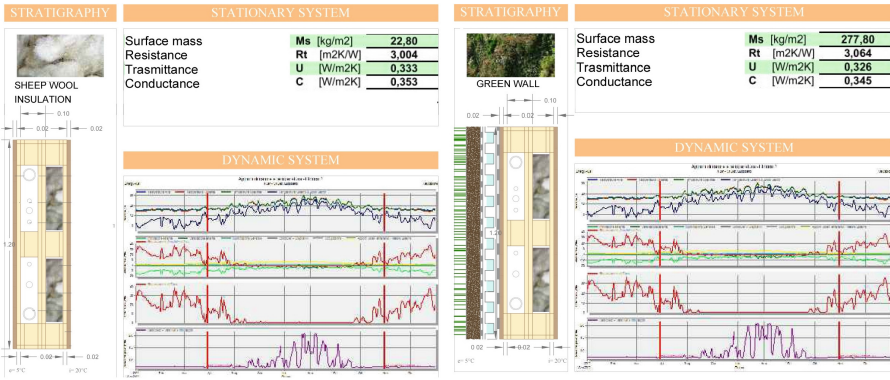


Fig. 4. Construction flexibility of the system. Thermal analysis of two different types of vertical closures.

The construction system allows rapid assembly/disassembly of the building. Only reversible connections such as bolting and nailing were used in order to allow assembly to take place even by unskilled labor. Horizontal and vertical closures are assembled on site in order to allow not only the use of local materials but also the reuse of waste materials. The supporting structure is integrated into the pallet cavities, so assembly steps proceed from the bottom up by simultaneously assembling the supporting structure and closures. Therefore, for the construction of a temporary module, it is necessary to follow the following steps (see Fig. 5):

1. construction of the lower horizontal closure
2. realization of the outer layer of the walls
3. realization of upper horizontal closure
4. insertion in the pallets of sheep wool insulation
5. screwing the insulated pallets on the yet mounted pallets in the internal side in the following order: walls, lower horizontal closures and upper horizontal closures
6. screwing the wooden planks in correspondence of the longitudinal openings of the pallets
7. assembly of the installations and assembly of the finishes (windows, doors, pavement, etc.) and painting
8. realization of the independent coverage.

The construction of a prototype made it possible to verify constructability. In particular, it was possible to verify the air and water tightness of the horizontal and vertical connections and the manoeuvring spaces available for assembly. The pallet, in fact, has standardized dimensions that impose predetermined spaces for the movement of tools (such as screwdriver, hammer, etc.). The construction process was designed in order to allow assembly using the hollow part of the pallet as the handling space. The construction of a prototype also verified that the connections designed both between the panels and between the panels and the load-bearing structure were adequate for the weight of the components and had enough durability to allow the module to be assembled/disassembled at least three times without having to replace the connective elements.

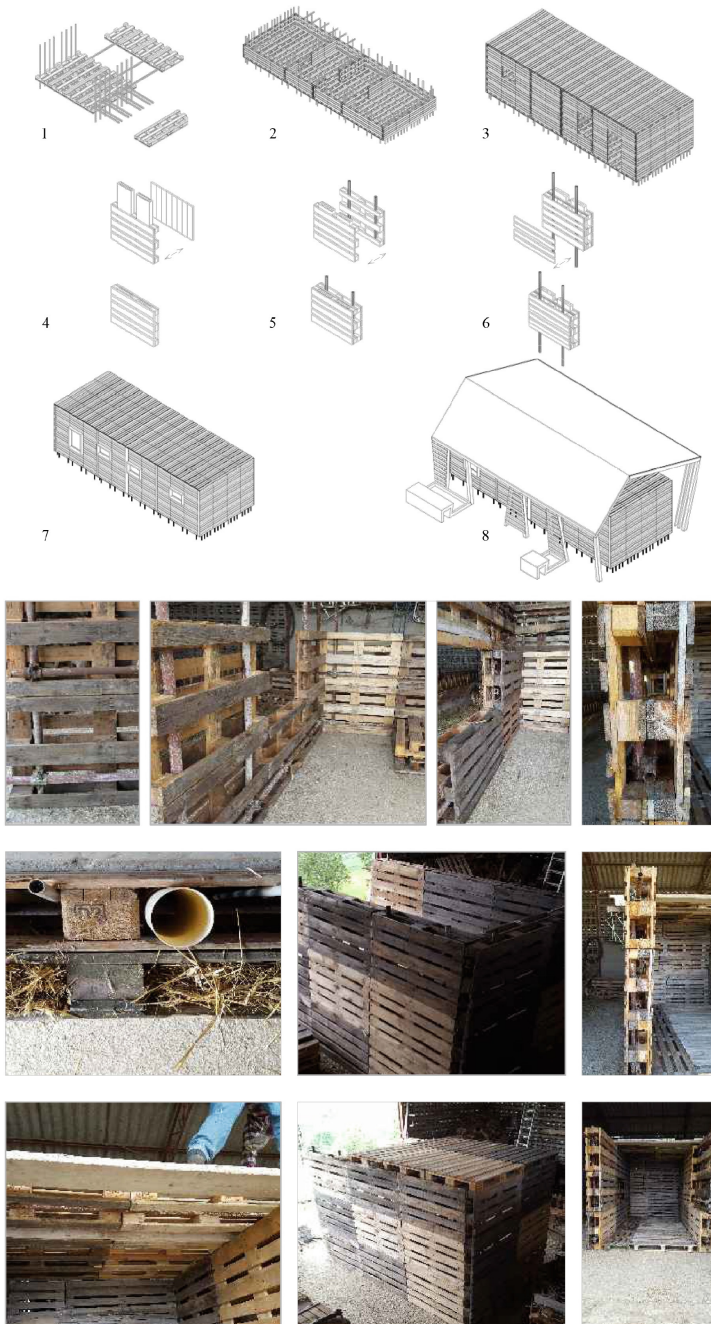


Fig. 5. Construction stages of a housing module (top) and prototype construction stages to test how vertical and horizontal closures are connected (bottom)

The prototype made it possible to verify the plant arrangements, showing that it is convenient for the purpose of facilitating realization to pre-assemble in the workshop “plant modules” that can be more easily assembled during the construction phase. The prototype also demonstrated the difficulty of achieving water tightness of the top horizontal closure without adding additional layers over the pallet (such as plastic material panels or sheathing). Therefore, to simplify the construction process, increase its flexibility, and ensure a link to the actual locally available resources, the water tightness of the upper horizontal closure was released from the panels made from the pallets and entrusted to an additional cover, which can be made from different materials (depending on local availability) and can achieve varying performance depending on the intended use of the building body. The roof can also be used for clean energy production through the installation of solar panels (thermal and photovoltaic) (see Fig. 6).

In the intervention on the built environment, the temporary module relates to the pre-existence, and it is therefore necessary to identify the values of the building (historical



Fig. 6. Design of the local building organism. Case study with residential use: plan, and detail of facilities and insulation of the pallet module.

and artistic) that constitute its invariant, to identify its formal and spatial aspects and building type (which will condition the way the temporary module is accessed), and to analyze the construction equipment in order to identify how to relate the construction system of the pre-existence to that of the temporary building organism.

The case study involves an unrestricted building located in the earthquake-damaged historic center of L'Aquila. From a typological point of view, it is a building with a central stairwell. The decision to place a temporary building organism at the roof top of the building with a smaller surface area than the underlying floor has two purposes: the first is to use the building's stairwell to reach the building organism as well, and the second is to create an accessible space on the roof. Constructively, the pre-existence is made of load-bearing masonry, so the temporary organism rests on a steel substructure (resulting from the reuse of the UPN beams from the shoring) that is functional in off-loading the weight onto the load-bearing structure of the pre-existence. This substructure also allows the systems of the pre-existing building to be connected to the temporary building body, taking advantage of the solar systems on the roof for the benefit of the entire building (see Fig. 7).



Fig. 7. Intervention of densification of the built-up area by placing the local temporary building organism in place of the roof of an existing building. Existing building before intervention (top left), densification intervention with the temporary module (bottom left and right).

When intervening in emergency or constrained contexts, the temporary-neo building organism has no size limits precisely because of its temporary nature. The only constraint is that it must not irreversibly damage the soil. Therefore, the project involves the use of foundations on propeller driven piles and the presence of off-grid facilities such that self-sufficiency is guaranteed for a specified number of days. Therefore, the project involves the presence of a larger installations space than the intervention on the pre-existing (see Fig. 8).



Fig. 8. Render of temporary building organism with residential use used in a constrained context.

5 Discussion and Conclusions

“Local temporariness” seems an antithetical and paradoxical concept, otherwise it represents a response to the two major challenges we are facing: liquid society and its continuous and rapid change and the need to safeguard the environment, which is severely compromised by anthropogenic action.

Local temporariness is thus the sustainable declination of liquid architecture, capable of following the dynamism of man but in a sustainable way, in which the anthropic space does not stand in contrast to the environment, but, on the contrary, becomes a tool for the enhancement of local excellence, transforming itself into an economic and cultural driver. The building is compared to the living organism with its own metabolism, which is born, grows and dies. The local project imposes the planning of the place of the “birth” and “death” of the building, in order, jointly with the requirements that by nature characterize temporariness, to ensure the sustainability of the life cycle of the building process.

The illustrated methodology, verified through a case study in the territory of L’Aquila, defines through three phases (analysis of local potentialities, identification of requirements, design phase), how to design and implement local temporariness, both when the building organism interfaces with pre-existing buildings and when it interfaces with virgin soil, in a constrained or emergency context.

Future research developments may involve the verification of the method through a significant number of case studies located in diverse spatial contexts, also verifying the environmental comfort of the temporary building organism especially when it intervenes on the pre-existence. A further field of research development is the creation of harvest maps useful for facilitating the phase of identifying local resources (the first phase of the method) and consequently enhancing the relationship between the territory and the building organism.

The project of local temporary buildings is the result of analyses that start from the territory allowing its promotion and sustainable development (in terms of resource

enhancement, development of a sustainable industry and specialization of local operators on products of excellence and identity) and at the same time the environmental and economic cost of the building intervention is reduced. A benefit, therefore, for both the community and the individual, in a scalar and cyclical process guaranteeing that sustainable development can involve environmental, economic and social aspects.

Acknowledgement. The case study described in paragraph “4. Result” was partly developed in the thesis in Building Engineering-Architecture, University of L’Aquila, title: “L’architettura dei materiali di recupero: progettazione modulare”, student: Valentini Michini, supervisors Pierluigi De Berardinis and Stefania De Gregorio. The authors thanks V.M. for her contribution in the designing of macromodule.

Author Contributions. Conceptualization, S.D.G. and P.D.B.; methodology, S.D.G.; software, S.D.G.; validation, S.D.G.; formal analysis S.D.G., investigation, S.D.G. and P.D.B.; data curation S.D.G.; writing—original draft preparation, S.D.G.; writing—review and editing S.D.G.

References

1. Bauman, Z.: *La solitudine del cittadino globale*, vol. 287. Feltrinelli Editore (2000)
2. Bauman, Z.: *Liquid modernity*. John Wiley & Sons (2013)
3. Pollio, V., Cesariano C.: *Vitruvio De architectura: Libri II-IV: i materiali, i templi, gli ordini*, vol. 16. Vita e pensiero (2002)
4. UNEP: <https://www.unep.org/>. Last accessed 3 Feb 2023
5. Giardiello, P.: *Smallness: abitare al minimo*. Smallness (2009)
6. Magnaghi, A.: *La rappresentazione identitaria del territorio*. Alinea, Firenze (2005)
7. De Gregorio, S., De Vita, M.: *Temporaneamente architettura. Aspetti costruttivi e tecnologici per l’organismo edilizio*. Aracne editrice (2020)
8. Latouche, S.: *La scommessa della decrescita*. Feltrinelli Editore (2014)
9. Qin, M., et al.: Characteristic analysis and improvement methods of the indoor thermal environment in post-disaster temporary residential buildings: a systematic review. *Build. Env.* **235**, 110198 (2023)
10. Ye, R., Wang, J., Jiang, H., Xie, N.: Numerical study on thermal comfort and energy-saving potential of a prefabricated temporary house integrated with composite phase change materials. *Energ. Build.* **268**, 112169 (2022)
11. Zheng, P., Wu, H., Liu, Y., Ding, Y., Yang, L.: Thermal comfort in temporary buildings: a review. *Build. Environ.* **221**, 109262 (2022)
12. De Vita, M., Duronio, F., De Vita, A., De Berardinis, P.: Adaptive retrofit for adaptive reuse: converting an industrial chimney into a ventilation duct to improve internal comfort in a historic environment. *Sustainability* **14**(6), 3360 (2022)
13. Bhandari, S., Riggio, M., Jahedi, S., Fischer, E.C., Muszynski, L., Luo, Z.: A review of modular cross laminated timber construction: implications for temporary housing in seismic areas. *J. Build. Eng.* **63**, 105485 (2023). <https://doi.org/10.1016/j.jobbe.2022.105485>
14. Chen, D., Wang, G., Chen, G.: Lego architecture: research on a temporary building design method for post-disaster emergency. *Front. Archit. Res.* **10**(4), 758–770 (2021)
15. De Vita, M., Panunzi, S., Fabbrocino, G., Mannella, A.: A discussion on the conceptual design of multifunctional exoskeletons for sustainable regeneration of buildings in urban areas. *Buildings* **12**(8), 1100 (2022)

16. Grosso, M., Thiebat, F.: Life cycle environmental assessment of temporary building constructions. *Energ. Procedia* **78**, 3180–3185 (2015)
17. UNEP: 2021 Global status report for Buildings and construction, globalabc.org. Last accessed 3 Mar 2023
18. Agenda 2030: <https://www.undp.org/sustainable-development-goals/>. Last accessed 5 Jan 2023
19. Gangemi, V. (ed.): *Riciclare in architettura. Scenari innovativi della cultura del progetto*. Clean Edizioni, Napoli (2004)
20. Verducci, P.: *Sezioni Guida. Progettare Architetture Temporanee*, pp. 1–142. Gangemi Editore, Roma (2020)
21. Concu, G., et al.: Local supply chains and circular economy for building materials. The PLES project in Sardinia. In: Gervasi, O., et al. (eds.) *ICCSA 2021. LNCS*, vol. 12958, pp. 44–58. Springer, Cham (2021). https://doi.org/10.1007/978-3-030-87016-4_4
22. Meloni, A.: New sustainable building solutions in Sardinia. *Sustainable Mediterranean Construction. Sustainable Environment in the Mediterranean Region: from Housing to Urban and Land Scale Construction* 83 (2012)
23. Parlato, M.C.M., Porto, S.M.C., Valenti, F.: Assessment of sheep wool waste as new resource for green building elements. *Build. Env.* **225**, 109596 (2022)
24. De Gregorio, S.: The rehabilitation of buildings. Reflections on construction systems for the environmental sustainability of interventions. *VITRUVIO-Int. J. Archit. Technol. Sustain.* **4**(2), 247–257 (2019)
25. Gorgolewski, M., Morettin, L.: The process of designing with reused building components. *Lifecycle Des. Build. Syst. Mater.*, 105–109 (2009). CIB Report 323
26. Cradle to Cradle: <https://c2ccertified.org>. Last accessed 30 Jan 2023
27. Sereda, P.J.: *Durability of Building Materials and Components*, vol. 691. ASTM International, West Conshohocken, PA (1980)
28. Ginelli, E.: *La flessibilità techno-tipologica nelle soluzioni progettuali e costruttive. Abitare. Il progetto della residenza sociale fra innovazione e tradizione*. Maggioli Editore, Santarcangelo di Romagna (2010)
29. Slaughter, E.: Design strategies to increase building flexibility. *Build. Res. Inform.* **29**(3), 208–217 (2001)
30. Mandolesi, E.: *Edilizia*. Utet (1983)
31. Chabrowe, B.: On the significance of temporary architecture. *Burlingt. Mag.* **116**(856), 385–391 (1974)
32. Protocollo Itaca: <https://www.itaca.org/nuovosito/index.asp>. Last accessed 3 Feb 2023
33. Cresme: <https://agenziasviluppoaq.eu/annuario-delle-industrie-abruzzesi-2021/>. Last accessed 20 Jan 2023
34. Mastrodonardo, L., Mastrodonardo G.: Local resources and sustainable industrial production for the post earthquake reconstruction in the territory of L'Aquila In: Conference: SB10 Finland Regional Conference Sustainable Community–building SMART, Abruzzo, Italy (2010)
35. De Gregorio, S., De Berardinis, P., Palmero, L.: The Enhancement of local resources: Research, teaching and experimentation in L'Aquila. *Tech. Eng. Mater. Archit.* **6**(1), 86–95 (2020)
36. Regione Abruzzo: <https://www.regione.abruzzo.it/bollettini-agrometeorologici/dati-meteorologici-giornalieri>. Last accessed 25 Nov 2022



Monitoring of Bridges Damage Based on the System Transfer Function Maps from Sensors Datasets

Dangui Guo¹, Weixing Hong², and Wael A. Altabey³(✉)

¹ Boshen Branch of Guangdong Boda Expressway Co., Ltd., Guangzhou, Guangdong, China

² Nanjing Zhixing Information Technology Co., Ltd., Nanjing, Jiangsu, China
wilson.hong@zhixingit.com

³ Department of Mechanical Engineering, Faculty of Engineering, Alexandria University,
21544, Alexandria, Egypt
wael.altabey@gmail.com

Abstract. To ensure the normal service of the bridge, it is necessary to detect and evaluate the health status of the bridge structure. This work provides a novel framework for damage detection in trusses bridges through analyzing of displacement sensors datasets and plotting the frequency maps of bridge system transfer function (TF). First, the bridge finite element model under random load is analysis, and the cumulative damages are considered and introduced to bridge model. The datasets of the sensors installed in bridge are compiled in both static and transient types. Finally, the bridge structure TF is determined by applying the principles of open loop control system on bridge structure and then plotting the frequency maps. The results show that the system becomes unstable in frequency maps when damage evolves in bridge structure.

Keywords: Bridges Structure Systems · Damage Detection · Displacement · Open Loop System · Transfer Function · Frequency Analysis

1 Introduction

In recent years, the construction of bridge structures has developed rapidly, and the health monitoring of bridge structures has become a research hotspot at home and abroad. Reasonable configuration of sensors is the premise to ensure the quality of bridge structure health monitoring, and it is very important to obtain accurate and real-time information on the health status of bridge structures and realize the monitoring and evaluation of bridge structures [1–12].

Bridges have been under the heavy pressure of vehicles for many years, and the judgment of whether it is "healthy" is mainly based on manual inspections. It is difficult to achieve real-time, continuous and uninterrupted monitoring, and the efficiency is low and there are visual blind spots. Nowadays, more and more traffic managers use intelligent and digital means to automatically capture various structural safety-related data such as environmental temperature and humidity, expansion joint displacement, etc.

through the bridge and tunnel structural health monitoring system, identify and record the development of existing diseases in real time, Discover new diseases and report to the police, assist in decision-making and judgment, reduce maintenance costs, and improve monitoring efficiency and quality [13–25].

The bridge structure of the time-frequency domain characteristics is detected, but the number of frequency domain features in the original time is large, which adversely affects the efficiency of the health state detection of the bridge structure. In the process of the health state of the bridge structure, the selection of the detection algorithm is also very important [10–12].

A frequency response function (FRF) of the system using a signal of conventional valve closing is proposed to study the different faults effects, the viscoelasticity, and friction of pipe wall on that function and then compare it with corresponding influences the time domain [26]. The appropriateness of FRF in transient mode method for complex pipelines leakage detection is investigated [27]. A FRF method that requires measuring pressure and fluctuations of discharge at single location was used to detect the possibility of leaks in real piping systems carrying various types of fluids [28]. The simplification method of FRF system's analytically based approach was performed to determine the key blocking parameters that controlling on the frequency shift. It was shown that the of blockage severity follows that the increases of frequency shift magnitude related to wave propagation, and impedance of the pipe coefficients such as pipe diameter, thickness and/or wave velocity [29].

This paper discusses a new strategy of damage detection of bridges structure in static and transient sensing methods using displacement sensors, the displacement as system inputs and outputs of TF system is proposed, and the “open loop” bridge system is applied. As far as the author knows, no work has been done on new damage indicators based on “systems control theory” for bridge structures. By applying static and dynamic load to the displacement sensor distributed on bridge, damage area of the bridge.

2 Bridge Modeling

2.1 Bridge Description

Figure 1 shows a graphical representation of the truss bridge. The bridge is a combination of I-shaped, U-shaped, box-shaped and other cross-sections. The bridge's height is 4.25 m, its total length is 33.5 m, and its wide is 5.5 m. The truss high is 4.4 m. The average daily traffic is about 19066 vehicles northbound and 231748 southbound. The random excitation (–300–300 kN) is shown in Fig. 2, The corresponding elastic modulus value was, $E = 210$ GPa, and the Shear modulus value was $G = 10.64$ GPa, Poisson coefficient was $\nu = 0.3$, and the density was $7,860$ kg/m³. Various sensors were installed on the trusses and longitudinal deck of bridge as shown in Fig. 3 the sensors positions in red boxes. An appropriate finite element is selected, i.e. the LINK1 element is used to model the structural behavior with material model EX 210000.

Figure 4 shows the acceleration responses of random excitation measured from the various sensors installed on the trusses and longitudinal deck of bridge.

Changes in acceleration response due to damage effect on structural. Therefore, the response of the acceleration in time-history is sensitive to structural damage and can be considered as a damage indicator.



Fig. 1. General View of truss bridge.

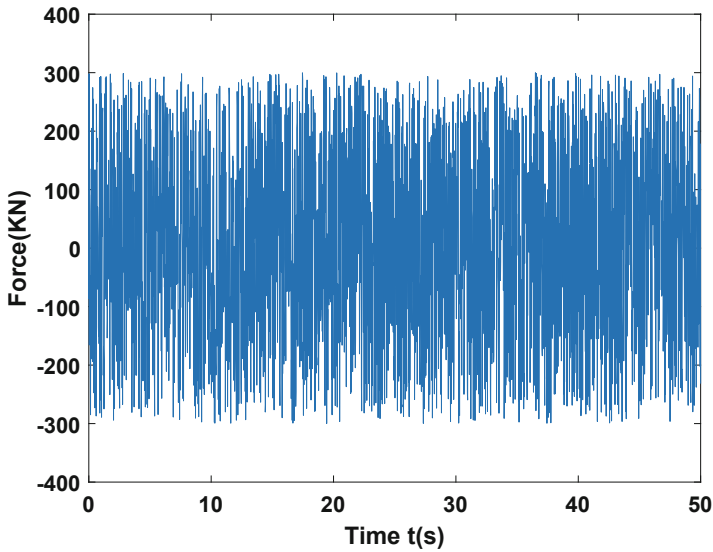


Fig. 2. Random Excitation.

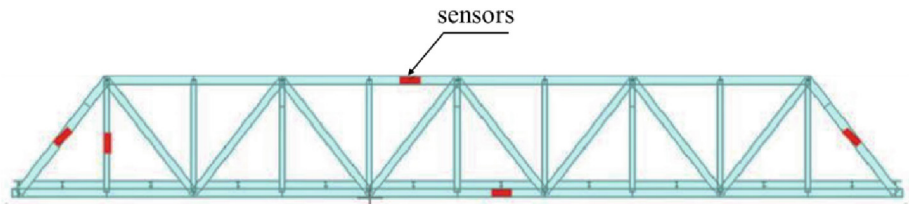


Fig. 3. Finite Element Bridge Modeling.

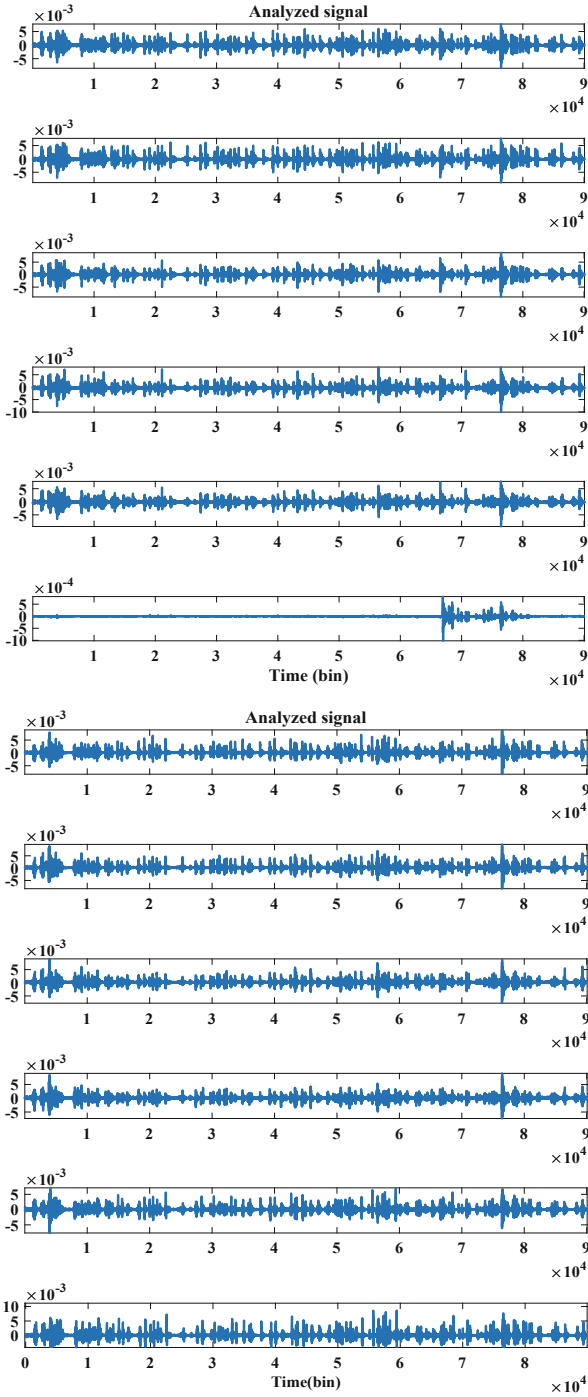


Fig. 4. The acceleration of random excitation.

Table 1. Structural frequency.

Frequency Order	D0 (Hz)	D1 (Hz)
1st order (Lateral Bending)	233.55	232.85
2nd order (Vertical Bending)	315.62	312.67
3rd order (shear)	824.38	822.90

Figure 5 shows the energy variations strength or shows at which frequencies variations are strong and at which frequencies variations are weak. Any changes in the PSD can be used as indicator of damage. Also, it can be used to reduce the effect of noise in the signal and also can be used to trace the damage through the curvature of the power spectrum energy. If tracking the ridge though time-frequency energy distribution and show any change due to damage. The energy variations strength or shows at which frequencies variations are strong and at which frequencies variations are weak. Any changes in the PSD can be used as indicator of damage. Also, it can be used to reduce the effect of noise in the signal and also can be used to trace the damage through the curvature of the power spectrum energy.

Table 1 lists all the values of frequency orders for different damage case (D0 & D1).

3 Results and Dissections

3.1 Acceleration Responses Analysis in the Frequency Domain

Accounting for modeling uncertainty, typical fitting curve (Mean) of acceleration select change response (Eq. 2) for output description of the structure system field excitation by random input, where the Cubic, Quadratic, Linear, and Constant terms of the fitting equation are 0.0287, -0.0016 , 0.0063, 0.0005, respectively.

$$X(t) = 0.0287t^3 - 0.0016t^2 + 0.0063t + 0.0005 \quad (1)$$

The differential equation can represent herein:

$$\begin{aligned} a_0x_o^{(n)}(t) + a_1x_o^{(n-1)}(t) + \dots + a_{n-1}x_o^{(1)}(t) + a_nx_o(t) \\ = b_0x_i^{(m)}(t) + b_1x_i^{(m-1)}(t) + \dots + b_{m-1}x_i^{(1)}(t) + b_mx_i(t), n \\ \geq m \end{aligned} \quad (2)$$

where x_o is the system output, x_i is the system input.

$$G(s) = \frac{X_o(s)}{X_i(s)} = \frac{b_0s^m + b_1s^{m-1} + \dots + b_{m-1}s + b_m}{a_0s^n + a_1s^{n-1} + \dots + a_{n-1}s + a_n} \quad (3)$$

System input can be expressed as:

$$X_i(s) = \frac{2232\pi}{s^2 + 35642\pi^2} \quad (4)$$

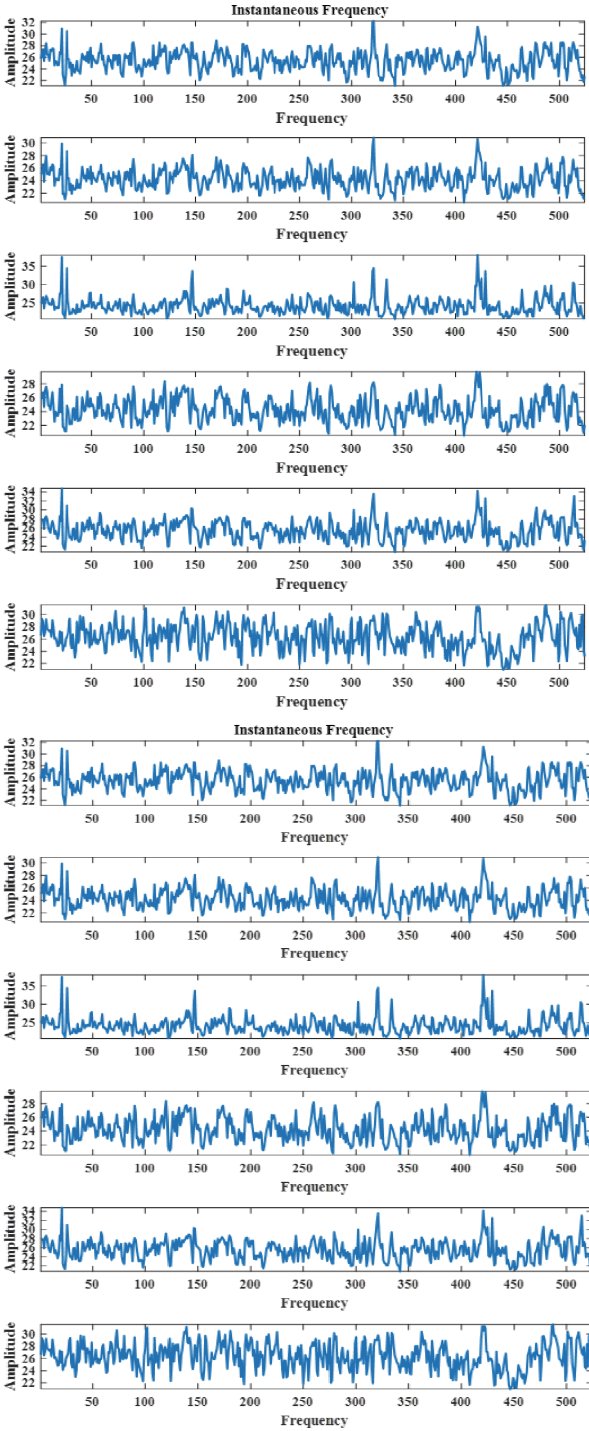
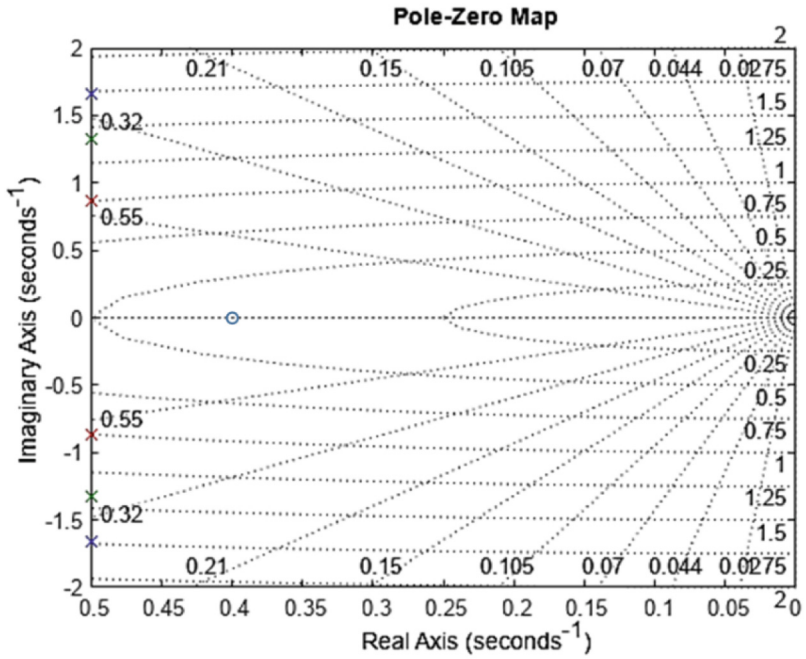
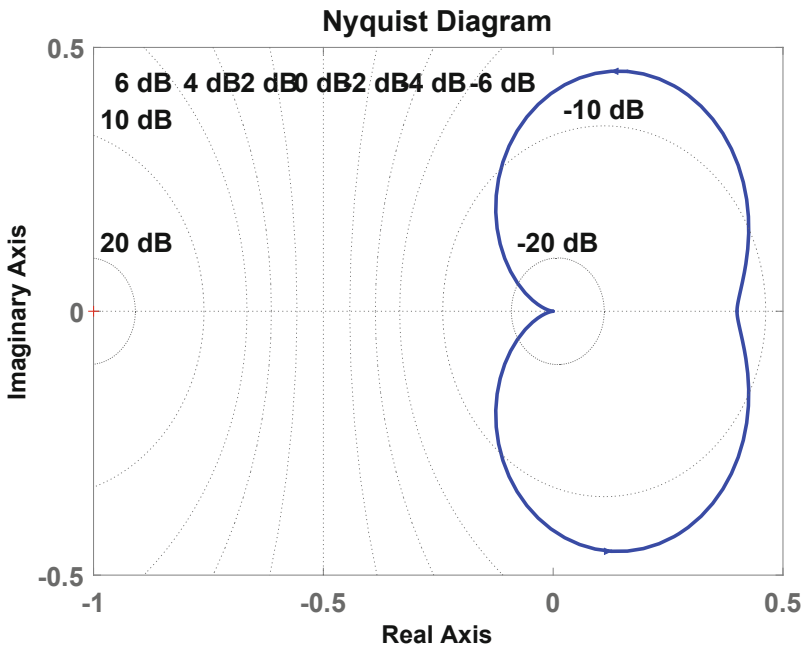


Fig. 5. The Power spectral density.

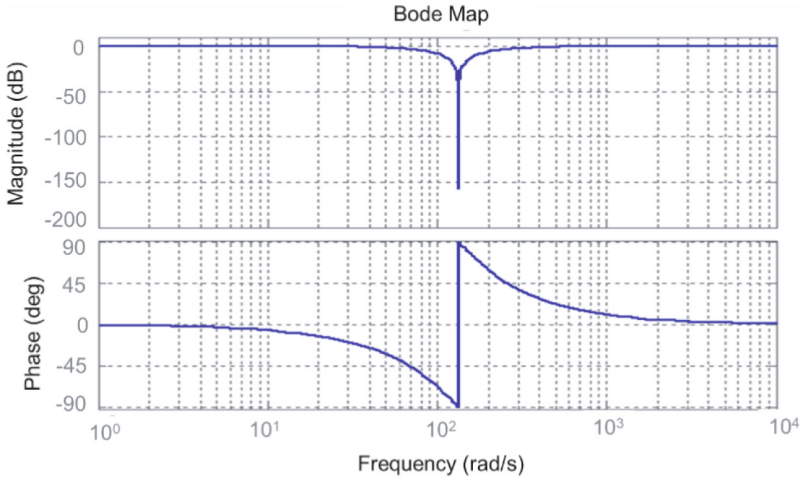


(a) Pole-Zero Map

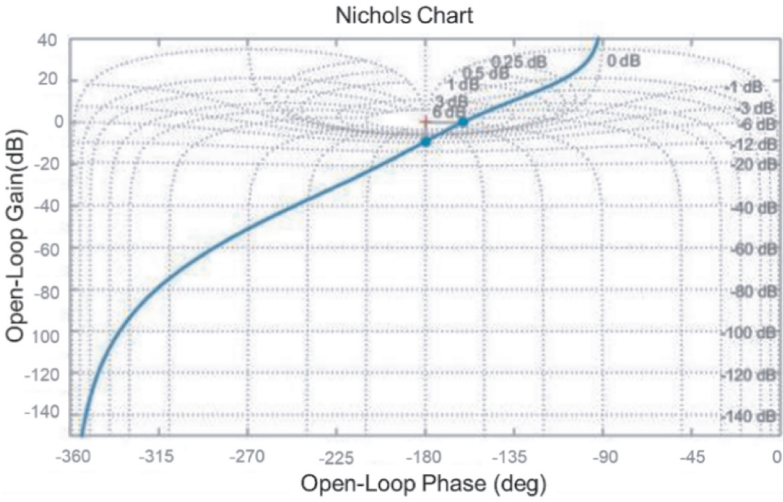


(b) Nyquist Map

Fig. 6. The frequency domain analysis methods for steel truss bridge.



(c) Bode Map



(d) Nichols Map

Fig. 6. (continued)

System output can be expressed as:

$$X_o(s) = \frac{213}{854s^4} - \frac{1}{2232s^3} \quad (5)$$

System TF can be expressed as follows according to the presented damage case (D1).

$$G_1(s) = \frac{(s^2 + 35642\pi^2)(854s - 11160)}{2.5E9\pi s^4} \quad (6)$$

3.2 Bridge System Analysis in Frequency Domain

The bridge system subjected to different conditions of damage features when excited by a random signal input. Let us regard it as a "control system" with an input excitation and an output measurement sensors. When considering the system as an open loop control system, this means that no feedback from output to the system, the main control on the system is from input only. The frequency domain analysis methods (Zero-Pole, Nyquist, Bode, Nichols) are applied to measure the dynamic response characteristics of the system regarding damage using Simulink software.

The Zero-Pole Point Map analysis for the presented damage case is plotted in Fig. 6(a). For the presented damage we can see that the Zero point of system TF (0.4) moves towards zero when the damage range increases. The Nyquist map analysis for the presented damage case is plotted in Fig. 6(b). As shown in the Figure, for the presented damage we can see the variation of the endpoint trajectory of the vector $G(j\omega) = A(\omega)e^{j\varphi(\omega)}$ (Where shows $A(\omega_i)$ appears the vector magnitude $G(j\omega_i)$ when the frequency equals ω_i , and The case of polar coordinates is $\varphi(\omega)$) when frequency ω changes from $0 \rightarrow \infty$. The Nyquist diagram shows in the non-overlapped part the system frequency of G is -11.4 . The system frequency decreases as the damage range increases. The Bode map analysis for the presented damage case is plotted in Fig. 6(c). As shown in the Figure, for the presented damage we can see the frequency of the excitation signal is 100π . In detail, when damage occurs the absolute value of magnitude increases over 153 dB, and the corresponding phase changes more than 180° . The Nichols map for the presented damage case is plotted in Fig. 6(d). As shown in the Figure, for the presented damage phase reaches about -180 , accordingly G change at the inflection point with Gain -10 at the frequency is 100π .

4 Conclusions

This paper established a FEM of steel truss bridge damage system from the traffic effect, by extracting the measurements of sensors and loaded with random signal. Results show that the signal magnitude will suddenly and sensitively change when the damage starts. The bridge system TF and the frequency domain are established and applied to reflect damage evolution through plotting the zero-pole points map, Nyquist Map, Bode Map, and Nichols Map. The most motivating conclusion in this work is that, instead of using the vibration signals of the responses of the structural system, the variation of the frequency is used to observe the time and displacement characteristics variation of the system due to structural damage.

References

1. Ghiasi, R., Noori, M., Altabey, W. A., Wang, T., Wu, Z.: Structural damage detection under uncertain parameters using non-probabilistic meta-model and interval mathematics. In: *Lifeline 2022: Advancing Lifeline Engineering for Community Resilience*, pp. 670–679. ASCE Library (2022)

2. Ghiasi, R., Noori, M., Altabay, W. A., Wang, T., Wu, Z.: Uncertainty handling in structural damage detection using non-probabilistic meta-model and interval mathematics. In: International Conference on Structural Health Monitoring of Intelligent Infrastructure: Transferring Research into Practice, SHMII 2021, vol. 2021-June, pp. 819–824 (2021)
3. Li, Z., Feng, D., Noori, M., Basu, D., Altabay, W.A.: Dynamic response analysis of Euler-Bernoulli beam on spatially random transversely isotropic viscoelastic soil. *Proc. Inst. Mech. Eng., Part L: J. Mater.: Des. Appl.* **236**(5), 1037–1052 (2022)
4. Li, Z., Noori, M., Basu, D., Taciroglu, E., Wu, Z., Altabay, W.A.: Dynamic analysis of soil structure interaction shear model for beams on transversely isotropic viscoelastic soil. *Proc. Inst. Mech. Eng., Part L: J. Mater.: Des. Appl.* **236**(5), 999–1019 (2022)
5. Ghabdian, M., Seyed, B.B.A., Noori, M., Altabay, W.A.: Reliability of reinforced concrete beams in serviceability limit state via microprestress-solidification theory, a structural health monitoring strategy. *Proc. Inst. Mech. Eng., Part L: J. Mater.: Des. Appl.* **236**(5), 1077–1093 (2022)
6. Seyed, B.B.A., Ghabdian, M., Noori, M., Altabay, W.A.: Simultaneous effect of temperature, shrinkage, and self-weight creep on RC beams: a case study. *Proc. Inst. Mech. Eng., Part L: J. Mater.: Des. Appl.* **236**(5), 1020–1036 (2022)
7. Arash, R., et al.: A simplified beam model for the numerical analysis of masonry arch bridges-A case study of the Veresk railway bridge. *Structures* **45**, 1253–1266 (2022)
8. Noori, M., Altabay, W.A.: Hysteresis in engineering systems. *Appl. Sci.* **12**, 9428 (2022)
9. Silik, A., Hong, W., Li, J., Mao, M., Noori, M., Altabay, W.A.: Develop a health monitoring technique for analysis a big data of bridges. *Lect. Notes Civ. Eng.* **292**, 59–78 (2023)
10. Silik, A., Noori, M., Altabay, W.A., Ji, D., Ghiasi, R.: A new denoising technique via wavelet analysis of structural vibration response for structural health monitoring applications. In: *Lifeline 2022: Advancing Lifeline Engineering for Community Resilience*, pp. 691–706. ASCE Library (2022)
11. Altabay, W.A., Wu, Z., Noori, M., Fathnejat, H.: Structural health monitoring of composite pipelines utilizing fiber optic sensors and an AI-based algorithm-A comprehensive numerical study. *Sensors* **23**(8), 3887 (2023)
12. Mohebian, P., Seyed, B.B.A., Noori, M., Lu, N., Altabay, W.A.: Visible particle series search algorithm and its application in structural damage identification. *Sensors* **22**(3), 1275 (2022)
13. Yanliang, X., et al.: Research of pavement crack detection system based on image processing. In: *Proceedings of the SPIE 12590, Third International Conference on Computer Vision and Information Technology (CVIT 2022)*, p. 1259007 (2023)
14. Altabay, W.A., Noori, M., Wu, Z., Al-Moghazy, M.A., Kouritem, S.A.: Studying acoustic behavior of bfrp laminated composite in dual-chamber muffler application using deep learning algorithm. *Materials* **15**(22), 807 (2022)
15. Altabay, W.A., Kouritem, S.A., Abouheaf, M.I., Nahas, N.: Research in image processing for pipeline crack detection applications. In: *IEEE Conference, 2nd International Conference on Electrical, Computer, Communications and Mechatronics Engineering (ICECCME-2022)*, Maldives, 16–18 November 2022
16. Altabay, W.A., Noori, M.: A dynamic analysis of smart and nanomaterials for new approaches to structural control and health monitoring. *Materials* **16**(9), 3567 (2023)
17. Altabay, W.A., Noori, M., Wu, Z., Al-Moghazy, M.A., Kouritem, S.A.: A deep-learning approach for predicting water absorption in composite pipes by extracting the material's dielectric features. *Eng. Appl. Artif. Intell.* **121**, 105963 (2023)
18. Silik, A., Noori, M., Altabay, W.A., Ghiasi, R., Wu, Z., Dang, J.: Evaluation of analytic wavelet parameters effect for data analyses in civil structural health monitoring. In: *International Conference on Structural Health Monitoring of Intelligent Infrastructure: Transferring Research into Practice, SHMII 2021*, vol. 2021-June, pp. 813–818 (2021)

19. Weixing, H., et al.: Artificial intelligence technique for pavement diseases identification. In: Proceedings of the 4th International Conference on Intelligent Science and Technology (ICIST'22), ACM Digital Library, pp. 66–72 (2022)
20. Hong, W., Noori, M., Jiang, H., Liu, Y., Altabey, W.A.: Machine vision-based structural diagnosis application. *Lect. Notes Civ. Eng.* **292**, 79–88 (2023)
21. Silik, A., et al.: Dynamic wavelet neural network model for damage features extraction and patterns recognition. *J. Civil Struct. Health Mon.* (2023)
22. Wang, T., Li, H., Noori, M., Ghiasi, R., Kuok, S., Altabey, W.A.: Seismic response prediction of structures based on Runge-Kutta recurrent neural network with prior knowledge. *Eng. Struct.* **279**, 115576 (2023)
23. Fathnejat, H., Ahmadi-Nedushan, B., Hosseinijad, S., Noori, M., Altabey, W.A.: A data-driven structural damage identification approach using deep convolutional-attention-recurrent neural architecture under temperature variations. *Eng. Struct.* **276**, 115311 (2023)
24. Altabey, W.A., Noori, M.: Artificial-intelligence-based methods for structural health monitoring. *Appl. Sci.* **12**(24), 12726 (2022)
25. Li, Z., Noori, M., Wan, C., Yu, B., Wang, B., Altabey, W.A.: A deep learning-based approach for the identification of a multi-parameter BWBN model. *Appl. Sci.* **12**(19), 9440 (2022)
26. Lee, P.J., Duan, H., Ghidaoui, M.S., Karney, B.: Frequency domain analysis of pipe fluid transient behavior. *J. Hydraul. Res.* **51**(6), 609–622 (2013)
27. Duan, H., Lee, P.J., Ghidaoui, M.S., Tung, Y.: Leak detection in complex series pipelines by using the system frequency M.S. Ghidaoui y response method. *Hydraulic Res.* **49**(2), 213–221 (2011)
28. Mpesha, W., Gassman, S.L., Chaudhry, M.H.: Leak Detection in pipes by frequency response method. *Hydraulic Eng.* **127**(2), 127–134 (2001)
29. Duan, H., Lee, P.J., Kashima, A., Lu, J., Ghidaoui, M.S., Tung, Y.: Extended blockage detection in pipes using the system frequency response, analytical analysis and experimental verification. *Hydraulic Eng.* **139**(7), 763–771 (2013)



Bridges Damage Assessment Techniques Improvement Through Machine Learning Algorithm

Liping Zhou¹, Weixing Hong², and Wael A. Altabay³✉

¹ Guangdong Provincial Highway Construction Co., Ltd., Guangzhou, Guangdong, China

² Nanjing Zhixing Information Technology Co., Ltd., Nanjing, Jiangsu, China

wilson.hong@zhixingit.com

³ Department of Mechanical Engineering, Faculty of Engineering, Alexandria University, Alexandria 21544, Egypt

wael.altabay@gmail.com

Abstract. The main goal of this paper is improving bridges structures health detection results to solve the problems of large errors of detection and poor efficiency of detection in the traditional models of detection. A bridge structural health monitoring (SHM) model based on data classification technique is designed by using the k-Nearest Neighbor (k-NN) algorithm. First, the sensor network is used to collect the health status data of the bridge structure, and the kernel principal component analysis is used to process the sensor datasets to remove the redundant features and reduce the classification feature scale. Second, adopt on the k-NN algorithm, the learning of the sensor datasets, and the optimum parameters of the bridge structure health state (SHS) to establish the optimal bridge SHS detection model. The optimum parameters of classification model are determined by the genetic optimization algorithm (GOA). Finally, the bridge SHM model is analyzed by using the most significant indexes of testing for its effectiveness and superiority. The results show that the proposed model has a classification results of the bridge SHS with higher precision, lower modeling time. The overall performance of proposed classification model is significantly better than exists methods, and the current method performance are recorded 97.4%, 93.7%, and 91.3%, for accuracy rate, recall rate, and F-score respectively. This indicates that the current SHM model provides an effective tool for bridge structure health research.

Keywords: k-Nearest Neighbor · Structural Health Monitoring · Data Classification · Machine Learning · Genetic Optimization Algorithm

1 Introduction

Due to the accelerated operating speed of the vehicle, the large number of vehicle load-bearing, and the invasion of the medium, it has brought a certain damage to the bridge structure. To ensure the normal service of the bridge, it is necessary to detect and evaluate the health status of the bridge structure [1–3]. In response to the test of bridge SHS,

domestic and foreign scholars and experts conducted a series of studies. Due to the SHS detection of bridge structure, it is a mode of identification [4–6]. First of all, we must extract the characteristics of the health state of the bridge structure, such as the displacement of the bridge structure and the speed of the bridge structure, etc., can describe the corresponding health status of the bridge structure, but there are insufficient [7–9]. The bridge structure of the time-frequency domain characteristics is detected, but the number of frequency domain features in the original time is large, which adversely affects the efficiency of the SHS detection of the bridge structure. In the process of the health state of the bridge structure, the selection of the detection algorithm is also very important [10–12]. At present, the main use of neural networks to model the health state of the bridge structure, and the neural network is a learning algorithm based on minimizing experience risk. State training samples make the cost of the health state of the bridge structure high [13–19]. k-NN is a classification algorithm based on minimizing structural risk. There is no large sample condition limit for the sample requirements of bridge SHS. The classification ability is also better than the neural network. It provides a new construction for the health state of the bridge structure model method [20–25].

In order to obtain better bridge SHS classification results, there are problems such as large classification errors and poor efficiency such as the health state classification model of the current bridge structure, and a bridge structure health state classification model (k-NN) based on data classification technology is designed. Test the effectiveness and superiority of the present bridge SHS model is analyzed by using the most significant indexes.

2 Bridge Structure Health State Classification Model Based on K-NN Algorithm

2.1 A K-Nearest Neighbor (K-NN) Algorithm

k-NN is one of machine learning algorithms in supervised types for regression and classification application. It is using the training data for processing, and testing data for classifying according to the distance metric. It finds the k-NNs of the test data and then classifies based on the majority class label. It is always a challenge for data scientists to choose the optimal value of k to achieve the maximum accuracy of the model. Figure 1 presents the k-NN algorithm principal in classification [26, 27].

Calculating Distance Metrics. The active hyperparameter in k-NN is a distance metric that measure the space from the feature value to new test inputs. Euclidean method is usually use to measure that distance between training data values and test samples. We measure the distance of the points along the straight line from point (x_1, y_1) to point (x_2, y_2) [27].

$$Euclidean\ Distance = \sqrt{\sum_{i=1}^n (x_i - y_i)^2} \quad (1)$$

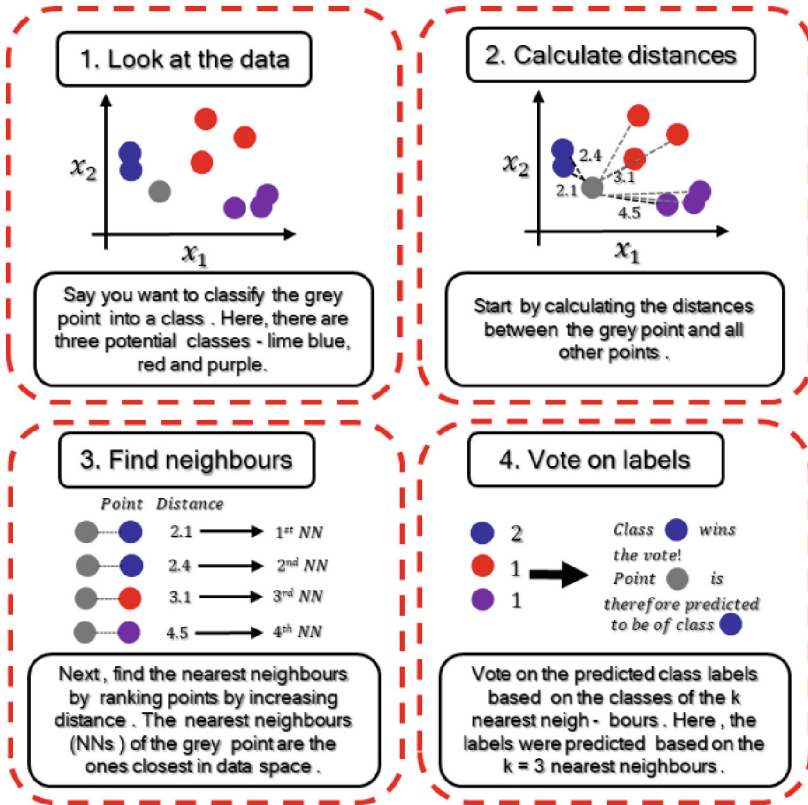


Fig. 1. A k-NN algorithm principal.

K Value Selection. The k value represents the count of nearest neighbors. We have to calculate the distance between labeled training and test points. The processes for distance metric updating are expensive every epoch computationally. As shown in Fig. 2, Two classes in the Figure A and B, by proceeding with $k = 3$ and $k = 7$, we can predict that the test input data follow class B and A respectively. This is how you can see the value of k to have a strong impact on k-NN performance [27].

Figure 3 illustrates largely how the decision boundary (indicated by the dashed line) is influenced by smaller or larger values of k. Smaller values allow more complex decision boundaries to be fitted more carefully to the training data. The issue is that we don't know if the straight border or the curved border better represents the real implicating concept to be learned. [26, 27].

2.2 Bridge Description

The case study here is a truss bridge type shown in the Fig. 4. The bridge is constructed of I-shape, U-shape, and box sections with dimensions and material properties listed in Table 1. The bridge is loaded by random excitation (−300–300 kN) is shown in

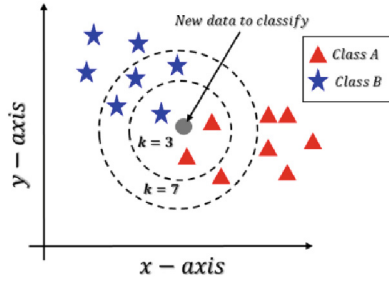


Fig. 2. Choose a k value.

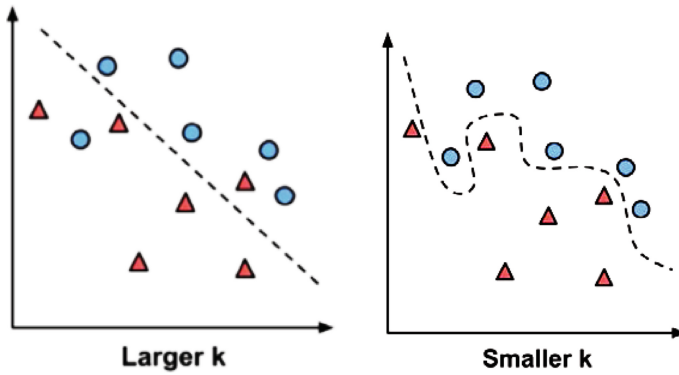


Fig. 3. Different between large k and smaller k in classification accuracy.

Fig. 5. An appropriate finite element is selected, i.e. the LINK1 element with material model EX 210000. Several accelerometers sensors in various positions on the trusses and longitudinal deck of bridge are installed as shown in Fig. 6, the red boxes indicates the sensors positions.

Table 1. The Main properties of Bridge.

Bridge properties	Value
Height	4.25 m
Total length	33.5 m
Wide	5.5 m
Truss high	4.4 m
Elastic modulus (E)	210 GPa
Shear modulus (G)	10.64 GPa
Poisson coefficient (ν)	0.3
Density	7,860 kg/m ³



Fig. 4. Truss bridge General View.

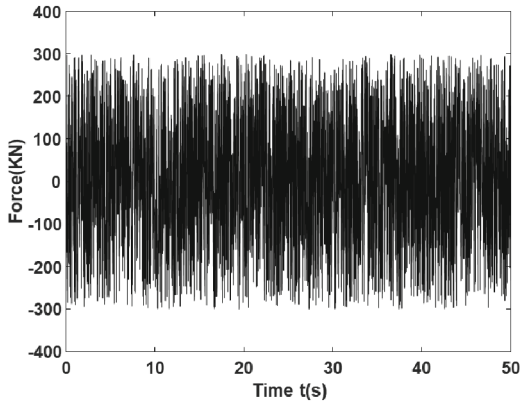


Fig. 5. Random Excitation.

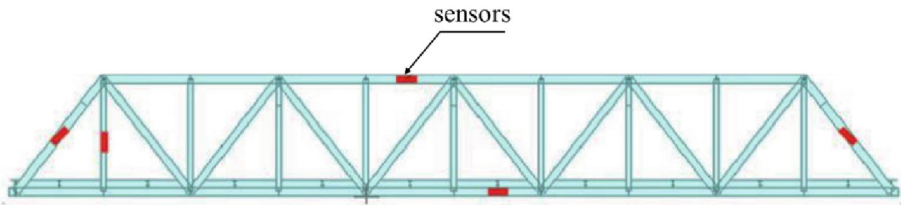


Fig. 6. Finite Element Modeling of Truss Bridge.

3 Results and Dissections

3.1 The Sensor Network Collection Bridge SHS Data

The responses of the distributed sensors installed on the trusses and longitudinal deck of bridge is presented in Fig. 7. As shown in the Figure the structural damage is leads to change of the acceleration responses. So, the time history acceleration responses are sensitive to structural damage and can be used as a damage indicator.

3.2 Steps of Health Status of Bridge Structure Based on Data Classification Technology

The work frame of the bridge SHS based on data classification technology is shown in Fig. 8.

The main steps of this work frame are presented as follows:

- (1). The sensor network collection bridge SHS vibration signal, and noise processing of the vibration signal of the original bridge SHS, eliminating some useless signals.
- (2). Extract the statistical characteristics of the time domain of the bridge structure from the health state signal of the bridge structure. Due to the difference in the statistical characteristics of the time domain of the bridge structure, the range of the value range is very different.
- (3). Because there is a certain correlation between the statistical characteristics of the time domain of the bridge, that is, there are some characteristic redundancy information, the analysis of the main element of the kernel function is used to analyze the health status characteristics of the bridge structure, and select the most effective bridge SHS of classification characteristics.
- (4). The health status characteristics of the bridge structure as the input of the k-NN algorithm, the health state of the bridge structure as the output of the k-NN algorithm, and the relationship between the health state and characteristics of the bridge structure by supporting the principal in classification of the k-NN algorithm (see Sect. 2.1). The genetic optimization algorithm (GOA) is used to determine the k parameter of the k-NN algorithm, and the bridge SHS detection model is established, the flowchart of GOA to choose for selecting the optimum k is shown in Fig. 9.
- (5). Test the sample of the health state of the bridge structure to analyze the performance of the healthy state detection model based on the data-based classification structure.

3.3 K-NN Data Classification Technology

As the aiming of this work, the response of acceleration sensor will be used as the input for health state classification of the bridge. After select the optimum value of parameter k . The sensor dataset is normalized by min-max normalization and z-score as following [26, 27]:

$$\text{Min - Max normalization}(X) = \frac{(X - \min(X))}{(\max(X) - \min(X))} \quad (2)$$

$$\text{z-score standardization}(X) = \frac{(X - \text{main}(X))}{\text{StdDev}(X)} \quad (3)$$

The distance metric is very important for accurate classification due to when features pair is input, k-NN will use the Euclidean distance to search for the nearest k pairs of features on the same scale, we can measure the distance from Eq. (1). Table 2 presents the k-NN intrinsic parameters of the present research [26, 27].

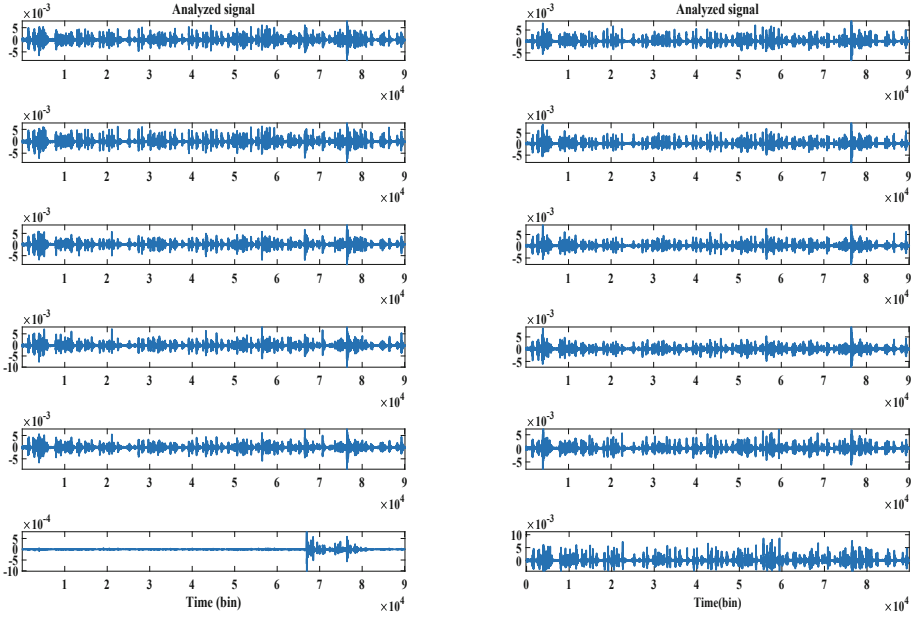


Fig. 7. The acceleration responses of sensors due to random excitation.

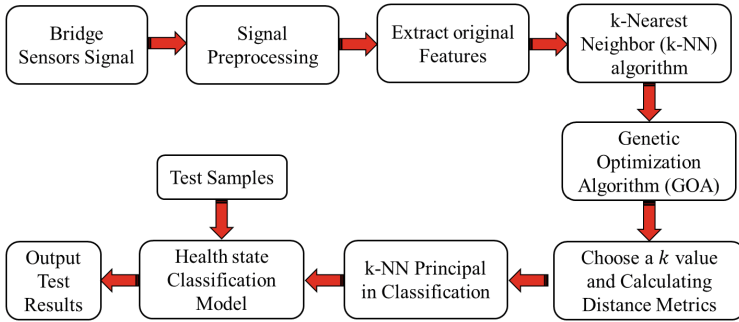


Fig. 8. The Work frame of bridge structure health condition detection model based on data classification.

3.4 Accuracy and Reliability Evaluation of Suggested Algorithm

To evaluate the suggested algorithm of health status of bridge structure, we computed the most significant indexes of performance measures for k-NN output of data classification sets Including the true-positive rate (TPR), true-negative rate (TNR), false-positive rate (FPR), and false-negative rate (FNR) [14, 17]. The performance indicators of suggested algorithm of health status of bridge structure can be found by calculating the accuracy rate ($P\%$), regression rate ($R\%$), and F-score ($F\%$) from the following equations:

$$P\% = \frac{N_{TPR}}{N_{TPR} + N_{FPR}} \tag{4}$$

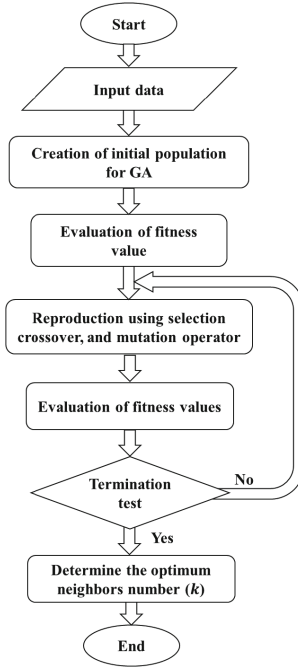


Fig. 9. Flowchart of GOA to choose for selecting the optimum k .

$$R\% = \frac{N_{TPR}}{N_{TPR} + N_{FNR}} \quad (5)$$

$$F\% = \frac{2N_{TPR}}{2N_{TPR} + N_{FNR} + N_{FPR}} \quad (6)$$

Used a convolutional Neural Network (CNN), Support Vector Machine (SVM), and K-NN for training the samples of the health state of the bridge structure, then establish the corresponding bridge SHS classification model, and then test the sample of the health state of the bridge structure to assess the present bridge SHS. Table 3 Comparing and analyzing the test results of the bridge structure from where classification time, accuracy rate, regression rate, and F-score.

In general, for all indexes ($P\%$, $R\%$, $F\%$, and Classification time), using CNN over the input datasets achieves lower average accuracy than SVM configuration, present approach k-NN achieve better results than the SVM and CNN. As a general conclusion, the proposed approach k-NN consistently outperforms the SVM, and CNN with all indexes.

Table 2. k-NN intrinsic parameters.

Parameters	Value
Optimum Neighbors number (k)	73
Optimization method	GOA
Distance	<i>Euclidean</i>
Bucket size	50
Include ties	0
Distance weight	equal
Break ties	smallest
Standardize data	1
Type	Prediction
min (X)	[3.735E-3,8.684E-3]
StdDev (X)	[0.656,1.008]
Weight (W)	106.58E-03

Table 3. Identification Testing Detailed Results.

Indexes	AI Method	Label
$P\%$	SVM	93.11%
	CNN	90.58%
	k-NN	96.4%
$R\%$	SVM	90.74%
	CNN	89.66%
	k-NN	93.7%
$F\%$	SVM	88.21%
	CNN	86.35%
	k-NN	91.3%
Classification time (s)	SVM	29.0
	CNN	12.0
	k-NN	7.0

4 Conclusions

Bridge SHS detection is an important technology to ensure bridge safety. There is a large amount of redundant information in the original bridge structure health data, which affects the bridge efficiency SHS detection. To improve the accuracy of health status detection, a bridge structure health status detection model based on data classification technology is designed. Firstly, the sensor network collects the health state data of the bridge structure, and uses the kernel principal component analysis to process the bridge

structure health data, removes the bridge structure health data redundancy, reduce the health scale of bridge structures, and then uses the k-NN algorithm to analyze the bridge structure, and the genetic optimization algorithm (GOA) is introduced to determine the bridge SHS detection parameters model, and the optimal bridge SHS detection model is established. Finally, the efficiency and superiority of the health model of the bridge structure are tested by comparison between the present bridge SHS detection model using k-NN and another two algorithms are a convolutional Neural Network (CNN) and Support Vector Machine (SVM) where from indexes (P%, R%, F%, and Classification time). The results show that the model in this paper has obtained the detection results of the bridge SHS with higher accuracy, bridge structure health modeling time is reduced, bridge SHS detection efficiency is improved, and overall bridges SHS detection performance is better than other present bridge structures It is healthy and has certain practical application value.

References

1. Ghiasi, R., Noori, M., Altabay, W. A., Wang, T., Wu, Z.: Structural damage detection under uncertain parameters using non-probabilistic meta-model and interval mathematics. In: *Lifeline 2022: Advancing Lifeline Engineering for Community Resilience*, ASCE Library, pp. 670–679 (2022)
2. Ghiasi, R., Noori, M., Altabay, W.A., Wang, T., Wu, Z.: Uncertainty handling in structural damage detection using non-probabilistic meta-model and interval mathematics. In: *International Conference on Structural Health Monitoring of Intelligent Infrastructure: Transferring Research into Practice, SHMII 2021*, vol. 2021-June, pp. 819–824 (2021)
3. Li, Z., Feng, D., Noori, M., Basu, D., Altabay, W.A.: Dynamic response analysis of Euler-Bernoulli beam on spatially random transversely isotropic viscoelastic soil. *Proc. Inst. Mech. Eng., Part L: J. Mater.: Des. Appl.* **236**(5), 1037–1052 (2022)
4. Li, Z., Noori, M., Basu, D., Taciroglu, E., Wu, Z., Altabay, W.A.: Dynamic analysis of soil structure interaction shear model for beams on transversely isotropic viscoelastic soil. *Proc. Inst. Mech. Eng., Part L: J. Mater.: Des. Appl.* **236**(5), 999–1019 (2022)
5. Ghabdian, M., Seyed, B.B.A., Noori, M., Altabay, W.A.: Reliability of reinforced concrete beams in serviceability limit state via microprestress-solidification theory, a structural health monitoring strategy. *Proc. Inst. Mech. Eng., Part L: J. Mater.: Des. Appl.* **236**(5), 1077–1093 (2022)
6. Seyed, B.B.A., Ghabdian, M., Noori, M., Altabay, W.A.: Simultaneous effect of temperature, shrinkage, and self-weight creep on RC beams: a case study. *Proc. Instit. Mech. Eng., Part L: J. Mater.: Des. Appl.* **236**(5), 1020–1036 (2022)
7. Arash, R., et al.: A simplified beam model for the numerical analysis of masonry arch bridges—A case study of the Veresk railway bridge. *Structures* **45**, 1253–1266 (2022)
8. Noori, M., Altabay, W.A.: Hysteresis in engineering systems. *Appl. Sci.* **12**, 9428 (2022)
9. Silik, A., Hong, W., Li, J., Mao, M., Noori, M., Altabay, W.: A: Develop a health monitoring technique for analysis a big data of bridges. *Lect. Notes Civ. Eng.* **292**, 59–78 (2023)
10. Silik, A., Noori, M., Altabay, W.A., Ji, D., Ghiasi, R.: A new denoising technique via wavelet analysis of structural vibration response for structural health monitoring applications. In: *Lifeline 2022: Advancing Lifeline Engineering for Community Resilience*, ASCE Library, pp. 691–706 (2022)
11. Altabay, W.A., Noori, M.: A dynamic analysis of smart and nanomaterials for new approaches to structural control and health monitoring. *Materials* **16**(9), 3567 (2023)

12. Mohebian, P., Seyed, B.B.A., Noori, M., Lu, N., Altabay, W.A.: Visible particle series search algorithm and its application in structural damage identification. *Sensors* **22**(3), 1275 (2022)
13. Yanliang, X., et al.: Research of pavement crack detection system based on image processing. In: Proceedings of the SPIE 12590, Third International Conference on Computer Vision and Information Technology (CVIT 2022), p. 1259007 (2023)
14. Altabay, W.A., Noori, M., Wu, Z., Al-Moghazy, M.A., Kouritem, S.A.: Studying acoustic behavior of BFRP laminated composite in dual-chamber muffler application using deep learning algorithm. *Materials* **15**(22), 807 (2022)
15. Altabay, W.A., Kouritem, S.A., Abouheaf, M.I., Nahas, N.: Research in image processing for pipeline crack detection applications. In: IEEE Conference, 2nd International Conference on Electrical, Computer, Communications and Mechatronics Engineering (ICECCME-2022), Maldives, 16–18 Nov 2022
16. Altabay, W.A., Wu, Z., Noori, M., Fathnejat, H.: Structural health monitoring of composite pipelines utilizing fiber optic sensors and an AI-based algorithm-A comprehensive numerical study. *Sensors* **23**(8), 3887 (2023)
17. Altabay, W.A., Noori, M., Wu, Z., Al-Moghazy, M.A., Kouritem, S.A.: A deep-learning approach for predicting water absorption in composite pipes by extracting the material's dielectric features. *Eng. Appl. Artif. Intell.* **121**, 105963 (2023)
18. Silik, A., Noori, M., Altabay, W.A., Ghiasi, R., Wu, Z., Dang, J.: Evaluation of analytic wavelet parameters effect for data analyses in civil structural health monitoring. In: International Conference on Structural Health Monitoring of Intelligent Infrastructure: Transferring Research into Practice, SHMII 2021, vol. 2021-June, pp. 813–818 (2021)
19. Weixing, H., et al.: Artificial intelligence Technique for Pavement Diseases Identification. In: Proceedings of the 4th International Conference on Intelligent Science and Technology (ICIST'22), pp. 66–72. ACM Digital Library August (2022)
20. Hong, W., Noori, M., Jiang, H., Liu, Y., Altabay, W.A.: Machine vision-based structural diagnosis application. *Lecture Notes Civ. Eng.* **292**, 79–88 (2023)
21. Silik, A., et al.: Dynamic wavelet neural network model for damage features extraction and patterns recognition. *Civ. Struct. Health Monit.* (2023)
22. Wang, T., Li, H., Noori, M., Ghiasi, R., Kuok, S., Altabay, W.A.: Seismic response prediction of structures based on Runge-Kutta recurrent neural network with prior knowledge. *Eng. Struct.* **279**, 115576 (2023)
23. Fathnejat, H., Ahmadi-Nedushan, B., Hosseininejad, S., Noori, M., Altabay, W.A.: A data-driven structural damage identification approach using deep convolutional-attention-recurrent neural architecture under temperature variations. *Eng. Struct.* **276**, 115311 (2023)
24. Altabay, W.A., Noori, M.: Artificial-intelligence-based methods for structural health monitoring. *Appl. Sci.* **12**(24), 12726 (2022)
25. Li, Z., Noori, M., Wan, C., Yu, B., Wang, B., Altabay, W.A.: A deep learning-based approach for the identification of a multi-parameter BWBN Model. *Appl. Sci.* **12**(19), 9440 (2022)
26. Gallego, A.-J., Pertusa, A., Calvo-Zaragoza, J.: Improving convolutional neural networks' accuracy in noisy environments using k-nearest neighbors. *Appl. Sci.* **8**, 2086 (2018)
27. Jeon, H.-K., Yang, C.-S.: Enhancement of ship type classification from a combination of CNN and KNN. *Electronics* **10**, 1169 (2021)



Numerical and Theoretical Study on Shear Capacity of Segmental Joints in UHPC-RC Composite Beam Bridge

Yun Shen¹(✉) and Jianluan Li²

¹ Anhui Transportation Holding Group Co., Ltd., Hefei 230000, China
1968391009@qq.com

² Anhui Transport Consulting and Design Institute Co., Ltd., Hefei 230000, China

Abstract. Excellent shear performance of Ultra-High Performance Concrete (UHPC) beam segmental joints is dependent on the shear keys. To investigate the shear performance of segmental joints, the existing shear capacity prediction equation were evaluated based on the design of a bridge. Moreover, a refined finite element model (FEM) of UHPC beam bridge segmental joints was established and discussed in detail. The obtained results shown that the shear capacity predicted value of Chen equation is 57% and 18% lower than AASHTO and JSCE codes, indicating that Chen equation can predict the shear capacity of UHPC joints safely. By developing a refined model of the segmental joints, the loads it bears in different directions are calculated. Both tensile and compressive stresses are small, which satisfies the requirements of basic combination loads and ensures the safety of the structure.

Keywords: Ultra-High Performance Concrete (UHPC) · Shear Keys · Shear Performance and Capacity · Finite Element Analysis · Predictive Equations

1 Introduction

For segmental bridges, joints are vulnerable structural components that usually require special attention and treatment – particularly regarding their shear performance and capacity. In view of the use of joints in segmental bridges, significant differences between the two bridges would appear when the ultimate state is reached. Buyukozturk, O, et al. reported that the integrality of segmental bridges is the main factor affecting its flexural and shear capacity [3]. Since the early segmental bridges were built with normal concrete (NC), the early research mainly focused on the shear capacity and integrity of NC joints in segmental bridges. Zhou et al. [6]. Conducted a series of shear-off tests to investigate the shear capacity of NC joints. Mohsen A. Issa, et al. [7] studied the behavior of single-keyed joints through amounts of shear-off tests. Balamurugan A. et al. [8] established a finite element model to investigate the structural behavior of NC keyed dry joints. Currently, the *American Association of State Highway and Transportation Officials* (AASHTO) [2] and the *Japan Society of Civil Engineers* (JSCE) [5] have different approaches for predicting the shear capacity of UHPC-RC segmental shear keys [1]. However, there is a lack of consensus on the most appropriate method to use.

Based on the above discussion and analysis, this study aims to compare the shear performance with that of existing equations. In addition, the paper uses finite element software ABAQUS to analyze the stress distribution and shear capacity of UHPC-RC shear keys in detail. The results of this study provide insights into the mechanical behavior of UHPC-RC shear keys and contribute to give guide for UHPC-RC composite structures.

2 Segmental Joints of UHPC-RC Composite Beam Bridge

The span of UHPC-RC box-shaped segmental girder is arranged as a 1x40m simple support structural system, which is designed according to Class A prestressed concrete components. The main beam adopts the prestressed UHPC “U-shaped beam” prefabricated structure, with a cross-section consisting of one piece of UHPC “U-shaped beam”. The height of the beam is 1.6 m, and the thickness of the web is 16 cm. UHPC “U-beam” with a span of 40m is divided into three sections, the length of which are 12.975 m, 14 m and 12.975 m, respectively. The adjacent segments are connected using shear keys, as shown in Fig. 1.

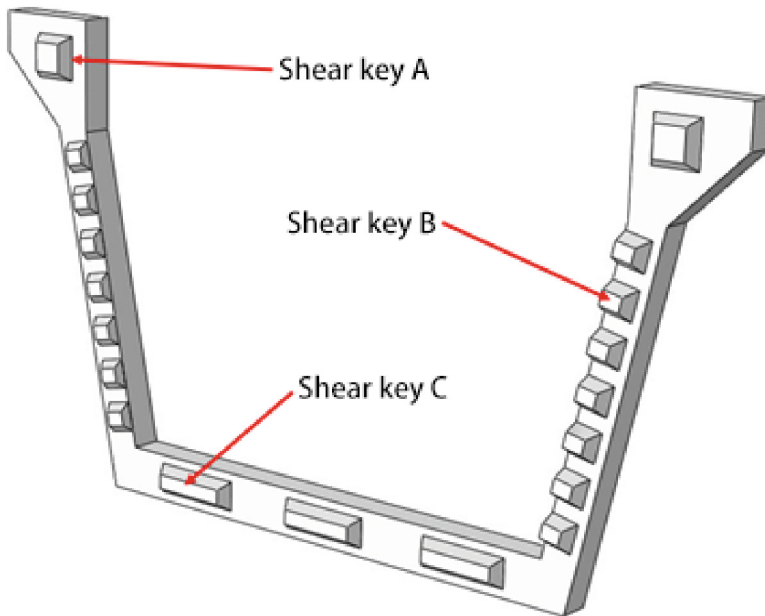


Fig. 1. Schematic diagram of U-shaped beam shear key with UHPC segment.

3 Shear Resistance Calculation of Segment Joints Based on Codes

Prefabricated segmental assembly of concrete bridges has become a significant direction in the development of concrete bridges. Pre-stressed steel strands are typically arranged longitudinally between the concrete segments, without continuous shear reinforcement.

The shear force between segments is mainly transmitted through shear keys on the compressed joint surface. Therefore, the mechanical behavior and load transfer mechanism of the shear keys on the joint surfaces are critical issues in the design and construction of prefabricated segmental assembly concrete bridges.

There have been many studies on the shear resistance of keyways both domestically and abroad, but few norms provide specific descriptions of them. Currently, the two most representative shear resistance prediction norms for keyways are AASHTO and JSCE. Therefore, based on the AASHTO and JSCE codes, this section calculates the shear resistance of the UHPC-RC bridge segment joints, and this study also proposes a new formula for predicting the shear resistance of keyways.

3.1 Shear Capacity Prediction of Segment Joints Based on the AASHTO Codes

According to the AASHTO *Guide Specifications for Design and Construction of Segmental Concrete Bridge* (1999), the shear bearing capacity of the joint surface includes two parts: one is the provided by the shear keys, and the other is the frictional force provided by the concrete in the flat part. The equation for calculating the shear capacity is as follows,

$$V_u = A_k \sqrt{f_{ck}} (0.2048\sigma_n + 0.9961) + 0.6A_{sm}\sigma_n \quad (1)$$

where, A_k is the root area of the shear key (mm^2), A_{sm} denotes the contact area of concrete (mm^2), f_{ck} is the standard compressive strength of concrete (MPa), which is taken as 135 MPa in this study, σ_n is the confining stress on the interface, which is calculated by multiplying the external prestressing force by a reduction factor of 0.8, resulting in a value of 11.25 MPa.

Shen Yin [4] has pointed out that the uneven distribution of shear stresses in multi-keyed dry joints can lead to inaccurate calculations of the shear performance of the joint surface in precast segmental assembled concrete bridges. Neglecting this non-uniform distribution characteristic may result in overestimated shear capacity calculation results, posing potential safety risks. Therefore, the shear capacity of section shear keys calculated based on the American AASHTO specification is prone to bias towards overestimation (Table 1).

Table 1. Calculation table for shear key based on AASHTO specifications.

	Shear key A	Shear key B	Shear key C
A_k (mm^2)	22500	9000	/
A_{sm} (mm^2)	15625	3250	/
V_{\sin} (kN)	968.25	367.05	/
N_{sk}	2	14	/
V_u (kN)	7075.2		

Note: where V_{\sin} represents the single bond bearing capacity, N_{sk} means the number of shear keys

For this, Shen [4] proposed that when calculating the bearing capacity during the operation phase, the recommended formula from AASHTO specifications can be used with modifications, and the equation for calculating the shear capacity after considering the correction coefficient of uneven shear stress distribution can be expressed as:

$$V_u = A_k \frac{\sqrt{f_{ck}}}{k} (0.2048\sigma_n + 0.9961) + 0.6A_{sm}\sigma_n \quad (2)$$

where, k represents the shear key shear resistance calculation correction factor.

After calculation, the correction factor for calculating the shear resistance of the shear key is determined to be 1.56. The corrected shear resistance capacity of the section with the shear key is 4721.35 kN, which satisfies the shear resistance requirements of the section under the basic combination.

3.2 Shear Capacity Prediction of Segment Joints Based on the JSCE Codes

According to the Japanese JSCE (2010) specifications, the shear capacity of a joint surface consists of two components: firstly, the contribution of the shear key, and secondly, the contribution of the concrete friction at the contact surface. The formula for calculating the shear capacity is as follows:

$$V_{cw} = 0.1A_k \cdot f'_{cd} + \mu \cdot f'_{cd} \cdot \sigma_{nd}^{1-b} \cdot A_{cc} \quad (3)$$

where, A_k represents the root area of the shear key (mm^2); A_{cc} represents the shear area of the compressed zone (mm^2); f'_{cd} represents the designed compressive strength of concrete, which is taken as 93.5 MPa in this case; σ_{nd} represents the average compressive stress on the interface surface of UHPC-RC beam bridges (MPa), which is calculated by multiplying the external prestressing force by a reduction factor of 0.8, resulting in a value of 11.25 MPa; b represents the coefficient of the planar structure (with a value range of 0–1, and a value of 0.5 if adhesive is used to connect prefabricated components).

The original form of the equation first appeared in the previous version of “Standard Specifications for Concrete Structures” (JSCE 2010), and was also mentioned in “Guidelines for Design and Construction of Ultra-High Performance Fiber-Reinforced Concrete Structures” (JSCE 2004). This equation indicates that the strength of concrete can not only affect the strength of shear keys, but in some cases, it can also affect the frictional properties.

It should be noted that the definition of A_{cc} is inconsistent with the definition of A_{sm} in AASHTO, whereas the meaning of A_k is equivalent to that of A_k in AASHTO. Additionally, the friction coefficient of 0.45 used in the JSCE formula is 25% smaller than the value of 0.6 used in AASHTO. Therefore, the calculated results using the JSCE formula are relatively smaller compared to those obtained using the AASHTO method (Table 2).

3.3 Shear Capacity Prediction Equation for Segment Joints Based on the Chen [1]

The equation proposed by Chen [1] is as follows (Table 3):

$$V_u = \alpha \cdot [\sqrt{f'_c} \cdot A_k \cdot (1.6 + 0.1\sigma_n) + (0.55 - 0.01 \cdot \sigma_n) \cdot \sigma_n \cdot A_{sm} + \tau \cdot A_{sm}] \quad (4)$$

Table 2. Calculation table for shear key based on JSCE specifications.

	Shear key A	Shear key B	Shear key C
A_k (mm ²)	22500	9000	/
A_{cc} (mm ²)	15625	3250	/
V_{sin} (kN)	577.77	178.50	/
N_{sk}	2	14	/
V_{cw} (kN)	3654.54		

Note: where V_{sin} represents the single bond bearing capacity, N_{sk} represents the number of shear keys

$$\alpha = \begin{cases} 1 & n=1 \\ -0.03711 \cdot n + 0.75518 & 2 \leq n \leq 7 \end{cases} \quad (5)$$

Table 3. Calculation table for shear key based on formulas proposed in this study.

	Shear key A	Shear key B	Shear key C
A_k (mm ²)	22500	9000	/
A_{sm} (mm ²)	15625	3250	/
V_{sin} (kN)	836.10	310.68	/
N_{sk}	2	14	/
V_u (kN)	3010.86		

Note: where V_{sin} represents the single bond bearing capacity, N_{sk} represents the number of shear keys

Table 4 shows that the bearing capacities obtained using the American AASHTO specifications and the Japanese JSCE specifications are 7075.2 kN and 3654.54 kN, respectively. The values calculated using the modified AASHTO formula and the proposed formula in this study are 4721.35 kN and 3010.86 kN, respectively.

Table 4. Summary table for shear resistance calculation of segment joints.

	Equations	Shear Capacity(kN)
Segmental Joint	The formula proposed in this study	3010.86
	AASHTO (American standards)	7075.20
	Revised AASHTO Formula (Tongji University)	4721.35
	JSCE (Japanese standards)	3654.54
Shear Resistance Section (Integral Beam)	AFGC (French standards)	3011.04
	JSCE (Japanese code)	4072.93
	“Code for Application of Ultra-High Performance Concrete in Highway Bridges and Culverts” (Draft for Comments)	4126.94

The formula proposed in this study calculates a value of 3010.86 kN, which is close to the French standard value of 3011.04 kN for the shear resistance verification section of the entire bridge. The French standard is considered to be more conservative in shear design standards. Given that the calculated value of the proposed formula in this study is smaller than the values calculated by the formulas in the American and Japanese standards, it is suggested to include the proposed formula in this study in the reference range.

4 Refined Analysis of segmental joints in UHPC-RC Composite Beam Bridge

A refined model of a UHPC-RC composite beam bridge segment was established using ABAQUS finite element software. The purpose of the model is to verify the safety of the shear key at the spliced joint of the U-shaped beam segment under basic load combinations. The mesh at the segment beam joint is using 3D reduced integration elements (C3D8R) with a size of 15 mm × 15 mm × 15 mm. The stress-strain relationship of UHPC is modelled in consistent with that in the study of Chen et al. [1], as shown in Fig. 2. The peak compressive stresses of UHPC is taken as 133 MPa, whereas the peak tensile stresses are 7.5 MPa (Fig. 3).

Based on Fig. 4, it can be seen that under the basic combination, the maximum tensile stress of the shear key's concave and convex surfaces is 7 MPa, which precisely reaches the design value of the tensile strength of UHPC material. Meanwhile, the maximum compressive stress on the contact surface is 78.12 MPa, which is less than the design value of the compressive strength of UHPC material, 93.5 MPa. Therefore, it can be concluded that under the basic combination, the shear key at the segment joint can meet the load requirements.

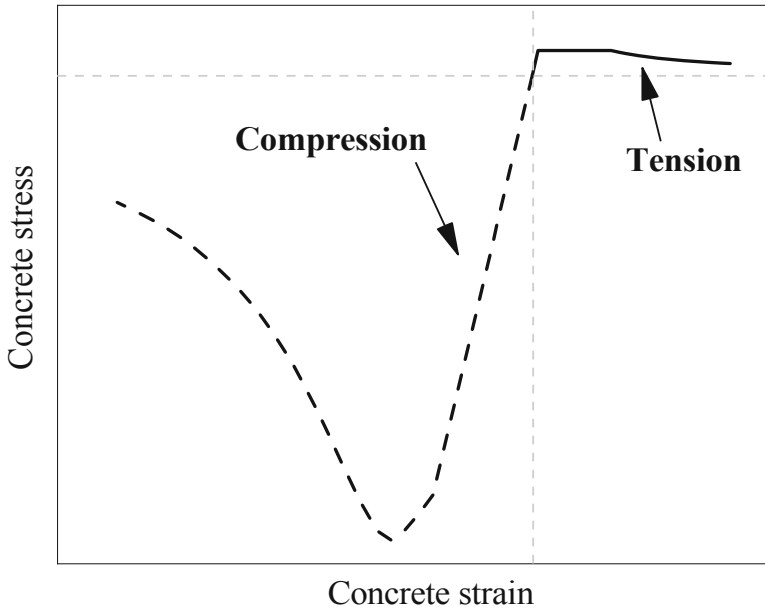


Fig. 2. Stress-strain relationships of UHPC.

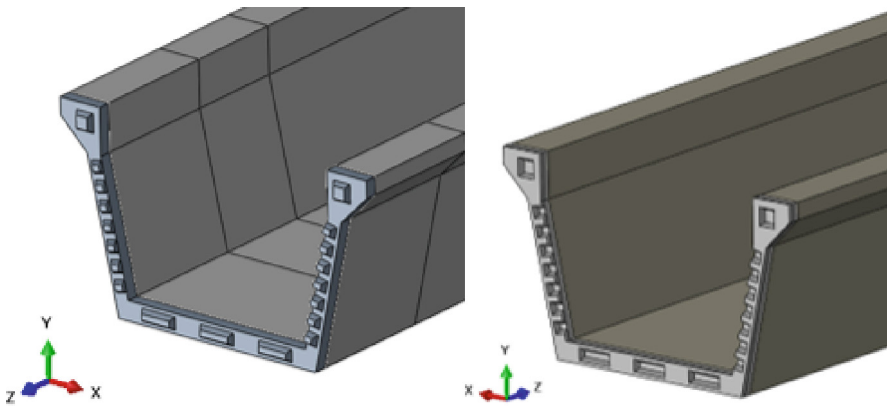
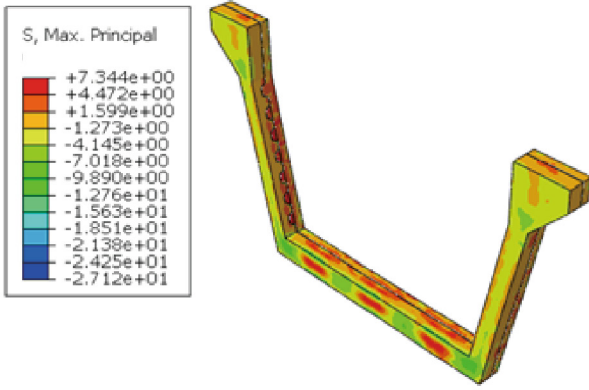
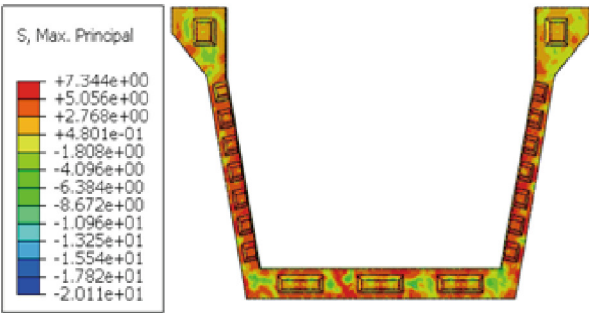


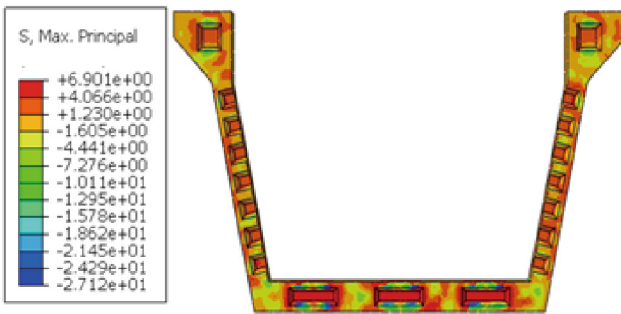
Fig. 3. U-shaped beam shear groove diagram.



(a)



(b)



(c)

Fig. 4. Results of FEM (unit: MPa): (a) Maximum principal stress of joints, (b) Maximum principal stress of male-key, (c) Maximum principal stress of female-key.

5 Conclusions

In this study, the predicted shear capacities equations various national standards, including the AASHTO specification and the JSCE codes, are compared. Additionally, the modified formulas proposed by other scholars are analyzed. Furthermore, a refined model of the UHPC-RC segmental joints is established using finite element analysis software ABAQUS to analyze the key mechanical properties of the structure. In summary, the following conclusions are drawn:

- (1) The shear capacity predicted value of Chen equation is 57% and 18% lower than AASHTO and JSCE codes, indicating that Chen equation can predict the shear capacity of UHPC joints safely.
- (2) By developing a refined model of the segmental joints, the loads it bears in different directions are calculated. Both tensile and compressive stresses are small, which satisfies the requirements of basic combination loads and ensures the safety of the structure.

References

1. Chen, L., Yan, J., Xiang, N.L., Zhong, J.: Shear performance of ultra-high performance concrete multi-keyed epoxy joints in precast segmental bridges. *Structures* **46**, 1696–1708 (2022)
2. Aashto LRFD: bridge design specifications, 6th edn. American Association of State Highway and Transportation Officials (AASHTO), Washington, DC (2015)
3. Buyukozturk, O., Bakhoun, M.M., Beattie, S.M.: Shear behavior of joints in precast concrete segmental bridges. *J. Struct. Eng.* **116**(12), 3380–3401 (1990)
4. Shen, Y., Cai, P., Chen, L., et al.: Shear strength of keyed joints in segmental precast concrete bridges. *J. Tongji Univ. (Nat. Sci.)* **102**, 3–11 (2019)
5. JSCE. Standard specifications for concrete structures-design. Japan Society of Civil Engineers, Tokyo (2010)
6. Zhou, X., Mickleborough, N., Li, Z.: Shear strength of joints in precast concrete segmental bridges. *ACI Struct. J.* **102**(1), 3 (2005)
7. Mohsen, A.I., Hiba, A.: A: Structural behavior of single key joints in precast concrete segmental bridges. *J. Mater. Civ. Eng.* **12**(3), 315 (2007)
8. Shamass, R., Zhou, X., Alfano, G.: Finite-element analysis of shear-off failure of keyed dry joints in precast concrete segmental bridges. *J. Bridg. Eng.* **20**(6), 04014084 (2015)



Study on the Influence of Temperature Rise on the Stress Change of Prefabricated Cantilever Composite Subgrade (PCCS)

Xiaoxiang Cao¹, Liang Yin², Cheng Peng¹, Zhigang Wu², and Shengwei Yang³(✉)

¹ Anhui Transportation Holding Group Co., Ltd., Hefei 230088, China

² Anhui Transport Consulting and Design Institute Co., Ltd., Hefei 230088, China

³ Hefei University of Technology, Hefei 230009, China

3024319405@qq.com

Abstract. In this paper, a new type of precast cantilever composite foundation structure for mountainous highway is studied, and the influence of temperature rise on the stress of the structure is analyzed. Under the load of temperature rise, the stress state of the PCCS structure is significantly improved, and its value is greater than the stress of the structure under static load. The temperature load mainly has great influence on the stress state of the connecting steel bar and bolt, but has little influence on the concrete members. The stress state of the connected steel bar and bolt under the global temperature rising case has little difference with that under the local temperature rising case, while the stress state of the concrete members under the global temperature rising case is greater than that under the local temperature rising case.

Keywords: PCCS · Global Temperature Rising · Local Temperature Rising

1 Introduction

Cantilevering subgrade structure forms an embankment with wall-pillar retaining wall within the range of stable subgrade, and makes up the under width of the road with the cantilevering structure. The stable subgrade is used to minimize the post-construction settlement, and the artificial foundation excavation avoids the disturbance of surrounding soil to the maximum extent. In the subgrade engineering, it can protect the ecological environment, excavate and fill small, cost low, and construction is simple, which is suitable for different terrain and geological conditions [1]. Although this method has greatly improved the performance of the structure, as a mass concrete structure, its mechanical response under temperature load can not be ignored.

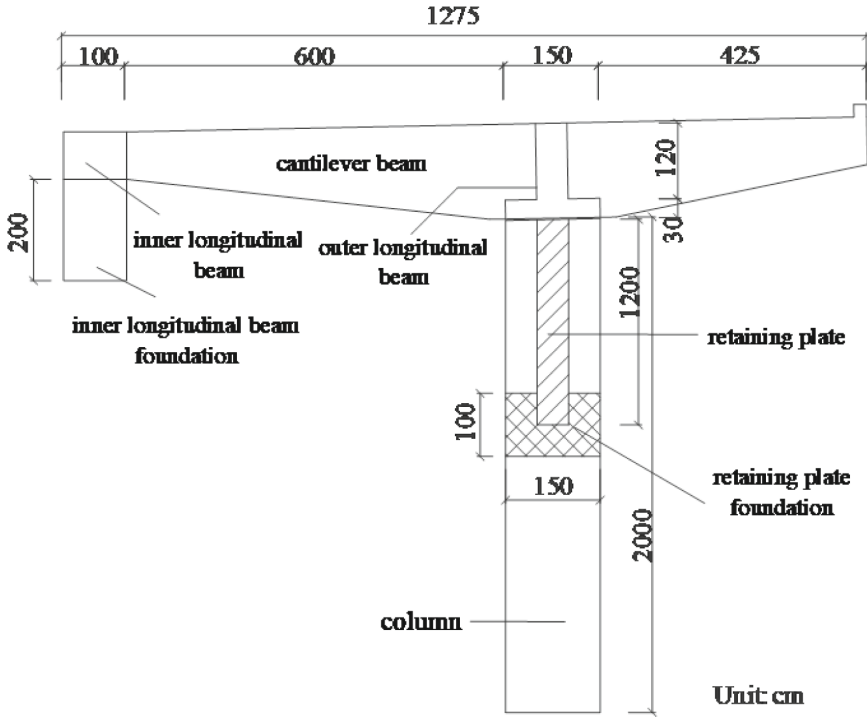
Hou [2] et al. artificially studied the time-varying temperature effect in hydration reaction process of mass concrete, taking Tianinggou Bridge, the second highest pier in Asia in the loess region, as the research object, and analyzed the time-varying temperature effect of hydration heat of mass concrete cap. The influences of concrete entry temperature, thermal conductivity and surface convection coefficient on the adiabatic

temperature rise, surface temperature rise and inner surface temperature difference of mass concrete cap are analyzed. Yan [3] et al. set another concrete strength test block with the same mix ratio under the condition of same insulation at the side of a large volume concrete slab, and experimentally studied the development law of concrete strength with time under different insulation measures and the influence of insulation curing time on concrete strength. Based on the test results, the thermal insulation and maintenance scheme of large volume concrete suitable for the severe cold area represented by Harbin is determined, and the relevant construction suggestions are put forward. He [4] et al., considering the large volume and high hydration heat of the concrete on the pylon cap, led to large temperature difference between the internal temperature and the inner surface, which easily resulted in temperature cracks and other conditions, conducted numerical simulation on different pouring schemes of the concrete on the pylon cap of Rongjiang Bridge, analyzed the influences of pouring thickness, cooling water and cooling water temperature on the temperature and stress of the concrete, so as to select appropriate pouring and temperature control schemes. The field measured data is compared with the calculated data. The research results have a certain reference value for the pouring and temperature control of mass concrete for tower bearing. The thawing and freezing of seasonal permafrost due to temperature fluctuations can cause safety hazards to the stability of roadbeds. He [5] et al. conducted on-site monitoring of temperature and water content on typical roadbed sections in the Naqu-Yangbajain segment. They performed regression analysis utilizing 2020 ground temperature data and analyzed the ground temperature amplitude, time lag, and soil thermal diffusivity of the monitored section through indoor experiments. With support from the Kun-Chu Expressway expansion project, Zhao [6] established a numerical model of asphalt pavement for the expressway using finite element software. He analyzed the effect of environmental temperature on asphalt pavement deformation, evaluated the significant factors affecting the deformation of asphalt pavement under continuous temperature changes using the gray correlation method, and estimated the permanent deformation of the asphalt pavement.

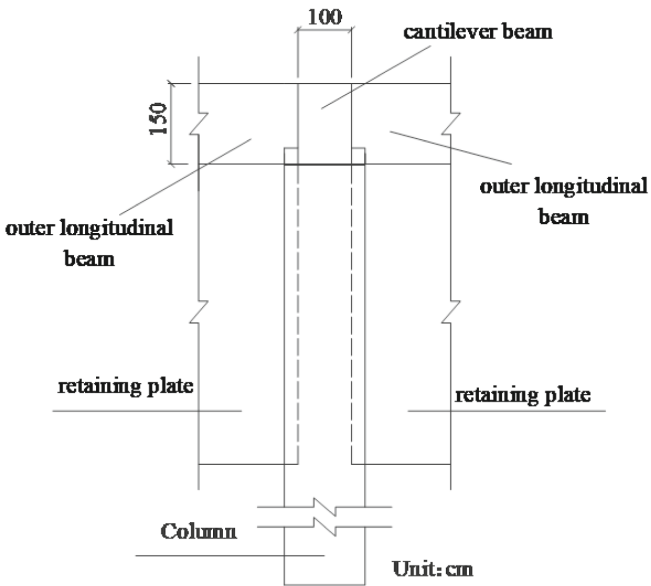
At present, Zhou [7–9] and his team have conducted a large number of researches on the application of cantilever structure in China, and the researches on the influence of temperature effect on concrete structure at home and abroad also tend to be mature and perfect, but the influence of temperature effect on cantilever structure is rarely reported. Therefore, this paper takes the PCCS structure of mountain highway as the research object, analyzes the influence of temperature rise on structural stress, and provides reference for the application and theoretical design of such structures.

2 Prefabricated Cantilever Composite Subgrade (PCCS) Structure

PCCS structure is composed of column, outer longitudinal beam, cantilevering beam, lapping plate, inner longitudinal beam, inner longitudinal beam foundation, retaining plate, retaining plate foundation and anchor rod. The cantilever beam, retaining board, outer stringer and lapping board are constructed with prefabricated standard components, while the column, inner stringer, inner stringer foundation and retaining board foundation are constructed with on-site pouring. The inner side of the beam is placed on the excavated subgrade, and the outer side is suspended on the outer side of the column. The inner



(a) Main elevation



(b) Left elevation

Fig. 1. Layout of prefabricated cantilever composite subgrade.

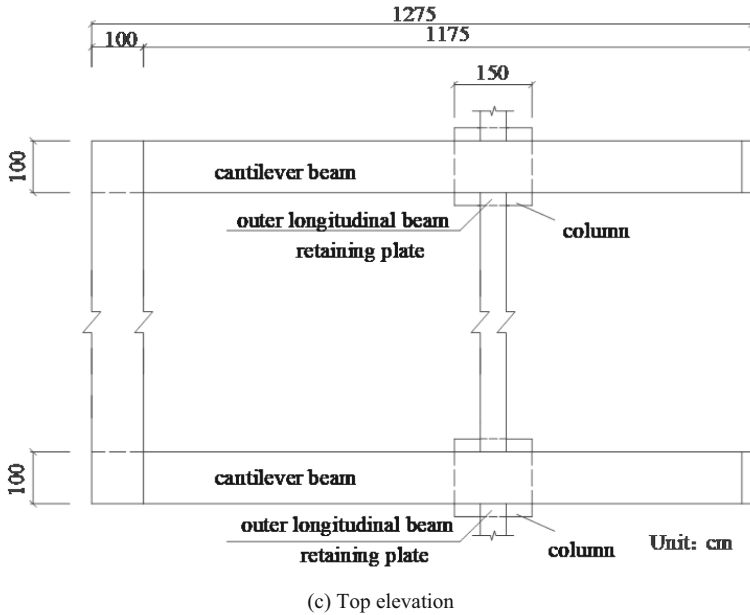


Fig. 1. (continued)

longitudinal beam is arranged longitudinally at the end of the cantilever beam along the route and connected with the cantilever beam by cast-in-place; The outer longitudinal beam is arranged in the beam position at the top of the column, and the retaining plate is arranged between the columns above the ground. In order to ensure the safety and stability of the whole structure, the anchor rod embedded in the rock layer is set at the end of the beam. The PCCS structure is shown in Fig. 1. And the Prefabricated cantilever composite subgrade structure is shown in Fig. 2.

3 Detailed Nonlinear Solid Finite Element Model Establishment

In this paper, ABAQUS is used to establish a refined finite element model of prefabricated cantilever composite subgrade structure. A total of 15 solid units including cantilever beam, outer longitudinal beam, inner longitudinal beam, inner longitudinal beam foundation, retaining wall, retaining wall foundation, column, foam concrete and soil were established. The bolt and reinforcement were simulated by truss unit. C3D8R eight-node linear hexahedron element was used to simulate the solid element, and T3D2 two-node linear three-dimensional truss element was used to simulate the truss element.

The model mainly adopts HPB300 steel bar, HRB400 steel bar, soil mass, foamed concrete, C50 concrete and C30 concrete. The steel bar adopts the double broken line constitutive model, the concrete adopts the plastic damage model, and the foamed concrete adopts the ideal elastic material model considering the calculation efficiency and the actual situation.



Fig. 2. Prefabricated cantilever composite subgrade structure.

The detailed finite element model of prefabricated cantilever composite subgrade structure is shown in Fig. 3.

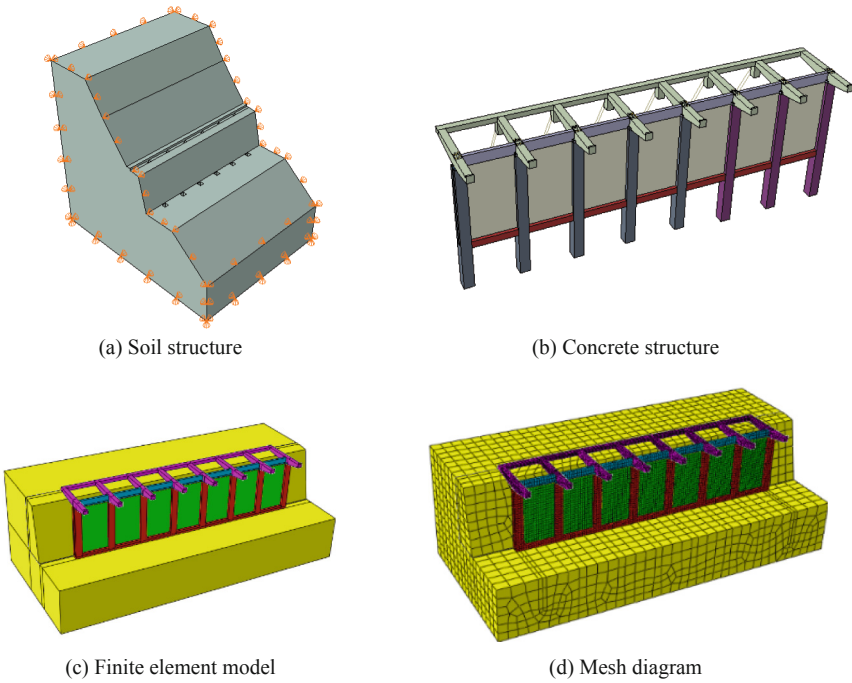


Fig. 3. Detailed nonlinear solid finite element model of PCCS.

This paper mainly discusses the influence of temperature rise on the structure of PCCS. The temperature rise of the structure is 25° . The stress of columns, beams, connecting rods and bolts in PCCS structure before and after temperature rise is analyzed to obtain the influence of temperature rise load on PCCS members. The global temperature rise is the overall temperature rise of the structure by 25° , and the local temperature rise is the temperature rise of the components except the retaining plate, retaining plate foundation and column by 25° .

4 Results Analysis

The stress states of column, beam, connecting steel bar and anchor rod in PCCS structure under various working cases are shown as follows.

4.1 Global Temperature Rising Case

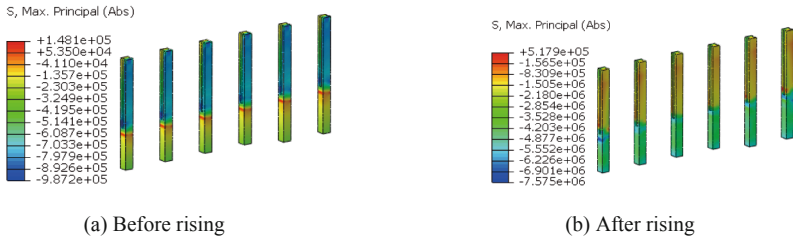


Fig. 4. Stress state of column (Pa).

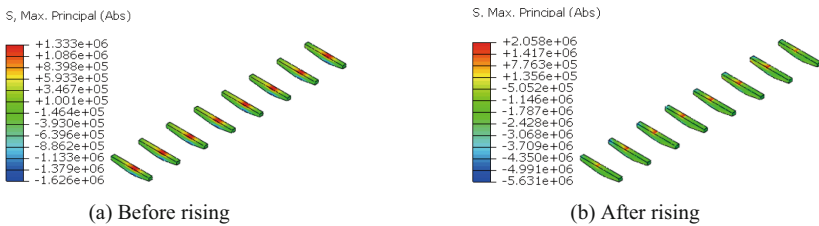


Fig. 5. Stress state of cantilever beam (Pa).

A comparative analysis of Figs. 4, 5, 6 and 7. Shows that the global temperature rise has an impact on the stress state of the column, beam, connecting steel bar and bolt. The maximum tensile stress and compressive stress of the column before temperature rise are 0.148MPa and 0.987MPa, while the maximum tensile stress and compressive stress of the column after temperature rise are 0.518MPa and 7.575MPa, and the ratios between the two groups are 3.50 and 7.67, respectively. The maximum tensile stress and compressive stress of cantilever beam are 1.333MPa and 1.626MPa before temperature rise. After temperature rise, the maximum tensile stress and compressive stress of cantilever

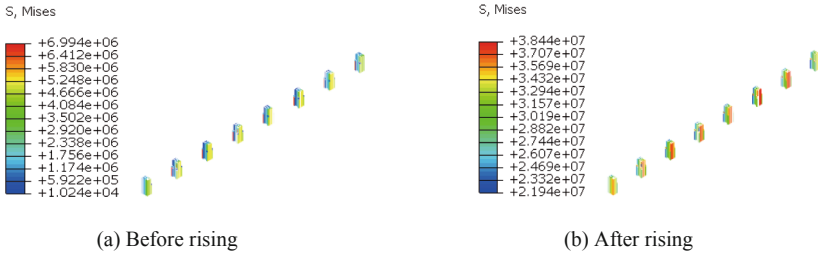


Fig. 6. Stress state of connecting bars (Pa).

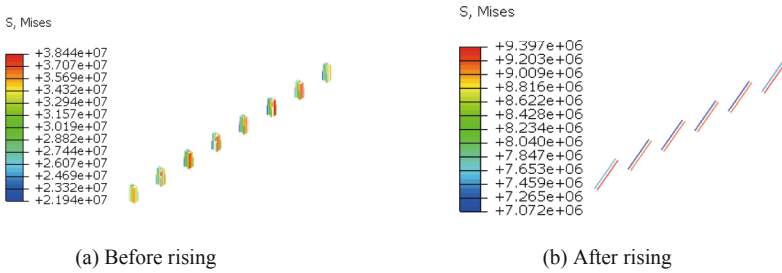


Fig. 7. Stress state of bolt (Pa).

beam are 2.058MPa and 5.631MPa, and the ratios between the two are 1.22 and 2.74, respectively. The maximum stress of the connected steel bar before temperature rise is 6.994MPa, and that of the connected steel bar after temperature rise is 38.440MPa, and the ratio between after temperature rise and before temperature rise is 5.50. The maximum stress of bolt is 0.078MPa before temperature rise, and 9.397MPa after temperature rise, and the ratio between after temperature rise and before temperature rise is 120.00. The research shows that the global temperature rise has a great influence on the stress of PCCS structure, and it is necessary to keep it in a safe state under the influence of temperature when designing the structure.

4.2 Local Temperature Rising Case

A comparative analysis of Fig. 8, 9, 10 and 11. Shows that the local temperature rise has an impact on the stress state of the column, beam, connecting steel bar and bolt. The maximum tensile stress and compressive stress of the column before temperature rise are 0.148MPa and 0.987MPa, while the maximum tensile stress and compressive stress of the column after temperature rise are 0.186MPa and 1.610MPa, and the ratios between the two groups are 1.25 and 1.63, respectively. The maximum tensile stress and compressive stress of cantilever beam are 1.333MPa and 1.626MPa before temperature rise. After temperature rise, the maximum tensile stress and compressive stress of cantilever beam are 0.465MPa and 3.332MPa, and the ratios between the two are 0.35 and 2.05, respectively. The maximum stress of the connected steel bar before temperature rise is 6.994MPa, and that of the connected steel bar after temperature rise is 37.280MPa, and

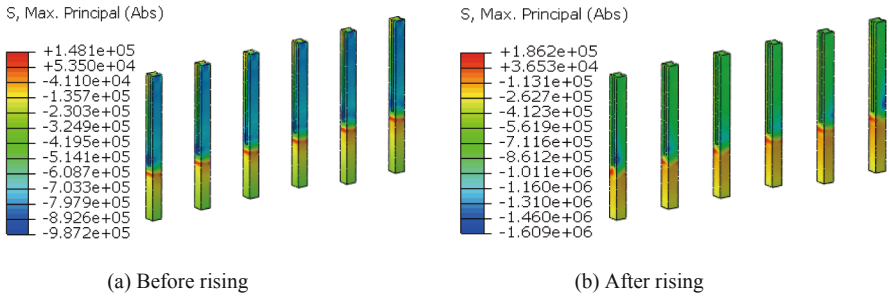


Fig. 8. Stress state of column (Pa).

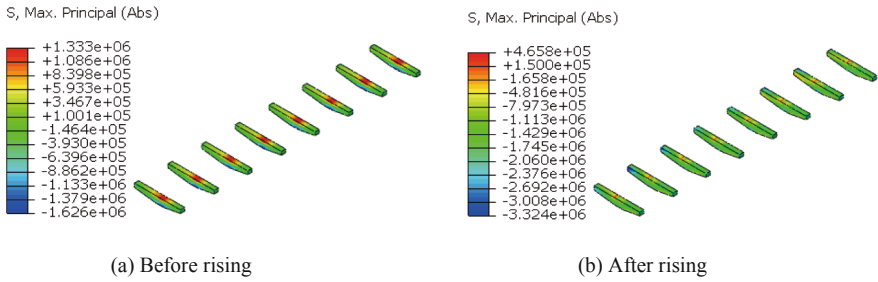


Fig. 9. Stress state of cantilever beam (Pa).

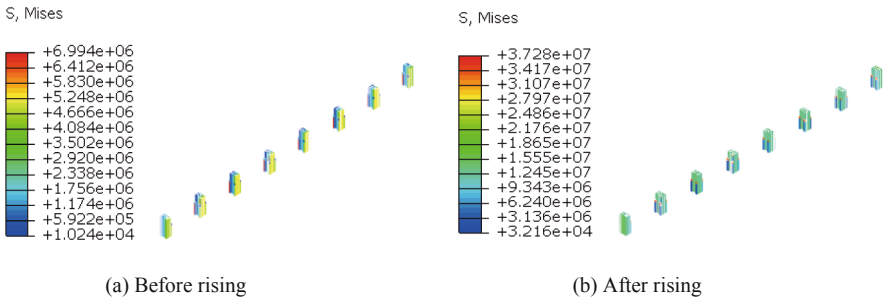


Fig. 10. Stress state of connecting bars (Pa).

the ratio between after temperature rise and before temperature rise is 3.33. The maximum stress of bolt is 0.078MPa before temperature rise, and 9.266MPa after temperature rise, and the ratio between after temperature rise and before temperature rise is 118.79. The research shows that the local temperature rise has a great influence on the stress of the PCCS structure, and it is necessary to keep it in a safe state under the influence of temperature when designing the structure.

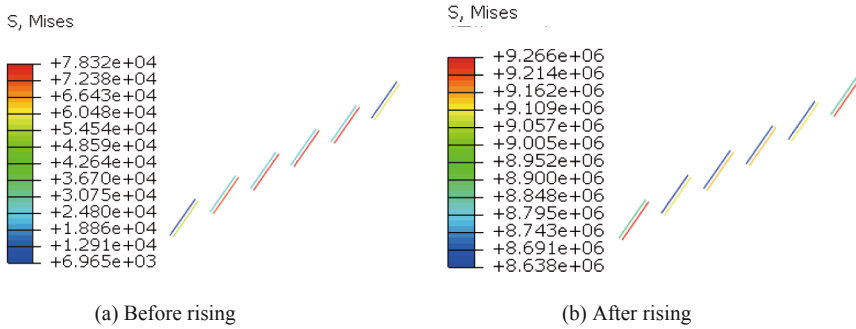


Fig. 11. Stress state of bolt (Pa).

According to the global temperature rise case and local temperature rise case, the temperature load mainly has the greatest influence on the stress state of the connected steel bar and bolt. This is because when the temperature rises, the structure is heated and expanded, and the connecting steel bars and bolts play their own design performance, restricting the deformation of the structure. Therefore, the stress state of the connecting steel bars and bolts increases.

For concrete members, the influence of global temperature rise is greater than that of local temperature rise. This is because the global temperature rise takes into account the temperature rise of the structure under seasonal changes, while the local temperature rise only considers the temperature rise of the structure under sunshine changes, and the two have different ranges of action on the concrete area. The larger the temperature load range is, the greater the influence on the structure, and the smaller the temperature load range is, the smaller the influence on the structure is.

5 Conclusions

Based on ABAQUS, a fine finite element model of precast cantilever composite foundation structure in mountainous highway is established, and the influence of temperature rise on structural stress is studied. The main conclusions are as follows:

- (1) The overall temperature rise and local temperature rise have a great influence on the stress of the precast cantilever composite foundation structure. Under the action of temperature load, the stress state of PCCS structure is significantly improved, and its value is greater than that of the structure under static load.
- (2) The temperature load mainly has great influence on the stress state of the connecting steel bar and bolt, but has little influence on the concrete member. The stress state of the connected steel bar and bolt under the global temperature rise case has little difference with that under the local temperature rise case, while the stress state of the concrete member under the global temperature rise case has a big difference with that under the local temperature rise case. The stress state of concrete member under the global temperature rise condition is greater than that under the local temperature rise case.

References

1. Zhou, Z.X., Zheng, W., You, T.: Widening mountainous highway with half-bridge and slope base composite embankment structures. *J. Chongq. Jiaotong Univ. (Natural Science)* **30**(04), 743–746 (2011)
2. Hou, W., Song, Y.F., Ma, C.: Time varying temperature effect of hydration heat of mass concrete based on pipe cooling system. *J. Chang'an Univ. (Natural Science Edition)* **41**(04), 65–77 (2021)
3. Yan, X.W., Liu, C.Y.: Development of temperature and strength for mass concrete under different insulation measures when constructed in severe cold area. *Concrete* (07), 135–140+144 (2020)
4. He, Y., He, J.L., Yu, P., Zhang, B.J., Fu, X.D.: Study on temperature control of mass concrete for tower pile cap. *J. Railw. Sci. Eng.* **17**(02), 372–378 (2020)
5. He, X.Z., Zeng, C., Gao, Z.Q., et al.: Study on the variation law of temperature field in the subgrade of the Nagqu-Yangbajing seasonal frozen soil area highway. *J. Safe. Envir. Eng.* **30**(02), 92–100 (2023)
6. Zhao, C.S.: Factors and estimation of asphalt pavement deformation under temperature variation on highways. *Railw. Constr. Technol.* **01**, 191–195 (2023)
7. Zhou, Z.X., Li, F., Awang Q.J.: Laterally cantilevered space frame for the roadway widening in steep-sloped mountainous areas. *Struct. Eng. Inte. (IABSE)* **18**(3), 254–258 (2008)
8. You, T., Zhou, Z.X., Zhen, W.: New technology of widening mountainous highway with side slope trellis base cantilevered structures. *J. Chongq. Jiaotong Univ. (Natural Science)* **30**(01), 74–77+106 (2011)
9. Liu, C.G., Zhou, Z.X., Mao, J.Q.: Interaction between integral cantilever structure and rock-soil. *J. Chongq. Jiaotong Univ. (Natural Science)* **30**(06), 1303–1305+1362 (2011)



Construction Technology of Tunnel Lining Vault Embedded Pipe Timely Grouting

Dongshan Zhang¹(✉) and Bin Yang²

¹ No. 1 Engineering Co., Ltd. of FHEC of CCCC, Beijing 102205, China
zds198711101@163.com

² China Railway 19th Bureau Group Corporation Limited, Beijing 100176, China

Abstract. In order to solve the grouting problem of tunnel lining vault cavity and local uncompacting, based on the project example of Qing-shiling tunnel and Yin-dongxia tunnel of Baoping Expressway, combined with the existing tunnel vault grouting construction technology, a construction method of embedded pipe grouting for tunnel lining vault is proposed, and the key construction technology and the best parameter index of pipe grouting are given. The engineering practice proves that the grouting method has good construction effect and can provide technical reference for similar tunnel lining defect treatment construction.

Keywords: Tunnel Engineering · Vault Cavity · Embedded Heel Tube · Timely Grouting · Key Technology

1 Introduction

In recent years, with the rapid development of highway construction in our country, more and more tunnels built in mountainous areas, due to the construction technology of tunnel lining concrete, the cavity and uncompact cement layer on the outside of the vault are common, it is also the key to affect the construction quality of the tunnel lining. Therefore, it is necessary to backfill the voids and non-dense areas with cement slurry, and the traditional grouting process is difficult to deal with in place at one time, and the effect is not good. Experts and scholars have done a lot of research on grouting construction of lining vault. Chengming Gong et al. [1] studied the process of timely grouting with forms of railway tunnel lining trolley vault; Zheli An et al. [2] studied the complete set technologies for mold grouting for the secondary lining vault of new railway tunnels; Bo Min et al. [3] studied the influence of cavity behind the vault of asymmetric arch tunnel on the damage law of lining structure; Dongming Li [4] studied and proposed a construction method of tunnel lining vault grouting with forms; Yongjie Fan et al. [5] studied the treatment technology of the long cavity behind the vault lining of the operating railway tunnel, and proposed three reinforcement technologies, such as foam concrete block plus grouting filling, PE-sphere plus grouting filling and PVC pipe plus grouting filling; Fuhai Li et al. [6] studied the experimental study on the influence of tunnel secondary lining cavity-belt mold grouting on the stress of lining structure, and verified the safety of application of independently developed cement-based filling

materials; Wenjun Liu [7] studied the cause analysis and remediation measures of the secondary lining vault caving in the hard rock tunnel. Although some achievements have been made in the study of vault cavity, there is no content that grouting can be done in time without drilling or without reforming the lining trolley.

Based on the lining grouting construction cases of Qing shiling Tunnel and Yin dongxia tunnel of the ninth contract of Baoping high-speed Project, this paper proposes a kind of timely embedded pipe grouting technology for tunnel lining vault, which overcomes the shortage of existing technology and provides an effective solution to the problems of cavity and local uncompacting in tunnel secondary lining vault.

2 Project Overview

Shanxi Baoji-Pingkan expressway is continuously connected by 9 tunnels, the bridge-tunnel ratio is 98.6%, forming the Qinling Mountain tunnel group. The starting point of Baoping Expressway LJ-9 contract section is K147 + 780, the end is K152 + 409, and the total length is 4.6 km. The right line of Qing-shiling Tunnel is 3,619 m, and the left line is 3,499 m. The right line of Yin-dongxia Tunnel is 816 m, and the left line is 793 m. The surrounding rock of the tunnel is 60 cm for Grade V, 45 cm for Grade IV and 35 cm for Grade III. The quality of the secondary lining of the two tunnels is the key control project in construction, there are different degrees of holes and incompacts in the pouring construction of the tunnel lining.

3 Overall Construction Scheme

3.1 Comparison and Selection of Grouting Scheme

At present, the main grouting methods of tunnel lining are borehole grouting and mold grouting, the most common method is borehole grouting, and mold grouting is a kind of grouting method by modifying lining trolley and installing flange and vertical pipe. Through investigation, it is found that the existing lining grouting method has not reached the ideal treatment effect. In order to better deal with the grouting of the vault cavity, the project refers to the construction technology of the pipe drilling [8–10], and proposes a method of the embedded pipe grouting in the tunnel lining vault. The comparison and selection of the three grouting methods are shown in Table 1.

After comparison and selection, the pipe grouting has a significant effect advantage over the other two method, and the third method is finally adopted for construction.

3.2 Technology Principle of Pipe Grouting

No.1. During the construction of the tunnel secondary lining, the longitudinal grouting pipe and exhaust pipe should be embedded close to the waterproof plate in the center of the vault, and a diameter of 4 mm holes should be drilled every 20 cm on the pipe wall, and the holes should be temporarily sealed with PE plastic wrap and adhesive tape. The vertical grouting and exhaust pipe are buried near the high point of the tunnel longitudinal slope, and the pipe body is not perforated. PVC elbow is connected with

Table 1. Comparison of grouting methods.

Construction method	Advantages	Disadvantages
Borehole grouting	Relatively simple operation	No.1 Construction requires a separate trolley or platform No.2 Low construction efficiency and poor effect No.3 Drilling holes can easily puncture the waterproof layer
Mold groutin	No.1 Working face is simple, construction difficulty is small No.2 Lining trolley is available for grouting	No.1 Lining trolley needs to be modified No.2 Trolley needs periodic maintenance No.3 There are local small cavities requiring secondary treatment
Pipe grouting	No.1 Small amount of material, low cost input No.2 Grouting reinforcement in time, good compactness No.3 High efficiency, small construction difficulty	Construction requires a separate trolley or platform

the longitudinal embedded pipe, the upper end is against the waterproof plate, and the lower end is blocked against the roof surface of the secondary lining trolley.

No.2. In the final setting of the secondary lining concrete, the secondary lining concrete cavity is grouted through the longitudinal grouting pipe, and improve the integrity of secondary lining concrete and serous fluid, and repair a variety of concrete defects, effectively prevent the waterproof plate of the vault perforating and falling off, and ensure the construction quality of the secondary lining.

4 Tunnel Lining Vault Embedded Pipe Grouting Construction

4.1 Construction Process of Pipe Grouting

Pipe grouting construction of tunnel vault mainly consists of two parts: embedding construction of vault grouting pipe and grouting construction. The prerequisite of pipe grouting construction is that the secondary lining concrete should be poured completely, and it is not allowed to use late grouting instead of lining concrete construction. The main process of pipe grouting construction (see Fig. 1).

4.2 Construction Process of Pipe Grouting

Embedded Installation Construction

Grouting Pipe and Exhaust Pipe Processing. The grouting pipe, exhaust pipe, elbow connection and end sealing plug shall be processed by the specified manufacturer according

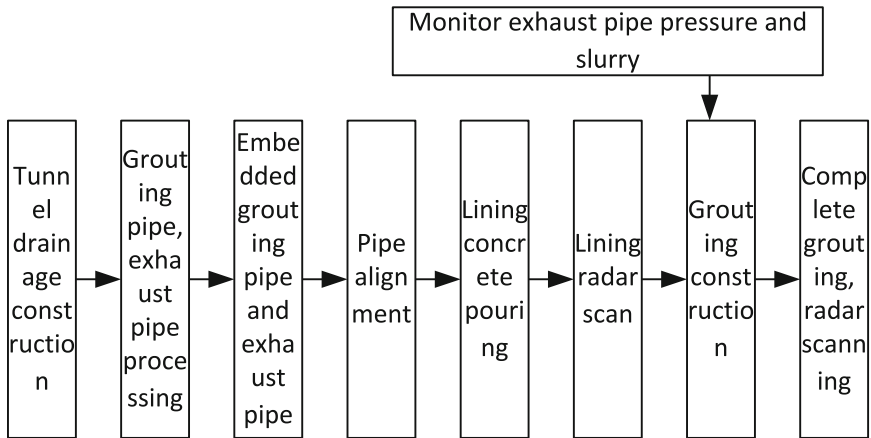


Fig. 1. Construction process of pipe grouting construction.

to the design requirements and the secondary lining pouring length. The length of longitudinal grouting and exhaust pipe should be greater than the pouring length of the secondary lining, and the length of vertical grouting and exhaust pipe should be greater than the thickness of the secondary lining, and sufficient working length should be reserved. Both longitudinal and vertical pipes are PVC pipes with Diameter 25 mm and thickness 1.5 mm, and three 4 mm grouting holes are drilled every 20 cm in the position of 90°, 180° and 270° on the wall of the longitudinal grouting pipe, and two 4 mm exhaust holes are drilled every 20 cm in the position of 45° and 315° on the wall of the longitudinal exhaust pipe. The outer wall of the longitudinal pipe is wrapped with two layers of PE wrap, and then seal it with adhesive tape, and the sealing position should be in the area without holes (see Fig. 2). Encapsulation sealing should ensure that the concrete grout will not flow into the grouting pipe when the secondary lining is poured, and the PE film can be pressurized to break through at the reserved orifice during the later grouting to ensure the grout and air circulation. Vertical grouting and exhaust pipe body need not open holes.

Three-Way and Vertical Pipe Connection When the vertical grouting pipe and exhaust pipe are embedded, the upper part is connected with the longitudinal embedded pipe by PVC elbow, the upper end is close to the waterproof plate in the middle line of the secondary lining vault to be poured, the lower end is blocked against the roof surface of the secondary trolley, and the vertical grouting pipe and exhaust pipe are embedded in the high side of the tunnel longitudinal slope. In order to ensure that the embedded pipe does not deviate, it can be fixed firmly by means of secondary lining reinforcement and positioning bars, and positioning marks can be made on the poured secondary lining concrete.

Embedded Construction. Tunnel vault longitudinal grouting pipe is embedded before the binding of secondary lining reinforcement after the completion of hanging and qualified relaxation test of geotextile and waterproof plate. When embedded, the hole of discharge slurry should be buried downward, and the exhaust hole should be buried

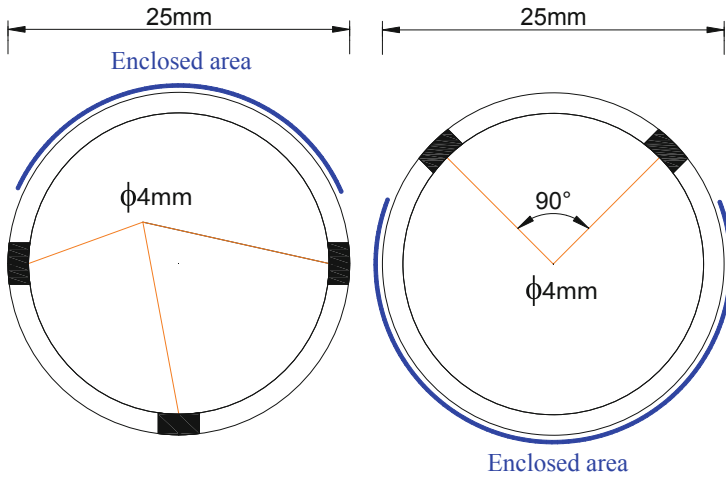


Fig. 2. Schematic diagram of grouting pipe and exhaust pipe processing.

upward. The exhaust pipe is buried at the highest point of the vault, and the grouting pipe is 2 cm away from it and slightly lower than the exhaust pipe (see Fig. 3). Elbows, plugs and tees should be connected by hot melt on site, and the quality of connection should be controlled.

Embedded Pipe Fixation. In order to ensure the position and alignment of the longitudinal embedded pipe, a longitudinal positioning steel bar can be added to bind and fix the two pipes, at the same time, it is connected and fixed with the secondary lining steel bar to ensure the accurate positioning of the longitudinal grouting pipe and exhaust pipe (see Fig. 4). After the construction of the tunnel secondary lining is completed, the radar wave detection is made in time to determine the existence of cavity or uncompacted situation behind the secondary lining concrete, and if there is a cavity or local uncompacting, the embedded pipe is used for grouting.

Grouting Construction.

Simple Grouting Mold and Grouting Material Selection. Considering that the process of pipe grouting is consistent with that of mold grouting, the project made a simple grouting mold to study the parameters and indexes of pipe grouting (see Fig. 5).

The selection of grouting material mainly refers to the requirements of water plugging and reinforcement of lining cavity. In order to overcome the defects of traditional grouting material, the cement-based grouting material with certain micro-expansibility is selected as grouting material for pipe grouping, and early strength cement slurry is a kind of cement-based slurry. As the grouting material of secondary lining concrete, it also needs to meet the requirements of strength, setting time, consistence, density, expansion amount and other indicators. Through continuous testing with grouting mold, the optimum water cement ratio is determined to be between 1:1.6 and 1:1.7, and slurry weight ratio is cement: admixture: water reducing agent: expansion agent: sand = 1:1.31:0.012:0.08:2.43. Among them, the admixture is highly active fly ash, the water

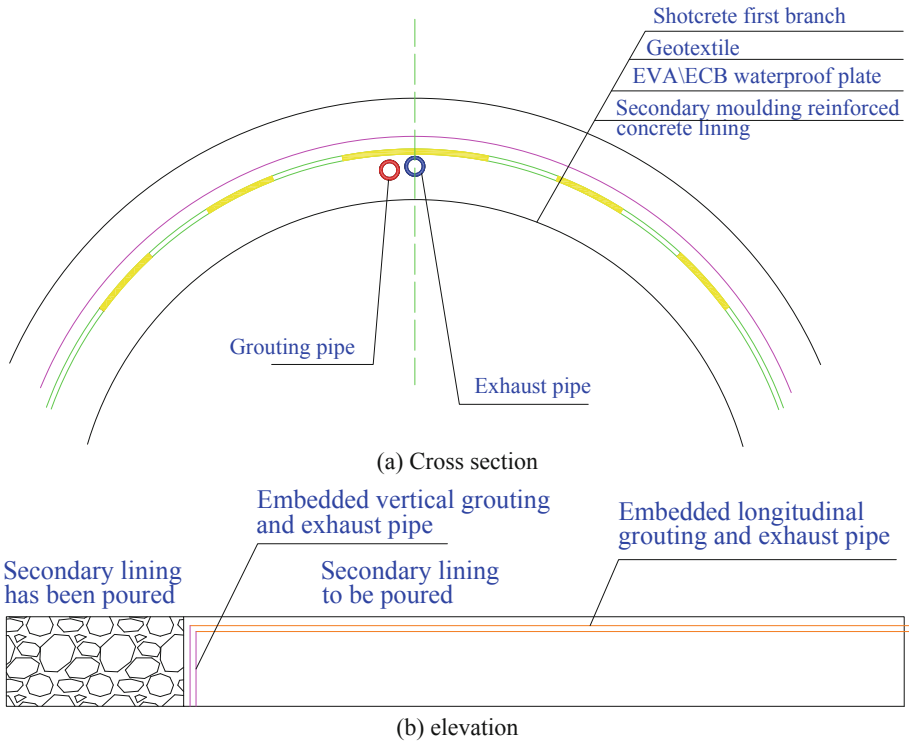


Fig. 3. Schematic diagram of grouting pipe and exhaust pipe buried.



Fig. 4. Photo of embedded pipe fixation in tunnel vault.

reducing agent is PCA-I type polyhydroxyacid water reducer, and the expansion agent is HME-III low alkali type concrete expansion agent. PE film is verified by experiment that the bearing pressure is less than 0.15 Mpa. The early strength cement slurry can be



Fig. 5. Tunnel lining grouting simple mold.

mixed with water to form a high fluidity micro-expanded cement slurry, and it has the advantages of fast preparation, low operation difficulty and reliable quality assurance.

Hollow Grouting Construction. Through the joint operation of the grouting machine and the mixer, the cement slurry should be continuously mixed, strictly control the amount of material, to ensure the quality of the cement slurry. After the cement slurry is prepared and mixed evenly, the grouting pipe of the grouting machine is connected to the grouting valve of the grouting pipe reserved in the vault, and the stop valve of the exhaust pipe is installed. The pressure gauge is installed on the stop valve, the exhaust stop valve is closed, after the preparation work is completed, the cement slurry is pressed into grouting pipe through the high pressure. The grouting pressure in the early stage is controlled at about 0.2 MPa to ensure that the cement slurry can break through the PE plastic film wrapped in the hole of the grouting pipe and flow into the hole. With the increase of pressure in the cavity, through the longitudinal slope of the pipe body and the principle of hydraulic emptying, the air breaks through the PE film wrapped in the hole of the exhaust pipe and enters the exhaust pipe, and then the cement slurry can be processed synchronously with all the holes in the layout range of the pipe. The pipe grouting process can also be used for multi-plate joint grouting by connecting the external suspension end with the next segment grouting pipe and exhaust pipe. Considering the grouting efficiency, equipment and pressure, it is recommended that the length of synchronous grouting be no more than 30 m.

The key of grouting construction is the control of grouting pressure. During the grouting process, the pressure gauge on the stop valve of exhaust pipe should be monitored in real time. When the pressure reaches 0.15 MPa, the stop valve should be opened and the air in the pipe should be discharged. As the grouting time lengthens, 0.1 MPa grouting pressure should be increased every 2 h, but the maximum pressure should not

exceed 0.4 MPa. When the cement slurry in the stop valve continues to flow out and no air is discharged, the stop valve is closed to stabilize the pressure, and then the grouting construction of the hollow part is completed (see Fig. 6).

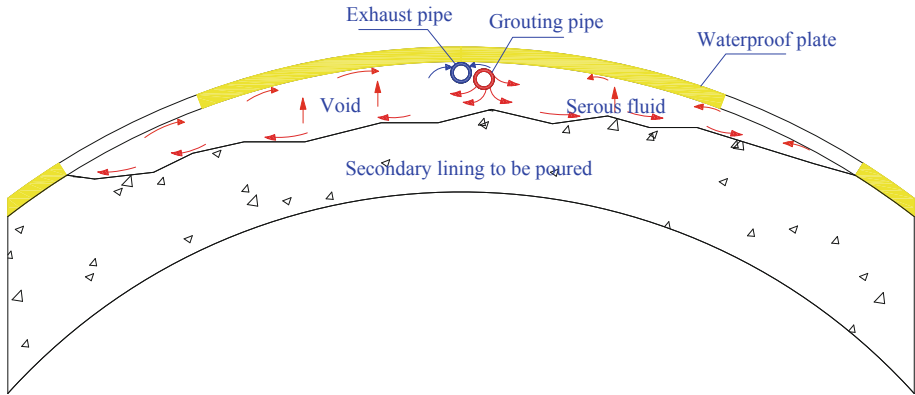


Fig. 6. Schematic diagram of tunnel vault grouting construction.

5 Grouting Effect and Benefit Analysis

5.1 Grouting Effect Detection

After the tunnel secondary lining pipe grouting is completed, ultrasonic radar scanning of the whole section of the secondary lining can be carried out at a selected time. For vault area with special section, surveying lines can be added from one surveying line to three surveying lines to cover all vault areas. After completion of detection, line analysis should be carried out in time, and the location of suspected cavity problem should be marked. Retest or drilling method is adopted to verify (see Fig. 7). The test results of this project after pipe grouting meet the quality acceptance standards, and the grouting effect is good.

5.2 Benefit Analysis

No.1. Prescription aspect. Compared with the traditional grouting method, the pipe grouting has less damage to the waterproof plate and secondary lining, and the number of reserved holes is less. Moreover, through the collection and analysis of construction data, the one-time success rate of treating the secondary lining cavity with the pipe grouting method is 97.6%, avoiding the secondary or multiple treatment caused by inadequate treatment of the same part, and greatly improving the construction efficiency.

No.2. Cost aspect. Compared with the traditional grouting process, the pipe grouting is simple to operate and has lower requirements for construction personnel. Pipeline processing, embedding and the secondary lining construction are carried out simultaneously, saving time and labor, will not destroy the waterproof system, and reduce the construction cost of the secondary lining cavity treatment, as shown in Table 2.



Fig. 7. Radar scan of tunnel vault.

Table 2. Comparative benefit analysis.

Selected items	Pipe grouting	Ordinary grouting
Speed	0.08 m ³ /min	0.05 m ³ /min
Cost	PVC plus PE plastic wrap = 1,000 yuan	Drilling plus anchoring grouting valve = 1,500 yuan
Safety	Good safety pre-control effect	Safety pre-control effect is general
Quality	The grouting effect is very remarkable	Grouting effect is general, there is not dense
Principle	Pre-embedded grouting pipe	The average cost under the same conditions is 6,000 yuan
Comprehensive economic index	The average cost under the same conditions is 4,000 yuan	The average cost under the same conditions is 6,000 yuan
Amount saved	Compared to ordinary grouting, the cost savings of pipe grouting are about 199000 yuan	

6 Conclusion

In the tunnel lining construction of Baoping expressway LJ-9 contract section, the construction method of tunnel vault embedded pipe grouting is adopted, and the cavity grouting is carried out in time. The Qing-shiling Tunnel was completed on August 23, 2019, the Yin-dongxia Tunnel on December 5, 2019, and the tunnel was completed and opened to traffic on September 30, 2021. The effect of the lining cavity treatment by this technology is good, which not only guarantees the quality of the tunnel lining, but also meets the requirements of the main tunnel construction, and reduces the cost input, at the same time, it has been praised by the owners. The valuable experience accumulated in construction can provide reference for similar construction projects.

Acknowledgments. This research reported in this paper was partially supported by enterprise class subject about “Study on construction technology of tunnel lining vault embedded pipe grouting” (No. KT2019-03).

References

1. Gong, C.M., Zhu, X.B., She, H.L.: Timely grouting with forms at the crown of a railway tunnel via a lining trolley. *Modern Tunnelling Technology* **54**(01), 180–185 (2017)
2. An, Z.L., Ma, W.B., Guo, X.X., Zhou, W.H., Wang, Y.: Complete set of technologies for immediately grouting into crown void with formwork after secondary lining concrete pour for new railway tunnels. *Railway Engineering* **57**(11), 48–52 (2017)
3. Min, B., Zhang, C.P., Zhang, X., Gong, Y.P., Yuan, T.F.: Failure laws of asymmetrical double-arch tunnels under effects of voids behind vault. *J. Centr. South Univ. (Science and Technology)* **50**(07), 1686–1695 (2019)
4. Li, D.M.: Tunnel lining construction technology of vault grouting with formwork. *Journal of Changchun University* **30**(08), 5–8+14 (2020)
5. Fan, Y.J., et al.: Remediation technology for the long segment and large-scale cavity behind vault linings of an operating railway tunnel. *Railway Standard Design* **64**(11), 116–121+135 (2020)
6. Li, F.H., Li, R., Jiang, Y.L., Gao, H., Wang, Y.B., Wang, P.X.: Experimental study on the mechanical behaviors of the lining structure affected by grouting in tunnel secondary lining cavities through molds. *Modern Tunnelling Technology* **58**(05), 147–158 (2021)
7. Liu, W.J.: Causes analysis on the vault void of the second lining of the hard rock tunnel and research on the treatment measures. *Railway Construction Technology* **342**(09), 134–139 (2021)
8. Guo, X., Wang, Y.C., Chen, J.B., Kang, J.M., Zhong, X.Y.: Application of pipe drilling and grouting technology in water treatment system of Dongming Open-pit Coal Mine. *Opencast Mining Technology* **32**(06), 30–33+36 (2017)
9. Liu, J.C.: Drilling and construction of anchor cable technology in fractured mountain area. *Building Technology Development* **46**(18), 100–101 (2019)
10. Wang, H.B., Zhang, H.Y., Chen, C.H., Ma, C.: Tunnel pipe shed casing construction technique. *Architecture Technology* **51**(10), 1182–1183 (2020)



Numerical Study on Performance of Single-Keyed Dry Joint of Ultra-High Performance Concrete (UHPC) Under Combined Shear and Torsion Load

Zening Xu¹, Yun Shen¹, and Jing Yan²(✉)

¹ Anhui Transportation Holding Group Co., Ltd., Hefei 230000, China

² School of Civil Engineering, Hefei University of Technology, Hefei 230009, China

yanjing12321@163.com

Abstract. Under the vehicle load, segment joints are subjected to coupling effects of bending, shear, and torsion, while for dry joints, they are mainly subjected to a combination of shear and torsion, making them more prone to failure. In this study, to investigate the performance of single-keyed dry joint of ultra-high performance concrete (UHPC) under combined shear and torsion load, finite element model (FEM) was carried out considering the effect of confining pressure. Then AASHTO code equations was chosen to predict the shear-torsion capacity of UHPC single-keyed dry joints. The results of FEM indicated that the increase of confining pressure can effectively improve the shear-torsional load capacity of the dry joints. Whereas the increase of confining pressure has little effect on the improvement of stiffness. From the failure mode of specimens, the specimens are damaged in the root of the shear key when confining pressure is less than 18 MPa. However, in view of the high confining pressure (when the confining pressure is greater than 18 MPa), the damaged surface of the specimen changes from the root of the male key to the feminine key. In addition, the evolution of AASHTO equation shows that the AASHTO code equations were overestimated the ultimate capacities of UHPC single-keyed dry joints under shear-torsion load.

Keywords: Precast Bridge · Ultra-High Performance Concrete (UHPC) · Dry Joint · Finite Element Model (FEM) · Combined Shear and Torsion Load

1 Introduction

With the advancement of bridge industrialization, assembled precast bridges have been promoted and applied widely. As a new type of bridge, Ultra high performance concrete (UHPC) segmental girder bridge is an important study direction to promote the industrialization of bridges. However, the structural integrity of segmental bridges is the main issue affecting its flexural and shear performance [1, 2]. In actual bridge operation, segment joints are subjected to coupling effects of bending, shear, and torsion, while for dry joints, they are mainly subjected to a combination of shear and torsion, making them more prone to failure. Therefore, for segmental pieced bridges, joints are fragile

structural components that require special attention and treatment, especially in terms of shear resistance and load capacity. In the past decade, a large number of scholars have conducted test to study UHPC dry joints. The shear strength of segmental joints (especially dry joints) is mainly provided by shear keys, and the shear key material properties have a significant effect on enhancing the strength of the key and improving the shear resistance of the joints. In order to reasonably reflect the effect of shear keys materials on shear strength, the mechanical properties such as strength were measured in the study, literatures [8] investigated different specimens f_c and shear strength based on the push-off test. To understand the shear characteristics of UHPC dry joints, Tongxu Liu [3, 4] found that the multi-tooth bond dry joint reduction coefficient gradually increased with the increase of lateral pressure under high lateral pressure, and the reduction coefficient was greater than 1 when the lateral stress reached a certain size and remained basically constant through direct shear tests of UHPC dry joints. In addition, in order to predict the shear load capacity of UHPC dry joints accurately, Yuqing Hu [5] of Southeast University proposed a load capacity prediction formula for UHPC large-tooth bond dry joints considering the effect of steel fiber bridging based on the modified pressure field theory, and the method was proved to have high prediction accuracy.

From on the above discussion, past research on joints has focused on shear resistance, while little research has been done on the mechanical properties of joints under shear-torsional coupling. To investigate the performance of single-keyed dry joint under combined shear and torsion load, a total of 10 specimens were conducted, which took into account the three influential factors of offset distance, normal stress, width-to-depth radiate the combined shear and torsion effect on the shear capacity of the single shear key. And concluded that both the cracking load and ultimate capacity were enhanced with the confining pressure increased. However, there is limited study on the mechanical properties of UHPC dry joints under shear-torsional composite action.

Based on the above discussion, to investigate the performance of single-keyed dry joint of ultra-high performance concrete (UHPC) under combined shear and torsion load, numerical study was carried out considering effect of confining pressure.

2 Specimen Design

Based on the literature [1], considering the load moving space of shear-torsion compound action, the upper part of the specimen is set 200 mm thick area, and a 200 mm × 200 mm × 200 mm trigonal concrete axil is designed to strengthen the projection area; the size of the lower part of the specimen is 500 mm × 1, 250 mm × 200 mm, and the size of this part is increased to prevent the whole load process. In order to ensure that the joint position is destroyed before the non-key area, the specimen is equipped with HRB400 reinforcement, except for two $\phi 18$ mm bars in the lower part of the specimen, the rest are $\phi 16$ mm bars in each group, the specimen size are shown in Figs. 1 and 2. Of note, load eccentricity is 200 mm in specimens (see Figs. 1 and 2).

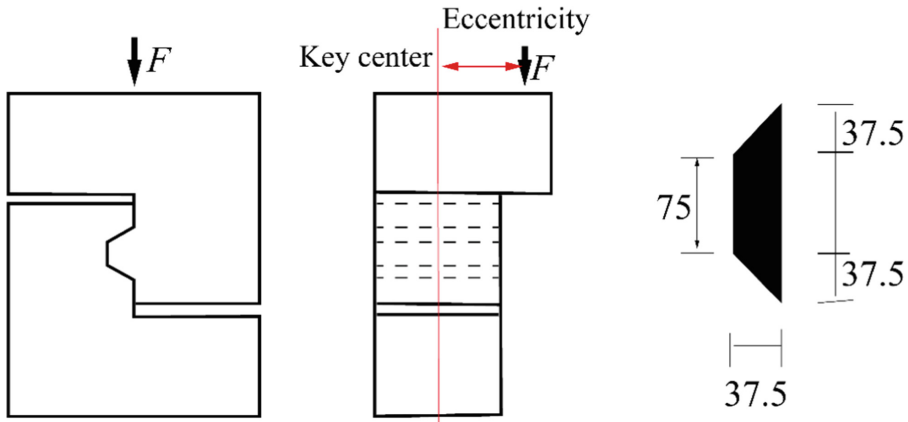


Fig. 1. Structural drawing of specimens [1].

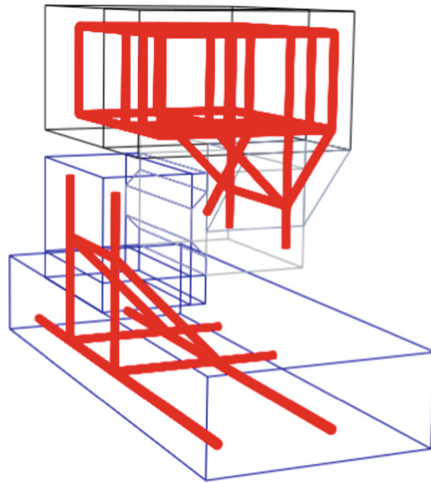


Fig. 2. 3D rendering of specimens.

3 Finite Element Analysis

3.1 Finite Element Model (FEM)

To understand the shear-torsion behavior of UHPC epoxy joint interface, finite element modeling and analysis were conducted based on the Abaqus platform (2020). 3D finite element models of the tested specimens were established in Abaqus (see Fig. 3), which considers the effect of confining pressure, namely, 2 MPa, 6 MPa, 10 MPa, 14 MPa, 18 MPa, 20 MPa, 25 MPa, and 30 MPa.

Using concrete damage plasticity material model (CDP) to simulate the stress-strain constitutive behavior of UHPC. In detailed, the stress-strain relationship of UHPC is

modelled in consistent with that in the study of Chen et al. [6], and the detailed information are illustrated in Fig. 3 and Eq. 1–3. Of note, the peak compressive and tensile stresses of UHPC are taken as 133 MPa, 7.0 MPa, respectively.

The C3D8R solid elements are used to present the UHPC part (see Figs. 4 and 5), while the T3D2 truss elements are chosen to simulate the behavior of steel reinforcement. Fraction model is chosen to simulate the interface between male part and female part in dry joints, and the fraction fact is 0.65 based on AASHTO codes [7].

For reinforcement,

$$\sigma_s = \begin{cases} E_s \varepsilon_s & (0 \leq \varepsilon_s \leq \varepsilon_y) \\ f_y & (\varepsilon_y \leq \varepsilon \leq \varepsilon_u) \end{cases} \quad (1)$$

For the compression model of UHPC,

$$y = \begin{cases} ax + (6 - 5a)x^5 + (4a - 5)x^6 & 0 \leq x \leq 1 \\ \frac{x}{b(x-1)^2+x} & x \geq 1 \end{cases} \quad (2)$$

$$y = \sigma/f_c, x = \varepsilon/\varepsilon_0, \varepsilon_0 = 3500\mu\varepsilon,$$

$$a = \frac{E_0}{E_c}$$

For tension model of UHPC,

$$\begin{cases} E_c \varepsilon_t & 0 \leq \varepsilon_t \leq \varepsilon_{t0} \\ f_t & \varepsilon_{t0} < \varepsilon_t \leq \varepsilon_{tp} \\ \frac{f_t}{[1+(\varepsilon_t - \varepsilon_{tp})l_c/\omega_p]} & \varepsilon_{tp} < \varepsilon_t \end{cases} \quad (3)$$

In which, $f_t = 8 \text{ Mpa}$, $\varepsilon_{tp} = 0.002$, $\omega_p = 1.0 \text{ mm}$, $l_c = 400 \text{ mm}$, $p = 0.95$.

3.2 FEM Results

Figure 5 plots the load-displacement curves of finite element model, obviously, the increase of confining pressure can effectively improve the shear-torsional load capacity of the dry joints (see Fig. 6). Whereas the increase of confining pressure has little effect on the improvement of stiffness. Compared with specimen m2 (confining pressure is 2 MPa), the ultimate load of specimens m6, m10 and m14 are increased by 134 kN, 239 kN and 302 kN. Respectively. And more detailed information about ultimate load is presented in Fig. 7.

The failure mode of specimens is present in Fig. 7, the specimens are damaged in the root of the shear key when confining pressure is less than 18 MPa. However, in view of the high confining pressure (when the confining pressure is greater than 18 MPa), the damaged surface of the specimen changes from the root of the male key to the feminine key (see Fig. 8f-g). Thus, to enhance the shear-torsion behavior of UHPC dry joints, reinforcements can be used in structures.

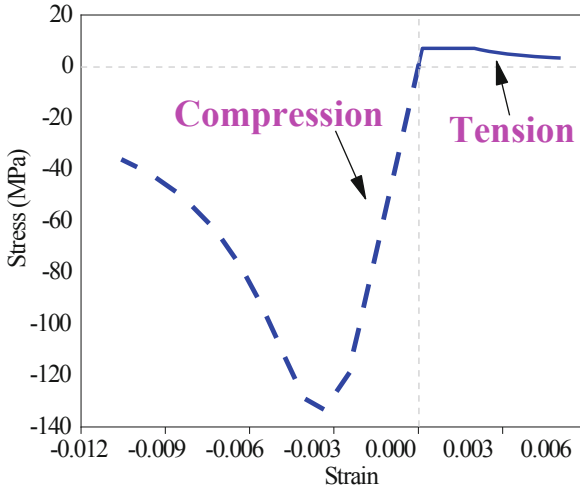


Fig. 3. The stress-strain relationship of UHPC.

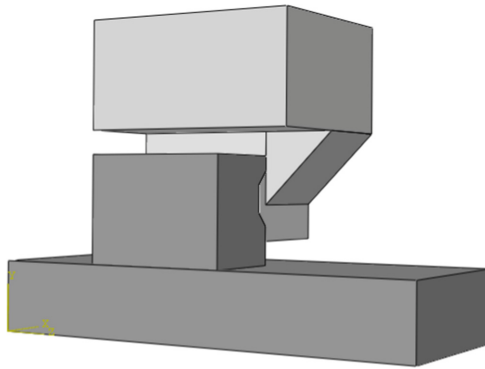


Fig. 4. Model schematic.

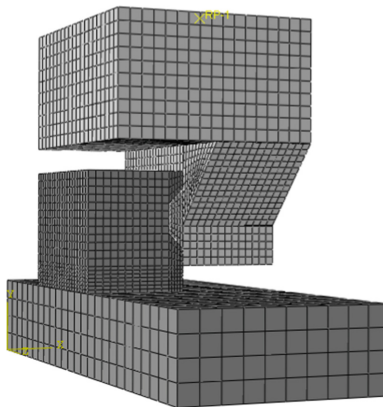


Fig. 5. Mesh schematic of FEM.

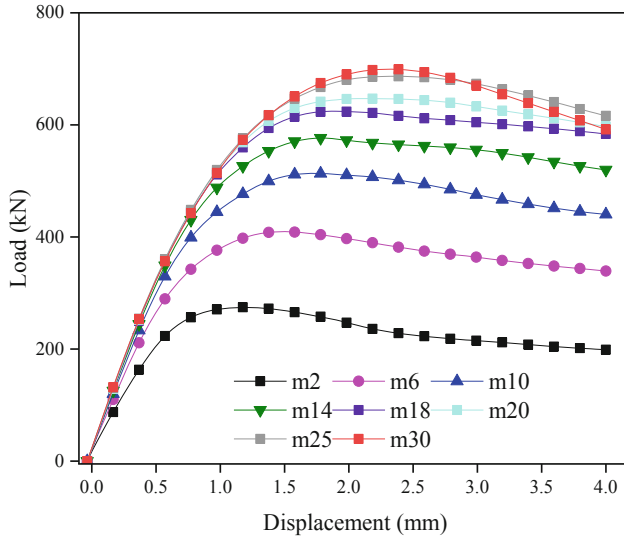


Fig. 6. Load-displacement curves of UHPC single-keyed dry joint.

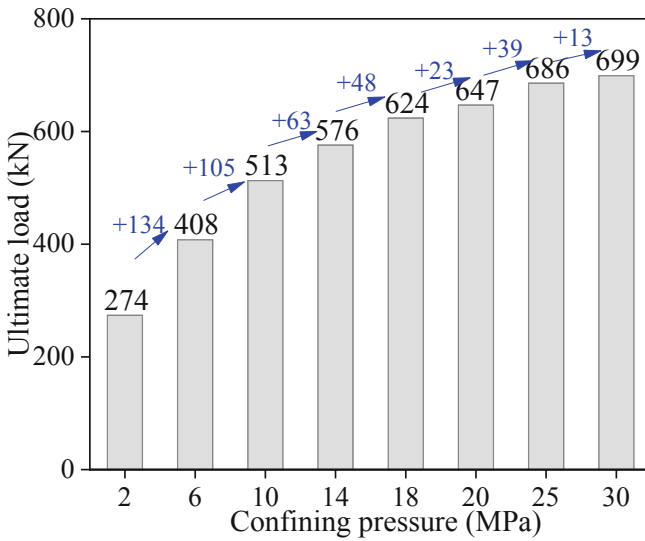


Fig. 7. Ultimate load of UHPC single-keyed epoxy joint.

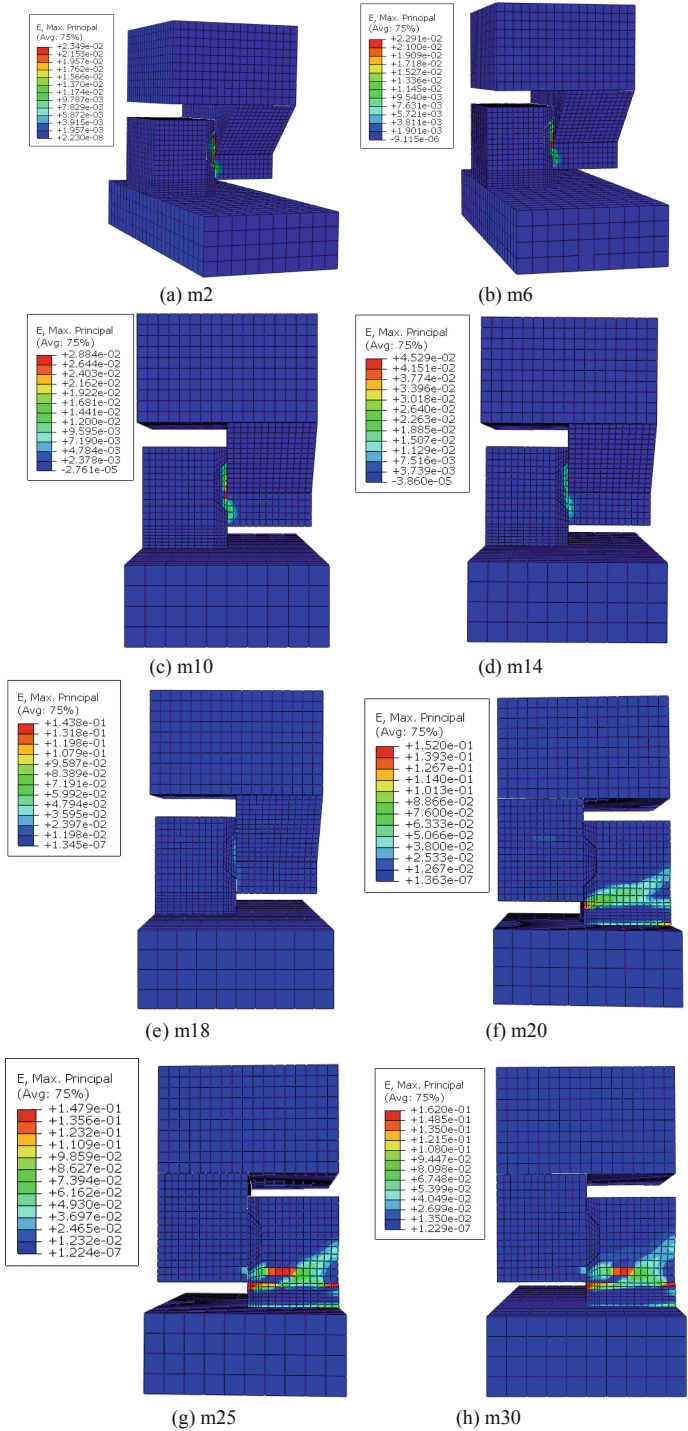


Fig. 8. Failure mode of dry joint specimens

4 Bearing Capacity Prediction of Joints Based on the AASHTO Code

According to the AASHTO *Guide Specifications for Design and Construction of Segmental Concrete Bridge* (1999) [7], the shear bearing capacity of the joint surface includes two parts: one is the provided by the shear keys, and the other is the frictional force provided by the concrete in the flat part. The equation for calculating the shear bearing capacity is as follows,

$$V_u = A_k \sqrt{f_{ck}} (0.2048 \sigma_n + 0.9961) + 0.6 A_{sm} \sigma_n \quad (4)$$

In which, V_u is nominal joint shear capacity (N), A_k is the root area of the shear key (mm^2), and $A_k = 60000 \text{ mm}^2$, $f_{c'}$ is compressive cylinder strength of concrete (MPa), which is approximately equal to $f_{ck} = 147.7 \text{ MPa}$ based on past research [6]. σ_n is the compressive stress of concrete (MPa). A_{sm} denotes the contact area of concrete (mm^2), and $A_{sm} = 33600 \text{ mm}^2$.

In order to investigate the applicability of AASHTO equations to UHPC dry joints under shear-torsion load, the calculated shear capacities of specimens were compared with the FEM results, as depicted in Fig. 9.

For UHPC single-keyed dry joints under shear-torsion load, the difference between predicted value and FEM results was great than 100% in AASHTO equations. Thus, the calculated ultimate capacities of the joints showed significant discrepancies from the FEM values. The AASHTO code equations were found to overestimate the ultimate load of UHPC single-keyed dry joints under shear-torsion load.

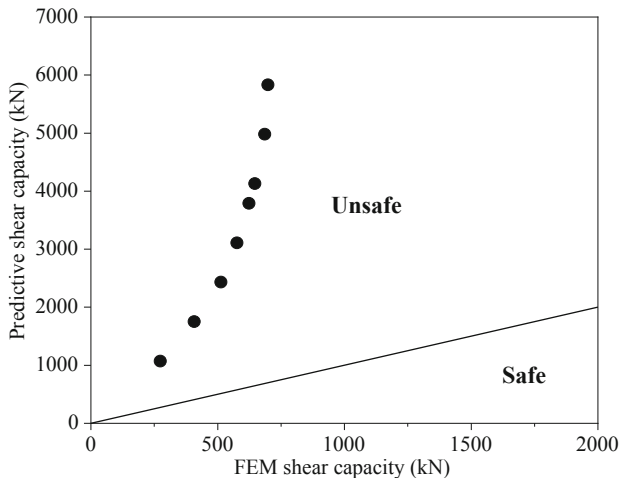


Fig. 9. Comparisons of the AASHTO equations to FEM results.

5 Conclusion

Based on the FE results of UHPC single-keyed dry joints under shear-torsion load, the following conclusions are obtained:

- (1) The increase of confining pressure can effectively improve the shear-torsional load capacity of the dry joints. Whereas the increase of confining pressure has little effect on the improvement of stiffness. From the failure mode of specimens, the specimens are damaged in the root of the shear key when confining pressure is less than 18 MPa. However, in view of the high confining pressure (when the confining pressure is greater than 18 MPa), the damaged surface of the specimen changes from the root of the male key to the feminine key.
- (2) For UHPC single-keyed dry joints under shear-torsion load, the difference between predicted results and fem data was great than 100% in AASHTO equations. Thus, the calculated ultimate capacities of the joints showed significant discrepancies from the FEM values. The AASHTO code equations were found to overestimate the ultimate capacities of UHPC single-keyed dry joints under shear-torsion load.

References

1. Wang, H.L., Li, B.H., Guo, X., et al.: Experimental study on shear behavior of single-keyed dry joint of ultra-high performance concrete (UHPC) under combined shear and torsion. *Bridge construction* **52**(02), 31–38 (2022). (in Chinese)
2. Shamass, R., Zhou, X.M., Giulio, A.: Finite-element analysis of shear-off failure of keyed dry joints in precast concrete segmental bridges. *J. Bridg. Eng.* **20**(6), 04014084 (2015)
3. Liu, T.X.: Experimental and theoretical research on shear behavior of joints in precast UHPC segmental bridges. Southeast University, Nanjing (2017). (in Chinese)
4. Liu, T.X., et al.: Shear strength of dry joints in precast UHPC segmental bridges: experimental and theoretical research. *J. Bridg. Eng.* **24**(1), 04018100 (2019)
5. Hu, Y.Q., et al.: Shear strength prediction method of the UHPC keyed dry joint considering the bridging effect of steel fibers. *Eng. Struct.* **255**, 113937 (2022)
6. Chen, L., et al.: Shear performance of ultra-high performance concrete multi-keyed epoxy joints in precast segmental bridges. *Structures* **46** (2022)
7. Aashto, L.: bridge design specifications, sixth edition. Association of State Highway and Transportation Officials (AASHTO), American, Washington, DC (2015)
8. Rombach, G., et al.: Shear strength of joints in precast concrete segmental bridges. *ACI Struct. J.* **102**(1), 3–11 (2005)



First Master-Permanentization Solution for Telecommunication Tower

Hastining Bagyo Astuti^{1,4}, Rosadi Makhdor^{2,4}, Detriana Margita Sari^{3,4}(✉),
and Soekhatta Setiawan^{3,4}

¹ Operation and Construction Department, Mitratel, Jakarta 12710, Indonesia
Hastining.b.astuti@mitratel.co.id

² Operation and Maintenance Department, Mitratel, Jakarta 12710, Indonesia
720204@telkom.co.id

³ Technology Solution and Operation Improvement, Mitratel, Jakarta 12710, Indonesia
{detriana.margita,soekhatta.setiawan}@mitratel.co.id

⁴ Daya Mitra Telecommunication, Jakarta, Indonesia

Abstract. Telecommunications development in Indonesia is growing rapidly, as it is in other emerging countries. With the expansion of this business, there is a very tight level of competition among Indonesian cellular operators as well as in the Tower Provider sector as a provider of supporting infrastructure services. Furthermore, the demand for infrastructure to support telecommunication systems has increased dramatically over the last decade, as the need to erect more towers. As a consequence, these two factors contribute to an increase in the demand for land to build the new tower. Need a solution to take advantage of the existing site, particularly the guyed mast tower, so that no new land is required. The novelty of this paper presents the First Master solution developed by Mitratel, one of Indonesia's largest tower providers. This solution has been used in several locations and proven to use the existing guyed mast tower without turning off the tower transmission to ensure that the telecoms tower can still function.

Keywords: First Master · Solution · Erection · Tower · Telecom

1 Introduction

Telecommunications is still one of the mainstay businesses, especially in developing countries. Over the past three decades, the technology, standards, and development of the Chinese mobile communications industry have gone through a process of introduction, absorption, digestion, and innovation, and it has already become a leader rather than a follower and a pursuer [1]. Economic growth in Sub-Saharan Africa has been increasing over the last two decades [2]. Adela reports some compelling and robust findings which substantiate that ICT has a statistically significant influence on economic growth in Africa [3]. As evidenced by the tremendous construction of telecommunications tower infrastructure. Considering the explosive services demand in cities as a result of population increase, the need for more support structures to be installed [4]. Because of the increasing need for telecom tower construction, developing countries such as Indonesia

continue to make the telecommunications business a cornerstone. New telecommunication technologies have flooded into Indonesia, within a highly competitive market structure. Local firms such as Telkomsel, Indosat, and Mobile-8 (Smartfren), supported by multinational companies such as Samsung, LG, and Nokia, are now prominent in the market, offering all kinds of discounts on mobile phones and advertising widely [5]. On the other hand, with the growing need for telecommunications infrastructure, there is a limited amount of land available for the building of telecommunications towers. Aside from limited land, there has been an increase in land leasing prices for tower development; the larger the area required, the higher the rent.

However, as building or land permits become more difficult to obtain, aesthetics become increasingly important. Nowadays, it is difficult to find new land to build telecommunications infrastructure, such as towers, so innovation is needed to find new ways to use the existing land and towers while also adding height and new devices. Innovation is complex, uncertain, somewhat disorderly, and subject to changes of many sorts. Innovation is also difficult to measure and demands close coordination of adequate technical knowledge and excellent market judgment to satisfy economic, technological, and other types of constraints – all simultaneously [6]. In this case, related to the telecoms infrastructure, steel is still a commonly used material for steel lattice towers and is typically made from tubular or angular profiles. Steel lattice towers are extensively utilized in the telecommunication industry as supporting structures providing services such as telephoning, wireless internet, or television [7]. Lattice structures for telecommunication purposes are mainly erected in mountainous terrain, where transportation of the building materials can be extremely challenging and costly [8]. When there is a high demand for a specific type of structure, the projects become more unique, with different focus areas from site to site. In addition, because this type of project is now a specialized market, it becomes harder to find real-world experience in terms of both design and execution [9]. Aside from lattice towers, which require specific land, a guyed mast can be used as an alternative solution. Apart from its lightweight, other advantages include the fact that it does not require a significant size of land, the erection time is quicker, and the overall costs are more affordable. Guyed masts have been applied within the field of telecommunications for many years. Previous comparisons of the advantages of guyed masts over self-supporting towers highlight that positive properties of the guyed mast include: lower cost with height, less erection time, and cost-effective foundations [10]. Mitratel, one of Indonesia's largest tower providers provides the solution, to how to use the existing guyed mast structure with minimize strengthening to add more antennas and other ancillaries is called First Master. This solution has been used in several locations and proven to use the existing guyed mast tower without turning off the tower transmission to ensure that the telecoms tower can still function.

2 Background

Telecommunications development in Indonesia is growing rapidly, as it is in other emerging countries. With the expansion of this business, there is a very tight level of competition among Indonesian cellular operators as well as in the Tower Provider sector as a provider of supporting infrastructure services. Furthermore, the demand for infrastructure to support telecommunication systems has increased dramatically over the last decade, as the

need to erect more towers. As a consequence, these two factors contribute to an increase in the demand for land to build the new tower. Nowadays, it is difficult to find new land to build telecommunications infrastructure, such as towers, so innovation is needed to find new ways to use the existing land and towers while also adding height and new devices. Need a solution to take advantage of the existing site, particularly the guyed mast tower, so that no new land is required. Mitratel has the largest tower portfolio in Indonesia spread across strategic locations. Of 35,051 towers, less than 2% or 724 sites are guyed mast structures. Guyed masts are common structures to support telecommunication devices used worldwide. They are slender and light structures frequently exposed to high winds which are determinant loads in their structural design [11]. Guyed masts are telecom towers that have guy wires, which are tensioned cables used to stabilize the tower [12]. Guyed masts are extensively used in the telecommunications industry, and the size, shape, and topology optimization can significantly benefit their transportation and installation [13]. The analysis and design of masts and towers require specific knowledge and expertise, particularly concerning guyed masts. Towers are lightweight structures with high slenderness and high flexibility [11]. This paper presents a solution regarding the use of existing towers especially guyed masts to support demand from operators with additional equipment.

3 Methodology

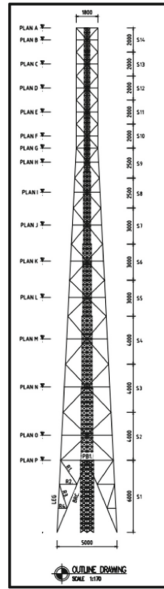
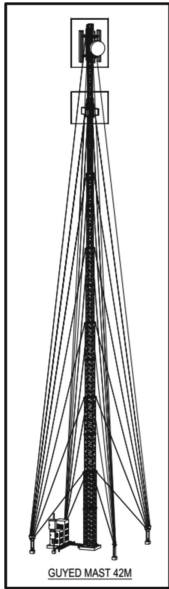
Used of existing guyed mast structure becomes the main object in this study. The concept of the First Master solution is to keep using the existing guyed mast by modifying by replacing the guyed wire and covering it with steel angle. The purpose of using this steel angle is to ensure that the guyed mast structure can still accept force from either the existing load or an additional load. The guyed mast structure used is 42 m tall, with the following material list below (Table 1):

Table 1. Material List of Guyed Mast.

Member	Material	Dimension	Unit
Horisontal	Roundbar	φ 19	mm
Bracing	Roundbar	φ 19 and φ 16	mm
Leg	Pipe	1	inch

Source: Detail Drawing [14].

Furthermore, to obtain the most efficient tonnage from the use of steel angle, an analysis was performed using the MS Tower version 222 G and this program can be used for linear and non-linear analysis, static and dynamic analysis of communication and transmission towers [15–17]. Standard drawing and drawing modification for the guyed mast is presented below,



REVISIONS		REVISIONS	BY	DATE
1	ISSUED FOR CONSTRUCTION	1.000000	1.000000	1.000000
2	ISSUED FOR CONSTRUCTION	1.000000	1.000000	1.000000
3	ISSUED FOR CONSTRUCTION	1.000000	1.000000	1.000000
4	ISSUED FOR CONSTRUCTION	1.000000	1.000000	1.000000
5	ISSUED FOR CONSTRUCTION	1.000000	1.000000	1.000000
6	ISSUED FOR CONSTRUCTION	1.000000	1.000000	1.000000
7	ISSUED FOR CONSTRUCTION	1.000000	1.000000	1.000000
8	ISSUED FOR CONSTRUCTION	1.000000	1.000000	1.000000
9	ISSUED FOR CONSTRUCTION	1.000000	1.000000	1.000000
10	ISSUED FOR CONSTRUCTION	1.000000	1.000000	1.000000
11	ISSUED FOR CONSTRUCTION	1.000000	1.000000	1.000000
12	ISSUED FOR CONSTRUCTION	1.000000	1.000000	1.000000
13	ISSUED FOR CONSTRUCTION	1.000000	1.000000	1.000000
14	ISSUED FOR CONSTRUCTION	1.000000	1.000000	1.000000
15	ISSUED FOR CONSTRUCTION	1.000000	1.000000	1.000000
16	ISSUED FOR CONSTRUCTION	1.000000	1.000000	1.000000
17	ISSUED FOR CONSTRUCTION	1.000000	1.000000	1.000000
18	ISSUED FOR CONSTRUCTION	1.000000	1.000000	1.000000
19	ISSUED FOR CONSTRUCTION	1.000000	1.000000	1.000000
20	ISSUED FOR CONSTRUCTION	1.000000	1.000000	1.000000
21	ISSUED FOR CONSTRUCTION	1.000000	1.000000	1.000000
22	ISSUED FOR CONSTRUCTION	1.000000	1.000000	1.000000
23	ISSUED FOR CONSTRUCTION	1.000000	1.000000	1.000000
24	ISSUED FOR CONSTRUCTION	1.000000	1.000000	1.000000
25	ISSUED FOR CONSTRUCTION	1.000000	1.000000	1.000000
26	ISSUED FOR CONSTRUCTION	1.000000	1.000000	1.000000
27	ISSUED FOR CONSTRUCTION	1.000000	1.000000	1.000000
28	ISSUED FOR CONSTRUCTION	1.000000	1.000000	1.000000
29	ISSUED FOR CONSTRUCTION	1.000000	1.000000	1.000000
30	ISSUED FOR CONSTRUCTION	1.000000	1.000000	1.000000
31	ISSUED FOR CONSTRUCTION	1.000000	1.000000	1.000000
32	ISSUED FOR CONSTRUCTION	1.000000	1.000000	1.000000
33	ISSUED FOR CONSTRUCTION	1.000000	1.000000	1.000000
34	ISSUED FOR CONSTRUCTION	1.000000	1.000000	1.000000
35	ISSUED FOR CONSTRUCTION	1.000000	1.000000	1.000000
36	ISSUED FOR CONSTRUCTION	1.000000	1.000000	1.000000
37	ISSUED FOR CONSTRUCTION	1.000000	1.000000	1.000000
38	ISSUED FOR CONSTRUCTION	1.000000	1.000000	1.000000
39	ISSUED FOR CONSTRUCTION	1.000000	1.000000	1.000000
40	ISSUED FOR CONSTRUCTION	1.000000	1.000000	1.000000
41	ISSUED FOR CONSTRUCTION	1.000000	1.000000	1.000000
42	ISSUED FOR CONSTRUCTION	1.000000	1.000000	1.000000
43	ISSUED FOR CONSTRUCTION	1.000000	1.000000	1.000000
44	ISSUED FOR CONSTRUCTION	1.000000	1.000000	1.000000
45	ISSUED FOR CONSTRUCTION	1.000000	1.000000	1.000000
46	ISSUED FOR CONSTRUCTION	1.000000	1.000000	1.000000
47	ISSUED FOR CONSTRUCTION	1.000000	1.000000	1.000000
48	ISSUED FOR CONSTRUCTION	1.000000	1.000000	1.000000
49	ISSUED FOR CONSTRUCTION	1.000000	1.000000	1.000000
50	ISSUED FOR CONSTRUCTION	1.000000	1.000000	1.000000
51	ISSUED FOR CONSTRUCTION	1.000000	1.000000	1.000000
52	ISSUED FOR CONSTRUCTION	1.000000	1.000000	1.000000
53	ISSUED FOR CONSTRUCTION	1.000000	1.000000	1.000000
54	ISSUED FOR CONSTRUCTION	1.000000	1.000000	1.000000
55	ISSUED FOR CONSTRUCTION	1.000000	1.000000	1.000000
56	ISSUED FOR CONSTRUCTION	1.000000	1.000000	1.000000
57	ISSUED FOR CONSTRUCTION	1.000000	1.000000	1.000000
58	ISSUED FOR CONSTRUCTION	1.000000	1.000000	1.000000
59	ISSUED FOR CONSTRUCTION	1.000000	1.000000	1.000000
60	ISSUED FOR CONSTRUCTION	1.000000	1.000000	1.000000
61	ISSUED FOR CONSTRUCTION	1.000000	1.000000	1.000000
62	ISSUED FOR CONSTRUCTION	1.000000	1.000000	1.000000
63	ISSUED FOR CONSTRUCTION	1.000000	1.000000	1.000000
64	ISSUED FOR CONSTRUCTION	1.000000	1.000000	1.000000
65	ISSUED FOR CONSTRUCTION	1.000000	1.000000	1.000000
66	ISSUED FOR CONSTRUCTION	1.000000	1.000000	1.000000
67	ISSUED FOR CONSTRUCTION	1.000000	1.000000	1.000000
68	ISSUED FOR CONSTRUCTION	1.000000	1.000000	1.000000
69	ISSUED FOR CONSTRUCTION	1.000000	1.000000	1.000000
70	ISSUED FOR CONSTRUCTION	1.000000	1.000000	1.000000
71	ISSUED FOR CONSTRUCTION	1.000000	1.000000	1.000000
72	ISSUED FOR CONSTRUCTION	1.000000	1.000000	1.000000
73	ISSUED FOR CONSTRUCTION	1.000000	1.000000	1.000000
74	ISSUED FOR CONSTRUCTION	1.000000	1.000000	1.000000
75	ISSUED FOR CONSTRUCTION	1.000000	1.000000	1.000000
76	ISSUED FOR CONSTRUCTION	1.000000	1.000000	1.000000
77	ISSUED FOR CONSTRUCTION	1.000000	1.000000	1.000000
78	ISSUED FOR CONSTRUCTION	1.000000	1.000000	1.000000
79	ISSUED FOR CONSTRUCTION	1.000000	1.000000	1.000000
80	ISSUED FOR CONSTRUCTION	1.000000	1.000000	1.000000
81	ISSUED FOR CONSTRUCTION	1.000000	1.000000	1.000000
82	ISSUED FOR CONSTRUCTION	1.000000	1.000000	1.000000
83	ISSUED FOR CONSTRUCTION	1.000000	1.000000	1.000000
84	ISSUED FOR CONSTRUCTION	1.000000	1.000000	1.000000
85	ISSUED FOR CONSTRUCTION	1.000000	1.000000	1.000000
86	ISSUED FOR CONSTRUCTION	1.000000	1.000000	1.000000
87	ISSUED FOR CONSTRUCTION	1.000000	1.000000	1.000000
88	ISSUED FOR CONSTRUCTION	1.000000	1.000000	1.000000
89	ISSUED FOR CONSTRUCTION	1.000000	1.000000	1.000000
90	ISSUED FOR CONSTRUCTION	1.000000	1.000000	1.000000
91	ISSUED FOR CONSTRUCTION	1.000000	1.000000	1.000000
92	ISSUED FOR CONSTRUCTION	1.000000	1.000000	1.000000
93	ISSUED FOR CONSTRUCTION	1.000000	1.000000	1.000000
94	ISSUED FOR CONSTRUCTION	1.000000	1.000000	1.000000
95	ISSUED FOR CONSTRUCTION	1.000000	1.000000	1.000000
96	ISSUED FOR CONSTRUCTION	1.000000	1.000000	1.000000
97	ISSUED FOR CONSTRUCTION	1.000000	1.000000	1.000000
98	ISSUED FOR CONSTRUCTION	1.000000	1.000000	1.000000
99	ISSUED FOR CONSTRUCTION	1.000000	1.000000	1.000000
100	ISSUED FOR CONSTRUCTION	1.000000	1.000000	1.000000

Fig. 1. Existing Guyed Mast. Modification Guyed Mast

Fig. 2. Outline Drawing

Figure 1 show the original Guyed Mast modification, the modifications include removing the guy wire and replacing it with a steel angle, popularly known as Self Supporting Tower (SST) [18]. Figure 2 shows the material list for Guyed Mast and the modification or SST. Figure 3 presented a view of the guayed mast including detail of the connection. Before undertaking a guayed mast modification with SST, make sure the guy wire is tight [19]. To keep the guy wire, a Helical pile will be installed immediately, this function as a temporary foundation to attach those guy wire to it [19]. Helical piles are now widely used in many fields, both onshore and offshore, and have proven to be very useful and efficient. Large diameter piles at cohesive and cohesionless sites in western Canada using three-helix were successfully implemented [20]. Helical piles are used mainly to resist tension forces generated by uplift and overturning moments of various structures, therefore they have been suggested as a potential alternative to driven piles as offshore piles because they provide a large uplift capacity due to the anchor effect of the helix [20]. M. Muthukumar and Sanjay Kumar Shukla also did deep research regarding the use of Helical piles in expansive soil [21]. Tests were carried out on helical pile foundations where there were similarities between helical collisions and pile collisions [22].

To get a better understanding, will explain how the Helical pile is used to support this solution.

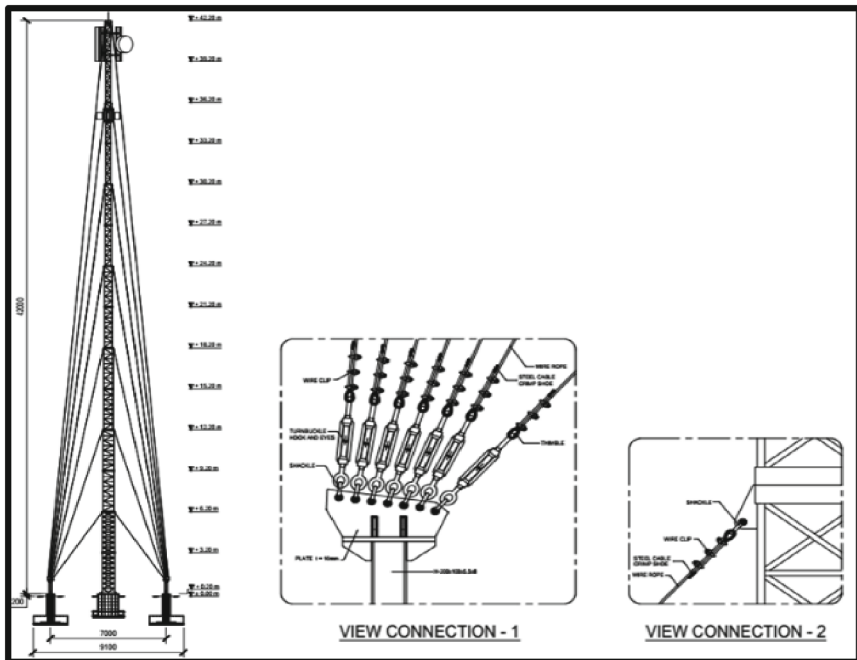


Fig. 3. GUYED Mast view.

Figures 4 and 5 show the GUYED mast 42 m high view and section which will be permanently modified into SST 42 m using the existing gUYED mast. Figure 6 presented a strengthening plan using a Helical pile to keep the GUYED mast still standing during the transformation from GUYED mast to SST.

The general process regarding the First master is already described in the paragraph above, furthermore, the picture below will present all processes or activities starting from beginning until finish. Starting from the fabrication process, site opening, using Helical pile, pouring concrete for a new foundation, tower installation, and finally equipment installation on the existing GUYED mast site without dismantling and shutting down the power (Fig. 7).

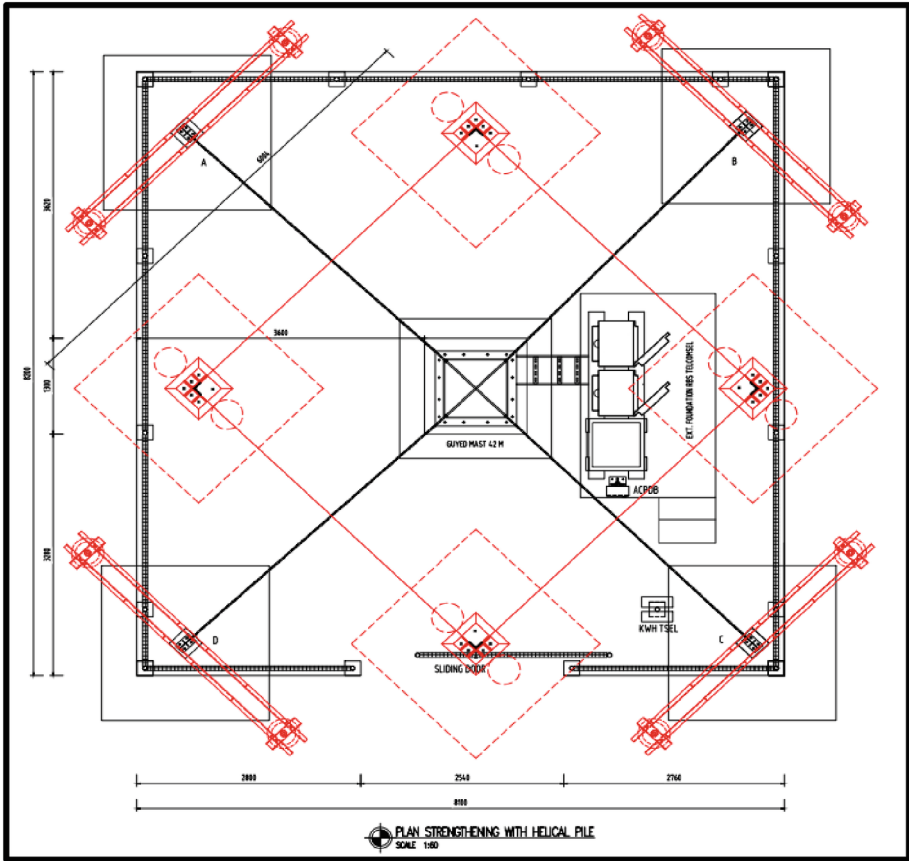


Fig. 5. Strengthening plan with Helical pile [23, 24]

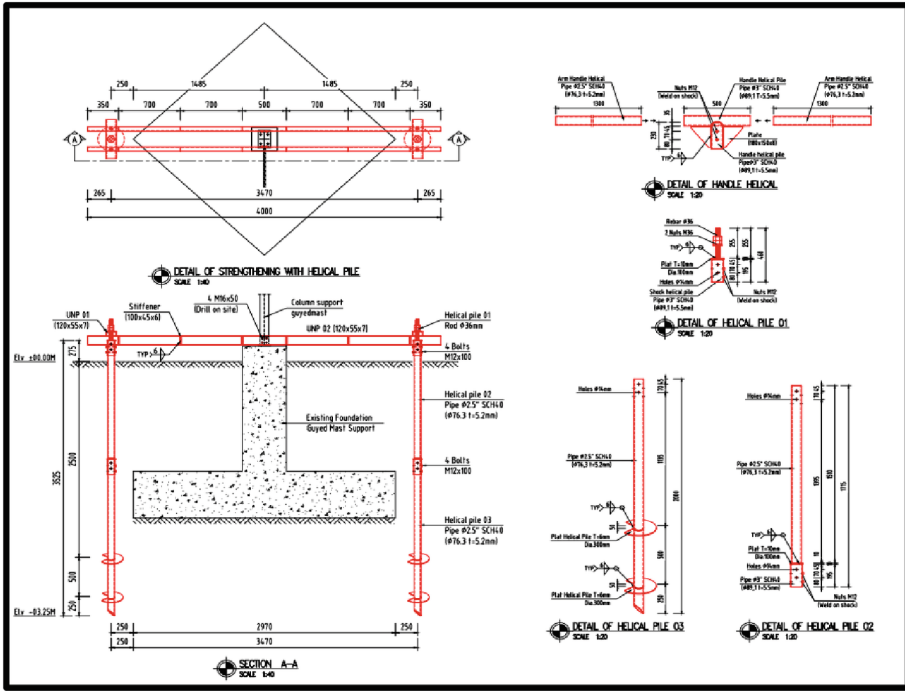


Fig. 6. Detail of Helical Pile [23, 24]

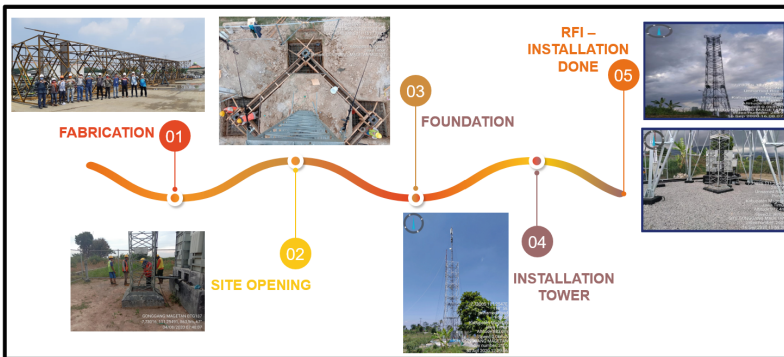


Fig. 7. The first Master construction process is on-site [25].

4 Conclusion

The first master staging consists of the following milestones as shown in the Table below (Table 2):

Table 2. First master Stages.

First period	Second period	Third period
Guyed mast Permanentization planning Overload and over quota database for Guyed mast tower	Review and design selection Approval for design Tower first master mockup	Tower’s first master fabrication Delivery to site Tower implementation

Each of the milestones completed shows that there is a difference in duration/time between the first master and the standard process. In general, the first master approach is 24 days faster than the conventional method (Built to Suite or B2S). The following figure shows the time difference between First Master and the typical B2S method (Fig. 8):

Timeline Planning-Actual **FIRST MASTER** vs Standard B2S

ACTIVITY	PLANNING	ACTUAL	REMARKS
SITAC	35	41	PROGRAM FIRST MASTER
Survey, Soil Test & Design	10	7	Design 4 Tenant Operator
Community information	5	4	Local Community, Local Government, Land Lord
Permit and legal aspect	20	30	Permit and legal aspect
Construction	70	54	
Fabrication	30	21	Horizontal check
Construction	40	33	Construction
TOTAL DURATION TIME	105	95	

V

S

ACTIVITY	PLANNING	REMARKS
SITAC-SIS B2S	44	B2S (New Site)
SIS, Soil Test & Design	14	
Community information	5	Process of Site Acquisition new site
Permit and legal aspect	25	
CME B2S	75	
Fabrication	30	Implementation process new site
Construction	45	Construction process
TOTAL DURATION TIME	119	

Fig. 8. Time Planning Actual First Master vs Standard [25]

Aside from the reduced time duration, the other benefits of the First Master solution are described in the figure below (Fig. 9).

NO	Scope of Work	FIRST MASTER	STANDARD TOWER (SST 4 LEG/3LEG)
1	Land lease for support Combat (Max 3 month)	No Need	Need
2	Combat	No Need	Need
3	Dismantle Equipment	No Need Equipment On at Tower GM-Existing	No Need
4	Dismantle Tower	No Need	Need – New Tower installation
5	Dismantle Sling	No Need	Need – New Tower installation
6	SACME	Need	Need
7	RPI-On Air Equipment	Easy to move the equipment directly	Equipment move after Erection Tower (RPI) done
8	Structural point of view	From Guyed Mast to 4 Leg tower Design calculation suitable for tenant capacity or existing Load	Standard Tower SST (4 Leg-3 Leg) Design calculation base on type of tower (New Light, Light, Medium, Back Bone)
9	Pro - Contra	No turn off equipment No new land Easy to move existing equipment Structural design more flexible and suitable for existing load	Turn off equipment Tower existing mandatory to dismantle New land Structural design refer to standard design
10	Equipment	4 Tenant : Ø 1.2 MW (8 Pcs) - 2.580 x 0.260 x 0.120 Antenna Sector (12 Pcs) - 0.550 x 0.550 x 0.150 RRU (24 Pcs)	2 Tenant (6RF + 6RRU + 2MW 0.6m + 1MW 1,2m)

Fig. 9. First Master Pro Cont [25].

We realize that the first master is not ideally yet; further improvements are required to ensure that this solution is truly the best answer in terms of implementation method, cost, and time.

References

1. Qin, H.: Chapter 7 from follower to leader: China and THE. World Sci. 117–134 (2013)
2. Donou-Adonsou, F., Lim, S., Mathey, S.A.: Technological progress and economic growth in Sub-Saharan Africa: evidence from telecommunications infrastructure. *Int. Adv. Econ. Res.* **22**(1), 65–75 (2016)
3. Adeleye, N., Eboagu, C.: Evaluation of ICT development and economic growth in Africa. *NETNOMICS Econ. Res. Electron. Netw.* (2019)
4. Tsavdaridis, K.D., Nicolaou, A., Mistry, A.D., Efthymiou, E.: Topology optimisation of lattice telecommunication tower and performance-based design considering wind and ice loads. *Structures* **27**, 2379–2399 (2020)
5. McCawley, P.: Infrastructure policy in Indonesia, 1965–2015: a survey. *Bull. Indones. Econ. Stud.* **51**(2), 263–285 (2015)
6. Kline, S.J.: An overview of innovation. *Stud. Sci. Innov. Process* 173–204 (2009)
7. Szafran, J.: An experimental investigation into failure mechanism of a full-scale 40 m high steel telecommunication tower. *Eng. Fail. Anal.* **54**, 131–145 (2015)
8. Spiliopoulos, A., Dasiou, M.E., Thanopoulos, P., Vayas, I.: Experimental tests on members made from rolled angle sections. *Steel Constr.* **11**(1), 84–93 (2018)
9. Holmstrøm, P., Nielsen, M.G., Lindgren, O.: Replacement of two 320 m masts in Sweden. *Ce/Papers* **3**(3–4), 791–796 (2019)
10. Jespersen, M., Støttrup-Andersen, U.: Guyed wind turbine towers: developments and outlook. *Ce/Papers* **3**(3–4), 779–784 (2019)
11. Elena Parnás, V., Martín Rodríguez, P., Castañeda Hevia, A.E.: Structural behavior of guyed mast with asymmetrical anchors. *J. Braz. Soc. Mech. Sci. Eng.* **35**(2), 61–67 (2013)
12. Cucuzza, R., Rosso, M.M., Aloisio, A., Melchiorre, J., Lo Giudice, M., Marano, G.C.: Size and shape optimization of a guyed mast structure under wind, ice and seismic loading. *Appl. Sci.* **12**(10) (2022)
13. Travanca, R., Varum, H., Vila Real, P.: The past 20 years of telecommunication structures in Portugal. *Eng. Struct.* **48**, 472–485 (2013)
14. Mitratel: 2021 Structural analysis of SST 42m (permanenization of existing guyed mast 42m) (2021)
15. Saudi, G.: Structural assessment of a guyed mast through measurement of natural frequencies. *Eng. Struct.* **59**, 104–112 (2014)
16. A./TIA, TIA-222-G: Structural standard for antenna supporting structures and antennas
17. Meshmesha, H.M., Kennedy, J.B., Sennah, K., Moradi, S.: Static and dynamic analysis of guyed steel lattice towers. *Struct. Eng. Mech.* **69**(5), 567–577 (2019)
18. Pte, T.I., Page, C.: Standard operating procedure (SOP) for the replacing or re-positioning turnbuckles installed to guyed masts. *Poles Tool Box Talks*, pp. 7–11
19. Li, W., Zhang, D.J.Y., Sego, D.C., Deng, L.: Field testing of axial performance of large-diameter helical piles at two soil sites. *J. Geotech. Geoenviron. Eng.* **144**(3), 2–6 (2018)
20. Spagnoli G., de Hollanda Cavalcanti Tsuha, C.: A review on the behavior of helical piles as a potential offshore foundation system. *Mar. Georesour. Geotechnol.* **38**(9), 1013–1036 (2020)
21. Muthukumar, M., Shukla, S.K.: Comparative study on the behaviour of granular pile anchors and helical pile anchors in expansive soils subjected to swelling. *Int. J. Geotech. Eng.* **14**(1), 49–54 (2020)
22. Elkasabgy, M., El Nagggar, M.H.: Lateral vibration of helical and driven steel piles installed in clayey soil. *J. Geotech. Geoenviron. Eng.* **144**(9), 1–8 (2018)
23. Mitratel: Temporary support for existing guyed mast foundation. no. Option 02
24. Mitratel: Temporary support foundation design report of existing guyed mast 42 m checked by: Gin Gin Ginanjar (2020)
25. Mitratel O&M Team: First master site gonggang magetan, installation permanentization GM to SST 42 (2021)

Environmental Monitoring and Risk Assessment



Impacts of Tibetan Plateau Vortex Activities on the Ecological Environment in the Yellow River Basin

Shuhua Yu¹(✉), Jun Peng¹, and Wenliang Gao²

¹ Chengdu Institute of Plateau Meteorology, China Meteorological Administration, Chengdu 610072, China
scshuhuayu@163.com

² Ya'an City Meteorological Bureau, China Meteorological Administration, Ya'an 625000, China

Abstract. The Tibetan Plateau vortex (TPV) is the main rain-producing system over the Tibetan Plateau. Once it moves out of the plateau, it can cause heavy rainfall and even lead to flooding, soil erosion, and other impacts on the ecological environment to the east of the plateau, especially in the Yellow River Basin (YRB). Based on sounding data, ground-based observations and Tibetan plateau vortex (TPV) and shear line yearbooks from 1998 to 2018, and using synoptic analysis and statistical analysis methods, the activities and the precipitation of high-influence Tibetan Plateau vortices (HITPVs) activities and their impact on the ecological environment in the YRB are analyzed. The results indicate that the Tibetan Plateau vortices (TPVs) that did not move out of the plateau brought moderate rain and above to the upper reaches of the YRB in 1998 which are beneficial to enrich the water resources of the “water tower” of the YRB. Most of the moving-out TPVs (MTPVs) in 1998 caused moderate rain and above in the upper-middle reaches of the YRB or in the whole YRB, contributing to the enrichment of the water resources of the “water tower” of the YRB. However, the activities of the MTPVs were likely to cause heavy rainfall such as rainstorms and heavy rainstorms, which could result in local flooding and other natural disasters and damage to the local ecological environment in the middle reaches of the YRB. The HITPVs mostly moved eastward and northeastward during late May to mid-August, mainly affecting the middle or lower reaches of the YRB. In addition, these HITPVs had southeastward paths, spinning in the Hetao region. The HITPVs with eastward paths and spinning in the Hetao region influenced the whole YRB, mainly causing rainstorms and heavy rainstorms in the middle or lower reaches. All of the HITPVs resulted in damage to the local ecological environment of the YRB.

Keywords: Tibetan Plateau Vortex · Yellow River Basin · Ecological Environment

1 Introduction

Tibetan Plateau vortices (TPVs) are essential low-pressure systems affecting China, and once the TPVs move eastward out of the Tibetan Plateau, they can cause disaster weather (such as torrential rain and downpour) over a wide range of China [1–5]. Therefore, the eastward-moving TPVs have become the focus of TPV research.

Several previous studies revealed the impact of the eastward-moving TPVs on precipitation in China. For example, Yu et al. [6] indicated that the TPVs generally resulted in rainfall with an intensity of moderate rain or above after moving out of the plateau, and 60% of them that were active for a long time (≥ 36 h) caused torrential rain or downpour. Zhang et al. [7] pointed out that a TPV spinning over the Hetao region caused a downpour in northern Shaanxi. Yu et al. [4] noted that the TPVs maintained east of the Tibetan Plateau have a wide range of influence on China and can even affect the Korean Peninsula, Japan and Vietnam. The TPVs lasting for a long time after moving out of the Tibetan Plateau greatly influence heavy precipitation in China and even in East Asia [8].

The Yellow River Basin (YRB) crosses eight provinces in China. Its upper reaches are the water resources of the Yellow River, called the “water tower”. The precipitation in this area is vital and directly impacts agriculture, ecology and human survival in the Hexi Corridor region. In addition, it affects the agricultural and livestock production in the Hetao region of the YRB (mid-latitude arid and semi-arid regions) and is closely related to the people’s production and livelihood in the lower reaches of the YRB. Further investigation of the relationship between TPV activities and heavy rainfall in China is of great significance for the use of water resources and ecological and environmental protection. However, studies on the impacts of TPV activities on the upper, middle and lower reaches of the YRB are scarce and deserve to be further carried out.

Therefore, in this study, we analyze the impacts of the TPVs in 1998 and the TPVs lasting for a long time after moving out of the Tibetan Plateau during 1998–2018 on precipitation in the YRB, in order to explore how the TPVs affect the ecological environment of the YRB. The remainder of this paper is organized as follows. Section 2 introduces the data and methods used in this research. Section 3 investigates the impacts of the TPVs in 1998 on precipitation and ecology in the YRB. Section 4 describes the activities and impacts of the high-influence TPVs (HITPVs) in the YRB. The main conclusions are presented in Sect. 5.

2 Data and Methods

The data used in this study include the ground-based observations and sounding data at 08:00 and 20:00 (Beijing time, the same as below) from 1998 to 2018 provided by the National Meteorological Information Center of the China Meteorological Administration. The yearbooks of the TPVs and the shear lines from 1998 to 2018 are also used in this research [9, 10].

The synoptic analysis and statistical analysis methods [4] are used to analyze the activities of the moving-out TPVs (MTPVs), the activities of the TPVs not moving out of the plateau (NMTPVs) in 1998 and their relationships with precipitation. Also, the activities and precipitation of the TPVs with a longer activity periods (more than 24

h after moving out of the plateau) from 1998 to 2018 are investigated. The impact of HITPVs in the YRB on the ecological environment is explored as well.

The TPVs are generated on the Tibetan Plateau and appear at 500 hPa, which refers to low-pressure systems with closed contours or with cyclonic circulations in terms of the wind direction at three stations [11]. Their number is composed of the letter “C” at the beginning, the second and third digits are the last two digits of the year, and the fourth and fifth digits are the two digits of the low vortex sequence in the corresponding year [9].

A HITPV refers to a TPV activity process that can cause precipitation of 100 mm or more in the upper, middle or lower reaches of the YRB after moving out of the plateau for more than 24 h.

3 Impacts of the TPVs in 1998 on Precipitation and Ecology in the Yellow River Basin

During the floods in the Yangtze River Basin in 1998 (from late June to August), there were 13 heavy rainfall events corresponding to eight flood peaks in the upper reaches of the Yangtze River, all of which were caused by low vortices with shear lines formed by the combination of a TPV and a westerly trough [12]. The impacts of TPV activities were considerable on the Yangtze River floods in 1998. Therefore, the TPV activities and the impacts of the MTPVs and the NMTPVs on precipitation and ecology in the YRB during 1998 are discussed as follows.

3.1 TPV Activities in 1998

Figure 1 presents the monthly occurrences of the TPVs, MTPVs and NMTPVs in 1998. The results indicate that the earliest occurrence of the TPVs in 1998 was in early March, and the last appeared in early December. Except for January, February and November, the TPVs appear in each month. June to August is the peak period for the occurrence of the TPVs, especially for the NMTPVs, while the MTPVs are more frequent in July–August.

The source locations of the TPVs, MTPVs and NMTPVs are also analyzed in this research, as shown in Fig. 2. It can be found that in 1998, most of the TPVs and MTPVs were generated in the east and south of the Tibetan Plateau. However, the TPVs generated in the northeastern and central plateau have higher probabilities of moving out of the plateau, with probability values of 67% and 50%, respectively.

3.2 Impacts of the NMTPVs in 1998 on the Precipitation and Ecology in the Yellow River Basin

Table 1 presents the precipitation situation in the YRB affected by the NMTPVs in 1998. Obviously, the NMTPVs in 1998, most of which (19/26) brought precipitation to the YRB, affected the upper reaches, with 37% (7/19) resulting in drizzle (≤ 10 mm) and 63% (12/19) causing moderate rain and above (> 10 mm). In addition, the maximum rainfall caused by the NMTPVs is 38 mm. Most of the NMTPVs resulting in moderate rain and above appeared in June and July (8/12 = 67%). Compared with Fig. 1, it can

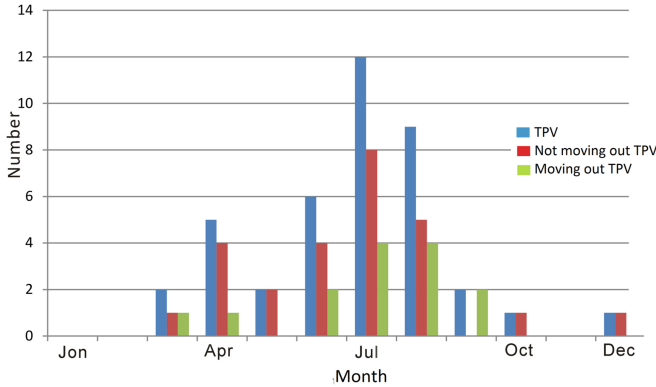


Fig. 1. Monthly occurrence of the Tibetan Plateau vortices (TPVs), moving-out TPVs (MTPVs) and TPVs not moving out of the plateau (NMTPVs) in 1998.

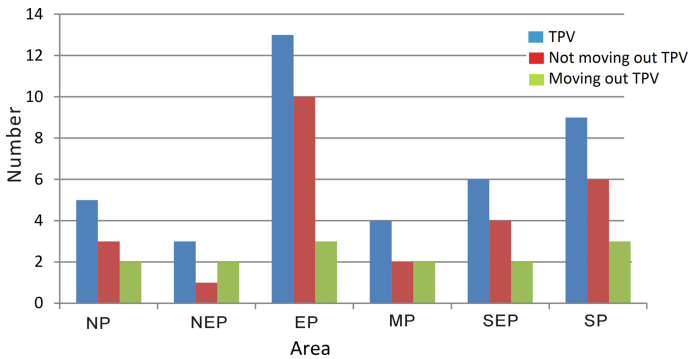


Fig. 2. Numbers of the TPVs, MTPVs and NMTPVs with various source locations. “NP” represent the northern plateau, “NEP” the northeastern plateau, “EP” the eastern plateau, “MP” the middle part of the Tibetan Plateau, “SEP” the southeastern plateau, and “SP” the southern plateau.

be found that the majority of the NMTPVs in June and July (11/12) brought rainfall to the upper reaches of the YRB, and most of them (8/12) caused moderate rain and above. These NMTPVs generally stayed at the source or moved southeastward. This result suggests that the NMTPVs greatly influence the precipitation in the upper reaches of the YRB, mostly causing rainfall with an intensity of moderate rain and above, especially in June and July.

Moreover, in 1998, the activity periods of the NMTPVs resulting in precipitation in the YRB were relatively short, mostly within 24 h (17/19), with 63% (12/19) of 24 h and the longest of 36 h (only two cases). There were only two NMTPVs causing more than 30 mm of precipitation, and their activity periods were 12 h and 24 h. As can be shown from Fig. 2, the NMTPVs generated in the northeastern and southeastern plateau in 1998 all could bring rainfall to the upper reaches of the Yellow River, and the majority of the NMTPVs (3/4) generated in the southeastern plateau caused rainfall of moderate rain and above, with an activity period of 24 h. The majority (9/10) of the

NMTPVs generated in the eastern plateau could bring rainfall to the upper reaches of the YRB, with more than half of them causing moderate rain and above. These results demonstrate that the activity periods of the NMTPVs are relatively short, and regardless of the activity periods, the influences of the NMTPVs should be taken into account. In particular, the NMTPVs generated in the northeastern, southeastern and eastern plateau should receive more attention as they can bring precipitation to the upper reaches of the YRB, especially for the NMTPVs originating from the southeastern plateau.

Table 1. Precipitation situation in the Yellow River Basin (YRB) affected by the Tibetan Plateau vortices not moving out of the plateau (NMTPVs) with different source locations.

Source locations	Number	Generation time	Activity period	Affected area of the YRB	Maximum rainfall (mm)	Path
		(month/day/hour.)	(hours)		(UR MR LR)	
Northern plateau	C9802	3/24/08	12	UR	2.7	
	C9808	5/11/20	12	UR	14.6	
Northeastern plateau	C9825	7/24/08	12	UR	8.2	
Eastern plateau	C9803	4/13/20	12	UR	13.5	
	C9807	4/22/08	12	UR	<10	
	C9809	5/28/08	12	UR	33.6	
	C9810	6/3/08	12	UR	11.4	
	C9815	6/30/20	12	UR	21.8	
	C9820	7/15/20	24	UR	<10	Southeastward
	C9822	7/10/08	24	UR	16.6	Southeastward
	C9826	7/26/08	12	UR	10	
	C9827	7/27/20	36	UR	16.1	Southeastward
Central plateau	C9819	7/14/20	12	UR	26.7	
Southeastern plateau	C9804	4/14/08	12	UR	<10	
	C9811	6/4/20	24	UR	12.5	Southeastward
	C9813	6/8/20	24	UR	26.3	Southwestward
	C9816	7/5/20	24	UR	38.0	Eastward
Southern plateau	C9829	8/7/08	36	UR	21.9	Eastward
	C9839	10/3/20	12	UR	<10	

Note: "UR", "MR" and "LR" denote the upper, middle and lower reaches of the Yellow River Basin, respectively

Overall, the activities of the NMTPVs are favorable for enriching the water resources of the “water tower” of the Yellow River. Especially in June–July when the agricultural and pastoral water use reaches its peak in the YRB, the NMTPV activities increase the water volume in the upper reaches of the YRB, positively regulating the water resources in the middle and lower reaches of the YRB.

3.3 Impacts of the MTPVs in 1998 on the Precipitation and Ecology in the Yellow River Basin

As illustrated in Table 2, the precipitation in the YRB affected by the MTPVs in 1998 indicates that the majority ($12/14 = 86\%$) of the MTPVs brought precipitation to the YRB, mostly affecting the upper and middle reaches of the YRB, only one influencing the whole basin, and 42% ($5/12$) impacting only the upper reaches of YRB. In terms of the MTPVs, only 17% ($2/12$) of the MTPVs resulted drizzle (≤ 10 mm), 83% of the cases caused precipitation with an intensity of moderate rain and above (> 10 mm), and one third led to downpour (maximum rainfall of 178.9 mm). The MTPVs that caused moderate rain and above mainly appeared in June–September ($9/10$), with two in June, July and September, respectively, and three in August. Compared with Fig. 1, it can be found that the MTPVs in both June and September brought precipitation with an intensity of moderate rain or above to the upper or upper to middle reaches of the YRB. Half of the MTPVs in August caused moderate rain or above in the upper to middle reaches of the YRB, with torrential rain in the upper or middle reaches. Half of the MTPVs in July resulted in torrential rain or downpour in the middle reaches. Therefore, it can be concluded that both in terms of rainfall area and intensity, the influence of the MTPVs on precipitation in the YRB is greater than that of the NMTPVs. Most of the MTPVs can cause moderate rain and above in the upper to middle reaches of the YRB, especially in July and August when half of the MTPVs caused torrential rain or downpour, which should be considered a concern.

Moreover, the activity periods of the MTPVs affecting precipitation in the YRB in 1998 are relatively longer, mostly more than 36 h ($8/12$), of which more than 48 h account for 76% ($6/8$). Three MTPVs have the longest activity period of 60 h. One of them caused heavy rain in the whole YRB, and the other resulted in moderate and heavy rain in the upper to middle reaches of the YRB, accompanied by downpours in the upper or middle reaches. Only two MTPVs led to precipitation greater than 90 mm, both with an activity period of 48 h. Combined with Fig. 2, we can find that the 1998 MTPVs generated in the northern, northeastern, eastern, central and southeastern plateau all brought precipitation to the upper or upper to middle reaches of the YRB. Except the MTPVs generated in the southeastern plateau, which only brought drizzle to the upper reaches of the YRB, most of the MTPVs ($6/9$) generated in the northern, northeastern, eastern and central plateau caused moderate rain and above in the upper to middle reaches or the whole YRB, with an activity period of 36–60 h, which mostly moved eastward or northeastward. This result indicates that the MTPVs with an activity period of more than 48 h deserve our attention, especially for those with an activity period of 60 h. The MTPVs generated in the northern and eastern plateau can cause moderate to heavy rain and above in the upper-middle reaches or middle-lower reaches of the YRB, especially for those generated in the eastern plateau.

Overall, the MTPV activities are beneficial to the enrichment of the water resources of the Yellow River “water tower”. However, the MTPV activities are prone to cause heavy rainfall such as torrential rain and downpour in the middle reaches of the YRB on the Loess Plateaus, leading to local flooding and other natural disasters, damaging the already fragile ecological environment. In particular, in July and August when agricultural and pastoral water use reaches its peak in the YRB, the activities of the MTPVs can increase more water volume than the NMTPVs in the upper reaches of the YRB, with more positive impacts on water regulation in the middle and lower reaches of the YRB. However, it is not favorable to the local ecological environment in the middle reaches of the YRB.

Table 2. Precipitation situation in the YRB affected by the moving-out Tibetan Plateau vortices (MTPVs) generated in different source locations.

Source location	Number	Generation time	Activity period	Affected area of the YRB	Maximum rainfall (mm)	Path
		(month/ day/ hour)	(hours)		(UR MR LR)	
Northern plateau	C9801	3/7/08	60	Whole YRB	<10 32.8 33.2	Eastward
	C9831	8/18/08	60	UR and MR	52.8 27.6	Southeastward
Northeastern plateau	C9814	6/10/08	24	UR	12.7	Northeastward
	C9838	9/3/20	36	UR and MR	18<10	Eastward
Eastern plateau	C9812	6/5/20	60	UR and MR	24.2 45.7	Northeastward
	C9818	7/8/20	48	UR and MR	36.7 178.9	Northeastward
	C9837	9/2/08	24	UR	11.8	Eastward
Central plateau	C9817	7/7/08	24	UR and MR	<10 77.3	Eastward
	C9834	8/27/08	48	UR	17.5	Northeastward to southeastward
Southeastern Plateau	C9823	7/21/20	36	UR	<10	southeastward
	C9833	8/23/08	24	UR	<10	Northeastward
Southern Plateau	C9828	8/4/08	48	UR and MR	17.2 91.4	Eastward

Note: “UR”, “MR” and “LR” denote the upper, middle and lower reaches of the Yellow River Basin, respectively

4 Activities and Impacts of the HITPVs in the Yellow River Basin

Based on the identification criteria for the HITPVs described in Sect. 2, the TPVs with high impacts on the YRB from 1998 to 2018 and their paths are shown in Table 3. It can be found that there was a total of thirteen HITPVs from 1998 to 2018, i.e., the annual average was less than 1. 2000 and 2002 are the years with the most HITPVs, both with two. Additionally, in nearly half of the years (10/21), no HITPVs were observed. The relative concentration periods of the HITPVs are 1999–2002 and 2007–2010, suggesting that the occurrences of the HITPVs are related not only to the weather systems affecting TPV activities, but also to atmospheric circulations. Moreover, the HITPVs were mostly

Table 3. High-influence Tibetan Plateau vortices in the YRB from 1998 to 2018.

Path	Number	Activity period	Source	Activity period	Maximum rainfall (mm)
	number	(month/day/hour–month/day/hour)	location	(hours)	(UR MR LR)
Northeastward	C0526	6/23/08–6/28/08	Southeastern plateau	72	103.0 157.8
	C0730	6/19/20–6/25/20	Eastern plateau	84	111.8
	C1026	7/17/20–7/19/20	Southeastern plateau	24	217.8
	C1321	5/24/08–5/27/20	Central plateau	60	123.0 132.2
Southeastward	C9922	7/14/08–7/16/20	Northern plateau	36	104.0
	C0223	8/12/08–8/20/08	Northeastern plateau	168	108.0
Eastward	C0010	6/17/08–6/23/08	Northeastern plateau	108	129.0
	C0319	7/12/20–7/14/20	Northeastern plateau	36	114.1
	C0831	7/20/08–7/23/08	Eastern plateau	24	116.0
	C0943	8/2/08–8/4/08	Northeastern plateau	24	141.0
	C1741	7/25/20–7/29/08	Central plateau	36	103.6
Spinning in the Hetao region	C0014	7/2/20–7/7/20	Eastern plateau	72	409.0
	C0216	7/1/20–7/5/08	Eastern plateau	108	341.9

Note: “UR”, “MR” and “LR” denote the upper, middle and lower reaches of the Yellow River Basin, respectively

generated in the eastern or northeastern plateau, mainly moving eastward or northeastward. The majority of the HITPVs remained active for 24 h to 72 h after moving out of the plateau, mainly affecting the middle or lower reaches of the YRB.

Additionally, the HITPVs for the YRB from 1998 to 2018 mainly moved eastward and northeastward, and also some of them had a southeastward paths or spun in the Hetao region.

The HITPVs with an eastward path (Figs. 3a, b, c, d and e) mainly occurred from the second half of June to early August and affected the whole YRB, generally resulting in moderate to torrential rain. These HITPVs were generally generated in the northeastern plateau and caused torrential rain or downpour in the middle or lower reaches of the YRB, leading to local flooding and other natural disasters in the middle or lower reaches of the YRB and causing severe ecological damage.

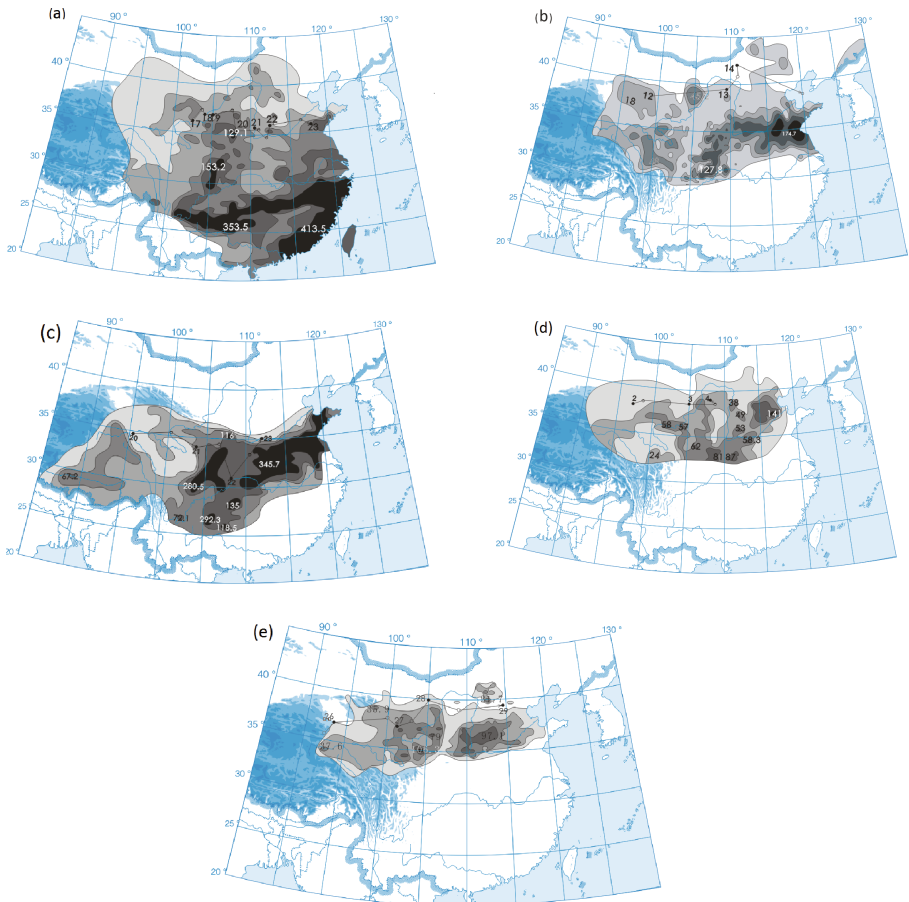


Fig. 3. The total rainfall caused by the high-influence Tibetan Plateau vortices (HITPVs) with an eastward path in the YRB, i.e., (a) C0010, (b) C0319, (c) C0831, (d) C0943 and (e) C1741.

The HITPVs with a northeastward path (Figs. 4a, b, c and d) mostly appeared from late May to mid-July and generally generated in the southeastern and eastern plateau. Half of them caused torrential rain or downpour in the middle and lower reaches of the YRB, and the other half resulted in torrential rain or downpour in the lower reaches of the YRB, leading to natural disasters such as local flooding in the middle and lower reaches of the YRB, especially in the lower reaches. The ecological damage brought by the northeastward-moving HITPVs is greater than that of the eastward-moving ones in the middle and lower reaches of the YRB.

The HITPVs with a southeastward path (Figs. 5a and b) typically occurred from late July to mid-August, causing moderate to torrential rain in the upper and middle reaches of the YRB. These TPVs were generated in the northern and northeastern plateau, leading to torrential rain in the upper or middle reaches of the YRB, resulting in natural disasters such as local flooding and thereby bringing ecological damage to these areas. However, the impact of the southeastward-moving HITPVs is weaker than that of the northeastward-moving and eastward-moving HITPVs.

The HITPVs spinning in the Hetao region in the YRB (Figs. 6a and b) mainly occurred in early July and had impacts on the entire YRB, with widespread drizzle to torrential rain. They were generated in the eastern plateau, leading to torrential rain and downpour in the middle or lower reaches of the YRB and thereby causing local flooding and other natural disasters in these areas. The impact of the HITPVs spinning in the Hetao region on the ecological environment in the middle or lower reaches of the YRB is greater than that of the eastward-moving HITPVs.

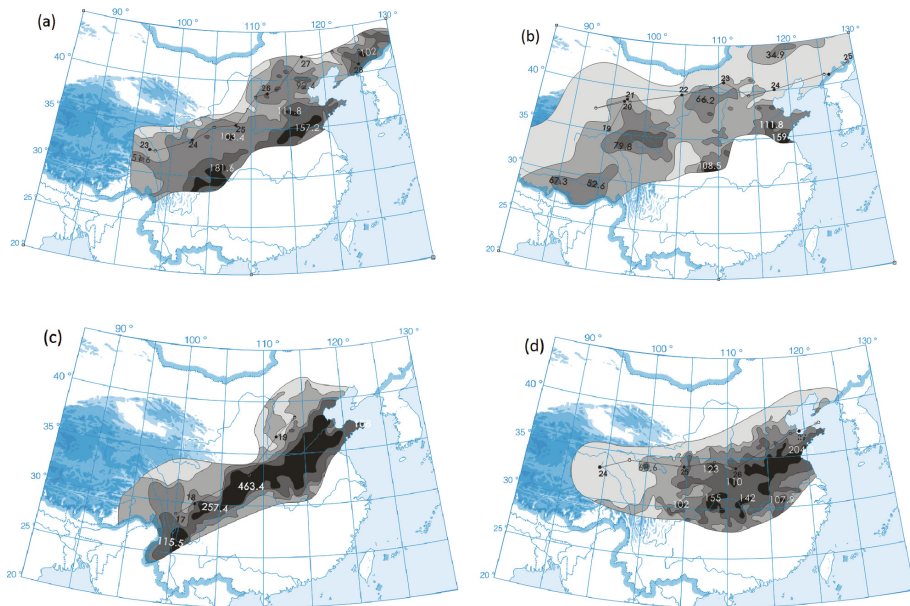


Fig. 4. Same as Fig. 3, but for the HITPVs with a northeastward path, i.e., (a) C0526, (b) C0730, (c) C1026 and (d) C1321.

Therefore, it can be concluded that the generation locations are different for the HITPVs with different paths. The eastward-moving HITPVs were generated in the northeastern plateau, the northeastward ones were generated in the southeastern and eastern plateau, the southeastward ones were generated in the northern and northeastern plateau, and the HITPVs spinning in the Hetao region were generated in the eastern plateau. Moreover, the impacts of the HITPVs with different paths on the YRB vary in range and intensity, causing different severity of ecological damage to the YRB. Specifically, the damage to the local ecological environment in the middle and lower reaches of the YRB was the greatest caused by the HITPVs with northeastward paths, followed by the TPVs spinning in the Hetao region, the third for the eastward-moving HITPVs, and the weakest for the HITPVs with southeastward paths.

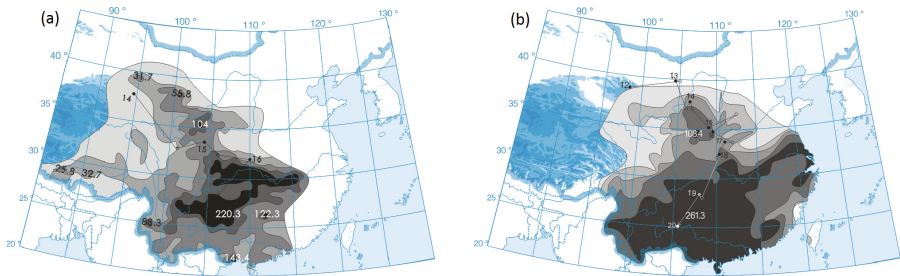


Fig. 5. Same as Fig. 3, but for the HITPVs with a southeastward path, i.e., (a) C9922 and (b) C0223.

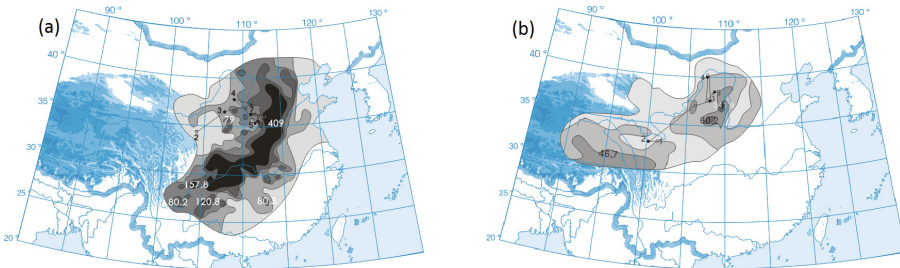


Fig. 6. Same as Fig. 3, but for the HITPVs spinning in the Hetao region, i.e., (a) C0014 and (b) C0216.

5 Conclusions

In this study, the impacts of TPVs activities in 1998 on the ecological environment of the YRB are investigated by analyzing the activities and precipitation of the MTPVs and NMPVs in 1998. The HITPV activities in the YRB and the precipitation caused by them from 1998 to 2018 are also discussed, and finally their impacts on the ecological environment of the YRB are obtained. The study is of great significance for the use of water resources and ecological and environmental protection. The main conclusions are as follows.

All the NMTPVs generated in the northeastern and southeastern plateau in 1998 brought rainfall to the upper reaches of the YRB. The NMTPVs generated in the southeastern plateau caused precipitation with an intensity of moderate rain and above. The NMTPVs generated in the eastern plateau mostly brought precipitation to the upper reaches of the YRB, more than half of which caused moderate rain and above. Therefore, these NMTPVs are conducive to enriching the water resources in the “water tower” of the YRB, which can increase the water volume in the upper reaches of the YRB and play a positive role in regulating water volume in the middle and lower reaches of the YRB.

All the MTPVs in 1998 brought rainfall to the upper or upper-middle reaches of the YRB. The MTPVs originating from the northern, northeastern, eastern and central plateau mostly caused precipitation with an intensity of moderate rain and above in the upper-middle reaches of the YRB or the whole YRB, mainly moving eastward or northeastward. The MTPVs with a longer activity periods (60 h or more), especially for those generated in the eastern plateau, resulted in stronger rainfall intensities. Compared with the NMTPVs, the increase of the water volume increase caused by the MTPVs activities is more, especially during July–August when agricultural and pastoral water use reaches its peak in the YRB. Thus, the MTPVs are more favorable to enriching the water resources in the “water tower” of the YRB. However, in terms of the middle reaches of the YRB, the MTPVs are likely to cause heavy rainfall such as torrential rain and downpour, leading to local flooding and other natural disasters and resulting in damage to the local ecological environment in these areas.

Most of the HITPVs in the YRB were generated in the eastern and northeastern plateau and generally moved eastward or northeastward. Their main activity periods were 24–72 h after moving out of the plateau, and the major influenced areas were the middle or lower reaches of the YRB.

The HITPVs mostly moved eastward and northeastward, and some of them moved southeastward or spun in the Hetao region. These TPVs mainly appeared from late May to mid-August, and the occurrence periods are different for the HITPVs with different paths, successively for the northeastward-moving HITPVs, the eastward-moving HITPVs, the HITPVs spinning in the Hetao region and the southeastward-moving HITPVs.

The impacts of the HITPVs with different paths on the YRB varied in range and intensity. The eastward-moving HITPVs and those spinning in the Hetao region had influences on the whole YRB, mainly causing torrential rain and downpour in the middle or lower reaches. The impacts of the eastward-moving HITPVs were greater than those spinning in the Hetao region. The northeastward-moving HITPVs caused torrential rain and downpour in the middle and lower reaches of the YRB, especially in the lower reaches. The HITPVs with southeastward paths led to moderate rain and above in the upper and middle reaches of the YRB.

This research also indicates that the HITPVs with different paths in the YRB all resulted in damage to the local ecology in the YRB, but the severity of the damage was different. The damage to the local ecological environment in the middle and lower reaches of the YRB was the greatest caused by the northeastward-moving HITPVs, followed by the HITPVs spinning in the Hetao region, the third for the eastward-moving HITPVs, and the weakest for the southeastward-moving HITPVs.

Acknowledgement. Thanks to Nanjing Hurricane Translation for the help in the translation of this paper. This research was supported by the National Natural Science Foundation of China (Grant Nos. 91937301).

References

1. Tao, S.Y., Ding, Y.H.: Observational evidence of the influence of the Qinghai-Xizang (Tibet) Plateau on the occurrence of heavy rain and severe convective storms in China. *Bull. Amer. Meteor. Soc.* **62**(1), 23–30 (1981)
2. Zhang, S.L., Tao, S.Y., Zhang, X.L.: Meteorological and hydrological characteristics of severe flooding in China during the summer of 1998. *Q. J. Appl. Meteorol.* **12**(4), 442–457 (2001)
3. Liu, X.C., Chen, Y.R.: Comparative analysis of two heavy rainfall processes under interaction of Plateau Vortex and Southwest Vortex. *Plateau Mt. Meteorol. Res.* **34**(1), 1–7 (2014)
4. Yu, S.H., Gao, W.L., Peng, J., Xiao, Y.H.: Observational facts of sustained departure plateau vortexes. *Meteor. Res.* **28**, 296–307 (2014)
5. Chen, B., Gao, W.L.: The causing storm rain in Southwest Sichuan basin characteristic analysis of Tibetan Plateau vortex. *Plateau Mt. Meteorol. Res.* **35**(1), 9–15 (2015)
6. Yu, S.H., Gao, W.L.: Observational analysis on the movement of vortices before/after moving out Tibetan Plateau. *Acta Meteor. Sinica* **64**(3), 392–399 (2006)
7. Zhang, H., Chen, W.D., Sun, W.: Analysis of the influence of a Typhoon and mesoscale vortex in inner-mongolia irrigation area of Yellow River on rainstorm in north Shaanxi. *Plateau Meteor.* **25**(1), 52–59 (2006)
8. Yu, S.H., Gao, W.L., Xiao, D.X., Peng, J.: Observational facts regarding the joint activities of the Southwest Vortex and Plateau Vortex after its departure from the Tibetan Plateau. *J. Adv. Atmos. Sci.* **33**(1), 34–46 (2016)
9. Li, Y.Q., et al.: *Tibetan Plateau Vortex and Shear Line Yearbook 1998*. China Scientific Press, Beijing (2010)
10. Institute of Plateau Meteorology, China Meteorological Administration, Chengdu, and Plateau Meteorology Committee of Chinese Meteorological Society.: *Tibetan Plateau Vortex and Shear Line Yearbook 2018*. China Scientific Press, Beijing (2020)
11. The Lhasa Focus Group on Tibetan Plateau Meteorology Research.: *The Research of Vortex and Shear Line on 500 hPa of Tibetan Plateau in Summer Half Year*. Science Press, Beijing (1981)
12. Yang, K.M., Bi, B.G., Li, Y.A., Dong, L.Q.: On flooding-causing torrential rainfall in the upstream district of Changjiang River in 1998. *Meteor. Mon.* **27**(8), 9–14 (2001)



Assessment of Wind Energy Resources in Fujian Sea Areas Based on WRF Model

Dawei Ji¹, Lianjie Guo¹, Na Wang¹(✉), Feifei Jiang², Yingzhi Cao¹, and Hong Deng³

¹ National Marine Data and Information Service, Tianjin 300171, China
{guolianjie, caoyingzhi}@mail.nmdis.org.cn,
wangna0305151187@126.com

² College of Engineering, Ocean University of China, Qingdao 266100, China

³ National Center of Ocean Standards and Metrology, Tianjin 300112, China

Abstract. Wind energy is an important energy source with a strong potential for development. China's Fujian Sea areas is a key area for the development of offshore wind power. In this study, WRF model was used to simulate the wind field in Fujian Sea areas from 2019 to 2021, and the simulation data of WRF fit well with the measured data of buoy. According to the analysis, the maximum wind energy density in Fujian Sea areas is concentrated in the Taiwan Strait, the annual average wind energy density is distributed in the range of 400–700 W/m², the seasonal average wind energy density distribution is small in spring and summer, large in autumn and winter, the monthly average wind energy density is the largest in October, November and December, and the maximum is more than 2000 W/m². The main wind direction are NE and NNE. The results show that Fujian Sea areas is rich in wind energy, which is conducive to the promotion of offshore wind power development process.

Keywords: WRF Model · Fujian Sea Areas · Wind Energy Resources Assessment

1 Introduction

With the development of economy, the existing energy sources crisis is approaching, and the development and utilization of renewable energy are increasingly important [1–3]. As a kind of renewable energy, wind energy has the advantages of clean and environmental protection, large reserves and wide distribution range, and has a strong development potential. In the utilization of wind energy, it can be divided into onshore wind power and offshore wind power. Offshore wind power has more advantages, including higher wind speed, more stable wind direction, and higher annual utilization hours of wind speed [4–6].

Many scholars have analyzed the wind resources in different sea areas through WRF model. Matter et al. predicted the wind energy density in the central coastal area of Chile, and demonstrated the feasibility of installing wind turbines at this location [7]. Shimada et al. studied the offshore area of Shirahama, Japan, and found that improving

the wind speed simulation error is the key to improve the simulation accuracy, which can enhance the effect of wind energy assessment [8]. Mengsen Luo et al. analyzed the distribution of wind resources in Jiangsu Sea areas, which was the largest in spring and the smallest in summer, and the spatial distribution increased from inland areas to coastal areas [9]. Donghui Li simulated the wind fields in the Shandong Peninsula coastal area, and through comparison with data from actual observation stations, conducted a comprehensive assessment of the wind energy resources in this region [10]. Sheng Dong et al. conducted a simulation and analysis of wind fields in the Yangtze River Delta region, which showed that wind energy density in spring was the lowest, and it increased gradually in other seasons, and the prevailing wind directions that have the most significant impact on the Yangtze River Delta region are from the northwest and north [11].

The main research area of this study is the Fujian Sea areas, China, which have relatively high annual average wind speeds, mainly from the northeast direction with stable wind direction, and the abundant wind energy resources are conducive to the long-term operation of wind turbines [12–14]. Section 2 introduces the wind data and WRF model information used. Section 3 presents the analysis and assessment of wind energy resources, and Sect. 4 is the conclusion.

2 Methodology

2.1 Wind Data

The wind data used in this study can be divided into ERA5 reanalysis data and buoy data. ERA5 assimilates historical observation results into model data to meet researchers' requirements for studying various aspects of atmospheric conditions. The horizontal resolution of the wind data is $0.25^\circ \times 0.25^\circ$, it covers the entire globe.

In this study, four buoy data in the sea areas are selected, provided by Fujian Marine Forecasts (http://www.fjhyyb.cn/Ocean863Web_MAIN/default.aspx#hygc), and the temporal coverage ranges from 0:00 on January 1, 2020 to 0:00 on January 1, 2021. The schematic diagram of longitude and latitude information and location distribution is as follows. Because the four points where the buoy is located are missing in different time periods, the number of data is different. P2 points may be due to external factors such as instrument maintenance or buoy shift, the data is completely missing in the second half of November and December, so the number of data is less than the other points, accounting for slightly less than 75%, the other buoy data accounted for more than 75%, and the data integrity rate is high. The integrity of P3 points is the highest, accounting for 88.32%.

2.2 Wind Energy Calculation Method

Wind energy can be defined as the air energy that passes vertically through the cross section at a given wind speed:

$$E_k = \frac{1}{2}mv^2 \quad (1)$$

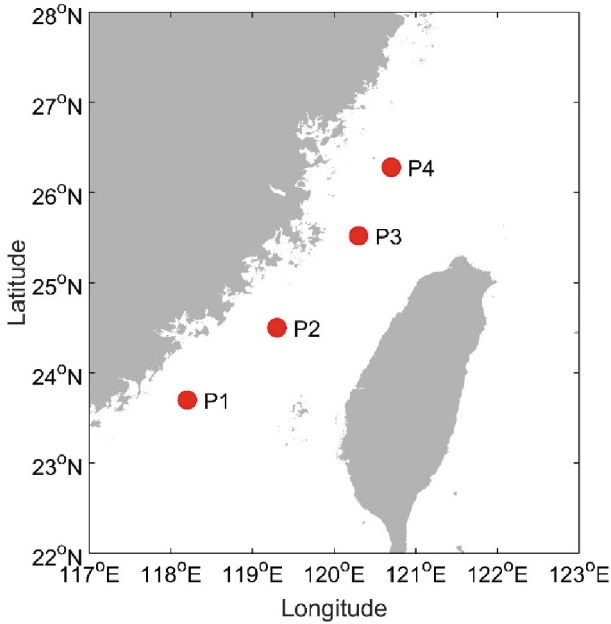


Fig. 1. Geographic location map of the buoy.

Table 1. Latitude and longitude of buoys.

Point	Longitude	Latitude	Number	Proportion
P1	118.20°E	23.70°N	6979	79.44%
P2	119.30°E	24.50°N	6502	74.01%
P3	120.30°E	25.52°N	7759	88.32%
P4	120.70°E	26.28°N	7439	84.68%

E_k , m and v represent wind energy, air quality and wind speed, respectively. The air quality can be rewritten as the product of the air density and the air volume passing through the cross section during that time period. Therefore, formula (1) can also be written as follows:

$$E_k = \frac{1}{2}(\rho Avt)v^2 = \frac{1}{2}\rho Av^3 t \quad (2)$$

In the above formula, ρ , A , v and t are the air density, cross-sectional area, wind speed and time, respectively.

According to formula (2), the relationship between wind potential and wind speed is the third power, and wind potential can be expressed as:

$$P(v) = \frac{1}{2}\rho Av^3 \quad (3)$$

According to formula (3), the wind energy density can be written as:

$$P_d(\rho, v) = \frac{1}{2}\rho v^3 \quad (4)$$

Here, the air density of the sea surface is 1.292 kg/m^3 in the Fujian Sea areas. All the equations used above are quoted from the literature [11].

2.3 Configuration of WRF Model

WRF model was developed by a number of research centers, as well as various universities and research institutions in the United States, in the year 2000 [15]. The WRF model can meet the needs of various operational forecasting and academic research under different spatial scales. It mainly focuses on weather forecasting and simulation research in the mesoscale.

In this study, the WRF4.1.2 version was used for simulation and analysis of the research areas, and ERA5 reanalysis data were used as input meteorological data. The simulation uses three two-way nested domains, the center of the study area is 119°E and 24°N , the horizontal resolution is 27 km, 9 km and 3 km, with grid numbers of 120×120 , 232×232 , and 304×304 , respectively. Data was output every 3 h for the outer layer and every hour for the middle layers and inner layers. The simulation adopts the Mercator projection, with a time integration step of 120 s for the outer layer, 37 vertical layers, and a top pressure of 5000 Pa. Based on preheating experiments and relevant literature review, the simulation was started 6 h in advance, that is, each simulation lasted for 30 h, and the simulated results of the innermost nested domain in the last 24 h were compared with the observed data [16, 17]. The simulation time is from 0:00 on January 1, 2019 to 0:00 on January 1, 2022, a total of three years. The physical parameterization schemes are shown in Table 2 and the simulation domain is shown in Fig. 2. The cumulus parameterization scheme of the innermost d03 domain is turned off [18]. The outer domain d01 covers a latitude range of 8.16°N to 38.12°N and a longitude range of 102.45°E to 135.55°E . The middle domain d02 covers a latitude range of 16.01°N to 35.27°N and a longitude range of 110.49°E to 132.00°E . The inner domain d03 covers a latitude range of 19.89°N to 28.47°N and a longitude range of 115.04°E to 124.45°E .

2.4 WRF Model Performance Evaluation

In this section, the measured data and simulated data of wind speed from 0:00 on January 1, 2020 to 0:00 on January 1, 2021 are selected. In the selection of simulated data, the nearest neighbor interpolation method is used to compared with the measured wind speed, and the time series diagram is shown in Fig. 3. The error analysis index used R, MAE, RMSE, rMAE and rRMSE, and the error analysis results are shown in Table 3.

From Fig. 3, the simulated wind speed and the measured wind speed fit well on the overall trend, and the WRF model can better capture the actual wind speed change situation, and the two have a strong correlation. In the comparison of wind speed, the deviation in summer is relatively large, and the trend of other seasons is consistent.

WPS Domain Configuration

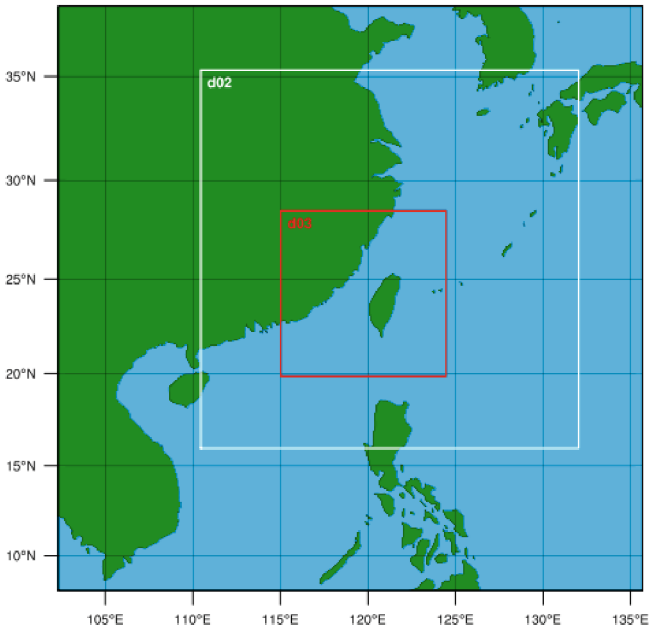


Fig. 2. Settings of the simulated sea areas.

Table 2. Configuration of the WRF model.

Parameterization	Configuration
Microphysics	Purdue Lin
Cumulus Parameterization	Kain-Fritsch
Longwave Radiation	RRTM
Shortwave Radiation	Dudhia
Planetary Boundary layer	Yonsei University (YSU)
Surface Layer	Revived Monin-Obukhov (Revised MM5)
Land Surface	Unified Noah land surface layer

According to Table 3, the R values are around 0.86 at P4 and above 0.90 at all other points, with an average of 0.91. The MAE values are all less than 1.50 m/s, with the best simulation performance at P1 (1.19 m/s) and the worst at P4 (1.48 m/s), with an average of around 1.31 m/s. The RMSE is less than 2.00 m/s, with an average of 1.75 m/s. In terms of rMAE, P2 has the smallest value at only 13.03%, while P4 has the largest value at 16.54%, fluctuating around 15%. The average value of rRMSE is 19.79%, P2 has the smallest value at only 18.07%.

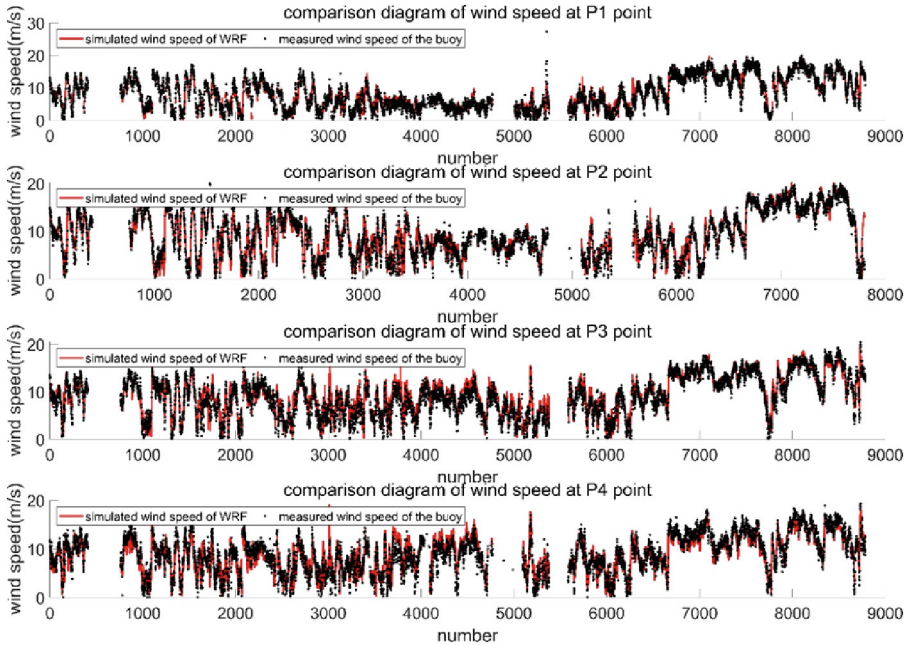


Fig. 3. Comparison diagram of the WRF model wind speed and the measured wind speed of the buoy.

Table 3. Error index of the wind speed.

Point	R	MAE(m/s)	RMSE(m/s)	rMAE	rRMSE
P1	0.9443	1.1859	1.5926	14.37%	19.30%
P2	0.9338	1.2078	1.6756	13.03%	18.07%
P3	0.9094	1.3682	1.8069	15.29%	20.19%
P4	0.8664	1.4778	1.9296	16.54%	21.60%
Average	0.9135	1.3099	1.7512	14.81%	19.79%

3 Results

3.1 Annual Average Wind Energy Characteristics Analysis

In this section, the 10 m height wind data was simulated for three years. From Fig. 4, the annual average wind energy density is mainly between 400–700 W/m², with the maximum value appearing in the Taiwan Strait, which can reach over 1000 W/m² and gradually decreases towards the surrounding areas.

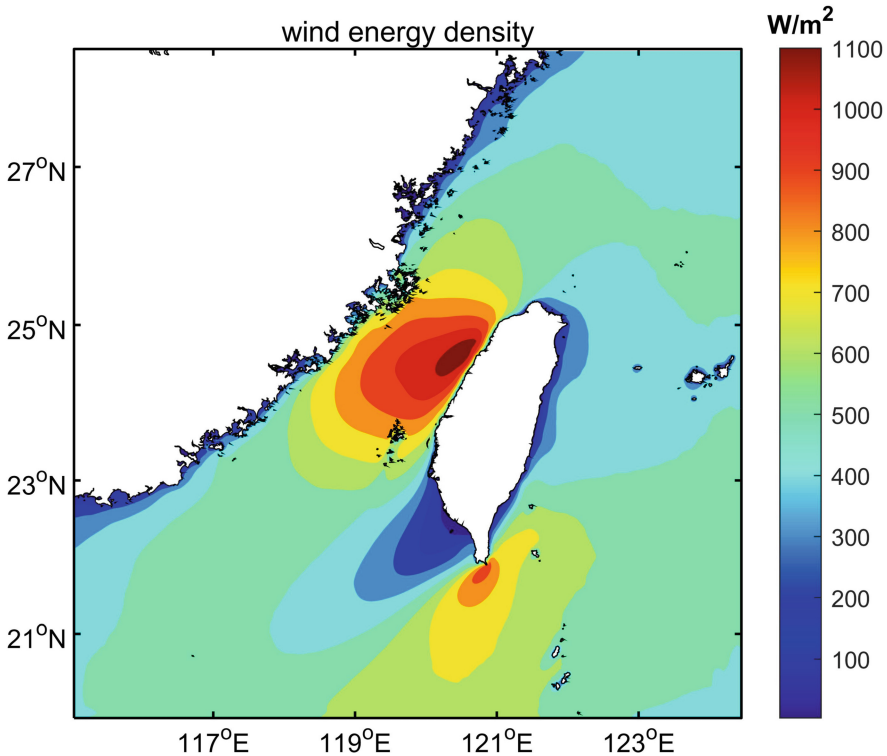


Fig. 4. Annual average wind energy density distribution in Fujian Sea areas.

3.2 Seasonal Average Wind Energy Characteristics Analysis

According to Fig. 5, the wind energy density in autumn and winter is the largest, with a maximum value of $1500 W/m^2$, and it in spring and summer is relatively small, with a maximum value of only $700 W/m^2$. In winter, it is mainly distributed in the range of $600\text{--}1000 W/m^2$, in spring in the range of $300\text{--}500 W/m^2$, in summer in the range of $200\text{--}450 W/m^2$, and in autumn within the range of $400\text{--}800 W/m^2$. The maximum wind energy density is distributed near the Taiwan Strait. The relatively large values in spring and summer are distributed in the eastern of the Fujian Sea areas, and in autumn and winter are distributed in the southwest of the Fujian Sea areas.

3.3 Monthly Average Wind Energy Characteristics Analysis

According to Fig. 6, the monthly average wind energy density is highest in October, November, and December, with the maximum value reaching over $2000 W/m^2$. Moreover, the wind energy density distribution during these three months is similar in spatial position, with the maximum value appearing in the Taiwan Strait, while the other high values are located in the southwest of Fujian Sea areas. In January, it is relatively high in the southwest of Fujian Sea areas and small in the eastern of Fujian Sea areas, with the

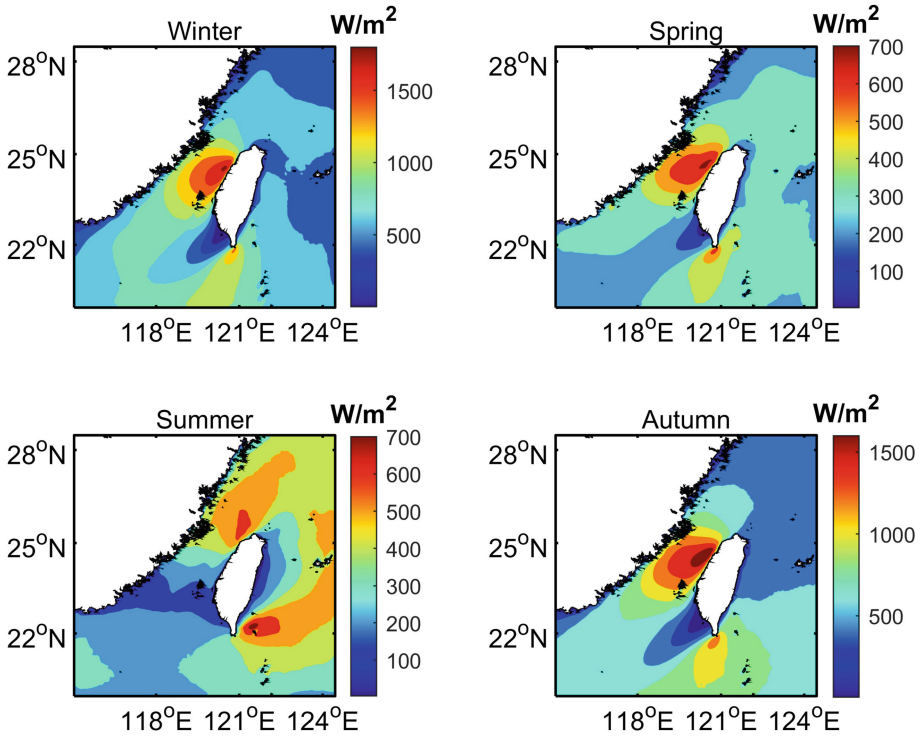


Fig. 5. Seasonal average wind energy density distribution in Fujian Sea areas

maximum value reaching over 1400 W/m^2 . In February, it is distributed around $400\text{--}800 \text{ W/m}^2$. The distribution of wind energy density in March and April is similar, with the maximum value around 800 W/m^2 . It is the lowest in May, with the maximum value only reaching 400 W/m^2 . In the four months of June, July, August, and September, the spatial distribution of wind energy density shows a trend of being small in the southwest of Fujian Sea areas and large in the eastern of Fujian Sea areas.

3.4 Analysis of the Wind Energy Density Rose Diagram

This section analyzes the WRF simulation data at four locations in the sea areas. The location distribution and coordinate positions of the points are shown in Fig. 1 and Table 1. The wind energy density rose diagrams of WRF data for the four points are shown in Fig. 7, with the first row showing the P1 and P2 points, and the second row showing the P3 and P4 points. According to Fig. 7, the dominant wind direction of P1 and P3 is NE direction, while the dominant wind direction of P2 and P4 is NNE direction. Compared with other points, P2 has the highest wind energy density, indicating that it has the most abundant wind energy resources. The main wind directions for the four points are NE and NNE, indicating that the northeast wind has a wide impact on the sea areas.

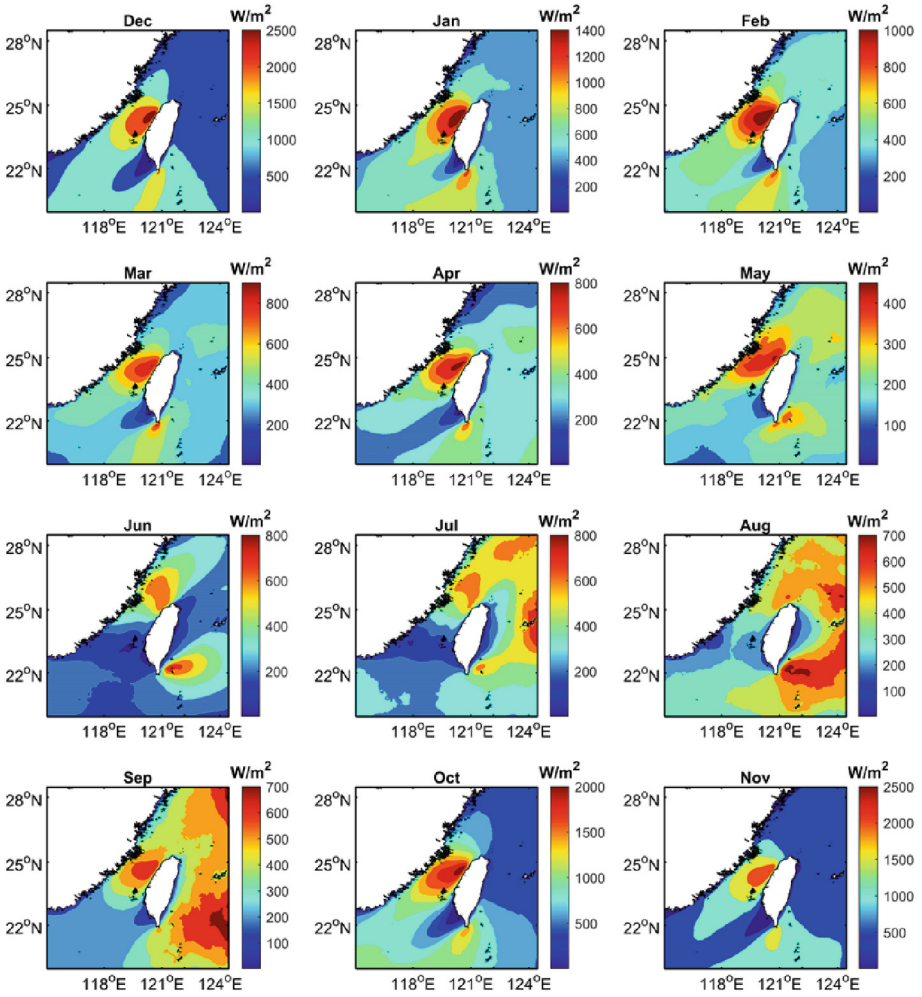


Fig. 6. Monthly average wind energy density distribution in Fujian Sea areas

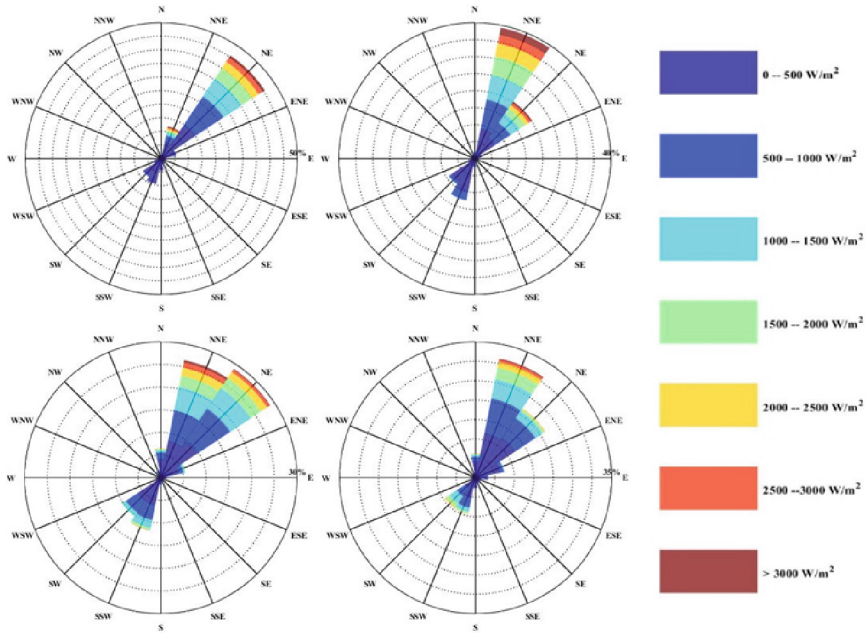


Fig. 7. Wind energy density rose diagram of WRF simulation data at P1, P2, P3 and P4 points.

4 Conclusion

This study uses the WRF model to evaluate the wind energy in the Fujian sea areas from 2019 to 2021. The buoy data is used for validation, and the agreement between the two is good, with MAE less than 1.5 m/s and RMSE less than 2.0 m/s. The results indicate that:

- (1) The maximum wind energy density in the Fujian Sea areas is distributed in the Taiwan Strait, with an annual average wind energy density distributed in the range of 400–700 W/m^2 , and the maximum value can reach over 1000 W/m^2 . The seasonal average wind energy density distribution is small in spring and summer, and large in autumn and winter. The monthly average wind energy density is highest in October, November, and December, with a maximum value exceeding 2000 W/m^2 , while it is lowest in May, only reaching 400 W/m^2 .
- (2) According to the wind energy density rose diagram, the main wind directions in the Fujian Sea areas are NE and NNE. The wind energy in Fujian Sea areas is abundant, which is conducive to the development of offshore wind power. When constructing wind farms, the incoming winds in the direction of NE and NNE should be given priority to improve the utilization efficiency of wind energy resources.

References

1. Chang, L., Saydaliev, H.B., Meo, M.S., et al.: How renewable energy matter for environmental sustainability: evidence from top-10 wind energy consumer countries of European Union. *Sustain. Energy Grids Netw* **31**, 100716 (2022)
2. Siram, O., Sahoo, N., Saha, U.K.: Changing landscape of India's renewable energy and the contribution of wind energy. *Clean. Eng. Technol.* **8**, 100506 (2022)
3. Zheng, C.W., Pan, J.: Assessment of the global ocean wind energy resource. *Renew. Sustain. Energy Rev.* **33**, 382–391 (2014)
4. Chen, Y., Lin, H.: Overview of the development of offshore wind power generation in China. *Sustain. Energy Technol. Assess.* **53**, 102766 (2022)
5. Zheng, C., Pan, J., Li, J.: Assessing the China Sea wind energy and wave energy resources from 1988 to 2009. *Ocean Eng.* **65**, 39–48 (2013)
6. Saidur, R., Islam, M.R., Rahim, N.A., et al.: A review on global wind energy policy. *Renew. Sustain. Energy Rev.* **14**(7), 1744–1762 (2010)
7. Mattar, C., Borvarán, D.: Offshore wind power simulation by using WRF in the central coast of Chile. *Renewable Energy* **94**, 22–31 (2016)
8. Shimada Susumu, O.T.: Accuracy and characteristics of offshore wind speeds simulated by WRF. *Sci. Online Lett. Atmos.* **7**, 21–24 (2011)
9. Luo, M.S., He, L., Peng, H.Q.: Assessment of Jiangsu coastal wind resources based on the WRF model. *Jiangsu Agric. Sci.* **39**(3), 486–549 (2011). (in Chinese)
10. Li, D.H.: Numerical Assessment of Wind and Wave Energy Resources in the Blue and Yellow Area of Shandong Peninsula. Ocean University of China (2015) (in Chinese)
11. Dong, S., Gong, Y., Wang, Z., et al.: Wind and wave energy resources assessment around the Yangtze River Delta. *Ocean Eng.* **182**, 75–89 (2019)
12. Dong, S., Gong, Y., Wang, Z.: Long-term variations of wind and wave conditions in the Taiwan Strait. *Reg. Stud. Mar. Sci.* **36**, 101256 (2020)
13. Wen, Y., Kamranzad, B., Lin, P.: Joint exploitation potential of offshore wind and wave energy along the south and southeast coasts of China. *Energy* **249**, 123710 (2022)
14. Guo, X., Han, Z., Liao, K.: Assessment of wind energy potential in shallow water offshore China based on ERA5 reanalysis data. *Mar. Sci. Bull.* **41**(3), 325–335 (2022). (in Chinese)
15. Mao, Q.R., Zhang, Q.H., Chen, T.Q.: Application of a coupled atmosphere-ocean-wave model in typhoon process simulation. *Mar. Sci. Bull.* **39**(3), 309–315 (2020). (in Chinese)
16. Gholami, S., Ghader, S., Khaleghi-Zavareh, H., et al.: Sensitivity of WRF-simulated 10 m wind over the Persian Gulf to different boundary conditions and PBL parameterization schemes. *Atmos. Res.* **247**, 105147 (2021)
17. Che, Y., Salazar, A., Peng, S., et al.: A multi-scale model for day-ahead wind speed forecasting: a case study of the Houhoku wind farm, Japan. *Sustain. Energy Technol. Assess.* **52**, 101995 (2022)
18. Zhong, X., Wei, K., Shen, Z.H., Ti, Z.L.: WRF-based simulation of wind field and asymmetry feature of radius to maximum winds during typhoon Maria. *Eng. Mech.* **39**(S1), 389–396 (2022). (in Chinese)



Case Analysis of a Squall Line Process in Beijing Area in 2021

Jianjun Geng^(✉) and Lei Lei

Beijing Weather Forecast Center, Beijing 100097, China
77933297@qq.com

Abstract. From 18:00 June 25, 2021 to 01:00 June 26, 2021 a squall line appeared in Beijing. Synoptic scale environment conditions, physics parameters fields, Beijing Doppler radar products are analyzed. Results are as follows. 1) At 500 hPa, Beijing was in front of trough which from mid-eastern inner Mongolia to central Hebei. Temperature trough lagging behind height trough over the baroclinic zone in the troposphere is favorable to system developing. Surface chart shows high east and low west situation. 2) Beijing located in the center of 850 hPa θ_{se} high energy zone, which does benefit to accumulate and trigger of unstable energy for convective weather. 3) Sounding analysis at 14:00 June 25 showed that the curve of temperature and dew point temperature was trumpet shape from bottom to top. The distribution form of upper dry and lower wet and the appropriate height of 0° layer and -20° layer were beneficial to the occurrence of large hail. The vertical shear of the wind direction was a clockwise rolling flow, when the low-level water vapor supply was sufficient, convection development was an important indicator of severe convective weather. 4) Reflectivity factor profile showed obvious echo wall, highly suspended strong echo, bounded weak echo region, the obvious jump of VIL, the appearance of Z_{DR} column and K_{DP} $4.3^\circ/\text{km}$ at corresponding time indicated the occurrence of hail. Analysis of radial velocity map showed that the ambiguity of radial velocity is closely related to the extreme wind at ground stations.

Keywords: θ_{se} High Energy Zone · Bounded Weak Echo Region · Z_{DR} Column · Velocity Ambiguity

1 Introduction

Due to its vast territory, diverse terrain, and unique geographical and environmental factors, China has been affected by various natural disasters for a long time. Among them, meteorological natural disasters have the greatest impact, characterized by numerous types, high frequency of occurrence, wide distribution area, and long duration. The losses caused by strong convective weather account for more than half of the total losses caused by meteorological disasters. Squall lines, as a mesoscale weather system that causes severe convective weather, are usually composed of multiple active thunderstorm cells arranged in a quasi linear mesoscale convective system. They are about tens to hundreds of kilometers in length, 20 to 50 km in width, and have a life cycle of several

to ten hours, leading to serious meteorological disasters [1–3]. With the application of advanced detection technologies such as Doppler weather radar and the development of mesoscale numerical models, the study of squall line cases has become more in-depth. Foreign scholars have analyzed the statistical characteristics of squall lines and mesoscale convective organization models using radar echo data [4–6], and provided a conceptual model of mature squall lines. Domestic scholars have also done a lot of research from the ground mesoscale physical characteristics, diabatic heating process, boundary layer mesoscale convergence line, terrain induced and maintained squall line structure, and the impact of initial convection and cloud physics schemes on the numerical simulation results of squall line [7–12].

From 18:00 on June 25 to 01:00 on June 26, 2021, a squall line weather process occurred in the Beijing area, accompanied by strong convective weather such as thunderstorms, strong winds, short-term heavy rainfall, and hail. This article uses conventional observation data, Doppler dual polarization radar data, and automatic station data to analyze the causes and characteristics of a squall line weather process that occurred in the Beijing area on June 25, 2021, in order to contribute to the nowcasting of the squall line weather process.

2 Real-Time Weather Data

On June 25, 2021 at 19:42, a squall line was formed in the northern region of Beijing, and then moved southeast by east. At 01:00 on June 26, the precipitation echo basically moved out of Beijing. Affected by the squall line, there are 22 stations with rainfall exceeding 50 mm in the city, and 2 stations with rainfall exceeding 70 mm (70.2 mm in Zhenluoying, Pinggu and 81.2 mm in Chazigou, Miyun). At 20:20 in Yanqing, a hailstone with a diameter of 4.5 cm appeared. The maximum wind speed at Yanqing Racing Station 1 reached 27.4 m/s.

3 Environmental Condition Analysis

A comprehensive analysis of the data from various layers at 08:00 on the 25th shows that the hailstorm area is located in front of the 500 hPa temperature trough (see Fig. 1). The eastward movement of the temperature trough cools the upper atmosphere, increases the vertical decrease rate of temperature, and increases the potential instability of the atmosphere. The 500 hPa temperature trough lags behind the height trough, and the system has strong baroclinic properties. Beijing is located in front of the trough, and the positive vorticity advection is obvious. There is a cyclonic circulation near Beijing at 700 hPa, which is conducive to upward movement; at 850 hPa Beijing is also located in front of the height trough, and the temperature trough lags behind the height trough. At the same time, it has a dry and cold upper layer structure and a warm and wet lower layer structure, which is conducive to further exacerbating the instability of the stratification. On the sea level pressure field at 08:00 on the 25th (see Fig. 2), Beijing is in a situation of high in the east and low in the west. Under the influence of the easterly wind behind the high pressure, high-energy and high humidity from the East China Sea and Bohai Sea flows towards Beijing, which is conducive to precipitation generation.

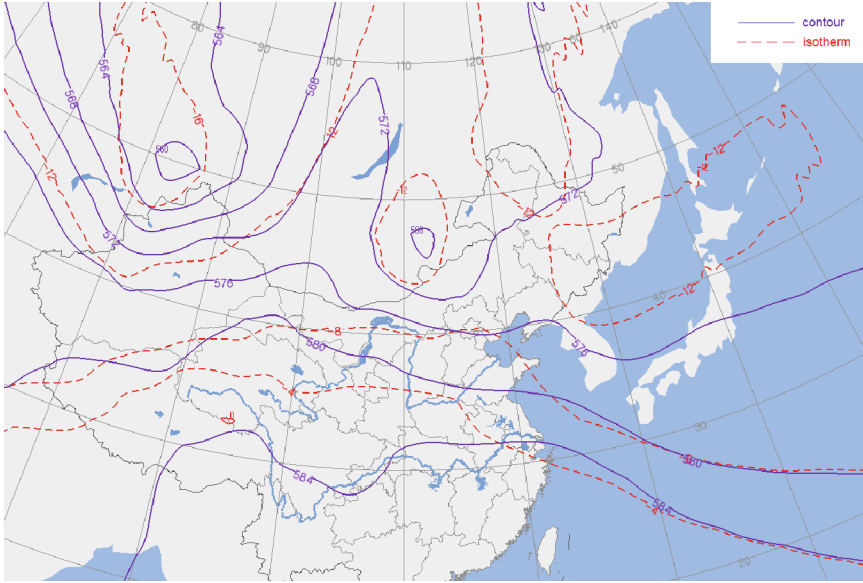


Fig. 1. 500 hPa high altitude situation field at 08:00 on June 25, 2021.

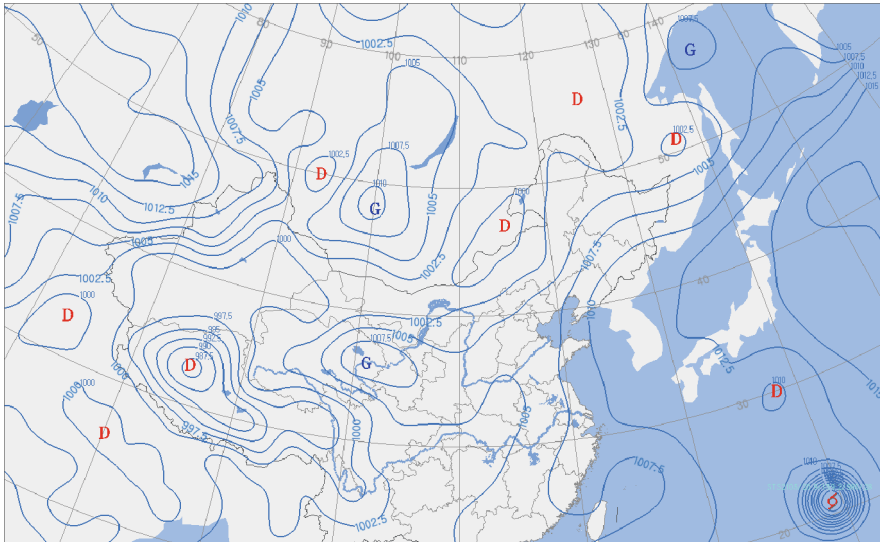


Fig. 2. Sea level pressure field at 08:00 on June 25, 2021.

The occurrence of heavy precipitation requires sufficient water vapor supply in the lower layers. The richer the water vapor, the greater the corresponding precipitation under the same conditions. Therefore, the specific humidity of 1000 hPa and the corresponding level of water vapor flux divergence were analyzed at 08:00 on the 25th. From the

1000 hPa specific humidity and water vapor flux divergence, it can be seen that the specific humidity in Beijing is greater than 14 g/kg, providing abundant water vapor for subsequent precipitation. At the same time, the water vapor flux divergence in Beijing reaches $-10 \times 10^{-7} g \cdot s^{-1} \cdot cm^{-2} hPa^{-1}$ is conducive to the convergence and horizontal transport of water vapor, and has a positive impact on the maintenance of precipitation.

θ_{se} (pseudo equivalent potential temperature) is a comprehensive characteristic quantity that characterizes atmospheric temperature, pressure, and humidity, and its distribution reflects the distribution of energy in the atmosphere. From the θ_{se} distribution map of 850 hPa at 08:00 on the 25th (see Fig. 3), it can be seen that Beijing is located in the center of the southwest northeast direction θ_{se} high energy zone with a central intensity of 64 °C, which is conducive to the occurrence of strong precipitation.

From the sounding curve of 14:00 54511 (Beijing) station (see Fig. 4), it can be observed that the temperature and dew point temperature curves show a trumpet shaped shape from bottom to top, and the distribution of dry and wet from top to bottom is conducive to the occurrence of large hail. The Convective Available Potential Energy (CAPE) jumped from 35.1 J/kg at 08:00 to 949.5 J/kg at 14:00, with lower elevated condensation height (840 hPa), convective condensation height (927 hPa), and free convection height (999 hPa), making it easy to trigger convection. The high value of the K index (33.4 °C) indicates good conditions for convection to occur. The height of the 0 °C layer is 3944 m, and the height of the -20 °C layer is 7408 m, which is conducive to the formation of hail. A SHEAR0-6 km speed of 16.1 m/s is conducive to the formation of organized storms. According to the calculation of sounding data from station 54511 at 14:00, the temperature difference between the 850 hPa and 500 hPa layers reaches 26.4 °C, which is converted into a vertical temperature reduction rate of about 6.1 °C/km. A larger vertical temperature reduction rate is beneficial for hail and thunderstorm weather [13].

V represents the observed data of wind direction and speed in the sounding data (see Fig. 5), while 3 θ Refers to θ (potential temperature) θ_{sed} (pseudo equivalent potential temperature based on dew point) and θ^* (saturated pseudo equivalent potential temperature). Therefore, comparing the vertical distribution of the three lines through horizontal wind direction not only enables us to understand the sources of wind and the vertical shear characteristics of airflow at different heights, but also the instability of the troposphere and the water vapor characteristics of the atmosphere. The precursor information of atmospheric instability is reflected in the bending of the characteristic layer, and abnormal bending in the middle and upper troposphere usually corresponds to cold stratiform clouds or ultra-low temperature phenomena, which also means the development of strong convective conditions. The 3 θ potential temperature line has multiple twists and turns, indicating that the vertical structure of the atmosphere is extremely uneven and accumulates unstable energy in this figure.

The vertical shear of the wind direction in the atmospheric wind direction can also be observed in V-3 θ . As reflected in the figure, the vertical direction of wind direction circulation is called rolling flow. In the northern hemisphere, when the lower level is easterly or southerly, and the upper level is westerly or northerly, it is called a forward rolling flow. At this time, the water vapor supply in the lower level is sufficient, and

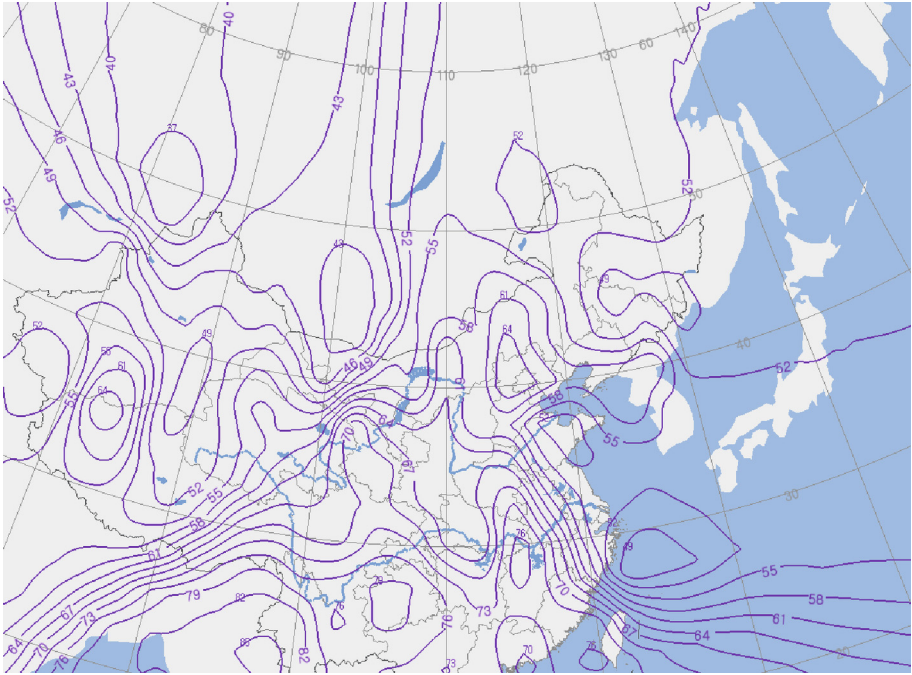


Fig. 3. The pseudo equivalent temperature field at 850 hPa at 08:00 on June 25, 2021.

convection develops, which is an important sign of strong convective weather. The V-30 figure at 14:00 on June 25, 2021 conforms to the characteristics of the logo.

4 Analysis of This Process by Dual Polarization Radar

4.1 Analysis of Radar Reflectivity Factor

It can be seen from the radar reflectivity factor intensity map at different times observed by the radar in the southern suburbs of Beijing on June 25 that since 18:30 (see Fig. 6(a)), the echo of convection cell with a central intensity of 55 dBZ is about 165 km away from the northwest of the radar station, and the echo of convection cell with a central intensity of 59 dBZ is about 150 km away from the north of the radar station, moving southeast at a speed of about 50 km/h. During the movement, the echo intensity located in the northwest of the radar is continuously strengthened to 61 dBZ, the echo intensity located in the north of the radar station remains basically stable. At 18:48 two echoes simultaneously entered the northern regions of Huairou and Yanqing in Beijing (see Fig. 6(b)). Subsequently, the individual continued to develop and move towards a southerly direction, while echoes continued to mature in the northwest and gradually merged with the aforementioned echoes. At 19:42, a squall line with a length of about 200 km and a width of about 30 km was formed (see Fig. 6(c)), with a strong central intensity of 63 dBZ. Subsequently, the squall line moved southeast at a speed of 130 km/h, and its intensity remained basically

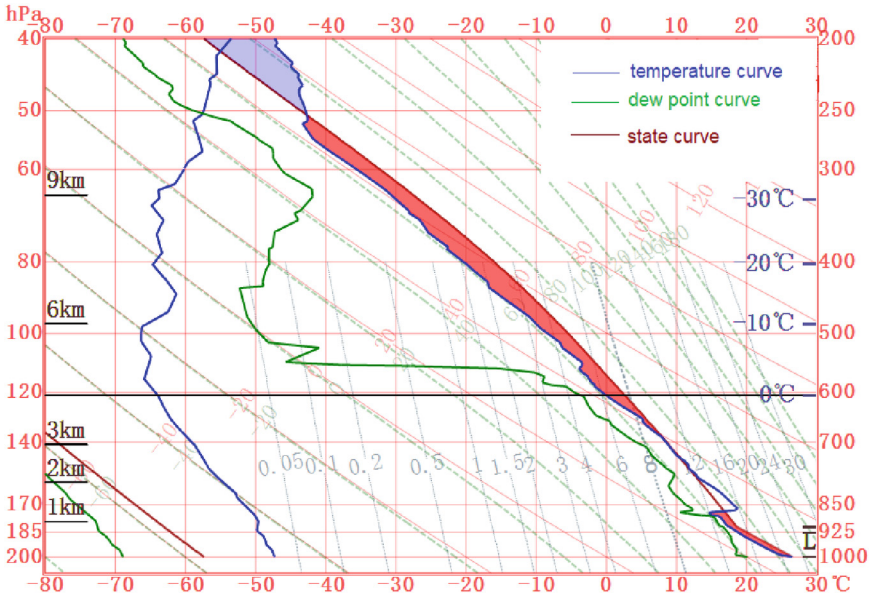


Fig. 4. Sounding diagram of station 54511 at 14:00 on June 25, 2021.

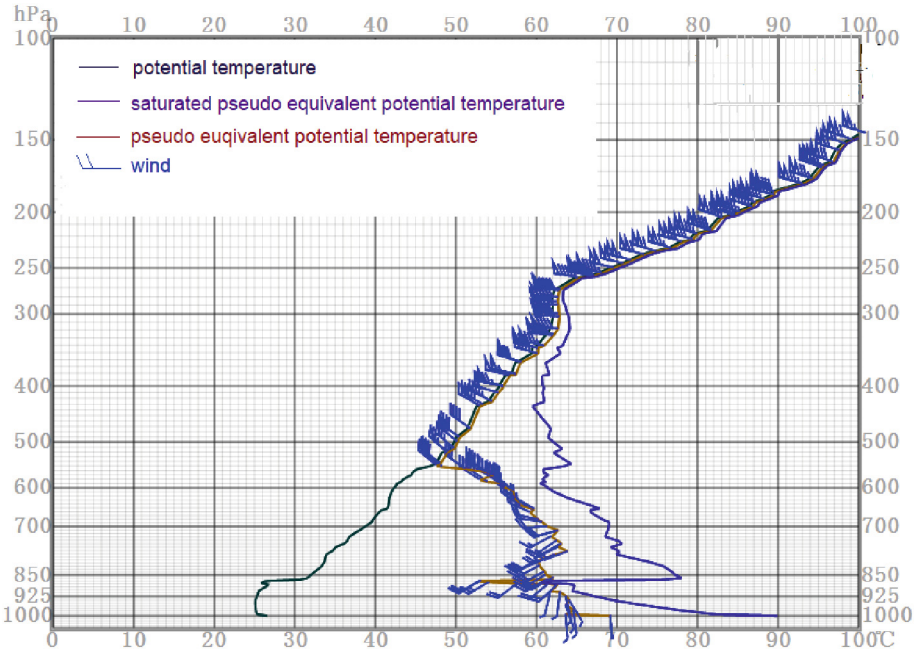


Fig. 5. V-3 θ chart of station 54511 at 14:00 on June 25, 2021.

stable. At 01:12 on the 26th, the precipitation echo moved out of Beijing (see Fig. 6 (d)). The squall line caused severe convective weather such as hail, local rainstorm, thunderstorm and gale in Beijing during its movement.

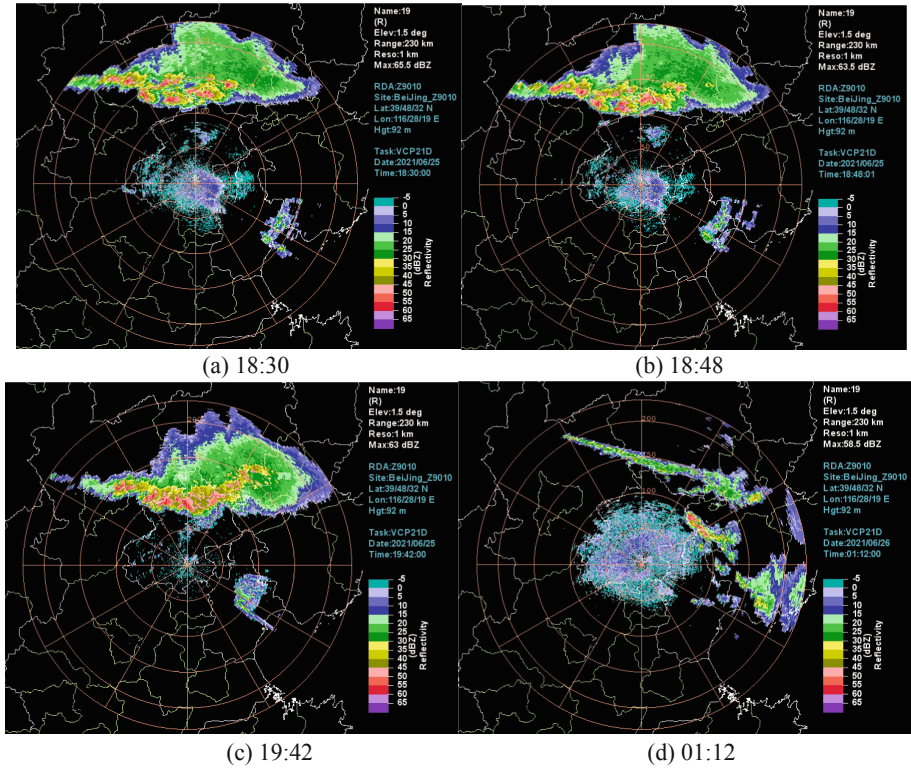


Fig. 6. 1.5° reflectivity factor intensity map.

4.2 Vertical Profile Analysis of Reflectivity Factor

The vertical profile of the 20:18 reflectivity factor along the blue line (see Fig. 7) shows a clear echo wall (with a strong echo center extending to over 10 km), a highly suspended strong echo, and a bounded weak echo region structure, indicating the occurrence of hail (see Fig. 8).

4.3 Radial Velocity Analysis

It can be seen that there is a velocity ambiguity zone in the red ellipse (see Fig. 9), which is a possible sign of strong ground winds. Ground observations have also confirmed this. At 20:15, the maximum wind speed of Yanqing Racing Station 1 near this velocity ambiguity zone is 26.4 m/s.

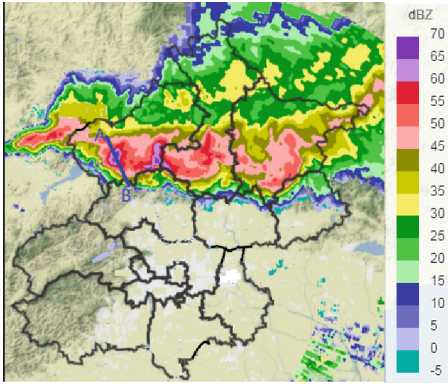


Fig. 7. Reflectivity factor diagram at 20:18.

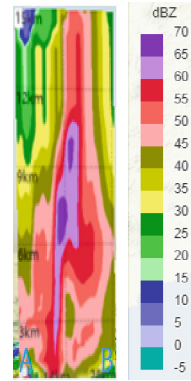


Fig. 8. Vertical profile of reflectivity factor at 20:18.

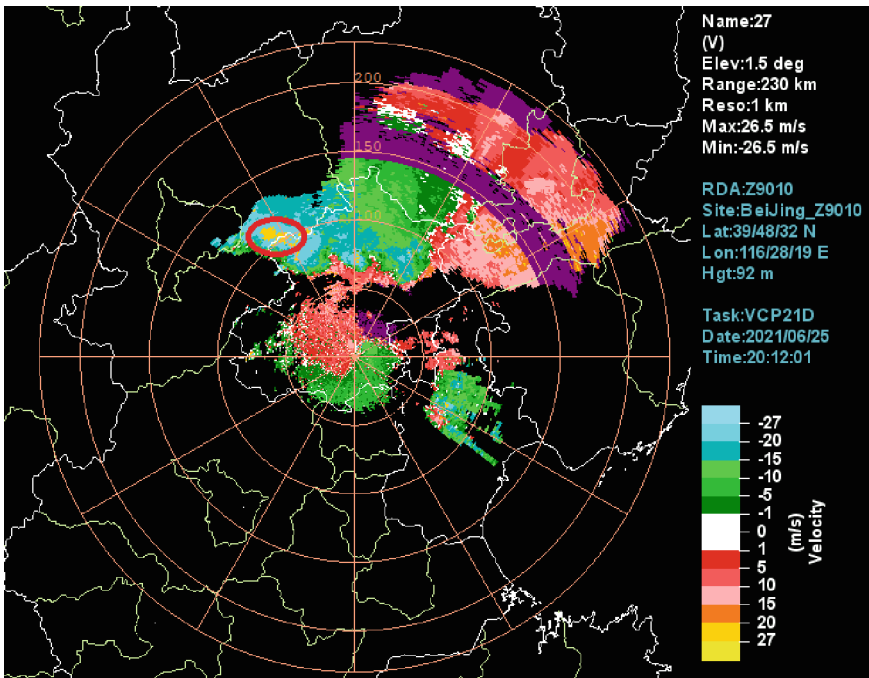


Fig. 9. 1.5° radial velocity map at 20:12.

4.4 Analysis of Vertically Integrated Liquid Water Content

In the early 1970s, Greene et al. [14] proposed a new predictive factor – Vertical Integrated Liquid (VIL) water content - for studying strong storms. VIL refers to the conversion of the radar reflectivity factor value into an equivalent amount of liquid water, reflecting the total amount of liquid water in a vertical column of precipitation clouds

at a certain base area. In 1986, Winston et al. [15] found that VIL had a good indicating effect on the presence of hail.

A significant jump in VIL from 20:06 to 20:18 near Yanqing, from 25.5 kg/m^2 to over 60 kg/m^2 , maintaining the scanning time of the two individuals (see Fig. 10). This coincides with the timing of hail in Yanqing.

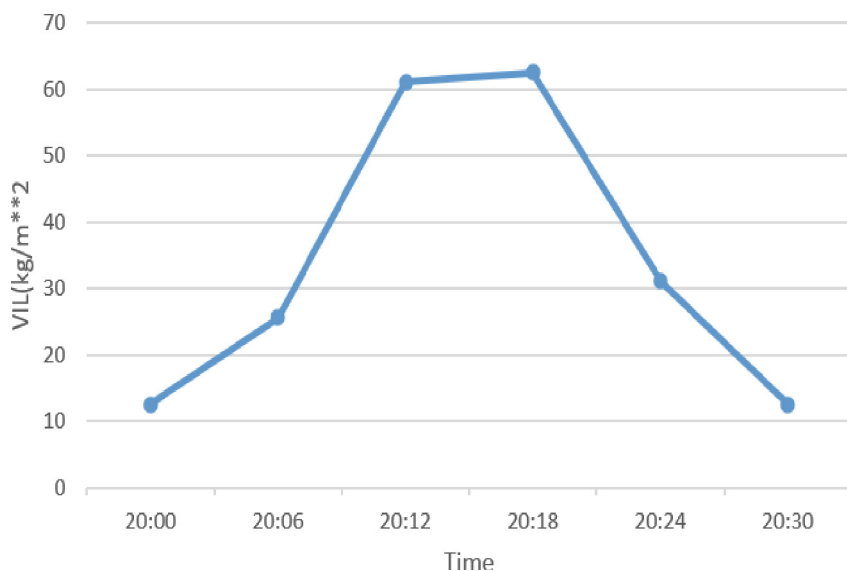


Fig. 10. VIL evolution map.

4.5 Differential Reflectivity Analysis

Dual-polarization Doppler weather radar can transmit and receive polarized waves in both horizontal and vertical directions. In addition to the reflectivity intensity, radial velocity and velocity spectrum width of conventional Doppler weather radar, the parameter such as Z_{DR} 、 K_{DP} of precipitation system can also be obtained. The radar's ability to detect strong convective weather such as hail has been significantly improved.

The variation of differential reflectivity in radar echoes is roughly consistent with the variation of reflectivity factor echoes. At 20:06, the central intensity of the strong echo near Yanqing reached 62 dBZ, with a corresponding Z_{DR} value of 4 dB (see Fig. 11). Its horizontal height is above 4 km, higher than the 0° layer height (3944 m). The differential reflectivity factor Z_{DR} column shows a high value range of Z_{DR} above the 0° layer height in the environment, located in the strong updraft zone of the storm. The appearance of this feature and the corresponding K_{DP} at $4.3^\circ/\text{km}$ (see Fig. 12) indicate the occurrence of hail, followed by hail at Yanqing Station, Huairou Liulimiao, and Yanqi Town.

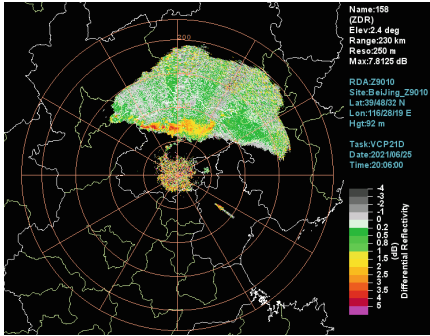


Fig. 11. 2.4° Differential reflectivity at 20:06.

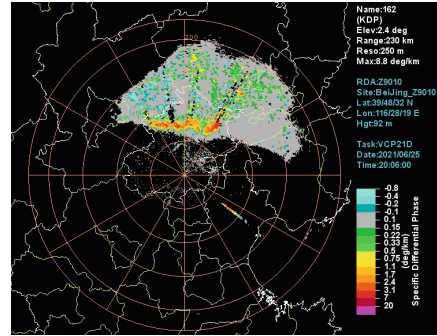


Fig. 12. 2.4° differential phase constant at 20:06.

5 Summary

- (1) On the high-altitude map, the temperature trough lags behind the height trough, and the system has strong baroclinic properties. Beijing is located in front of the trough, and the positive vorticity advection is obvious. On the ground map, Beijing is located in a situation of high in the east and low in the west. Under the influence of easterly winds at the back of high pressure, high-energy and high humidity from the East China Sea and Bohai Sea flow to Beijing, which is conducive to the generation of precipitation.
- (2) According to the analysis of the 1000 hPa physical field at 08:00 on the 25th, the specific humidity in the Beijing area is greater than 14 g/kg, providing abundant water vapor for subsequent precipitation. The performance of water vapor flux divergence is conducive to the convergence and horizontal transport of water vapor, and also has a positive impact on the maintenance of precipitation. Beijing is located in the center of the southwest northeast direction θ_{se} high energy zone, which is conducive to the occurrence of strong precipitation.
- (3) At 14:00, the sounding analysis showed that the temperature and dew point temperature curves showed a trumpet shape from bottom to top, and the distribution of dry and wet from top to bottom was conducive to the occurrence of large hail. Elevated condensation height, convective condensation height, and free convection height are all relatively low, which can easily trigger convection. The appropriate height of the 0° and -20° layers is conducive to the formation of hail. SHEAR0-6 km is conducive to the formation of organized storms. From V-30 as can be seen from the figure, the vertical shear of the wind direction shows a forward rolling flow. At this time, the low-level water vapor supply is sufficient, and convection develops, which is an important sign of the occurrence of strong convective weather. The V-30 figure at 14:00 on the 25th conforms to the characteristics of the logo.
- (4) The vertical profile of the reflectivity factor shows obvious echo walls (with echo centers extending to over 10 km), highly suspended strong echoes, bounded weak echo region structures, significant VIL jumps, differential reflectivity factor Z_{DR}

columns, and the corresponding occurrence of K_{DP} at $4.3^\circ/\text{km}$ indicate the occurrence of hail. The analysis of the radial velocity map shows that the ambiguity of radial velocity is closely related to extreme winds at ground stations.

References

1. Li, Z.C.: Pay attention to the research and prevention of meteorological disasters. *Technol. Rev.* **26**(8), 10 (2008)
2. He, J.H., Guo, P.W., Yin, Y., et al.: *Introduction to Atmospheric Science*. China Meteorological Press, Beijing (2012)
3. Shou, S.W., Li, S.S., Shou, Y.X., et al.: *Mesoscale Atmospheric Dynamics*. Higher Education Press, Beijing (2009)
4. Houze, R.A., Jr.: Structure and dynamics of a tropical squall line system. *Mon. Wea. Rev.* **105**(12), 1540–1567 (1977)
5. Chen, G.T., Chou, H.C.: General characteristics of squall lines observed in TAMEX. *Mon. Wea. Rev.* **121**(3), 726–733 (1993)
6. Parker, M.D., Johnson, R.H.: Organizational modes of midlatitude mesoscale convective systems. *Mon. Wea. Rev.* **128**(10), 3413–3436 (2000)
7. Gao, K., Zhang, D.L.: The role of non-adiabatic physical processes in simulating the medium β -scale structure of a squall line system. *J. Meteorol.* **52**(3), 321–331 (1994)
8. Dong, H., Xu, H.M., Luo, Y.L.: The effect of cloud condensation nodule concentration on squall line precipitation simulation in WRF model: a comparative study of different cloud microphysics parameterization schemes. *Atmos. Sci.* **36**(1), 145–169 (2012)
9. Shen, H.F., Zhai, G.Q., Zhu, B.Q., et al.: Numerical experiments on the impact of mesoscale convergence lines on the development of squall lines along the Zhejiang coast. *Atmos. Sci.* **34**(6), 1127–1139 (2010)
10. Wang, C., Wei, M.: Diagnostic analysis and numerical simulation for the birth of squall line in Jiangsu. *Sci. Technol. Eng.* **20**(2), 481–488 (2020)
11. Li, B., Wu, L.G.: Application of automatic meteorological station data in the simulation of a squall line in north Jiangsu. *J. Trop. Meteorol.* **35**(6), 789–800 (2019)
12. Yuan, Z.H.: Sensitivity of a nocturnal squall line to atmospheric conditions. *Acta Meteor. Sin.* **79**(6), 977–1001 (2021)
13. Zheng, Y.G., Tao, Z.Y., Yu, X.D.: Some essential issues of severe convective weather forecasting. *Meteorol. Monthly* **43**(6), 641–652 (2017)
14. Greene, D.R., Clark, R.A.: An indicator of explosive development in severe storms. In: 7th Conference on Severe Local Storms, Missouri (1971)
15. Winston, H.A., Ruthi, L.J.: Evaluation of RADAP II severe storm detection algorithms. *Bull. Amer. Meteor. Soc.* **61**(2), 142–150 (1986)



Research on Ecological Environment Impacts Assessment During the Construction Period of Railway Projects

Jieyu Zhang¹, Yitong Yin², Xiuhong Li²(✉), Yanrong Lu², and Yuying Zhang²

¹ Energy Saving and Environmental Protection and Occupational Safety and Health Research Institute, China Academy of Railway Sciences Co., Ltd., Beijing 100081, China

zhangjy@rails.cn

² State Key Laboratory of Remote Sensing Science, Faculty of Geographical Science, Beijing Normal University, Beijing 100875, China

lixh@bnu.edu.cn

Abstract. In recent years, with the rapid development of the national economy, China's railway construction industry has flourished, becoming the period with the most completed railway construction since the founding of the People's Republic of China. However, while greatly promoting the rapid development of regional economy, the construction of railway might lead to land occupation, vegetation destruction, changes in the natural environment within the construction area and the ecological environment along the line, and also might change the original landscape structure and ecosystem function, bringing certain pressure to the ecological environment. By establishing ecological environmental quality as assessment index system and taking Nanping-Longyan Railway as the study case, this study calculated the quality index of ecological environment and ecological environment assessment index of railway construction project during the construction period, and carried out classification and change analysis of the ecological environment status. The results showed as follows: the railway ecological environment quality index is continuously increasing, indicating that the engineering construction has a small impact on the ecological environment, standardized construction, and high environmental governance, boosting the continuous improvement of ecological environment quality. The purpose of this paper is to find out the real changes in the ecological environment in the process of railway construction, provide basic data for railway environmental protection, and evaluate the quality of railway ecological environment, in order to provide technical support for railway environmental management decision.

Keywords: Railway Construction Projects · Construction Period · Nanping-Longyan Railway · Ecological Environmental Quality

1 Introduction

With the rapid development of the global transportation network, many developing countries and regions have increasingly strong demands for infrastructure projects such as highways and railways [1]. China's 13th Five-Year Plan calls for strengthening railway

construction to drive national construction. The 14th Five-Year Plan upgraded the “four vertical and four horizontal” railway network proposed in 2008 to the “eight vertical and eight horizontal” high-speed railway main channel, committed to the construction of a modern comprehensive transportation system [2]. As the main artery of national economy, key infrastructure and major livelihood projects [3, 4], railway plays an increasingly important role in economic and social development [5, 6].

There are abundant researches on ecological evaluation abroad. In 2012, IREM UCAL SARI et al. [7] used fuzzy analytic Hierarchy Process (FAHP) to evaluate Istanbul urban rail transit system under different risk factors, revealed the critical risk criteria of these systems, and carried out multi-criteria evaluation on the existing railway system to allocate scarce resources. In 2015, Mårten Karlson and UllaMörtberg [8] used GIS technology and FRAGSTATS software to evaluate the spatial ecology of road network fragmentation and disturbance in Sweden. In 2016, Erika Igondova proposed a “three-step” approach to the impact of road construction on the ecological environment in Slovakia, namely “investigation ecological resource assessment - ecological impact assessment”. By finding out specific criteria, such as duration, reversibility and road scale, the significance scale of ecological impact assessment is found for each criterion, so as to make the assessment results more detailed and reasonable. At the same time, foreign scholars have also conducted rich and extensive studies on the index system of eco-environmental impact assessment [9]. In 2018, Richard Damania, Jason Russ and others [10] simulated the interaction within the Democratic Republic of Congo through two simulations, the impact of infrastructure construction on ecological environment has been quantitatively studied. In 2018, ten recent environmental impact assessments conducted by Cathryn Clarke Murray et al. [11] in British Columbia, Canada, systematically reviewed and scored significance tests and methods used by assessors, the use of thresholds in significance tests, threshold exceedances and results. Governments and institutions can better protect resources in the above ways, so that the threshold set by the government has legal effect and accountability. In 2020, Cristina Mata et al. [12] built wildlife corridors on roads and railway lines to rebuild connectivity. However, little is known about whether predator-prey interactions bring down the effectiveness of cross structures. Finally, it is concluded that the number of more extensive structures can be increased during the construction process to bring down the risk of predator-prey encounter, and structural heterogeneity and shelter can be added to reduce the possibility of predator-prey interaction. To sum up, foreign countries attach great importance to the protection of the ecological environment, and researchers try different evaluation methods to establish a scientific index system. However, most of the environmental detection research during the construction period is still focused on the road, while the railway research is relatively few, so more attention should be paid to the railway.

The research and exploration on the protection of ecological environment in transportation engineering projects in China started relatively late, but the development speed is relatively fast. However, it is often concentrated on the environmental protection of highway, and the impact assessment of railway ecological environment is rarely studied. In 2006, Liu Li [13] found that the ecological impact assessment index was difficult to quantify, and adopted the dominance principle in landscape ecology to analyze the

changes of dominance before and after construction, so as to complete the impact assessment of the ecosystem. In 2007, Li Botao [14] established the PSR model, selected the impact indicators of railway ecological environment from the three aspects of “pressure”, “state” and “response”, and used the fuzzy analytic hierarchy process to evaluate the impact of railway ecological environment and obtained the evaluation results. In 2010, Zhang Xiaoyu [15] used the PSR model to establish the ecological risk index system of high-speed railway, and used the graph overlay method in GIS technology to evaluate each index respectively. Finally, grey clustering method was adopted to evaluate the overall impact of ecological environment. In 2016, Feng Caimin [16] adopted DSR model to select environmental risk indicators of railway from three aspects: “driving force”, “state” and “response”. In 2018, Hao Jingwen [17] used the improved BP neural network algorithm to establish an ecological environment evaluation index system from three aspects: ecology, environment and landscape, and evaluated the ecological impact of railway engineering on nature reserves.

The ecological environment monitoring plan for railway construction projects [18–20], including monitoring indicators, monitoring methods, monitoring scope, monitoring points, monitoring frequency, etc., is used to guide the design, implementation, and reporting of specific ecological environment monitoring plans for railway construction projects, especially the monitoring indicators and data acquisition methods. It can be integrated with national and regional ecological environment monitoring. In the process of railway construction projects, it is necessary to timely assess the impact of railway construction on the ecological environment and feed back to the environmental protection management of railway construction projects, so as to better guide the construction and help decision-making. In monitoring indicators and data acquisition methods [19, 21–25], it requires the guidance of ecological professional engineers to get such as vegetation coverage, vegetation index, biomass, and biodiversity acquisition and analysis, etc. Therefore, it is necessary to study more simple and feasible evaluation indicators, data acquisition methods and evaluation methods. Even if there is a lack of ecological professionals, general staff can still carry out the implementation, and use data collection, field investigation and rapid monitoring methods to assess the ecological environment of railway construction projects more quickly and concisely. At the same time, from the perspective of railway environmental protection management, it may be possible to realize the comparison between the same construction project in different periods and different construction projects, so as to better promote the ecological environmental protection level of railway construction projects.

2 Materials and Methods

2.1 Ecological Environment Quality Evaluation Index System of Railway Construction Project

With reference to the Technical Specification for Assessment of Ecological Environment Status (HJ/T 92-2015) issued by the Ministry of Environmental Protection in March 2015 (<https://www.mee.gov.cn/>), based on the ecological environment monitoring indexes of railway construction projects and in accordance with the principles of operability and feasibility, the second selection and modification of the selected monitoring indexes are

carried out. The ecological environmental quality evaluation Index system of railway construction projects is established (Table 1). Ecological environmental quality Index (REI) of railway is used to assess the ecological environmental status of railway construction projects, reflecting the impact and restoration of railway construction on the overall state of regional ecological environment to a certain extent.

Table 1. Ecological environmental quality as assessment index system of railway construction project.

Type	Evaluation content	Evaluation index
Land occupation and restoration	Land occupation	Normative land occupation index
	Temporary land restoration	Temporary land protection and restoration index
	Land desertification	Land desertification control index*
Environmental governance	Sewage control	Sewage control index
	Dust control	Dust control index
Plants and vegetation	Vegetation protection	Vegetation protection index
	Key plant protection	Key plant protection index*
Wild animal	Key wild animal protection	Wild animal protection index*
Ecological water demand	Natural water	Ecological water demand protection index*
Restrictive factors	Environmental limiting factor	Environmental restriction index

* Note: the index of land desertification control degree, key plant protection degree, wild animal protection degree and ecological water demand protection degree are the characteristic monitoring indexes, that is, the indexes to be adopted if the railway construction project has the necessary monitoring and evaluation of the content.

2.2 Evaluation Methods of Ecological Environmental Quality of Railway Construction Projects

(1) Calculation method of ecological environment quality index

The Ecological Environment Quality Index (REI) of railway construction projects = (Normative land occupation index+ Temporary land protection and restoration index+ Land desertification control index+ Sewage control index+ Dust control index+ Vegetation protection index+ Key plant protection index+ Wild animal protection index+ Ecological water demand protection index)/n - Environmental restriction index.

Among them, Land desertification control index, key plant protection index, wild animal protection index and ecological water demand protection index are optional characteristic monitoring indicators, and n is the number of monitoring indicators.

(2) Calculation method of ecological environment evaluation index

The calculation methods of 10 evaluation indicators (<https://www.mee.gov.cn/>) are shown in Table 2. Each indicator ranges from 0 to 100. As a binding index, the environmental restriction index refers to the limitation and regulation of the ecological environment status according to the severe destruction of ecological balance and environmental contamination caused by railway construction projects within the scope of evaluation. The specific contents are shown in Table 3.

Table 2. Calculation method of REI of railway construction project.

Evaluation index	Calculation method	Positive/negative
Normative land occupation index	The number of construction points of normative land occupation / Total number of points in the survey \times 100%	Positive
Temporary land protection and restoration index	The temporary land protected and restored / Total temporary land use \times 100%	Positive
Land desertification control index*	The length of lines to take control measures of desertification / Length of railway line located in extremely sensitive area of desertification \times 100%	Positive
Sewage control index	The number of monitoring points with the sewage up to the standard / Total number of monitoring points \times 100%	Positive
Dust control index	The number of points with the difference between monitoring points and reference points less than 0.5 mg/m ³ / Total number of monitoring points \times 100%	Positive
Vegetation protection index	The number of points with the biodiversity loss less than 10% / Total number of monitoring points \times 100%	Positive
Key plant protection index*	The number of points with no damage to key plants / Total number of monitoring points \times 100%	Positive
Wild animal protection index*	The number of points with no wild animal being hunted or habitat destroyed / Total number of monitoring points \times 100%	Positive

(continued)

Table 2. (continued)

Evaluation index	Calculation method	Positive/negative
Ecological water demand protection index*	The number of points with no ecological water loss / Total number of monitoring points × 100%	Positive
Environmental restriction index	Limiting factor	Negative

* Note: land desertification control index, key plant protection index, wild animal protection index and ecological water demand protection index are optional characteristic monitoring indicators.

(3) Classification and change analysis of ecological environment status

According to the ecological environment status index (EI), the ecological environment is classified into five levels, namely excellent, good, average, poor and worst (Table 4). According to the change of the ecological environment status index and the base value, the change amplitude of the ecological environment quality is classified into four levels, namely no obvious change, slight change, obvious change, significant change (Table 5). The grading evaluation method of the change of each sub-index can refer to the grading of the change degree of ecological environment status (<https://www.mee.gov.cn/>).

Table 3. The specific constraint content of environmental restriction index.

Classification		Reason of judgment	Constraint content
Emergent environmental incident	Very large environmental event	According to the “Emergency Plan for Environmental Emergencies”, if there is an emergency environmental event of very large, major, larger or general grade caused by railway construction project in the region, if there is more than one emergency environmental event in the evaluation region, the most serious grade shall prevail	The ecological environment cannot be classified “excellent” or “good”, and the quality level of the ecological environment should be reduced by one level
	Major environmental event		
	Larger environmental event		The quality level of ecological environment is reduced by one level
	General environmental events		

(continued)

Table 3. (continued)

Classification		Reason of judgment	Constraint content
Ecological damage and environmental pollution incidents and cases	Environmental pollution	There are cases of environmental pollution or ecological damage caused by railway construction projects notified by competent department of environmental protection or reported by state media (including areas exceeding standards in public environmental quality reports)	If there are environmental pollution or ecological damage events reported by the Ministry of Environmental Protection, the ecological environment cannot be classified “excellent” or “good”, and the quality level of the ecological environment should be reduced by one level; For other types of environmental pollution or ecological damage, the ecological environment level is reduced by one level
	Ecological destruction		
	Ecological environment illegal cases	There are violation cases of ecological environment caused by railway construction projects reported by competent department of environmental protection or listed for supervision	The ecological environment quality level is reduced by 1 level

Table 4. Classification of ecological environment status.

Classification	Excellent	Good	Average	Poor	Worst
Index	$EI \geq 75$	$55 \leq EI < 75$	$35 \leq EI < 55$	$20 \leq EI < 35$	$EI < 20$

Table 5. Classification of change degree of ecological environment status.

Classification	No obvious change	Slight change	Obvious change	Significant change
Variation	$ \Delta EI < 5$	$5 \leq \Delta EI < 10$	$10 \leq \Delta EI < 20$	$ \Delta EI \geq 20$

3 Results and Analysis

The Nanping-Longyan railway laying in the Fujian province opened On Dec. 25th, 2018. This study takes Nanping-Longyan railway as an example to study its ecological environment status and changes through ecological environmental quality evaluation, so as to promote the environmental protection level of railway construction projects. The data source selected the evaluation index of Nanping-Longyan railway from the third quarter of 2016 to the fourth quarter of 2017, the calculation results are shown in Table 6.

Table 6. Evaluation result of ecological environment quality of Nanping-Longyan Railway.

Evaluation index	2016		2017			
	Third quarter	Fourth quarter	First quarter	Second quarter	Third quarter	Fourth quarter
Normative land occupation index	85	90	85	93	95	95
Temporary land protection and restoration index	55	60	60	65	70	80
Sewage control index	78	80	85	90	95	100
Dust control index	75	85	95	95	100	100
Vegetation protection index	80	85	85	90	100	100
Ecological water demand protection index	80	80	80	100	100	100
Environmental restriction index	0	0	0	0	0	0
REI	75.5	80.0	81.7	88.8	93.3	95.8

Through monitoring and calculation (Table 6 and Fig. 1), the REI of Nanping-Longyan railway during the simulation period (from the third quarter of 2016 to the fourth quarter of 2017) was 75.5, 80.0, 81.7, 88.8, 93.3 and 95.8, respectively. The overall score was high and showed a trend of improvement. According to the ecological environment status index, the ecological environment of Nanping-Longyan railway in 2016–2017 is the highest level, that is, excellent. Due to the construction standards, the impact on the ecological environment and land resources is relatively small, with a high degree of environmental governance and better protection of animals and plants, ultimately bringing an improvement in the quality of the ecological environment.

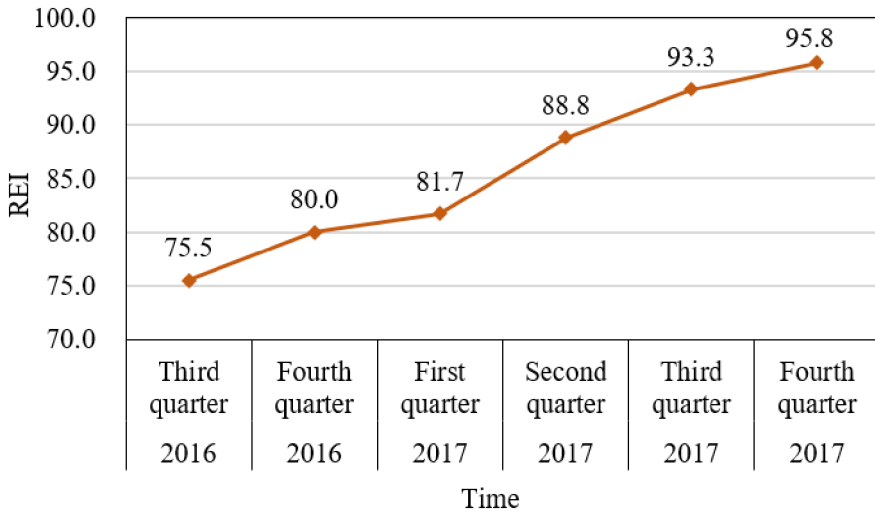


Fig. 1. Evaluation result of ecological environment quality of Nanping-Longyan Railway.

4 Discussion and Conclusion

- (1) From the perspective of guiding environmental impact assessment, construction and management, data collection is the fastest for engineering data, graphical overlay method is the most practical for ecological monitoring content, and standard analysis method is the most practical for environmental monitoring content. In short, simple and practical evaluation methods are easier to accept and realize in actual monitoring work. However, it is necessary to pay attention to the credibility of the collected data and conduct checks.
- (2) This study puts forward indicators, data acquisition methods and evaluation methods suitable for guiding the ecological environment quality evaluation of railway construction projects. Compared with existing monitoring schemes and monitoring indicators, they are simpler and more feasible, and can be implemented by general staff even in the absence of ecological professionals. At the same time, from the perspective of railway environmental protection management, it may be possible to realize the comparison between the same construction project in different periods and different construction projects, so as to better promote the ecological environmental protection level of railway construction projects [5, 6].
- (3) In this study, the index used for the ecological environment quality evaluation of railway construction projects adopts the calculation method of uniform weight, that is, the indexes based on land occupation and restoration, environmental governance, plant and vegetation, wild animal, ecological water demand are equally important in the evaluation of railway ecological environment quality. In the next research, weight analysis can be carried out on these ecological environment quality evaluation indicators, so as to make it more convenient for ecological environment evaluation of railway construction projects.

Author Contributions. J.Z. and X.L. contributed to all aspects of this work; Y.Z. and Y.L. conducted the data analysis; Y.Y. wrote the main text of the manuscript. All the authors have reviewed the manuscript. All the authors have read and agreed to the published version of the manuscript.

Funding. Research on Key Technologies of “Intelligent Environmental Butler” Service System for Railway Construction Project (Key research project of China Academy of Railway Sciences Co., Ltd. (Grant No. 2022YJ211).

Data Availability Statement. The data presented in this study are available on request from the author.

Conflicts of Interest. The authors declare no conflict of interest.

References

1. Parag, C.: Supply chain: the next national competitive advantage. *Discovery* **10**, 24–26 (2017)
2. Zhao, L., Zhang, H., Zhang, G.: Prediction of water gushing in Muzhailing tunnel and analysis of groundwater environment impact. *Environment and Development* **30**(12), 14–16 (2018)
3. Wang, A.: China’s railway construction needs innovative development under the new normal. *China Investment* **09**, 42–44 (2016)
4. Fu, Z., Liu, Z., Li, Z.: China railway development and innovation in the past century. *China Railway* **709**(07), 1–7 (2021)
5. Liu, W.: Effects of Ecological Environment Evolution Along the Gusher Path of Typical Mountain Railway Tunnel. Harbin Normal University (2022)
6. Xu, C.: The Cold Northwest Drought Region During the Construction of Ecological Environment Impact Assessment of Railway Bridges and to Study. Lanzhou Jiaotong University (2021)
7. Irem, U.S., Hulya, B., Cengiz, K.: Risk governance of urban rail systems using fuzzy AHP: the case of Istanbul. *Int. J. Uncertainty Fuzziness Knowl. Based Syst.* **20**(supp01), 67–79 (2012)
8. Mårten, K., Ulla, M.: A spatial ecological assessment of fragmentation and disturbance effects of the Swedish road network. *Landsc. Urban Plan.* **134**, 53–65 (2015)
9. Erika, I., Katarina, P., Oto, M.: The ecological impact assessment of a proposed road development (the Slovak approach). *Environ. Impact Assess. Rev.* **59**, 43–59 (2016)
10. Richard, D., Jason, R., David, W., Alvaro, F.B.: The road to growth: measuring the tradeoffs between economic growth and ecological destruction. *World Dev.* **101**, 351–376 (2018)
11. Cathryn, C.M., et al.: The insignificance of thresholds in environmental impact assessment: an illustrative case study in Canada. *Environ. Manage.* **61**(6), 1062–1071 (2018)
12. Cristina, M., Jesús, H., Juan, E.M.: Attraction and avoidance between predators and prey at wildlife crossings on roads. *Diversity* **12**(4), 166 (2012)
13. Liu, L.: Study on Landscape Ecology Method of Traffic Engineering Eco-environmental Impact Assessment. Southwest Jiaotong University (2006)
14. Li, B.: Study on the Index System of Railway Eco-environmental Impact Assessment. Southwest Jiaotong University (2007)
15. Zhang, X.: Research on Ecological Risk Assessment of High-Speed Railway Construction based on GIS. Central South University (2010)
16. Feng, C.: Research on Railway Environmental Risk Assessment Based on DSR Model. Southwest Jiaotong University (2016)

17. Hao, J.: Study on Ecological Impact of Jingyue Railway Project on East Dongting Lake Nature Reserve. Southwest Jiaotong University (2018)
18. Tian, J.: Comprehensive Evaluation of Ecological Environment Impact of Railway Long Tunnel. Southwest Jiaotong University (2005)
19. Wen, Y.: Study on Ecological Environment Assessment and Greening Model Design of Highway Domain in Ecologically Fragile Area. Northeast Forestry University (2013)
20. Song, Z.: Research on railway scheme evaluation model based on full line ecological impact. *Environ. Sustain. Dev.* **40**(2), 85–87 (2015)
21. Guo, Q., Jiang, W., Wang, Z.: Effects of high-speed railway on spatial-temporal changes of land use in surrounding areas. *J. Chongqing Jiaotong Univ. (Natural Science Edition)* **34**(04), 133–139 (2015)
22. Liu, Y.: Study on the impact of railway construction on ecological environment in ecologically fragile area: a case study of Hongliu river to Nuomaohu railway. *Railway Stand. Des.* **60**(10), 141–144 (2016)
23. Xue, C., Zhang, H., Zou, T., et al.: Ecological quality and its relationship with human activities in the economic corridor of China-Laos railway. *Chin. J. Appl. Ecol.* **32**(02), 638–648 (2021)
24. Liu, Y.: Research on Landscape Construction along Railway. Hunan University of Technology (2019)
25. Liu, Y., Zhao, X., Hu, Y.: Ecological assessment of landscape along Beijing-Guangzhou railway in Zhuzhou County. *J. Hunan City Univ. (Natural Science Edition)* **28**(01), 40–46 (2019)



Analysis of the Spatial Changes and Influencing Factors of Landscape Patterns Along the Fujian-Guangdong Interconnection

Jianxun Zhang¹, Guowei Chen², and Chang Lu¹ (✉)

¹ Construction Branch of State Grid Fujian Electric Power Co., Ltd., Fuzhou 350011, China
luchang_fz@163.com

² State Grid Fujian Electric Power Co., Ltd., Fuzhou 350003, China
chen_guowei@fj.sgcc.com.cn

Abstract. The Fujian-Guangdong Power Grid Project is of significant importance for the research on the changes in landscape patterns and the impact factors on biodiversity along the Fujian-Guangdong interconnection line, as it is a key project in the national “14th Five-Year Plan” for power development. This study aims to combine forest disturbance observation to assess the extent of forest destruction and recovery along the line and to analyze the influencing factors of landscape patterns and biodiversity changes using relevant indices. We utilized the COLD algorithm to monitor forest disturbances and calculated three landscape indices, including patch number, largest patch index, and Shannon’s diversity index. We found that the power grid project has caused certain damage to the forests, but they have been able to recover within 3 to 4 months after construction completion. Through index analysis, we observed that a 1000-m buffer zone is most suitable for analyzing the landscape pattern around the power station. Furthermore, factors such as the power of wind turbines and the age classification of the surrounding forests have an impact on the landscape pattern. These findings can provide assistance for ecological conservation and restoration along the Fujian-Guangdong interconnection line, as well as serve as a reference for future environmental analysis of power grid projects.

Keywords: Forest Disturbance · Landscape Pattern · Forest Age

1 Introduction

On September 30, 2022, the key project of the national “14th Five-Year Plan” for power development, the Fujian-Guangdong Interconnection Project, was officially completed and put into operation [1]. This milestone signifies the first-ever interconnection of power grids between Guangdong and Fujian provinces. The project has significant implications for regional energy security, resource allocation, and the green transformation of energy. Spanning through Zhangpu, Yunxiao, and Pinghe counties in Zhangzhou City, within the province of Fujian, the project traverses diverse ecological landscapes, experiences variable climates, and possesses abundant biodiversity. Consequently, the study of landscape pattern variations and factors influencing biodiversity along the Fujian-Guangdong interconnection line holds significant scientific value and practical significance.

Forest disturbance detection is one of the essential means to study landscape ecology, utilizing multi-source remote sensing data for monitoring and management of forest cover changes [2]. It enables the detection and monitoring of forest disturbances by comparing changes between images captured at different time periods or through time-series change patterns. Landscape patterns refer to the spatial organization and distribution characteristics of surface landscape elements [3]. By analyzing landscape patterns, we can investigate the factors and mechanisms of spatial pattern changes along the construction of the Fujian-Guangdong Interconnection Project, and determine the characteristics of landscape evolution. Biodiversity encompasses the diversity of species, genes, and ecosystems [4]. The regions along the Fujian-Guangdong Interconnection Project exhibit abundant biodiversity.

In this study, we utilized Landsat and high-resolution satellite imagery to analyze the Fujian-Guangdong interconnection line. Employing the COLD algorithm, we monitored surrounding disturbances and observed the forest's degradation and recovery. Three landscape pattern indices, including patch count, were computed to analyze the changes in landscape patterns across different spatial scales. Additionally, the changes in three landscape pattern indices were also compared between different tower base power and different forest age structures. Subsequently, the influencing factors of the landscape pattern along the corridor were analyzed. Based on the results, we conducted an analysis of the ecological conditions along the line and provided assistance for subsequent ecological conservation efforts.

2 Data and Study Area

2.1 Study Area

The study area is located within the boundaries of Fujian Province and forms part of the Fujian-Guangdong interconnection power grid line, spanning approximately 70 km in length (Fig. 1). Geographically, it lies between 23°24'N and 25°15'N latitude, and 116°51'E to 118°08'E longitude. The area boasts a unique geographical position, characterized by diverse and complex topography, encompassing high mountains, hills, plains, and coastal regions. Within Fujian Province, the region traversed by the Fujian-Guangdong interconnection project mainly includes Zhangpu, Yunxiao, and Pinghe counties, all of which fall within the subtropical monsoon marine climate zone. This area exhibits a variety of ecological types, experiences diverse climatic changes, and boasts a rich biodiversity, abundant with plant and animal resources [5].

2.2 Data

In this study, Landsat 8 and Gaofen-1 imagery were employed as data sources for analysis, playing a crucial role in Earth observation and environmental monitoring. The Landsat 8 imagery is acquired by the joint operation of the National Aeronautics and Space Administration (NASA) and the United States Geological Survey (USGS) through the Landsat satellite series [6]. With a spatial resolution of 30 m, this study primarily utilized the red, green, blue, and near-infrared bands. The Gaofen-1 imagery belongs to

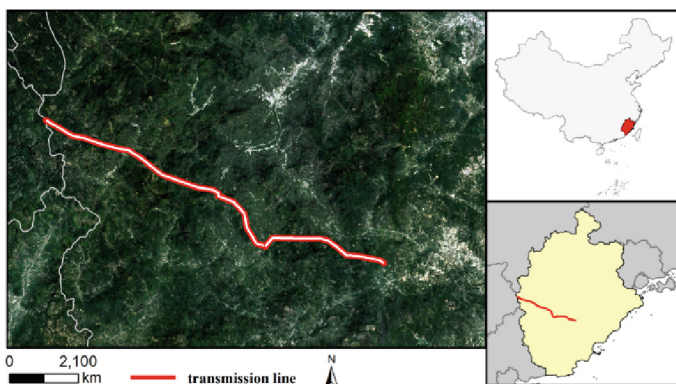


Fig. 1. The location of the study area. The red part in the picture is a part along the Fujian-Guangdong grid.

the High-Resolution Earth Observation Satellite series, launched by the China National Space Administration. Equipped with high-resolution optical sensors, the Gaofen satellite provides imagery data at a higher spatial resolution [7]. In this study, the Gaofen-1 imagery used had a resolution of 2 m, allowing for clearer observation of changes in the surrounding features of the tower base.

3 Methods

3.1 COLD Algorithm

The COLD (Continuous monitoring of Land Disturbance) algorithm is an enhanced algorithm used for land disturbance monitoring, which builds upon and improves the Continuous Change Detection and Classification (CCDC) algorithm [8]. It is designed to monitor various types of land disturbances. It offers several advantages over existing methods. Firstly, it provides high spatial (30 m) and temporal (up to four days) resolution automated accurate maps of land disturbance. Secondly, unlike many other disturbance algorithms that rely heavily on the availability of training data or inputs from several complicated algorithms, COLD detects land disturbance fully automated with Landsat time series as the only input data. This streamlined approach simplifies the process and improves efficiency. Thirdly, most of the rules and techniques used in COLD are based on ecological and biophysical processes that can be generalized for large areas and different kinds of environments. This generalizability enhances the algorithm's applicability and robustness. Lastly, with some adjustments (e.g., region-based thresholds), the COLD algorithm should have the capability of providing land disturbance maps for different regions. This flexibility further extends its utility in various geographical contexts.

The COLD algorithm primarily consists of three stages: data preparation, model initialization, and continuous monitoring. A normalized change vector magnitude is used as the threshold for change detection (Formula (1)). By continuously updating the model and observing new data, the COLD algorithm enables the continuous monitoring and extraction of land disturbances. With its optimized algorithmic workflow and rational

judgment criteria, the COLD algorithm effectively monitors various types of land disturbances, including subtle changes, thereby providing more accurate and comprehensive information on land changes.

$$\sum_{i=1}^k \left(\frac{\rho_i - \hat{\rho}_i}{RMSE_i} \right)^2 \sim \chi^2(k) > \chi_{0.99}^2 \quad (1)$$

where i is the i th band; k is Number of bands used for change detection; ρ_i is observed value for the i th band; $\hat{\rho}_i$ is predicted value for the i th band.

3.2 Landscape Pattern Index

When assessing landscape pattern changes, landscape pattern indices are commonly used to characterize landscape fragmentation. In this study, three indices, namely patch number (N), largest patch index (LPI), and Shannon's diversity index (SHDI), were selected to describe landscape pattern changes. The N represents the total number of heterogeneous landscape elements in the landscape [9]. The LPI reflects the dominant patch types in the landscape, indirectly indicating the direction and magnitude of human-induced disturbances (Formula (2)) [10]. Shannon's diversity index is an important indicator of landscape heterogeneity, accurately identifying the spatial uneven distribution of different patch types in the landscape. A higher value indicates a more diverse land use and a more fragmented landscape (Formula (3)) [11].

$$LPI = \frac{Max(a_1, \dots, a_n)}{LA} \quad (2)$$

where a_n represents the area of the n th patch, and LA represents the total landscape area of the study area.

$$SHDI = - \int_{i=1}^n (p_i \ln p_i) \quad (3)$$

where p_i represents the proportion occupied by the landscape patch type i .

4 Results

4.1 Analysis of Forest Disturbance and Recovery

Based on high-resolution time-series remote sensing images, this study utilized the COLD algorithm to detect disturbance patterns around each tower base. Overall, within a $1.5 \text{ km} \times 1.5 \text{ km}$ area surrounding each tower base, undisturbed areas were predominant, indicating the accuracy of the detection results. Regarding the disturbed areas, the largest extent of disturbance occurred during the construction phase of each tower base, aligning with the actual construction timeline. By combining the time-series imagery with the disturbance results, the analysis reveals that the forests in each area experienced three stages: pre-construction stability, forest disturbance during construction, and gradual recovery after construction completion. Furthermore, the extent of disturbance in each area exhibited varying patterns due to different construction conditions, operational status, and terrain characteristics.

We selected two representative regions for analysis, utilizing remote sensing imagery before and after the disturbance. In the first region, the northwestern part shows the disturbed area caused by construction activities (Fig. 2). By examining the extent of disturbance and the occurrence of disturbance events in this area, it can be observed that the construction of the tower base occurred in three stages. The first stage began in November 2021 with tree felling, followed by the second and third stages in February and March 2022, respectively. Based on the area of disturbance, it is evident that the third stage had the largest construction scope, with the disturbance trend gradually increasing from November 2021 and peaking in March 2022, followed by a decline indicating the start of recovery. Furthermore, due to a temporary suspension of construction activities and subsequent resumption the following year, the time span of disturbance in this area was prolonged. It is possible that vegetation, which had started to recover after the first stage, experienced repeated disturbance when construction activities resumed. Lastly, based on the post-construction remote sensing imagery, despite experiencing prolonged and multiple disturbances, some areas that experienced earlier disturbances (e.g., in November of the previous year) showed signs of vegetation greening and recovery by June 2022.

In the second region, combining the analysis with remote sensing imagery (Fig. 3), it can be observed that the central part of the area consists of scattered disturbed areas arranged horizontally from east to west. These point-like areas correspond to tower bases required for the construction of the power line. The disturbed areas are linearly aligned, following the alignment of the power line. Based on the occurrence time of disturbance in these areas, it is evident that several tower bases were disturbed simultaneously during the period from February to April 2022, suggesting synchronized construction with a relatively short duration. The disturbed areas are relatively small and generally consistent with the size of the tower bases. The terrain in this region exhibits minimal variation, making construction less challenging and allowing for a shorter construction period. Therefore, in the post-construction imagery from June 2022, it can be observed that the majority of the areas that underwent disturbance have already started to recover.

In conclusion, the forest disturbances within the study area exhibit various patterns influenced by construction conditions, difficulty, terrain, and other factors. Although the degree of disturbance, duration, and frequency of repetitions vary, resulting in varying degrees of damage to the forest, it is noteworthy that the majority of the areas begin to recover within 3 to 4 months after construction completion.

4.2 Changes in Landscape Pattern Across Different Spatial Scales

Tables 1–3 display the results of four indices calculated within buffer zones of 500 m, 1000 m, and 1500 m around the tower bases. The majority of tower base points show an increasing trend in the N index as the buffer zone expands. This is because as the range increases, the complexity within the area increases, resulting in a higher number of fragmented patches in the environment. Therefore, in larger buffer zones, the analysis includes a greater variety of land cover types and landscape features, leading to an increase in the N index. However, there are a few tower base points, such as 1#-P1 and 41#-P1 plots, that exhibit a decreasing trend followed by an increasing trend as the range expands. This is because, within the 1000-m range of these plots, the proportion

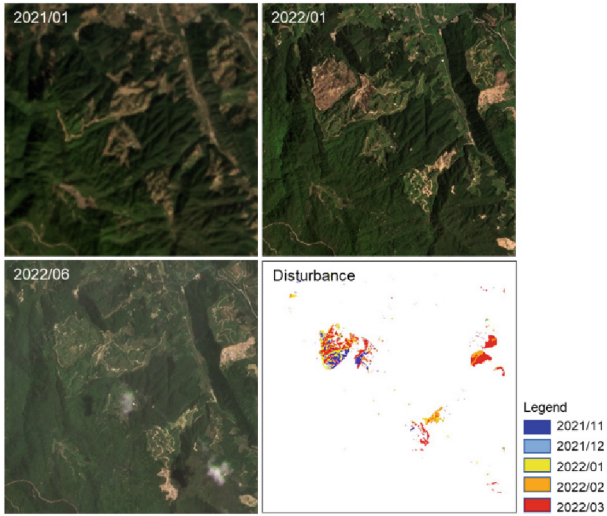


Fig. 2. Temporal imagery and disturbance map around the tower base (bottom right). From left to right, top to bottom: 2021/01 – no construction, 2022/01 – construction begins with disturbances, 2022/06 – construction completed and vegetation recovery initiates.

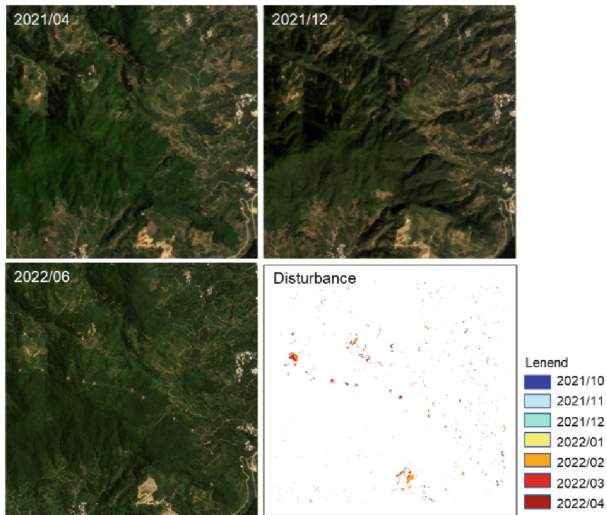


Fig. 3. Temporal imagery and disturbance map around the tower base (bottom right). From left to right, top to bottom: 2021/01 – no construction, 2022/01 – construction begins with disturbances, 2022/06 – construction completed and vegetation recovery begins.

of forests is higher and more concentrated. Thus, when the range expands from 500 m to 1000 m, these two indices decrease due to the inclusion of relatively fewer land cover types. However, when the range expands from 1000 m to 1500 m, the land cover types

become more complex and fragmented, resulting in an increase in the indices. This variation indicates that the differences in landscape features and land cover distribution within different tower base plots can lead to varying trends in the indices across different ranges.

The variation of the LPI and the SHDI does not exhibit a clear pattern compared to the first two indices. This is because the LPI is determined by the largest patch within each tower base, and the size of the index varies as the range expands due to the different largest patches in each area. Additionally, the LPI is also influenced by other factors such as landscape shape and layout. In contrast to the LPI, the SHDI depends on the location of the tower base. If the tower base is located at the edge of a town, the inclusion of the town will increase the SHDI as the range expands. This is because areas at the edge of towns typically have higher landscape heterogeneity, and as the range expands, a greater variety of land cover types enter the range, thereby increasing the landscape heterogeneity. Therefore, the variation of the maximum patch index and the SHDI may exhibit different patterns in different situations, depending on the location of the tower base and the characteristics of the surrounding landscape.

Based on the above analysis, it can be observed that when studying the spatial landscape pattern of tower bases, selecting a range that is too large can easily be influenced by factors outside the tower bases, such as urban areas, leading to distorted analysis results. On the other hand, choosing a range that is too small may overlook the influence of some tower bases on the surrounding environment, failing to capture the complete picture of these impacts and limiting a comprehensive understanding of the tower base landscape pattern. Therefore, using a 1000-m buffer zone around the tower bases as an appropriate spatial range for landscape pattern analysis is reasonable. This range takes into account the influence range of the tower bases themselves while avoiding excessive interference from non-tower base factors.

Table 1. Results of Four Indices within the 500-m Buffer Zone of Each Tower Base.

Tower Number	N	LPI	SHDI
1#-P1	401	0.020877747	1.589290704
41#-P1	411	0.015906553	1.520274484
45#-P1	359	0.011628534	1.77377741
46#-P1	400	0.013777854	1.768775916
49#-P1	356	0.016420486	1.572914525
50#-P1	337	0.018135183	1.526265123
51#-P1	411	0.013625577	1.617397436
1#-P1	432	0.014973859	1.617760735

Table 2. Results of Four Indices within the 1000-m Buffer Zone of Each Tower Base.

Tower Number	N	LPI	SHDI
1#-P1	354	0.011939432	1.573959316
41#-P1	405	0.022186374	1.543204838
45#-P1	393	0.021334577	1.770785108
46#-P1	468	0.012851505	1.754516155
49#-P1	389	0.015122963	1.630979635
50#-P1	379	0.009883699	1.610842823
51#-P1	439	0.010979773	1.56191216
1#-P1	434	0.011149497	1.625540084

Table 3. Results of Four Indices within the 1500-m Buffer Zone of Each Tower Base.

Tower Number	N	LPI	SHDI
1#-P1	372	0.014042752	1.513284449
41#-P1	414	0.018599944	1.592059453
45#-P1	377	0.016241244	1.767096902
46#-P1	465	0.008903419	1.741417489
49#-P1	369	0.012960954	1.682751152
50#-P1	366	0.02286686	1.659907154
51#-P1	461	0.021139473	1.600264799
1#-P1	443	0.011530189	1.60429509

4.3 Influence of Different Factors on the Landscape Pattern Along the Line

While the selection of spatial range indirectly affects the distribution of landscape patterns, there are other factors that directly impact the degree of landscape fragmentation. Based on While the selection of spatial range indirectly affects the distribution of landscape patterns, there are other factors that directly impact the degree of landscape fragmentation. Based on this, this study investigates the influence of tower base power and forest age structure on landscape patterns. We selected three different tower base power levels (110 kV, 220 kV, 500 kV) and calculated the changes in three landscape indices within a 1000-m buffer zone (Fig. 4). From the figure, it can be observed that both the number of patches and Shannon's diversity index increase with the increase in tower base power. However, the maximum patch index initially decreases and then increases with the increase in tower base power. This indicates that as the tower base power increases, the surrounding landscape becomes more fragmented, leading to greater disturbance. The reason for this may be that low-power tower bases have smaller land areas, and the

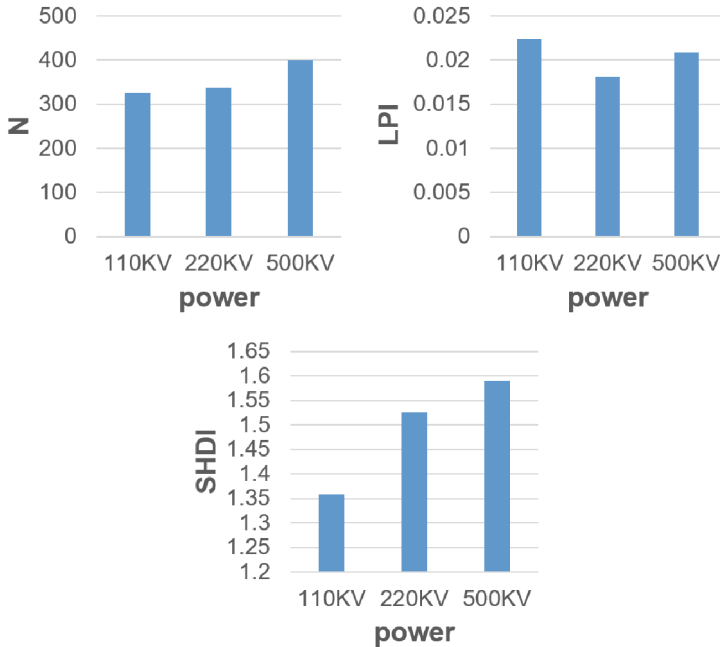


Fig. 4. Changes in landscape pattern indices around three different tower base power levels.

construction process involves minimal entry of large vehicles, resulting in lower vegetation disturbance. This study investigates the influence of tower base power and forest age structure on landscape patterns. We selected three different tower base power levels (110 kV, 220 kV, 500 kV) and calculated the changes in three landscape indices within a 1000-m buffer zone (Fig. 4). From the figure, it can be observed that both the number of patches and Shannon's diversity index increase with the increase in tower base power. However, the maximum patch index initially decreases and then increases with the increase in tower base power. This indicates that as the tower base power increases, the surrounding landscape becomes more fragmented, leading to greater disturbance. The reason for this may be that low-power tower bases have smaller land areas, and the construction process involves minimal entry of large vehicles, resulting in lower vegetation disturbance.

Two tower bases were selected with different surrounding forest age levels (average age of 15 years and 30 years), and the three landscape pattern indices for January 2021 and March 2023 were compared (Fig. 5), representing the period before and after the construction of the power project, respectively. From the figure, it can be observed that the number of patches decreases with higher forest age levels. The maximum patch index and Shannon's diversity index increase with increasing forest age during the period of maximum disturbance, but decrease with increasing forest age at the current stage. Areas with higher forest age levels tend to be densely wooded forest areas. Therefore, constructing power projects in these areas may be more challenging. Additionally, the recovery rate in these areas may be slower compared to areas with lower forest age,

possibly because mature forests take longer to recover from the damage caused by construction activities.

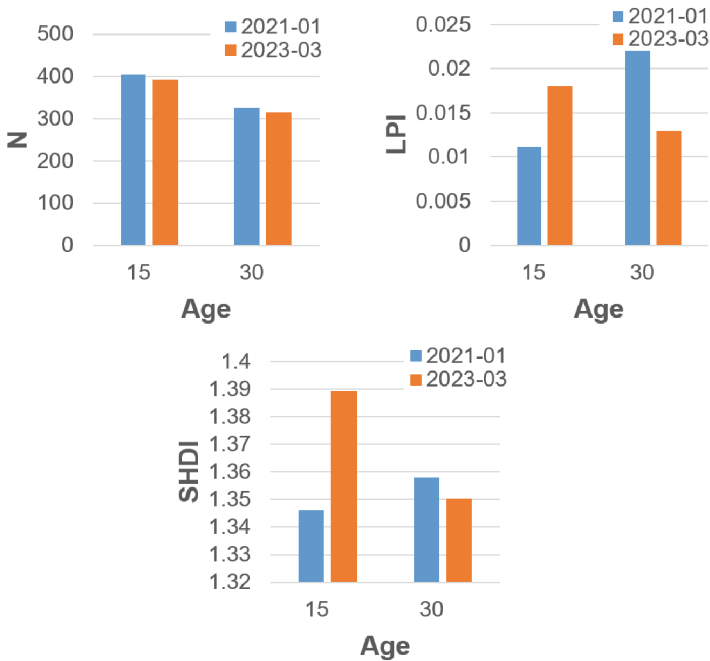


Fig. 5. Changes in three landscape pattern indices under different surrounding forest age levels.

5 Discussion

This study analyzed the forest disturbance around multiple tower sites and assessed the degradation and recovery of three forest regions. However, there are uncertainties associated with the forest disturbance results, primarily stemming from both the imagery and the algorithm used. In terms of imagery, we utilized high-resolution imagery from the GF-1 satellite [12]. However, variations in reflectance between adjacent images due to factors like clouds and sensor quality may lead to erroneous detection results. Despite selecting high-quality imagery data, these influences still persist. Additionally, we employed the COLD algorithm for forest disturbance monitoring, which has some limitations such as temporal lag and potential errors in threshold adjustments, leading to some degree of inaccuracy. Nevertheless, these errors have a minor impact on the final disturbance monitoring results and do not significantly affect the reliability of the findings. Therefore, despite the uncertainties and limitations associated with the imagery and algorithm, the results of this study still maintain a high level of credibility. We selected high-quality imagery data and employed a reliable disturbance monitoring algorithm to ensure the accuracy and reliability of the results. However, when interpreting and

discussing the results, it is important to acknowledge these uncertainties and limitations and provide appropriate discussions and explanations to better understand and interpret the research findings.

The power grid project has achieved good results in vegetation restoration, and the restoration will basically take 3–4 months. At the same time, the 1000-m buffer zone is most suitable for analyzing the landscape pattern around the power station, which takes into account the environment around the tower and can be applied to most power stations. The article also found that the power of wind turbines and the age class of surrounding forests can have an impact on landscape patterns and that for high-power and older forest environments, increased forest restoration efforts are needed. Taking different restoration measures according to the power of the power station and the surrounding environment can improve the restoration efficiency and contribute to the ecological restoration of the power grid project.

6 Conclusion

This study focused on a section of the Fujian province along the Fujian-Guangdong Interconnection Project as the research area. Based on high-resolution time-series remote sensing imagery, the COLD algorithm was used to detect disturbance maps at each tower site, enabling the analysis of forest degradation and recovery around the tower sites. Additionally, comparisons were made regarding landscape pattern changes at different spatial scales and the impact of various factors on landscape patterns. The following conclusions are drawn:

- (1) The electrical grid construction projects in the study area caused varying degrees of forest damage, but most areas began to recover within 3 to 4 months after construction completion.
- (2) Landscape pattern changes varied across different spatial scales, with the 1000-m buffer zone being the most suitable for analyzing landscape patterns around the power projects.
- (3) The power of wind turbines and the age class of surrounding forests can have an impact on the landscape pattern. Under different power and age class combinations, the extent to which the landscape pattern around wind turbines is affected varies. Higher turbine power results in a more fragmented landscape. Older surrounding forests take longer to recover the landscape pattern.

The results of this study indicate that although the Fujian-Guangdong Interconnection Project caused some degree of forest damage along the transmission lines, the forests have shown signs of recovery, likely due to the implemented restoration measures. The findings on landscape patterns and biodiversity not only provide valuable insights for the ecological restoration of the interconnection project but also serve as a reference for future power engineering projects. Therefore, this research holds scientific and practical value, contributing to both scientific understanding and guiding practices in the field.

Author Contributions. Methodology, Jianxun Zhang; software, Jianxun Zhang; validation, Guowei Chen and Chang Lu; formal analysis, Jianxun Zhang; data curation, Guowei Chen; writing – original draft preparation, Chang Lu. All authors have read and agreed to the published version of the manuscript.

Funding. This work is supported by the State Grid Fujian Electric Power Co., LTD (52130T220007).

Conflicts of Interest. The authors declare no conflict of interest. The funders had no role in the design of the study; in the collection, analyses, or interpretation of data; in the writing of the manuscript, or in the decision to publish the results.

References

1. Ling, W., Ming, L., Fangjie, W.: Research on control strategy of canceling tap changer in back to back dc project. In: 10th Renewable Power Generation Conference, pp. 678–683 (2021)
2. Chen, X., Zhao, W.Z., Chen, J.G., Qu, Y., Wu, D.H., Chen, X.H.: Mapping large-scale forest disturbance types with multi-temporal CNN framework. *Remote Sens.* **13**(24), 5177 (2021)
3. Wu, Z.F., Wei, L.Z., Lv, Z.Q.: Landscape pattern metrics: an empirical study from 2-d to 3-d. *Phys. Geogr.* **33**(4), 383–402 (2012)
4. Syrbe, R.U., Michel, E., Walz, U.: Structural indicators for the assessment of biodiversity and their connection to the richness of avifauna. *Ecol. Ind.* **31**(5), 89–98 (2013)
5. Ma, Z.G., et al.: Recent changes in temperature and precipitation of the summer and autumn seasons over Fujian Province, China. *Water* **13**(14), 1900 (2021)
6. Reuter, D., et al.: The operational land imager (OLI) and the thermal infrared sensor (TIRS) on the Landsat data continuity mission (LDCM). In: Algorithms and Technologies for Multispectral, Hyperspectral, and Ultraspectral Imagery XVII 8048, pp. 382–388 (2011)
7. Liu, Q.Y., Yu, T., Zhang, W.H.: Validation of gaofen-1 satellite geometric products based on reference data. *J. Indian Soc. Remote Sens.* **47**(8), 1331–1346 (2019)
8. Zhu, Z., et al.: Continuous monitoring of land disturbance based on Landsat time series. *Remote Sens. Environ.* **238**, 111–116 (2020)
9. Xu, Z.H.: Parallel calculation method of patch area landscape art index based on surface coverage data. *Secur. Commun. Netw.* **2021**, 1–10 (2021)
10. Zhao, F., Li, H., Li, C.H., Cai, Y.P., Wang, X., Liu, Q.: Analyzing the influence of landscape pattern change on ecological water requirements in an arid/semiarid region of China. *J. Hydrol.* **578**, 124098 (2019)
11. Yeboah, D., Chen, H.Y.H., Kingston, S.: Tree species richness decreases while species evenness increases with disturbance frequency in a natural boreal forest landscape. *Ecol. Evol.* **6**(3), 842–850 (2016)
12. Wang, X.F., Zhou, C.W., Feng, X.M., Cheng, C.W., Fu, B.J.: Testing the efficiency of using high-resolution data from GF-1 in land cover classifications. *IEEE J. Sel. Top. Appl. Earth Observ. Remote Sens.* **11**(9), 3051–3061 (2018)



Impact of Electric Power Grid Projects on Bird Diversity and the Suggestion of Bird Conservative Technology

Chang Lu¹(✉), Xi Li², Ying Deng³, Jian Wang⁴, Huaizhou Zheng⁴,
and Mingfeng Zhang⁴

¹ Construction Branch Company of State Grid Fujian Electric Power Co., Ltd., Fuzhou 350011, China

luchang_fz@163.com

² Electric Power Research Institute of State Grid Fujian Electric Power Co., Ltd., Fuzhou 350007, China

³ Nanping Electric Power Supply Company of State Grid Fujian Electric Power Co., Ltd., Nanping 353000, China

⁴ School of Geographical Sciences, School of Carbon Neutrality Future Technology, Fujian Normal University, Fuzhou 350117, China

jwang@fjnu.edu.cn

Abstract. The increasing number of power lines each year has a significant impact on bird biodiversity, while the control of birds at high risk from power grid projects is a guarantee of safe and reliable power grid operation. From both the perspective of safety and biodiversity conservation, how to achieve harmonious coexistence between birds and power grid projects has become an urgent scientific problem to be solved. This study investigates the impact of power grid projects on bird diversity by investigating birds in and around power grid projects in Fujian Province, and proposes suggestions for power grid projects to protect bird diversity. The results show that future power grid projects should try to avoid increased forest fragmentation, and temporary construction roads should be restored as soon as possible in order to preserve animal passage. The affected migratory birds in the power grid deployment area under study are mainly finches and a few raptors, and according to the migration pattern of these two types of birds, construction during the bird migration season in March and October should be avoided as much as possible during the construction of power grid, especially the night-time construction of large converter stations and substations.

Keywords: Electric Power Grid Projects · Pylon · Electric Power Lines · Bird Diversity · Bird Conservation

1 Introduction

The control of birds at high risk from power grid projects is essential for the safe and reliable operation of power grids [1], while the increasing number of transmission lines each year also has a significant impact on bird biodiversity [2, 3]. The lines and pylons

of the power grid project are known to cause injury to wildlife, mainly birds, through collisions [4], electrocution [5] and electromagnetic fields [6]. On the positive side, electricity pylons are used as nesting platforms by birds, raptors such as the white stork *Ciconia ciconia* [2] and as calling posts, resting and roosting sites [5]. However, most of these studies have focused on Europe and the United States, and there are fewer studies in China. How to achieve harmonious coexistence between birds and power grid projects is an urgent scientific question, both from the perspective of safety and wildlife conservation. At the same time, the conservation of biodiversity in the course of large-scale linear construction projects has become a global initiative, attracting the attention of all sectors of society, including companies and biodiversity public interest groups [7–9]. How to move from early grid protection to harmonious coexistence with the ecological environment is one of the urgent tasks to be carried out for future power grids. This study investigates power grid projects under construction in Fujian Province and the birds in their vicinity to clarify the impact of power grid projects on bird diversity and to suggest power grid projects to protect bird diversity.

2 Materials and Methods

2.1 Study Area

The present study site is Zhangzhou City and Nanping City, Fujian Province, China. Zhangzhou City is located in the southernmost part of Fujian Province, between longitude 116°54′–118°08′ East and latitude 23°34′–25°15′ North, with a land area of 12,600 square kilometers and a sea area of 18,600 square kilometers. It is a southern subtropical maritime monsoon climate type, with an average annual temperature of 21 °C and an annual rainfall of 1,500 mm. Nanping City is the northern gate of Fujian, located in the southeast of the Wuyi Mountains and the upper reaches of the Min River, with longitude 117°00′–119°25′ east and latitude 26°30′–28°20′ north. It's a central subtropical monsoon climate, with an average annual temperature of 19.3 °C and an annual rainfall of 1660 mm. The subjects of this study are the Min-Yue Power Project (line length in Fujian 48.8 km) within the Zhangzhou city area and the Xiangshan Power Project (total length 31.2 km) within the Nanping city area (Fig. 1).

Min-Yue Power Project, also known as the Fujian-Guangdong networking project is the sixth back-to-back project in China, a landmark project to deepen cooperation between the State Grid and the Southern Power Grid, and is the second interconnection channel between the State Grid and the Southern Power Grid [10]. Upon completion, the Min-Yue interconnection project realizes the interconnection of the power grids of Fujian and Guangdong provinces. The project enables the power grids of the two provinces to complement each other's surplus and the two provinces to standby each other. The Min-Yue interconnection project can bring certain peak-shaving benefits and allow for a greater scope of optimized resource allocation. In addition, the interconnection of the two power grids will provide additional "blood" to resist natural disasters such as typhoons and rainstorms. At the same time, it is conducive to giving full play to the advantages of clean energy resources in Fujian Province, further optimizing the energy structure of the Guangdong-Hong Kong-Macao Greater Bay Area and the Economic Zone on the West Coast of the Taiwan Strait, and is an important demonstration for building a clean,

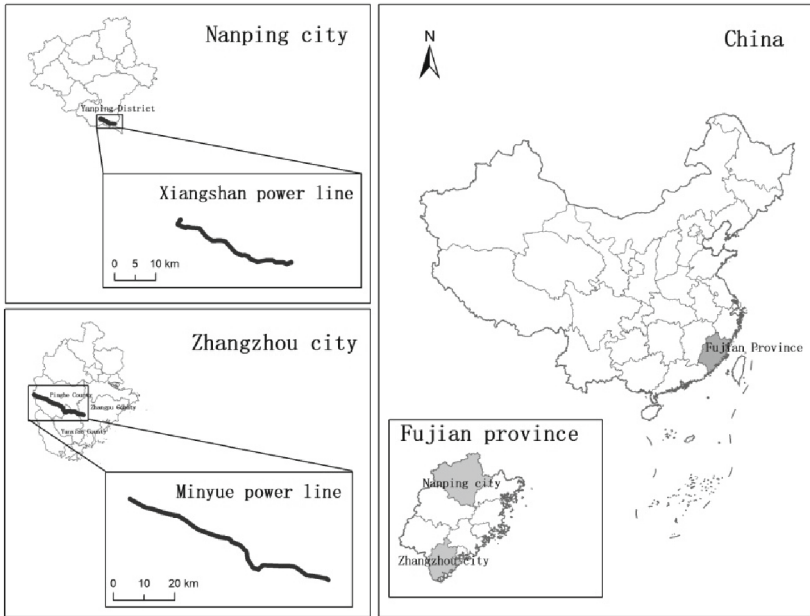


Fig. 1. Map of study area. Locations of power grid projects are shown.

low-carbon, safe and efficient energy system to ensure regional energy security. The project is of great significance to the implementation of the new national energy security strategy, the realization of a larger optimal allocation of energy resources, the service of carbon peaking and carbon neutral objectives, and the construction of a new power system with new energy as the mainstay.

The Xiangshan Transformation Project is located in the Yanping District of Nanping, Fujian Province, which is an important ecological function area for water conservation and biodiversity protection of river sources. At the same time, Yanping District is the core of Nanping's economic development, with a concentration of industrial users in the area and is the load center of Nanping's power grid. And the project can be for driving the development of peripheral townships, advance planning and construction, and guarantee the township power construction steadily, so planning Nanping Xiangshan change project is necessary for local development.

2.2 Data Handling

From February to April 2023, two representative high-voltage transmission lines in Fujian Province, the Min-Yue Interconnection Project (500 kV) and the Xiangshan Transformation Project (110 kV), were selected for bird surveys based on bird phenological characteristics. The sample line method was mainly used to survey the areas along the power grid projects and the birds residing on the pylons. Based on the sample line method, a total of 615 bird data were collected along the power grid projects involved in the project (Table 1).

Three indices of conservation status were used: (1) a modified category of IUCN conservation status, (2) the protected birds at national level defined by List of National Key Wildlife Protection and (3) three valuable animals defined by National Forestry and Grassland Administration [11–13].

The study was conducted (1) to compare the impact of different levels of power grid projects (500 kV and 110 kV) on bird diversity, (2) to compare the diversity of birds at different distances (within 1 km and beyond 1 km) from power grid projects, (3) to compare the diversity of birds at different stages of power grid projects such as construction (within 1 km) and maintenance (within 1 km), (4) and to compare the diversity of birds using power grid project hardware (e.g., power lines and pylons). (5) Finally, the possible impact of the power grid project on the migration of migratory birds in the area is explored.

Table 1. Characteristics of bird diversity along the power grid project area.

No.	Site	Data	Bird diversity	Migratory bird	Protected birds at national level II	ICUN status	Three valuable animals
1	ZZ	443	8 Order 23 Family	7	<i>Centropus sinensis</i>	LC	68%
					<i>Spilornis cheela</i>	LC	
2	NP	172	11 Order 27 Family	9	<i>Lophura nycthemera</i>	LC	50%
					<i>Centropus sinensis</i>	LC	
					<i>Spilornis cheela</i>	LC	
					<i>Ictinaetus malaiensis</i>	LC	
					<i>Buteo japonicus</i>	LC	
					<i>Glaucidium brodiei</i>	LC	
					<i>Glaucidium cuculoides</i>	LC	

Note: ZZ stands for Zhangzhou Min-Yue Interconnection 550 kV Project and NP stands for Nanping Xiangshan Transformation 110 kV Project. The three valuable animals refer to wild animals that are beneficial, have important economic value and scientific research value.

3 Results

3.1 Characteristics of Bird Diversity Along the Electric Power Grid Project Area

There were significantly more bird diversity and “three valuable animals” of birds recorded along the 500 kV power grid project than the 110 kV power grid project, which is significantly related to the length of the line. The species of national protected birds and migratory birds along the 110 kV power grid project were higher than those of the 500 kV power grid project, which may be related to the area where the 110 kV power grid project is located (Table 1).

A higher proportion of the birds in Zhangzhou are “three valuable animals”. This is probably due to the warmer and more humid climate in Zhangzhou, more economic forests such as orchard, and more densely populated surrounding villages, where birds are more closely related to human activities and their food needs (especially pest species) are more diverse. In order to increase awareness of the need to protect the “three valuable animals”, it is recommended that in the future, in more economically developed areas, grid companies increase education on biodiversity conservation for local residents.

Compared with the Zhangzhou area, the Nanping area is richer in bird diversity, with more species of birds protected at national level and more species of migratory birds than in the Zhangzhou area, which is in line with the characteristics of the Nanping area as a biodiversity-rich area, indicating that forests with a higher degree of protection are more suitable for the survival of birds. The construction area of the Nanping Xiangshan Power Grid Project is smaller, and maintaining a continuous forest helps to protect endangered birds. Future power grid projects should try to avoid increased forest fragmentation, and temporary construction roads, for example, should be restored as soon as possible in order to preserve animal passage.

3.2 Spatial and Temporal Effects of Electric Power Grid Projects on Bird Diversity

Spatial: Characteristics of Bird Diversity at Different Distances from Power Grid Projects. A comparison of bird diversity characteristics between the pylon area (within 1 km) and the control area (beyond 1 km) (Table 2) shows that the pylon area has a lower diversity of plant life available for nesting birds and is subject to a higher intensity of human disturbance, resulting in a lower bird species and numbers than the control area. Bird species in the pylon area are predominantly finches (Fig. 2) and are all resident birds, with zero migratory birds (Fig. 3).

Temporal: Characteristics of Bird Diversity at Different Stages of Power Grid Projects. A comparison of the birds in the construction stage (1 km range) and the maintenance stage (1 km range) shows that the diversity of birds within 1 km of the construction and maintenance stages of the pylons is dominated by finches, with few differences in species (Table 3, Fig. 4). The main change is the decrease in the number of national priority animals during the construction phase, especially raptors, which are more sensitive to environmental changes and require a longer period of time to recover after the cessation of human disturbance (Fig. 5).

Table 2. Characteristics of birds in the power pylon area and control area.

Sample site	The species of birds	The number of birds	Protected birds at national level
Pylon area (<1 km)	7	21	None
Control area (> 1 km)	44	441	2 (Class II)

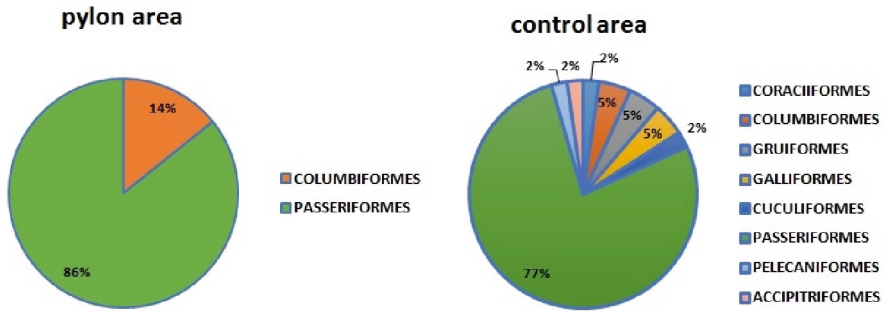


Fig. 2. The classification of birds of the pylon area and control area.

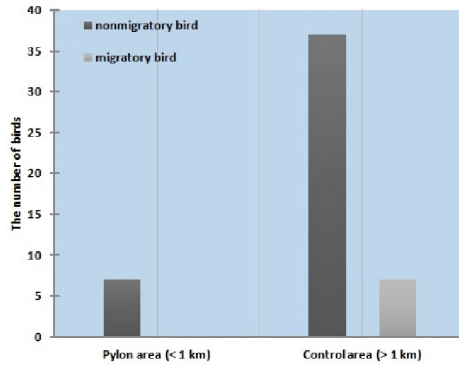


Fig. 3. The number of migratory birds of the pylon area and control area.

Table 3. Characteristics of birds at different stages of power grid projects.

Stages of Project	The species of birds	The number of birds	Species of protected birds at national level
Construction stage	29	128	1 (Class II)
Maintenance stage	36	151	6 (Class II)

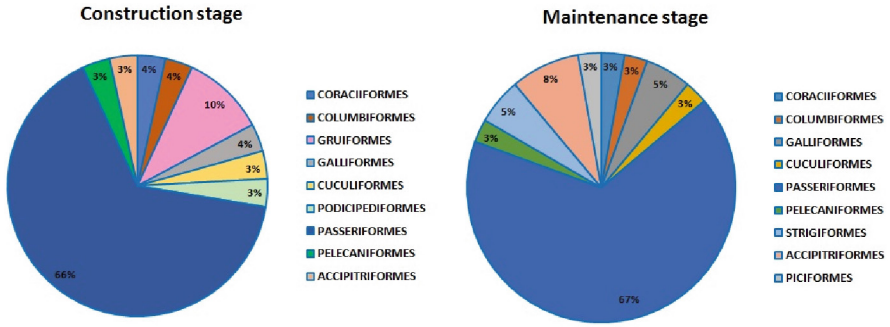


Fig. 4. The classification of birds at different stages of power grid projects.

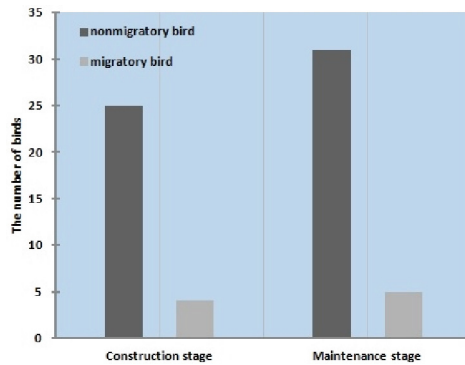


Fig. 5. The number of migratory and nonmigratory birds at different stages of power grid projects.

3.3 Utilization of Power Lines and Pylons by Birds in the Power Grid Project Area



Some birds use pylons or power lines as important habitats for their behaviors such as roosting and foraging (Table 4), especially resident birds of the order Finch, as a behavioral feature of their adaptation to the environment (Figs. 6 and 7).

3.4 The Impact of Power Grid Project Construction on Migratory Birds

Migratory Bird Species Affected by the Construction of Power Grid Projects. Migratory bird species – dominated by finches, only three species were observed on power lines, mostly individuals moving around on grass or shrubs on the ground (Table 5).

Migratory Bird Migration Routes. There are nine known global bird migration routes: 1) the ‘Atlantic Migration Route’ which crosses the entire Atlantic Ocean linking Western Europe, eastern North America and a narrow strip of West Africa; 2) the ‘Black Sea/Mediterranean Migration Route’ linking Eastern Europe and West Africa; 3) the ‘East African West Asia Migration Route’ which crosses the Indian Ocean linking West

Table 4. The different types birds of utilized powerline and pylon.

No.	Types of behavior using powerlines	Species	Examples
1	Perching on a powerline	26	
2	Nesting electric pylon	2	

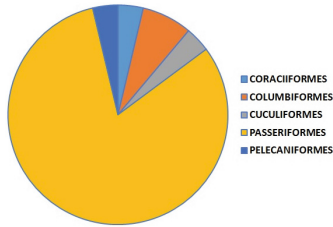


Fig. 6. The classification of birds of utilized power grid.

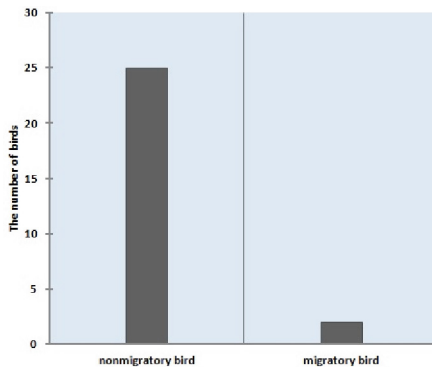


Fig. 7. The number of migratory and nonmigratory bird of utilized power grid.

and East Africa; and 4) the ‘Central Asian Migration Route’ which crosses the entire Asian continent from south to north; 5) The ‘East Asia/Australia Migration Route’, which crosses the Indian, Arctic and Pacific Oceans and connects the continents of East Asia and Australia; 6) The ‘American Pacific Migration Route’, which runs along the

Table 5. Migratory bird species affected by the construction of power grid projects.

No.	Species	Scientific Name	Genus	Activity
1	Black Bulbul	<i>Hypsipetes leucocephalus</i>	<i>Passeriformes</i>	Yes
2	Dusky Warbler	<i>Phylloscopus fuscatus</i>	<i>Passeriformes</i>	No
3	Pallas's Leaf Warbler	<i>Phylloscopus proregulus</i>	<i>Passeriformes</i>	No
4	Arctic Warbler	<i>Phylloscopus borealis</i>	<i>Passeriformes</i>	No
5	Daurian Redstart	<i>Phoenicurus auroreus</i>	<i>Passeriformes</i>	Yes
6	Blue Whistling Thrush	<i>Myophonus caeruleus</i>	<i>Passeriformes</i>	No
7	Olive-backed Pipit	<i>Anthus hodgsoni</i>	<i>Passeriformes</i>	Yes
8	Black-faced Bunting	<i>Emberiza spodocephala</i>	<i>Passeriformes</i>	No
9	Yellow-browed Warbler	<i>Phylloscopus inornatus</i>	<i>Passeriformes</i>	No
10	Gray Wagtail	<i>Motacilla cinerea</i>	<i>Passeriformes</i>	No
11	Little Bunting	<i>Emberiza pusilla</i>	<i>Passeriformes</i>	No
12	Black-faced Bunting	<i>Buteo japonicus</i>	<i>Accipitriformes</i>	No

Notes: Activity means whether there is a habit of using power lines or pylons.

entire Pacific coast of North and South America; 7) The 'American Mississippi Migration Route', which runs along the entire west-central part of North and South America; 8) The 'American Atlantic Migration Route', which connects the entire eastern part of North and South America and 9) 'Pacific Rim Migration Route'. Eastern China, especially the coastal areas, is right on the 'East Asia/Australia Migration Route' [14].

Unlike waterbirds, the migration routes of forest birds are more complex and different populations have different migration patterns, so it is difficult to judge their specific migration times and routes. According to previous research data, there are two main migration routes for forest birds arriving in Fujian Province, one by land, along the Wuyi Mountains into Fujian, and one along the coastline from Zhejiang into Fujian (Fig. 8).

Migratory Bird Migration Times. Summer migrant birds: start arriving in March to begin preparing for breeding and leave after September, winter migrant birds: start arriving in October and start leaving in March. Smaller birds of the order Finches often migrate at night (Table 6).

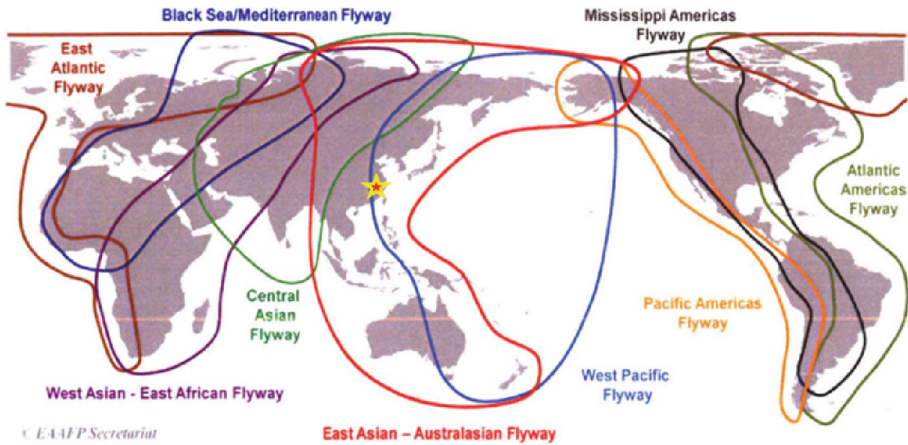


Fig. 8. Migratory bird migration routes affected by the construction of the power grid project (Modifications on the basis of the web page [15]). Notes: Yellow star mark survey plots for this study (Color figure online).

Table 6. Species of nocturnal migratory birds affected by power grid projects.

No.	Species	Scientific Name	Genus	Activity
1	Black Bulbul	<i>Hypsipetes leucocephalus</i>	<i>Passeriformes</i>	Yes
2	Dusky Warbler	<i>Phylloscopus fuscatus</i>	<i>Passeriformes</i>	No
3	Pallas's Leaf Warbler	<i>Phylloscopus proregulus</i>	<i>Passeriformes</i>	No
4	Arctic Warbler	<i>Phylloscopus borealis</i>	<i>Passeriformes</i>	No
5	Daurian Redstart	<i>Phoenicurus auroreus</i>	<i>Passeriformes</i>	Yes
6	Blue Whistling Thrush	<i>Myophonus caeruleus</i>	<i>Passeriformes</i>	No
7	Olive-backed Pipit	<i>Anthus hodgsoni</i>	<i>Passeriformes</i>	Yes
8	Black-faced Bunting	<i>Emberiza spodocephala</i>	<i>Passeriformes</i>	No
9	Yellow-browed Warbler	<i>Phylloscopus inornatus</i>	<i>Passeriformes</i>	No
10	Gray Wagtail	<i>Motacilla cinerea</i>	<i>Passeriformes</i>	No
11	Little Bunting	<i>Emberiza pusilla</i>	<i>Passeriformes</i>	No

Notes: Activity means whether there is a habit of using power lines or pylons.

4 Discussion

Our study shows that bird species richness is higher along 500 kV power grid project than 110 kV power grid project, indicating that grid linear projects increase landscape diversity and habitat diversity, which is consistent with the results of Kajzer-Bonk et al. [8] on bird diversity along railway lines in southern Poland. Also, the impact of the different phases of the power grid project on bird diversity shows that bird diversity

increases significantly during the maintenance phase, indicating that some birds are accustomed to the pylons and power lines, while the degree to which power grid projects still attracts some birds for nesting and stopping, which also indicates that power grid projects increase the heterogeneity of the homogeneous landscape from a landscape perspective. These results confirm that such human-constructed environments, at least in some cases, may not be harmful or may even be beneficial for biodiversity and should not be neglected in modern nature conservation [16, 17]. It seems that power grid projects do not introduce new functional properties into forest landscapes, but they also do not diminish existing properties, which is also worth noting in light of studies demonstrating the opposite effects in other linear manmade habitats [8, 9]. The effect may also depend on the landscape context. It is possible that in areas with more intense natural forest, the differences in biodiversity would be higher.

5 Conclusion

The specific impact of power grid projects on migratory birds in the Fujian region is subject to further study. According to the results of the current survey, future power grid projects should try to avoid increased forest fragmentation, and temporary construction roads should be restored as soon as possible in order to preserve animal passage. The affected migratory birds in the power grid deployment area under study are mainly finches and a few raptors, and according to the migration pattern of these two types of birds, construction during the bird migration season in March and October should be avoided as much as possible during the construction of power grid, especially the night-time construction of large converter stations and substations.

Author Contributions. Designed the research and constructed survey plots by Chang Lu and Xin Deng. Data analyzed and improved the manuscript by Xi Li. Writing the manuscript by Chang Lu and Jian Wang. Data and photo collected by Huaizhou Zheng. Tables and figures prepared by Mingfeng Zhang. All authors contributed to the article and approved the submitted version.

Funding. This work is supported by the State Grid Fujian Electric Power Co., LTD (52130T220007).

Conflicts of Interest. The authors declare no conflict of interest. The funders had no role in the design of the study; in the collection, analyses, or interpretation of data; in the writing of the manuscript, or in the decision to publish the results.

References

1. Ferrer, M., Morandini, V., Baumbusch, R., Muriel, R., De Lucas, M., Calabuig, C.: Efficacy of different types of “bird flight diverter” in reducing bird mortality due to collision with transmission power lines. *Global Ecol. Conserv.* **23**, e01130 (2020)
2. Garrido, J.R., Fernández-Cruz, M.: Effects of power lines on a white stork *Ciconia ciconia* population in central Spain. *Ardeola: Int. J. Ornithol.* **50**, 191–200 (2003)
3. Jenkins, A.R., Smallie, J.J., Diamond, M.: Avian collisions with power lines: a global review of causes and mitigation with a South African perspective. *Bird Conserv. Int.* **20**, 263–278 (2010)

4. Savereno, A.J., Savereno, L.A., Boettcher, R., Haig, S.M.: Avian behavior and mortality at power lines in coastal South Carolina. *Wildl. Soc. Bull.* **24**, 636–648 (1996)
5. Janss, G.F.E.: Avian mortality from power lines: a morphologic approach of a species-specific mortality. *Biol. Conserv.* **95**, 353–359 (2000)
6. Balmori, A.: Possible effects of electromagnetic fields from phone masts on a population of white stork (*Ciconia ciconia*). *Electromagn. Biol. Med.* **24**, 109–119 (2005)
7. Kajzer-Bonk, J., et al.: The effect of railways on bird diversity in farmland. *Environ. Sci. Pollut. Res.* **26**, 31086–31089 (2019)
8. Fahrig, L., Rytwinski, T.: Effects of roads on animal abundance: an empirical review and synthesis. *Ecol. Soc.* **14**, 21 (2009)
9. Morelli, F., Jerzak, L., Pruscini, F., Santolini, R., Benedetti, Y., Tryjanowski, P.: Testing bird response to roads on a rural environment: a case study from Central Italy. *Acta Oecol.* **69**, 146–152 (2015)
10. Back-to-back DC projects in China. International Electricity Network. <https://power.in-en.com/html/power-2376675.shtml>. Accessed 28 Sep 2020
11. IUCN: The IUCN Red List of Threatened Species. Version 2022-2 (2022). <https://www.iucnredlist.org>
12. National Forestry and Grassland Administration: List of National Key Wildlife Protection. Version 2021-02-01
13. National Forestry and Grassland Administration: List of terrestrial wildlife of national conservation, beneficial or economically or scientifically important value. Version 2017-03-15
14. National Forestry and Grassland Administration: The world's largest migratory route for migratory birds passes through China. <https://www.forestry.gov.cn/main/5462/20210123/093445680189938.html>. Accessed 26 Jan 2021
15. EAAFP Homepage. <https://www.eaaflyway.net>. Accessed 30 May 2023
16. Martínez-Abraín, A., Jiménez, J.: Anthropogenic areas as incidental substitutes for original habitat. *Conserv. Biol.* **30**, 593–598 (2016)
17. Maclagan, S.J., Coates, T., Ritchie, E.G.: Don't judge habitat on its novelty: assessing the value of novel habitats for an endangered mammal in a peri-urban landscape. *Biol. Conserv.* **223**, 11–18 (2018)



Methodology for Monitoring the Ecological Environment of Railway Construction

Jieyu Zhang¹, Yuying Zhang², Xiuhong Li²(✉), Yanrong Lu², and Yitong Yin²

¹ Energy Saving and Environmental Protection and Occupational Safety and Health Research Institute, China Academy of Railway Sciences Co., Ltd., Beijing 100081, China
zhangjy@rails.cn

² State Key Laboratory of Remote Sensing Science, Faculty of Geographical Science, Beijing Normal University, Beijing 100875, China
lixh@bnu.edu.cn

Abstract. As a linear project, the ecological environment along the railway construction project is complex and changeable, with a high proportion of tunnels and bridges, which makes ecological environmental protection management difficult and requires regular investigation and monitoring of the impact of construction on the ecological environment. Based on the characteristics of railway engineering, this study analyzes and summarizes the ecological environment monitoring scheme and technical methods during railway construction, and then puts forward relevant environmental protection measures. The results show that the ecological environment monitoring of railway construction is generally divided into four stages: preliminary investigation and analysis, monitoring sites, data collection and work results. The monitoring content from macro to micro, from ecosystem to plants, animals and other specific indicators. The main monitoring methods include manual investigation, remote sensing monitoring, infrared trigger camera trap, etc. According to the specific ecological characteristics and ecological problems, the construction of a scientific and complete ecological environment monitoring program for railway construction is conducive to mastering the trend of the ecological environment change in the process of railway construction, and implement the environmental protection measures and construction project environmental protection policies more pertinently.

Keywords: Ecological Environment Monitoring · Railway Construction · Ecosystem · Wild Animals and Plants

1 Introduction

In order to solve the contradiction between railway construction and ecological environment, it is necessary to carry out ecological environment monitoring for railway construction projects, so as to grasp the change trend of ecological environment in the process of railway construction and implement various environmental protection measures and construction project environmental protection policies more pertinently [1]. For railway construction projects, ecological environmental protection monitoring mainly

includes the monitoring of environmental factors within a certain range along the railway, the environmental impact and protection measures of main engineering and temporary engineering such as roadbed, bridge and tunnel, the impact of construction process on ecological environmental factors and pollution environmental factors and restoration [2]. However, the railway construction period is long, the proportion of Bridges and tunnels is high, and the region along the railway has the characteristics of significant terrain elevation difference and fragile ecological environment, which brings various difficulties to the scientific investigation and environmental management along the railway, and also puts forward new demands for railway construction and environmental protection. Therefore, it is necessary to study the ecological environment monitoring of railway construction, so as to provide reference scheme design and technical methods for railway environmental protection.

In 1965, the United States formulated the “Highway Beautification Regulations”, paying attention to the visual coordination between the highway and the environment. From the design to the construction stage, the requirements on environmental protection are very strict. Try to avoid high filling and deep digging in the design, and carry out the road landscape design, and set up monitoring systems in the key sections to detect the air quality and environmental quality. In 1975, the 15th International Road Conference in Mexico established a working group on “Road and Environment Problems”, which proposed that new highways must consider environmental problems and carry out environmental impact assessment, and put forward corresponding ecological environmental protection measures in view of the impact. In the late 1970s, some countries established laws and management mechanisms for highway environmental protection, taking ecological environmental factors into account in the planning, design, construction and operation stages, reflecting the principle of ecological priority from beginning to end, with special emphasis on the study of wild animals and their habitats [3]. In the planning and construction of highway network, environmental impact assessment is firstly carried out, and then landscape design, environmental restoration and governance are carried out. Ecological protection measures and highway construction are unified in planning, design, construction and operation, and corresponding environmental investigation and monitoring mechanisms are established at each stage.

The monitoring of macroscopic ecological changes around road areas before and after road construction is an important research direction of road ecological monitoring. Remote sensing technology, due to its greater selectivity in time and space, can provide decision-making basis for route selection and construction design influenced by ecological environment, and provide data support for ecological environmental evolution research and ecological environmental protection along the road during and after construction. Therefore, remote sensing technology is more and more applied in road ecological monitoring to provide a comprehensive picture of the actual situation and change process of the ecological environment in the process of highway construction and operation. Bai et al. used remote sensing images to construct a potential-connectedness-resilience framework and evaluated the landscape ecological risk level of China-Laos Railway [4]. Guo et al. and Liu et al. analyzed the spatio-temporal dynamic changes

of land use, vegetation types, desertification and soil erosion in the areas surrounding Beijing-Tianjin intercity high-speed railway and Hongliu River to Nuomao Lake Railway by using remote sensing images [5, 6].

In addition to the above macro monitoring by satellite remote sensing images, fauna, flora and biodiversity are important components of the ecological environment. The changes of vegetation coverage and growth, animal population and habitat, biodiversity and other micro indicators before and after operation have also attracted wide attention. Researchers usually use artificial field survey combined with technology to analyze the changes of vegetation along the road, its species diversity and plant physiological characteristics, which can reflect the impact of road construction or operation on the ecological environment. Ma et al. set up a vegetation survey quadrat on both sides of Tongpu Railway to analyze vegetation diversity and environmental gradient on both sides, and the monitoring index was the change of species diversity index, uniformity index and richness index of shrub layer and herb layer [7]. Impacts of road construction on animals are mostly shown as impacts on wildlife habitat quality. Zhang et al. compared satellite remote sensing data before and after the construction of passenger dedicated lines between Xi'an and Chengdu in 2010 and 2014 to analyze changes in vegetation type, area and spatial distribution. Combined with the data of the fourth panda survey, the impact of the Xicheng Passenger Dedicated Line on the panda habitat was evaluated. The results showed that the direct impact of the construction period on the panda habitat vegetation was small [8].

In the research process of monitoring and evaluation indicators, Huang and Wen selected the indicators of comprehensive evaluation of road ecological health into five aspects: engineering design class, land resources class, ecological environment class, landscape greening class, management class [9, 10]. Zou et al. selected natural causes (soil erosion, vegetation coverage, etc.) and impact performance (engineering interference) to evaluate ecosystem integrity in the study of ecosystem evaluation in the Minle to Yumen section of the second line of Lanzhou-Xinjiang Railway [11]. Li proposed a remote sensing monitoring index system for road ecological environment, including road network density, affected area, road length, width, affected width, land use type/area, vegetation type/area/coverage, etc. [12]. Song established evaluation criteria from three aspects of sensitive area protection, service function value and landscape change, selected 16 indicators to construct a comprehensive evaluation system, and used ecological impact comprehensive evaluation index to represent the impact degree of railway engineering scheme design on the ecosystem [13].

The ecological environment monitoring of construction projects, especially highway construction projects, is mainly macro monitoring during the construction process and after operation. It mainly uses macro technical means to compare vegetation, land use and landscape before and after construction, while there are relatively few researches on micro monitoring of vegetation and soil along the route by artificial investigation. With the emergence of new technologies such as unmanned aerial vehicles (UAVs), low-altitude remote sensing monitoring of UAVs has also been applied to railway construction projects, most of which use UAVs to directly monitor the range of soil erosion and soil conservation measures [14]. Compared with satellite and manned aircraft and other aerospace ground information acquisition platforms, UAV near ground remote sensing

platform has the advantages of fast image acquisition speed, large coverage area, short application cycle, high image definition (accuracy can reach centimeter level), easy analysis, less constraints from natural environment, low cost, easy operation, and low operation and maintenance cost. It makes up for the deficiency of traditional satellite remote sensing and ordinary aerial remote sensing.

This study analyzes and summarizes the research on ecological environment monitoring of railway construction from macro to micro monitoring methods, monitoring scope and monitoring distribution, so as to provide a basis for the systematic implementation of construction projects and environmental protection.

2 Method

The ecological environment monitoring of railway construction projects should be in line with the principles of comprehensive overview, reasonable deployment, strong representation, reliable methods, economic feasibility and quality assurance. With the environmental impact assessment report and its approval as the main basis and relevant materials of railway engineering technical documents as reference, ecological methods are used to monitor the impact of engineering construction on ecology on the basis of the preliminary investigation of ecological status and the preliminary analysis of the construction and operation of the project. The ecological environment monitoring of railway construction projects is generally divided into four stages, which are preliminary survey and analysis, monitoring deployment, data collection and work results. The specific technical process is shown in Fig. 1.

- (1) In the preliminary investigation and analysis stage, the main work is to investigate the regional ecological environment, engineering and construction, determine the monitoring scope, and propose monitoring programs or plans.
- (2) In the monitoring the deployment stage, it is necessary to further determine and complete the layout of various monitoring points within the monitoring scope. Monitoring points should be integrated with the impact factors, select representative, reflecting the environmental impact of the railway construction period location.
- (3) In the data acquisition stage, monitoring data can be obtained through on-site sampling, detection, observation, collection of satellite remote sensing data, aerial photography of UAV, etc., according to the planned monitoring frequency.
- (4) In the work results stage, carry out data analysis and processing, and form monitoring charts, reports and other results.

2.1 Monitoring Indicators and Monitoring Content

(1) Ecosystem

According to the “National Ecological Condition Survey and Assessment Technical Specification – Project Scale Ecological Impact Assessment HJ 1175-2021” [15], the project scale ecological impact survey and assessment index system is divided into two parts: ecologically sensitive targets and ecosystems, as detailed in Table 1.

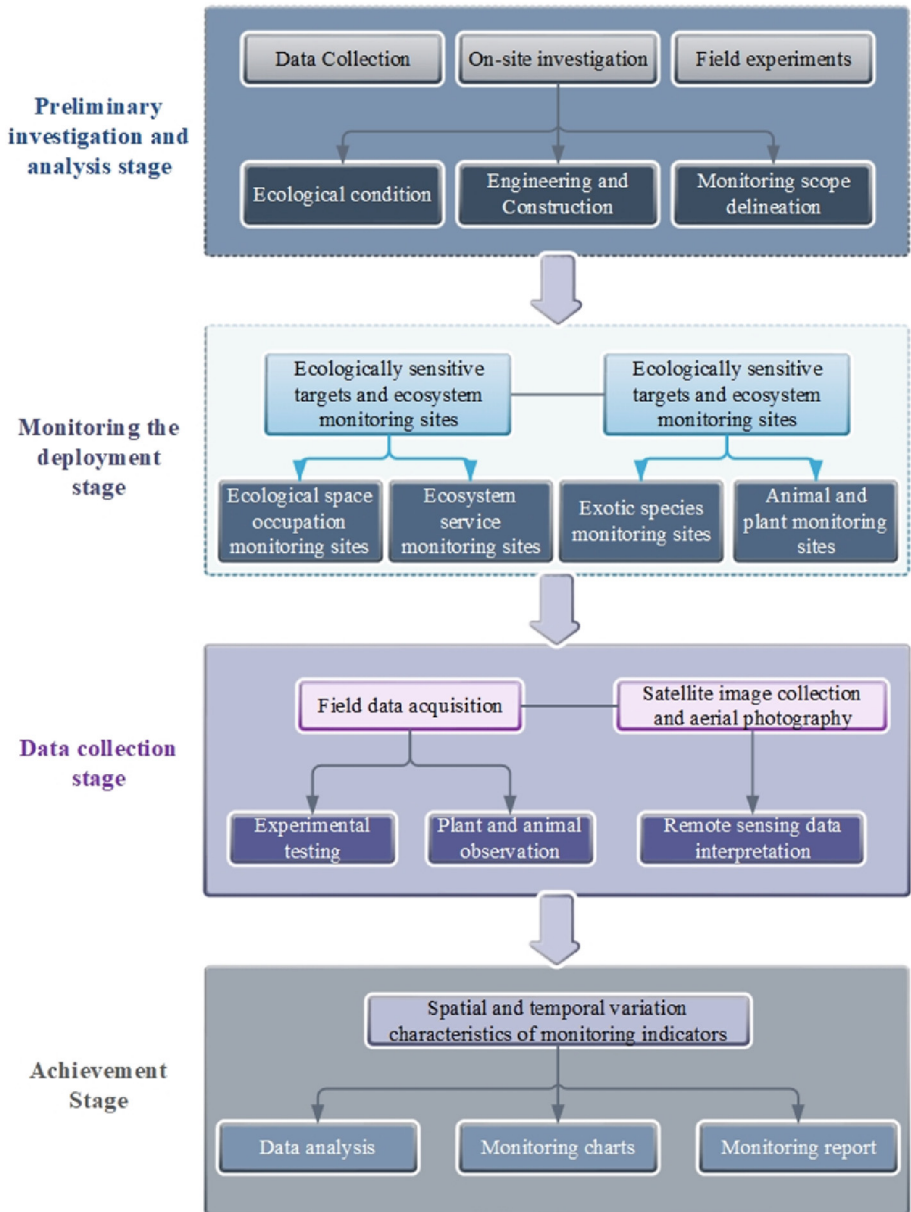


Fig. 1. Basic flow chart for ecological monitoring of railway construction projects.

(2) Plants and Vegetation

Fractional vegetation cover is obtained by vegetation index calculation, and the most commonly used is the normalized difference vegetation index (NDVI), which reflects the background influence of the green plant canopy. Vegetation index is usually used

Table 1. Project scale ecological impact survey and assessment index system.

Types	Indicators	Meaning
Ecologically sensitive targets	Distance or overlap with construction area relationship	Distance or overlapping area and length of the project construction area and surrounding ecologically sensitive targets
	Occupied area	The area of ecologically sensitive areas occupied by the project, including the main project, temporary works, etc.
Ecosystem	Occupied area	The area of the project construction area occupying different types of ecosystems, including the specific amount and proportion
	Ecosystem change	Changes in typical ecosystem characteristics factors in the construction area of the adjacent railway project during the monitoring cycle

to evaluate regional ecological environment status. NDVI adopts the maximum value of vegetation growth period, and takes the whole growth period of vegetation as the time scale for monitoring, that is, it is appropriate to monitor once a year in the growing season. It should be noted that the railway is a linear construction project, and the climate and regional differences from the starting point to the end point will be very obvious, and the differences in vegetation index will also be significantly different. Therefore, the spatial differences in vegetation index cannot be used to directly determine the impact of railway construction on vegetation. Instead, the impact of railway construction and artificial restoration on vegetation along the line can be reflected through the difference of vegetation index in different years in the same section.

Vegetation biodiversity is used as a monitoring indicator for nature reserves with biodiversity as the main conservation object. In this study, the species diversity of plant communities along the railway line was used as a specific indicator of biodiversity. The proportion of species diversity reduction is the proportion of species reduction to the original species, that is, the impact of project construction and operation on habitat quality.

(3) Wild Animal

In this study, the quantity and habitat changes of wild animals near the railway before and after the railway construction are selected as monitoring indicators, which can basically reflect whether wild animals are affected by the railway. The monitoring objects are mainly key national protected animals, and the number of animals is the

number of wild animals near the railway. Animal habitat, also known as habitat, is an important place for animals to live and breed. It is mainly monitored whether it is occupied, divided or otherwise affected by railway land or temporary land, and whether the area is reduced or the quality is reduced as a result.

2.2 Monitoring Scope, Location and Method

(1) Monitoring Scope

The monitoring scope includes time range and space range, which should be determined according to the characteristics of railway construction project and the ecological characteristics of the region. The scope of ecological monitoring should be no less than the project construction area and the area within 1000m away from the central line of railway and the outer boundary of station. If there are ecologically sensitive targets within 2000m of the surrounding the main project and temporary project, they should be included in the monitoring scope.

(2) Monitoring Deployment

Vegetation monitoring sites should be laid according to the influence range of the project on vegetation, taking into account the topography and geomorphology, vegetation distribution and vegetation flora along the route, including the types of forest, shrub and meadow vegetation in typical altitudes and climatic zones, covering major project types. The specific point location can be adjusted according to the detailed project layout, vegetation distribution characteristics, traffic conditions and location of sensitive areas. Protection level in the state II and above the key protection plants should also be distributed.

Wildlife monitoring sites should be set up on roads near ecologically sensitive targets and key wild animal distribution roads in the background survey, focusing on tunnel entrances and exits, bridges, roadbeds, stations, auxiliary adit exits, construction roads, large temporary projects, etc.

(3) Monitoring Method

A background ecological survey and monitoring should be carried out before the construction of railway construction projects. Ecologically sensitive areas, plants and animals should be monitored quarterly or semi-annually, and ecosystems should be monitored every 1 to 2 years. The monitoring frequency of different monitoring contents can be adjusted according to the progress of project construction. The monitoring indicators can be carried out by the following monitoring methods:

Area of ecosystem type occupied by the project construction area: define the total area of the project and the area type and proportion of different ecosystems. The specific method should meet the requirements of technical specifications [15]. The analysis focuses on the ecosystem types with higher ecological service functions, including forest, wetland, grassland, etc.

Ecosystem change: whether the natural ecosystem near the railway project construction area has undergone significant changes in structure and function due to railway

construction. Specific methods should meet the requirements of technical specifications [15].

Changes in plant diversity: survey and statistics are adopted to count the number of wild plant species within the monitoring range and compare with the number of species before the construction of the project. For specific methods, refer to the Technical Guidelines for biodiversity observation [16].

Protection of key plants: monitoring the species, distribution and growth of key protected wild plants and whether they are affected by railway construction projects by means of site survey and data collection.

Changes in animal diversity: infrared triggered camera traps and manual survey and statistics can be used to count the number of wild animal species within the monitoring range, and compare the number of species before the construction of the project, whether it is affected by the railway construction project. For specific methods, refer to the Technical Guidelines for biodiversity observation [16], which can be divided into mammals, birds, amphibians, reptiles and fishes.

Protection of key wild animals: infrared trigger camera traps and manual investigation and statistics can be used to compare the species, distribution and activities of key protected wild animals with the number of species before the construction of the project, and whether they are affected by the railway construction project.

Invasive risk of alien species: monitoring the species and distribution of alien species and whether the railway construction has caused the expansion of the distribution range of alien species or the introduction of new alien species by on-site survey and data collection. Alien invasive species refer to the List of Alien Invasive Species under State Key Management [17].

3 Conclusion

Based on the quantitative indicators of ecology, soil science, railway engineering, soil and water control, environmental assessment, completion acceptance and other disciplines, combined with the characteristics of railway engineering process and the needs of monitoring data acquisition methods, this study distinguished different monitoring indicators under the conditions of background and process, conventional and special, along and sensitive areas, daily and emergency, etc. The conclusions are as follows. Ecological monitoring of railway construction projects should take into account the ecological and environmental, biological and abiotic contents, and then adjust according to the ecological status of specific regions. The biological and abiotic contents of ecological monitoring include various indicators, and the specific ecological impact of the contents should be described from different aspects. According to specific ecological characteristics and ecological problems, as well as different indicators, a scientific, complete and feasible indicator system should be constructed through reasonable refinement and screening, so as to increase the persuasion of monitoring results.

Author Contributions. Writing-original draft, J.Z.; Formal analysis, Y.Z.; Conceptualization, X.L.; Investigation, Y.L. and Y.Y. All authors have read and agreed to the published version of the manuscript.

Funding. This research was supported by Research on Key Technologies of “Intelligent Environmental Butler” Service System for Railway Construction Project (Key Research Project of China Academy of Railway Sciences Group Co., LTD. 2022YJ211).

Data Availability Statement. The data presented in this study are available on request from the author.

Declaration of Competing Interest. The authors declare that they have no known competing financial interests or personal relationships that could have appeared to influence the work reported in this study.

References

1. Wang, P., Yang, N., Quintero, J.D.: China: The Environmental Challenge of Railway Development. World Bank Group, Washington, D.C. (2012)
2. Karlson, M., Karlsson, C.S.J., Mörtberg, U., et al.: Design and evaluation of railway corridors based on spatial ecological and geological criteria. *Transp. Res. Part D: Transp. Environ.* **46**, 207–228 (2016)
3. Qiu, W., Liu, Y., Lu, F., et al.: Establishing a sustainable evaluation indicator system for railway tunnel in China. *J. Clean. Prod.* **268**, 122150 (2020)
4. Bai, H., Weng, L.: Ecological security pattern construction and zoning along the China-Laos Railway based on the potential-connectedness-resilience framework. *Ecol. Ind.* **146**, 109773 (2023)
5. Guo, Q., Jiang, W., Wang, Z.: Effect of high-speed railway on the spatial-temporal changes of surrounding area land use. *J. Chongqing Jiaotong Univ. Nat. Sci. Ed.* **34**(4), 133–139 (2015)
6. Liu, Y.: The impact analysis of peripheral ecological environment of railway construction in ecological fragile region. *Railway Stand. Des.* **60**(10), 141–144 (2016)
7. Ma, J.: Gradient analysis of environment and vegetation diversity on both sides of Tongpu railway. *Shanxi Forest. Sci. Technol.* **40**(3), 20–23 (2011)
8. Zhang, H., Zhang, W., Hu, H., et al.: Assessment of the construction period of Xi’an-Chengdu high speed railway impact on the giant panda habitats. *Chin. J. Wildl.* **42**(1), 192–198 (2021)
9. Huang, Y.: The Influence of Expressway Construction on the Stability of Natural Ecosystem. Central China Normal University (2011)
10. Wen, Y.: Study on Ecological Environment Evaluation and Greening Pattern Design of Highway Domain in Ecologically Fragile Area. Northeast Forestry University (2013)
11. Zou, C., Shen, W., Zhou, L., et al.: Ecological system integrity assessment of railway construction in Cold and arid regions of Northwest China: a case study of Minle to Yumen section of Lanzhou-Xinjiang railway second line. *J. Ecol. Rural Environ.* **28**(6), 633–637 (2012)
12. Li, H., Wang, Y., Guan, L., et al.: Study on index system of highway ecological environment monitoring by remote sensing. *China Achiev. Sci. Technol.* **5**, 35–37 (2014)
13. Song, Z.: Research on railway scheme evaluation model based on ecological impact of whole line. *Environ. Sustainable Dev.* **40**(2), 85–87 (2015)
14. Wang, Z., Fu, G., Wei, L., et al.: Application of UAV low altitude remote sensing technology in soil and water conservation monitoring of linear engineering – a case study of the newly built Chongqing-Wanzhou Railway. *Sci. Soil Water Conserv.* **13**(4), 109–113 (2015)
15. Technical Specification for National Ecological Status Investigation and Assessment – Project-Scale Ecological Impact Assessment (HJ 1175–2021)

16. Technical guidelines for biodiversity observation: Terrestrial vascular Plants (HJ 710.1-2014), Terrestrial Mammals (HJ 710.3-2014), Birds (HJ 710.4-2014), Reptiles (HJ 710.5-2014), Amphibians (HJ 710.6-2014), Fish in inland waters (HJ 710.7-2014)
17. List of Alien Invasive Species under National Priority Management (First Batch), Announcement No. 1897 of the Ministry of Agriculture of the People's Republic of China (2012)



Analysis and Suggestions on Agricultural Non-Point Source Pollution-Yongchuan District, Chongqing as an Example

Yanrong Lu¹, Rongjin Yang², Zhang Le², Meiyong Sun², and Xiuhong Li¹(✉)

¹ State Key Laboratory of Remote Sensing Science, Faculty of Geographical Science, Beijing Normal University, Beijing 100875, China

202131490009@mail.bnu.edu.cn, lixh@bnu.edu.cn

² State Key Laboratory of Environmental Criteria and Risk Assessment, Chinese Research Academy of Environmental Sciences, No. 8, Da Yang Fang, An Wai, Chao Yang District, Beijing 100012, China

{yangrj, zhangle, sun.meiyong}@craes.org.cn

Abstract. Among various types of pollution, agricultural non-point source pollution (AGNPS), as an important component of water pollution, has received significant attention from countries around the world in the past forty years. Especially after the effectiveness of point source pollution prevention and control, AGNPS prevention and control has become an international problem, and the overall research on AGNPS prevention and control has also become a hot topic. The 14th Five Year Plan period is a period of in-depth promotion of AGNPS prevention and control, and China has also conducted many studies on AGNPS in recent decades. This study focuses on research and policies on AGNPS in recent years in China, and summarizes the existing problems in the field of agricultural non-point source, such as the lack of top-down full chain technology and a lack of comprehensive evaluation standards. At the same time, Taking Yongchuan District of Chongqing City as an example, the study analyzed the relationship between the concentration of major pollutants and rainfall, fertilizer and pesticide application, planting and livestock breeding in the Zhu Tuo section of AGNPS. Finally, the factors that need to be focused on controlling AGNPS are proposed, and the governance work should be carried out based on the full chain technology of monitoring, tracing, calculation, governance, and management. The study proposes that the entire system of AGNPS needs to be improved and targeted policies should be introduced in order to provide basic support for the control of AGNPS, thereby improving the ecological environment and achieving sustainable ecological development.

Keywords: Non-Point Source Pollution · Agriculture · Governance · Policy Suggestion

1 Introduction

Pollution prevention and control has always been a topic of concern to the world. According to statistics, 30%–50% of the global earth's surface has been affected by surface source pollution [1–3]. Surface source pollution, also known as non-point source pollution (NPS), consists mainly of soil particles, nutrients such as nitrogen and phosphorus, atmospheric particles, pesticides, etc., which enter the water, soil or atmosphere through surface runoff, agricultural drainage, etc. It has the characteristics of randomness, extensiveness, vagueness and lagging. Compared with point source pollution, the source of point source pollution is clear, and the monitoring and management objectives are high and clear, so the international management of point source pollution has been quite effective in recent years. And NPS, especially AGNPS is widely distributed, pollution is difficult to trace the source, in different land type areas, flood, non-flood pollution elements are different, increasing the difficulty of monitoring and management.

In the 1960s, the study of AGNPS started abroad, the United States, Japan, the United Kingdom and some other developed countries on the basis of point source pollution prevention and control began to tackle AGNPS, they first from the concept and then to the theory, model gradually developed [4]. In the 1970s, the United States issued a series of laws to control AGNPS, determining the implementation of the Clean Water Act, and ushering in a new era of AGNPS control [5]. Developed countries such as Europe and America have conducted early research on the assessment of AGNPS and related policies and laws. As early as 1936, the United States enacted the first domestic AGNPS control law, which made clear provisions for rural environmental quality and held accountable for illegal activities that undermine rural environmental quality [6]. In terms of AGNPS policies, the Best Management Practices (BMPs) program implemented in the United States has been widely applied in the identification process of key source areas [7]. The United States began implementing AGNPS BMPs as early as the 1970s and has achieved significant results. The BMPs in the United States have developed measures for agricultural and urban BMPs based on the sources of AGNPS, and each management measure is the most suitable governance measure based on the characteristics of AGNPS [8]. At the same time, regulations, policies, and guarantee systems have been established for the entire process of supervision, including “source target constraints – full factor governance requirements – regulatory means – governance mechanisms – end point governance requirements” [9]. European Union countries reduce the impact of agricultural non-point sources by enacting registration and use systems for fertilizers and pesticides, providing high subsidies to farmers who adopt environmentally friendly production technologies, and increasing funding for environmental protection at all levels of government [10]. Both the European Union and the United States attach great importance to increasing farmers' enthusiasm in controlling AGNPS, and have introduced relevant policies to guide and cultivate farmers to voluntarily learn new skills and use new technologies, in order to control AGNPS from the source [11]. Overall, research has been conducted on prevention and control technologies, policies, and guarantee systems for AGNPS in foreign countries, and good results have been achieved. However, there is still room for further research on the evaluation of various technologies and policies.

Research on AGNPS in China is later than that of foreign countries. Since the 1980s, scholars began to carry out systematic research on Agricultural pollution. Policy system

in China based on the prevention and control of AGNPS was initially established [12]. Since 2000, the issue of AGNPS has been given national attention, and the policy system for preventing and controlling AGNPS has gradually been established. At the same time, evaluation plans based on statistical models have also begun to be established. During this period, policies were more inclined towards macro prevention and control, with relatively single evaluation plans. The “Regulations on the Prevention and Control of Pollution from Livestock and Poultry Scale Breeding” issued in 2013 is a milestone document for the prevention and control of AGNPS in China. From this time on, the prevention and control of AGNPS in China began to form a systematic policy pattern for AGNPS prevention and control [13]. In 2015, the Ministry of Agriculture issued the “Implementation Opinions on Fighting the Battle of Agricultural Non-point Source Pollution Prevention and Control”, which was the first special policy introduced to address the issue of agricultural non point source pollution prevention and control. It was not until 2021 that the country officially introduced the targeted plan “Implementation Plan for the Control and Supervision of Agricultural Non-point Source Pollution (Trial)”. However, at present, prevention and control of AGNPS in China focuses more on research on agricultural non-point sources, and there is a lack of specific development of relevant standards for non-point source prevention and control, as well as technical standards for evaluation of prevention and control effects. For a long time to come, research on AGNPS should combine GIS technology, model simulation, and on-site monitoring methods, and develop specific standards and policies based on evaluation.

Foreign research on AGNPS management has achieved fruitful research results and practical experience, which has strong significance for the improvement of AGNPS management in China. At this stage, China has made some academic achievements in AGNPS management research, but the research on the prevention and control of AGNPS in China is still very limited, and there is still a lack of perfect whole-chain technology and assessment structure system for prevention and control. This study is based on the existing problems of AGNPS and conducts statistical analysis of non-point source related factors in the research area. Explore the key factors affecting AGNPS in the data results and propose prevention and management suggestions based on this.

2 Research Method

To study the prevention and control of AGNPS, it is necessary to have a detailed understanding of the situation in the research area in the early stage, and to analyze the relevant data of AGNPS through various methods, establish a comprehensive and systematic assessment system, promote the orderly and precise implementation of AGNPS prevention and control work, and overcome the difficulty of AGNPS as soon as possible.

(1) Remote sensing and geographic information system analysis

Remote sensing and geographic information system analysis methods are one of the main and fundamental research methods. Based on multi temporal and cross-sectional data on the concentration and flux of major non-point source pollutants, analyze the spatial changes of long time series in typical regions, and analyze the spatiotemporal changes in the concentration and flux of major pollutants in different typical regional

cross-sections. Conduct single factor spatial pattern analysis and multi factor spatial correlation analysis using environmental data and socio-economic data. Use principal component analysis, analytic hierarchy process, and other methods to screen indicators and construct an evaluation index system.

(2) Field research method

Based on different typical cross-sections, methods such as field research and discussions were used to understand the situation of AGNPS and its control measures, as well as economic and social development in typical areas. The research and discussion content includes the quality status of cross-sectional water environment, the current situation of AGNPS, measures for controlling AGNPS, the current situation of economic and social development, and the current situation of land use.

(3) Literature research method

Regarding the research on the policy system and normative system for preventing and controlling AGNPS, a literature review method was used to analyze the current status, historical changes, and future plans of the policy system for preventing and controlling AGNPS at home and abroad, as well as the current status and future plans of the policy system and standards for preventing and controlling AGNPS in relevant provinces, regions, and sub basins of the Yangtze and Yellow River basins, as well as the policy system and standards for preventing and controlling AGNPS in China, Research on policies, systems, and norms for the prevention and control of AGNPS on the existing basis.

(4) Model simulation method

Mainly applied to analyze the spatiotemporal changes in concentration and flux of major pollutants in the cross-section, identify the main driving factors of spatiotemporal changes, and construct an assessment system for AGNPS prevention and control. Based on environmental data, SWAT/HSPF/AGNPS/LOADEST and other models are selected as needed to analyze the characteristics of AGNPS in the watershed, and to study the main driving factors of spatiotemporal changes in the concentration and flux of major pollutants in the cross-section.

(5) Monitoring analysis method

Based on the relevant data obtained from the agricultural non-point source monitoring network, targeted and supplementary monitoring of the concentration and flux of major pollutants will be carried out according to the assessment and evaluation objectives, in order to meet the needs of the assessment and evaluation of land plots and research areas.

3 Research Results

3.1 Overview of the Research Area

Yongchuan District of Chongqing is located in the north bank of the upper reaches of the Yangtze River, southwest of Chongqing, $105^{\circ} 38' - 106^{\circ} 05' E$, $28^{\circ} 56' - 29^{\circ} 34' N$ (Fig. 1). The landform of Yongchuan District is complex and diverse, and the terrain is

relatively flat. It is dominated by low mountains and hills. The altitude of the whole area is 172–990 m. Five low mountains and mountains cross the whole area in the form of “Sichuan” from north to south. Hills, gentle hills and terraces are distributed alternately, making it a typical hilly area in Chongqing. The planting area of grain crops in the entire region is 980000 mu, with a total yield of 481000 tons; The grain crops planted in Yongchuan District include rice, wheat, corn, sorghum, soybeans, beans and potatoes. The Cash crop planted include peanuts, rapeseed, sesame, vegetables (including edible fungi), melons and fruits, tea, pepper, etc. The livestock and poultry farming in the region is mainly based on live pigs and poultry.

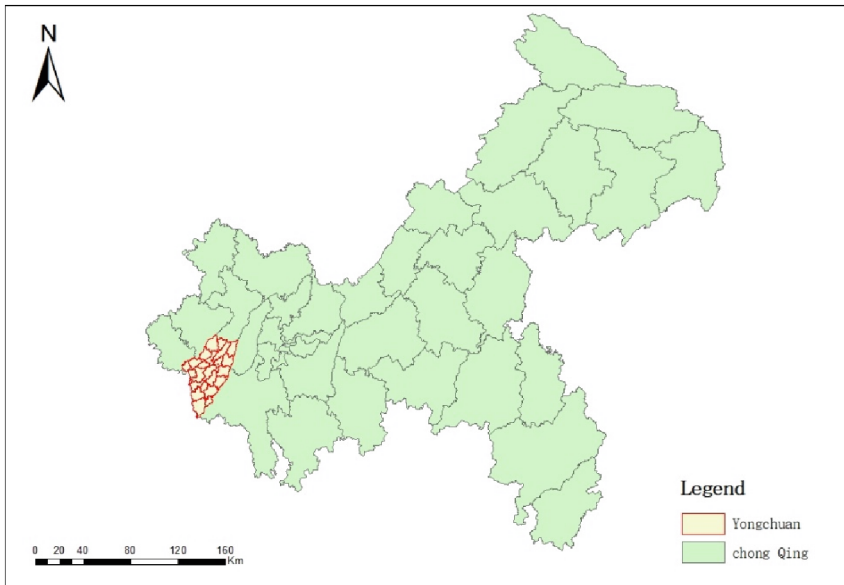


Fig. 1. Regional Map of Chongqing and Yongchuan District.

3.2 Analysis of Agricultural Non-Point Source Pollution in the Research Area

According to the analysis on the planting area and yield of various agricultural crops in Yongchuan District from 2014 to 2021(Figs. 2 and 3), the Plantation industry in Yongchuan District is dominated by food crops and vegetable crops, and the planting area of vegetable crops is increasing. At the same time, from the perspective of crop yield, vegetable yield is the highest and increasing year after year, while other crop yields show a stable trend. The change in crop area planted over the years indicates a change in regional planting types, which directly affects the sources of agricultural non-point source pollutants.

The use of chemical fertilizers in Yongchuan District has shown a downward trend year by year from 2015 to 2021(Figs. 4 and 5), of which nitrogen, phosphorus and potassium fertilizers have the same trend, and the downward trend of nitrogen fertilizer is

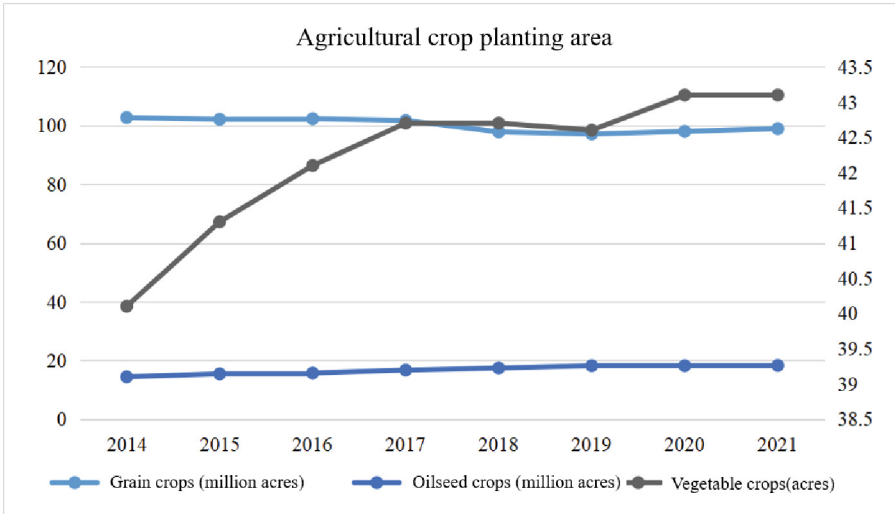


Fig. 2. Crop planting area in Yongchuan District from 2014–2021.

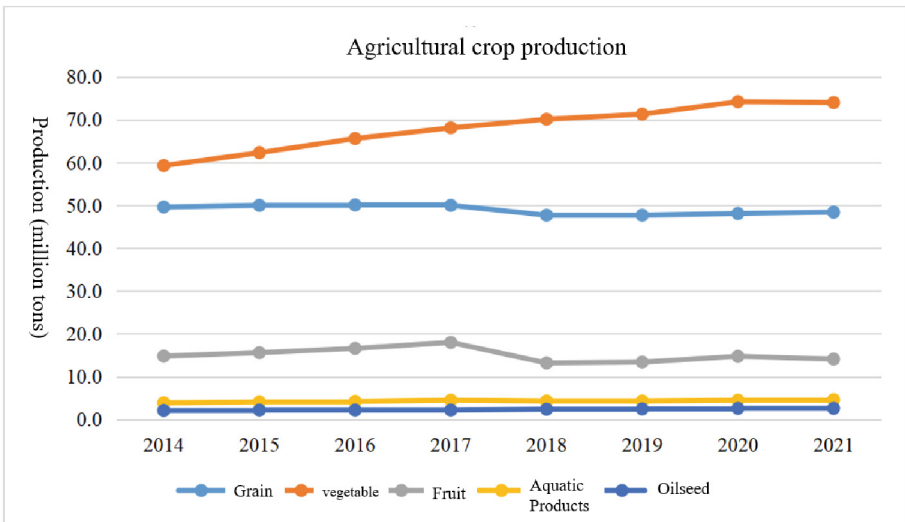


Fig. 3. Crop yield in Yongchuan District from 2014–2021.

obvious, especially from 2017 to 2018. The use of pesticides has also shown a downward trend in recent years. To sum up, the use of fertilizers and pesticides in Yongchuan District has shown a downward trend year after year, which indicates that Yongchuan District has accurately implemented the policy of fertilizer and pesticide reduction after the issuance of the policy of fertilizer and pesticide reduction, and has obvious reduction effect. It is necessary to combine this important measure in the analysis of AGNPS to

study the practical role of fertilizer and pesticide reduction in the prevention and control of AGNPS in the basin.

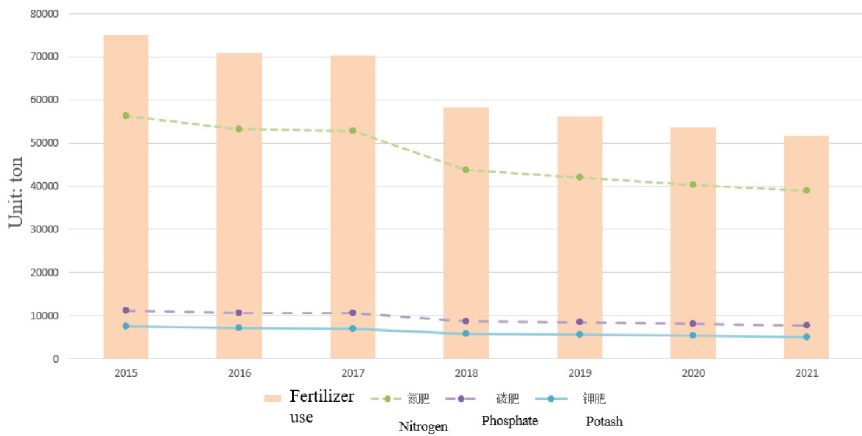


Fig. 4. Fertilizer Application in Yongchuan District from 2015–2021.

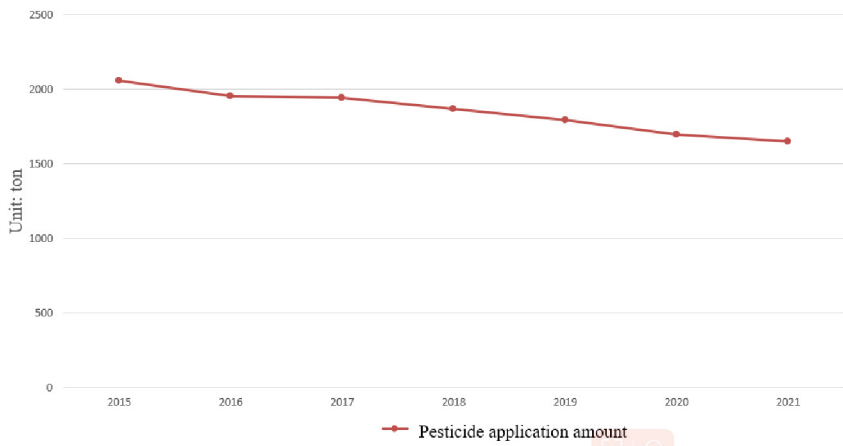


Fig. 5. Use of Pesticides in Yongchuan District from 2015–2021.

Rainfall is an important factor affecting the inflow of agricultural non-point source pollutants into rivers. The rainfall data of Yongchuan District were collected and analyzed. From the Precipitation figure (Fig. 6), it can be seen that the annual rainfall in Yongchuan District is mainly concentrated in June September, which is also the flood season of Yongchuan District. Most of the maximum rainfall comes from July, and some years will be in August and September. The rainfall during the flood season of 2019 was low. In general, Yongchuan District is dry and has little rainfall in non flood season, so attention should be paid to the precipitation index when studying AGNPS.

On the basis of rainfall data, the pollutant monitoring data of the ZhuTuo section from 2019 to 2021 were selected for the study, and the monthly data of pollutant content was organized (Fig. 7). Zhu Tuo section is located in the southeast of Yongchuan District, belongs to the national control section, the data is publicly released, accurate and easy to obtain. Between 2019 and 2021, the water quality changes were relatively stable, mostly in Class II and III water. The changes in pollutants highlighted the lag of agricultural non-point sources, and concentration accumulation occurred during non flood seasons. During the flood season, the concentration decreased due to rainwater erosion. In addition, in August 2019, the water quality deteriorated to IV and total phosphorus exceeded the standard, indicating that agricultural non-point source pollutants in the region should focus on total phosphorus.

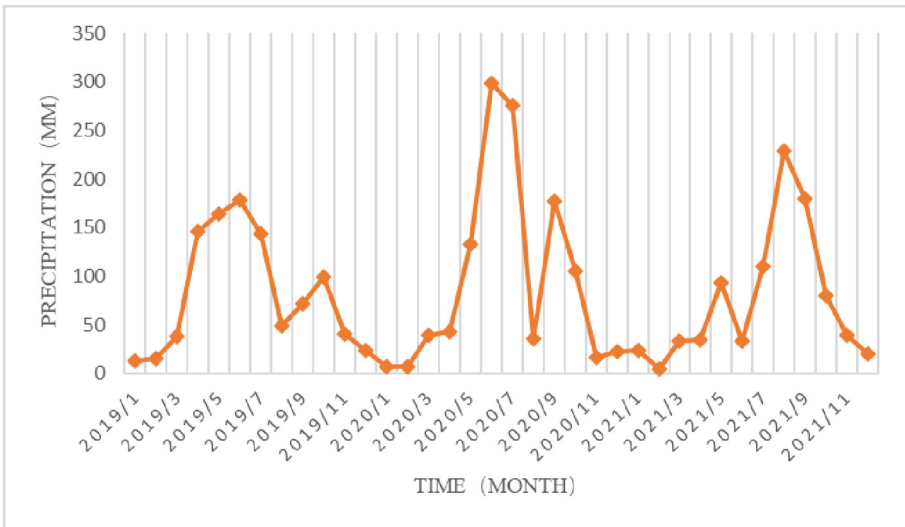


Fig. 6. Precipitation in Yongchuan District from 2019–2021.

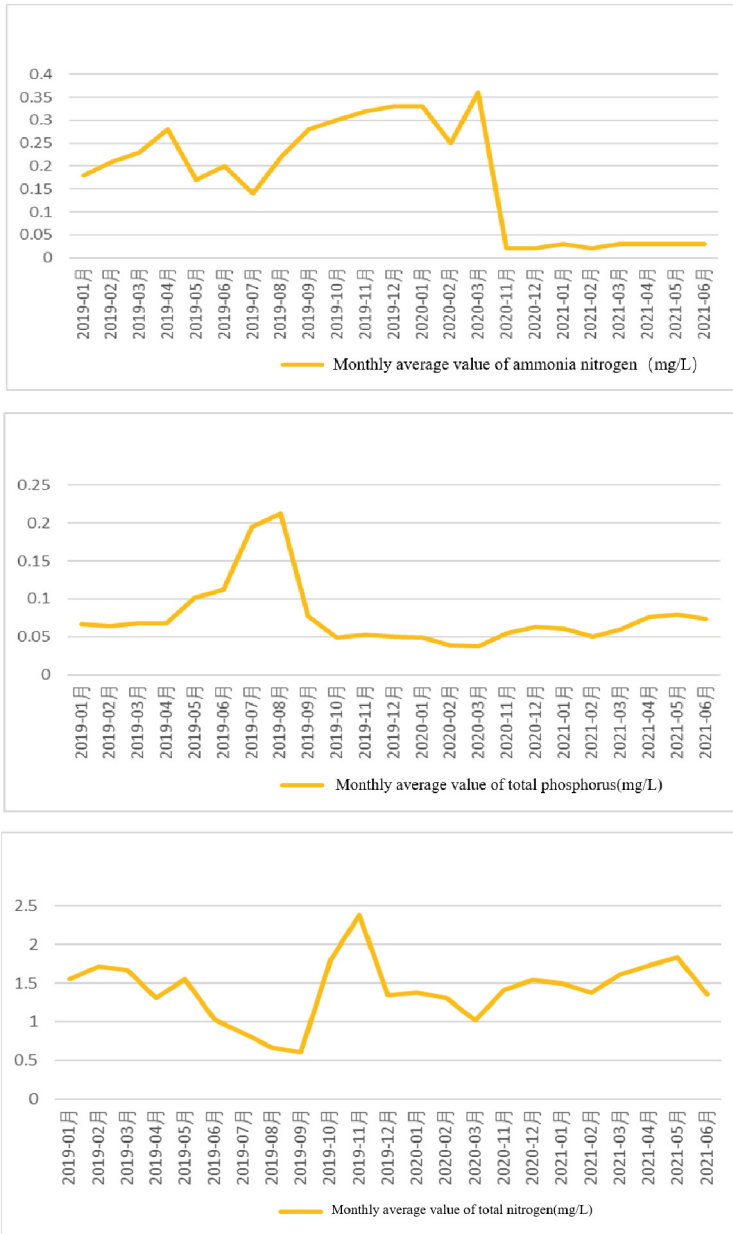


Fig. 7. Change of Ammonia Nitrogen, Total Phosphorus and Total Nitrogen at Zhutuo Section in Yongchuan District from 2019 to 2021.

4 Conclusion and Outlook

This study first studied the policies and methods of AGNPS control at home and abroad, and then analyzed AGNPS in Yongchuan District of Chongqing, and obtained the following conclusions: 1. AGNPS should be deeply studied based on planting types; 2. The use of fertilizers and pesticides remains an important factor affecting AGNPS; 3. For AGNPS in different regions, the main pollutants need to be selected for research based on monitoring data analysis, and analysis needs to be carried out in combination with precipitation, flood season, and non flood season.

Based on the current situation and research analysis of AGNPS, this study proposes relevant suggestions for AGNPS, in order to provide basic support for the prevention and control of AGNPS: 1. AGNPS needs to be studied through monitoring, tracing, calculation, governance, and management to connect the technological chain; 2. The assessment and evaluation of AGNPS requires a complete system as the standard; 3. According to local conditions, research on AGNPS needs to be targeted at different terrain areas, focusing on the main influencing factors, and achieving precise analysis and research.

Due to limited data collection and shallow research and analysis at this stage, data will continue to be collected in future studies to conduct in-depth correlation analysis and more accurately analyze agricultural non-point source pollutants and pollution sources. Based on the data results, open up a technological chain for the prevention and control of AGNPS, and explore the assessment and evaluation system standards for AGNPS prevention and control.

Author Contributions. Writing-original draft, R.Y. and Y.L.; Formal analysis, Y.L.; Conceptualization, X.L.; Investigation, L.Z. and M.S. All authors have read and agreed to the published version of the manuscript.

Funding. This research was supported by Funding: This research was supported by the National Key Research and Development Project of China (No. 2021YFC3201505).

Data Availability Statement. The data presented in this study are available on request from the author.

Declaration of Competing Interest. The authors declare that they have no known competing financial interests or personal relationships that could have appeared to influence the work reported in this study.

References

1. Dennis, L., Corwin, D.L., et al.: Non-point pollution modeling based on GIS. *Soil Water Conserv.* **1**, 75–88 (1998)
2. Meybeck, M.: Nitrogen and phosphorus transport by world rivers. *Acad. Manag. J.* **282**, 401–450 (1982)
3. Meybeck, M., Chapman, D., Helmer, R.: Global freshwater quality: a first assessment. *Global Environmental Monitoring System/UNEP/WHO* (1989)

4. Gromaire, M.C., Grmsud, F., Saad, M., et al.: Attribution of different sources to the pollution of wet weather flows in combined sewers. *Water Res.* **35**, 521–533 (2000)
5. Sartor, J.D.: A short course in cloud physics/clouds, rain, and rainmaking (Book Review). *Phys. Today* **42**(2), 354–361 (1976)
6. Chang, M., Crowley, C.M.: Preliminary observations on water quality of storm runoff from four selected residential roofs. *Jawra J. Am. Water Resour. Assoc.* **29**(5), 777–783 (2007)
7. Carpenter, S.R., Correll, D.L., Howarth, R.W., et al.: Nonpoint pollution of surface waters with phosphorus and nitrogen. *Ecol. Appl.* **8**(3), 134–143 (1998)
8. Gromaire, M.C., Garnaud, F.: Contribution of different sources to the pollution of wet weather flow sin combined sewers. *Water Res.* **35**(2), 521–533 (2001)
9. Wang, H.M., Qiu, Z.Y.: The best management measures for non-point source pollution in the United States and its implications for China. *Rural Econ. Sci. Technol.* **24**(11), 5–7 (2013). (In Chinese)
10. Mishra, S.K., Singh, V.P.: Soil conservation service curve number (SCS-CN) methodology. *Water Sci. Technol. Libr.* **22**(3), 355–362 (2007)
11. Zhang, X.Y.: Evaluation of Farmland Non-Point Source Pollution in Liaohe River Basin. Shenyang University (2021) (in Chinese)
12. Wang, Y.G., Wang, H.Y., Zheng, Y.L., Sun, X.Y.: Research methods and control technology of agricultural non-point source pollution. *Agric. Resour. Region. China* **42**(1), 25–33 (2021). (in Chinese)
13. Chuan, L.M., Zheng, H.G., Zhao, T.K., Wang, A.L., Zhao, J.J., Yan, Z.H.: Research progress and trend of prevention and control technology of agricultural non-point source pollution in China. In: *Proceedings of the 2020 Annual Conference of Science and Technology of the Chinese Society for Environmental Sciences*, vol. 1 (2020) (in Chinese)



Role of Rare Taxa in the Structure and Function of Soil Fungal Community

Jianfei Guan^(✉)

School of History and Culture, Mudanjiang Normal University, Mudanjiang 157000, China
bangeshiji@126.com

Abstract. Rare taxa are the potential force influencing function and structure of fungal communities and play an over-proportional role in soil ecosystems. We studied the typical Chernozem soil in Heilongjiang Province using high-throughput analysis techniques to investigate the role of rare taxa in function and structure of fungal communities in Chernozem. Coexistence of various low-abundance rare fungal taxa and few high-abundance fungal taxa were observed in Chernozem. Most of the rich and rare fungal taxa belonged to the phyla Ascomycota and Basidiomycota. No rare fungus from the phylum Mortierellomycota was detected. The primary environmental factor affecting the structure of rare fungal taxa was found to be soil pH, followed by water content. The rich fungal taxon *Mortierella* had a significantly positive correlation with total phosphorus and organic carbon ($P < 0.05$). The function prediction revealed 72 significantly different MetaCyc pathways in the two plots, and the rare taxa accounted for 80.56% of the total microbial community. The sulfate reduction pathway I was significantly different at $P < 0.001$, the octane oxidation pathway and the adenine and adenosine pathway were significantly different at $0.001 \leq P < 0.01$, and the remaining pathways were significantly different at $0.01 \leq P < 0.05$. In summary, the rare fungal taxa are of great significance to maintaining functional diversity and microbial structure of soil.

Keywords: Fungal Community Structure · Rare Taxa · Physical and Chemical Properties

1 Introduction

Microbial communities and their succession processes are an important aspect of the foundation of ecosystem development. Microbes in the environment shows a typical skewed abundance distribution, with few abundant groups coexisting with various rare groups [1]. The portion of low-abundance groups is denoted as the “microbial rare biosphere” [2]. So far, the research on soil microbes has mainly focused on the abundant groups [3], but with the continuous improvement of high-throughput sequencing technology [4], it has become possible to further determine and analyze the rare microbial groups. Extensive research on rare microbial groups is crucial for full understanding of the microbial ecology, as well as prediction of the ecological roles.

Rare microbial groups are known to exhibit significant impacts on the ecosystem services as key microbial species [5]. Indeed, rare microbial groups play a disproportionately significant role in the biogeochemical cycles and ecosystem functions [6]. Nevertheless, their ecological role remains unclear. Previous studies of rare microbial groups in soil focused on the bacteria [7, 8], with little research on fungi and other microorganisms. Unlike bacteria, which grow as single cells, fungi grow as mycelium and have larger body size [9], and play an important ecological role in the nutrient cycle of soil by alleviating nutrient limitations for other organisms and regulating mineral nutrition of plants [10]. In this pursuit, the role of rare fungal groups in soil fungal community structure and function was analyzed in this study. Specifically, the typical black soil in the Heilongjiang Province was employed for this study using high-throughput sequencing analysis technology. Our results can lay a foundation for understanding the rare fungal types, analyzing the succession patterns of the rare groups, and exploring the assembly process of rare biospheres.

2 Materials and Methods

2.1 Study Area and Sample Collection

Heilongjiang Province has an obvious temperate continental monsoon climate, located at N43°26′–53°33′ and E121°11′–135°05′. The sampling sites of this study were located in the Tailai County, Heilongjiang Province (N 46°34′42″, E 123°16′30″), where Chernozem soil is the main soil type. Samples (depth = 0–20 cm) of two types of agricultural soil (Site A and Site B) were collected in August 2020 by random sampling, subjected to the removal of debris liked stones, and stored in sterile sealed bags. Some soil samples were air-dried indoor to determine the features, while the remaining samples were subjected with dry ice for the microbial community amplification and sequencing analysis. Nine replicates were collected for each sampling site.

2.2 Physical and Chemical Properties of Soil Samples

The moisture content, the pH value, the organic carbon level, the total nitrogen level, and the total phosphorus level of the soil was measured by the vacuum oven method (NY525-2012/5.6), the potentiometric method (NY/T1377-2007), the $K_2Cr_2O_7$ oxidation-spectrophotometric method (NY/T1121.6-2006), the semi-micro Kjeldahl method (NY/T53-1987), and the NaOH fusion-MoSb anti-colorimetric method (NY/T88-1988), respectively.

2.3 High-Throughput Sequencing

The extraction of total fungal DNA, design of PCR primers, PCR reaction system and conditions, as well as the quantitative detection process in soil samples was performed according to an earlier report [11]. The Illumina MiSeq platform was employed for paired-end sequencing of the sequencing samples, while splicing, denoising, quality control, and remove chimerization were executed on all raw sequences of the samples to

develop OUT. This was aligned with the UNITE database to obtain the species annotation information. This experiment was performed at the Shenzhen Microecology Technology Co., Ltd.

2.4 Data Processing and Analysis

According to existing literature and the actual field conditions, the OTUs with a sequence abundance of more than 0.1% of the total sequence measured by high-throughput sequencing were denoted as the “abundant” groups, while those with relative abundance lower than 0.1% of the total sequence were denoted as the “rare” groups. Bacterial genera with annotation information obtained through the comparison of database that accounting for more than 1% of the same taxonomic level were defined as the “abundant” groups, while those below 1% were defined as “rare” groups [12, 13]. The basic data were processed and analyzed using software such as Microsoft Excel 2010, OriginPro 2019b, and SPSS. The Chao1, Faith_pd, Shannon index, and Simpson index were employed to evaluate the α diversity of samples, while the Kruskal Wallis method was employed to clarify significant differences in the α diversity among the different groups based on grouping information. The Circos plot was drawn using the Microbial Ecological Bioinformatics Cloud website (<https://www.bioincloud.tech/>). RDA analysis of the relationship between the microbial communities and the environmental factors was executed using the R language VEGAN package, and visualization was performed using ggplot2. The correlation heatmap was mainly drawn using the R language heatmap package. Based on the principle of PICRUSt2, the metabolic functions of the fungal microbial communities were predicted, and significant differences in the predicted microbial community functions among the groups were determined using ANOVA.

3 Results

3.1 Physical and Chemical Properties of Soil Samples

Sample analysis revealed negligible differences in the soil moisture content (SMC) between the sampling sites A and B (Fig. 1). The pH value of samples collected at site A (8.16 ± 0.27) was significantly higher than that of samples collected at site B (7.81 ± 0.06). The total nitrogen (TN), soil organic carbon (SOC), and total phosphorus (TP) in the soil at sampling point B were significantly higher than that at point A, higher than 0.66 g/kg, 7.13 g/kg, and 0.68 g/kg respectively.

3.2 High-Throughput Sequencing

In this study, 1,203,526 original sequences were determined and 692,817 OTUs belonging to 12 phyla, 28 classes, 66 orders, 119 families, and 169 genera were generated. The α diversity rarefaction curve was flat, suggesting that the diversity of samples in this study can be reflected by the sequencing results. Furthermore, an increase in the sequencing depth could not realize the detection of abundant undiscovered OTUs. The number of unique OTUs at sampling sites A and B were 1,047 and 916, respectively, with a total of 134 OTUs observed. The differences in α diversity indexes at the two sampling sites were not significant (Table 1).

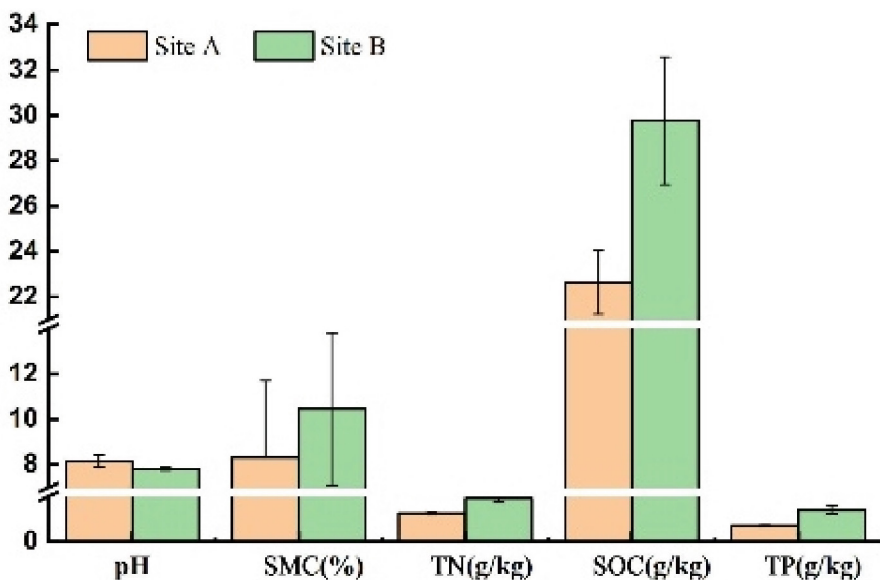


Fig. 1. Physical and chemical properties of soil.

Table 1. α diversity of samples collected at different sites.

Sample site	Chao1 index	Faith_pd index	Shannon index	Simpson index
Site A	173.33 \pm 39.24a	32.53 \pm 5.75a	5.31 \pm 0.56a	0.91 \pm 0.06a
Site B	159.33 \pm 65.13a	29.18 \pm 11.03a	4.91 \pm 1.51a	0.87 \pm 0.16a

3.3 Community Structure and Composition

At sampling sites A and B, the proportion of rare groups with an OUT count lower than 0.1% of the total was found to be 85.67% and 80.55%, respectively, while the abundance of rare groups was 24.08% and 19.85%, respectively. This indicates that there were many rare groups at each sampling point, but their abundance was low, and a large number of rare groups with relatively low abundance coexisted with a small number of rich groups with relatively high abundance. Identification analysis through OUT sequence alignment revealed that *Mortierella*, a genus of *Mortierellomycota*, was a rich group in the black soil, with a relative abundance of 29.45% and 19.67% at sampling points A and B, respectively. No rare groups were found in this phylum. In *Ascomycota* and *Basidiomycota*, the rich group genera were relatively high, with *Fusarium*, *Unspecified_Pyronemataceae*, *Unspecified_Chaetomiaceae*, *Unspecified_Sordariomycetes*, and *Unspecified_Onygenales* in *Ascomycota* exhibiting an average relative abundance of over 2.7% in both types of soil, making them rich genera. *Chytridiomycota* and *Kickxellomycota* were the two rare phyla found at both sampling points, and the genera under each phylum were also rare groups.

RDA was employed to analyze the correlation of species with environmental factors at the genus level, and the results are shown in Fig. 2. Soil pH, SMC, SOC, TN, and TP had negligible effects on the fungal abundance in black soil ($P = 0.252$), but significant effect on the rare fungal groups ($P = 0.014$), with soil pH being the main environmental factor affecting rare fungal groups, followed by moisture content. Correlation analysis between the identifiable fungal genera (top 30 in abundance) and soil properties (Fig. 3) showed that the *Mortierella* genus in the abundant group had a significantly positive correlation with SOC and TP ($P < 0.05$). In the rare group, identifiable fungal genera such as *Tulostoma*, *Geastrum*, *Debaryomyces*, *Coprinopsis*, *Leucoagaricus*, *Ramicandelaber*, and *Geopora* had a significant correlation with these features, as shown in Fig. 3.

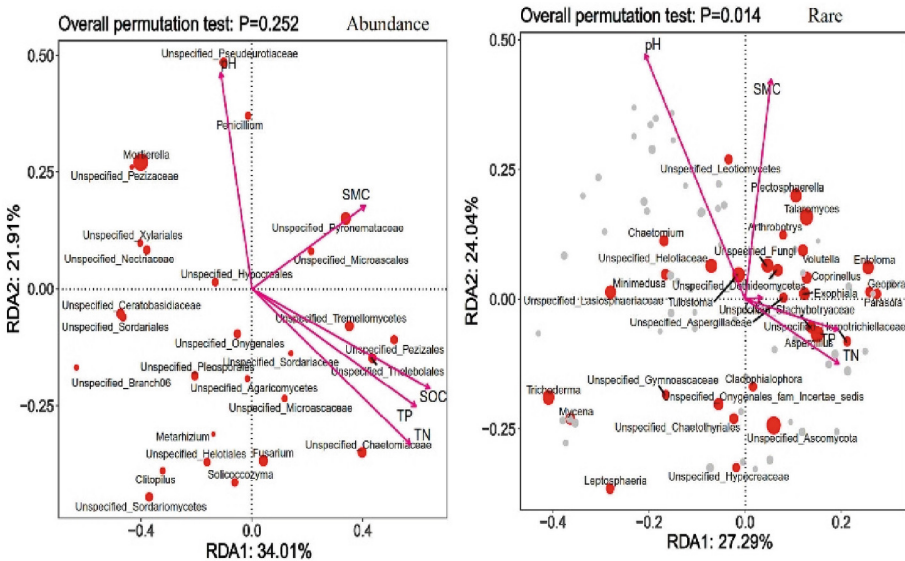


Fig. 2. RDA results of species at genus level.

3.4 Community Structure and Functionality

Based on the analysis of MetaCyc pathways with significant differences obtained from the test, a total of 72 pathways with significant differences were obtained at sampling points A and B, including 14 pathways with significant differences in the enriched taxa. The sulfate reduction I (SO₄ASSIMPWY) pathway showed considerable differences at the $P < 0.001$ level, while the octane oxidation (P221-PWY) pathway and the adenine and adenosine pathway (PWY-6609) showed considerable differences at the $0.001 \leq P < 0.01$ level. The remaining pathways showed significant differences at $0.01 \leq P < 0.05$ level. Analysis of the significantly different pathways in 58 rare taxa showed that the pathways with significant differences were all at $0.01 \leq P < 0.05$ level, this showed that the rare taxa contributed considerably to the auxiliary functions of the fungal community.

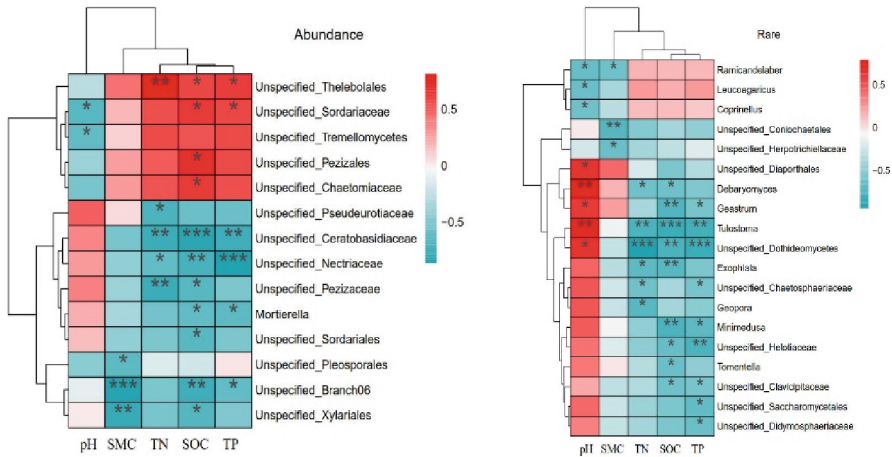


Fig. 3. Heatmap of the correlation of fungi with environmental factors at genus level.

4 Discussion

Ascomycota, *Basidiomycota*, and *Mortierellomycota* are often detected as dominant groups in the soil ecosystem. In this study, most of the species belonged to *Ascomycota* and *Basidiomycota*, whether it was a rich group or a rare group. The results were consistent with the existing research results [13]. *Mortierella* of *Mortierellomycota*, as a rich group at the genus level in black soil degrade chitin, while some species can degrade hemicellulose into sugars. Thus, *Mortierella* can serve as an indicator species for changes in the fungal community of soil, with a relative abundance changing significantly with TN and moisture content [14]. Herein, *Mortierella* had a significantly positive correlation with SOC and TP ($P < 0.05$). Analysis of rare groups at the genus level found that some rare fungal genera, such as *Unspecified_Ceratobasidiaceae* had an average relative abundance of 0.18% ($n = 9$) at site B, while the average relative abundance at site A was 7.84% ($n = 9$). *Mycena* was only detected at the fourth sampling point in A, with a relative abundance of 0.25%. The presence of *Aspergillus* was detected at all sampling points, except at the second sampling point in B. For rare microbial groups in soil, their rarity can be a random process [15], an inherent trade-off of the life history strategies [16], or the result of biotic and abiotic interactions [17]. Rare groups are the “seed bank” of microorganisms, and under appropriate conditions, they can become dominant groups, increasing the functional role of ecosystems and the resilience to the environmental disturbances. Conditionally rare groups can effectively explain the dynamics of overall community of rare biospheres and tend to become the dominant communities under desired environmental conditions [5]. Additionally, the random processes (e. g. diffusion limitation) dominated the assembly of fungal rich groups, while deterministic assembly (e. g. homogeneous selection) controlled the assembly process of the rare groups [13].

Environmental changes have been reported to influence ecosystem functions by mediating dynamic balance of microbial communities in soil. Currently, studies of

the impacts of environmental factors on the microbial community composition in soil focused on bacteria. For instance, Jiao [13] found that soil pH is the main determinant of the geographic distribution of rare and abundant subgroups in a model ecosystem of rice soil in China. Soil pH, SOC, TN, TP, and moisture content can also affect the composition of fungal communities to a certain extent. In this study, soil pH was also found to be a key environmental factor affecting composition and abundance of rare and abundant fungal groups in black soil, indicating that soil pH has significant impacts on the distribution of microbial communities in soil. Other environmental factors also have influences on abundance and composition of rare and abundant groups. SOC, TN, and TP have higher impacts on the abundant groups, SMC is another major factor influencing the distribution of rare groups.

In this study, rare taxa account for a higher proportion (80.56%) in distinguishing the different fungal community structures and functions. Predictive functional analysis shows unique predictive functional traits of rare taxa compared with their common peers, and rare taxa have significant impacts on the functional diversity [18], with huge genetic and functional diversity [6]. Although their abundance is low, some rare microorganisms have been identified as major contributors to the processes such as degradation of polycyclic aromatic hydrocarbon [19] and carbon cycling [20]. In this study, the sulfate reduction pathway of two abundant taxa differed significantly at the $P < 0.001$ level. It is known that the available sulfur in soil is essentially a dominant factor regulating the balance of the random and deterministic combinations of abundant and rare fungal subgroups in agricultural ecosystems [13]. Sulfur is a necessary nutrient for microbial growth, and fungi participate in the sulfur metabolism and cycling [21]. Soil sulfur may affect the composition of fungal communities by either directly influencing fungal growth or indirectly influencing fungal community composition by affecting plants [13].

5 Conclusions

The role of rare fungal groups in soil fungal community structure and function was analyzed using high-throughput sequencing analysis technology. The following conclusions can be drawn: (1) In chernozem soil, a large number of rare fungal groups with relatively low abundance coexisted with a small number of rich fungal groups with relatively high abundance. Most of the species in the rich and rare groups belonged to *Ascomycota* and *Basidiomycota*, and there were no rare groups in *Mortierellomycota*. Further, *Chytridiomycota* and *Kickxellomycota* were found to be the two fungal phyla with rare groups present at two sampling points. (2) There were significant differences in the soil pH, TN, SOC, and TP of samples collected at different sampling sites. The abundant genus *Mortierella* had a significantly positive correlation with SOC and TP ($P < 0.05$). Also, soil pH was the dominant environmental factor for the rare fungal groups, followed by SMC. (3) Based on the results, 72 MetaCyc pathways with significant differences were obtained, and 14 MetaCyc pathways with significant differences were enriched in the abundant taxa. The SO_4 ASSIMPWY pathway for sulfate reduction I showed significant differences at the $P < 0.001$ level. Rare taxa accounted for 80.56% of the pathways with significant differences.

Acknowledgments. This project was financially supported by Basic Research Project of Heilongjiang Provincial Department of Education (1451ZD003) and National Project Cultivation Project of Mudanjiang Normal University (GP2021004).

References

1. Nemergut, D.R., Costello, E.K., Hamady, M., et al.: Global patterns in the biogeography of bacterial taxa. *Environ. Microbiol.* **13**(1), 135–144 (2011)
2. Hamasaki, K., Taniguchi, A., Tada, Y., et al.: Active populations of rare microbes in oceanic environments as revealed by bromodeoxyuridine incorporation and 454 tag sequencing. *Gene* **576**(2), 650–656 (2016)
3. Zhou, Q., Zhang, X.M., He, R.J., et al.: The composition and assembly of bacterial communities across the rhizosphere and phyllosphere compartments of phragmites *Australis*. *Divers. Basel* **11**(6), 98 (2019)
4. Gokul, J.K., Cameron, K.A., Irvine-Fynn, T.D.L., et al.: Illuminating the dynamic rare biosphere of the Greenland ice sheet's dark zone. *FEMS Microbiol. Ecol.* **95**(12), fiz177 (2019)
5. Yang, S.Z., Winkel, M., Wagner, D., et al.: Community structure of rare methanogenic archaea: insight from a single functional group. *FEMS Microbiol. Ecol.* **93**(11), fix126 (2017)
6. Lynch, M.D.J., Neufeld, J.D.: Ecology and exploration of the rare biosphere. *Nat. Rev. Microbiol.* **13**(4), 217–229 (2015)
7. Jiao, S., Wang, J.M., Wei, G.H., et al.: Dominant role of abundant rather than rare bacterial taxa in maintaining agro-soil microbiomes under environmental disturbances. *Chemosphere* **235**, 248–259 (2019)
8. Hou, J.Y., Wu, L.H., Liu, W.X., et al.: Biogeography and diversity patterns of abundant and rare bacterial communities in rice paddy soils across China. *Sci. Total Environ.* **730**, 139116 (2020)
9. Powell, J.R., Karunaratne, S., Campbell, C.D., et al.: Deterministic processes vary during community assembly for ecologically dissimilar taxa. *Nat. Commun.* **6**, 8444 (2015)
10. Hug, L.A., Thomas, B.C., Sharon, I., et al.: Critical biogeochemical functions in the subsurface are associated with bacteria from new phyla and little studied lineages. *Environ. Microbiol.* **18**(1), 159–173 (2016)
11. Guan, J.F., Li, X.L., Cao, Y., et al.: Fungal community structure in top layer of frozen soil in Heilongjiang Province. *Chin. J. Ecol.* **39**(9), 2904–2911 (2020)
12. Liu, L.M., Yang, J., Yu, Z., et al.: The biogeography of abundant and rare bacterioplankton in the lakes and reservoirs of China. *ISME J.* **9**(9), 2068–2077 (2015)
13. Jiao, S., Lu, Y.: H: Abundant fungi adapt to broader environmental gradients than rare fungi in agricultural fields. *Glob. Change Biol.* **26**(8), 4506–4520 (2020)
14. Zhang, H.F., Liu, H.M., Zhao, J.N., et al.: Response of soil fungal community structure to nitrogen and water addition in *Stipa baicalensis* steppe. *Acta Ecol. Sin.* **38**(1), 195–205 (2018)
15. Ai, D.X.C., Chu, C.J., Ellwood, M.D.F., et al.: Migration and niche partitioning simultaneously increase species richness and rarity. *Ecol. Model.* **258**, 33–39 (2013)
16. Gudelj, I., Weitz, J.S., Ferenci, T., et al.: An integrative approach to understanding microbial diversity: from intracellular mechanisms to community structure. *Ecol. Lett.* **13**(9), 1073–1084 (2010)
17. Narisawa, N., Haruta, S., Arai, H., et al.: Coexistence of antibiotic-producing and antibiotic-sensitive bacteria in biofilms is mediated by resistant bacteria. *Appl. Environ. Microbiol.* **74**(12), 3887–3894 (2008)

18. Li, P.F., Liu, J., Jiang, C.Y., et al.: Distinct successions of common and rare bacteria in soil under humic acid amendment – a microcosm study. *Front. Microbiol.* **10**, 2271 (2019)
19. Teira, E., Lekunberri, I., Gasol, J.M., et al.: Dynamics of hydrocarbon-degrading Cycloclasticus bacteria during mesocosm-simulated oil spills. *Environ. Microbiol.* **9**(10), 2551–2562 (2007)
20. Neufeld, J.D., Schafer, H., Cox, M.J., et al.: Stable-isotope probing implicates Methylophaga spp. and novel Gammaproteobacteria in marine methanol and methylamine metabolism. *ISME J.* **1**(6), 480–491 (2007)
21. Holt, S., Kankipati, H., De Graeve, S., et al.: Major sulfonate transporter Soa1 in *Saccharomyces cerevisiae* and considerable substrate diversity in its fungal family. *Nat. Commun.* **8**, 14247 (2017)

Hydraulics, Hydrology and Water Resources Engineering



Experimental Study on Flow Capacity of a Typical Side Weir

Xiaowei Han^{1,2}(✉), Haifeng Zhang³, Nan Yi¹, and Guanglei Gao¹

¹ Zhejiang Institute of Hydraulics and Estuary (Zhejiang Institute of Marine Planning and Design), Hangzhou 310017, China

hanxiaowei64@outlook.com

² Zhejiang Provincial Key Laboratory of Estuary and Coast, Hangzhou 310017, China

³ Jinyun County Water Conservancy and Hydropower Construction Management Co. Ltd., Jinyun 321400, China

Abstract. The flow capacity of a side weir is an important factor to consider in its study, as it can significantly impact the relevant hydraulic parameters near the weir. In this study, a 1:50 scale physical model of a river was used to investigate the flow capacity of a side weir with a flood diversion angle of 31° and a height of 1 m. The results indicate that the discharge coefficient C_w of the side weir decreases with an increase in parameter h_2/P , and increases with an increase in Fr_1 . Furthermore, the side weir outflow efficiency η decreases with an increase in downstream Fr_2 , but increases with an increase in parameter h_2/P . The η has a stronger correlation with Fr_2 and a relatively weaker correlation with parameter h_2/P . The discharge coefficient C_w and outflow efficiency η of the side weir were fitted, and corresponding calculation formulas were proposed. The fitting formula for the discharge coefficient shows good correlation, with an error within 8%. However, the split ratio fitting formula has a relatively large error, with a maximum of about 28%. These findings can be used as a reference for design and operational management.

Keywords: Side Weir · Flow Capacity · Discharge Coefficient · Outflow Efficiency

1 Introduction

Side weirs are widely used for flood, agricultural, sewage, and urban runoff management. They are effective in relieving flood pressure in target areas by diverting over-standard floodwater into subsidiary channels or flood storage areas. To make the most of the flood diversion benefits of a side weir, its ability to divert floodwater under different flow conditions is particularly important.

Flow analysis at side weirs has been the focus of many researchers, with most studies on the hydraulic characteristics of water intakes by domestic and foreign scholars focusing on right-angle intakes. de Marchi [1] was the first to systematically analyze discharge coefficients at side weirs, but with large errors. Uyumaz and Muslu [2] carried out an in-depth study of flow over side weirs in circular channels and proposed a

slow and rapid flow condition based on energy relations, which is a calculation method of discharge coefficients. Considering the complexity of side weir flow, Castro-Orgaz and Hager [3] proposed a method based on the evaluation of the momentum and energy equations in both longitudinal and transverse directions, arguing that the momentum approach provides better results and that the effect of velocity distribution is significant. Crispino et al. [4] modeled supercriticality over a double lateral low weir in a circular channel based on model tests and numerical simulations. Lindermuth [5] used FLOW3D and a physical model to analyze the flow characteristics of a porous side weir under normal water depth conditions in the main channel and derived correction equations for coefficients using multivariate regression analysis, which can be applied to side weirs with multiple holes.

The angle between the side weir and the center line of the upstream channel, known as the diversion angle θ , is often different. It is generally believed that the smaller the diversion angle, the more evenly distributed the flow velocity of the side weir, the smoother the flow into the channel, and the smaller the energy loss when diverting the flow. Smaller diversion angles do not result in a larger bend in the flow line in front of the intake, in line with the principle of frontal intake [6]. Common diversion angles for acute side weir arrangements are shown in Fig. 1 [7]. This paper combines an actual project with an experimental study of the overflow capacity of side weirs when the diversion angle is acute.

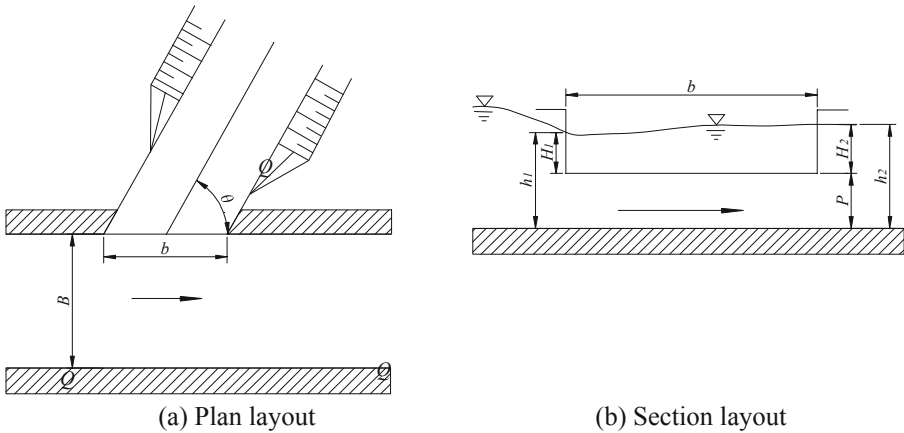


Fig. 1. Side weir with acute angle of diversion.

2 Theoretical Background

The water surface line in the main canal along the side weir direction can be described by a one-dimensional equation based on the theoretical principle of conservation of energy as follows [8]:

$$\frac{dh}{dx} = \frac{I_S - I_E + \frac{\alpha q Q_x}{gA^2}}{1 - \frac{\alpha B Q_x^2}{gA^3}} \quad (1)$$

Where: A is the overflow area (m^2); B is the main canal water surface width (m); g is the acceleration of gravity (m/s^2); Q_x is the flow rate in the channel at position x along the weir (m^3/s); q side weir single width flow rate (m^2/s); I_S is the main canal bottom slope drop; I_E is the energy specific drop; dh/dx is the rate of change of the main canal water depth h with x and α is the kinetic energy correction factor.

Where the single width flow rate of the side weir can be calculated according to the conventional weir flow equation.

$$q = -\frac{dQ}{dx} = \frac{dQ_w}{dx} = C_d \sqrt{2g} (h - P)^{1.5} \quad (2)$$

Integration of q along the length b of the side weir gives the side weir flow equation:

$$Q_w = C_d \sqrt{2g} \int_0^b (h(x) - P)^{1.5} dx \cong C_d \sqrt{2g} \sum_i (h(x) - P)^{1.5} \Delta b_i \quad (3)$$

In view of the more complex changes in water depth along the side weir, it is more difficult to discretize the calculation, using the downstream water depth h_2 as the characteristic water depth instead of $h(x)$, the above equation can be re written as:

$$Q_w = C_w b \sqrt{2g} (h_2 - P)^{1.5} \quad (4)$$

Where: C_w is the discharge coefficient considering the influence of water depth variation along the course, under the neglect of water Weber number and Reynolds number influence, this discharge coefficient is related to the following factors, including the slope drop at the top of the side weir, the water depth of the main channel h_2 , the width of the main channel B , the width of the weir b , the number of river Fr , the angle of diversion θ , the height of the weir P , etc., can be written as:

$$C_w = f_1(\Theta, B, b, h_2, \theta, P, Fr_1) \quad (5)$$

Using the weir height P as the characteristic length, dimensionlessizing the above equation yields:

$$C_w = f_2(\Theta, \frac{B}{P}, \frac{b}{P}, \frac{h_2}{P}, \theta, Fr_1) \quad (6)$$

Since $\Theta = 0$ and the variables B , b , P and θ remain unchanged, the above equation can be rewritten for this example as:

$$C_w = f_3(\frac{h_2}{P}, Fr_1) \quad (7)$$

At this point, the side weir discharge coefficient is a function of both h_2/P and Fr_1 .

3 Experimental Plan

3.1 Project Layout

The study was carried out based on a physical model of the lateral inlet of a flood diversion tunnel. The width of the main channel in the study area is approximately 135 m. The angle between the centreline of the lateral weir and the centreline of the channel is approximately 31° . Downstream of the lateral weir is the open channel section, with the left-hand retaining wall at a contraction angle of 10° and the right-hand retaining wall at a contraction angle of 12° ; downstream of the open channel section is the control gate, which is a double-casement gate with a chamber size of 12.00 m x 10.30 m (net width x net height), and the bottom plate elevation of the gate is 4 m lower than the top elevation of the lateral weir. See Fig. 2 for engineering plan layout and Fig. 3 for section layout.

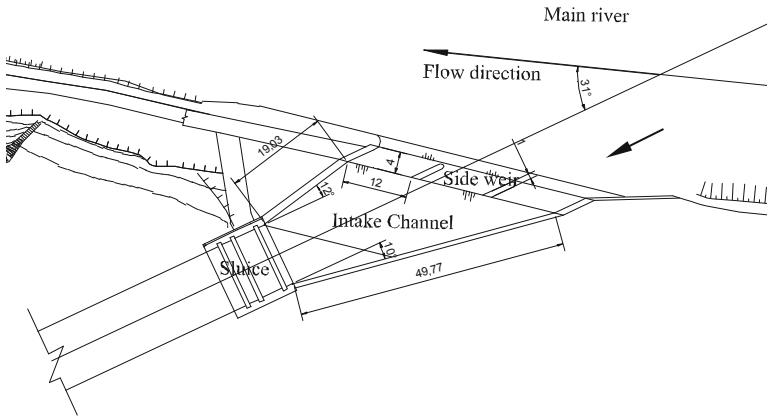


Fig. 2. Layout of the project.

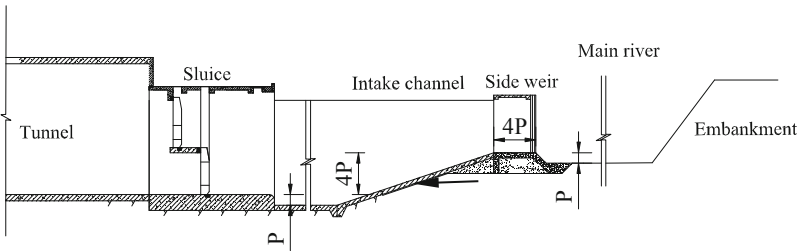


Fig. 3. Section layout of the project.

3.2 Model Scales

The physical model is based on a normal hydraulic model, designed according to the Fr number similarity law, with the model satisfying gravity similarity and drag similarity

respectively. Considering the model flow rate, water depth, flow velocity and resistance squared area and other hydraulic parameters comprehensive factors research based on a tunnel inlet model, physical use by gravity similarity criteria design, model scale for 1:50, the corresponding physical volume scale is shown in Table 1.

Table 1. Law of similitude.

Physical quantity	Length L_r	Time T_r	Velocity V_r	Discharge Q_r	Roughness n_r
Ratio	1:50	$1:L_r^{1/2}$	$1:L_r^{1/2}$	$1:L_r^{5/2}$	$1:L_r^{1/6}$

3.3 Model Range and Production

The physical model was designed as a self-circulating system, with simulations covering the underground reservoir, inlet forebay, valves, flow meters, river channel, and flood gates. The model layout is shown in Fig. 4. The conditions were simulated by controlling different upstream flows and downstream tailgate levels in the main river channel, with the channel downstream of the side weir being free outflow to ensure maximum overflow capacity.

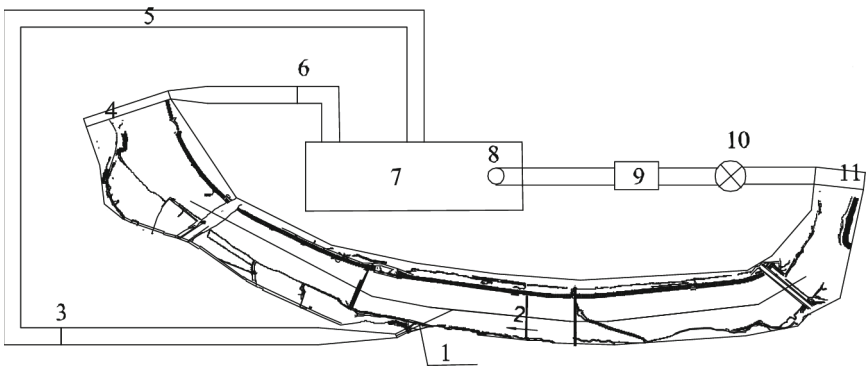


Fig. 4. Schematic layout of the model.

Figure 4 shows the schematic layout of the model, including the side weir (1), main river (2), measuring weir (3), tailgate (4), return channel (5), another measuring weir (6), underground reservoir (7), pump (8), electromagnetic flow meter (9), valve (10), and intake tank (11).

4 Results and Analysis

4.1 Results

All experiments presented in this paper are conducted based on dimensionless weir lengths $\frac{b}{P} = 36$, $\frac{B}{P} = 135$, and $\theta = 31^\circ$. Table 2 displays the test results for the 26 constant flow experimental conditions investigated, with different flow rates (Q_1 ranging from 886 to 2,200 m^3/s), tailwater conditions (h_2/P ranging from 3.45 to 7.46), and upstream Fr_1 ranging from 0.12 to 0.56. The test results can be found in Table 2.

Table 2. Test results.

NO.	P/m	$Q_1/\text{m}^3\cdot\text{s}^{-1}$	h_1/m	Fr_1	$Q_2/\text{m}^3\cdot\text{s}^{-1}$	h_2/m	Fr_2	h_2/P	$Q_W/\text{m}^3\cdot\text{s}^{-1}$	C_w	η
1	1	2 195.9	4.42	0.56	1 804.8	4.50	0.45	4.50	391.1	0.374	0.178
2	1	2 194.2	5.19	0.44	1 756.2	5.35	0.34	5.35	438.0	0.303	0.200
3	1	2 160.3	5.85	0.36	1 676.2	6.00	0.27	6.00	484.1	0.271	0.224
4	1	2 166.0	6.51	0.31	1 636.8	6.65	0.23	6.65	529.2	0.247	0.244
5	1	2 200.1	6.86	0.29	1 643.1	7.00	0.21	7.00	557.1	0.238	0.253
6	1	2 180.0	7.32	0.26	1 593.0	7.46	0.18	7.46	587.1	0.224	0.269
7	1	1 843.3	4.12	0.52	1 508.2	3.96	0.45	3.96	335.2	0.412	0.182
8	1	1 922.5	5.02	0.40	1 511.2	5.13	0.31	5.13	411.3	0.308	0.214
9	1	1 950.9	5.74	0.34	1 482.3	5.87	0.25	5.87	468.6	0.274	0.240
10	1	1 940.0	6.46	0.28	1 420.5	6.58	0.20	6.58	519.5	0.247	0.268
11	1	1 948.3	7.35	0.23	1 367.1	7.45	0.16	7.45	581.3	0.222	0.298
12	1	1 469.5	3.88	0.46	1 188.7	3.66	0.40	3.66	280.9	0.405	0.191
13	1	1 463.6	4.95	0.31	1 085.1	5.02	0.23	5.02	378.5	0.295	0.259
14	1	1 467.1	5.85	0.25	1 015.3	5.93	0.17	5.93	451.8	0.259	0.308
15	1	1 479.8	6.56	0.21	970.5	6.64	0.13	6.64	509.3	0.238	0.344
16	1	1 441.5	7.20	0.18	889.4	7.24	0.11	7.24	552.1	0.222	0.383
17	1	1 254.0	4.02	0.37	973.1	3.99	0.29	3.99	280.9	0.340	0.224
18	1	1 253.9	5.00	0.27	881.9	5.05	0.18	5.05	372.1	0.286	0.297
19	1	1 174.7	5.75	0.20	742.0	5.79	0.13	5.79	432.6	0.259	0.368
20	1	1 173.9	6.45	0.17	683.4	6.49	0.10	6.49	490.5	0.239	0.418
21	1	1 171.1	7.32	0.14	615.3	7.35	0.07	7.35	555.8	0.218	0.475
22	1	886.0	3.95	0.27	636.6	3.45	0.24	3.45	249.4	0.408	0.281
23	1	889.2	4.71	0.21	563.7	4.74	0.13	4.74	325.5	0.282	0.366
24	1	886.9	5.34	0.17	503.3	5.36	0.10	5.36	383.5	0.264	0.432
25	1	891.1	6.22	0.14	426.5	6.24	0.06	6.24	464.7	0.243	0.521
26	1	890.5	6.94	0.12	364.4	6.95	0.05	6.95	526.2	0.227	0.591

4.2 Analysis

Discharge Coefficient. The discharge coefficients C_w obtained in the tests ranged from 0.20 to 0.45. Equation (7) shows that the discharge coefficient of the side weir in this project depends on Fr_1 (upstream Fr number) and the dimensionless water depth h_2/P . Figures 5 and 6 illustrate the relationship between C_w and h_2/P and C_w and Fr_1 , respectively. It can be observed from these figures that the discharge coefficient C_w decreases as h_2/P increases and increases as Fr_1 increases. These findings are in general agreement with the conclusions presented in the paper [9]. By fitting the data, the relationship between the discharge coefficient C_w and Fr_1 and h_2/P is obtained as follows:

$$C_w = Fr_1^{0.135} \left(h_2/P \right)^{-0.599} - 0.02 \quad (8)$$

A deviation analysis of the discharge coefficient formula is presented in Fig. 7, showing good correlation between the calculated and measured discharge coefficients, with a correlation coefficient of $R = 0.978$ and an average error of approximately 3% and a maximum error of 7%.

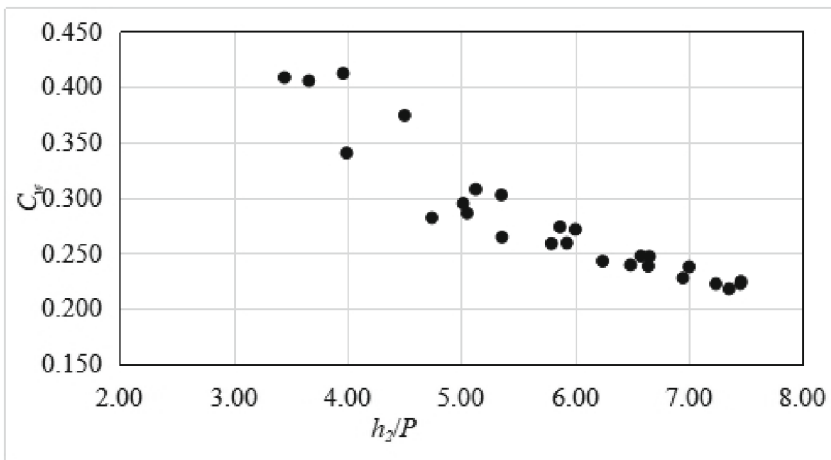


Fig. 5. Plot of h_2/P vs. C_w .

Outflow Efficiency. When determining the type of side weir body, the paper [10] suggests that the Outflow Efficiency η ($\eta = Q_w/Q_1$) of the side weir is related to factors such as Fr_2 (downstream Fr number) and the dimensionless water depth h_2/P . Figure 8 shows the relationship between the Outflow Efficiency η and Fr_2 . The test results show that the Outflow Efficiency correlates well with the downstream Fr_2 , and the Outflow Efficiency decreases as the downstream Fr_2 increases, indicating that the intake efficiency of the side weir is relatively low when the main channel is flowing rapidly. Figure 9 shows the relationship between the Outflow Efficiency η and h_2/P , and the overall correlation between the Outflow Efficiency η and h_2/P is relatively poor, although the correlation is positive.

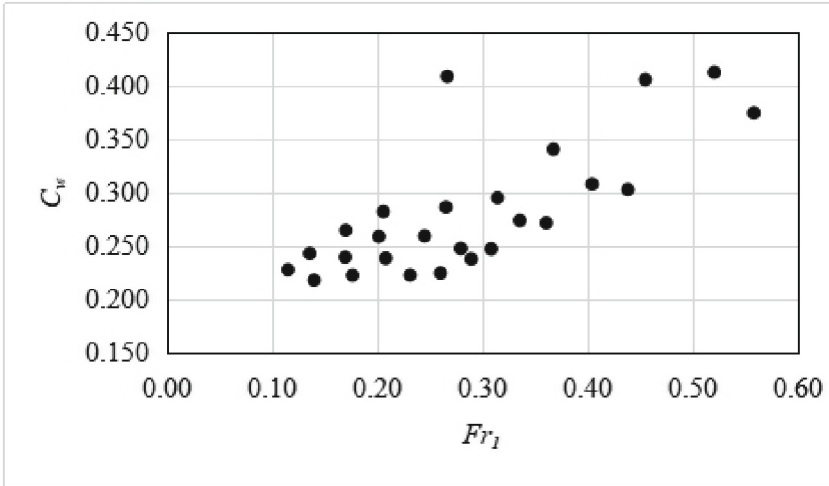


Fig. 6. Plot of Fr_1 vs. C_w .

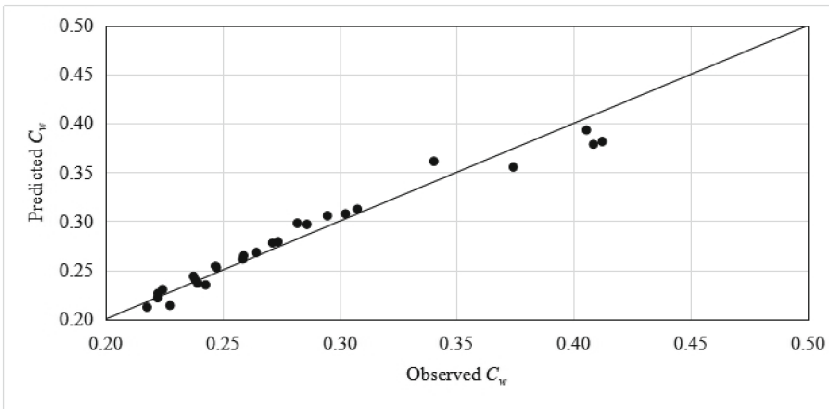


Fig. 7. Comparison between observed and predicted Discharge Coefficient.

Defining dimensionless parameters:

$$\chi = 1/(Fr_2)(h_2/P) \tag{9}$$

It is widely accepted that the outflow efficiency η is significantly correlated with the dimensionless parameter χ [10], which is defined as:

$$\eta = 1 - \frac{1}{c\chi^\delta} \tag{10}$$

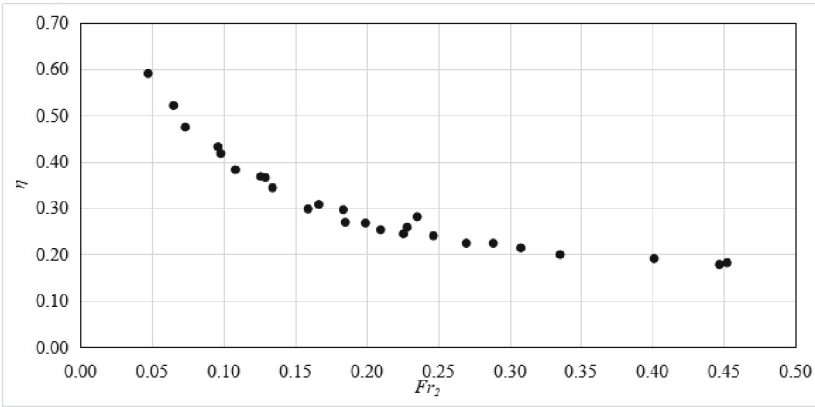


Fig. 8. Plot of Outflow Efficiency η versus Fr_2 .

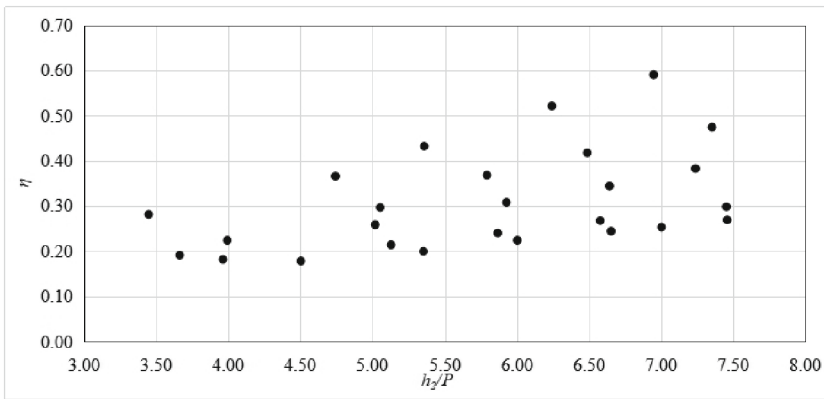


Fig. 9. Plot of Outflow Efficiency η versus h_2/P .

where c and δ are the parameters in the regression model. Using the least squares method to fit the above parameters, the values of c and δ for this project are obtained as 0.778 and 0.182, respectively. The correlation coefficient R is 0.88, and the fitting results are presented in Fig. 10. The comparison between the measured and predicted values of Outflow Efficiency η is shown in Fig. 11. The overall relationship between the test value and the fitted value is more consistent, but there is still some error, with a maximum error of approximately 28%.

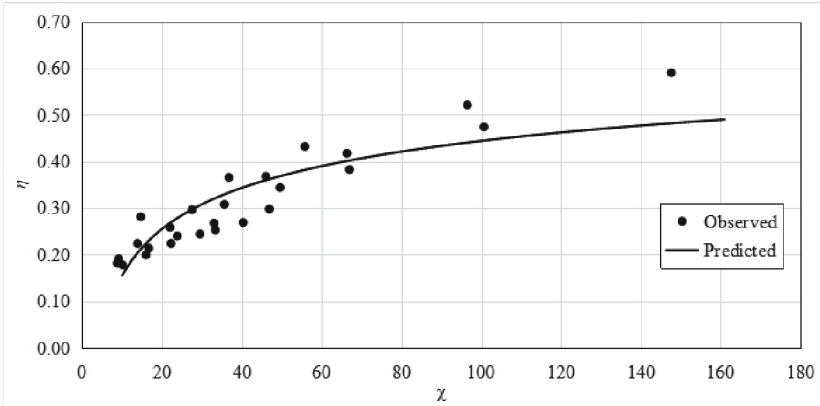


Fig. 10. Relationship between Outflow Efficiency η and χ .

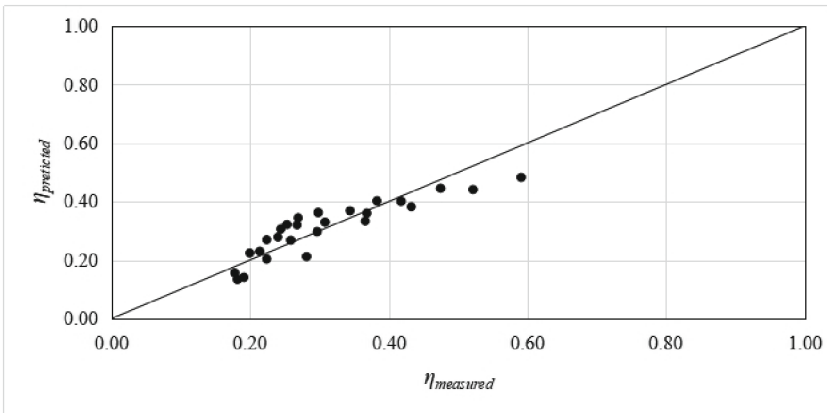


Fig. 11. Comparison between observed and predicted outflow efficiency.

5 Conclusion

Side weirs are common hydraulic structures in many industrial and agricultural applications, and their importance has been demonstrated in relevant scientific and technical papers. In this paper, a series of tests on side weir diversion discharge coefficients and outflow efficiency based on a 1:50 normal channel physical model are conducted. All tests are based on dimensionless weir length $\frac{b}{P} = 36$, $\frac{B}{P} = 135$, and $\theta = 31^\circ$, where Fr_1 ranges from 0.12 to 0.56 and tailwater conditions h_2/P range from 3.45 to 7.46.

- (1) In the case of the determined side weir body type, the discharge coefficient C_w decreases as h_2/P increases and increases with the increase of Fr_1 . Formula (8) is used to calculate the discharge coefficient C_w , with a correlation coefficient $R = 0.978$. After analysis, the calculated discharge coefficient and the measured discharge coefficient correlation are good, and the error is within 8%. Similar projects can use

this fitting formula to calculate the discharge coefficient of the side weir applicable to their project.

- (2) There is a relationship between the side weir outflow efficiency η and factors such as Fr_2 (the downstream Fr number) and the dimensionless water depth h_2/P . The correlation between the outflow efficiency η and Fr_2 is good, with the outflow efficiency decreasing as Fr_2 increases, indicating that the faster the flow, the lower the outflow efficiency of the side weir at the same flow rate. The correlation between the outflow efficiency η and h_2/P is positive, but the correlation is relatively poor. Reference [10] gives the relationship between the outflow efficiency and the dimensionless parameter χ , see Eq. (10), where $c = 0.778$ and $\delta = 0.182$ for this project, and the correlation coefficient $R = 0.88$. The test value and the fitted value are generally more consistent, but there is still a certain error, with the maximum error being about 28%. The definition of the dimensionless parameter χ needs further study.
- (3) Many factors influence the flood diversion capacity of side weirs, and this paper only focuses on a specific project, which still has certain limitations. Further series of studies can be conducted on the slope drop at the top of different side weirs Θ , weir width b , diversion angle θ , weir height P , and other factors.

Acknowledgement. This research was supported by Zhejiang Water Conservancy Science and Technology Plan Project under Grant No. RB2201 and ZIHE21Y002 of Zhejiang Institute of Hydraulics and Estuary (Zhejiang Institute of Marine Planning and Design).

References

1. De Marchi, G.: Saggio di teoria sul funzionamento degli stramazzi laterali. *L'Energia Elettr* **11**(11), 849–854 (1934)
2. Uyumaz, A., Muslu, Y.: Flow over side weirs in circular channels. *J. Hydraul. Eng.* **111**(1), 144–160 (1985)
3. Castro-Orgaz, O., Hager, W.H.: Subcritical side-weir flow at high lateral discharge. *J. Hydraul. Eng.* **138**(9), 777–787 (2012)
4. Crispino, G., Cozzolino, L., Della Morte, R., et al.: Supercritical low-crested bilateral weirs: hydraulics and design procedure. *J. Appl. Water Eng. Res.* **3**(1), 35–42 (2015)
5. Linderemuth, A., Ostrander, T.S.P., Achleitner, S., et al.: Discharge calculation of side weirs with several weir fields considering the undisturbed normal flow depth in the channel. *Water* **13**(13), 1717 (2021)
6. Fan, Y.: Study on “Diversion Angle Effect” of Lateral Intake Flow. China Institute of Water Resources and Hydropower Research, Beijing (2007). (In Chinese)
7. Wei, L.: Hydraulic Calculation Manual, 2nd edn. China Water & Power Press, Beijing (2006). (In Chinese)
8. May, R.W.P.: Hydraulic Design of Side Weirs. Thomas Telford, London (2003)
9. Wang, X.X., Lu, Q.N., Zhuang, T.G., Xu, L.: A study on hydraulic performance parameters of rectangular side weir. *Water Saving Irrig.* **0**(3), 85–88 (2021). (In Chinese)
10. Maranzoni, A., Pilotti, M., Tomirotti, M.: Experimental and numerical analysis of side weir flows in a converging channel. *J. Hydraul. Eng.* **143**(7), 04017009 (2017)



The Sustainable Development Model of Rural Domestic Sewage Treatment in China

Xinying Fan^{1,2}(✉), Xiaotao Gao^{1,2}, Ming Cai^{1,2}, Hao Ma^{1,2}, Jian Fu^{1,2},
and Zhengwei Li^{1,2}

¹ Yellow River Engineering Consulting Co., Ltd., Zhengzhou 450003, China
fanxinying1234@126.com

² Key Laboratory of Water Management and Water Security for Yellow River Basin,
Ministry of Water Resources (Under Construction), Zhengzhou 450003, China

Abstract. With the successive promulgation of rural environmental governance policies in China, rural sewage treatment has become a hot topic. In response to the problem of traditional unified sewage collection and treatment model being difficult to adapt to in rural China, this article systematically investigates academic literature and engineering projects in China since 2000. The main problems existing in the existing rural governance are: the design scale of the project is too large; the water quality of the project inlet design is too high; the sewage pipe network is blocked and damaged; the sewage treatment facilities are not acclimated to the local conditions. Therefore, this article proposes a new model of rural sewage treatment and resource utilization that is 'source separation, classified discharge, qualitative treatment, and recycling', and provides three utilization scenarios and suitable technologies. In addition, it also explores the economic performance of this new model. The new sewage treatment concept proposed in this study will provide reference for further improving the rural sewage treatment rate in China.

Keywords: Rural Domestic Sewage · Treatment Model · Rural Environment · Domestic Sewage · China

1 Introduction

China has invested a large amount of construction funds, aiming to create a beautiful ecological and livable countryside, so that farmers can have a greater sense of gain and happiness in rural revitalization [1]. According to research data from the Prospective Industry Research Institute, the investment in rural sewage treatment in China has shown a rapid growth trend, with a cumulative investment of over 300 billion RMB (Renminbi) from 2016 to 2021. At present, rural areas in China involve 520000 administrative villages, with a population of 55.4% in the country. The annual sewage volume exceeds 10 billion tons [2], accounting for nearly 50% of urban sewage. According to the Bulletin of the Second National Pollution Source Survey of China, the discharge of chemical oxygen demand, ammonia nitrogen, total nitrogen and total phosphorus in rural domestic sewage reached 4.9962 million tons, 245 million tons, 446.5 million tons

and 36.9 million tons respectively. According to data from the Ministry of Ecology and Environment of China in 2023, the average treatment rate of rural sewage in China is 31%, with economically developed areas ranging from 30% to 90% (see Fig. 1). The current urban domestic sewage treatment rate in China has reached 97.89% [3], while the rural domestic sewage treatment rate is much lower than that in urban areas. Compared with the popularization rate of rural tap water in China [4], the statistical rural sewage treatment rate is much lower than the popularization rate of tap water. Therefore, a large amount of rural sewage cannot be effectively treated, and China’s rural sewage still needs to increase its treatment efforts.

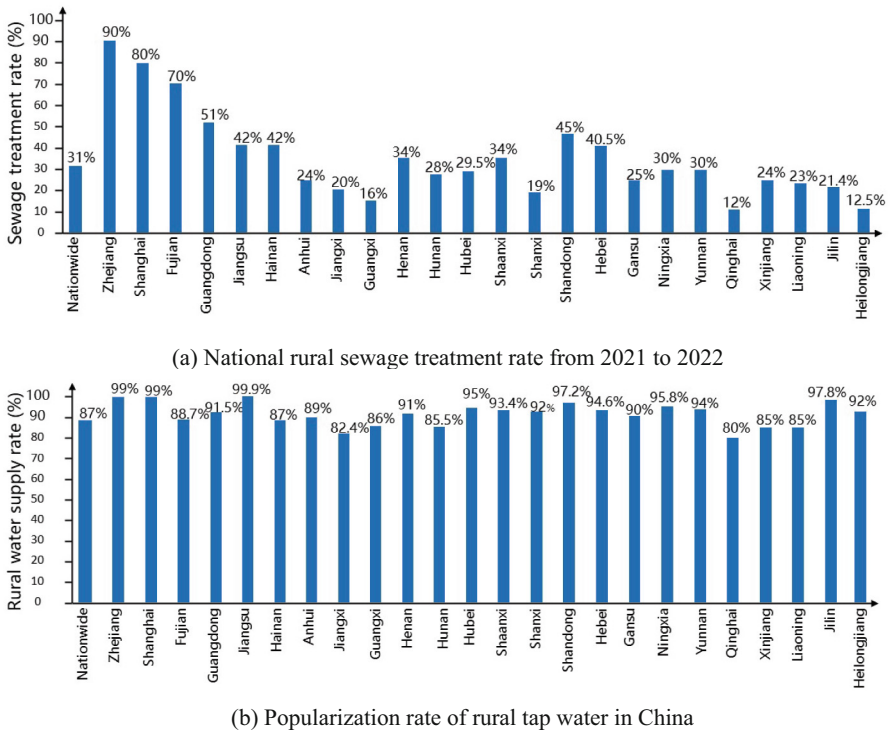


Fig. 1. Current situation of rural water supply and sewage treatment in China.

In order to comprehensively promote the improvement of rural living environment, China has issued a series of policy documents and standards. Overall, our rural sewage treatment has gone through three stages (see Fig. 2): the embryonic stage (before 2015), the growth stage (from 2015 to 2021), and the mature stage (after 2021). Overall, the foundation of rural domestic sewage treatment is weak, and the task remains arduous. Between 2016 and 2021, the rural sewage treatment rate in China only increased by about 6%, and the rural sewage treatment rate is still at a relatively low level. Therefore, through literature research (Period: since 2000; Tool: Citespace) and on-site investigation, this article summarizes many main aspects that restrict rural sewage treatment:

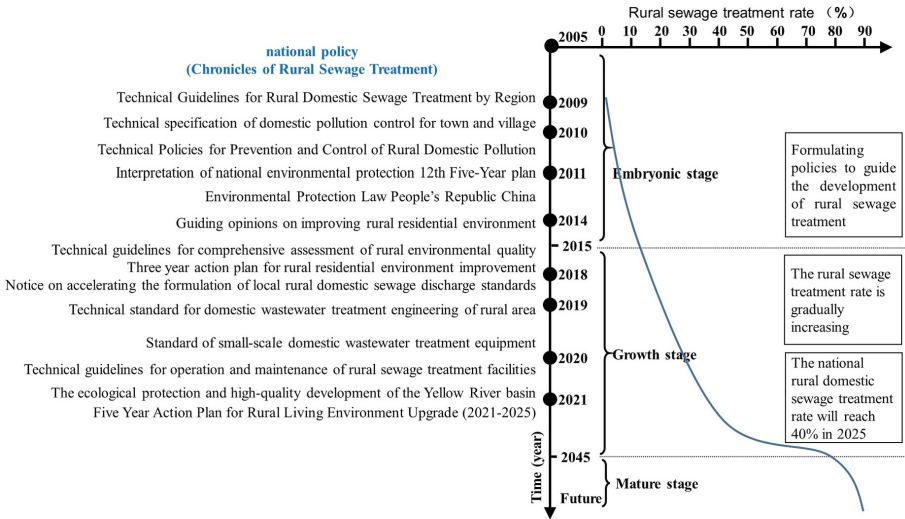


Fig. 2. Development history of rural sewage treatment of China.

- The engineering design scale is too large.** At present, the designed discharge volume of rural domestic sewage is 100–150 L/ (person · day) for calculation, but the actual value is only 50% of the design value. This is mainly because the construction of rural sewage pipelines in China is relatively small, and latrine pits are commonly used in rural areas, where feces and urine are directly utilized as resources. However, some miscellaneous water such as laundry water in daily life is directly discharged through courtyard infiltration, only kitchen water and bath water are discharged through the sewer. The inflow of sewage treatment facilities depends on the actual rural population and water usage habits. The large designed water volume leads to high investment, sedimentation of sewage pipe networks, and difficulty in normal operation of treatment facilities.
- The design water quality of the engineering inflow is relatively high.** The design of sewage treatment engineering is based on the mixed concentration of black water and gray water, usually with a COD concentration of 250-300mg/L in the influent, which deviates greatly from the actual situation. The inlet water quality of sewage treatment facilities depends on the discharge path of sewage from farmers' homes, and the inlet water quality of each row of the project should be reasonably designed based on the actual drainage habits of local residents.
- The sewage pipe network is blocked or damaged.** The construction and maintenance of rural sewage pipelines are not in place, and there are serious issues of mixed connection, wrong connection, and damage. The problem of not building household collection pipes in the construction of sewage pipe networks is quite common, and treatment facilities cannot receive sewage. A large number of villages have not built sewage collection pipelines, and sewage is transported through rainwater pipelines, polluting surrounding water bodies.

- (4) **Sewage treatment facilities are not suitable for rural areas.** The normal operation rate of rural domestic sewage treatment facilities is not high, and the situations that cannot operate normally include large design scale, abnormal operation of facilities, shutdown of facilities, substandard effluent quality, incomplete or damaged pipeline network, and low inlet water quality (see Fig. 3).

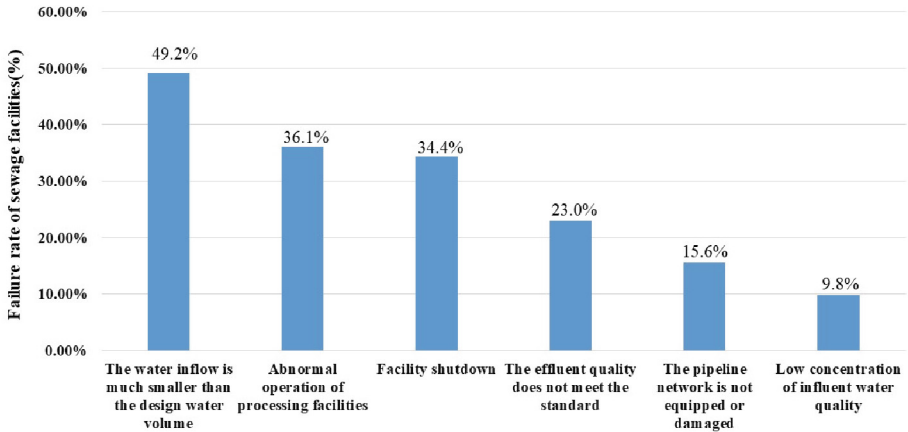


Fig. 3. Proportion of abnormal operation of rural sewage treatment facilities.

The reasons for the above-mentioned problems in rural domestic sewage are mainly due to copying the urban drainage treatment model and neglecting rural water usage habits from the source (see Fig. 4). The traditional mixed discharge mode of sewage makes it difficult to fully utilize organic resources and pollute the environment. Urine and feces are internationally recognized as the second phosphate rock, and the traditional drainage mode of phosphorus is extremely wasted in landfills. Phosphorus is a non-renewable resource, and the existing phosphorus resources can only be used for 100 years. In recent years, China has emphasized resource recycling in rural sewage treatment, especially feces and water resources [5].

Based on the concept of resource recycling, combined with the practice of existing rural sewage treatment projects, this paper proposes a new low-carbon ecotype treatment model of “classified treatment and recycling” of rural sewage, which aims to provide a reference for the future development of differentiated treatment and resource utilization of rural sewage in different regions of China.

2 Comparative Analysis of the Characteristics of Rural Sewage Treatment Models at Home and Abroad

Various countries have attempted various operational models to achieve rural sewage treatment. For example, there are five rural sewage treatment modes in the United States [6], namely, homeowner awareness mode, maintenance contract model, operating permit

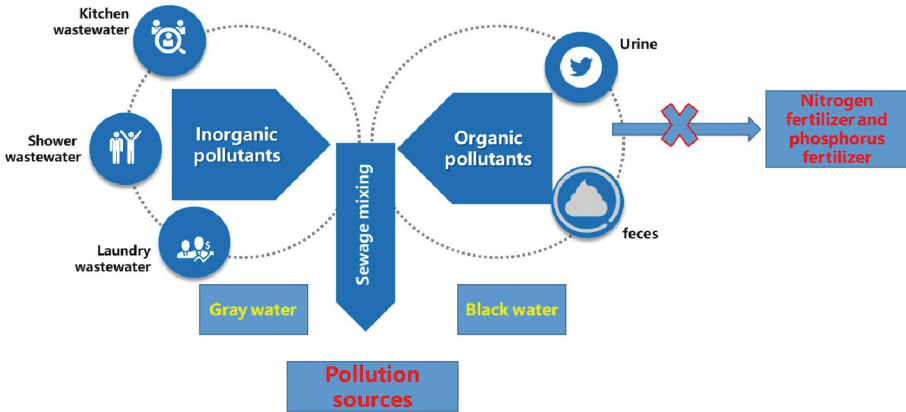


Fig. 4. Unified sewage discharge mode.

model, responsible management entity (RME) operation, responsible management entity (RME) ownership model, which are mainly determined according to water environment sensitivity and process complexity [7, 8]. The operation mode of rural sewage treatment in South Korea is divided into direct management by local governments and entrusted management [9]. The infrastructure of EU countries is well-established, and they mainly use centralized management to treat rural sewage [10]. Rural areas are charged 30% of the standard for urban residents, ensuring the good operation of the system. In Japan, rural sewage is mainly treated jointly by the government, third-party institutions, and users. There are three modes of treatment: piped treatment, centralized treatment in villages and towns, and purification tanks [7, 10]. The operation is mainly carried out by third-party companies, and farmers are required to pay pollution discharge fees. The successful experiences of various countries provide valuable experience for China to carry out rural sewage treatment in the future.

At present, there are three main types of sewage treatment models in China [11], namely the piped treatment model (connected to the urban sewage pipeline network for unified treatment), the centralized treatment model (constructing centralized sewage treatment facilities), and the decentralized treatment model (constructing decentralized sewage treatment facilities). The characteristics of each model [12] are shown in Table 1. (1) The operation effect of the Nanotube processing model is relatively good, and it should be adopted in rural areas within 3km of urban sewage treatment plants (sewage treatment pipelines can usually extend for about 5km [9], and investment in pipelines beyond this range will greatly increase). (2) The centralized processing mode often lacks professional facility operation and post maintenance [13], requires large investment, and is not suitable for rural areas with low population density and dispersed population. In addition, there are significant differences in the production and lifestyle of rural areas compared to urban areas. The daily fluctuations in the quality and quantity of rural domestic sewage [7] have led to an increase in the difficulty of sewage treatment. Finally, many centralized sewage treatment systems in China do not operate or have poor operational effects. (3) For the decentralized treatment model, it is unrealistic to

build sewage treatment plants in many rural areas due to low population density and dispersed households, but the construction cost of decentralized treatment is relatively high. Therefore, cost-effective decentralized sewage treatment technology is sustainable and necessary for rural areas [15]. In addition, the difficulty of operating sewage treatment technology is also a major factor limiting the decentralized treatment of rural sewage. Although some researchers have attempted to develop low-cost and easy to operate sewage treatment devices, such as a multi soil layered sewage treatment system (MSL) [16], its practical application effect still needs to be verified.

Table 1. Characteristics of rural sewage treatment mode in China.

Model	Connotation	Characteristic	Applicable conditions
Nanotube processing	Incorporate rural domestic sewage pipelines into the municipal pipeline network for unified treatment by urban sewage treatment plants	Low investment, short construction cycle, fast efficiency, and convenient management	Suitable for areas close to urban sewage plants (about 3 km [14])
Centralized processing	Build a new supporting sewage pipe network collection system to collect and treat residential sewage uniformly	Unified collection, transportation, and processing	Suitable for central villages, residential areas, or natural villages with a certain population and relatively concentrated residential areas
Decentralized processing	Sewage is collected by multiple households or single households and then treated separately	Flexible layout, cost saving of pipeline network, and simple structure	Suitable for non ecologically sensitive areas, villages with scattered populations, or villages with unsuitable elevation and terrain for laying pipeline networks

3 New Models for Rural Sewage Treatment

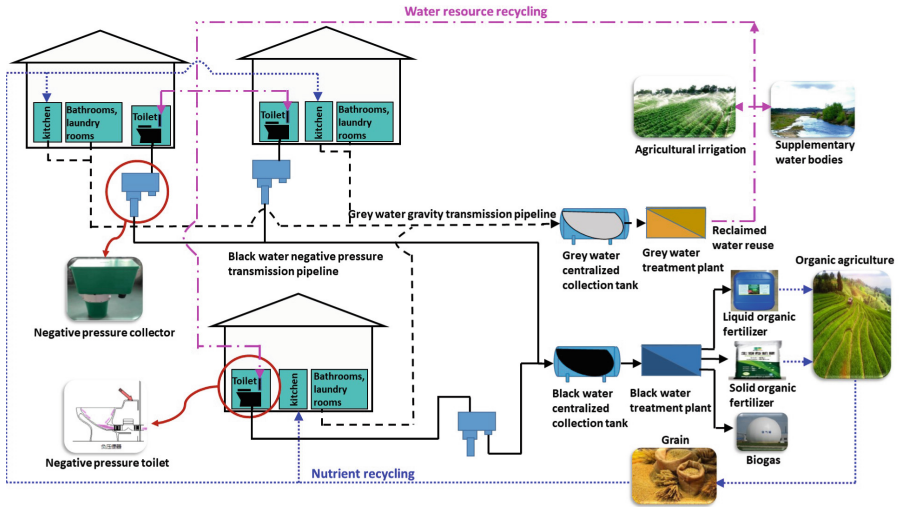
3.1 Model and Concept

This article proposes a new rural sewage treatment model of “source separation, classified discharge, qualitative treatment, and recycling”, and its technical schematic is shown in see Fig. 5. There are three specific models based on the size of the rural population served.

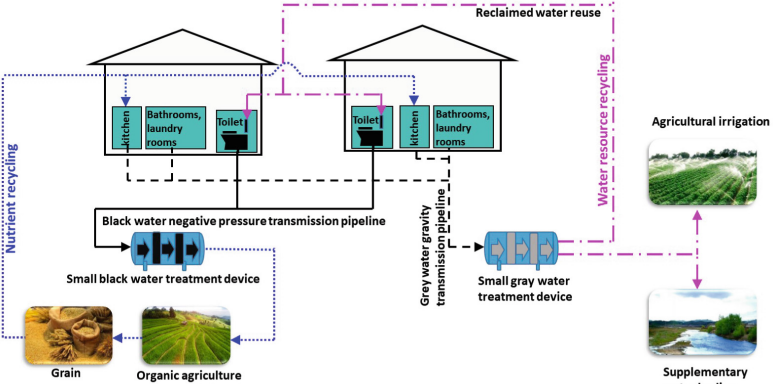
- **Centralized collection and processing model.** The characteristic of this model is to classify and collect domestic sewage from the source, forming two sewage transmission pipelines. The first pipeline is to mix and collect kitchen washing sewage, shower sewage, and other lightly polluted domestic miscellaneous water. After being collected through the pipeline, it is transported to the gray water treatment station. After simple and low consumption “physicochemical + ecological” treatment, the effluent quality can reach the standard of recycled water quality, which can be reused for agricultural irrigation nearby sprinkling, flushing or supplementing natural water bodies to achieve the recycling of water resources. The second pipeline mainly collects toilet drainage, and the toilet is a negative pressure collection toilet (the water consumption of stool/urination is 1L/0.1L each time). The collected black water is transmitted to the black water treatment station (black water recycling center) through the negative pressure collection and transmission system, where the rural agricultural wastes such as straw, livestock manure and kitchen waste are mixed in proportion to produce solid organic fertilizer and liquid organic fertilizer through anaerobic/aerobic fermentation, The fermented fertilizer should be applied to nearby farmland to achieve a virtuous ecological cycle of nutrients such as C, N, and P.
- **Decentralized collection and processing model.** This mode is similar to the centralized collection and processing mode, with the main difference being that the number of people serving is relatively small. Therefore, small gray water and black water treatment devices are used, and after treatment, they are directly reused on site.
- **Decentralized collection and centralized processing model.** When farmers are scattered, it is recommended to use an anhydrous toilet for black water collection. The generated feces and urine are packaged and stored in biodegradable bags in a fecal collector. Professional operators collect feces regularly and return the produced organic fertilizer to the countryside in proportion to the amount of recovered feces and urine, achieving a virtuous cycle of this model.

3.2 Performance Analysis

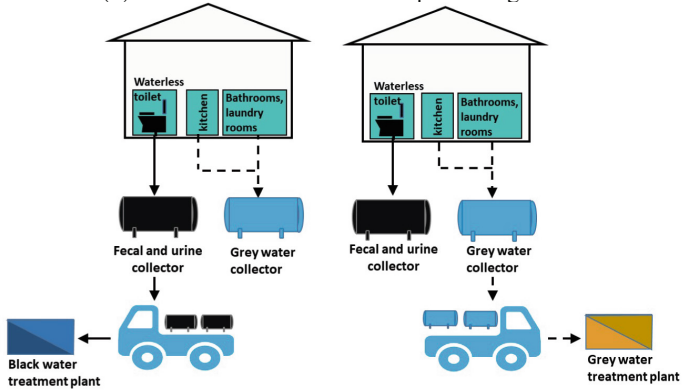
To further elaborate on the economy of the rural sewage treatment model proposed in this study, this study takes a rural area with 300 people and a centralized collection and treatment model as an example for economic accounting analysis. According to the reference values of gray water design discharge and black water design discharge in the “Design Standards for Building Water Supply and Drainage” GB50015-2019, the treatment scale of gray water and black water in this project is calculated to be 33.15 m³/d and 1.775 m³/d respectively, with an investment of approximately 4.34 million RMB (Table 2). The annual operating cost of black water and gray water is 127400 RMB, and the investment recovery period is 8.31 years. It can be seen that the investment benefits of this new model are significant and have strong promotion and application value.



(a) Centralized collection and processing model



(b) Decentralized collection and processing model



(c) Decentralized collection and centralized processing model

Fig. 5. The new rural sewage treatment model based on source separation.

Table 2. Benefit analysis of new model of rural sewage treatment.

Investment, operation and maintenance, and benefits of the project		Cost/10000 RMB
Initial investment	Grey water collection system, black water collection system	134
	Black water and gray water resource utilization treatment stations (separate resource utilization, gray water pre-treatment + artificial wetland; black water production organic fertilizer)	300
Operation and maintenance expenses	The direct operating cost of grey water resource treatment is generally 0.4–0.6 RMB/ton of water	1.21
	The direct operating cost of black water resource treatment is generally about 0.2 RMB/ton of sewage	0.064
Benefit analysis	Water saving benefits	1.564
	Energy Saving benefits	7.2
	Economic performance	0.036
		0.3024
	15.9	27.4

Note: Water and electricity prices are calculated based on Zhengzhou city.

4 Conclusions

This paper has been proposed a new rural sewage treatment model based on the intensive and economical utilization of water resources, namely “source separation, classified discharge, negative pressure collection, and resource utilization”. The major differences from the existing rural sewage treatment models can be addressed as below:

- (1) The new sewage treatment model has achieved the full resource utilization of sewage. Grey water can be used for irrigation and domestic miscellaneous water after being treated to reach recycled water; Black water is made into organic fertilizer and ultimately returns to farmland.
- (2) Compared with traditional sewage treatment models, the new sewage treatment model has good water saving benefits, energy saving benefits, and economic performance.

However, the following limitations of the study should be noted. Firstly, further research and development are needed to develop black water solid-liquid separation technology with high water content to improve the efficiency of fecal and urine treatment and better achieve resource utilization. Secondly, the model proposed in this study was only demonstrated in some regions and did not involve rural areas in all climate regions of China.

Acknowledgment. I acknowledge support from the National Key Research and Development Program of China (2021YFC3201302), China Postdoctoral Science Foundation (No. 2022M711288), Advanced Technology Demonstration Project of the Ministry of Water Resources of the People's Republic of China (SF-202206), and Yellow River Engineering Consulting Co., Ltd. Project (2022KY007).

References

1. Yang, B., Wen, W.: Treatment and technology of domestic sewage for improvement of rural environment in China. *J. King Saud Univ. - Sci.* **34**(7), 102181 (2022)
2. Wang, C., et al.: Revealing factors influencing spatial variation in the quantity and quality of rural domestic sewage discharge across China. *Process Saf. Environ. Prot.* **162**(6), 200–210 (2022)
3. Xu, Z.X., Xu, J.: Establishing an Assessment Index System for Sewage Treatment Works in China. In Press, *Engineering* (2022)
4. Wang, T., Sun, D.L., Zhang, Q., Zhang, Z.Z.: China's drinking water sanitation from 2007 to 2018: a systematic review. *Sci. Total Environ.* **757**(8), 143923 (2021)
5. Zhou, X., et al.: China should focus beyond access to toilets to tap into the full potential of its Rural Toilet Revolution. *Resour. Conserv. Recycl.* **178**(3), 106100 (2022)
6. Huang, W.F., Wei, Y.F., Wang, H.X., Jia, Q.: The revelations on decentralized rural sewage disposal policy and technology of the United States. *Environ. Prot.* **44**(7), 63–65 (2016)
7. Kong, D., Zhang, X.L.: International experience study and suggestions on rural sewage treatment operation model in China. *Environ. Prot.* **47**, 61–64 (2019)
8. U.S. Environmental protection agency: Handbook for management of onsite and clustered (decentralized) wastewater treatment systems, U.S. (Environmental Protection Agency, 2003)
9. Zhou, L., Li, B.H., Li, J.L.: Construction and management of rural drainage system in Korea. *Environ. Pollut. Cont.* **31**(6), 89–91 (2009)
10. Shen, Z., Huang, J., Liu, P.Y.: International experience in the treatment of rural domestic sewage-Based on the comparison of the models of the United States, the European Union and Japan. *Price Theory Pract.* **33**(2), 49–50 (2013)
11. Han, G.Y.: Problems and optimization measures of rural domestic sewage treatment. *Heilongjiang Huanjing Tongbao.* **35**(1), 114–116 (2022)
12. Wang, T.X.: Study on rural domestic sewage treatment scheme. *IOP Conf. Ser. Earth Environ. Sci.* **781**(3), 32040 (2021)
13. Li, P.F., et al.: Analysis on the present situation and discussion on its treatment mode of rural sewage treatment in China. *Water Wastewater Eng.* **57**(12), 65–71 (2021)
14. Wang, Z.L., Cheng, Y., Shen, S.H., Fu, D.D.: Selection of rural domestic sewage treatment mode and process. *China Resour. Compr. Utilization.* **39**(5), 189–191 (2021)
15. Hong, Y.Y., et al.: Enhanced nitrogen removal in the treatment of rural domestic sewage using vertical-flow multi-soil-layering systems: experimental and modeling insights. *J. Environ. Manage.* **240**(15), 273–284 (2019)
16. Xu, Y., et al.: Systematically assess the advancing and limiting factors of using the multi-soil-layering system for treating rural sewage in China: from the economic, social, and environmental perspectives. *J. Environ. Manage.* **312**(12), 114912 (2022)



Comparative Study on Real-Time Economic Operation Algorithm of Three Gorges Hydropower Station

Kui Huang¹, Zhenyu Mu², Xuanyu Shi^{2(✉)}, Xueshan Ai^{2,3,4}, Jiajun Guo²,
and Jie Ding²

¹ Power Dispatching Control Center, Guangxi Power Grid, Guangxi 530023, China

² School of Water Resources and Hydropower Engineering, Wuhan University, Wuhan 430072, China

1035518773@qq.com, xsai@whu.edu.cn

³ State Key Laboratory of Water Resources Engineering and Management, Wuhan University, Wuhan 430072, China

⁴ Hubei Key Laboratory of Water System Science for Sponge City Construction (Wuhan University), Wuhan 430072, China

Abstract. The study of flood season stage has significant scientific significance and value in achieving the dual goals of flood control and drought resistance in reservoirs. However, existing research on staging schemes often focuses on a single hydrological indicator for staging calculations, which makes it difficult to comprehensively measure the hydrological characteristics of the basin and is not closely integrated with reservoir scheduling. In response to this problem, this study takes the Longtan Reservoir in Guangxi as the research object, first analyzing the three indicators of rainfall, flood, and flow in the Longtan Basin, and then using circular distribution method, fuzzy statistical test method, and the fuzzy set analysis method and the multi-index identification method are used to calculate the flood season staging. Finally, the flood season staging scheme of Longtan Reservoir is determined based on the reservoir operation mode, and the advantages and disadvantages of the four staging methods are analyzed in all aspects. The results show that the staging scheme combined with the reservoir operation mode can not only consider the nodes of hydrological index changes in the flood season, but also take into account the shipping and water storage needs of the reservoir, compared to directly using nodes for staging, it has stronger applicability. This study can provide theoretical basis and reference for the determination of reservoir flood season staging plans.

Keywords: Longtan Reservoir · Flood Season Stage · Hydrological Indicators · Reservoir Regulation

1 Introduction

Under the premise of ensuring dam safety and downstream flood control safety, implementing phased scheduling of reservoirs is an important measure to improve the profitability of reservoirs. Studying flood season staging has significant scientific significance

and value for achieving the dual goals of flood control and drought resistance in reservoirs [1, 2]. After analyzing and improving existing research results, there are basically two types of analysis methods for flood season staging: qualitative analysis method and quantitative analysis method [3, 4]. The qualitative analysis method mainly analyzes the change law of hydrological elements such as rainstorm and flood in the basin, and selects the mutation points of each element in the flood season by applying mathematical statistics and other methods. This method is simple and clear, but subjective, and the results are highly uncertain; The quantitative analysis method is based on mathematical calculations, with clear principles and strong objectivity, thus receiving more widespread attention [5]. Among them, the clustering analysis method [6, 7] comprehensively considers the influence of various factors on the flood season staging, and uses the similarity coefficients in the calculation elements of feature factors to form a fuzzy similarity matrix as the staging basis; The change point analysis method [8, 9] is objective and reliable, and the staging results can be accurate to the day; The relative frequency method [10] can intuitively represent the probability and trend of flood occurrence, and the calculation steps are relatively simple. Zhou et al. [11] used the probability change point analysis method for flood season staging. Li et al. [12] first processed the flood process, and then used the circular distribution method for flood season staging, achieving certain results.

Overall, statistical methods need to be used to process indicators such as rainfall, flood, and flow during the flood season staging process. The magnitude and occurrence time of these indicators are the primary considerations in the flood season staging process. However, existing staging schemes often focus on one hydrological indicator for staging calculations, making it difficult to comprehensively measure the hydrological characteristics of the basin and not closely integrated with reservoir scheduling. To address this issue, this paper takes Longtan Reservoir in Guangxi as the research object. First, it analyzes the three types of indicators such as rainfall, flood and flow in Longtan Basin. Then it calculates the flood season by stages using circular distribution method, fuzzy statistical test method, fuzzy set analysis method and multi-indicator identification method in turn. Finally, it determines the flood season staging scheme of Longtan Reservoir in combination with the reservoir operation mode. This study can provide theoretical basis and reference for the determination of reservoir flood season staging plans.

2 A Subsection Sample

In order to cover the three stage indicators and compare and analyze their characteristics, this study uses circular distribution method, fuzzy statistical test method, fuzzy set analysis method and multiple indicator identification method to calculate the flood season stage. The circular distribution method uses flood indicators, fuzzy statistical test method and fuzzy set analysis method use flow indicators, and the multiple indicator identification method uses rainfall indicators, flow indicators and flood indicators.

2.1 A Subsection Sample

D_i is the peak occurrence time, and Q_i is the magnitude of the flood peak of the flood sample i , so the flood time coordinate values (x_i, y_i) are [13]:

$$(x_i, y_i) = \begin{cases} (\cos \alpha_i, \sin \alpha_i), & \text{without considering flood magnitude} \\ (q_i \cos \alpha_i, q_i \sin \alpha_i), & \text{considering flood magnitude} \end{cases} \quad (1)$$

$$(\bar{x}, \bar{y}) = \left(\sum_{i=1}^N x_i/N, \sum_{i=1}^N y_i/N \right) \quad (2)$$

In which N is the sample size; $\alpha_i = D_i \frac{2\pi}{T}$ is the occurrence time of the flood i (angle), $0 \leq \alpha_i \leq 2\pi$.

$\bar{\alpha}$ is the concentration period of the flood, which is:

$$\bar{\alpha} = \begin{cases} \arctan \bar{y}/\bar{x} & \bar{x}>0, \bar{y}>0 \\ 2\pi + \arctan \bar{y}/\bar{x} & \bar{x}>0, \bar{y}<0 \\ \pi + \arctan \bar{y}/\bar{x} & \bar{x}<0 \\ \pi/2 & \bar{x} = 0, \bar{y}>0 \\ 3\pi/2 & \bar{x} = 0, \bar{y}<0 \\ / & \bar{x} = 0, \bar{y}=0 \end{cases} \quad (3)$$

And the concentration r is:

$$r = \begin{cases} \sqrt{\bar{x}^2 + \bar{y}^2}, & \text{without considering flood magnitude} \\ \sqrt{\bar{x}^2 + \bar{y}^2}/\bar{q}, & \text{considering flood magnitude} \end{cases} \quad (4)$$

Where \bar{q} is the mean of N sample flood peaks.

The relationship between r and the standard deviation s of α_i is as follows:

$$s = \sqrt{-2 \ln r} \quad (5)$$

The starting and ending days D_1 and D_2 of the main flood season in the calculation period are respectively:

$$D_1 = \frac{\bar{\alpha} - s}{2\pi} T \quad (6)$$

$$D_2 = \frac{\bar{\alpha} + s}{2\pi} T \quad (7)$$

2.2 Fuzzy Statistical Test Method

The formula of Fuzzy statistical test method is [14]:

$$D_t = \left[\sum_{i=1}^N (Q_{i,t} - Q_y)/Q_y \right] / N \quad (8)$$

Where $Q_{i,t}$ is the average daily runoff on the day t of the year i ; Q_y is the multi-year daily average flow; N is total years.

Select an appropriate positive number as the membership threshold, and if the membership exceeds the threshold, it is the member of the flood season.

2.3 Fuzzy Set Analysis Method

Firstly, the threshold Q_T is determined based on the actual situation of the watershed. Then, for the i year flood season, the flood season time of the i year is determined based on the start and end times greater than or equal to the threshold Q_T . After years of calculation, for a certain time t , the number of times it is covered by the flood season is m_i , and its membership degree $U_A(t)$ can be calculated by: $U_A(t) = m_i/N$, and an empirical membership function can be drawn. Then, the start time a_1 and end time a_1 of the main flood season can be determined based on the threshold Q_T , and perform function fitting on the obtained empirical membership function, which is [15]:

$$U_A(t) = \begin{cases} \exp[-(\frac{a_1-t}{b_1})^2] & t < a_1, b_1 > 0 \\ 1 & a_1 \leq t \leq a_2 \\ \exp[-(\frac{t-a_2}{b_2})^2] & t > a_2, b_2 > 0 \end{cases} \quad (9)$$

$$b_1 = \sqrt{-\sum_{i=1}^{a_1} (a_1 - i)^2 / \sum_{i=1}^{a_1} \ln u_i} \quad (10)$$

$$b_2 = \sqrt{-\sum_{i=a_2}^{T_0} (i - a_2)^2 / \sum_{i=a_2}^{T_0} \ln u_i} \quad (11)$$

Where T_0 is the last time of flood season, and u_i is the empirical membership in day i .

Draw the curve of fitting membership function. Keep the threshold λ unchanged and determine the main flood season $A'_\lambda = [a'_1, a'_2]$ in the figure. Where a'_1 and a'_2 are the starting and ending time of main flood season determined by the fitting curve of empirical membership function. The final main flood season can be obtained by taking A_λ and A'_λ compromise values.

2.4 Multiple Indicators Identification Method

The calculation steps for the multiple indicators identification method are [16]:

Set the eigenvalues matrix of m indicators during the flood season as

$$X = (x_{it}), i = 1, 2, \dots, m \quad (12)$$

Where x_{it} is the characteristic value of the time series t indicator i .

For the larger and smaller optimal indicators in the indicator eigenvalue matrix, there are:

$$k_{i1} = \max x_{it}, k_{i2} = \min x_{it} \quad (13)$$

$$k_{i1} = \min x_{it}, k_{i2} = \max x_{it} \quad (14)$$

Where $\max x_{it}$ 、 $\min x_{it}$ are the maximum and minimum eigenvalues of the time series set indicators respectively.

According to the matrix X and the above equation, the matrix can be obtained:

$$K = (k_{ih}), i = 1, 2, \dots, m; h = 1, 2 \tag{15}$$

The relative membership formula is:

$$\mu_{i1}(u_t) = \frac{x_{it} - k_{i2}}{k_{i1} - k_{i2}} \tag{16}$$

The comprehensive relative membership degree is:

$$v_t(u_t) = \frac{1}{1 + \left\{ \frac{\sum_{i=1}^m [\omega_i(1-\mu_{i1}(u_t))]^p}{\sum_{i=1}^m [\omega_i\mu_{i1}(u_t)]^p} \right\}^{\frac{\alpha}{p}}} \tag{17}$$

Where α, p are parameters; $\alpha = 1$ is the least one squares optimization criterion parameters; $\alpha = 2$ the least two squares optimization criterion parameters; $p = 1, p = 2$ are Hamming distance and European distance parameters respectively, ω_i are variable indicator weights, such as using equal weights, the above formula is simplified as:

$$v_t(u_t) = \frac{1}{1 + \left\{ \frac{\sum_{i=1}^m [1-\mu_{i1}(u_t)]^p}{\sum_{i=1}^m [\mu_{i1}(u_t)]^p} \right\}^{\frac{\alpha}{p}}} \tag{18}$$

The time series with a comprehensive relative membership degree of 0.5 is the node corresponding to the flood season stage.

3 Case Study

The Longtan Reservoir is located 15 km upstream of Tiane County in Guangxi, and was fully put into operation and completed by the end of 2009. This study analyzes the daily flow data from 2010 to 2022 after the completion of the Longtan Reservoir, providing reference for its actual scheduling in the event of changes in water conditions after its completion.

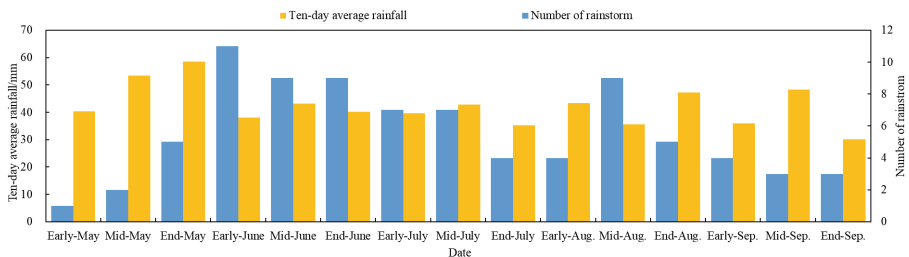
3.1 Analysis of Hydrological and Meteorological Indicators in River Basins

Based on the rainfall data of Longtan Basin, this study takes ten days as the unit, uses the number of heavy rainstorm and the average rainfall of ten days as the rainfall indicators, and counts the index values, as shown in Table 1 and Fig. 1:

In terms of flood indicators, this study adopts flood peak size indicators and annual maximum flood peak occurrences within ten days. The flow indicators adopt multi-year

Table 1. Statistics of rainfall index values.

Indicator type	Early-May	Mid-May	End-May	Early-June	Mid-June	End-June
Number of rainstorm	1	2	5	11	9	9
Ten-day average rainfall	40.30	53.50	58.50	38.10	43.10	40.20
Indicator type	Early-July	Mid-July	End-July	Early-Aug	Mid-Aug	End-Aug
Number of rainstorm	7	7	4	4	9	5
Ten-day average rainfall	39.70	42.90	35.30	43.30	35.60	47.2
Indicator type	Early-Sep	Mid-Sep	End-Sep			
Number of rainstorm	4	3	3			
Ten-day average rainfall	35.90	48.30	30.20			

**Fig. 1.** Statistics of rainfall index values.

average inflow and daily inflow indicators. The historical flood information of each site is shown in Table 2. The annual maximum flood peak occurrences within ten days, i.e. multi-year average inflow, are shown in Table 3 and Fig. 2. The daily average inflow curve during the flood season is shown in Fig. 3.

Obviously, the change trend of the two rainfall indicators of heavy rainstorm frequency and ten day average rainfall in the Longtan basin is basically consistent, which better reflects the rainfall law in the basin. At the same time, the ten day average rainfall at both ends of June and early July is higher, and forms a corresponding relationship with the peak of the daily average inflow curve around July 1, indicating that the corresponding time of rainfall runoff in the Longtan basin is shorter in the middle of June and July, which is more likely to cause floods. In addition, in recent years, the distribution of floods in the Longtan Basin has been relatively scattered, but most of them still occur in July, which corresponds to rainfall and flow indicators.

On the other hand, in terms of the multi-year average inflow index, there is a peak period at the end of September, which to some extent indicates that the end of flood season is not only a critical time for water storage, but also a high risk of flood control.

Table 2. Historical flood information of each event.

Date	Peek (m ³ /s)	Date	Peek (m ³ /s)
2010/6/30	8932	2020/6/10	5421
2010/7/26	5385	2020/6/25	6392
2014/7/5	6370	2020/7/4	5972
2014/7/19	6167	2020/9/18	8949
2014/9/21	6932	2022/5/31	9023
2015/6/22	6957	2022/6/6	7090
2015/8/30	6073	2020/6/10	5421
2016/6/13	6271	2020/6/25	6392
2017/7/2	6429	2020/7/4	5972
2017/7/22	5598	2020/9/18	8949
2017/9/8	6758	2022/5/31	9023
2018/6/24	6232	2022/6/6	7090

Table 3. Statistics of average annual inflow and frequency of flood peaks over ten years.

Indicator type	Early-May	Mid-May	End-May	Early-June	Mid-June	End-June
Average ten days inflow	1049.8	1399.7	1706.4	2074.1	2471.9	2783.6
Number of annual maximum peak in ten days	0	0	1	0	3	2
Indicator type	Early-July	Mid-July	End-July	Early-Aug	Mid-Aug	End-Aug
Average ten days inflow	2804.7	2345.1	2488.9	2036.8	1971.8	1768.1
Number of annual maximum peak in ten days	2	1	1	0	0	0
Indicator type	Early-Sep	Mid-Sep	End-Sep			
Average ten days inflow	1786.4	1776.7	1679.0			
Number of annual maximum peak in ten days	1	1	1			

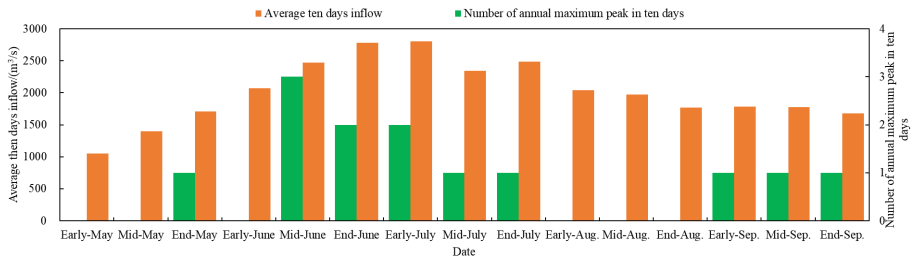


Fig. 2. Statistics of the index values of average annual inflow and frequency of flood peaks over ten years.

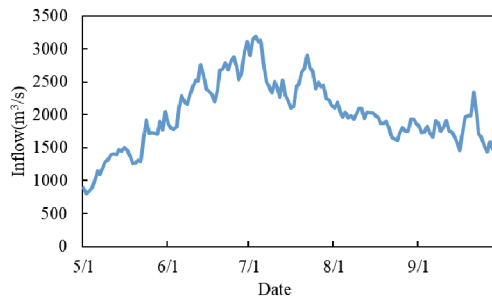


Fig. 3. Multi-year daily average flow hydrograph.

3.2 Comparison and Analysis

Based on the above three indicators, circular analysis method, fuzzy set analysis method, fuzzy statistical test method and multi indicator identification method are used for calculation. The calculation results are shown in Figs. 4, 5, 6 and 7, and the calculation stage nodes of each method are shown in Table 4:

Based on the analysis of the principles, calculation processes, and results of the four staging methods, it can be concluded that:

- (1) The circular distribution method and fuzzy set analysis method can effectively divide the stage of low flow and low number of floods before the flood season and the impounding stage at the end of the flood season, with strong objectivity, but it is difficult to reflect the change process of flow and flood frequency during the flood season. In addition, except that the flood peak corresponding to the field flood on June 23, 2010 is higher, the rest of the peak flows have little difference, so the results of considering the peak and not considering the peak are only one day different;
- (2) The fuzzy statistical experimental method takes traffic as the direct statistical object, with a simple principle and intuitive image, which is easy to operate. However, when dealing with complex traffic changes, this method has a certain degree of subjectivity in selecting membership threshold and stage node operations, and the method results are not convincing enough;
- (3) The fuzzy set analysis method takes the flow as the index, and the method itself has a strong objectivity. However, since the start time and end time of the flood season are

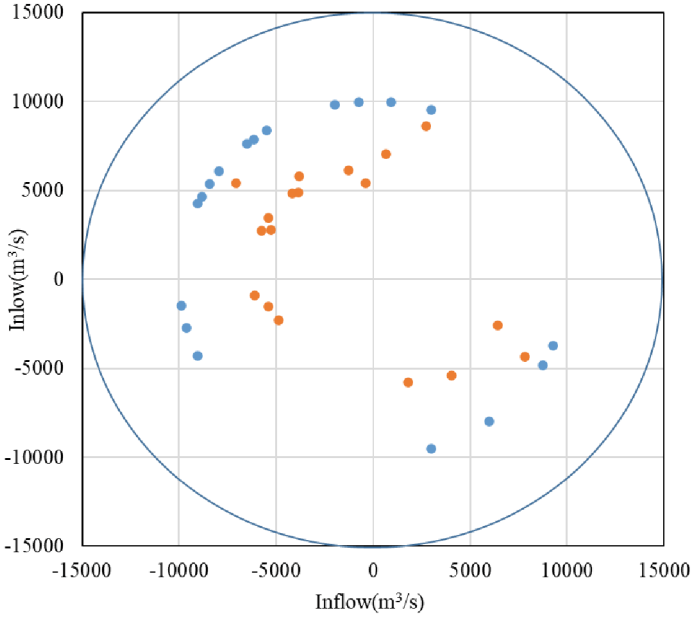


Fig. 4. Calculation results of circular distribution method.

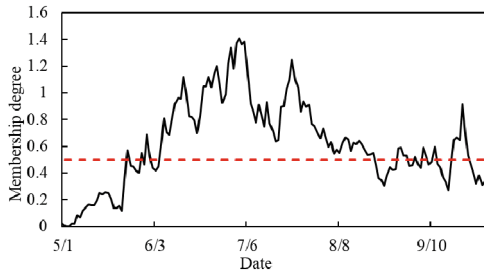


Fig. 5. Calculation results of fuzzy statistical experimental method.

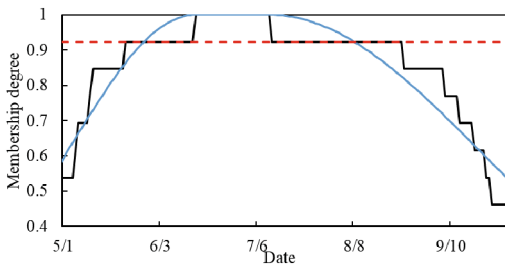


Fig. 6. Calculation results of fuzzy set analysis method.

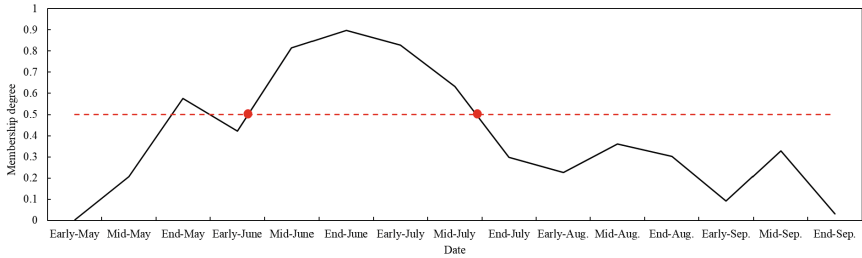


Fig. 7. Calculation results of multiple indicators identification method.

Table 4. Four staging methods for calculating staging nodes.

Method	First node	Second node
Circular distribution method (Considering flood peaks)	May 22nd	July 27th
Circular distribution method (Without considering flood peaks)	May 23rd	July 26th
Fuzzy statistical test method	June 5th	August 21st
Fuzzy set analysis method	May 28th	August 9th
multiple indicators identification method	June 7th	July 20th

determined by the average annual runoff, there may be a large gap between different years, which is difficult to unify;

- (4) The multi indicator recognition method can use multiple different types of indicators for decision-making, covering a wide range of content and having strong objectivity and comprehensiveness. However, this method is more suitable for using indicators with the same changing trend. When using indicator types with different changing trends for calculation, the membership degree of the time period calculated by this method often fluctuates greatly and the law is not obvious, Enhance subjectivity in the final selection of staging nodes.

3.3 Final Installment Plan Determination

According to the chronological order of the nodes obtained by the above three methods, they can be roughly divided into two sets: the first node selection set: May 22nd, May 22nd, May 28th, June 5th, and June 7th; The second node selection set: July 20th, July 26th, July 27th, August 9th, and August 21st. Considering the shipping demand at the beginning of the reservoir operation flood season, the power generation demand at the end of the flood season, and the water storage demand, the time of the first and third sub flood seasons should be extended as much as possible, and the flow corresponding to the transition period between the second and third sub flood seasons should be as large as possible. At the same time, for the convenience of actual operation of the reservoir, it should be divided into ten days, based on this, two initial stages were selected: June 1st and July 20th. The stage results are shown in Table 5.

Table 5. Final stage plan.

	First sub-season	Second sub-season	Third sub-season
Final Stage Plan	May 1st–May 31st	June 1st–July 20th	July 21st–September 30th

4 Conclusion

Taking Longtan Reservoir in Guangxi as the research object, this paper analyzes three types of indicators of rainfall, flood and flow in this area, and calculates them by using circular analysis method, fuzzy set analysis method, fuzzy statistical test method and multi indicator identification method according to the characteristics of indicators, compares and analyzes the calculation results of each method, and finally determines the staging scheme in combination with the actual operation of the reservoir. The conclusions are as follows:

- (1) The circular distribution method has strong objectivity, but it is difficult to reflect the changes in flow and flood frequency during the flood season; The fuzzy statistical experimental method takes the flow rate as the direct statistical object, with a simple principle and intuitive image, which is easy to operate but has a certain degree of subjectivity; The fuzzy set analysis method takes the flow as the indicator, and the method itself has strong objectivity, but there may be a large gap between different years, which is difficult to unify; The multi indicator recognition method covers a wide range of content and has strong objectivity and comprehensiveness, making it more suitable for using indicators with the same trend of change.
- (2) The staging plan combined with the purpose of reservoir scheduling can not only consider the nodes with changes in hydrological indicators during the flood season, but also take into account the shipping and water storage needs of the reservoir. Compared to directly using nodes for staging, it has stronger adaptability.

References

1. Dong, Q., Wang, X., Wang, J., Fu, C.: Application of fractal theory in the stage analysis of flood seasons in Three Gorges reservoir. *Resour. Environ. Yangtze Basin* **3**, 400–404 (2007)
2. Jiang, H., Mo, C., Wei, D., Sun, G., Wei, W.: Review of reservoir flood season staging. *Adv. Sci. Technol. Water Resour.* **32**(3), 75–80 (2012)
3. Yu, T., Guo, S., Liu, P., Li, W0.: Study on method and application of reservoir flood season staging. *China Rural Water Hydropower* (8), 24–26+56 (2006)
4. Liu, K., Wang, Y., Hu, S.: Comparative study on application of quantitative analysis methods to division of flood seasonal phases for reservoir. *Water Resour. Hydropower Eng.* **09**, 76–78+82 (2006)
5. Wang, X.: Study on the Flood Season Staging and Limited Water Level of Xidayang Reservoir. Northwest A&F University, Yangling (2021)
6. Mo, C., et al.: Stage application of Chengbihe reservoir in flood season based on jump analysis. *Yellow River* **39**(2), 38–41 (2017)

7. Wang, Z., Wang, Y., Hu, S.: Effective fuzzy cluster method for dividing reservoir flood season. *Adv. Water Sci.* **4**, 580–585 (2007)
8. Li, W., Su, C., Chen, X., Liu, K., Dai, L.: Research on the application of flood season staging in Hongze lake. *Controlling Huai River* **11**, 80–82 (2020)
9. Liu, Z., Zhang, J., Wen, T., Cheng, J.: Research on the flood season staging in Xiajiang reservoir of Ganjiang river. *China Rural Water Hydropower* **487**(05), 124–128 (2023)
10. Bo, H., Dong, X., Deng, X.: Study on the method of flood season staging for the Three Gorges Reservoir. *Yellow River* **33**(2), 43–44 (2011)
11. Zhou, K.: Flood season segmentation and scheme optimization in the Yellow River. *J. Water Clim. Change* **13**(1), 274–286 (2022)
12. Li, X., Zhang, Y., Tong, Z., Niu, G.: Reservoir flood season segmentation and risk–benefit cooperative decision of staged flood limited water level. *Water Resour. Manage* **36**(10), 3463–3479 (2022)
13. Guo, J., Guo, Q., Wu, X.: Study on flood season staging based on fuzzy set analysis method and circle distribution method. *Water Resources Power* **31**(03), 50–53 (2013)
14. Wan, J.: *Staged Control and Operation of Dongjiang Reservoir*. Science Press, Beijing (2009)
15. Wang, Y., Wang, B., Pan, H., Hou, G., Li, Y.: Study on flood season staging of different stations in Xijiang River based on fuzzy set analysis. *Pearl River* **41**(4), 8–14 (2020)
16. Li, M., Chen, S., Wang, Y., Zhou, R.: Multi-criteria recognition method for flood seasonality based on variable sets. *J. Hydraul. Eng.* **44**(12), 1420–1424 (2013)



Flood Forecast and Control for Urban Rivers Using LSTM Neural-Network

Lars-Eric Ertlmeier¹, Zhenyu Yang¹(✉), and Benjamin Refsgaard²

¹ AAU Energy, Aalborg University, Esbjerg Campus, 6700 Esbjerg, Denmark
yang@energy.aau.dk

² Vejle Spildevand, Toldbodvej 20, 7100 Vejle, Denmark
benre@vejlespildevand.dk

Abstract. To make better prediction and control of river water navigation in a Danish city - Vejle, the Long-Short-Term-Memory (LSTM) neural-network model is adopted to predict the water-level nearby a high flooding-risk area using correlated historical data. A set of feedback control solutions are developed based on the extension of the obtained LSTM model to automatically regulate a distribution-gate system, which guides the coming stream-flow into separated urban rivers. The proposed control solutions are tested in simulation based on four historic events, and it can be observed that two floods at the critical areas since 2017 could have been prevented by balancing flow-splits using automatic feedback control, which was manually controlled in the past. This study demonstrates a clear and promising potential to use machine learning methods for supporting development of smart cities and their climate adaption strategies.

Keywords: Urban rivers · flood prediction · LSTM · flood control

1 Introduction

In July 2021, some part of the western Europe, particularly in Germany and Belgium, experienced severe floods along the rivers of Rhine and Meuse, due to a record-breaking precipitation. This catastrophic event led to a loss of more than 200 lives [1]. According to IPCC's report [2], the frequency of extreme rainfalls has significantly increased since 1950s, and this trend has been evidenced by more and more flood events in recent decades. The climate change is one of the drivers behind these extreme precipitation events [3]. Analyzed by The World Meteorological Organization, 44% of disasters reported worldwide between 1970 and 2019 has been associated with floods, which caused 16% of reported deaths and 31% of reported economic losses. Corresponding to the river floods specifically, it is about 24% of disasters, leading to 6% of deaths and 21% of reported economic losses. It has also been noticed that about 66% of reported disasters in Africa between 2000 and 2019 were due to floods [4].

Precise prediction of water-levels or stream-flows in urban rivers has become crucial in climate adaptation of global municipalities. The EU commission issued the European Flood Awareness System (EFAS) after the flooding catastrophe of Danube and Elbe rivers in 2002 [5]. The EFAS did not issue a warning for the Rhine River Basin four days before the 2021 flooding occurred [6]. Besides that, the European Commission issued the European Floods Directive in 2007 which instructed its member states to evaluate which areas are at risk of floods and to prepare flood risk management plans for these areas accordingly [3].

Conventional approach for river/lowland flood prediction and warning is to use hydro-meteorological models which often require accurate and sufficient hydro- and meteorological information [7]. In recent decades the data-driven AI technologies, such as deep neural networks and machine learning, are causing more and more attentions for relevant climate adaptation studies, thanks to the fact that this type of models can be built up based on just measurement data, while the detailed knowledge of underlying processes may not be required. As an extension of the standard Recurrent Neural Networks (RNN), the Long-Short Term Memory (LSTM) neural network, firstly proposed in [8] by Hochreiter and Schmidhuber, is considered as one of the most effective and efficient neural networks for modeling and prediction of time series data, primarily due to its capability to be able to catch potential long-term time dependencies present in the input-output data. This is quite relevant for the purpose of stream-flow or water-level forecasting in hydrological systems as the water can be held in some catchments for a long while.

A set of LSTM models are developed for a real-time water-level forecast of urban rivers at Fuzhou city [9]. This study showed that the LSTM forecast is pretty accurate in the leading time of 3–6 h. By coupling a LSTM model, developed using radar precipitation measurements, with a Storm Water Management Model, the accurate water-level predictions at Seoul is achieved for the leading time of 30–90 min in [10]. By including each basin's specific information into the LSTM's input, Shalev et al. proposed a single LSTM model for daily runoff prediction for several hundred basins in [11], and their study illustrated that the developed LSTM model outperformed the hydrological model which is calibrated with respect to individual basin. The study in [12] also discovered that a properly trained LSTM model can outperform the linear regression, multi-layer perception models, as well as the Support Vector Machines (SVM) models. The accuracy of these predictions heavily depends on basins' characteristics and meteorological conditions, which can be implicitly modelled by specific LSTM structure and parameters. The LSTM modeling method have also been applied on fast flowing rivers. For example, Luppichini et al. trained a LSTM model for water-level prediction at the Arno river basin in Italy, where parts of the basin

have runoff times of just four hours [13]. Li et al. investigated two small and medium sized basins in China, and discovered that the LSTM model can exhibit a much more precise prediction capability compared with the applied convolutional neural networks and SVM [14]. A cascaded LSTM model is proposed in [15] to forecast daily stream-flow over 49 watersheds in the Yangtze River, where the first LSTM is used to predict the future precipitation, and then the second LSTM is designed to predict the stream-flow using the predicted precipitation from the first LSTM.

It should be noticed that one major challenge of these data-driven models and methods particularly in the hydrology applications is the lack of understanding/explanation about how exactly these models work internally, with respect to the situation that these models have no direct connection to the underlying physical processes [16]. This open issue is common for many data-driven approaches. By focusing on a specific high flooding risk area in Danish city of Vejle, [17] proposed a Feed-Forward NN (FNN) model to make flood forecast for a prediction period from 30 min to 4 h. It has been noticed that this type of simple FNN model already showed an outperform compared with a commercial model applied at the utility. However, it has also been observed that the achieved results could be further improved in terms of its accuracy and computation loads.

This work focuses on the same concerned area and data as used in [17], but the LSTM neural network is applied instead of a simple FNN model. Furthermore a set of PI-based control solutions for a distribution-gate system is also developed using a transfer function model spinet out from the obtained LSTM model. Compared with most existing studies and literature, we believe that the novelties of this work lie in:

- Different from most reported work which focus on the stream-flow forecasts, here we focus on the direct forecast of water-levels at some critical flooding areas;
- The temporally dynamic behavior of some special locations is focused, instead from a spatial but steady-state perspective;
- An automatic control solution is proposed as a real-time proactive approach to mitigate flooding risks.

The following of the paper is organized as: Sect. 2 gives the description of the concerned area and challenge; Sect. 3 presents the LSTM modelling and its results; Sect. 4 proposes a set of automatic control solutions for a manipulable distribution system as a proactive approach to mitigate the flooding risks; and finally, we conclude the paper in Sect. 5.

2 Considered Area and Challenge

Vejele is a Danish city with approximately 58.000 inhabitants, located at the southern half of the Jylland peninsula. It is the merging point of the Vejele Å river and Grejs Å river. both rivers flow into the Vejele Fjord. The 22 km long valley of the Grejs Å is the Danish largest river valley. The catchment of the Vejele Å is around 245 km², whereas the catchment of the Grejs Å is about 78 km². Near Abeloness Plads in city of Vejele, the Grejs Å is separated into the Omløbsåen river and Mølleåen river via a controlled distribution system (“fordelerbygværk”), which is abbreviated as FBV in the following. The Omløbsåen river runs through the Vejele’s centre and ends into Vejele Å, while the Mølleåen flows through the city roughly parallel and to the east of Omløbsåen. The FBV system consists of three pipes of 140 cm in diameter and equipped with individually controllable gates. The opening percentage of these gates can be remotely controlled from the central control station. The upstream area surrounding both Omløbsåen and Mølleåen is considered as a high flooding risk area. The Omløbsåen is also protected against high water-levels in Vejele Havn by a sluice and a set of pumps installed there to pump water from Omløbsåen into Vejele Å when needed. The water-levels in Vejele Å are uncontrollable. A map of the concerned rivers and area is illustrated in Fig. 1.

From the municipality point of view, there are three prioritized expectations regarding to the flood forecast and control of the river flows:

- First of all, the potential flood in the risk area at Aagade needs to be prevented as much as possible;
- Secondly the flooding risk of Mølleåen also need to be prevented as much as possible;

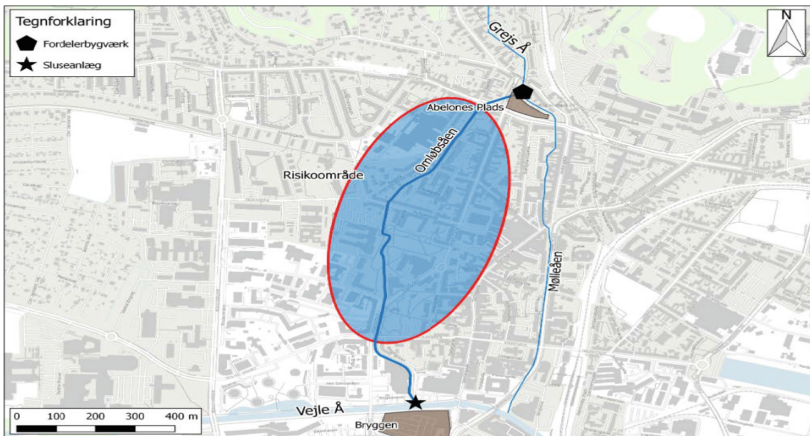


Fig. 1. Map of Vejle and its relevant rivers, where Risikoområde is the risk area

- Thirdly, the FVB gates are preferred to be open as long as possible, with respect to the concern that the Grejs Å is often seasonally visited by salmon for spawn.

For the purpose of controlling the FVB, sluice and pumps, a set of water-level measurements are installed at a number of stations as shown in Fig. 2. A set of rain measurements are also taken in some of these stations. Table 1 provides the concerned stations denoted by their reference numbers and their ground and bank levels, respectively.

The first step in the flood forecast and control is to develop a LSTM model to predict the dynamic behavior of the water-level at Aagade (ST. 32.21) and also Abelones Plads (ST. 32.20) in a more precise real-time manner than the conventional models can do. Because of the rapid response of the Grejs Å catchment and the availability of a 2-h precipitation rainfall, we will limit this level forecast to 4–12 h in this study.

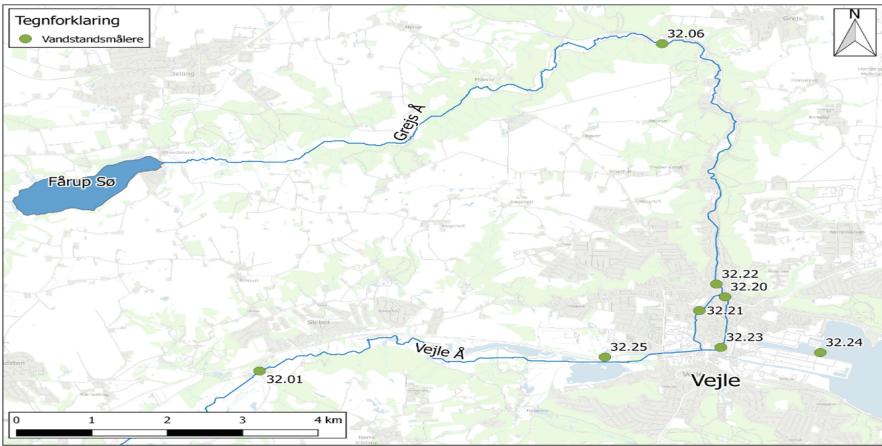


Fig. 2. Locations of water-level measurement stations

Table 1. Locations of measurement stations with their ground and bank levels (G-level & C-level)

Reference No.	Location	Unit	G-Level	C-Level
ST. 32.06	Grejsdalens Planteskole	[m]	27.35	29.4
ST. 32.20	Abelones Plads, Mølleåen	[m]	1.47	2.8
ST. 32.21	Aagade, Omløbsåen	[m]	0.28	1.4
ST. 32.22	Ny Grejsdalsvej, Grejs Å	[m]	1.67	3.6
ST. 32.23	Dæmningen, Mølleåen	[m]	-0.46	2

3 LSTM Modelling

3.1 LSTM Neural Network

The LSTM neural network is a type of RNN equipped with the capability to be able to catch potential long-term time dependencies in time series data, thereby the risk of exploding/vanishing of gradients can be significantly mitigated [18].

As shown in Fig. 3, one typical LSTM cell consists of two types of internal states, which are named as the hidden state denoted as h_t , and the cell state denoted as c_t . These states follow the computations illustrated in Eq. (1) to evolve from t th time instant into the next ($t+1$ th) time instant. σ represents the sigmoid function, \tanh presents the hyperbolic tangent function, and \odot denotes the Hadamard (element-wise) product. There are three different gates defined inside the LSTM cell, represented by i_t, f_t, o_t , with the names of input, forget, and output gates, respectively. The output of the LSTM cell is the hidden state h_t .

$$\begin{aligned}
 i_t &= \sigma(W_{ii}x_t + b_{ii} + W_{hi}h_{t-1} + b_{hi}) \\
 f_t &= \sigma(W_{if}x_t + b_{if} + W_{hf}h_{t-1} + b_{hf}) \\
 g_t &= \tanh(W_{ig}x_t + b_{ig} + W_{hg}h_{t-1} + b_{hg}) \\
 o_t &= \sigma(W_{io}x_t + b_{io} + W_{ho}h_{t-1} + b_{ho}) \\
 c_t &= f_t \odot c_{t-1} + i_t \odot g_t \\
 h_t &= o_t \odot \tanh c_t
 \end{aligned}
 \tag{1}$$

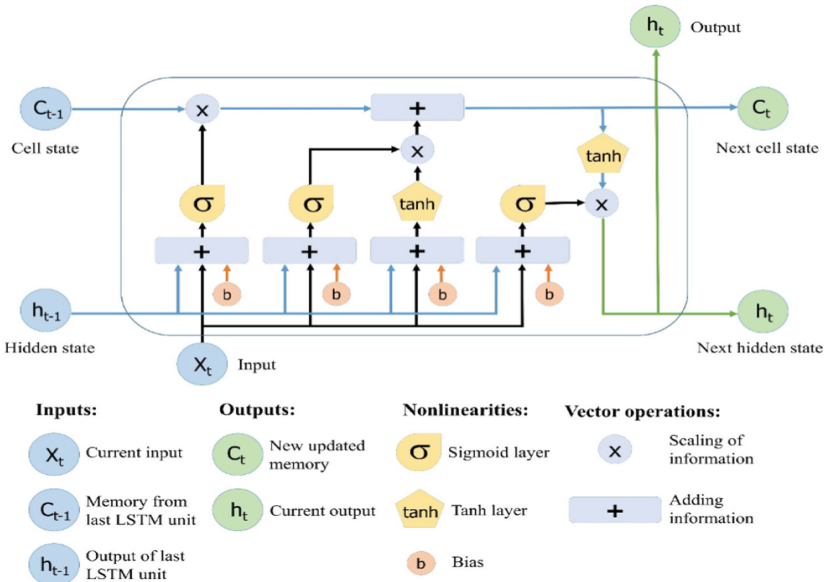


Fig. 3. A typical LSTM cell structure [8]

In the case of a multi-layer LSTM model, the input of a hidden layer is the hidden state of the previous layer as shown in Eq. (2). The Hadamard products indicate that the gates i_t, f_t, o_t , as well as the states c_t, h_t should have the same dimension. For example, the input dimension n denotes the dimension of the input $x_t \in R^n$ to the first layer, while the hidden dimension m denotes the dimension of the states $c_t, h_t \in R^m$ and the dimension of the input to all further LSTM layers.

$$h_t^{(l)} = \begin{cases} h_t^{(l-1)} & \text{if no dropout} \\ \delta_t^{(l-1)} \odot h_t^{(l-1)} & \text{if dropout applied} \end{cases} \quad (2)$$

Dropout is a very effective technique to protect neural networks from overfitting by randomly *dropping out* neurons. It has been shown that implementing dropout has the same effect as “bagging”, a machine learning technique where multiple versions of a model are trained and the over-all output is computed by averaging the individual outputs [19]. In Eq. (2), $\delta_t^{(l-1)}$, as a dropout coefficient, is a vector of random variables generated by following the Bernoulli distribution. It should be noted that dropout is only applied in the feed-forward direction and not the recurrent direction. Furthermore, dropout is only used during training. For evaluation, the dropout layers are disabled and the preceding weight matrices are scaled up (as the number of active neurons on average has increased). This process can be handled automatically by Pytorch after assigning a proper dropout rate [19].

3.2 LSTM Model Setup

In principle, the developed LSTM model represents a recursive function which calculates the model’s output corresponding to the physical meaning of the water-level at station ST. 32.21 or/and station ST. 32.20, using all relevant inputs including the controllable inputs (i.e., the FBV gate opening percentages) and uncontrollable inputs (i.e., the correlated up-stream and downstream measurements), and sometimes also possibly some previous output(s), depending on the dedicated model structure.

Without losing of generality, we denote y_t the water-level at station ST. 32.21, u_t/d_t all controllable/uncontrollable input/measurement, and h_t the LSTM hidden state at the t th instant. Three types of LSTM models are concerned in the following:

$$\hat{y}_{t+1}, h_{t+1}, c_{t+1} = f_{vir}(d_t, u_t, h_t, c_t). \quad (3)$$

$$\hat{y}_{t+1}, h_{t+1}, c_{t+1} = f_{obs}(y_t, d_t, u_t, h_t, c_t). \quad (4)$$

where $\hat{y}_{t+1}, h_{t+1}, c_{t+1}$ represents the model’s predicted output, hidden state and cell state(s) at $t + 1$ th instant respectively. We name model (3) as a Virtual-sensor type of LSTM (*Vir-LSTM*) which does not explicitly depend on any

previous output y_t for predicting the next output \hat{y}_{t+1} . The time-dependency is inherently embedded in the RNN principle. While the second model (4) named as Observer type of LSTM (*Obs-LSTM*), which explicitly request the previous output measurement as part of the model’s input besides the RNN feature. This kind of model acts like a observer or Kalman filter used in modern control theory [21]. A third model, we name it as Auto-Regression model (*AR-LSTM*), can be adapted from the Obs-LSTM as:

$$\hat{y}_{t+1}, h_{t+1}, c_{t+1} = f_{ar}(\hat{y}_t, d_t, u_t, h_t, c_t). \tag{5}$$

The only difference between Obs-LSTM and AR-LSTM lies in whether the measurement y_t or predicted \hat{y}_t is required for iterative computation. It should be noticed that, during the training and validation phase, the output prediction \hat{y}_{t+1} can be computed by the LSTM as a function of the actual output y_t due to the fact that these data are already available. However, when this model (4) is used for application purpose, e.g., to make multi-step prediction or closed-loop simulation, the predicted output from previous iteration may be needed for making next step’s prediction like (5), e.g., use of \hat{y}_{t+1} in Eq. (4) instead of y_{t+1} to generate prediction of \hat{y}_{t+2} and so on, as a kind of non-Teacher Forcing training [20]. Otherwise, the Obs-LSTM (4) needs to run parallel with the actual measurement to be able to recursively compute the next instant’s prediction, similar like the Teacher Forcing training [20]. In the following, the Vir-LSTM model is adopted and illustrated. We refer to one of our recent study [23] about other LSTM model applications.

Different data sets and hyper-parameters listed in Table 2 and Table 3 are investigated to obtain different Vir-LSTM models. The field *Trajectory Min. Value* specifies the smallest measurement value of the normalised data which will be collected for training with respect to the concern that we are more interested in peak flow scenarios than low flow scenarios.

Table 2. Data and hyper-parameters for Set-One

Inputs (water-level & control gate measurements)	SLUSE_FOER ST.32.22 FBV1 FBV2 FBV3
Output (water-level)	ST.32.21
model Architecture	LSTM Layer (5 to 20) Dropout (p=0.5) Linear Layer (20 to 1)
data duration	6 h
Trajectory Min. Value	0.5

Table 3. Data and hyper-parameters for Set-Two

Inputs (water-level & control gate measurements)	ST.32.22 SLUSE.FOER ST.32.23 FBV1 FBV2 FBV3
Outputs (water-level)	ST.32.21 ST.32.20
model Architecture	LSTM Layer (6 to 20) Dropout ($p = 0.5$) Linear Layer (20 to 1)
data duration	12 h
Trajectory Min. Value	0.5 (ST.32.21) 0.5 (ST.32.20)

3.3 Data Preparation

All water-level measurements are normalised with respect to ground and bank levels, and all actuators measurements are normalised with respect to the actuator limits (0–100%). The measurements from 2017-03-29 10:40:00 to 2021-10-11 15:35:00 are considered in this study. The sampling time is 1 min, and this counts to 2,386,376 data of each measurement.

3.4 LSTM Training and Validation

The training procedure is committed using Pytorch. The class *LSTM_Predictor* is used to construct the LSTM model subject to given structure and hyper-parameters. One hidden LSTM layer with both cell and hidden state dimension of 20 are developed, and a linear (output) layer is added to reduce the state dimension from 20 to the dimension of the output. The mean square error (MSE) by comparing the output tensor to the target tensor is used to evaluate the learning performance, and the optimiser Adam is employed for optimization. The dropout layer with dropout probability of 50% has been used to prevent possible over-fitting.

3.5 Prediction Capability

Figure 4 shows a comparison of the prediction of an obtained Vir-LSTM with validation data. The prediction performance is fairly accurate for peak-flow situations but it overestimates tidal behaviour for the low flow situations. This is not regarded as a problem, as the model is only intended to precisely model the peak-flow behaviour due to the flooding concern. The mean absolute error (MAE) over the whole month is given as 0.0215 and the mean square error (MSE) is given as 0.0007.

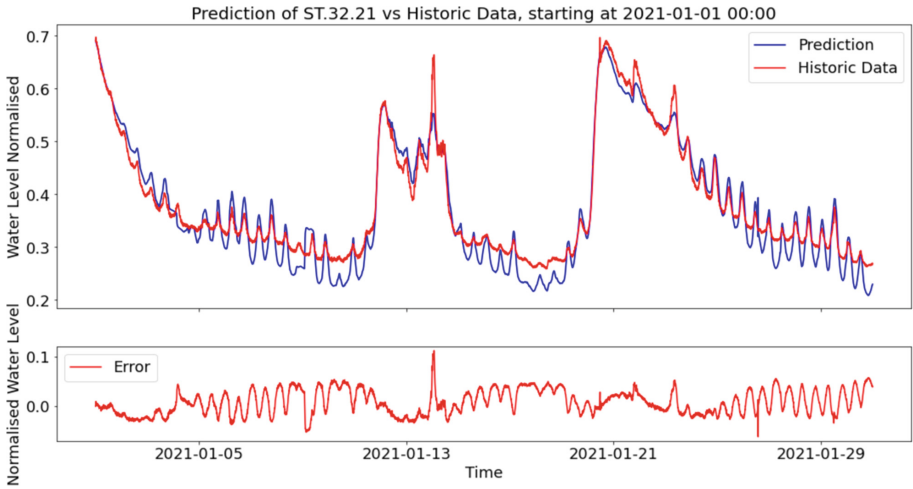


Fig. 4. Comparison of model prediction and historic data for January 2021

4 Flow Control

Because the concerned river network has a controllable distribution-gate system (FBV), which apparently is manually controlled remotely from the central station. Some automatic control solutions are designed and tested using conventional and advanced feedback control theories [21, 22]. In order to do so, some proper control-oriented model need to be further obtained from the developed LSTM model.

4.1 Transfer Function Model

A transfer function model is derived from the obtained LSTM model through an experimental approach. Firstly, the extraction of an interesting equilibrium point from a Vir-LSTM is committed by fixing the disturbance d_t and control input u_t to the LSTM model as some constants, then observe the final settle down performance of the model. Afterwards, a process model denoted as a first-order Transfer Function (TF-model) is estimated based on a unit-step response of LSTM model around the found equilibrium as:

$$P_u(s) = \frac{K_u}{\tau_u s + 1}, \quad P_d(s) = \frac{K_d}{\tau_d s + 1}, \quad (6)$$

where $P_u(s)$ and $P_d(s)$ represents the TF-model from the control and disturbance input u_t , d_t to the system output y_t respectively. One set of the TF-model parameters are obtained as $K_u = 0.49$, $K_d = 1.48$, $\tau_u \approx \tau_d \approx 600$ (Fig. 5).

The loop-shaping method [21] is picked up to design the cascaded controller $C(s)$, as a type of simple robust PI controller, for a given closed-loop's bandwidth ω_c and expected phase margin ϕ_m .

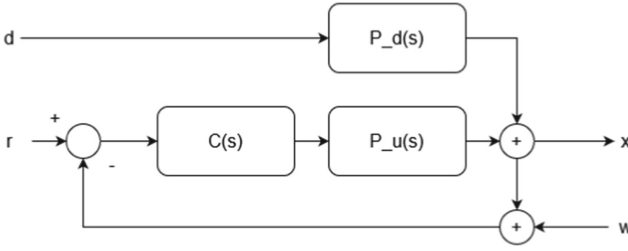


Fig. 5. TF-model based Feedback control

Subject to a predefined PI control structure, the Sensitivity Function $S(i\omega)$, and the Complementary Sensitivity Function $T(i\omega)$, are obtained as:

$$S(s) = \frac{\tau_u s^2 + s}{\tau_u s^2 + (1 + K_u k_p) s + k_i}, T(s) = \frac{K_u k_p s + k_i}{\tau_u s^2 + (1 + K_u k_p) s + k_i} \quad (7)$$

Assign both functions at ω_c have the expected property: $|S(i\omega_c)| = |T(i\omega_c)| = 1/2$, Then the PI control parameters can be calculated as

$$k_p = \frac{1}{K_u} \sqrt{\frac{1 + \tau_u^2 \omega_c^2}{1 + \tan^2(\phi_m + \arctan(\tau_u \omega_c))}}, k_i = \frac{\omega_c}{K_u} \frac{\sqrt{1 + \tau_u^2 \omega_c^2} \tan(\phi_m + \arctan(\tau_u \omega_c))}{\sqrt{1 + \tau_u^2 (\phi_m + \arctan(\tau_u \omega_c))}}. \quad (8)$$

4.2 Adaptive PI&FF Control

An adaptive control solution is further developed to handle potential large uncertainties, modelling errors and diverse operating conditions, using the Model-Reference Adaptive Control (MRAC) method [22] together with feed-forward structure [21], as shown in Fig. 6.

Assume the reference model is described as a state space formulation (9), where x_m/y_m is the reference model state/output:

$$\dot{x}_m = a_m x_m + b_{um} u, \quad y_m = x_m. \quad (9)$$

An adaptive combined feedback (PI) and feed-forward (FF) control is designed as:

$$\begin{aligned} u &= \theta_1(r - y) + \theta_2 x_2 + \theta_3 d \\ \dot{x}_2 &= r - y \\ \epsilon_1 &= y_m - y \\ \dot{\theta}_1 &= -\gamma b_{um} \epsilon_1 y \\ \dot{\theta}_2 &= \gamma b_{um} \epsilon_1 x_2 \\ \dot{\theta}_3 &= -\gamma b_{um} \epsilon_1 d \end{aligned} \quad (10)$$

where γ is the adaption size which needs to be properly tuned. θ_i , $i = 1, 2, 3$ are adaption coefficients for the P-, I- and feed-forward parts. The stability of this adaptive control solution is guaranteed by the Lyapunov stability analysis.

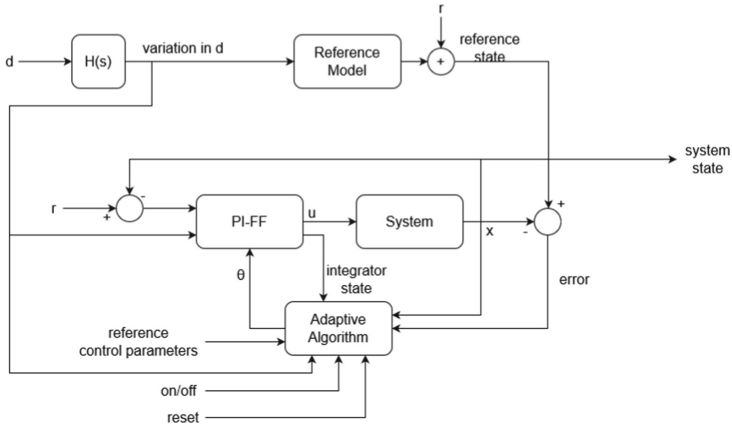


Fig. 6. Diagram of the Adaptive PI&FF controller with switch on/off mechanism

4.3 LSTM-Based Simulation

Figure 7 illustrates the LSTM-based control simulation diagram. The LSTM can be a Vir-LSTM (3) or an AR-LSTM model (5) and the controller is a digitized controller corresponding to either (8) or (10).

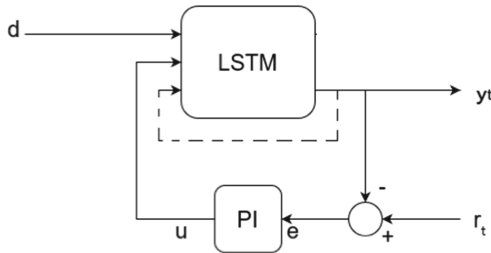


Fig. 7. LSTM-based feedback control diagram

4.4 Control Performance

For a given $\omega_c = 0.01$ rad/s and phase margin $\phi_m = 60^\circ$, a designed PI control solution according to (8) for a specific historic period is illustrated in Fig. 8. It can be noticed that the automatic control solution leads to a higher water-level without tricking the bank alarm, while the historic data (manual controlled by operator) shows a too conservative performance - far below the bank alarm level, if the third objective w.r.t. salmon prawn needs to be concerned as well.

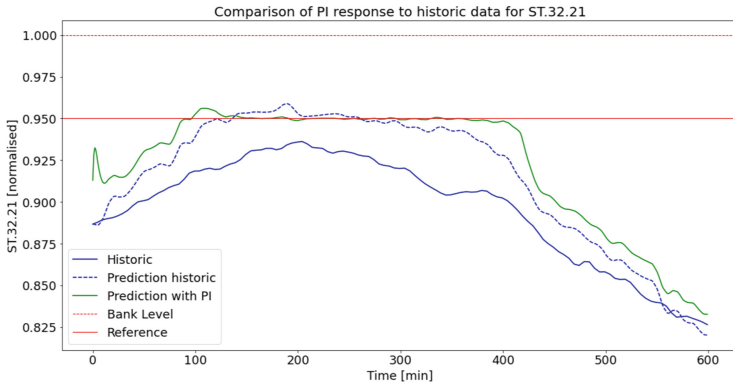


Fig. 8. Performance Comparison of automatic control vs. manual control (historic data)

Figure 9 shows a performance comparison of the reference model, PI controlled system and API controlled system, subject to some varying disturbance. It can be noticed that API control solution leads to a less oscillating performance than the PI control solution did, due to its adaptive flexibility.

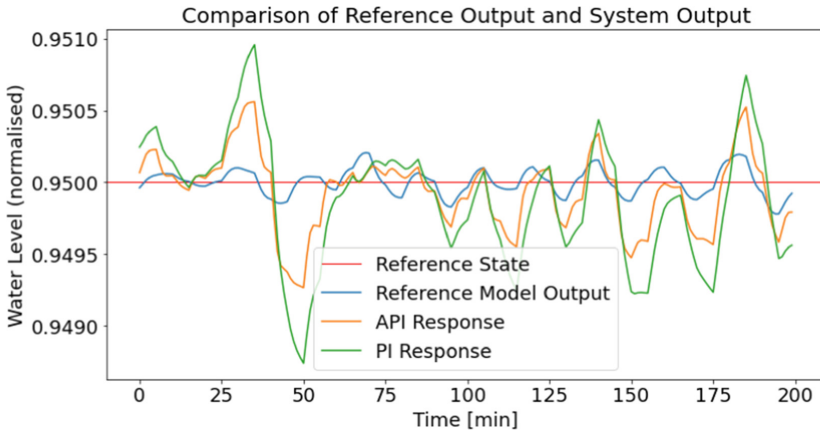


Fig. 9. Performance Comparison of different control solutions

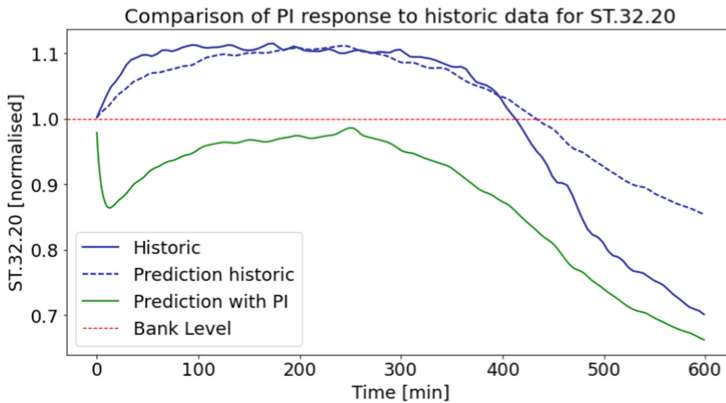
4.5 Flood Mitigation

The designed model and control solutions are tested for four historic flooding/near-flooding events at Abelones Plads (ST. 32.20) as listed in Table 4.

Table 4. Selected Flooding and Near-Flooding Events

Event no.	Starting Time	Status & location
1	2019-10-11 20:00	Flood at Abelones Plads (ST. 32.20)
2	2020-02-16 21:00	Flood at Abelones Plads (ST. 32.20)
3	2020-02-22 12:00	Near Flood at Abelones Plads (ST. 32.20)
4	2019-02-09 04:00	Near Flood at Abelones Plads (ST. 32.20)

The comparisons of water-levels at ST.32.20 for event-1 and event-2 are illustrated in Fig. 10 and Fig. 11, respectively. The historic data taken from Vejle Spildevand A/S is presented by the blue line. The LSTM's prediction (without control loop) using historic FBV's opening percentages and relevant historic upstream and downstream water-level measurements is illustrated by the dashed blue line. The discrepancy between the solid and dashed blue lines indicates how accurate the LSTM model's prediction from the actual measurement. The green line denotes the simulated performance of the closed-loop controlled LSTM system (as shown in Fig. 7) subject to the designed PI control solution 8, while the dashed red line represents the bank level. The water-levels are normalised with respect to ground and bank levels. Thereby a normalized water-level "0" means that there is no flow-stream, and a normalized water-level "1" indicates the situation that the water-level has reached the bank level - a near-flooding situation. When the normalized water-level exceeds "1", this clearly indicates a flooding situation. All simulations are carried out for 10 h durations.

**Fig. 10.** Historic and controlled behaviours of water-levels for Event-1.

It is very obvious, according to Fig. 10, that the flooding event-1 at Abelones Plads (ST.32.20) could have been avoided completely by splitting more flow-stream into the Omløbsåen river via the automatic control of the FBV system.

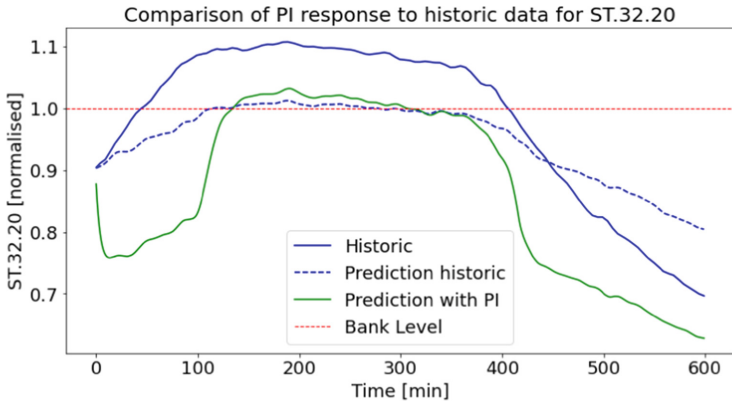


Fig. 11. Historic and controlled behaviours of water-levels for Event-2.

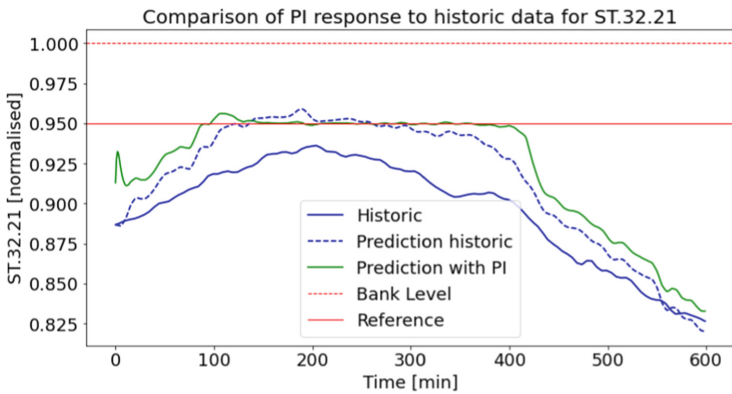


Fig. 12. Historic and controlled behaviours of the water-levels at ST.32.21 for Event-2.

As another flooding event shown in Fig. 11, the LSTM model’s prediction (without control loop) and the simulated controlled system exhibited quite similar behaviors, i.e., both water-levels are kept around the bank level (indicated by the red dashed line). This means that this flooding event-2 can not be completely avoided even with the feedback control in action. If we look at the water-level at Aagade area (ST.32.21) as shown in Fig. 12 during this period, which measurement is used as feedback signal for the developed control system, it can be observed that the controlled water-level at ST.32.21 is already around its set-point $r = 0.95$ denoted by the solid red line. This means that the upstream flow-stream under event-2 already made both rivers reach their saturation levels. Under this kind of circumstance, the automatic control could still mitigate the flooding impacts by better balancing the flow-stream split into both rivers.

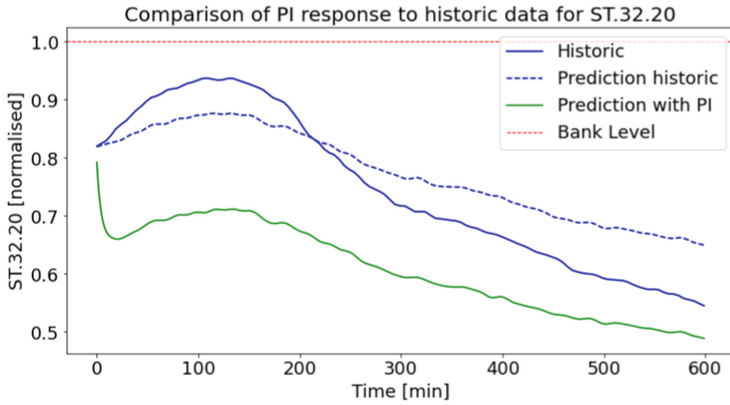


Fig. 13. Historic and controlled behaviours of water-levels at Abelones Plads for Event-3.

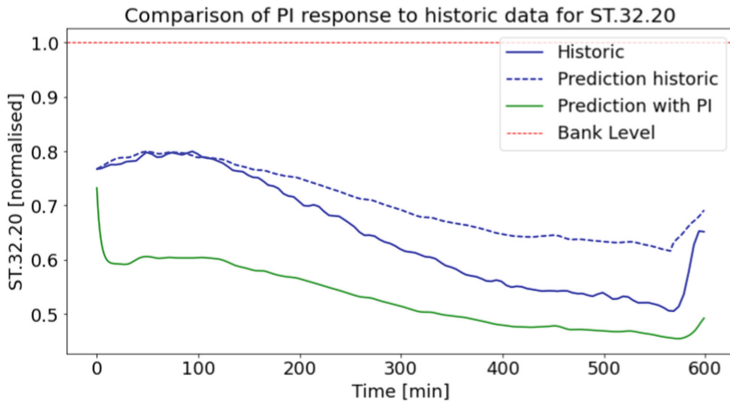


Fig. 14. Historic and controlled behaviours of water-levels at Abelones Plads for Event-4.

Both Events-3 and Event-4 indicated that the historic water-levels at Abelones Plads came close to its bank level, as shown in Fig. 13 and Fig. 14, respectively. The simulations of the controlled system showed better performances in terms of pushing down the water-level further. It can be observed that when the controller was into action, the water-level of the controlled system drops significantly since the beginning. The reason behind this situation is that the controlled distribution system FBV divided more stream-flow into Omløbsåen river. For both Event-3 and Event-4 scenarios, the historic data showed that the upstream stream-flow was not sufficient yet to drive the water-level at Omløbsåen (ST.32.21) to reach its reference water-level of 0.95. The designed control system needs to dispatch more stream-flow into Omløbsåen river, thereby the risk of near-flooding at Abelones Plads (ST.32.20) can be completely avoided.

5 Discussion and Conclusion

The LSTM model is developed and trained to predict the dynamic behaviours of water-levels at some critical areas of urban rivers in Vejle city. Different LSTM models are investigated using some water-level measurements at the up- and downstream stations, as well as the measurement from a stream-flow distribution system (FBV). The Vir-LSTM model, which only uses the input measurement (without requiring previous output measurement or prediction), is applied in this study. BY choosing data from 2021 year as a validation set for the developed model, the overall MAE of the LSTM prediction is 2.51 cm. Considering the situation that the physical distance between ground and bank at Aagade area is 112 cm, this MAE is equivalent to only 2.24% prediction error. From this perspective, the obtained LSTM model is super accurate compared with some previous work. Furthermore, compared with the commercial simulation model the utility is currently using, the proposed LSTM model is much more computationally efficient and also presents the opportunity for real-time monitoring.

It is clearly demonstrated that the flood prevention at both Aagade (ST.32.21) and Abelones Plads (ST. 32.20), with the third objective to keep maximal opening of FBV system, can be reliably and efficiently balanced by applying an automatic control to the FBV system in a dynamical manner. The varying behaviors can also be automatically mitigated via this real-time control, thereby significantly reducing the flooding potentials inside the city area. One of our future work is to investigate how to coordinate the rain gauge measurement into this LSTM-based framework.


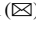

References

1. Copernicus: European State of the Climate 2021 - Flooding in Europe (2021). <https://climate.copernicus.eu/esotc/2021/flooding-july>
2. Intergovernmental Panel on Climate Change: Technical Summary. Accessed 1 Oct 2021. https://www.ipcc.ch/report/ar6/wg2/downloads/report/IPCC_AR6_WGII_FinalDraft_TechnicalSummary.pdf
3. European Commission: The EU Floods Directive. https://ec.europa.eu/environment/water/flood_risk/implem.htm
4. World Meteorological Organization: WMO Atlas of Mortality and Economic Losses from Weather, Climate and Water Extremes (1970–2019) (2021)
5. European Flood Awareness System - EFAS. <https://www.efas.eu/en/european-flood-awareness-system-efas>
6. Mathiesen, K., Posaner, J., Gehrke, L.: Europe's floods: how a modern warning system was overwhelmed. In: POLITICO (2021)
7. Mosavi, A., Ozturk, P., Chau, K.: Flood prediction using machine learning models: literature review. *Water* **10**(11), 1536 (2018)
8. Hochreiter, S., Schmidhuber, J.: Long short-term memory. *Neural Comput.* **9**(8), 1735–80 (1997)
9. Liu, Y., Wang, H., Feng, W., Huang, H.: Short term real-time rolling forecast of urban river water-levels based on lstm: a case study in Fuzhou City, China. *Int. J. Environ. Res. Public Health* **18**(17), 9287 (2021)

10. Lee, J., Yuk, G., Moon, H., Moon, Y.: Integrated flood forecasting and warning system against flash rainfall in the small-scaled urban stream. *Atmosphere* **11**(9), 971 (2020)
11. Shalev, G., El-Yaniv, R., Klotz, D., Kratzert, F., Metzger, A., Nevo, S.: Accurate hydrologic modeling using less information. In: *Second Workshop on Machine Learning and the Physical Sciences, NeurIPS* (2019)
12. Rahimzad, M., Nia, A., Zolfonoon, H., Soltani, J., Mehr, A., Kwon, H.: Performance comparison of an LSTM-based deep learning model versus conventional machine learning algorithms for streamflow forecasting. *Water Res. Manag.* **35**, 4167–4187 (2021)
13. Luppichini, M., Barsanti, M., Giannecchini, R., Bini, M.: Deep learning models to predict flood events in fast-flowing watersheds. *Sci. Total Environ.* **813**, 151885 (2022)
14. Li, K.: The applicability of ASCS.LSTM.ATT model for water-level prediction in small- and medium-sized basins in China. *J. Hydroinf.* **22**(6), 1693–1717 (2020)
15. Li, J., Yuan, X.: Daily streamflow forecasts based on cascade long short-term memory (LSTM) model over the Yangtze river basin. *Water* **15**, 1019 (2023)
16. Kratzert, F., Herrnegger, M., Klotz, D., Hochreiter, S., Klambauer, G.: NeuralHydrology – interpreting LSTMs in hydrology. In: Samek, W., Montavon, G., Vedaldi, A., Hansen, L.K., Müller, K.-R. (eds.) *Explainable AI: Interpreting, Explaining and Visualizing Deep Learning. LNCS (LNAI)*, vol. 11700, pp. 347–362. Springer, Cham (2019). https://doi.org/10.1007/978-3-030-28954-6_19
17. Refsgaard, B., Jensen, T.: Oversvømmelsesvarsling i Vejle - Prognostisering af vandstande med neurale netværk. Master Thesis, Aalborg Univeristy (2020). (in Danish)
18. Bengio, Y., Simard, P., Frasconi, P.: Learning long-term dependencies with gradient descent is difficult. *IEEE Trans. Neural Netw.* **5**(2), 157–166 (1994)
19. Labach, A., Salehinejad, H., Valaee, S.: Survey of dropout methods for deep neural networks (2019). <https://doi.org/10.48550/arXiv.1904.13310>
20. Sangiorgio, M., Dercole, F.: Robustness of LSTM neural networks for multi-step forecasting of chaotic time series. *Chaos Solitons Fract.* **139**, 110045 (2020)
21. Skogestad, S., Postlethwaite, I.: *Multivariable Feedback Control: Analysis and Design*. Wiley, Hoboken (2005)
22. Tao, G.: Multivariable adaptive control: a survey. *Automatica* **50**(11), 2737–2764 (2014)
23. Pajuro, K., Hansen, L., Odena, M., Jespersen, S., Yang, Z.: Modelling the oil-in-water separation dynamics in a de-oiling hydrocyclone system using LSTM neural network. In: *Proceedings of IEEE IECON2023* (2023)



Spatial Variation of Agricultural Drought Vulnerability in Eastern Agricultural Zone of Qinghai Province, China

Youwen Zhang^{1,2} , Xueqin Cao¹  , and Rentian Shu^{1,2}

¹ College of Geographical Sciences, Qinghai Normal University, Xining 810016, Qinghai, China

3164183141@qq.com

² Key Laboratory of Natural Geography and Environmental Processes of Qinghai Province, Xining 810008, Qinghai, China

Abstract. Based on the statistical indicators of 14 counties in the agricultural area of eastern Qinghai, the evaluation of exposure, sensitivity and adaptability were studied by using principal component analysis and weighted synthesis method. Then, the vulnerability of the risk-bearing body was analyzed by using GIS The barrier degree model was established to analyze the barrier degree of each indicator. The spatial distribution map of drought vulnerability in the eastern part of Qinghai and the barrier index of each indicator were obtained. The results show a trend of increasing from the central part to the north and south; drought vulnerability in the agricultural production environment shows the highest in the Naoshan area, followed by the Qianshan area, and the lowest in the Chuanshui area. According to the barrier degree index, precipitation, per capita net income of farmers and gross regional product are derived as the main causes of disaster management.

Keywords: Agricultural Zone in Eastern Qinghai Province · Agricultural Drought Vulnerability · Barrier Degree · GIS · Principal Component Analysis

1 Introduction

1.1 Research Background

Droughts are spatially widespread and long-lasting, posing a great threat to people's normal life. Droughts are caused by the interaction of external droughts faced by a region with its own internal factors [1].

Qinghai Province is located in the northeastern part of the Qinghai-Tibet Plateau and has a plateau continental climate. The eastern agricultural region of Qinghai province is the breadbasket of Qinghai [2]. In most places of the eastern agricultural region, it is spring and autumn with one harvest a year. In this region, the average annual temperature and precipitation is low, and summer is predominant. October to April is the season for farm harvesting, but with only 15% of the annual rainfall, drought is the main factor limiting spring wheat production [3–5].

1.2 Review of Chinese and International Research

The concept of vulnerability was first introduced by Burton [6] in 1960 and has played a large role in disaster research. Burton considers vulnerability as an exposure risk [6]. Cutter et al. [7] emphasize vulnerability as a social problem. Liverman [8] shows how vulnerability to natural hazards can be measured and analyzed and how drought vulnerability is linked to new agricultural technologies and land tenure in Mexico. Liverman shows how vulnerability to natural hazards can be measured and analyzed and how drought vulnerability is linked to new agricultural technologies and land tenure in Mexico. And he argues that the impact of drought on agricultural systems depends on both the technological, economic, and political characteristics of a region and the severity of meteorological events [8]. Some scholars argue that vulnerability can be measured in both temporal and spatial dimensions [9], and SÖNMEZ investigated the spatial and temporal dimensions of meteorological drought in Turkey from the concept of vulnerability [10]. Sahana et al. consider drought hazards in a multivariate framework and use reliable drought vulnerability indicators that consider exposure, sensitivity and adaptive capacity for a comprehensive, fine-grained, nationwide drought risk assessment, a three-level evaluation system widely used in drought vulnerability studies [11]. Vulnerability has been studied in a variety of ways, and in recent years there has been more research on vulnerability in conjunction with GIS. Aksoy et al. proposed a method using a standardised precipitation index to obtain empirical relationships between intensity and return periods using site-specific IDF curves [12]. Z Taheri uses percent normal precipitation index and GIS for hazard assessment of drought in Iran [13].

Domestic research on vulnerability started relatively late, but there are still many scholars who apply vulnerability to their research fields. Yanrui Shang conducted a statistical analysis of the effects of different factors on vulnerability based on rural survey subhousehold statistics separately [14]. Zhongyuan Li et al. analyzed the vulnerability of agricultural drought in Henan Province based on statistical and meteorological data of the province using several indicators and applying gray correlation analysis [15]. Yali Ma et al. conducted a vulnerability study by combining comprehensive weighting with GIS [16]. Yongqiang Dai et al. used the projection tracing model indicators to influence the weight coefficients, objectively reducing the influence of artificial weighting on the evaluation results, and analyzed and evaluated the main agricultural drought vulnerability indicators in 14 regions of Province to Gansu verify the feasibility of the method [17]. Jing Cheng et al. used principal component analysis to study the drought risk in the middle and lower reaches of the Yangtze River, and spatial variation was studied by using cluster analysis. Disaster vulnerability risk studies have also been explored for the agricultural areas in eastern Qinghai Province affected by global changes [18]. Liu Xuan et al. studied the ecological drought vulnerability in northwest China, they found that the local vulnerability in southern Qinghai was on the rise [19].

In summary, the novelty of this study lies in the following four aspects: (1) Using multidisciplinary theoretical approaches This study uses multidisciplinary theoretical approaches such as earth science, disaster science and statistics to study disaster vulnerability in the agricultural areas of eastern Qinghai Province through the theoretical basis of disaster vulnerability. (2) Constructing models and multi-methods Based on the

standardization of data, evaluation indicators are constructed from three aspects of exposure, sensitivity and adaptive capacity of the disaster-bearing system, and vulnerability is constructed to unfold the evaluation of agricultural drought vulnerability in the study area. (3) The study and analysis of spatial and temporal evolution not only assesses the natural and social vulnerability of the study area, but also further explores the temporal evolution of disaster vulnerability over the past 20 years and analyzes the spatial variability based on the county perspective. (4) The study will contribute to the construction of Qinghai and provide a practical basis for integrated disaster prevention and mitigation in the agricultural areas of eastern Qinghai and promote sustainable regional development.

1.3 Research Ideas

As shown in Fig. 1, the research ideas of the spatial differentiation of agricultural drought vulnerability and regulation measures in the eastern agricultural region of Qinghai Province are as follows: firstly, we review the information and read the literature to understand the concept of vulnerability, the current status of research and the general situation of the study area, and summarise the research significance of this study, with certain theoretical support; at the same time, we collect various relevant data and information through field surveys, internet data search and consultation with relevant departments, with certain data The study is supported by data. Afterwards, the research indicators were selected according to the specific conditions of the study area, and the research model was constructed. The weight of each indicator was determined by the principal component analysis method, which constituted the vulnerability evaluation system of the eastern agricultural area of Qinghai Province, and the indicators were divided into

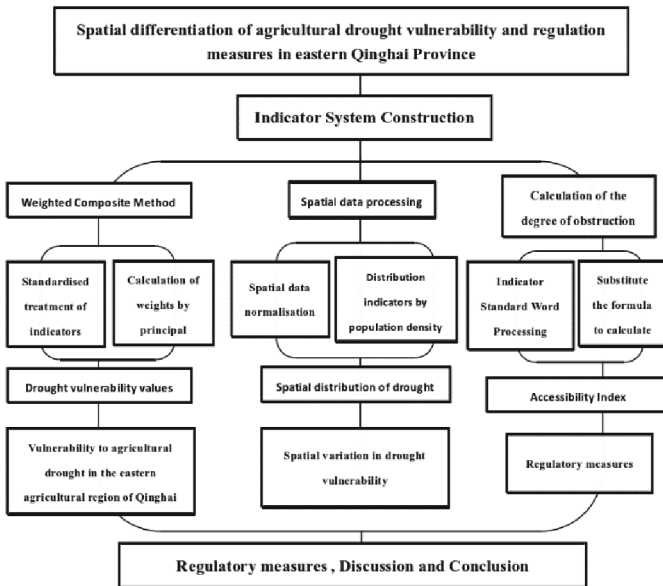


Fig. 1. Technology roadmap.

three subsystems: exposure, sensitivity and resilience. Finally, the results of vulnerability are calculated by standardising and weighting the indicators, summarising the main influencing factors of vulnerability and finally discussing and analysing the conclusions to achieve the aim of this study.

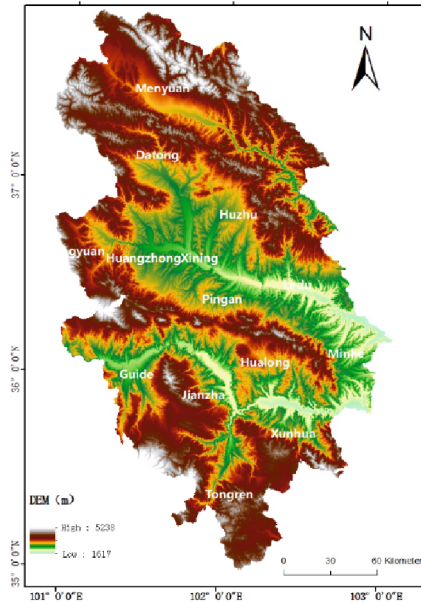


Fig. 2. Overview map of the study area.

2 Overview of the Study Area

As shown in Fig. 2, the eastern agricultural region of Qinghai Province is located south of Daban Mountain, a branch of Qilian Mountain, north of Longyang Gorge, east of Riyue Mountain and west of Sigou Gorge [24], at latitude and longitude $98^{\circ}54' \sim 103^{\circ}04'E$, $34^{\circ}48' \sim 38^{\circ}20'N$. The eastern agricultural region includes 14 counties, while the arable land area occupies 70% of the province, which is a region with a higher percentage of grain production and rapid development of agriculture in Qinghai Province compared with other regions.

The eastern agricultural region is relatively undulating, with the Yellow River and its tributaries Huangshui and Datong River running through it. Precipitation and temperature vary markedly with the altitude and topography of the region, thus creating different types of agricultural production environments. The first type is the Chuanshui area, this type of arable land is mainly located in the river valley terraces and alluvial fans, the soil layer is relatively thick, the soil type is mainly through the irrigation of the chestnut calcium soil. The second type is shallow Qianshan area, mainly located in areas with heights between 2000 and 2600 m, with loose soil texture and very serious soil erosion due to

the influence of the topographic slope. The third type is Naoshan area, located in areas with altitudes of 2600 to 3400 m, with high soil fertility but poor thermal conditions, so that mainly cold-tolerant crops are grown.

3 Research Methodology and Data Sources

3.1 Evaluation Indicator System Construction

Taking the drought vulnerability of the eastern agricultural region of Qinghai Province as the research background, the index system is constructed in three aspects: exposure, sensitivity and recovery ability based on previous researches [14, 15, 17, 19–25]. Exposure refers to the situation of people, livelihoods, environmental services and resources, infrastructure, and economic, social or cultural assets. Vulnerability is the tendency or propensity to be adversely affected. Resilience is the ability of a system and its components to quickly anticipate, withstand, adapt or recover from the impact of a potentially hazardous event. The indicators of the exposure subsystem include three kinds of grain production, crop sown area and total agricultural output value; the indicators of the sensitivity subsystem include precipitation, agricultural production environment (Chuanshui area, Qianshan area and Naoshan area), TVDI and effective irrigation area; the indicators of the adaptability subsystem are more numerous, including per capita net income of farmers, number of village committees, gross local product, total agricultural machinery power, population density and annual fertilizer application, as shown in Table 1 below:

Table 1. Drought vulnerability indicators and weights.

System layer	Indicator layer	Weighting index
Exposure (0.198)	Grain production	0.06
	Crop sown area	0.06
	Total agricultural output	0.078
Sensitivity (0.323)	Precipitation	0.078
	Agricultural production environment	0.081
	TVDI	0.082
	Effective irrigated area	0.082
Adaptability (0.479)	Per capita net income of farmers	0.081
	Number of village committees	0.081
	Gross Local Product	0.075
	Total power of agricultural machinery	0.077
	Population density	0.08
	Annual fertilizer application	0.085

3.2 Data Sources and Processing

Grain production, average land water resources, arable land area, population, agricultural GDP, per capita net income of farmers, agricultural population, total output value of primary industry, etc. are from *Qinghai Yearbook*, *Haidong Regional Statistical Yearbook*, *Xining Statistical Yearbook*, *Menyuan Statistical Yearbook*, *Huangnan Statistical Yearbook*, and related data public. Spatial data on agricultural areas in eastern Qinghai Province, TVDI, population density, etc. are from, and soil moisture is from China Meteorological Data Network, National Earth System Science Data Centre and National Qinghai-Tibet Plateau Science Data Centre.

Product Data Processing. TVDI, population density, DEM elevation data and land use data used in this paper are all existing data products that require a range of processing using the Arcgis.

The TVDI was applied to the global 1 km resolution TVDI dataset, and as this paper is based on a study of agricultural drought vulnerability, TVDI data was downloaded for June, July and August of the growing season. The data for the study area were first extracted by mask, then resampled to obtain 300 m precision TVDI data, and finally the average TVDI for June, July and August was calculated using raster operations.

The population density data was adopted from China, and the data needed to go through a series of processing after downloading. The population density data for the study area was first extracted from the national data and then resampled to obtain the population density data at 300 m precision.

The extraction of agricultural production environment data required the use of DEM elevation data and land use data from Qinghai Province. The agricultural production environment in the eastern part of Qinghai is divided into Naoshan area, Qianshan area and Chuanshui area according to the altitude. The DEM elevation map was reclassified according to the altitude range of the different arable land types, assigning a value of 1 to those between 2800 and 3200 m, 2 to those between 2200 and 2800 m, 3 to those between 1565 and 2200 m, and NoData to the rest. The raster data was then extracted by mask and the reclassified cropland layer was used to extract the processed DEM elevation map to obtain the raster data by cropland type.

Statistical Data Processing. The data in this paper all need to be converted into raster data for the study, so the county statistics were integrated into an Excel sheet and the statistics were converted into raster data after the statistics were completed, the steps are as follows: (1) Download the Chinese county vector dataset, import the downloaded data into Arcgis, select the study area required to extract the 14 counties contained in the study area. (2) Rasterise the vector data. The connected map is still a vector map of each indicator, so the vector map should be rasterised, and the accuracy is also set to 500 m. (3) Calculate the density of each raster. There are many ways to classify the density, but in this paper, we use population density to classify the density of each indicator, which is considered to be dense where there are many people and vice versa. Using the raster calculator, the density is obtained by dividing the product data of the population distribution by the data rasterised by county in step three. (4) The data for each indicator distributed by population density is obtained. The rasterised data for each indicator is multiplied by the area calculated in step three to obtain the raster distribution

results for each indicator. (5) The data are normalized, which means that the required data are processed and their range of values are restricted to a uniform range. The raster calculator's formulae are used to normalize each indicator to a range between 0 and 1.

3.3 Agricultural Drought Vulnerability Evaluation Methods

Standardization of Evaluation Indexes. The agricultural drought vulnerability evaluation factors were standardized and the required data were calculated by substituting the formula:

$$X_i' = (X_i - X_i \min)(X_i \max - X_i \min) \quad (1)$$

where X denotes the standardized data of the i -th indicator; X denotes the original value of the i -th indicator; $X_i \max$, $X_i \min$ denote the maximum and minimum values of the i -th index in the data, respectively.

In this paper, both textual data and spatial data are standardized. For the textual data, the data is substituted into SPSS software for processing; the spatial data is calculated by using a raster calculator with the formula.

Determination of Evaluation Index Weights. Since the evaluation of agricultural drought vulnerability is based on the comprehensive evaluation of multiple indicators, there are obvious differences in strengths and weaknesses between each evaluation indicator and drought vulnerability.

In this paper, principal component analysis is applied to calculate the weights of each agricultural drought vulnerability evaluation index in the eastern agricultural region of Qinghai. The principal component analysis method derives the main influencing components in the space of characteristics and can use mathematical methods to reveal the correlations among the evaluation indicators in order not to bias the results in favor of a certain indicator factor. For this reason, this paper uses principal component analysis to determine the weights of each evaluation index.

The following equation was used to calculate the common factor variance H for each drought evaluation index.

$$H_j = \sum_{k=1}^m \lambda_{jk}^2 \quad (2)$$

where H_j is the common factor variance; m is the number of principal components, taking $m = 3$; j is the original total number of indicators, and λ is the eigenvalue of the indicators on the principal components. After processing the common factor variance H of each evaluation index, the weights of each index are obtained [25]:

$$W_j = H_j / \sum_{j=1}^{11} H_j \quad (3)$$

where W_j is the weight, and each evaluation index and weight coefficient are shown in Table 1 in 3.1.

Agricultural Drought Vulnerability Evaluation Model Calculation. The vulnerability index was calculated using the weighted composite method with the following formula:

$$V_i = \sum_{j=1}^m W_j \times S_{ij} \quad (4)$$

where V denotes the drought vulnerability index, W_j is the weight corresponding to the j -th indicator, and S_{ij} is the standardized value of the j -th indicator in the i -th area. The corresponding ones are calculated based on the above equations for further analysis of drought vulnerability in the study area [26].

A weighted composite score was developed for the three dimensions of exposure, sensitivity and resilience, named exposure index (E), sensitivity index (I) and resilience index (A), respectively, and the vulnerability of the study area was calculated with the following equation:

$$V = E \times I \div A \quad (5)$$

Agricultural Drought Vulnerability Barrier Degree Evaluation Model. Analysis of the barriers to agricultural development in the eastern agricultural region of Qinghai Province using a barrier degree model and specific values values.

$$d_{ij} = 1 - y_{ij} \quad A_{ij} = \frac{W_{ij} \cdot d_{ij}}{\sum_{i=1}^n W_{ij} \cdot d_{ij}} \times 100\% , \quad (6)$$

$$U = \sum_{i=1}^n A_{ij}$$

where A_{ij} denotes the barrier degree of single indicator in the indicator layer, and is the degree of influence of the i -th indicator on early disaster vulnerability in agriculture; W denotes the contribution of the indicator to the overall target, and is the weight value of the i -th indicator. d_{ij} is the deviation degree of the indicator, which indicates the gap between the single indicator and the maximum target, set as the gap between the standardized value of the indicator and 1; y_{ij} is the standard value of the i -th indicator; U denotes the guideline level indicator barrier degree, which is the degree of influence of the guideline level indicator on agricultural drought vulnerability [27].

4 Results and Analysis

The three sub-modules of exposure, sensitivity and adaptability were evaluated first, and then the three were combined to obtain the evaluation results of the fragility within the insured body.

4.1 Spatial Variation in Agricultural Drought Vulnerability

The distribution of agricultural drought vulnerability index in the eastern agricultural area of Qinghai province was obtained by substituting the vulnerability formula as shown in the Fig. 3. The range of the index is between 0.003 and 0.47. From the regional distribution, each county in the study area has areas with high vulnerability, and the central

areas of Datong County, Huanzhong County and Huzhu County with high vulnerability are larger, and the vulnerability index near Huangshui River Valley is higher; the vulnerability index of Tongren County increased in 2004 and 2007.

The vulnerability distribution is gradually increasing in Huzhu and Menyuan counties and decreasing in Huanzhong district between 2009 and 2019.

To analyze the spatial variation of agricultural drought vulnerability, the spatial distribution of vulnerability strengths and weaknesses could not be obtained intuitively through the vulnerability result map. Therefore, the spatial distribution of vulnerability for each year was obtained by systematically classifying the average vulnerability of each county into five levels: the lowest vulnerability, Medium low vulnerability, moderate vulnerability, high vulnerability and the highest vulnerability.

As shown in Fig. 4, through the spatial distribution diagram of vulnerability in each year, it is obvious that between 2000 and 2007, the vulnerability of Menyuan County, Tongren County and Guide County is the highest, and the vulnerability of Datong County, Huzhu County and Jianzha County is high, while the vulnerability of Xining City is the lowest. From 2011 to 2019, the spatial distribution of vulnerability strength and weaknesses has changed significantly, with the vulnerability of Menyuan County, Tongren County, Guide County and Datong County weakening, but the vulnerability of Huzhu County, Pingan County, Huanzhong County and Ledu County gradually increasing. In conclusion, the spatial distribution pattern of vulnerability has changed significantly between 2000 and 2019, from low vulnerability in the central part and high vulnerability in the north and south to high vulnerability in the north and low vulnerability in the south.

The main reason for this development of vulnerability may be that the main impact on agriculture in the early years was water resources, the central part of the agricultural region of eastern Qinghai Province is crossed by the Huangshui River, whose banks are rich in water resources while water resources are scarce at the farther ends of the basin, resulting in a deterrent to agricultural development; in recent years the main factors affecting agricultural development have been excessive economic development, insufficient market supply and demand, and increased vulnerability due to excessive pressure on land.

4.2 Temporal Variation in Agricultural Drought Vulnerability

The temporal variation of agricultural drought vulnerability in the eastern agricultural region of Qinghai Province, after averaging the vulnerability raster sub-counties, shows that the vulnerability level mainly ranges from 0 to 0.4, with most counties showing a decreasing trend over time, with some counties gradually increasing in vulnerability after falling to a low point in 2011. The highest level of vulnerability is currently in Xunhua County, while the lowest level of vulnerability has been maintained in Jianzha County.

4.3 Analysis of Factors Influencing Vulnerability to Agricultural

Analysis of Meteorological Drought Factors in Agricultural Areas. The analysis was carried out from the TVDI. Due to the special local climatic conditions in Qinghai

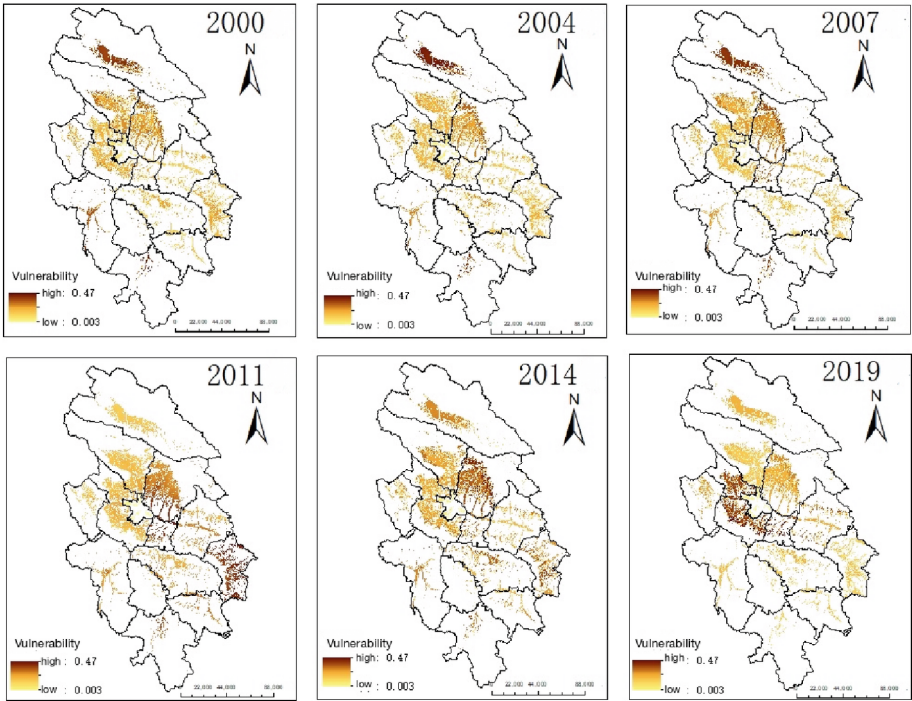


Fig. 3. Spatial distribution of drought vulnerability.

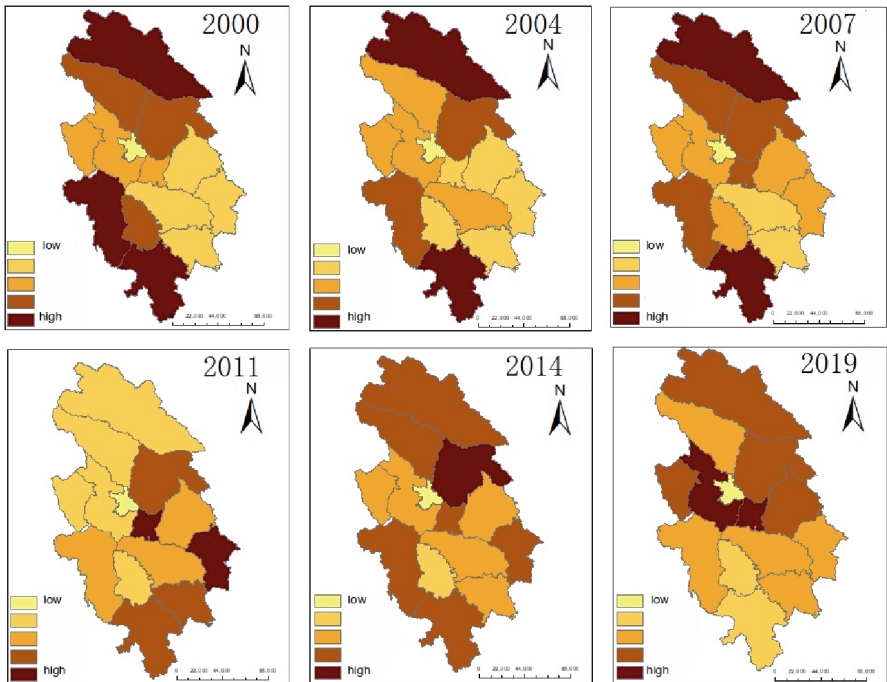


Fig. 4. County distribution of drought vulnerability.

Province, the growing season of crops in the eastern agricultural zone is from June to August, and the average TVDI data for crops from June to August for each county in the eastern agricultural zone of Qinghai Province from 2000 to 2019 were derived as shown in Table 2 below:

Table 2. TVDI for each county in the study area.

County Name	2000	2004	2007	2011	2014	2019
Xining	0.6654	0.6474	0.6328	0.6617	0.6273	0.6172
Datong	0.5402	0.5471	0.5323	0.5487	0.5101	0.5108
Huangzhong	0.5914	0.5683	0.5532	0.5813	0.5484	0.5397
Huangyuan	0.5892	0.5584	0.5373	0.5599	0.5367	0.5153
Ledu	0.6305	0.6238	0.6145	0.6445	0.5896	0.5695
Pingan	0.6407	0.6291	0.6047	0.6452	0.5938	0.5741
Minhe	0.6524	0.6458	0.6359	0.6734	0.6076	0.5772
Huzhu	0.5761	0.5672	0.5559	0.5832	0.5375	0.5273
Hualong	0.6587	0.6138	0.5885	0.6444	0.5934	0.5706
Xunhua	0.6303	0.5981	0.586	0.6253	0.5871	0.5619
Menyuan	0.5406	0.5422	0.5207	0.54	0.5093	0.4906
Tongren	0.6223	0.5792	0.5638	0.5838	0.5674	0.5598
Jianzha	0.6488	0.6022	0.5736	0.6099	0.5848	0.562
Guide	0.6566	0.6085	0.5769	0.6257	0.6056	0.5601

Table 3. Drought vulnerability data for the Kwarau, Shallow and Cerebral Mountains.

Year	Chuanshui area	Qianshan area	Naoshan area
2000	0.1359	0.1841	0.2255
2004	0.1163	0.1501	0.2089
2007	0.1036	0.1327	0.1772
2011	0.1243	0.0943	0.0789
2014	0.1217	0.1389	0.1544
2019	0.0941	0.1265	0.1292

It can be seen that the TVDI mostly lies between 0.5 and 0.7, and this data is in the range of 0 to 1.1 for the total TVDI taken globally, so it can be seen that the meteorological environment in the eastern agricultural zone is in a relatively dry state. The overall TVDI in the eastern agricultural zone shows a decreasing trend, but in the middle years there is a phenomenon of first decreasing and then increasing. by the nature of the TVDI, the

larger the TVDI, the lower the soil moisture, and the smaller the TVDI, the higher the soil moisture. From 2004 to 2007 the TVDI first decreases, the soil moisture increases, and from 2007 to 2011 it increases again, the soil moisture decreases, the precipitation, the changes in precipitation, grain production and total agricultural output also produced opposite fluctuations from 2004 to 2011. Thus, a decrease in the TVDI leads to a decrease in drought and a gradual weakening of the meteorological causes of drought (Table 3).

Analysis from the agricultural production environment. The agricultural production environment in Qinghai Province is divided into three types of agricultural production environment according to the special climatic environment and topography of Qinghai Province is Naoshan area, Qianshan area and Chuanshui area. The resulting vulnerability distribution data were extracted according to the three types of production environments to derive their respective vulnerability indices:

It can be seen that the vulnerability index is the lowest in the Chuanshui area, Qianshan area in the middle and Naoshan area is the highest vulnerable, with a general trend of weakening vulnerability between 2000 and 2019, with a sudden rise in 2014, but then a decline.

Analysis of Factors Influencing Drought Vulnerability. Reducing agricultural drought vulnerability in the eastern agricultural region is an important prerequisite for promoting agricultural development in the region. In order to further explore the main factors affecting agricultural development in the eastern agricultural region of Qinghai Province, the results of the barrier index calculation for each indicator are shown in Table 4 below:

Table 4. Barrier degree values for each indicator.

Indicators	Barrier degree index	Indicators	Barrier degree index
TVDI	5.671	Total power of agricultural machinery	-2.825
Precipitation	4.191	Gross Agricultural Product	0.447
Village Council Number	-0.445	Annual fertilizer application	1.353
Grain production	-1.093	Agricultural production environment	-0.667
Crop sown area	-0.926	Gross Regional Product	3.985
Population density	1.039	Effective irrigated area	-1.307
Per capita net income of farmers	4.578		

From the Table 4, it can be concluded that the variation of the barrier degree of each indicator on the vulnerability to drought in the eastern counties of Qinghai Province varies. The top four indicators in the barrier degree in the indicator layer are the TVDI, precipitation, net per capita income of farmers and gross regional product, which belong to the sensitivity and adaptive capacity subsystems respectively, indicating that these indicators have a greater impact on vulnerability and are the main influencing factors of agricultural drought in the region.

5 Discussion and Conclusion

This paper constructs an indicator system for drought risk analysis in the eastern agricultural region of Qinghai Province from the perspectives of geographical location and geomorphology, climatic conditions and water resources, geographical characteristics of agriculture, government management capacity and forecasting and mitigation capacity of disasters occurring in the eastern agricultural region of Qinghai Province. It is suggested that this index system is suitable for regional scales such as the eastern agricultural region of Qinghai Province. The system was established by applying standardization methods to normalize the relevant indicators and applying principal component analysis to determine the weights of each factor and indicator. In addition, the indicators were divided into three subsystems: exposure, sensitivity and resilience, according to the geographical characteristics of agriculture in the study area. Finally, by standardizing and weighting the indicators, the results of vulnerability were calculated and the key constraints to agricultural development were identified through a barrier model.

Existing studies on drought in the eastern agricultural region have mostly focused on natural factors such as meteorology and geography, and most of the measures for disaster mitigation and prevention are in the area of post-drought recovery. This paper presents an empirical analysis of drought vulnerability in the eastern agricultural region of Qinghai Province based on data obtained on the basis of the principles of scientific, representativeness and accessibility, which has certain feasibility and application value, but there is some subjectivity in the selection of indicators. Therefore, in order to make the evaluation results more reasonable and better used by government departments as reference for disaster prevention and mitigation policies, the indicator system and evaluation model of agricultural drought vulnerability in the eastern agricultural region of Qinghai Province still need continuous improvement. At the same time, a more precise scale and objective analysis of agricultural drought vulnerability in the eastern agricultural region of Qinghai Province are the directions to be considered in this paper. Based on the comprehensive study in this paper, the vulnerability of the eastern agricultural region of Qinghai Province was measured from 2000 to 2019, and the main conclusions are as follows:

(1) Agricultural drought vulnerability from the spatial distribution layout: from 2011 to 2019, the spatial distribution of vulnerability strengths and weaknesses has changed significantly. In summary, the spatial distribution pattern of vulnerability has changed significantly from 2000 to 2019, from low vulnerability in the central part and high in the north and south to high vulnerability in the north and low vulnerability in the south. (2) The layout of agricultural drought vulnerability in terms of temporal distribution: most

counties show a decreasing trend in vulnerability over time, with some counties showing a gradual increase in vulnerability after falling to the lowest point in 2011. At present, the highest vulnerability is in Xunhua County, while the vulnerability in Jianzha County has remained the lowest. (3) Agricultural drought vulnerability from the agricultural production environment, it can be seen that the vulnerability index is the largest in the Chuanshui area, with shallow mountainous areas in the middle and brain mountainous areas being the most vulnerable areas. Between 2000 and 2019, there was a general trend of weakening vulnerability, with a sudden rise in 2014, but then a decline. (4) Agricultural drought vulnerability in terms of influencing factors: the top 4 indicators in the indicator layer in terms of barrier degree are the TVDI, precipitation, net per capita income of farmers, and gross regional product, which belong to the sensitivity and adaptive capacity subsystems respectively, indicating that these indicators have a greater impact on vulnerability and are the main influencing factors of agricultural drought in the region.

References

1. Wang, N.: A study on the relationship between drought and desertification in the Guanzhong region during the Ming and Qing dynasties. Shaanxi Normal University (2016)
2. Wen, K.G.: China's Meteorological Disaster Dictionary. Meteorological Press (2008)
3. Zhang, S.: On the production of dryland potato crops in the mountainous areas of the Qinghai Plateau. *Agric. Sci. Technol. Newslett.* **498**(06), 34–36 (2013)
4. Yang, F., Liu, L.: Drought occurrence patterns and their trends in eastern Qinghai. *Arid Zone Res.* **29**(02), 284–288 (2012)
5. Zhao, H.M.: A preliminary study on the relationship between natural precipitation resources and spring wheat yield in semi-arid areas of southeastern Qinghai and its countermeasures. *Qinghai Agric. Extension* **1997**(4), 49–50 (1997)
6. Thomas, E.D., Burton, I., Robert, W.K., Gilbert, F.W.: The environment as hazard. *Contemp. Sociol.* **8**(3) (1979)
7. Cutter, S.L., Boruff, B.J., Shirley, W.L.: Social vulnerability to environmental hazards. *Soc. Sci. Q.* **84**(2), 242–261 (2003)
8. Diana, M.L.: Drought impacts in Mexico: climate, agriculture, technology, and land tenure in Sonora and Puebla. *Ann. Assoc. Am. Geogr.* **80**, 49–72 (1990)
9. Wilhelmi, O.V., Wilhite, D.A.: Assessing vulnerability to agricultural drought: a Nebraska case study. *Nat. Hazards* **25**(1), 37–58 (2002)
10. Sönmez, F.K., Kömüscü, A.Ü., Erkan, A., Turgu, E.: An analysis of spatial and temporal dimension of drought vulnerability in turkey using the standardized precipitation index. *Nat. Hazards* **35**(2), 243–264 (2005)
11. Sahana, V., Mondal, A., Sreekumar.: Drought vulnerability and risk assessment in India: sensitivity analysis and comparison of aggregation techniques. *J. Environ. Manag.* **299** (2021)
12. Hafzullah, A., et al.: Critical drought intensity-duration-frequency curves based on total probability theorem-coupled frequency analysis. *Hydrol. Sci. J.* **66**(8), 1337–1358 (2021)
13. Zahra, T., Masoudi, M., Fischer T.: Hazard assessment of drought using PNPI and GIS in Fars Province, Iran. *J. Environ. Assess. Policy Manag.* (2023)
14. Shang, Y.R.: Drought, agricultural drought, and drought vulnerability of farmers: a case study of typical farmers in Xingtai County. *J. Nat. Hazards* **02**, 55–61 (2000)
15. Li, Z.Y., Wang, G.C., Yang, D., Lu, Y.Z.: Analysis of agricultural drought vulnerability in Henan Province. *China Agron. Bull.* **37**(10), 101–106 (2021)

16. Ma, Y.L., Guo, J.P., Luan, Q., Liu, W.P.: Vulnerability assessment of agricultural droughts in the north of Jinjiang agricultural-pastoral interlacing zone. *Disaster Science* **35**(03), 75–81 (2020)
17. Dai, Y.Q., Wang, L.G., Hu, B.: Vulnerability assessment of agricultural drought in Gansu Province region. *J. Appl. Sci.* **36**(03), 515–523 (2018)
18. Cheng, J., Du, Z., Hu, J.L., Li, C.S.: Study on factors influencing agricultural drought vulnerability and spatial variation - empirical evidence based on six provinces and one city in the middle and lower reaches of Yangtze River. *Ecol. Econ.* **33**(09), 188–194 (2017)
19. Liu, X., Su, X.L., Liu, Y.H., Liang, X.X.: Assessment of ecological drought vulnerability in Northwest China. *Water Resour. Conserv.* **39**(03), 65–73 (2023)
20. Huo, T., Zhang, X., Zhou, Y., Chen, W.: Spatial and temporal variability evaluation and correlation analysis of ecological vulnerability based on the exposure-sensitivity-adaptation model - an example of the Suzhou section of the Grand Canal in China. *J. Ecol.* **42**(06), 2281–2293 (2022)
21. Jiang, T., Li, X.C., Chao, Q.D., Yuan, J.S., Lin, E.D.: Key findings and new insights from climate change 2014: impacts, adaptation and vulnerability. *Adv. Clim. Chang. Res.* **10**(03), 157–166 (2014)
22. Zheng, F., Sun, C., Li, J.P.: Understanding disaster risk, exposure, vulnerability and resilience from a new perspective of climate change. *Adv. Clim. Chang. Res.* **8**(02), 79–83 (2012)
23. Sun, D.: A GIS-based study of ecological vulnerability in Jilin Province. Northeast Normal University (2013)
24. Hou, G.L., Xiao, J.Y., Li, S.M.: Drought vulnerability assessment based on climate change - an example from eastern Qinghai. *J. Nat. Hazards* **21**(02), 163–168 (2012)
25. Yang, C.Y., Wang, J.A., Su, Y., Wang, Z.Q.: Vulnerability assessment of agricultural droughts: a case study of Xinghe County in the northern agro-pastoralist zone. *J. Nat. Hazards* **6**, 88–93 (2005)
26. Li, J.: Grey clustering assessment of agricultural drought vulnerability in Henan Province. North China University of Water Resources and Hydropower (2021)
27. Gao, S., Sun, H.H., Liu, W.: Vulnerability assessment and barrier analysis of marine economic systems based on entropy-weighted TOPSIS model. *Ecol. Econ.* **37**(10), 77–83 (2021)

Geotechnical Engineering



A Review on Application of Soft Computing Techniques in Geotechnical Engineering

T. V. Nagaraju¹ (✉), Mantena Sireesha², B. M. Sunil³, and Shaik Subhan Alisha⁴

¹ Department of Civil Engineering, S.R.K.R. Engineering College, Bhimavaram, India
varshith.varma@gmail.com

² Department of Geo-Engineering, Andhra University, Visakhapatnam, India

³ Department of Civil Engineering, National Institute of Technology, Karnataka, India
sunilbm@nitk.edu.in

⁴ Department of Civil Engineering, Vishnu Institute of Technology, Bhimavaram, India

Abstract. Numerous test results, mathematical relationships, and in-the-moment analysis and design are all components of geotechnical issues. Additionally, due to smart infrastructure and materials, the research trend in engineering nowadays is shifting toward intelligent tools and their ability to tackle engineering problems. Artificial neural networks (ANN), support vector machines (SVM), genetic algorithms (GA), and particle swarm optimization algorithms (PSO), among other soft computing techniques, have made significant progress in recent years in solving geotechnical issues. Based on a review of more than 800 published research, this study discusses the applicability of soft computing techniques in the current environment. Traditional methods, such as regression analysis and trial-and-error techniques, take time and could be more effective. Additionally, most geotechnical designs require considerable experimental data and may require laborious work. A novel methodology for soft computing approaches has emerged to solve the problems mentioned above. This paper presents soil problems and geotechnical challenges while examining recent developments and the potential applications of soft computing.

Keywords: Artificial Intelligence · Soft Computing · Geotechnical Engineering · Modeling

1 Introduction

Due to the complexity of soils and rocks, geotechnical engineering problems have more significant uncertainty. Geotechnical engineering is also essential for building pavement, sub-structure foundations, retaining walls, canal lining, earthen dams, mining, landfill development, and slope stability. Due to a three-phase system, soils display various characteristics depending on moisture presence. Any project estimating soil strength and durability involves costly laboratory work. Many parameters, including chemical composition, particle size, moisture content, soil layer thickness, and allowable pressure, influence soil strength and durability.

Many types of soil deposits were available worldwide, but lateritic soils, collapsible soils, expansive clays, and marine clays were problematic due to their complex characteristics [1]. Expansive clays exhibit significant swell-shrink changes when exposed to alternate wet and dry seasons. Additionally, according to statistics from the American Society of Civil Engineers (ASCE), expansive clay settlements cause damage to 25% of the lightweight dwellings in the United States. Expansive clays cost 2.3 billion dollars in damages, equal to the total cost of all-natural disasters like earthquakes, floods, and cyclones [2]. Due to abrupt changes in void ratio after soaking, collapsible soils enable severe damage to pavements, electricity lines, lightweight buildings, and retaining walls. There are significant hazards everywhere due to the abrupt shift in soil. Furthermore, due to the presence of iron oxides, lateral soils have distinct characteristics and are challenging to categorize. While it is uncommon during field structure, fractured iron oxides are commonly observed during laboratory testing of laterites. Understanding how soils behave in this regard depends on the type of project. Additionally, various elements, including the type of soil, the outcomes of laboratory and field tests, and the experience of the testing specialist, affect the soil attributes. However, measuring the engineering qualities of soils takes a lot of time and effort [3].

Regression and classification models based on correlations and relationships between complex and index variables have been developing since the 1990s to avoid time-consuming tests and save project expenses. Numerous researchers have contributed to developing empirical correlations between soil parameters. For example, Cubrinovski and Ishihara [4] reported an empirical correlation based on the SPT 'N' value to determine the relative density of the in-situ soils. The main conclusions of this work are well-established. According to Yilmaz [5], there is an empirical correlation between the clays' un-drained shear strength and plasticity index to avoid time-consuming shear tests. Swelling and shrinkage in expansive clays are vital issues, especially in chemically treated clays; the dosage of chemical additive was selected by swelling behavior. However, expanding clays primarily rely on chemical constituents and exchangeable ions. In this regard, Farrar and Coleman demonstrated the relationship between index characteristics and cation exchange capacity [6]. For building structures, the liquefaction of silty sand soils is a critical hazard. Therefore, several types of research have established relationships between in-situ penetration values and liquefaction potential.

Geotechnical engineering has seen the emergence of artificial intelligence (AI) and machine learning (ML) algorithms in recent years, offering hope for many challenging issues. The major geotechnical issues and adaptability of AI approaches are highlighted in this research to illustrate the relevance of soft computing techniques in geotechnical engineering.

2 Soft Computing (SC) Techniques

This section presents brief details of the different successful soft computing approaches in the geotechnical engineering domain.

2.1 Artificial Neural Network (ANN)

The most promising and well-known method that uses the neural network principle is called ANN. The appropriate features of models, including regression, classification, pattern generation, and clustering, are responsible for the network's appeal. ANN typically consists of three parts to analyze and process any model: the input layer, hidden layer, and output layer. Furthermore, the bias and weight functions determine how accurately the ANN model performs. For example, the linear regression equation in neural networks is $Y = mX + n$, where m and n are the coefficient and slope, respectively. Data will be learned and trained based on the function to produce appropriate predictions with the least inaccuracy. For example, the California bearing ratio (CBR) values of pavement subgrades, the unconfined compressive strength (UCS) of the soils, foundation settlements, liquefaction potential, landslide susceptibility, and unsaturated soils were all accurately predicted by ANN models [7, 8].

2.2 Convolutional Neural Network (CNN)

CNN is a unique tool used mostly for image processing using pattern recognition. CNN has shown promising results in numerous medical, environmental, and engineering domains. The CNN technique was extensively used in geotechnical engineering to classify soils, identify earthquakes, predict slope failure, strength assessment, and analyze clay crack patterns. Convolution, polling, flattening, fully linked, and output layers are all present in CNN. The convolution layer would aid in extracting features from the input layer and filtering each field in CNN models, including features like ANN models. Additionally, network neurons change to recognize and detect the overall answer [7].

2.3 Support Vector Machine (SVM)

SVM is one of the most sophisticated algorithms for making predictions using supervised training and pattern recognition. The most excellent technique for classifying and separating data after obtaining raw data is SVM. LINEAR, SIGMOID, and radial basis function (RBF) are the most frequently utilized kernel functions in SVM-based classification. The performance of classification models might be improved by using these kernel functions to produce non-linear surface separations. SVM successfully resolves pattern recognition and matter classification issues in geotechnical engineering. Soil categorization, landslide susceptibility, liquefaction potential, rock displacement, and soil deformation are important contributions of the SVM tool. Additionally, the dynamic behavior of soil-structure interaction is successfully analyzed by SVM. It was discovered that the SVM model might provide more accurate predictions than the finite element method (FEM) in a shorter amount of time [7, 8].

2.4 Random Forest (RF)

By using decision trees for training, random forests operate on the notion of resampling the original data. The decision trees are constructed using boosting so that each new decision tree works to minimize the errors of the prior one. Each decision tree updates

the residual mistakes based on what it has learned from its past. Consequently, the tree that develops later will likely gain knowledge from revised regressions. Additionally, the individual decision split received a random distribution of the RF properties. As a result, features decreased the correlation between the decision trees. Additionally, the learning process increases the model's performance and prediction power. With the help of additional features, RF can effectively model high-dimensional complex data that contains missing, category, and binary information. RF has been modified, and adaptive random forests (ARF) are the most effective classifier for data streams. The ARF's dynamic method can help the data as it changes and enables the training of new trees to provide the best overall answer. In geotechnical engineering, multi-linear regression prediction models have been effectively used to forecast soil water infiltration, the maximum seismic response of soil-pile interaction, soil salinity, soil erosion, and soil categorization [7, 8].

2.5 Genetic Algorithm (GA) And Particle Swarm Optimization Algorithm (PSO)

The most effective algorithms in history are genetic algorithms, which are widely used. In addition, GA is the first population-based algorithm. The GA searches for a global solution with convergence outcomes based on the genetic selection theory.

Due to the few performance parameters that could be changed, PSO is a successful algorithm that is inspired by nature in many fields. Similar to the population of random search, PSO operates on the GA principle. However, PSO searches the issue space using velocity coefficients that are given to random particles. PSO discovered accurate predictions in small datasets. Geotechnical engineering has successfully used the PSO to forecast a variety of geotechnical factors, including soil erosion susceptibility, foundation settlement, CBR of pavement subgrades, shear strength of soils, shield performance in tunneling, soil heavy metal content, pull-out behavior of piles, and seismic slope stability [7, 9, 10].

2.6 Fuzzy Logic (FL)

The four promising elements of fuzzy logic are fuzzification, rule base, inference engine, and defuzzification. Fuzzy logic is a well-known model. In the FL technique, the input data was first divided into various datasets (fuzzified), and then relationships between the input and output variables were developed (rule base). Learning with rule-based and reducing errors (inference engine) was then performed. Finally, the outputs were produced from the fuzzy inference (defuzzification). The FL system can approximate the data with its generalization behavior rather than duplicate the laboratory data. Due to the robust non-linear simulation performance and the inclusion of fuzzy language rules, the FL system has recently gained prominence. The geotechnical engineering field is drawn to these non-linear models. Unsaturated hydraulic conductivity, soil erosion, boring penetration rate, and slope stability were all correctly predicted by FL using fuzzy language rules [7, 8, 11].

3 Application of Soft Computing Techniques in Geotechnical Engineering

Researchers and professionals in the field of geotechnical engineering have successfully used soft computing and machine learning methods in recent years. Since soil qualities are the main consideration in the construction of any structure, geotechnical properties of soils have been extensively investigated. The use of soft computing techniques to forecast soil properties is briefly explained in this section.

Figure 1 illustrates the use of soft computing techniques for foundations, slope stability, liquefaction potential, landslides, and landfills. The literature reviews demonstrate that soft computing has a significant impact in many geotechnical engineering domains. In earlier investigations, several SC techniques were used, with a focus on modelling, simulating, and optimizing geotechnical features and issues [7, 11].

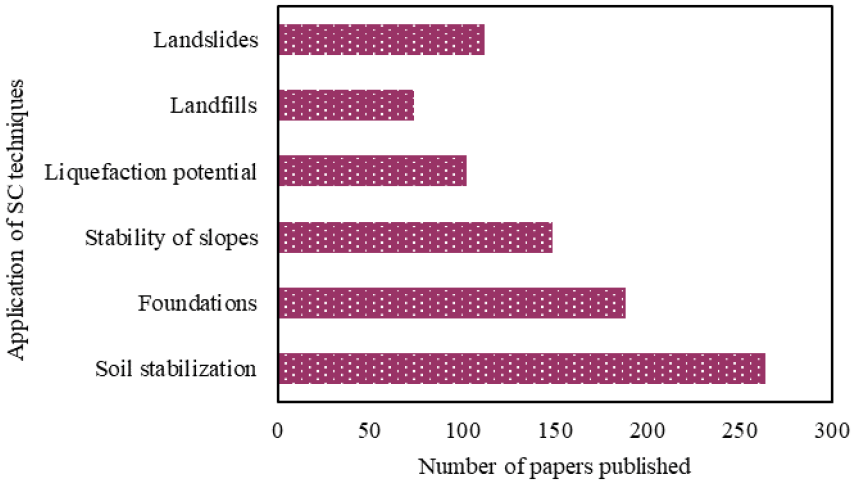


Fig. 1. Application of soft computing techniques in geotechnical engineering domain.

3.1 Soil Stabilization

Researchers' interest in soil stabilization has grown because of their achievements in the field. Additionally, there are numerous chemicals and pozzolanic additives in use today. However, careful additive dosage selection can prevent over- or underestimating additive dosage and reduce project costs. The swell-shrink behaviour of chemically altered clays, UCS of the stabilized soils, and the CBR values of the pavement subgrades are all predicted using various soft computing techniques [7, 9]. Figure 2 illustrates the use of SC approaches for soil stabilization.

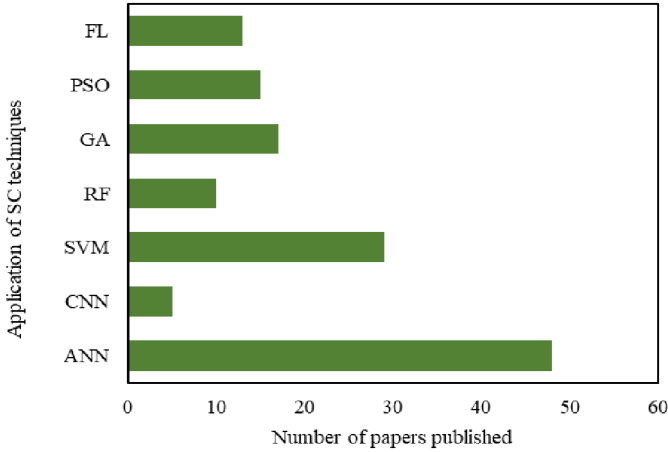


Fig. 2. Number of published papers with application of SC in soil stabilization.

The settling of foundations, bearing capacity of foundations, axial bearing capacity, and lateral load capacity of piles were all predicted using SC techniques in the field of foundations (see Fig. 3). Understanding the behaviour of the piles in pile foundations is exceedingly difficult and time-consuming. An increased number of tests will also impact on the project's final cost. Therefore, using intelligent technologies to forecast pile response could be useful. The effectiveness of the ANN technique in forecasting the piles' bearing capacity was reported by Moayed and Jahed [12]. The regression coefficient of determination (R^2) value of 0.974 in the prediction results shows that the ANN model successfully predicted the foundation's bearing capacity. A PSO-based model was put up by Ray et al. [13] to forecast the settlement of shallow foundations. According to the findings of the prediction, the PSO model can estimate foundation settlement in general.

3.2 Foundations

3.3 Stability of Slopes and Landslides

Maintaining appropriate highways to connect one region to another in the hilly terrains is a top government priority since stability is a big problem worldwide, particularly in northern India. In addition, numerous slope collapses have been reported due to various circumstances, including soil characteristics, slope aspect, slope size, geological conditions, and rainfall. Therefore, empirical relationships between these variables are required to estimate the slope condition using user-friendly and powerful tools. On the other hand, landslides are significant natural disasters in underdeveloped nations, causing over 17% of all fatalities worldwide [14]. Slope failure and slope stability utilizing ANN were successfully applied, according to Lin et al. [15] and Gordan et al. [16]. Figure 4 illustrates the use of SC approaches for stability of slopes and landslides.

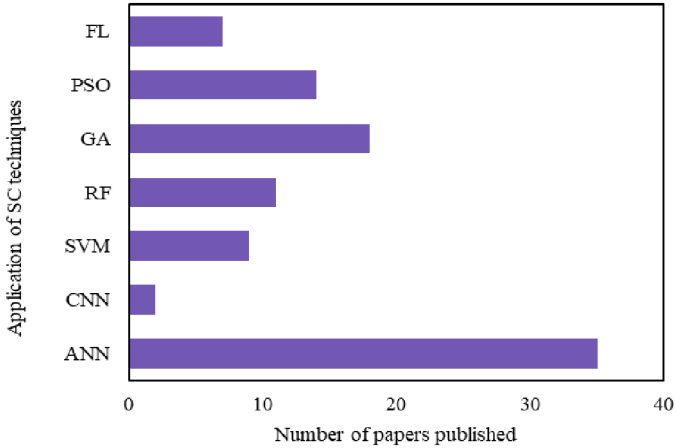


Fig. 3. Number of published papers with application of SC in foundations.

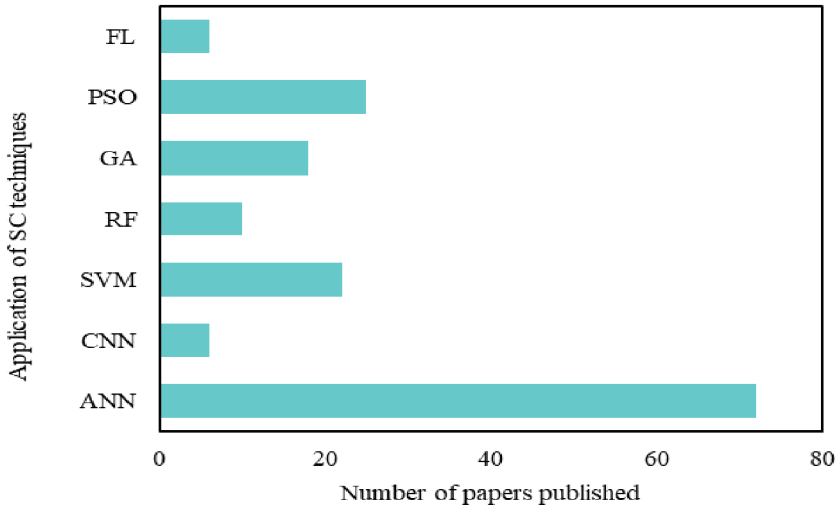


Fig. 4. Number of published papers with application of SC in slope stability and landslides.

3.4 Liquefaction

Soft computing has taken on predicting soil's seismic liquefaction potential as a classifying challenge [17, 18]. For determining the seismic liquefaction potential of soil, geotechnical engineers typically employ a variety of in situ techniques, such as the field standard penetration test and shear wave velocity approach. In addition, soft computing approaches have been applied to standard penetration N-values, shear wave velocity findings, stresses, earthquake intensity, and ground acceleration. To predict the seismic liquefaction potential of soil, various soft computation approaches are applied in Fig. 5.

Most researchers used ANN to categorize liquefiable and non-liquefiable soil [19]. For the final prediction, ANN uses the entire training dataset. SVM and RF, however, only use a small percentage of the training dataset for outcome prediction [20]. The established soft computing approaches provide charts for identifying liquefiable and non-liquefiable sands. Final predictions are made using kernel functions by SVM and RF. For output prediction, ANN uses an activation function. GA and PSO can use any function to determine the output [21–23].

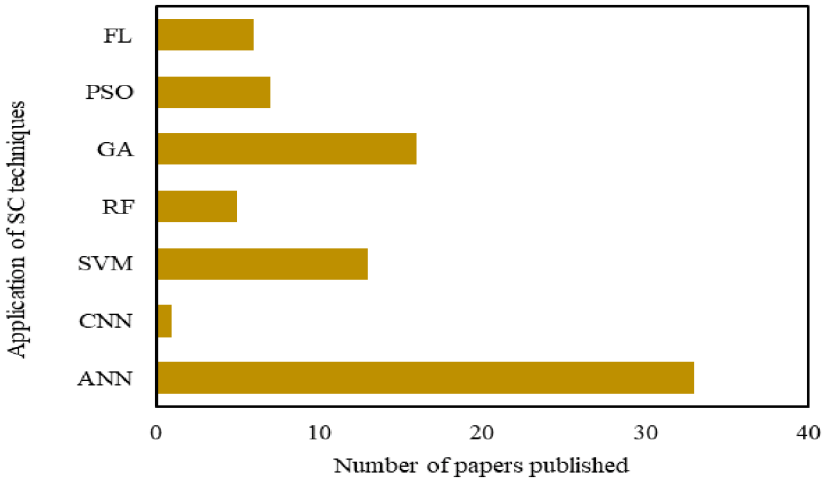


Fig. 5. Number of published papers with application of SC in slope stability and landslides.

Due to their capacity to handle nonlinear and complicated relationships, take large amounts of data, including incomplete information, learn from data rather than relying only on prior knowledge, manage multiple outputs, and adapt quickly to new data or changes, ANN models are becoming more and more important in geotechnical engineering. This makes them suitable for actual monitoring and forecasting tasks. As a result, they have been well-liked for jobs including soil categorization, soil property prediction, settlement prediction, and slope stability prediction [24–26].

4 Conclusions

The use of soft computing techniques in geotechnical engineering has been suggested in this study, robust techniques, including ANN, CNN, SVM, RF, GA, PSO, and FL.

According to a peer-review of the literature that has been published, SC techniques are becoming more promising. They may be able to address geotechnical issues in three dimensions through modeling, simulation, and optimization. Additionally, the adaptability and viability of these tools decreased time-consuming and labor-intensive tests, lowered project costs, increased the sustainable use of geomaterials, and produced easy predictions.

Additional applications of prediction models created utilizing SC techniques in geotechnical engineering are conceivable in addition to the main areas emphasized in the current work. They can make progress regarding the most recent concerns and issues about environmental and seismic geotechnics.

References

1. Vamsi Nagaraju, T., Satyanarayana, P.V.V.: Geotechnical aspects of various constructions along the canal embankment using rice husk ash as stabilizer. In: Thyagaraj, T. (eds.) *Ground Improvement Techniques and Geosynthetics*. Lecture Notes in Civil Engineering, vol. 14. Springer, Singapore (2019). https://doi.org/10.1007/978-981-13-0559-7_16
2. Gourley, C.S., Newill, D., Schreiner, H.D.: Expansive soils: TRL's research strategy. In: *Engineering Characteristics of Arid Soils*, pp. 247–260. CRC Press (2020)
3. Nagaraju, T.V., Gobinath, R., Awoyera, P., Abdy Sayyed, M.A.H.: Prediction of california bearing ratio of subgrade soils using artificial neural network principles. In: Sharma, H., Gupta, M.K., Tomar, G.S., Lipo, W. (eds.) *Communication and Intelligent Systems*. Lecture Notes in Networks and Systems, vol. 204. Springer, Singapore (2021). https://doi.org/10.1007/978-981-16-1089-9_12
4. Cubrinovski, M., Ishihara, K.: Empirical correlation between SPT N-value and relative density for sandy soils. *Soils Found.* **39**(5), 61–71 (1999)
5. Yilmaz, I.: Evaluation of shear strength of clayey soils by using their liquidity index. *Bull. Eng. Geol. Env.* **59**(3), 227–229 (2000)
6. Farrar, D.M., Coleman, J.D.: The correlation of surface area with other properties of nineteen British clay soils. *J. Soil Sci.* **18**(1), 118–124 (1967)
7. Baghbani, A., Choudhury, T., Costa, S., Reiner, J.: Application of artificial intelligence in geotechnical engineering: a state-of-the-art review. *Earth Sci. Rev.* **228**, 103991 (2022)
8. Shahin, M.A.: Artificial intelligence in geotechnical engineering: applications, modeling aspects, and future directions. In: *Metaheuristics in Water, Geotechnical and Transport Engineering*, pp. 169–204 (2013)
9. Nagaraju, T.V., Prasad, C.: Swarm-assisted multiple linear regression models for compression index (Cc) estimation of blended expansive clays. *Arab. J. Geosci.* **13**(9), 1–11 (2020)
10. Kaveh, A.: *Applications of Metaheuristic Optimization Algorithms in Civil Engineering*. Springer International Publishing, Basel, Switzerland (2017)
11. Ebid, A.M.: 35 Years of (AI) in geotechnical engineering: state of the art. *Geotech. Geol. Eng.* **39**(2), 637–690 (2021)
12. Moayedi, H., Jahed Armaghani, D.: Optimizing an ANN model with ICA for estimating bearing capacity of driven pile in cohesionless soil. *Eng. Comput.* **34**(2), 347–356 (2018)
13. Ray, R., Kumar, D., Samui, P., Roy, L.B., Goh, A.T.C., Zhang, W.: Application of soft computing techniques for shallow foundation reliability in geotechnical engineering. *Geosci. Front.* **12**(1), 375–383 (2021)
14. Moayedi, H., Khari, M., Bahiraei, M., Foong, L.K., Bui, D.T.: Spatial assessment of landslide risk using two novel integrations of neuro-fuzzy system and metaheuristic approaches; Ardabil Province Iran. *Geomatics Nat. Hazards Risk* **11**(1), 230–258 (2020)
15. Lin, H.M., Chang, S.K., Wu, J.H., Juang, C.H.: Neural network-based model for assessing failure potential of highway slopes in the Alishan, Taiwan Area: Pre-and post-earthquake investigation. *Eng. Geol.* **104**(3–4), 280–289 (2009)
16. Gordan, B., Jahed Armaghani, D., Hajihassani, M., Monjezi, M.: Prediction of seismic slope stability through combination of particle swarm optimization and neural network. *Eng. Comput.* **32**(1), 85–97 (2016)

17. Samui, P., Sitharam, T.G.: Machine learning modelling for predicting soil liquefaction susceptibility. *Nat. Hazard.* **11**(1), 1–9 (2011)
18. Kumar, D.R., Samui, P., Burman, A.: Prediction of probability of liquefaction using soft computing techniques. *J. Inst. Eng. (India): Ser. A* **103**(4), 1195–1208 (2022)
19. Abbaszadeh Shahri, A.: Assessment and prediction of liquefaction potential using different artificial neural network models: a case study. *Geotech. Geol. Eng.* **34**(3), 807–815 (2016)
20. Zhou, J., Huang, S., Wang, M., Qiu, Y.: Performance evaluation of hybrid GA–SVM and GWO–SVM models to predict earthquake-induced liquefaction potential of soil: a multi-dataset investigation. *Eng. Comput.* **38**(5), 4197–4215 (2022)
21. Kohestani, V.R., Hassanlourad, M., Ardakani, A.J.N.H.: Evaluation of liquefaction potential based on CPT data using random forest. *Nat. Hazards* **79**(2), 1079–1089 (2015)
22. Nagaraju, T.V., Prasad, C.D., Chaudhary, B., Sunil, B.M.: Assessment of seismic liquefaction of soils using swarm-assisted optimization algorithm. In: Sitharam, T.G., Jakka, R., Govindaraju, L. (eds.) *Local Site Effects and Ground Failures. Lecture Notes in Civil Engineering*, vol. 117. Springer, Singapore (2021). https://doi.org/10.1007/978-981-15-9984-2_25
23. Demir, S., Şahin, E.K.: Liquefaction prediction with robust machine learning algorithms (SVM, RF, and XGBoost) supported by genetic algorithm-based feature selection and parameter optimization from the perspective of data processing. *Environ. Earth Sci.* **81**(18), 1–17 (2022)
24. Şahin, M.A., Jaksa, M.B., Maier, H.R.: Recent advances and future challenges for artificial neural systems in geotechnical engineering applications. In: *Advances in Artificial Neural Systems* (2009)
25. Chao, Z., Ma, G., Zhang, Y., Zhu, Y., Hu, H.: The application of artificial neural network in geotechnical engineering. In: *IOP Conference Series: Earth and Environmental Science*, vol. 189, no. 2, p. 022054. IOP Publishing (2018)
26. Pradeep, T., GuhaRay, A., Bardhan, A., Samui, P., Kumar, S., Armaghani, D.J.: Reliability and prediction of embedment depth of sheet pile walls using hybrid ANN with optimization techniques. *Arab. J. Sci. Eng.* **47**(10), 12853–12871 (2022)



Study on Enhanced Oil Recovery Technology of Tight Reservoir Modified in Highly Deviated Well: A Case Study of the L183 Area in the Huaqing Oilfield Ordos Basin, China

Ce Wang^(✉), Xizhu Zhu, Tianhao Jiang, Libiao Li, Fangxin Song, Ping Zheng, and Jiuli Gu

No. 10 Oil Production Plant, Changqing Oilfield, Gansu 745100, China
1414701737@qq.com, {zxxz100_cq, jth100_cq, llb100_cq, sfx_cq, zp10_cq, gjli_cq}@petrochina.com.cn

Abstract. Chang 6 sandstone reservoir in Huaqing oilfield is a typical tight reservoir. The whole reservoir presents the characteristics of obvious non Darcy seepage, widespread development of natural fractures, large proportion of low production and low efficiency wells, and low production of single wells developed by conventional vertical wells. Based on the mechanism of highly deviated wells improving oil production rate, aiming at the problems of low recovery degree and fracture development induced by water injection during the development of tight reservoirs, this paper verifies the feasibility and superiority of highly deviated wells in tight reservoirs through indoor numerical simulation and field actual effect evaluation. The research results indicate that: (1) The highly deviated wells in the study area adopt advanced fine layered water injection development method, and the regional formation pressure is maintained at a level of over 120%. By utilizing the role of closed well infiltration and displacement, the seepage range is increased and the oil recovery rate is significantly improved. (2) Through numerical simulation combined with actual field test results, it has been proven that the concept of reducing the number of fracturing sections by combining cost control in highly inclined well areas, and the optimal perforation control degree is achieved at 10–20 m per well, with a reasonable flow to saturation ratio of less than 1.0, can maximize the benefits. It is concluded that the development of highly deviated wells in the L183 area of Huaqing oilfield provides strong support for the optimization design of fracturing parameters of thick reservoirs with tight interlayer, and provides theoretical guidance and technical support for their field application.

Keywords: Tight Reservoir · Imbibition Oil Recovery · Highly Deviated Well · Enhanced Oil Recovery

1 Introduction

Huaqing oilfield in Ordos Basin has large proved reserves and developed oil resources. The main layer length of 6 is a powerful battlefield for the exploration and development of Huaqing oilfield. The reservoir in this area is a typical tight reservoir (permeability

0.38md), with low formation pressure (pressure coefficient 0.6–0.8), large thickness of stable contiguous oil layer (23.6 m), large geological reserves controlled by a single well (106000 tons), relatively complex sedimentary environment, interaction of semi deep lake gravity flow channels in the middle, deep lake sandy debris flow mainly developed in the south, weak sand carrying capacity, interlayer development, and natural fractures in the reservoir, The maximum principal stress direction $NE50^\circ \sim NE90^\circ$. Therefore, it is urgent to explore a more suitable development mode for tight and thick reservoirs to further improve the oil recovery.

Highly deviated well means that the same oil production well can be exploited through multiple strata at the same time. At present, there is relatively little research on highly deviated wells in China [1–3]. Yang [4] proposed that reservoirs with small oil layer thickness and sufficient natural energy are suitable for long horizontal well development, with discontinuous sand body development, reservoirs with complex water drive conditions are suitable for short horizontal well development, and reservoirs with many oil layers and large thickness are suitable for highly deviated well development, Tang [5] developed the directional hydraulic injection technology to solve the technical problems of highly deviated wells, realizing the natural positioning of the spray gun and avoiding the problem of shooting through thin interlayer in the perforation process. Based on previous studies, on the basis of numerical simulation and field test analysis of Chang 6 reservoir in the L183 area of Huaqing oilfield, this paper discusses the transformation intensity, reasonable flow saturation ratio and advance water injection time of highly deviated wells, and finally realizes the scale benefit development of highly deviated wells in tight reservoirs. Its understanding has important reference significance for the benefit development of highly deviated wells in subsequent tight reservoirs.

2 Reservoir Profile

L183 area of Huaqing district is located in Huachi County, Gansu Province, with an area of about 300 square kilometers, belonging to the Loess Plateau landform. The surface is covered by 100–200 m thick Quaternary loess, with complex terrain, crisscross gullies and uneven ridges. Exposed rocks can be seen in the valley where the river cuts down deeply. The ground elevation is 1350–1660 m, and the relative elevation difference is about 310 m.

L183 area of Huaqing oilfield is located in the south of the slope of Ordos sedimentary basin in Northern Shaanxi [6]. It is a deep-water gravity flow deposit. The structure is a gentle west dipping monocline. The main development layer system is Triassic Yanchang Chang6 oil layer group. The oil layer is stable and thick. The South mainly develops deep Lake sandy debris flow with weak sand carrying capacity, small sand body development scale, thin oil layer, rapid change, interlayer development, reservoir burial depth of 2064 m, and 11.9 m oil layer, The poor oil layer is 4.6 m, the average porosity is 11.6%, the average permeability is 0.28 mD, the oil saturation is 56.87%, the resistivity is 55.41 Ω m, and the acoustic time difference is 225.8 us/m.

3 Well Pattern Transformation of Highly Deviated Well

3.1 Establishing a New Model of Imbibition Displacement in Highly Deviated Wells

According to the driving mechanism of matrix fracture network and Blasingame theory [7, 8], the unstable seepage model of highly deviated wells is derived. According to Fig. 1, the seepage area of highly deviated wells is divided into inner and outer areas. The inner area is artificial fracture network and matrix seepage, and the outer area is mainly matrix seepage. Combined with block reservoir parameters, the zonal seepage theory chart is established.

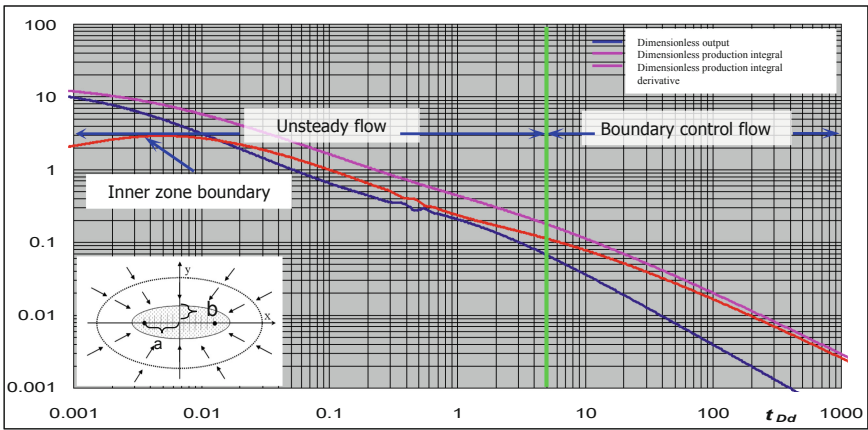


Fig. 1. Zonal seepage theory chart of highly deviated wells.

After high angle volume fracturing, a comprehensive characterization development mode of differential pressure mass transfer and imbibition displacement is established. The fracture network structure is the main control factor affecting matrix fracture mass transfer. After volume fracturing, the oil production rate is the sum of imbibition displacement and differential pressure mass transfer, that is:

$$Q_w = \Delta q + q_w \tag{1}$$

$$q_w = C_f \frac{K_w A}{\mu} (p_f - p_m) \tag{2}$$

where Q_w is the total mass transfer within the scope of large-scale volume transformation of horizontal well, m^3/d ; Δq is the imbibition production rate within the scope of large-scale volume reconstruction of horizontal well, m^3/d ; q_w is the differential pressure mass transfer and oil production rate, m^3/d .

Necessity of highly deviated well

The tight reservoir of the Huaqing oilfield has the characteristics of large oil layer thickness, developed interlayer, large proved undeveloped reserves, and sand body structure mainly of continuous superposition type, as shown in Fig. 2. In view of the development advantages of comprehensive vertical wells and horizontal wells in the reservoir physical properties of the study area, the development mode of highly deviated wells is innovatively proposed to make full use of each small layer, realize the development of multi-layer system, and improve the horizontal and vertical production degree of the reservoir.

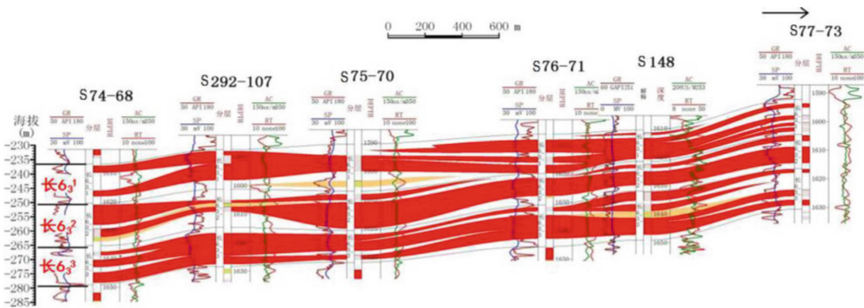


Fig. 2. Profile of Chang 6 reservoir in the L183 area of the Huaqing Oilfield.

The pressure distribution of water drive in 20a through numerical simulation in the study area is shown in Fig. 3. The figure shows that the pressure distribution of highly deviated wells is relatively uniform, and the start-up pressure gradient is higher than that of directional wells and horizontal wells. There is a wide range of low-pressure area near the wellbore of horizontal wells, and the pressure difference in the area is small. While the pressure distribution near directional wells is uneven, the pressure at the edge wells and corner wells of highly deviated wells is low, and the production pressure difference is larger than that of directional wells.

Consequently, the numerical simulation in the study area shows that the reservoirs with thick layers, multiple thin layers and relatively high permeability in Huaqing oilfield have good adaptability for highly deviated wells, greater plane sweep efficiency, greater start-up pressure gradient and more uniform seepage field.

According to Fig. 4, it can be proved theoretically that the highly deviated well on the plane has realized the transformation from conventional fracturing to single sand body volume fracturing. A single fracture is generated after conventional fracturing on the profile, while independent multiple fractures are formed in highly deviated wells.

In order to improve the production degree of reserves, oil production rate and single well production, the development mode of highly deviated wells is optimized for the thick oil reservoir developed in Huaqing Chang 6 inter-layer.

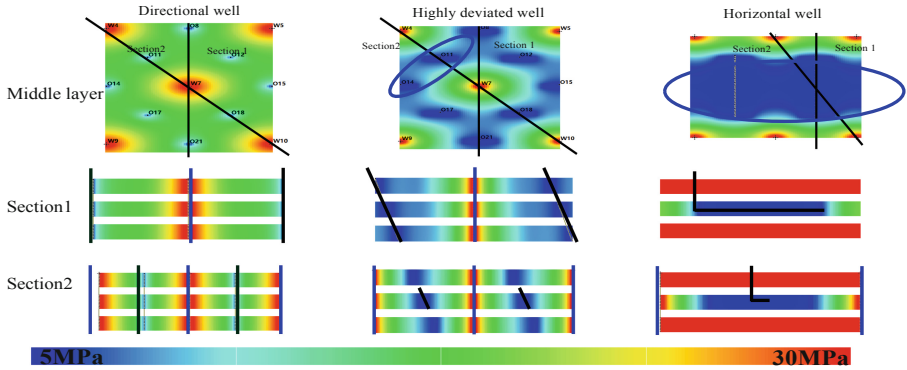


Fig. 3. Numerical simulation pressure distribution of Chang 6 in the L183 area of Huaqing oilfield (20 years of water drive).

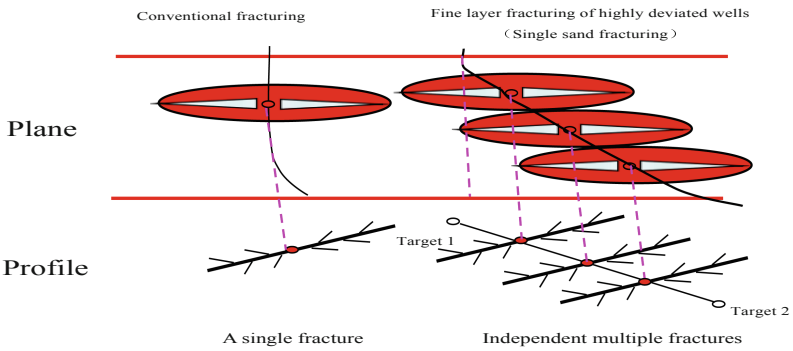


Fig. 4. Schematic diagram of theoretical volume fracturing for highly deviated wells.

3.2 Selection of Well Pattern

Selection of well pattern and well type the reservoir physical property of Huaqing oilfield is poor, and there are contradictions in the development process, such as slow establishment of effective displacement system and rapid production decline. Thus, the three well patterns of rhombus reverse nine-spot well pattern, five-spot well pattern and rectangular well pattern are optimized. The results of numerical simulation are shown in Fig. 5 and Fig. 6. The five-spot well pattern has a large number of water injection wells and a small distribution of residual oil. The rhombus reverse nine-spot well pattern and rectangular well pattern have obvious distribution of residual oil. Controlled by the well pattern, the residual oil is enriched near the corner well, but the pressure distribution of rectangular well pattern is more uniform than that of rectangular well pattern.

In combination with the development characteristics of natural fractures and the current principal stress direction in Huaqing area [9], the well pattern adjustment in this area is designed and optimized to make it easier to establish a displacement system between oil and water wells and extend the stable production time. The well pattern distribution of Huaqing tight reservoir is related to the fracture density and reservoir

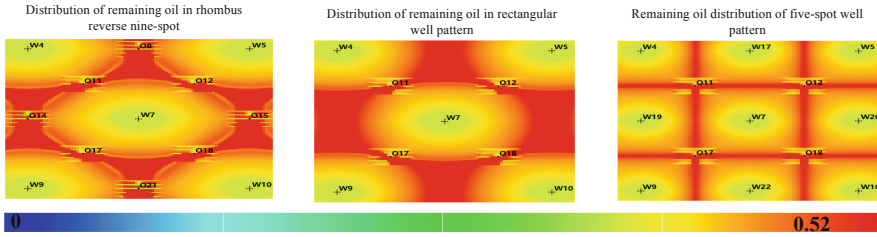


Fig. 5. Numerical simulation of Chang 6 in the L183 area of Huaqing Oilfield.

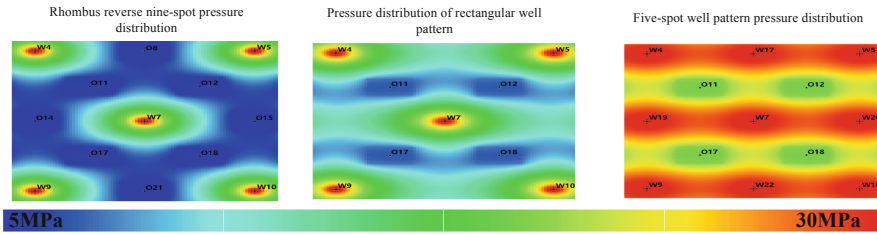


Fig. 6. Numerical simulation of Chang 6 in L183 area of Huaqing Oilfield.

matrix permeability, and the tight reservoir has obvious non Darcy seepage characteristics, Therefore, it is necessary to calculate the formation pressure distribution curves between water injection wells and oil production wells under different well row spacing. According to the starting pressure gradient under different permeability (Fig. 7), the well spacing of rectangular well pattern of highly deviated wells is determined to be 400 m. Draw the chart of the relationship between fracture bandwidth and single section production (Fig. 8), determine that the effective width of artificial fracture is about 10 m, and determine that the row spacing is 120–160 m in combination with the length of the inclined section of highly deviated wells of 80–100 m.

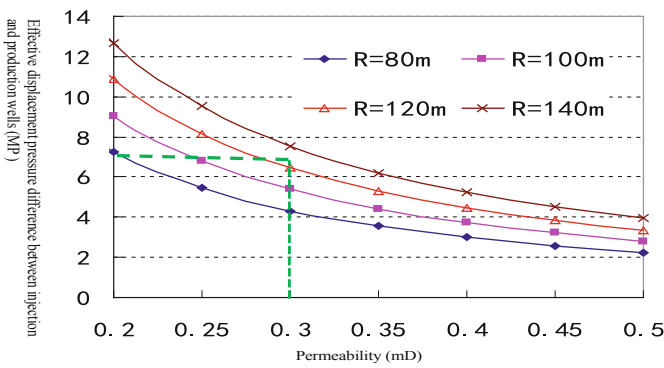


Fig. 7. Effective displacement injection production differential pressure and permeability chart.

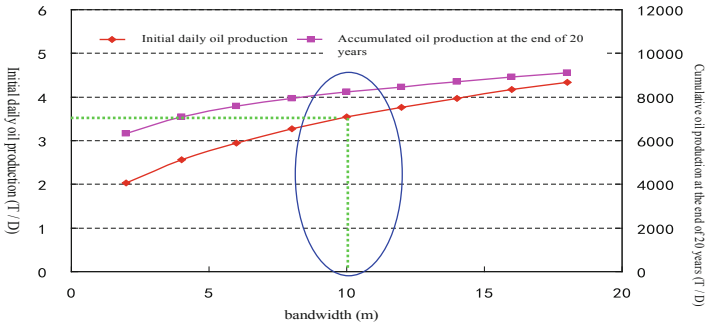


Fig. 8. Single section production with different average fracture bandwidth.

4 Large Scale Application of Highly Deviated Wells to Enhance Oil Recovery

4.1 Reconstruction Strength in the L183 Area

Referring to the idea of large-scale reservoir reconstruction of horizontal wells, aiming at the reservoir with multi-layer system production and high level of horizontal and vertical production, the technical idea of hydraulic injection, fine multi-stage and interference fracturing is adopted as a whole to form the development mode of highly deviated wells in tight reservoir of Huaqing Oilfield: (1) single point centralized perforation: the point source fracture is achieved through hydraulic multi-stage perforation, making the artificial fracture easy to be controlled and extended; (2) Vertical layered fracturing: use the reservoir at the geological “sweet spot” and the corresponding place of injection and production to realize fine multi-stage fracturing; (3) Large displacement fracturing: it is similar to multi-stage and multi cluster fracturing in the horizontal well layer, increasing the three-dimensional complexity of fractures.

By establishing the fracturing geological model in the study area, the numerical simulation software and fracturing software are comprehensively used to optimize the key parameters. See Fig. 9 and Table 1 for details, so as to realize the replacement of natural fractures by artificial fractures. Finally, it is determined that the reconstruction technology is mainly conventional hydraulic jet staged fracturing, with the fracturing fluid of biological glue and EM30 + fracturing fluid. The number of fracturing sections is 4–8, and the single well sanding section is 57–63 m³, the discharge capacity is 4–6 m³/min, the sand ratio is 19.0–25.0%, and the amount of liquid entering the ground is 2300–2500 m³.

Based on the mature experience of the test of changing the water injection development mode [10] (Fig. 10), the well is blocked after fracturing. The actual average number of fracturing sections of 139 highly deviated wells in the test area is 5.6, the average sand addition per well is 352 m³ (single section 63 m³), the average sand ratio is 19.6%, the displacement is 5.7 m³/min, the amount of ground fluid is 2500 m³ (single section 446 m³), and the average single well is blocked for more than 20 days.

It is proved that the scale of reservoir reconstruction is in direct proportion to daily oil production through the scatter relation diagram of single section fluid inflow and daily

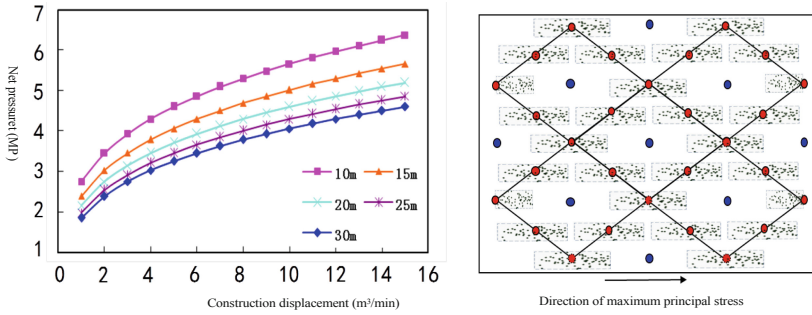


Fig. 9. Net pressure chart and large-scale molded fracture network matching chart of reservoirs with different thickness and different displacement in the study area.

Table 1. Parameters of volume fracturing in highly deviated well area.

well number	number of clusters	sand quantity m ³	sand ratio %	displacement m ³ /min	fracture pressure MPa	working pressure MPa	Single section liquid inflow m ³	flowback liquid volume m ³
1	6	42.5	17.9	6.0	91.3	63.9	479.2	54.6
2	5	52.0	19.8	6.0	71.2	54.4	354.1	71.0
3	6	60.8	18.6	5.0	79.4	58.2	496.5	86.3
4	6	43.3	19.5	6.0	72.0	43.9	318.6	59.7
5	6	54.2	18.2	5.0	75.9	57.8	398.5	72.7
6	5	64.0	19.6	6.0	68.3	47.2	430.2	81.1

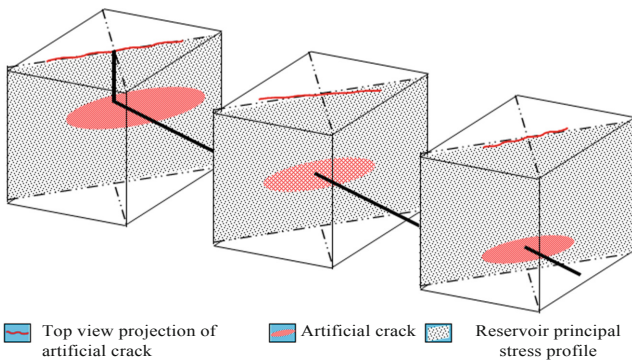


Fig. 10. Schematic diagram of highly deviated well + hydraulic jet staged fracturing process in the L183 area.

oil production and the scatter relation diagram of displacement and daily oil production (Fig. 11). Contrary to the conventional understanding, the greater the displacement in the study area, the lower the water cut. The large displacement reconstruction forms a wide fracture instead of extending the fracture to the far end. The transformation near the perforated section can be fully carried out without affecting the water cut while extracting the liquid.

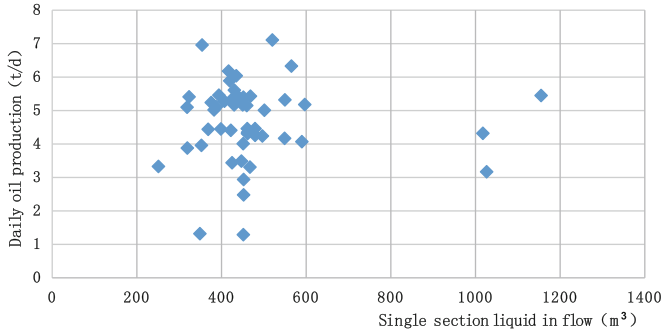


Fig. 11. Scatter diagram of single section liquid inflow and daily oil production.

The perforation control degree parameter introduced in this paper is shown in Fig. 12, that is, the effective oil layer length divided by the number of perforated sections represents that a single perforated section controls the oil layer length. The smaller the controlled oil layer length of a single perforated section, the better the reservoir reconstruction effect. Combined with the concept of reducing the number of fracturing sections by controlling the cost, the optimal result is 10–20 M/piece.

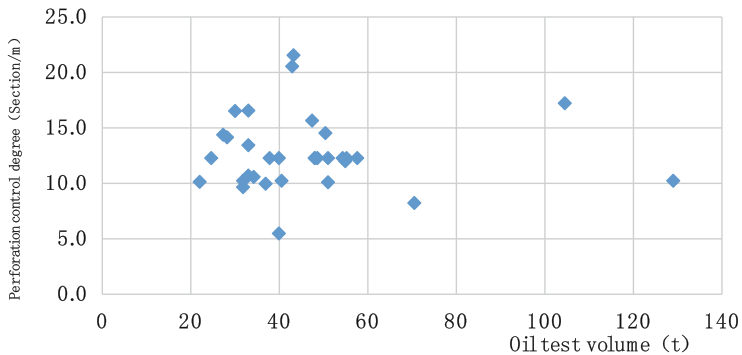


Fig. 12. Scatter diagram of perforation control degree and oil testing volume.

L183 area of the Huaqing oilfield adheres to the development technical policy of “fine layering, small water volume, long period and plane equilibrium” advanced water injection and coiled tubing + closed well. The pressure level is maintained at more than 120% (Fig. 13). The formation energy is sufficient, and all water injection wells adopt

separate injection in 2–3 layers. The vertical water absorption is uniform, the water drive control degree reaches 72.4%, and the dynamic liquid level is maintained at about 1000 m.

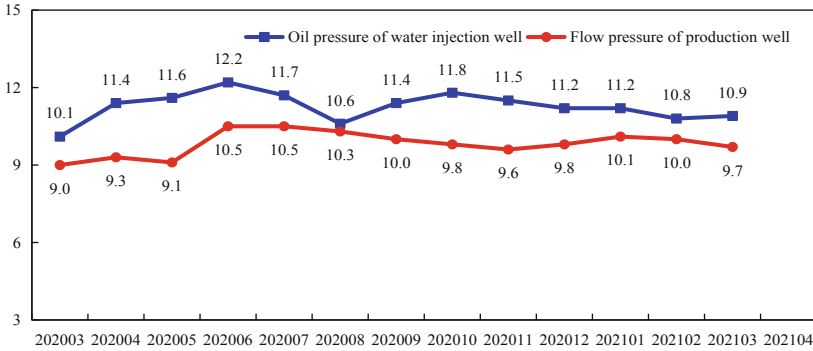


Fig. 13. Variation curve of oil pressure of water injection well and flow pressure of production well in highly deviated well in the L183 area.

4.2 Reasonable Flow Saturation Ratio in the L183 Area

The correlation analysis between the flow saturation ratio and single well production in the Chang 6 highly deviated area of the Huaqing L183 area shows that when the flow saturation ratio is less than 0.8, the single well production is between 4.0–5.0 t, and the benefit is maximized. According to the analysis of single well B299-54X, there is no obvious decline when the flow saturation ratio is about 1.0 (Figs. 14 and 15).

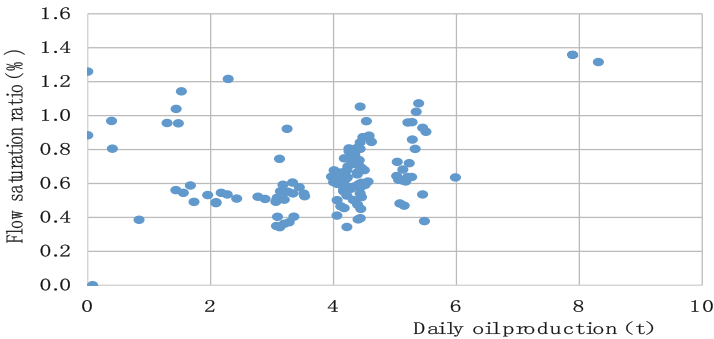


Fig. 14. Scatter diagram of well flow saturation ratio and daily oil production in the L183 area.

Through the industrial profile test (Table 2, Fig. 16), the vertical oil layers are fully utilized, and the vertical production degree of the reservoir is increased to more than 80%. Compared with adjacent horizontal wells, highly deviated wells produce 0.9t ↑ 3.5t oil in 100m horizontal section, and the initial oil production rate is 0.7% ↑ 1.8%.

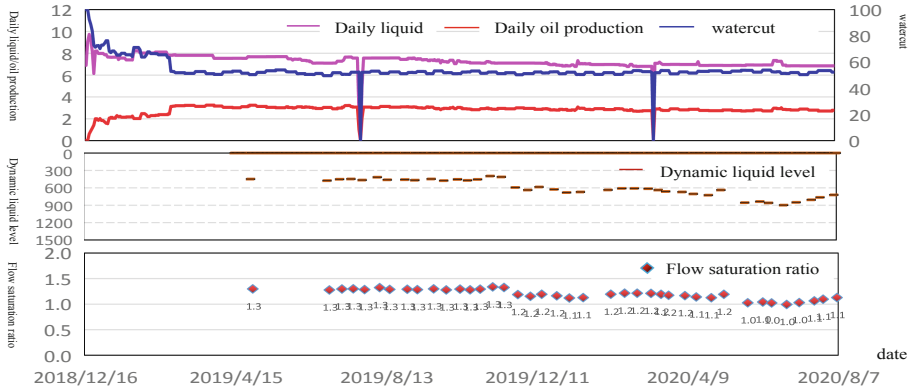


Fig. 15. Production curve of well B299-54X.

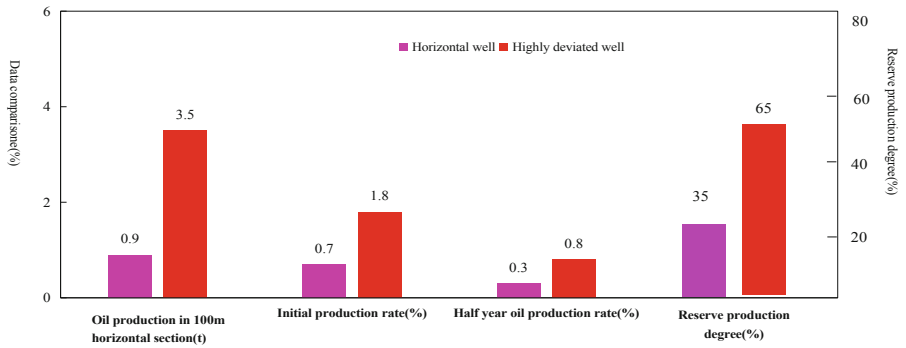


Fig. 16. Comparison histogram of highly deviated wells and surrounding horizontal wells.

Table 2. Production interpretation results of B184-107X well.

number	Perforation point m	Daily water production m ³ /d	Daily oil production m ³ /d	Liquid production m ³ /d	Moisture content %	Relative liquid production %
1	2223.0	0.61	1.74	2.35	26.11	24.33
2	2238.0	0.47	1.36	1.83	25.63	18.94
3	2265.0	0.49	1.40	1.89	25.77	19.57
4	2281.0	0.47	1.37	1.84	25.64	19.05
5	2294.0	0.45	1.30	1.75	25.63	18.12
total		2.49	7.17	9.66	25.78	100

Production decline law in the L183 area

The production change of highly deviated wells in the L183 area conforms to the law of exponential decline, as shown in Fig. 17. The production decline is 10.9% in half a year, 30.8% in one year, and the water cut is stable at about 25%, which is in the early decline stage as a whole.

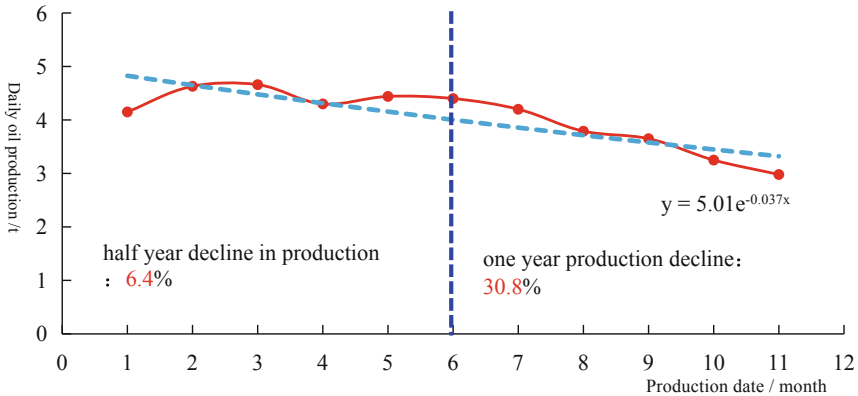


Fig. 17. Pull up curve of daily oil production and production of highly deviated wells in the L183 area.

5 Conclusion

- (1) The tight reservoir in the Huaqing oilfield has poor physical properties, strong heterogeneity and natural fractures, but relatively high permeability sections are developed in many sets of small layers in the study area. The numerical simulation results show that highly deviated wells have feasibility and superiority in the development of tight reservoirs.
- (2) The highly deviated wells in the study area are developed by advanced fine layered water injection, and the regional formation pressure is maintained at a level of more than 120%. The seepage range is increased and the oil production rate is greatly improved by using the imbibition displacement effect of closed wells.
- (3) The development of highly deviated wells in the study area changes the relationship between reservoir reconstruction fractures and oil layers from two-dimensional level to three-dimensional level through the change of well pattern. Through numerical simulation combined with actual field test results, it is proved that the idea of reducing the number of fracturing sections in highly deviated well area combined with cost control can maximize the benefit when the optimal perforation control result is 10–20 m/well and the reasonable flow saturation ratio is less than 1.0.
- (4) At the initial stage, the average daily oil production of a single well in the study area is 4.0 t, the initial production of highly deviated wells is 2.0–2.4 times that of surrounding directional wells, the initial oil production rate is increased from 0.8–1.0% to 2.0–2.3%, and the oil production rate and single well production of the block are significantly increased.

References

1. Li, K.: Dynamic Analysis of unstable pressure in highly deviated wells in fractured-vuggy carbonate gas reservoir. *Henan Sci. Technol.* **35**, 105–109 (2021)
2. Lai, Q., Tang, J., Wu, Y.Y.: Numerical simulation of dual laterolog response and resistivity anisotropy correction method in highly deviated wells. *Petrol. Geophys. Explor.* **57**, 706–712 (2022)
3. Yu, T.W.: Research and application of trajectory control technology for highly deviated well SX5056. *West-China Explor. Eng.* **34**, 68–70 (2022)
4. Song, J.Y., Yao, M., Jing, W.P.: Calcic interbed evaluation and multi-stage frac optimization for highdeviation wells in Chang7 reservoir. *Drill. Eng.* **48**, 29–35 (2021)
5. Tang, C.H.: Research and application of hydraulic jet fracturing in thin interlayer of highly deviated wells. *Inner Mongolia Petrochem. Indust.* **3**, 116–118 (2020)
6. Wang, C., Wang, M.Y., Chen, J.: Research and application of large-scale volume fracturing technology for horizontal wells in ultra-low permeability reservoirs. In: *Proceedings of 2021 International Conference on Oil and Gas Field Exploration and Development* (2019)
7. Jiang, H., Xu, Y., Wen, D.W.: Analysis of matrix fracture percolation law of volume fracturing in horizontal wells. *J. Xi'an Petrol. Univ. (Nat. Sci. Edn.)* **34**, 49–55 (2019)
8. Gong, L.H., Liu, J.Z., Wu, X.: Study on percolation characteristics of matrix fracture fluid in CO₂ huff and puff fractured tight reservoir. *Spec. Reserv.* **28**, 118–124 (2021)
9. Asai, P., Panja, P., Velasco, R.: Fluid flow distribution in fractures for a doublet system in Enhanced Geothermal Systems (EGS). *Geothermics* **75**, 171–179 (2018)
10. Wang, F.F., Yang, K.: Influence of pore throat size distribution on oil displacement by spontaneous imbibition in tight oil reservoirs. *Lithol. Reserv.* **33**, 155–162 (2021)



Suitability Evaluation of Subsurface Space Development and Utilization in Langfang North Three Counties, Hebei Province

Dong Du^{1,2,3,4}✉, Xinliang Guo⁵, Yaonan Bai^{1,2,3,4}, Chuanming Ma⁶,
Hongwei Liu^{1,2,3,4}, Jinjie Miao^{1,2,3,4}, and Jing Zhang^{1,2,3,4}

¹ Tianjin Center, China Geological Survey, Tianjin 300170, China
303540216@qq.com

² North China Center for Geoscience Innovation Precambrian Research Centre,
China Geological Survey, Tianjin 300170, China

³ Xiongan Urban Geological Research Center, China Geological Survey, Tianjin 300170, China

⁴ Tianjin Key Laboratory of Coast Geological Processes and Environmental Safety,
Tianjin 300170, China

⁵ Shandong Geo-Mineral New Energy Co., Ltd., Jinan 250102, Shandong, China

⁶ China University of Geosciences (Wuhan), Wuhan 430074, China

Abstract. This article is on the basis of the analysis of geological environmental factors such as topography, engineering geology, hydrogeology, and geological environmental issues in the Langfang north three counties, Hebei Province. According to the study of the interaction between geological environment elements and subsurface space development, a geological environment suitability evaluation index system for different depths of subsurface space development has been established. This article evaluates the suitability of the development and utilization of the shallow (0 ~ -18m), medium(-22 ~ -50 m) and deep (Below 70 m) subsurface space at different depths in this area according to the four levels of unsuitable, less appropriate, more appropriate and appropriate by the analytic hierarchy process. The results show that more than 70% of shallow and deep layers the study area is suitable or more suitable for the development and utilization of subsurface space. Among them, the suitable area for shallow subsurface space development accounts for 31.23%, the more suitable area accounts for 53.63%, the less suitable area accounts for 12.27%, and the unsuitable area accounts for 2.87%; The middle suitable area accounts for 7.45%, the more suitable area accounts for 46.61%, and the less suitable area accounts for 34.48%; The proportion of unsuitable areas is 11.95%; The deep suitable area accounts for 30.81%, the more suitable area accounts for 43.86%, and the less suitable area accounts for 22.72%; The proportion of unsuitable areas is 2.62%. The evaluation results can provide geoscientific basis for the planning of subsurface space development and utilization in the study area.

Keywords: Underground Space · Geological Environment · Analytic Hierarchy Process · Suitability · Langfang North Three Counties

1 Introduction

With the continuous deepening of the urbanization process, “urban diseases” such as population expansion, housing shortage, and traffic congestion are increasingly prominent. At the same time, the development of cities is also undergoing a transformation from extension expansion to connotation upgrading. Cities are no longer planar expansion, which requires scientific territorial space planning for development within limited space. Nowadays, the comprehensive utilization of subsurface space is considered to be an effective solution [1, 2]. As an effective way to solve the “city illness”, the development and utilization of underground space has reached an unprecedented scale [3], its development and utilization methods are becoming increasingly diverse [4]. Subsurface space resources are one of the precious natural resources in the surface substrate layer. As an important component of urban organisms, they will play a pivotal role in future urban construction [5]. The development and utilization of urban subsurface space plays an important role in improving land utilization efficiency, saving land resources, improving urban transportation, expanding infrastructure capacity, increasing urban green space, maintaining historical and cultural characteristics, reducing environmental pollution, and improving ecological landscape [6, 7]. However, as an important land space resource [8, 9], subsurface space development is irreversible, and unreasonable development will cause a huge waste of valuable underground resources [10, 11]. In order to improve the rational development and orderly utilization of underground space resources, it is necessary to conduct a preliminary evaluation of the suitability of underground space development and utilization [12, 13]. In the past process of geological environment assessment, the constant weight vectors calculated through Analytic Hierarchy Process, Principal Component Analysis, and other methods, although to some extent reflecting the effect of multi-factors on the target, ignored the impact of internal differences in indicators. In order to make up for this limitation of constant weight, this evaluation introduced the idea of using variable weights. With the proposal of the non-capital function alleviation strategy, the coordinated development planning of the northern three counties of Langfang in Hebei and Tongzhou District in Beijing has become an important undertaking area for the transfer and upgrading of non-capital function industries in Beijing. In order to fully improve land use efficiency, save land resources, and improve urban transportation, it is of great significance to conduct an evaluation of the suitability of subsurface space development and utilization in this area.

2 General Situation

The study area is located at the junction of Tongzhou District in Beijing and Tianjin City, including Sanhe City, Dachang Hui nationality County, Xianghe County, and other three counties (referred to as the North Three Counties of Langfang City). It is the east gate of the capital Beijing. Located 16 km north of Capital Airport and 100 km east of Tianjin Tanggu Port, it is the core hub of the Bohai Rim Economic Circle. The research area covers an area of about 1258 square kilometers, with an overall terrain that is high in the north and low in the south. The average altitude is generally 5.9 to 31.9 m, the natural longitudinal slope of the ground is about 0.66‰, and the annual average precipitation is 584.6 mm (Fig. 1).

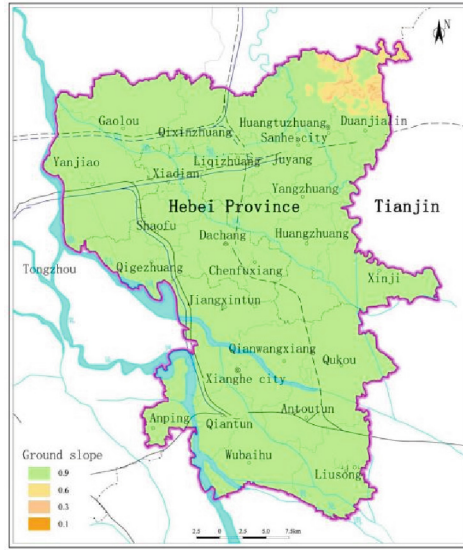


Fig. 1. Map of the study area and ground surface slope.

3 Geological Environmental Conditions

The study area is located in the north central part of the North China landmass, the western section of the Mesozoic Cenozoic intracontinental orogenic belt in the Yanshan Mountains. The main faults include Yanjiao fault, Xiadian fault, Nankou Sunhe fault, Xianghe fault, etc. Quaternary sediments are generally exposed on the surface, and the main strata buried at a depth of 50 m or less include artificial fill, modern riverbed alluvial, river alluvial, lacustrine deposits, and proluvial deposits [14, 15]. The area mainly exploits Quaternary aquifer pore groundwater with a buried depth of less than 300 m [16]. The main environmental geological issues existing in the area including active faults, ground subsidence, ground fissures, karst collapse, sand liquefaction, etc. [17].

The Quaternary system is widely distributed in the research area, consisting of the Chaobai River alluvial fan, and is divided into 8 engineering geological layers from top to bottom at a depth of 80 m. The engineering geological factors that have an impact on the development of subsurface space in the study area include the bearing capacity of rock and soil, soil uniformity, sand liquefaction, and crustal stability. Hydrogeology mainly includes factors such as groundwater level, aquifer thickness and Aquifer water abundance. The groundwater level in the study area has a great impact on the development and utilization of underground structures. Areas with aquifer thickness of huge thickness and strong water yield are mainly spread on both sides of the river. Karst areas are mainly distributed near Gaolou Town and Qixinzhuang Town. The areas with severe land subsidence are mainly distributed around Yanjiao Town.

4 Suitability Evaluation of Underground Space

4.1 Evaluation Method

Rational utilization of subsurface space is an important issue facing modern urban management [18, 19], especially with the continuous consumption of shallow and central underground space resources, the development and utilization of subsurface space will develop and extend to deeper layers [20], the evaluation of the suitability of subsurface space development and utilization is a complex systematic work under the influence of multiple sources of influencing factors [21], due to the different geological environment characteristics faced by different regions, the factors affecting the development and utilization of underground space are also different, so selected the evaluation index system and method are different. For example, the main factors affecting of the exploiting of subsurface space in bedrock areas are karst collapse, active faults, etc. The influencing factors in plain areas are much more complex, such as seawater intrusion and its corrosivity, the thickness of muddy soil and its engineering geological characteristics, and land subsidence in coastal areas [22]. This evaluation mainly involves factors affecting the topography, engineering geology, hydrogeology, geological environmental issues, and other aspects of the plain area. Each indicator includes several secondary evaluation indicators (Table 3). For the evaluation work under the influence of multiple sources and complex influences, it is necessary to conduct hierarchical decomposition of the overall evaluation under the guidance of system thinking [23]. This paper establishes a multi-level indicator system based on the idea of analytic hierarchy process. Variable weight theory is used to quantify and determine the weight of indicators. Finally, a sensitivity factor comprehensive index variable weight evaluation former is used to obtain the suitability evaluation results.

Method Selection. Analytic Hierarchy Process (AHP) is a systematic, hierarchical, qualitative and quantitative analysis method that combines simple principles and well-knit theory foundation. A large number of practical cases have also confirmed that Analytic Hierarchy Process is very practical and effective for solving complex multi-objective decision-making problems, especially for system problems with both qualitative and quantitative indicators [24]. The AHP is based on a systematic analysis of the essence and influencing factors of complex multi-objective decision-making problems, decomposing them into levels such as goals, criteria, and plans, and then conducting qualitative and quantitative analysis. The basic steps include: Establish a hierarchical model, construct a paired comparison matrix, calculate weight vectors under a single criterion, and verify consistency.

- (1) Hierarchy model establishment

Analyze the essential issues and influencing factors of the system, and then construct a multi-level model. A complete structural model contains target layer, criterion layer, and scheme layer. The division of importance is based on a 1–9 scale method (Table 1).

Table 1. Scale and meaning of judgment matrix.

Mark	Implications
1	Both factors are equally important
3	Compared to two factors, one is slightly more important than the other
5	Compared to two factors, one is significantly more important than the other
7	Compared to two factors, one is more important than the other
9	Compared to two factors, one is extremely important than the other
2 4 6 8	Intermediate value of the above two adjacent judgments
count backwards	If the importance of A_i compared to A_j is a_{ij} , then A_j compared to A_i is $a_{ji} = 1/a_{ij}$

Determine the relative importance of the influencing factors according to Table 1, and construct a judgment matrix A:

$$A = \begin{bmatrix} a_{11} & \cdots & a_{1n} \\ \vdots & \ddots & \vdots \\ a_{n1} & \cdots & a_{nn} \end{bmatrix}$$

- (2) Calculate weight vector

The weight vector is calculated using the geometric average method. First, the geometric average of each row vector of the judgment matrix A is calculated, and then the weight vector is obtained through normalization ω_i :

$$\omega_i = \frac{\left(\prod_{j=1}^n a_{ij}\right)^{\frac{1}{n}}}{\sum_{k=1}^n \left(\prod_{j=1}^n a_{kj}\right)^{\frac{1}{n}}} \quad i = 1, 2, 3, \dots, n$$

- (3) Checking the consistency of the judgment matrix

First, calculate the consistency indicator CI:

$$CI = \frac{\lambda_{\max} - n}{n - 1}$$

Find the average random consistency index RI and calculate the random consistency ratio CR according to Table 2.

When $CR = \frac{CI}{RI} < 0.1$, the judgment matrix is considered to meet the consistency requirements; When $CR \geq 0.1$, the judgment matrix should be modified again.

Evaluation Steps. 1. Based on the actual situation of protecting the aquifer in the research area and the principle of layered utilization of underground space in the “Urban Underground Space Planning Standard”, the geological environment assessment of

Table 2. Random consistency index.

Matrix order	1	2	3	4
RI	0	0	0.58	0.89
Matrix order	5	6	7	8
RI	1.12	1.26	1.36	1.41

underground space in the study area is separated into shallow layer (0 ~ -18 m), middle layer (-22 ~ -50 m), and deep layer (below 70 m).

2. Analyze and select the geological environmental factors that affect the development of subsurface space in each layer of the study area as evaluation indicators, divide them into sensitive factors and important factors, and classify and standardize the important factors.

3. The weight of evaluation indicators is determined using analytic hierarchy process.

4. Using MapGIS to vectorize the layers of each evaluation index, perform attribute assignment and spatial analysis to obtain the geological environment suitability evaluation unit.

5. Calculate the index variable weight of each evaluation unit based on the evaluation index grade.

6. Calculate the comprehensive index of each evaluation unit, formulate evaluation criteria, and partition to obtain a geological environment suitability zoning map.

7. The final evaluation result is obtained by stacking sensitive factors on the geological environment suitability zoning map.

4.2 Selection of Evaluation Index System

The evaluation index system for this project is according to the collection and organization of relevant data, summarizing the geological environment factors that affect the development of subsurface space, and then deeply analyzing their mutual constraints with the development of underground space. Combining the characteristics of the geological environment in the research area, a geological environment suitability evaluation index library for underground space development has been constructed. At the same time, the evaluation indicator system follows the three principles of “high potential risk, large impact range, and accessible data” to screen indicators [25–27]. The geological environment factors that affect the development of underground space in the study area are selected for this evaluation. The evaluation work has established an evaluation index system based on reflecting the special geological environment in the study area, the research level of the results and data, and comprehensive, scientific, reasonable, and practical aspects. It mainly includes four categories of first-class indicators, namely, terrain and geomorphology, engineering geological conditions, hydrogeological conditions, and environmental geological issues. The terrain and geomorphology mainly consider the terrain slope as a secondary indicator, the engineering geological conditions mainly consider the bearing capacity of rock and soil mass, soil homogeneity, crustal

stability (including sensitive indicators such as active fractures and karst collapse), and sand liquefaction as a secondary indicator, and the hydrogeological conditions mainly consider the phreatic water depth, aquifer water yield, aquifer thickness, and groundwater corrosivity as a secondary indicator, Geological environment issues mainly consider the ground elevation as a secondary indicator (Table 3).

4.3 Index Standardization and Determination of Weight

Based on the actual situation of relevant research and research areas at home and abroad, each index is divided four levels: I (excellent), II (good), III (average), and IV (poor) [28–31]. In order to facilitate the evaluation work, it is necessary to standardize and assign values. According to the classification of evaluation index grades, I (excellent), II (good), III (general), and IV (poor) are assigned values of 0.9, 0.6, 0.3, and 0.1, respectively. Based on the analytic hierarchy process, this study divides the evaluation indicators for the suitability of underground space development and utilization in the research area into target layer, primary index, and second level index. First, construct the judgment matrix of the secondary index, then construct the corresponding judgment matrix of the tertiary indicator layer within each secondary indicator, and finally obtain the weight of each evaluation indicator based on the judgment matrix (Table 3).

4.4 Comprehensive Evaluation

According to the actual situation of geological environment conditions of the study area, active faults and karst collapse areas are selected as sensitive indicators. The impact range of active faults refers to the minimum avoidance distance specified in the Code for Seismic Design of Buildings. Areas within 100 m of active faults are classified as sensitive factors, and areas where sensitive factors exist are directly classified as unsuitable areas. Comprehensive evaluation refers to the superposition of sensitive indicators on the basis of the evaluation results of various indicators to finally obtain suitable zones, which are divided into four levels, namely, unsuitable zones (evaluation score < 0.5), less suitable zones (evaluation score 0.5 to 0.6), more suitable zones (evaluation score 0.6 to 0.7), and suitable zones (evaluation score > 0.7).

5 Evaluation Results

The evaluation results show that: the suitable area for developing shallow underground space is 398.76 km², proportion 31.23%; The relatively suitable area is 684.86 km², proportion 63.63%; The area of the less suitable area is 156.73 km², proportion 12.27%; The area of the unsuitable area is 36.64 km², proportion 2.87%. Unsuitable areas for the development and utilization of shallow subsurface space are mainly distributed in Gaolou Town, Qixinzhuang Town, and some areas of Xianghe County in the south of the study area (Fig. 2). The main factors affecting unsuitability include poor crustal stability, land subsidence, high water yield in aquifers, active fractures, and liquefaction of sand.

The suitable area for the middle layer is 95.18 km², proportion 7.45%; The relatively suitable area is 595.21 km², proportion 46.61%; The area of the less suitable

area is 440.27 km², proportion 34.48%; The area of the unsuitable area is 152.59 km², proportion 11.59%. Unsuitable areas for the development and utilization of middle-level subsurface space are mainly distributed on both sides of the Yanjiao fault zone, in the southwest of Yangzhuang Town, in Qixinzhuang Town, Sanhe City, in the north of Gaolou Town, and in the south of Huangzhuang Town. The main factors affecting unsuitability include poor crustal stability, land subsidence, active fractures, karst collapse, and sand liquefaction (Fig. 3).

Table 3. Evaluation index system and weight. [32]

Target layer	1st index(B)	Secondary indicators(C)	Index grading standards and grades				Weight				
			Depth	I(excellent)	II (good)	III (General)	IV (poor)	Shallow	Middle	Deep	
Layered evaluation of the suitability of underground space development and utilization(A)	Geomorphological(B1)	Terrain slope/(°) (C1)	/	<5	5-15	15-25	>25	0.0465	0.0349	0.0279	
		Engineering geological conditions (B2)	Bearing capacity of rock and soil mass/KPa (C2)	/	>200	160-200	120-160	<120	0.1200	0.1200	0.1200
			Soil uniformity (C3)	/	Monolayer (Silt)	Double layer (fine sand, silt or silt, silty clay)	three layers (Silt, silty sand Interbedding)	Multilayer (upper silty clay, lower fines and, medium coarse sand nterbedding)	0.0645	0.0645	0.0645
			Crustal stability (including sensitive indicators such as active faults and karst collapse) (C4)	/	Stabilize	Relatively stable	Less stable	Instability	0.1200	0.1200	0.1200
			Sand liquefaction (C5)	/	No liquefaction	Slight liquefaction	Moderate liquefaction	Easily liquefiable	0.2234	0.2234	0.2234
	Hydrogeological conditions(B3)	Phreatic water depth/m (C6)	Shallow	>15	15-10	10-5	<5	0.0556			
			middle	>30	30-25	25-20	<20		0.0556		
		Aquifer water yield/m ³ /d (C7)	/	<500	500-1000	1000-3000	>3000	0.0393	0.0393	0.0543	
		aquifer thickness/m (C8)	/	<5	5-10	10-15	>15	0.0870	0.0870	0.0987	
	Geological environmental issues(B4)	land bsidence/mm/y (C10)	/	< 10	10-30	30-50	>50	0.0931	0.1047	0.1117	

Note: “/” Indicates that this indicator is used in the suitability evaluation of shallow, medium, and deep underground spaces

The deep suitable area is 393.38 km², proportion 30.81%; The relatively suitable area is 560.06 km², proportion 43.86%; The area of the less suitable area is 290.11 km², proportion 22.72%; The area of the unsuitable area is 33.43 km², proportion 2.62%. Unsuitable areas for the development and utilization of deep subsurface space are mainly distributed in Qixinzhuang Town, Sanhe City, in the north of Gaolou Town, and on both sides of the Yanjiao Fault and Xiadian Fault zones. The main influencing factors for

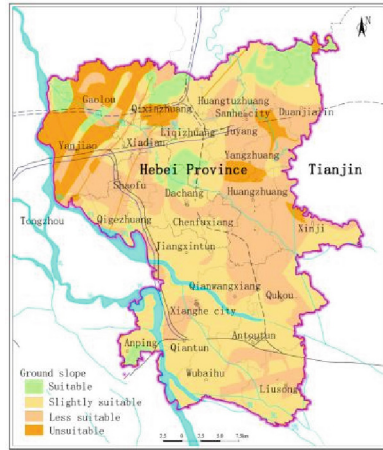
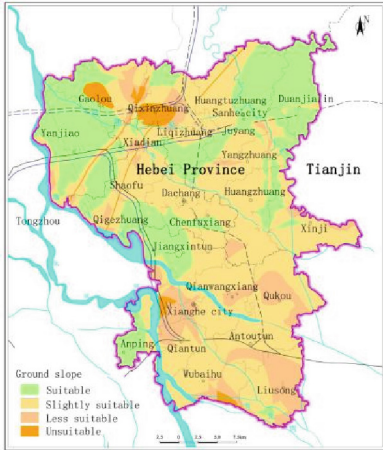


Fig. 2. Geological environment suitability zoning map for shallow depth underground space development.

Fig. 3. Geological environment suitability zoning map for development of middle depth subsurface space

unsuitability include karst collapse, high water yield in aquifers, land subsidence, active fractures, etc. (Fig. 4).

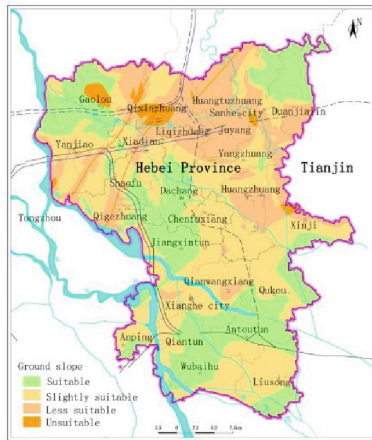


Fig. 4. Geological environment suitability zoning map for deep depth underground space development.

6 Recommendations

Based on the analytic hierarchy process, the suitability evaluation of subsurface space development and utilization in three different depths, namely shallow, medium, and deep, was conducted in the northern three counties of Langfang, Hebei Province. The results

showed that over 70% of the shallow and deep areas in the study area were suitable or more suitable for subsurface space development and utilization. For unsuitable areas, it is important to pay attention to the main factors affecting the development of subsurface space, such as active fractures, karst collapse, land subsidence, sand liquefaction, and ground fissures. Corresponding preventive measures should be taken when developing and utilizing subsurface space. The evaluation results can provide a reference for the rational development and utilization of subsurface space in this area.

Acknowledgements. This study was funded by the China Geological Survey (project DD20221727, DD20230438 and DD20190251).

References

1. Yang, W.C., Tian, G., Xia, J.H., et al.: Prospects for development and utilization of urban underground space in hilly areas of South China. *China Geol.* **46**(3), 447–454 (2019)
2. Li, X.Z., Wang, R., Gu, Q., et al.: Strategic needs for urban underground space development. *Earth Sci. Front.* **26**(3), 32–38 (2019)
3. Cheng, G.H., Wang, R., Zhao, M.H., et al.: Current situation and development trend of urban underground space development and utilization in China. *Earth Sci. Front.* **26**(3), 39–47 (2019)
4. Guo, C.B., Wang, Z.H., Liu, K., et al.: Application and research status of special underground space. *China Geol.* **46**(3), 482–492 (2019)
5. Tang, X., Gong, X.L., Xu, S.G., Zhang, Q.Q., Guo, H., Deng, F.L.: Current situation of urban underground space resources development and utilization in southern Jiangsu metropolitan area and countermeasures for geological investigation. *Geol. Rev.* **68**(2), 593–605 (2022)
6. Li, P.Y., et al.: Geological suitability evaluation of underground space development and utilization in mountain front alluvial flat prototype cities: a case study of Chengdu city. *Geol. Bull.* **40**(10), 1644–1655 (2021)
7. Wang, X.S., Li, B.X., Li, Y., Jiang, X., Jiang, C.X., Gao, J.: Chemical characteristics and genetic analysis of quaternary groundwater in Tongzhou district Beijing. *J. Irrig. Drain.* **41**(3), 92–97 (2022)
8. Xing, H.X., Dou, F.F., Ge, W.Y., Hua, J., Chang, X.J., Cai, X.H.: Study on the three-dimensional evaluation index system of geological suitability for urban underground space development and utilization: a case study of Hangzhou city. *Geol. Rev.* **68**(2), 607–614 (2022)
9. Yang, R.S., Wang, Y.B.: Understanding and thinking on service safety of underground space engineering. *J. Eng. Sci.* **44**(4), 487–495 (2022)
10. Ge, W.Y., Wang, R., Zhang, Q., Xing, H.X., Zhou, J.: Conception of comprehensive utilization evaluation of urban underground space resources. *Geol. Bull.* **40**(10), 1601–1608 (2021)
11. Tian, C., Su, J.W., Ni, H.Y., Wang, R.: Progress and prospect of urban underground space resource evaluation. *Geol. East China* **42**(2), 147–156 (2021)
12. Zhao, Y., Huang, F.M.: Study on the planning and management of urban underground space development and utilization: a case study of Jiangsu province. *Shanghai Urban Plan.* **1**, 89–92 (2013)
13. Lei, S.S., Huang, S.L.: Disturbance mechanism and control technology of underlying buildings (structures) in underground space. *Tunnel Construct. (Chin. English)* **42**(1), 1–8 (2022)
14. Du, D., Wang, G.M.: Evaluation of regional crustal stability at the junction of Beijing, Tianjin and Hebei. *Geol. Surv. Res.* **43**(3), 218–223 (2020)

15. Tianjin Geological Survey Center. Comprehensive Geological Survey Report of Main Towns along the Development Axis of Beijing, Tangshan, and Qinhuangdao Dynasties. 2019–2020
16. Miao, J.J., Liu, H.W., Guo, X., Du, D., Bai, Y.N.: Analysis and study on the blocking capacity of the upper aquifer of confined water to NH_4^+ and NO_3^- in plain area - Taking Tongzhou district of Beijing as an example. *Geol. North China* **45**(03), 62–68 (2022)
17. Du, D., et al.: Study on the characteristics and influencing factors of land subsidence in Tongzhou district of Beijing. *Acta Geol. Sin.* **96**(2), 712–725 (2022)
18. Zhao, Y.T., Wu, K.J., Shi, X.D.: Exploration of underground space planning and control methods under the territorial space planning system -Taking the underground space planning and control of Beijing urban sub center as an example. *Tunnel Construct. (Chin. English)* **42**(2), 313–319 (2022)
19. Gong, Q.: Some thoughts on developing “physical examination” of urban underground space. *Inform. Technol.* **46**(6), 44–4753 (2022)
20. Shi, Y.J., Zhang, X.L., Chen, D.P.: Geological environmental conditions and suitability evaluation of deep underground space development in Shanghai. *Geol. Surv. Res.* **39**(02), 130–135 (2016)
21. Li, P.Y., Han, H.D., Wang, D.H., Wang, C.S.: Current situation and development trend of suitability evaluation for the development and utilization of urban underground space resources. *Sediment. Tethyan Geol.* **41**(1), 121–128 (2021)
22. Wang, L.H., Ma, W.M., Li, M.M., Zhang, Y., Cui, K.P.: Suitability evaluation of underground space development in Tianjin Binhai New Area. *Geol. Surv. Res.* **38**(04), 299–304 (2015)
23. Yang, H.Y., Jiang, Y., Li, Z., Gao, J.J., Wang, B.C.: Research on the development strategy of comprehensive treatment of underground space development. *China Eng. Sci.* **23**(4), 126–136 (2021)
24. Xi, Y., Zhang, W.B., Li, P.N., Liu, B.L., Xu, B., Li, X.J.: Three-dimensional refined evaluation of urban underground space resource quality. *J. Zhejiang Univ. Eng. Edn.* **56**(4), 656–663710 (2022)
25. Du, D., Liu, F.T., Liu, H.W.: Study on stability evaluation of engineering geological environment in Caofeidian Island Area Hebei Province. *Geol. Surv. Res.* **42**(4), 299–304 (2019)
26. Ministry of Housing and Urban-Rural Development of the People’s Republic of China. Urban Underground Space Planning Standard. GB/T 51358 - 2019
27. Zhou, A.G., Zhou, J.W., Liang, H.C., et al.: Geological Environment Assessment. China University of Geosciences Press, Wuhan (2008)
28. Cai, H.S., Zhou, A.G., Tang, Z.H.: Expert analytic hierarchy process weight determination method in geological environment quality evaluation. *Earth Sci. J. China Univ. Geosci.* **23**(3), 299–302 (1998)
29. Saaty, T.L.: A scaling method for priorities in hierarchical structures. *J. Math. Psychol.* **15**(3), 234–281 (1997)
30. Saaty, T.L.: How to make a decision: the analytic hierarchy process. *Interfaces* **24**(6), 19–43 (1994)
31. Liu, K., Peng, J., Peng, F.L.: Evaluation model for suitability of underground space resources development and utilization. *J. Underground Space Eng.* **2**(7), 219–231 (2011)
32. Liu, H.W., et al.: Study on evaluation index system of suitability for development and utilization of underground space in sedimentary plain: a case study of Tongzhou district in Beijing and Langfang north three counties in Hebei Province. *Geol. North China* **45**(4), 68–74 (2022)



Spatial Distribution, Influencing Factors and Suitability Evaluation of Rural Tourism - An Example from Guizhou, China

Yan Xiang¹, Junwei Zhao², and Yanlin Hou³(✉)

¹ College of Tourism Management, Guizhou University of Commerce, Guiyang 550014, China

² Administration and Management Institute, Ministry of Agriculture and Rural Affairs, Beijing 102208, China

³ School of Management, Guizhou University of Commerce, Guiyang 550014, China
y1hoo@126.com

Abstract. Clarifying the spatial distribution, influencing factors, and spatial suitability of rural tourism is of great significance for the industry authorities to optimize the layout and practitioners to select sites scientifically. Using 1200 tourist villages in Guizhou Province as the research sample, the spatial distribution, influencing factors, and suitability of tourist villages are studied using the Nearest Neighbor Index, GeoDetector, and Suitability Evaluation Model. It is found that: the spatial distribution of tourist villages is neither random nor dispersed but shows a significant tendency to cluster in a specific local space. Multiple factors significantly influence the spatial heterogeneity of tourist villages. Distance to tourist attractions, accessibility to urban areas, distance to ethnic villages, distance to ecological villages, distance to main rivers, and distance to featured agri-products are the major factors affecting the spatial heterogeneity of tourist villages. Tourist villages mainly surround tourist attractions, neighboring cultural villages, conveniently accessible to urban areas, close to ecological villages, along with main rivers, and nearby featured agri-products. And the tourism village distribution is remarkably correlated with the above factors. It presents a distribution consistent with distance decay. It is estimated that the area suitable for developing rural tourism in Guizhou is limited. The highly suitable, relatively suitable, and generally suitable areas for developing rural tourism are only about 1.38%, 6.95%, and 11.35% of the total area, respectively. Approximately 80.32% of the area in Guizhou is still not suitable for developing rural tourism.

Keywords: Rural Tourism · Spatial Distribution · Influencing Factors · Spatial Suitability

1 Introduction

A thriving business environment is the basis for rural revitalization and resolving all of the issues facing rural areas. Rural tourism is a new industry that expands agricultural functions, explores rural values, and innovates business types [1, 2]. Rural tourism

development has a significant positive effect on promoting rural revitalization, poverty alleviation, and sustainable development [3–5]. Rural tourism is regarded as an essential method of revitalizing rural China in recent years. Research shows that rural tourism development can promote rural industrial and community development and is an effective path to consolidate the results of poverty alleviation and rural revitalization [6, 7].

The spatial distribution of rural tourism is a long-standing common concern among scholars. Since Wu et al. (2004) [8] conducted a study on the spatial distribution of rural tourism in China, the research in this field is gradually enriched and shows four diversified trends. Firstly, the research contents are diversified, involving the spatial distribution types, spatial patterns, and influencing factors of rural tourism [9–11]. Secondly, the research regions are diversified, there are studies based on administrative regions such as national [12], provincial [13] and municipal [14], and there are also studies based on geographical or economic regions [15, 16]. Thirdly, the research data are diversified, government-identified [7, 8], internet celebrities [9, 17] or POIs [18] are used to conduct research. Fourthly, the research methods are diversified, and quantitative research methods, such as Nearest Neighbor Index, Kernel Density Analysis, Buffer Analysis, and GeoDetector, have become significant current research methods [9–18]. In summary, recent research has yielded valuable results in the spatial distribution, pattern evolution, and influencing factors of rural tourism.

However, there still needs to be more research on how to evaluate the spatial suitability of rural tourism. The existing studies mainly set the spatial range of the sample relative to the agglomeration of certain geographical elements as the suitable interval for rural tourism. For single geographical features, existing studies mainly set the intercepted aggregation distribution intervals as reasonable intervals without considering the variation of sample distribution in different intervals. For various geographical factors, the existing studies thoroughly combine the relative agglomeration intervals of various factors without considering the strength of different factors' determinate power. For suitable interval settings, the current studies need the classification of the suitability level of each interval; otherwise, the suitability level of different intervals cannot be compared. Identifying and effectively exploring suitable areas for rural tourism is still a challenging problem for industry authorities and practitioners.

Accordingly, this study takes Guizhou province, where rural tourism is developing rapidly, as the study region, selects 1200 government-identified tourist villages as the study sample, using the Nearest Neighbor Index, GeoDetector, and Suitability Evaluation Model, exploring the factors influencing the spatial distribution of tourist villages and measuring the spatial suitability of rural tourism. To provide a reference for similar areas of rural tourism authorities to optimize the layout and practitioners to select sites.

2 Materials and Methods

2.1 Study Area

Guizhou Province is in southwest China, adjacent to Hunan to the east, Guangxi to the south, Yunnan to the west, and Sichuan and Chongqing to the north, and is a typical inland mountainous province. Guizhou jurisdiction Guiyang and other nine cities and

prefectures, its administrative area is 176,200 km². Guizhou Province is a highlight and challenging place for China to consolidate the results of poverty eradication and promote rural revitalization. In recent years, rural tourism in Guizhou has achieved rapid expansion, and according to the *Green Book of Rural Tourism 2022*, Guizhou's rural tourism development index has reached fifth place in the country. The analysis of spatial distribution, influencing factors, and suitability of rural tourism in Guizhou can provide a reference for the layout optimization by rural tourism authorities and rational site selection by practitioners in similar areas.

2.2 Methods

Nearest Neighbor Index. The Nearest Neighbor Index (*NNI*) can be used to characterize tourist villages' clustering and dispersion status. The Nearest Neighbor Index is expressed as the ratio of the Observed Mean Distance to the Expected Mean Distance. The formula for *NNI* is shown in Eq. (1) as follows.

$$NNI = \frac{\bar{R}_O}{\bar{R}_E} = \frac{\sum_{i=1}^n d_i / \sqrt{A/n}}{2} \quad (1)$$

where \bar{R}_O is the Observed Mean Distance; \bar{R}_E is the Expected Mean Distance; d_i is the distance between tourist village i and its nearest tourist village. n is the number of tourist villages; A is the area of the study region. When $NNI > 1$, the trend is toward dispersion or competition; When $NNI < 1$, the pattern exhibits clustering.

GeoDetector. The GeoDetector is proposed by Wang et al. [19], it can be used to detect the consistency of the spatial pattern between the dependent variable and the independent variable, whereby the determinate power of the independent variable on the dependent variable is measured. This study uses GeoDetector to analyze the factors influencing the spatial heterogeneity of tourist villages. The formula for GeoDetector is shown in Eq. (2) as follows.

$$q = 1 - \frac{1}{n\sigma^2} \sum_{i=1}^m n_i\sigma_i^2 \quad (2)$$

where q is the determinant power of influence factor; n and σ^2 are sample size and variance for the entire region; m and σ_i^2 are sample size and variance for sub-level regions. The value range of q is [0, 1], a higher q value indicates a more substantial determinant power of the influence factor, and the opposite is weaker.

Suitability Evaluation Model. In this study, a Suitability Evaluation Model is constructed to measure the spatial suitability of rural tourism. The formula is shown in Eq. (2) as follows.

$$S_{Cj} = \sum_{i=1}^n W_i C_{ij} \quad (3)$$

where S_{Cj} is the composite score of the j th grid; W_i is the weights of the i th explanatory variable; C_{ij} is the judging score of the i th explanatory variable in the j th grid. Judging the suitability grade of each grid for rural tourism based on the composite score. When $S \geq 85$ is a highly suitable area; When $85 > S \geq 70$ is a relatively suitable area; When $70 > S \geq 60$ is a generally suitable area; When $S < 60$ is an unsuitable area.

2.3 Data Sources

The research sample of this study is 1200 tourist villages in Guizhou Province which were identified by governments at or above the county level from 2011–2021. The data were obtained from the Guizhou provincial government data open platform and the official websites of government departments. The coordinates of the study samples were searched individually, and then the spatial distribution of tourist villages was mapped (see Fig. 1).

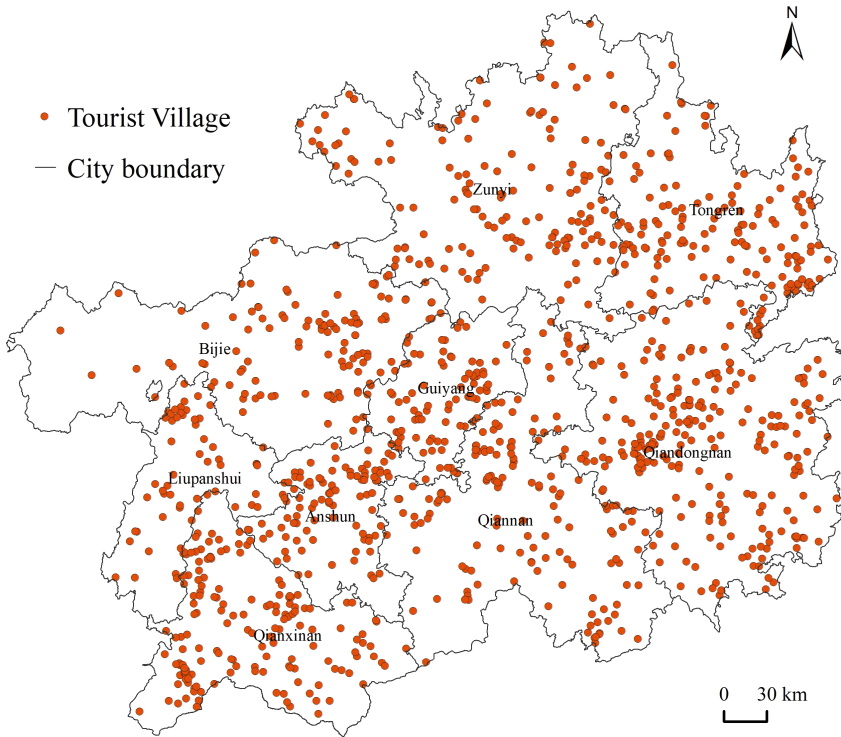


Fig. 1. Spatial distribution of tourist villages in Guizhou Province.

A variety of factors influence the spatial distribution of tourist villages. Concerning available studies, this paper screens out six-dimensional indicators, including cultural and tourism resources, traffic conditions, ecological conditions, natural conditions, industrial base, and socio-economic development, with 12 influencing factors to analyze the impact on the spatial distribution of tourist villages in Guizhou Province (see Table 1). In Guizhou Province, spatial data of administrative divisions, government sites, river systems, highways, etc., are obtained from the National Catalogue Service for Geographic Information 1: 1 million national geographic databases. The data on tourist attractions in Guizhou include 3A-level and above tourism attractions, totaling 499, which are from the Guizhou Provincial Department of Culture and Tourism. The data on ethnic villages are

in Guizhou include 1129 government-identified ethnic villages from the National Ethnic Affairs Commission and the Guizhou Provincial Ethnic Affairs Commission. The vegetation coverage was calculated based on the 2021 vegetation index (NDVI) data provided by Resource and Environmental Sciences and Data Center, CAS, concerning the method of Gan et al., with a resolution of 30m. The data on ecological villages in

Table 1. Influencing factors of tourist villages Guizhou.

Dimensions	Factors	Explanation
Culture and tourism resources	Distance to tourist attractions (km)	Tourism resources are attraction for rural tourism, and areas with rich tourism resources are suitable for developing rural tourism
	Distance to ethnic villages (km)	
Traffic conditions	Distance to main roads (km)	Traffic conditions guarantee rural tourism to connect with urban sources, and areas with convenient transportation are suitable for developing rural tourism
	Accessibility to urban areas (h)	
Ecological conditions	Distance to the ecological village (km)	Rural tourism development requires good ecological conditions, and areas with good environmental conditions are suitable for developing rural tourism
	Site vegetation coverage (%)	
Natural Conditions	Distance to main rivers (km)	Natural resources can affect rural tourism and areas with good natural resources are suitable for developing rural tourism
	Site elevation (km)	
Industrial foundation	Distance to featured agri-products(km)	Areas with prominent agricultural features and a high share of tertiary industries have a better foundation and are more suitable for developing rural tourism
	Share of tertiary industry (%)	
Socio-economic conditions	GDP per cantata (10^4 yuan)	Areas with better economic have a higher willingness of travel for residents to participate in rural tourism, which is conducive to developing rural tourism
	County resident population (10^4 person)	

Guizhou include 638 government-identified ecological villages from the China Eco-Culture Association and the Department of Ecological and Environment of Guizhou Province. Data on featured agri-products include professional agricultural villages, geographical indication products, regional public brands, etc., recognized by government departments from the Ministry of Agriculture and Rural Affairs and the Department of Agriculture and Rural Affairs of Guizhou Province. Socio-economic data from the *Guizhou Provincial Statistical Yearbook 2022*.

3 Results

3.1 Spatial Pattern of Tourist Villages

The spatial distribution of geographic data is classified as clustered, dispersed, and random. The nearest neighbor index can directly reflect the spatial pattern of the data. To explore the spatial pattern of tourist villages, the *NNI* was calculated. The result indicates that the *NNI* of tourist villages in Guizhou province is 0.76, $P < 0.01$, and z score < -2.58 . It demonstrates that the spatial distribution of tourist villages is neither random nor dispersed but shows a significant clustered. It is evident that tourist villages significantly tend to cluster in a specific local space. Intervals of distance to tourist attractions.

3.2 Spatial Heterogeneity of Tourist Villages

In this paper, the impact of each factor on the spatial differentiation of tourist villages was detected using a GeoDetector. The results reveal (see Fig. 2) that all factors significantly affect the spatial distribution of tourist villages. Of which, distance to tourist attractions

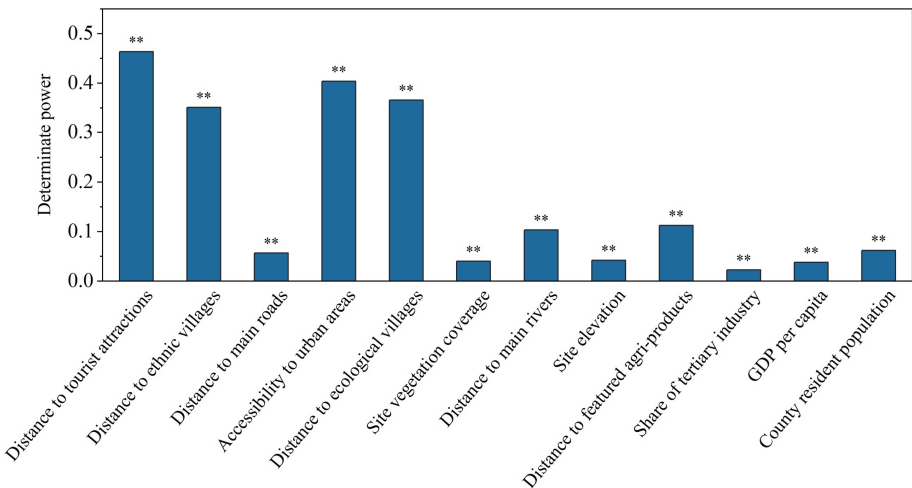


Fig. 2. The determinant power of influence factors on spatial heterogeneity of tourist villages in Guizhou. Where ** represents significance in 99% confidence.

(0.46), accessibility to urban areas (0.40), distance to ecological villages (0.37), and distance to ethnic villages (0.35) have more vital determinants and more significant influence on the spatial differentiation of tourist villages and are the dominant influence factors. Distance to featured agri-products (0.11) and distance to the main rivers (0.10) also have a significant effect and are secondary factors affecting the spatial differentiation of tourist villages. The remaining factors significantly impact the spatial heterogeneity of tourist villages, but the determinant power is minor and moderate. In Summary, distance to tourist attractions, accessibility to urban areas, distance to ethnic villages, distance to ecological villages, distance to main rivers, and distance to featured agri-products are the major factors affecting the spatial heterogeneity of tourist villages.

3.3 Spatial Correlation of Tourist Villages

The above 6 factors strongly influence the distribution of rural tourism, and further, this paper analyzes how tourist villages are distributed under the influence of the above factors (see Fig. 3).

Tourist Villages Mainly Surround Tourist Attractions and Decay with Distance. The mean distance between tourist villages and tourist attractions is 5.61 km, and 63.67% of the tourist villages locate within 6 km of tourist attractions. The results of equidistant grouping statistics with 2 km intervals showed a significantly high negative correlation between the number of tourist villages and the distance to tourist attractions ($P < 0.01$). The quantity of tourist villages gradually decays with the increase in distance to the tourist attractions (see Fig. 3A), and the fitted model is $y = 397.676e^{-0.305x}$ ($R^2 = 0.93$). It is noticeable that the distribution of tourist villages is significantly correlated with tourist attractions, showing a spatial distribution mainly distributed surrounding tourist attractions and decays with distance.

Tourist Villages Mainly Neighboring Cultural Villages with Distance-Decay. The mean distance between tourist villages and ethnic villages is 3.98 km, and about 64.50% of tourist villages locate within 4 km of ethnic villages. The results of equidistant grouping statistics with 2 km intervals showed a significant and highly negative correlation between the number of tourist villages and the distance to ethnic villages ($P < 0.01$). The quantity of tourist village distribution decreases with the increase of distance to the ethnic villages (see Fig. 3B), and the fitted model is $y = 507.033e^{-0.168x}$ ($R^2 = 0.96$). The distribution of tourist villages is significantly correlated with ethnic villages, presenting that the distribution is mainly neighboring ethnic villages and decays with distance.

Tourist Villages Mainly Locate Conveniently Accessible to Urban Areas with Distance Decay. The mean value of the accessibility of tourist villages to urban areas is 1.80 h, and about 65.17% of tourist villages locate within 2 h of accessibility to urban areas. In this paper, we use equal interval statistics with 1 h as the initiation and 0.5 h as the step for the tourist village, and the results show that a significant and high negative correlation was revealed between the number of tourist villages and the accessibility to urban areas ($P < 0.01$). With the increase in accessibility, the number of tourist village distribution tends to decay (see Fig. 3C), and the fitted model is $y = -31.418x + 297.236$

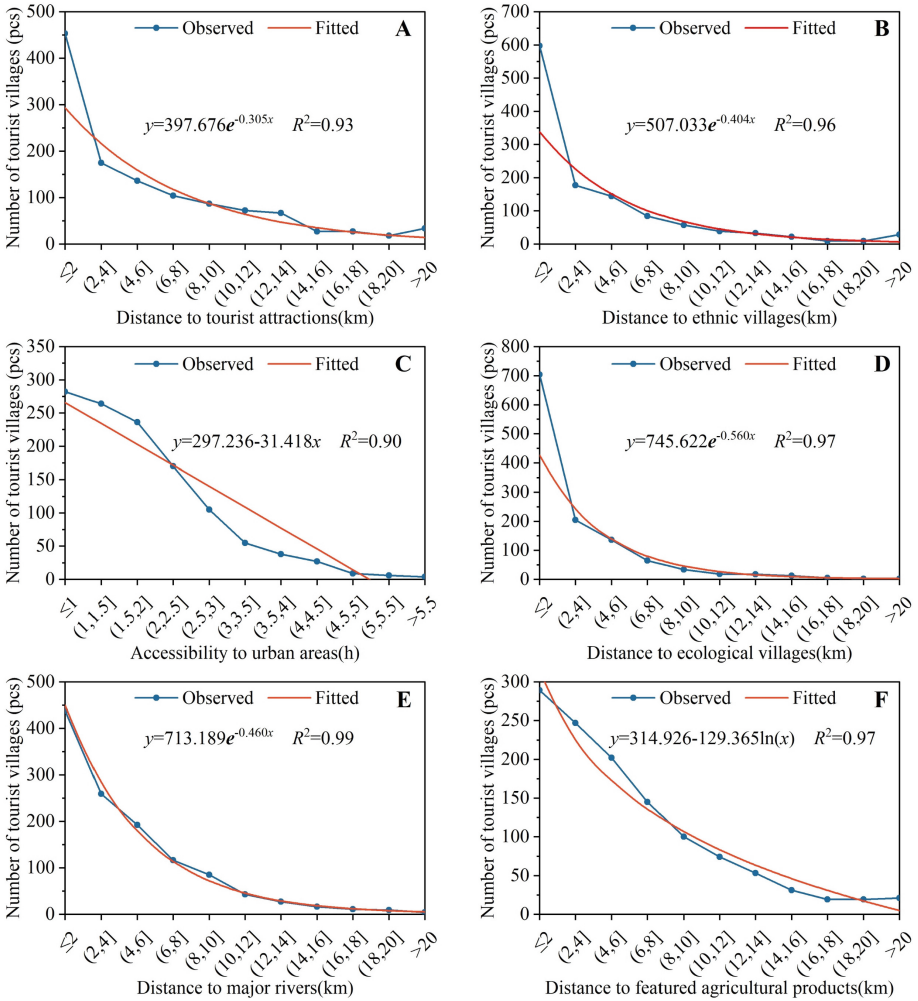


Fig. 3. Distribution of tourist villages under the influencing factors. The blue line is the observed curve of the tourist village distributed in intervals, and the red line is the fitted curve between the number of tourist villages and the intervals.

($R^2 = 0.90$). The distribution of tourist villages is significantly correlated with the accessibility to urban areas, showing that they are mainly located in areas with convenient access to urban areas and decaying with accessibility.

Tourist Villages Mainly Locate Close to Ecological Villages with Decay Distance. The mean distance between tourist villages and ecological villages is 2.60 km. About 75.67% of tourist villages distribute within 4 km of ecological villages. The results of equidistant grouping statistics with 2 km intervals showed a significant and highly negative correlation between the number of tourist villages and the distance to ecological villages ($P < 0.01$). The number of tourist villages decreases as the distance to the

ecological villages increases (see Fig. 3D), and the fitted model is $y = 745.622e^{-0.560x}$ ($R^2 = 0.97$). The distribution of tourist villages is remarkably correlated with ecological villages, showing the spatial distribution of clustering around ecological villages and decaying with distance.

Tourist Villages Mainly Locate Along with Main Rivers and Decay with Distance. The mean distance from the tourist village to the main rivers is 4.25 km, and 74.08% of the tourist villages distribute within 6 km of the main rivers. The results of equidistant grouping statistics with 2 km intervals revealed a significant and high negative correlation between the number of tourist villages and the distance to the main rivers ($P < 0.01$). The amount of tourist villages decreases as the distance to the main rivers increases (see Fig. 3E), and the fitted model is $y = 713.189e^{-0.460x}$ ($R^2 = 0.99$). The tourism village distribution is remarkably correlated with the main rivers, presenting a distribution along with the main rivers and decaying with distance.

Tourist Villages Mainly Nearby Featured Agri-Products with Distance-Decay. The mean distance from the tourist village to the featured agri-products is 5.76 km, and 61.50% of the tourist villages distribute within 6 km of the featured Agri-products. Equidistant grouping statistics with 2 km intervals showed a significant and highly negative correlation between the number of tourist villages and the distance to featured Agri-products ($P < 0.01$). The amount of tourist villages decreases as the distance to the Agri-products increases (see Fig. 3F), and the fitted model is $y = 314.926 - 129.365\ln x$ ($R^2 = 0.97$). Distribution of tourist villages is remarkably correlated with featured Agri-products. Demonstrates a spatial allocation primarily located near featured agri-products and diminishes with distance.

3.4 Suitability Evaluation of Tourist Villages

Model Construction. Factors such as distance to tourist attractions, accessibility to urban areas, distance to ethnic villages, distance to ecological villages, distance to main rivers, and distance to featured agri-products are the major factors affecting the spatial heterogeneity of tourist villages, have a strongly influencing impact on the spatial heterogeneity and correlation of tourist villages. Consequently, the above factors are selected as the explanatory variables for the Suitability Evaluation Model of tourist villages. Based on the determinant values of each factor on the spatial heterogeneity of tourist villages, the weights of each factor were obtained by a standardization process. The intervals of the factors were assigned according to the distributed characteristics presented by the fitted models of tourist villages and each factor (see Table 2).

Model Validation. Using the constructed Suitability Evaluation Model, the score of a selection with county-level above government-identified tourist villages is measured based on the assignments and weights. The results indicated that the mean score of was 80.35, and about 91.36% of the selections were distributed in suitable areas. Since the selected tourist villages are a typical case recognized by the high-level government, they should be in a better suitability grade. The evaluation is in line with reality and indicates that the model has a good performance.

Table 2. Assignment and weight of factors influencing the spatial distribution of tourist villages. Where Int is the interval and Asg is the Assignment.

Factor	Assignment										Weight	
	Int(km)	≤ 2	(2,4]	(4,6]	(6,8]	(8,10]	(10,12]	(12,14]	(14,16]	(16,18]		> 18
Distance to tourist attractions	Int(km)	≤ 2	(2,4]	(4,6]	(6,8]	(8,10]	(10,12]	(12,14]	(14,16]	(16,18]	> 18	0.257
	Asg	100	75	55	40	30	20	15	10	5	0	
Distance to ethnic villages	Int(km)	≤ 2	(2,4]	(4,6]	(6,8]	(8,10]	(10,12]	(12,14]	(14,16]	(16,18]	> 18	0.195
	Asg	100	75	60	40	30	20	15	10	5	0	
Accessibility to urban areas	Int(h)	≤ 1	(1,1.5]	(1.5,2]	(2,2.5]	(2.5,3]	(3,3.5]	(3.5,4]	(4,4.5]	(4.5,5]	> 5	0.225
	Asg	100	90	80	70	55	45	30	20	10	0	
Distance to ecological villages	Int(km)	≤ 2	(2,4]	(4,6]	(6,8]	(8,10]	(10,12]	(12,14]	(14,16]	(16,18]	> 18	0.203
	Asg	100	75	55	40	30	20	15	10	5	0	
Distance to main rivers	Int(km)	≤ 2	(2,4]	(4,6]	(6,8]	(8,10]	(10,12]	(12,14]	(14,16]	(16,18]	> 18	0.057
	Asg	100	75	55	40	30	20	15	10	5	0	
Distance to featured agri-products	Int(km)	≤ 2	(2,4]	(4,6]	(6,8]	(8,10]	(10,12]	(12,14]	(14,16]	(16,18]	> 18	0.062
	Asg	100	75	55	40	30	20	15	10	5	0	

Suitability Evaluation. The Guizhou province is divided into several $1 \text{ km} \times 1 \text{ km}$ grids, and Suitability Evaluation Model calculates the score of each grid. According to the score, the suitability grade of each grid is obtained (see Fig. 4). It is estimated that 80.32% of the areas in Guizhou are still unsuitable for developing rural tourism due to scarcity of tourism resources, insufficient cultural characteristics, poor ecological environment, or inconvenient traffic conditions. The highly suitable area for developing rural tourism in Guizhou is about $2,436 \text{ km}^2$, which accounts for only 1.38% of the total area; the relatively suitable area is about $12,243 \text{ km}^2$, which accounts for only 6.95%. Less than 10% of the area can provide better suitability for developing rural tourism. In addition, the generally suitable area is about $20,000 \text{ km}^2$, approximately 11.35% of the total area, suitable for developing rural tourism, but the suitable grade is low. The suitability level of this area should be upgraded to provide backup space for developing rural tourism.

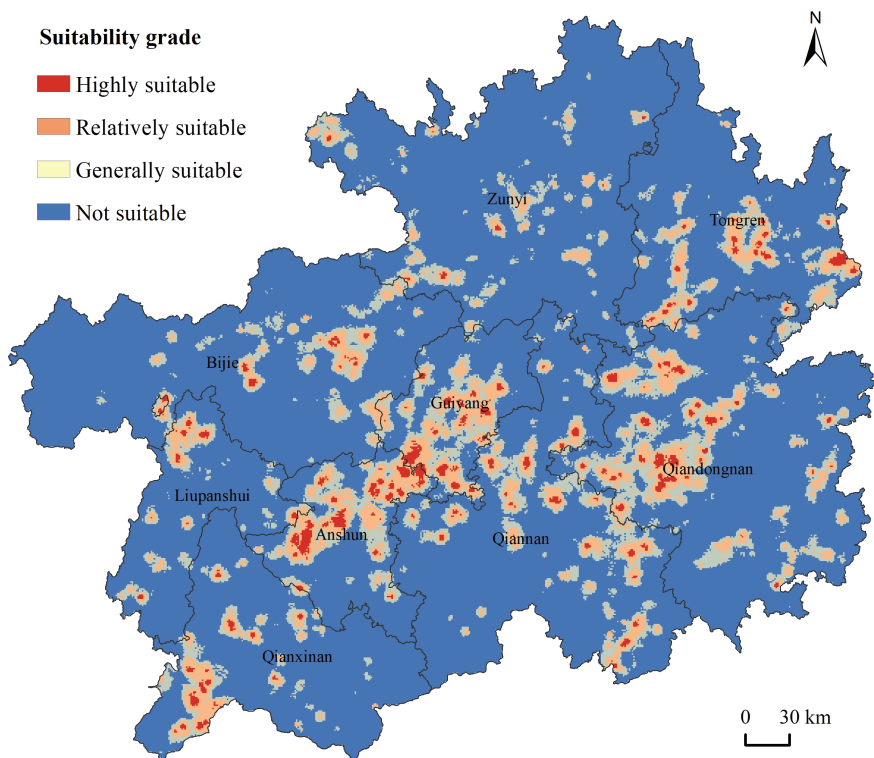


Fig. 4. Spatial distribution of suitability areas for developing rural tourism in Guizhou.

4 Conclusion

It is evident that the spatial distribution of tourist villages is neither random nor dispersed but shows a significant tendency to cluster in a specific local space.

Multiple factors significantly influence the spatial heterogeneity of tourist villages. Distance to tourist attractions, accessibility to urban areas, distance to ethnic villages, distance to ecological villages, distance to main rivers, and distance to featured agri-products are the major factors affecting the spatial heterogeneity of tourist villages.

Tourist villages mainly surround tourist attractions, neighboring cultural villages, conveniently accessible to urban areas, close to ecological villages, along with main rivers, and nearby featured agri-products. And the tourism village distribution is remarkably correlated with the above factors and presents a distribution consistent with distance decay.

It is estimated that the area suitable for developing rural tourism in Guizhou is limited. The highly suitable, relatively suitable, and generally suitable areas for developing rural tourism are only about 1.38%, 6.95%, and 11.35% of the total area, respectively. Approximately 80.32% of the area in Guizhou still needs to be suitable for developing rural tourism due to scarcity of tourism resources, insufficient cultural characteristics, poor ecological environment, or inconvenient traffic conditions.

5 Discussion

The spatial suitability evaluation of rural tourism development in Guizhou demonstrates that not all areas are appropriate for rural tourism development. According to the degree of suitability of rural tourism development, classification should adopt policy measures to optimize the spatial layout and promote high-quality development of rural tourism. This paper analyzes the spatial distribution, influencing factors, and suitability of rural tourism in Guizhou. However, there are still some shortcomings: the sample of this paper is the tourist villages recognized by the government, and other types of tourist villages are not investigated; the suitability evaluation model constructed in this paper established mainly based on the tourist villages in Guizhou, and the applicability of this model in other regions still needs further verification.

Foundation. This article is supported by Youth Science and Technology Talents Growth Project of General Universities of Guizhou Province (Qianjiaohe KY[2022] No. 320).

References

1. Yang, J., Yang, R., Chen, M.H., et al.: Effects of rural revitalization on rural tourism. *J. Hosp. Tour. Manag.* **47**, 35–45 (2021)
2. Gao, C., Cheng, L.: Tourism-driven rural spatial restructuring in the metropolitan fringe: an empirical observation. *Land Use Policy* **95**, 104609 (2020)
3. Steven, D.: Rural poverty, tourism and spatial heterogeneity. *Ann. Tour. Res.* **37**(1), 80–205 (2010)
4. Briedenhann, J., Wickens, E.: Tourism routes as a tool for the economic development of rural areas—vibrant hope or impossible dream? *Tour. Manage.* **5**(1), 71–79 (2004)
5. Lane, B., Kastenholz, E.: Rural tourism: The evolution of practice and research approaches—towards a new generation concept? *J. Sustain. Tour.* **23**(8–9), 1133–1156 (2015)
6. Qian, J.C., Zhang, B.L., Liu, H.W., et al.: Development differentiation of rural areas with tourism characteristics in eastern mountainous areas and its driving forces: a case study of Pingyang county, Zhejiang province. *Progress Geography* **39**(09), 1460–1472 (2020)

7. Xi, J., Wang, X., Kong, Q., et al.: Spatial morphology evolution of rural settlements induced by tourism: a comparative study of three villages in Yesanpo tourism area China. *J. Geograph. Sci.* **25**, 497–511 (2015)
8. Wu, B.H., Huang, Z.W., Ma, X.M.: Spatial structure of rural tourism attractions in suburban areas of China. *Scientia Geographica Sinica* **06**, 757–763 (2004)
9. Lee, S.H., Choi, J.Y., Yoo, S.H., et al.: Evaluating spatial centrality for integrated tourism management in rural areas using GIS and network analysis. *Tour. Manage.* **34**(2), 14–24 (2013)
10. Xiang, Y., Chen, Y.J., Hou, Y.L., et al.: Spatial distribution and influencing factors of leisure agriculture: a case from Hebei province. *Scientia Geographica Sinica* **39**(11), 1806–1813 (2019)
11. Kumar, S., Valeri, M.: Understanding the relationship among factors influencing rural tourism: a hierarchical approach. *J. Organ. Chang. Manag.* **35**(2), 385–407 (2022)
12. Xie, Y., Meng, X., Cenci, J., et al.: Spatial pattern and formation mechanism of rural tourism resources in China: evidence from 1470 national leisure villages. *ISPRS Int. J. Geo Inf.* **11**(8), 455 (2022)
13. Liao, C., Zuo, Y., Law, R., et al.: Spatial differentiation, influencing factors, and development paths of rural tourism resources in Guangdong province. *Land* **11**(11), 2046 (2022)
14. Lv, Li., Hu, J., Tian, X. B., et al.: Spatial agglomeration evolution characteristics and influencing factors of rural tourism in Wuhan. *Resourc. Environ. Yangtze Basin* **31**(06), 1234–1248 (2022)
15. González-Ramiro, A., Gonçalves, G., Sánchez-Ríos, A., et al.: Using a VGI and GIS-based multicriteria approach for assessing the potential of rural tourism in Extremadura (Spain). *Sustainability* **8**(11), 1144 (2016)
16. Qi, J., Lu, Y., Han, F., et al.: Spatial distribution characteristics of the rural tourism villages in the Qinghai-Tibetan Plateau and its influencing factors. *Int. J. Environ. Res. Public Health* **19**(15), 9330 (2022)
17. Song, H.F., Tao, Z.M.: Hotspot identification and cause analysis of rural tourism based on website data: take Jiangsu province as an example. *J. Nat. Resour.* **35**(12), 2848–2861 (2020)
18. Wang, J.Y., Xie, D.T., Wang, S., et al.: Research on spatial distribution of rural tourism in mountainous and hilly areas based on poi extraction—a case study of Chongqing city. *Chin. J. Agric. Resour. Region. Plan.* **41**(05), 257–267 (2020)
19. Wang, J.F., Li, X.H., Christakos, G., et al.: Geographical detectors-based health risk assessment and its application in the neural tube defects study of the Heshun region, China. *Int. J. Geogr. Inf. Sci.* **24**(1), 107–127 (2010)

Coastal Engineering and Fluid Mechanics



Coastline Change Monitoring by Remote Sensing in Coastal Zone of Bohai Bay in China

Hualiang Xie^{1,2,3}, Jie Han⁴, Huaiyuan Li^{1,2,3(✉)}, Shuhua Zuo^{1,2,3},
and Zhiyuan Han^{1,2,3}

- ¹ Tianjin Research Institute for Water Transport Engineering, Tianjin 300456, China
lhy07031@126.com
- ² National Engineering Research Center of Port Hydraulic Construction Technology,
Tianjin 300456, China
- ³ Key Laboratory of Engineering Sediment, Ministry of Transport, Tianjin 300456, China
- ⁴ School of Science, Tianjin University of Technology, Tianjin 300384, China
hanjie@email.tjut.edu.cn

Abstract. Coasts are the zone between the sea and the land, influenced by the dual effects of the exchange of materials between land and sea. It is an important reference for sea and land changes that reflect climate change and human activities. Monitoring shoreline changes has become an important task in the ecological environment protection, economic development of the bay. In this paper, coastline changes, bay area and shoreline characteristics of Bohai Bay in northern China were investigated over a 40-year period using multi-dated Landsat TM/ETM satellite image data from 1975 to 2015. The results show that the total coastline length of Bohai Bay increased by 761 km in the past 40 years, but the bay area showed a decreasing trend, which decreased by 18%; the artificial coastline showed a clear increasing trend year by year, while the natural coastline change was relatively weak and acutely disappeared, More than 95% of the coastline's length was made up of artificial coastline along Bohai Bay; the factors influencing the shoreline change of Bohai Bay had significant temporal heterogeneity, and then the leading factor was the anthropogenic development activities (reclamation engineering and port construction), mainly concentrated in the three key regions of Caofeidian Port, Tianjin Port and Huanghua Port in Bohai Bay. With the expansion of development and exploitation of marine activities, the impact of human activities on the evolution of coastal zone is becoming more and more obvious, according to an analysis of the change of the bay coast and the bay area under the influence of hydrodynamic, sedimentary, and natural evolution environment. The study reveals the characteristics and influencing factors of coastal change in Bohai Bay, which can provide the necessary scientific basis for the development and construction, comprehensive management and coastal environmental protection of the Bohai Bay region.

Keywords: Bohai Bay · Remote Sensing · Coastline Change · Human Activities · Reclamation Project

1 Introduction

The coastline is the dividing line between sea and land [1, 2]. Several elements, including human activity (reclamation, harbor projects, and so forth), sediment supply, sea level changes, the hydrodynamic environment, and storm surges, are linked to both long-term and short-term coastline alterations. Understanding the location of the coastline and its erosion and accretion patterns throughout time is crucial [3–5].

In the study of coastal zones all over the world, such as in the analysis of landforms, coastal erosion, and shoreline change, satellite remote sensing technology has been extensively used as a significant tool [6–13]. Further, because of their low cost, remote sensing images are easy to access and understand. Thematic Mapper (TM) and Enhanced Thematic Mapper (ETM+) imagery, which contains visible and infrared bands, is frequently used for mapping changes to coastlines due to the absorption of infrared wave-length area by water and its strong reflectance by soil and plant [6].

However, there is limited research on the long-term coastline changes in the entire Bohai Bay. Therefore, in this paper, using the method of remote sensing and geographic information system, nearly 40 years of coastline length changes, the bay area and Bohai Bay coast properties change are analyzed based on the Landsat TM/ETM satellite data of the entire Bohai Bay from 1975 to 2015 in order to provide necessary scientific basis for coast environmental protection, development and management.

2 Materials and Methods

Bohai Bay (see Fig. 1) is a large semi-enclosed sea in northern China. It is connected to Yellow Sea and the Pacific Ocean through a gap between Shandong Peninsula and Liaoning Peninsula.

Bohai coastal economic zone is the main part sea passage of national development plan “Circum-Bohai Sea Economic Circle” in north China, which brings rapid development to the regional economy and urban construction along Bohai Bay. Sea area reclamation engineering rapidly increases with social and economic development in coastal zone of Bohai Bay over recent years. In the last decade, nearly 300 km² of new land have been created around the bay coast due to this coastal development. [14, 15], which has made the coastline change of Bohai Bay and brought certain influence or chain reaction to the hydrodynamic, water environment and sedimentary environment of the bay.

Bohai Bay is surrounded by the provinces of Hebei, Tianjin, and Shandong, from its northernmost point at the Daqing Estuary in Hebei to its southernmost point at the LaoHuanghe Estuary in Shandong. On its more than 200 km of coastline, there are approximately 15900 km² of water [15]. Its coast type belongs to the typical silty gentle slope coast. The bay’s average sea depth is 12.5 m, and Tianjin Port’s average tidal range is 2.4 m.

Bohai Bay is located in mid-latitudes monsoon region and is close to the Mongolian plateau. The climate characteristics have obvious continental. The average annual temperature is 13.1 °C and there are 363.7 mm of rain on average per year. There are a few rivers that flow into Bohai Bay from the west, but since the 1960s, the majority of rivers

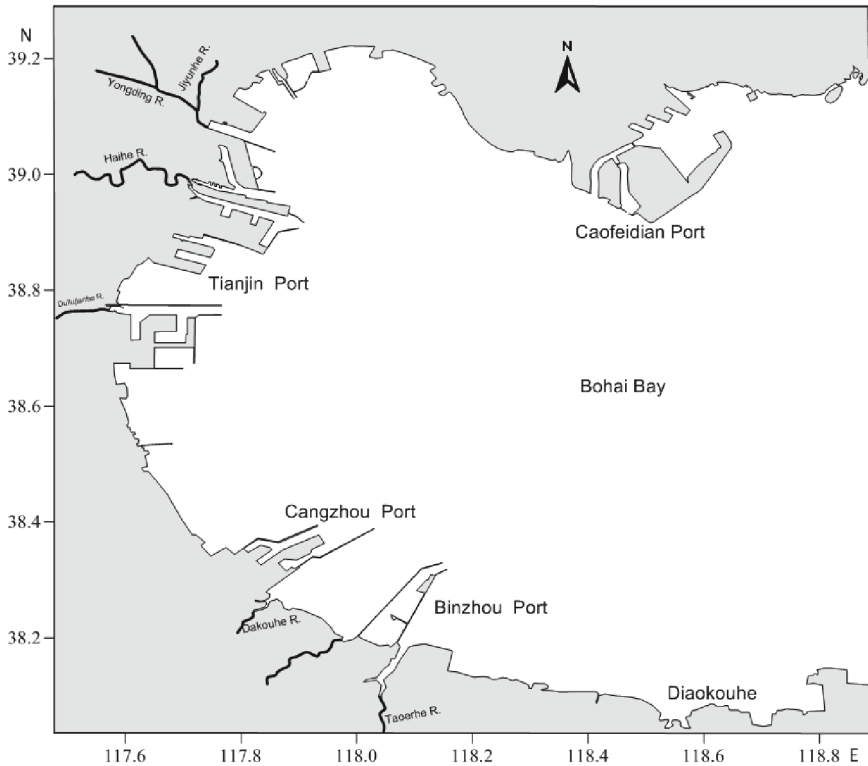


Fig. 1. The geographic location of Bohai Bay.

have significantly reduced the amount of sediment load reaching their estuaries due to upstream damming. The bay is situated between the Yellow River Delta and the Luan River Delta, and there are currently significant fluvial inputs.

The coastal region of Bohai Bay has gradually become one of China's key economic development areas. There are Caofeidian Port, Tianjin Port, Huanghua Port and Dongying Port. In order to adapt to the rapid economic development and make up for the shortage of land resources, large-scale land reclamation projects were carried out, especially starting from the tenth five-year plan.

To determine coastline change in studied areas, series remote sensing images of Landsat Multispectral Scanner (MSS), Landsat Thematic Mapper (TM), and Landsat Enhanced Thematic Mapper (ETM+) were used in the present study. Each image was acquired on different dates from 1975 to 2015. Landsat MSS image has four band and 78 m spatial resolution of pixel. Landsat TM image has pixel resolution of band 1, 2, 3, 4, 5, 7 in 30 m, ETM+ band 8 particularly in 15 m which were archived on the Global Land Cover Facility server [16]. The properties of the images are given in Table 1.

An analysis of coastline change in the study sea area was conducted using remote sensing and GIS technologies. The satellite remote sensing image is mainly processed by

Table 1. Information of the remote sensing images data.

Satellite	Senor	Track No	Spatial Resolution(m)	Acquisition Date
Landsat 2	MSS	122-33	78	1975-01-12
Landsat 5	TM	122-33	30	1984-09-10
Landsat 5	TM	122-33	30	1994-10-24
Landsat 7	TM	122-33	30	1999-12-09
Landsat 7	ETM	122-33	30	2000-06-10
Landsat 7	ETM	122-33	30	2002-05-31
Landsat 7	TM	122-33	30	2004-10-03
Landsat 5	TM	122-33	30	2005-04-13
Landsat 7	TM	122-33	30	2006-07-21
Landsat 7	ETM	122-33	30	2008-09-20
Landsat 7	ETM	122-33	30	2010-03-02
Landsat 8	ETM+	122-33	30	2015-06-12

geometric fine correction, coordinate system and projection transformation, band combination and radiation enhancement. The precision of geometric correction is controlled within 0.5 pixels.

The coastline reflected by satellite remote sensing images is generally the instantaneous boundary line between sea and land at a certain time (i.e., water frontier). In the identification of different types of coastline, water edge technology is mainly used. The water boundary line of artificial coastline is relatively clear. After simple enhancement treatment, artificial coastline is obtained through visual interpretation. Taking the high tide line as the standard, the external boundary of impervious structure is as artificial coastline.

In this paper, the bay area is the area surrounded by the mean low tide line and the inlet gate line, namely the sea area between the theoretical base level and two headlands of the bay.

3 Results

3.1 Varies with the Shoreline Length and the Bay Area

The Bohai Bay coastline from 1975 to 2015 is shown in Fig. 2. It can be seen from the figure that the overall length of Bohai Bay coastline in the past 40 years shows a trend of slight decrement, followed by a gradual increase.

Over the past 40 years, the coastline of Bohai Bay has grown by 761 km (Table 2), thereinto the length of coastline around Bohai Bay decreased by 31km from 1975 to 1984, it increased by 83 km, 53 km, 105 km, 398 km and 153 km from 1984 to 1994, from 1994 to 1999, from 1999 to 2005, from 2005 to 2010 and from 2010 to 2015 respectively.

While the overall length of the Bohai Bay coastline has increased, the bay area has been gradually decreasing and the rate of area reduction has gradually increased. In 1975, the bay area was about 11025 km² and it was 9305 km² in 2010, which was about 16% less than in 1975. But it reduced to 9016 km² by 2015. Thereinto from 2005 to 2010, the rate of reduction was the fastest. The survey shows the increasing extent of reclamation at this stage.

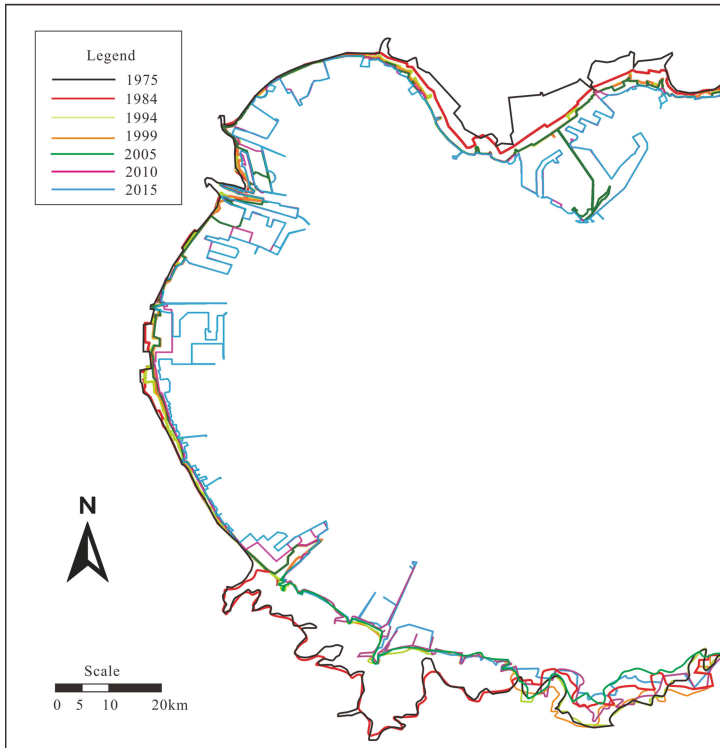


Fig. 2. Changes in the coastline of Bohai Bay.

3.2 Shoreline Attribute Change

From the perspective of the degree of shoreline artificialization, the Bohai Bay shoreline was developed and utilized earlier. In the early stage, a large number of salt fields and breeding ponds were built along the coast, which reduced the tidal flat area. In the later stage, the reclamation was mainly carried out along the coast, which changed the coastline shape and greatly reduced the tidal flat area.

As can be seen from Fig. 3, the whole artificial coastline of the research area shows an increasing trend year by year. By 2015, the artificial coastline accounts for over 95% of the total length, among which the artificial shoreline formed by port construction

Table 2. Coastline length, bay area changes in Bohai Bay.

Year	Coastline length(km)	Variable quantity(km)	Bay area (km ²)	Variable quantity (km ²)
1975	533		11025	
1984	502	-31	10840	-185
1994	585	+83	10655	-185
1999	638	+53	10230	-425
2005	743	+105	9924	-306
2010	1141	+398	9305	-619
2015	1294	+153	9016	-289

accounts for about 26% of the total shoreline. So the artificial coastline has become the main component of the Bohai Bay shoreline.

The natural shoreline is mainly around the estuary of part of the sea. The cardinal number of natural shoreline is small and the variation is relatively weak. For example, the old Yellow River Estuary which is located in the southern part of Bohai Bay entered the sea in the early period (1964–1976). Due to a large amount of sediment deposited, the sea from the Dakou River to the old Yellow River Estuary formed a large area of tidal beach. Before 1975, this part of the coastline was largely unaffected by human activities, and the coastal, seabed and surrounding geomorphology were basically in a state of natural evolution. There were a large number of coastal wetlands, and the coastline was dominated by natural shoreline. At that time, most of the coast of the Diaokou Estuary was in the natural state and has a strong erosion, which is affected by the natural environment conditions. The straight shoreline becomes a curved shoreline, so the shoreline length was fluctuating. After 2005, due to the influence of artificial exploitation and utilization, the natural shoreline was also gradually shrinking.

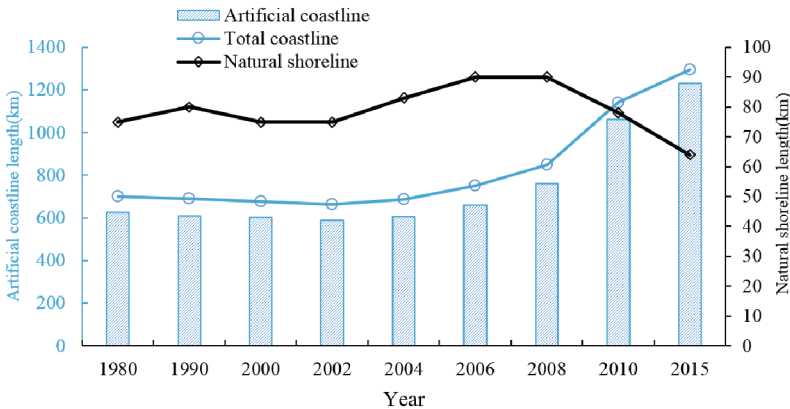


Fig. 3. Changes in different types of coastlines in Bohai Bay.

4 Discussion

While waves, currents, and a variety of natural processes frequently affect the coastal region, human activities like building coastal structures, dredging navigation channels, and reclamation have also had a significant impact [4].

4.1 Sediment Source Change

The Bohai Bay sediment source is mainly from the river into the sea sediment. Along the coast of Bohai Bay, there are many rivers, such as Jiyun River, Haihe River, Duliujian River, Qihe River, Dakouhe River and so on. However, other river basins (apart from Haihe River) are small, thus the influence on Bohai Bay is weak. In addition, the Yellow River and Luan River on the edge of Bohai Bay also have certain influence on the formation and evolution of Bohai Bay.

In this study region, the sediment load to the estuaries has reduced dramatically because of upstream damming during the last few years. The Haihe supplied 6×10^6 t/a before a dam was built in 1958. In the past few years, the runoff of Haihe River was respectively $729.9 \times 10^8 \text{ m}^3$ during the 1950s, $436 \times 10^8 \text{ m}^3$ during the 1960s, $100.9 \times 10^8 \text{ m}^3$ during the 1970s and about $22.7 \times 10^8 \text{ m}^3$ during the 1980s. The Haihe's sediment discharge decreased from $5213 \times 10^4 \text{ t}$ in the 1950s to $360 \times 10^4 \text{ t}$ in the 1970s [16]. The Haihe River currently supplies approximately $1.8 \times 10^5 \text{ t/a}$, while the Luanhe River supplies $2.7 \times 10^7 \text{ t/a}$ and Yellow River supplies $1.1 \times 10^9 \text{ t/a}$ [15]. The suspended sediment flux of these rivers has decreased to only 10% of what it was in the 1950s.

The total length of the coastline was also extended by sediment deposition in estuaries and sandbank extension as natural factors. However, the tidal flats expand at a slower rate as sediment sources continue to diminish.

4.2 Hydrodynamic Factors

Hydrodynamic conditions, including rivers and oceans, are important factors in shaping shoreline morphology and geomorphological features [1]. In this study, the coastal erosion is relatively obvious near the waste Yellow River delta, namely the waters near the Diaokou River. The coastal erosion of waste Yellow River delta is generally caused by the marine dynamic effect (especially wave and storm surge). The length of the coastline will be shortened due to coastal erosion as a result of an increase in the marine dynamic impact under the conditions of river migration and reduced sea sediment [1].

In addition, the variation of modern climate and the rise of sea level will increase the probability and intensity of storm surge disasters. Increased ocean dynamics such as storm surges will undoubtedly increase the risk of coastal erosion. If the sea level rises by 15 cm, the chance of storm surges will be about doubled [17]. The erosion effect of storm surges on the coast has a certain degree of suddenness, locality and harm. The storm surge affecting Bohai Bay is mainly temperate storm surges, which occur mainly along the southern or southwestern coast of the Bohai Sea.

4.3 Human Activities

Natural factors (sediment source and hydrodynamic factors) causing coastline change were mainly sedimentation and erosion, and the change rate was small. The variation of the Bohai Bay coastline length is closely related to the development and utilization of coastal tidal resources.

The findings show that from 1975 to 2015, reclamation, the development of harbors, and aquaculture ponds were the key human activities that led to changes in the coastline. The land area of Bohai Bay increased by a net 880 km² between 1975 and 2015, mostly as a result of human development. The Caofeidain Port of Tangshan City, Tianjin Port (or Tianjin Binhai New Area), Huanghua Port, Cangzhou Port and Binzhou Ports were among the coastal areas that were reclaimed to meet the needs of industry and commerce.

From 1975 to 2005, the land area of Bohai Bay increased slightly with an annual average reclamation area of 7.74 km². Since the 12th-Five-Year-Plan, the sea area reclamation in Bohai Bay stepped into a fast growth stage with an annual average reclamation area of 129.8 km² from 2005 to 2015. So human activity intensity is the main cause of the Bohai Bay coastline variation.

5 Conclusions

This paper analyzes the long-term coastline change of Bohai Bay by using Remote Sensing and GIS techniques in favor of facilitating rational planning, scientific management, and suitable regulation of coastal zones. The main conclusions were as follows.

The length and component of coastline changed dramatically in Bohai Bay during 1975–2015. The total length of the coastline in the Bohai Bay increased by 761 km, thereinto from 1975 to 1984, the length of Bohai Bay coastline decreased by 31 km, and the coastline growth was fastest in the phase from 2005 to 2010 with a growth of 398 km. Furthermore, the artificial coastline as a whole shows a clear increasing trend year by year. By 2015, the artificial coastline along the Bohai Bay coast accounted for over 95% of the total coastline length, while the natural coastline variation was relatively weak and disappeared acutely.

The Bohai Bay area has been gradually decreasing. In 1975, the bay area was about 11025 km², while it was reduced to 9016 km² by 2015.

The variation of the coastline length, bay area and coastline attributes of Bohai Bay is closely related to the continuous development and utilization of coastal beach resources by human beings. The factors affecting coastline change had significant temporal heterogeneity. The leading factor is anthropogenic development activities (reclamation engineering and port construction), which is mainly concentrated in the three key regions of Caofeidian Port, Tianjin Port and Huanghua Port.

However, this research has several limitations. Firstly, the study focused on the extraction of the instantaneous waterline, but lacked tidal correction and verification of accuracy. Second, the accuracy of shoreline extraction was not sufficiently verified.

Artificial shorelines are currently the mainstay in Bohai Bay, and the current extracted shoreline changes are sufficient to characterize the changes in Bohai Bay over the past 40 years. Therefore, future studies should collect as much measured tidal level data as

possible and correct the tidal level of the water's edge. Verification of the accuracy of the shoreline extraction will be achieved by using GPS data collected over the same period.

References

1. Xu, N., Gao, Z., Ning, J.: Analysis of the characteristics and causes of coastline variation in the Bohai Rim (1980–2010). *Environ. Earth Sci.* **75**, 719 (2016)
2. Alesheikh, A.A., Ghorbanali, A., Nouri, N.: Coastline change detection using remote sensing. *Int. J. Environ. Sci. Technol.* **4**(1), 61–66 (2007)
3. Narayana, A.C., Priju, C.P.: Landform and shoreline changes inferred from satellite images along the central Kerala coast. *J. Geol. Soc. India* **68**, 35–49 (2006)
4. Bai, Y.C., Shi, F.S., Xu, H.J., et al.: Coastline and tidal current changes responses due to large-scale reclamation in Bohai Sea. *Mar. Sci. Bull.* **40**(6), 621–635 (2021)
5. Xie, H.L., Han, Z.Y., Zuo, S.H., et al.: The application of parabolic headland-bay coast shape model to the Jinghai Bay, Guangdong Province. *J. Waterway Harbor* **39**(3), 269–274 (2018)
6. Kawakubo, F.S., Morato, R.G., Nader, R.S., et al.: Mapping changes in coastline geomorphic features using Landsat TM and ETM+ imagery: Examples in southeastern Brazil. *Int. J. Remote Sens.* **32**(9), 2547–2562 (2011)
7. Edwards, B.L., Namikas, S.L.: Changes in shoreline change trends in response to a detached breakwater held at grand Isle Louisiana. *J. Coast. Res.* **27**(4), 698–705 (2011)
8. Deepika, B., Avinash, K., Jayappa, K.S.: Shoreline change rate estimation and its forecast: remote sensing, geographical information system and statistics-based approach. *Int. J. Environ. Sci. Technol.* **11**, 395–416 (2014)
9. Chen, X.Y., Zhang, J., Ma, Y., et al.: Analysis of the spatial and temporal changes of the coastline in the Haizhou Bay during the past 40 years. *Adv. Marine Sci.* **32**(3), 324–334 (2014)
10. Zhang, W., Ruan, X., Zheng, J., et al.: Long-term change in tidal dynamics and its cause in the Pearl River Delta China. *Geomorphology* **120**, 209–223 (2010)
11. Sun, X.Y., Lu, T.T., Gao, Y., et al.: Driving force analysis of Bohai Bay coastline change from 2000 to 2010. *Resourc. Sci.* **36**(2), 413–419 (2014)
12. Suo, A.N., Zhang, M.H.: Sea areas reclamation and coastline change monitoring by remote sensing in coastal zone of Liaoning in China. *J. Coast. Res.* **1**(73), 725–729 (2015)
13. Xie, H.L., Yang, C.S., Han, Z.Y., et al.: Study on the characteristic and causes of the Deep-Water Channel siltation outside Zhanjiang Bay. *J. Waterway Harbor* **44**(1), 49–52 (2023)
14. Zhang, M., Jiang, X.Z., Zhang, J.R., et al.: Research progress of coastline feature extraction by remote sensing image. *Yellow River* **30**(6), 7–9 (2008)
15. Wang, F., Tian, L.Z., Jiang, X.Y., et al.: Human induced changes in recent sedimentation rates in Bohai Bay, China: implications for coastal development. *Sci. China Earth Sci.* **61**, 1–13 (2018)
16. Sener, E., Davraz, A., Sener, S.: Investigation of Aksehir and Eber Lakes (SW Turkey) coastline change with multitemporal satellite images. *Water Resource Manage* **24**, 727–745 (2010)
17. Gornitz, V., Lebedeff, S., Hansen, J.E., et al.: Global sea level trend in the past century. *Science* **215**(4540), 1611–1614 (1982)



The Progress and Management Suggestions for the Renovation and Restoration of Sea Area and Coastal Zone

Dawei Ji¹, Jian Zhang¹, Shiyue Fan¹(✉), Yuanjun Wang¹, Yingzhi Cao¹, and Hong Deng²

¹ National Marine Data and Information Service, Tianjin 300171, China
julia317fan@126.com

² National Center of Ocean Standards and Metrology, Tianjin 300112, China

Abstract. In recent years, the central government has invested in supporting 74 coastal zone renovation and restoration projects through sea area use funds, achieving a series of significant results. However, there are some problems such as a lack of comprehensive planning, incomplete management systems, unscientific implementation plans for some projects, and delayed implementation progress as well. Given the current progress and management status of coastal zone renovation and restoration projects, the article recommends the marine administrative departments to establish a management system, strengthen project supervision during and after the event, scientifically formulate and strictly implement renovation and restoration plans, broaden funding channels for renovation and restoration projects, innovate incentive mechanisms for renovation and restoration projects, promote the informatization construction of renovation and restoration project management, and proposed the ecological restoration concept of giving priority to natural restoration to promote the construction of marine ecological civilization and the development of marine economy in coastal areas.

Keywords: Sea Area and Coastal Zone · Renovation and Restoration · Marine Ecological and Environmental Protection

1 Introduction

The coastal zone is an important area of land sea interaction, containing abundant resources, and is a special zone with the most active and frequent human socio-economic activities. With the rapid development of the marine economy, the intensity of human activities in the development and utilization of coastal zones is also increasing. In order to protect the resources and environment of the sea area and coastal zone, the National Oceanic Administration issued the “Several Opinions on Carrying out the Renovation, Restoration and Protection of the Sea Area and Coastal Zone” in 2010, which pointed out that “further strengthening the renovation, restoration, and protection of the sea area and coastal zones, enhancing their environmental and ecological value and their support for the development of the marine economy.” The continuous implementation of the

renovation, restoration, and protection of the sea area and coastal zones can not only promote the transformation of the development mode of the marine economy, improve the ability of marine development, control, and comprehensive management, but also plays an important role in suppressing the deterioration of the marine ecological environment and promoting the construction of marine ecological civilization [1, 2].

The term “sea area and coastal zone renovation and restoration project” (hereinafter referred to as “renovation and restoration project”) in this article mainly refers to relevant projects supported by the return of central sea area use funds.

2 Investment in Central Sea Area Use Funds

From 2010 to 2013, the Ministry of Finance and the National Oceanic Administration refunded 1.67 billion yuan through sea area use funds, supporting a total of 74 renovation and restoration projects [3–5], involving 11 coastal provinces and 5 state plan cities (shown in Fig. 1 and Fig. 2), covering seven categories: beach restoration, returning aquaculture to sea area, dredging, seawall restoration, landscaping, structural demolition and renovation, and ecological restoration.

From the perspective of regional distribution, Shandong Province has the highest number of approved projects, with a total of 13 projects, while Ningbo and Shenzhen have the lowest number, with 1 project approved each. In terms of time span, in 2012, there were a maximum of 36 projects approved nationwide, while in 2013, only one project was approved. The single project with the most investment is the Bachimen returning the seawall to the sea area project in Zhangzhou City, Fujian Province, with a total approved sea area use funds of 70 million yuan, which is implemented over three years.

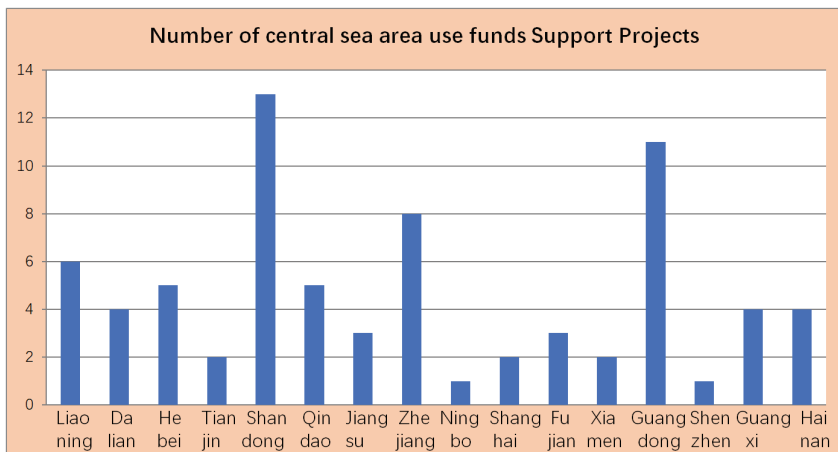


Fig. 1. A figure shows the distribution of accumulated projects supported by sea area use funds involving 11 coastal provinces and 5 state plan cities.

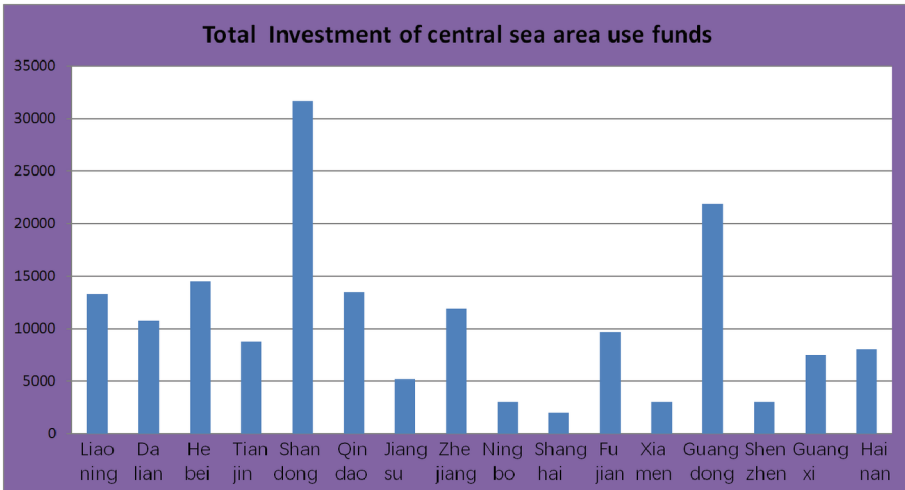


Fig. 2. A figure shows the distribution of total accumulated investment of sea area use funds involving 11 coastal provinces and 5 state plan cities.

3 Implementation of Renovation and Restoration Projects

The renovation and restoration projects reduce marine pollutants through pollution control, garbage removal, and the cleaning of abandoned and illegal aquaculture facilities in the sea area [6–9]. Improve nearshore hydrological and dynamic conditions, enhance self-purification capacity, and improve marine environmental quality through returning aquaculture to sea area, returning aquaculture to beaches, seabed dredging, and bottom quality improvement. Improve the ability to resist marine disasters and protect the safety of life and property along the coast by building breakwaters for shore protection and dredging, etc. Aim to create a coastal environment that is suitable for residents and tourists to enjoy water, improve the overall quality of marine landscapes, improve living environments, raise public awareness of marine ecology, and create a good social environment through the construction of coastal landscapes such as hydrophilic platforms, landscape corridors, and coastal squares. (The case effect after renovation and restoration is shown in Fig. 3.)

It is estimated that after the implementation of all renovation and restoration projects, a total of 188 km of coastline will be repaired, with a repaired coastal area of 58.76 million square meters, a dredging area of 11.57 million square meters, and a dredging volume of 11.11 million cubic meters. The “Comprehensive Renovation and Marine Environmental Protection Project of Beidaihe Sea Area” creatively proposed the “Cape Bay Sandy Tourism Beach Ecological Restoration Model” of “Sand Dunes Beach Sand Dams Submerged Embankments”, overcoming the problems of short beach life, loss of beach self-sufficiency, and conflicts between beach maintenance projects and habitat protection caused by traditional artificial beach maintenance models. The technical level has reached the international level and leading position in China. The “Beidaihe Model” has been created in the field of beach maintenance and has been applied to multiple beach



Fig. 3. A figure shows the status of the beach renovation of Beidaihe Dapu River to Xinkai River mouth section. The left is before and the right is after the renovation and restoration.

renovation and restoration projects, including Beidaihe West Beach Bathhouse, Laohushi Bathhouse, Expert Bathhouse, Langtao Sand Bathhouse, Donghai Beach Bathhouse, and so on.

4 Problems in Project Implementation

Through visits to relevant sea area management departments and project undertaking companies, as well as on-site inspections of the implementation effectiveness of renovation and restoration projects, some issues that cannot be ignored have been identified and need to be addressed urgently.

4.1 Management System Needs to Be Improved

The coastal zone renovation and restoration project belongs to public welfare projects itself, and the implementation of most projects will not change the natural attributes of the sea area. It improves the infrastructure and ecological environment of the coastal zone through renovation and restoration, and is a truly beneficial and popular project. After the implementation of the project, the sea area still belongs to an open space, without a specific owner of the sea area use rights, and will not be assigned to a certain organization or individual.

The project undertaking companies reported that the project often confronts with inspections from law enforcement agencies and requires relevant sea use procedures to be handled during the implementation process. In addition, the renovation and restoration project include many steps such as application, approval, supervision, and evaluation acceptance. In the specific implementation of the project, it is necessary to apply for project approval and handle relevant procedures such as planning, land use approval, environmental impact assessment, and bidding. After the project acceptance, it is necessary to accept government audits or entrust third-party audits. At present, there has been no clear management measures introduced at the national level, and the construction and management of project systems are disconnected. There is a lack of foundation for management during the project promotion process.

4.2 Insufficient Connection Between Some Projects and Related Planning

The National Marine Function Zoning (2012–2020) clearly requires: “to carry out the renovation and restoration of the sea area and coastal zone. The focus is on the renovation and restoration of the sea area and coastal zone where the natural landscape is seriously damaged, the ecological function is degraded, the disaster prevention ability is weakened, and the utilization efficiency is low. By 2020, the length of the completed renovation and restoration coastline should not be less than 2000 km.”

Most of the renovation and restoration projects currently implemented are only for part of the coastline and sea area. Comprehensive demonstration and analysis of the entire regional environment is deficient, and an overall restoration system has not been formed. Although the invested central sea area uses funds reached approximately 1.67 billion yuan, it is estimated that only 188 km of the coastline will be repaired after all the renovation and restoration projects are completed. Compared to a large number of damaged coastal areas, the renovation and restoration project is still in its early stages and requires persistent long-term investment. After the investigation and survey, it was found that some approved projects were not coordinated with special plans such as local development planning, port planning, and tourism planning, which hindered the implementation of renovation and restoration projects. Thus, the project implementation plans are required to be adjusted, which could not guarantee the predetermined renovation and restoration effects.

4.3 Project Execution Progress Generally Lags Behind

At present, the execution progress of various projects generally lags behind the planned time, mainly due to the following reasons:

Firstly, the designed implementation plan of some project is not comprehensive and detailed, so that the expected results cannot be achieved after the project implementation. For example, the coastal sediment foundation factors are not considered in detail in some projects, so that the original mudflat wetland are transformed into an artificial beach, ignoring the importance of mudflat wetland protection. The detailed demonstration of the hydrodynamic characteristics of the ocean is not provided in some beach restoration projects, and after a period of wave erosion and transportation, the effect of sand replenishment is basically ignored.

Secondly, some project construction involves regional special planning adjustments, demolition compensation, property rights disputes, etc., which has caused significant resistance to the implementation of the project. The design or the use of funds are required to be modified during the implementation process and resubmitted for approval, which affects the progress of project execution.

Thirdly, some projects need to be approved by the development and reform department during the implementation process, and the infrastructure procedures need to be followed again. The budget needs to be reviewed by the finance department, which is a long and inefficient process that affects the project execution progress.

4.4 Project Fund Raising and Utilization Need to Be Strengthened

The current funding support for renovation and restoration projects is mainly based on the return of central shared sea area use funds, lacking diversified funding support combining local financial support and enterprise investment. The funding source is single and the scale is limited, and the amount of funds for a single project is difficult to generate scale effects, resulting in limited restoration results.

In addition, after the central financial funds are transferred to the account, the project implementation progress is delayed, and there is a significant gap between the engineering estimates reported by some projects and the engineering budget at the time of project implementation.

Moreover, due to the increase in labor wages, transportation prices, material prices, and other reasons, the comprehensive cost of the project has changed, and the use of funds needs to be adjusted, which cannot fully utilize the benefits of central financial funds.

4.5 Low Social Participation

The public is both the user and protector of marine and coastal resources and environment. The current process of marine ecological renovation and restoration lacks publicity, education, and positive interaction with the public. Before and after the implementation of ecological restoration projects, the public's opinions and the design of objection expressions and rights relief procedures for relevant behaviors have not been fully listened to. Secondly, both national and local policy documents encourage the establishment of diversified investment mechanisms for coastal zone comprehensive governance and ecological restoration projects, but there is still great room for improvement in the incentive mechanisms and models for social capital participation.

4.6 Lack of Evaluation and Transformation of Ecological Restoration Effectiveness

At present, there is still no effective mechanism for evaluating the performance of marine ecological restoration. In terms of evaluating the effectiveness of ecological restoration projects, the current focus is only on the evaluation of wetland vegetation restoration and beach maintenance effects, lacking overall evaluation research on regional restoration effects. It is difficult to determine whether the restoration requirements have been met in practical work. At the same time, there is a lack of transformation work for ecological restoration effectiveness. Currently, the evaluation of ecological restoration effectiveness focuses on "quantity" rather than "price", which makes the value after ecological restoration unable to be reflected. This is not conducive to the realization of the value created by ecological restoration, but also reduces the motivation for social participation in ecological restoration.

5 Management Suggestions

In order to strengthen the comprehensive management of the coastal zone renovation and restoration project, improve the engineering quality and implementation effect of the project, and promote the engineering progress and completion acceptance of the project, the following suggestions are proposed regarding these problems above.

5.1 Improve Project Management System and Strengthen Full Process Supervision

Improve project management rules and regulations based on the management needs of different stages of the project. Introduce the “Key Directions and Project Application Guidelines for Sea Area and Coastal Zone Renovation and Restoration”, standardizing the key support directions and types of renovation and restoration projects, as well as the project application process. Introduce the “Implementation Plan (Model) for Sea Area and Coastal Zone Renovation and Restoration Projects” to standardize the content of project implementation plan preparation, design focus of different types of projects, and detail requirements of funding preparation, so that the overall project implementation plan meets the requirements of project construction and bidding. Introduce the “Interim Measures for the Management of Sea Area and Coastal Zone Renovation and Restoration Projects”, clarifying the main responsibilities of marine administrative departments at all levels and responsible companies in project management, planning and preparation, project library construction, application and implementation management processes, supervision and inspection, and acceptance management requirements.

After the project is approved, the project undertaking company shall comply with relevant national regulations and requirements strictly, and entrust qualified survey and design institutions to prepare preliminary designs to ensure the quality, content, and depth of the preliminary designs. The construction, supervision, and marine environmental monitoring institutions of the project, as well as the main materials for engineering construction, must undergo public bidding. The bidding activities must be carried out in accordance with the Bidding Law, Government Procurement Law, and other relevant national bidding regulations strictly. The construction company must strictly implement the relevant financial management regulations, comprehensively strengthen the management, supervision and inspection of the use of project funds, improve the efficiency of fund use, and no company or individual shall occupy, misappropriate, or intercept construction funds. During the project construction process, the construction company should simultaneously carry out the project archive construction work, and the formed archives should undergo archive acceptance. Those who have not undergone archive acceptance or fail the archive acceptance shall not pass the completion acceptance of the engineering project.

5.2 Prepare Scientifically and Implement Renovation and Restoration Plans Strictly

According to the actual situation of serious damage to the natural landscape of the coastal zone, degradation of ecological functions, and weakening of disaster prevention

and mitigation capabilities in the process of sea area development and utilization, and in combination with the requirements of coastal economic and social development and environmental protection, as well as the actual needs of marine development, utilization, protection, and comprehensive management, the renovation and restoration plan is scientifically prepared according to the national and provincial marine function zoning, and is in line with the urban and rural planning, infrastructure planning, water conservancy planning, ecological environment planning coordinate and connect tourism special planning, etc.

When planning a project, it is necessary to establish the concept of “regional renovation” for sea use, adhere to the overall approach of regionalization and integration, break through the limitations of fragmented and scattered areas, and effectively connect, reasonably layout, and plan scattered blocks as a whole. The plan should clearly propose the renovation and restoration goals for coastal protection, beach resource restoration, nearshore structure renovation, sea area dredging, coastal landscape beautification, etc., compile a list of renovation and restoration projects, propose coastline length and sea area indicators for the renovation and restoration plan, and develop implementation guarantee measures for the renovation and restoration plan. Once approved, the renovation and restoration plan must be strictly implemented. The approval and all kinds of activities of the renovation and restoration projects must be based on and comply with the plan for the renovation and restoration of the sea area and coastal zone. Marine administrative departments at all levels should coordinate and promote the renovation and restoration work, strengthen planning supervision and inspection, prohibit arbitrary modification of the plan, and effectively maintain the authority and seriousness of the plan.

5.3 Expand Funding Channels and Innovate the Operation Mode of Renovation and Restoration

Increase the transfer payment of central and local financial sea area use funds, while encouraging and guiding social funds to participate in the renovation and restoration of sea area and coastal zones based on the principle of “whoever invests, who benefits”. Research and explore market-oriented fund operation models for renovation and restoration, establish diversified investment and financing channels, and form a sea area and coastal zone renovation and restoration fund guarantee system led by government funds and attracting social funds. Develop preferential policies for social capital investment in renovation and restoration projects, comprehensively utilize measures such as reduction and exemption of sea area use fees, and mobilize the enthusiasm and initiative of social investment entities, sea area use rights holders, and local governments to participate in sea area and coastal zone renovation and restoration.

Implementing differentiated management based on the source of project funds (national financial funds, local financial funds, enterprise investment) and the nature of the project (public welfare, semipublic welfare, and profit making) will help to comprehensively promote the renovation and restoration projects, and implement the renovation and restoration goals proposed by the national marine function zoning.

5.4 Promote the Informatization Construction of Renovation and Restoration Project Management

On the basis of information security, according to the specific needs of the project management process, develop and construct a project library and management decision support system for coastal zone renovation and restoration [10–13].

The construction of project library mainly includes the basic information library, the application information library, the inspection and acceptance information library, the management information library and the policy specifications text library of renovation and restoration projects.

The management decision support platform includes an information release platform and a management application platform, which comprehensively controls the application, approval, implementation, inspection, acceptance, and other aspects of renovation and restoration projects. It realizes functions such as browsing and querying, data statistical analysis, graphic output, and visual effect display of renovation and restoration projects, rationalizes the efficiency of fund utilization, standardizes the implementation of renovation and restoration projects, improves the timeliness of management decisions and provides comprehensive information support.

5.5 Implement the Ecological Restoration Concept of Giving Priority to Natural Restoration and Supplemented by Artificial Restoration

At present, due to the large amount of engineering, high investment in funds, and heavy artificial traces, the restoration model mainly based on manual intervention has caused severe disturbance to the original ecosystem. Therefore, natural restoration should be prioritized and artificial restoration should be supplemented. Measures such as comprehensive water environment management, habitat improvement and biodiversity restoration, vegetation thickening and restoration, as well as shoreline protection and ecological restoration should be taken to enhance the self-purification and restoration capacity of the ocean, and improve the ecological environment quality and function of bays and islands. For natural wetlands that are densely connected, severely fragmented, and functionally degraded, measures such as returning them to the sea, returning them to beaches, and returning them to wetlands from cultivation should be taken to carry out restoration and comprehensive renovation; For typical ecosystems such as coral reefs, mangroves, seagrass beds, estuaries, bays, and islands, ecological conservation measures should be taken, and technologies such as enclosure, microorganisms, seed banks, and animals should be applied to ensure the safety of the ecosystem. Currently, how to implement natural based marine ecological restoration projects requires specific consideration from the degree of ecosystem degradation:

(1) Mild damage to the ecosystem, natural restoration is recommended.

When the degradation of natural ecosystems is not severe and the original system structure and function are basically maintained, natural restoration methods should be adopted. Most of these ecosystems are degraded or threatened by natural or human activities. As long as these disturbances are eliminated in a timely manner, ecosystems can recover on their own without the need for human intervention. In 2019, the United States temporarily closed the Kahalu Bay Marine Park in Hawaii to ensure that coral

breeding in the area was not disturbed by human activities, and it was opened to tourists after the coral breeding period ended. Research has shown that human activities can affect the fertilization process of coral sperm and eggs, posing a threat to coral reproduction. For example, Thailand will close the Maya Bay Marine Park until 2021 to restore the local coral reefs and surrounding ecological environment. Before the closure of Maya Bay, up to 5000 people visited every day. The garbage, pollution, and debris caused by these tourists damaged four fifths of the coral around the island, which grows about half a centimeter per year, indicating that recovery may take a long time.

(2) Moderate damage to the ecosystem, appropriate manual intervention.

When a natural ecosystem undergoes degradation or damage, and its own structure and function undergo significant changes that cannot be self-restored, artificial restoration measures need to be implemented to assist in the restoration of already degraded, damaged or destroyed ecosystems. For example, Shanghai Chongming Dongtan Wetland Restoration. Since the first discovery of *Spartina alterniflora* in Chongming Dongtan in 1995, the plant has gradually settled and rapidly spread in Dongtan, excluding local plants such as reeds. The area where *Spartina alterniflora* grows is difficult for birds to enter for food, and there are very few benthic animals, seriously damaging the biodiversity of Dongtan wetland. Therefore, it is necessary to harness and control *Spartina alterniflora* through human means, and restore damaged wetland habitats.

When implementing artificial intervention, it is necessary to explore natural restoration measures with the ultimate goal of improving the self-recovery ability of the original ecosystem, avoiding the construction of landscape engineering unrelated to ecosystem functions, such as using natural materials to build ecological seawalls, breeding and planting local vegetation, etc. These all require us to fully learn and learn from foreign related restoration projects, and strengthen our own research and development of restoration science and technology.

(3) Severe damage to the ecosystem, suitable for ecological reconstruction.

When the natural ecosystem is excessively damaged and the biological habitat is on the brink of destruction, and it is no longer possible to restore the original ecosystem through artificial restoration methods, ecological reconstruction is necessary. For example, the San Francisco Bay Wetland Construction Project in the United States. San Francisco Bay has a large area of intertidal zone wetlands with diversified habitats in history. In the past 150 years, serious wetland reclamation has led to large-scale loss of wetlands. Therefore, wetlands can only be restored through artificial reconstruction methods. In order to restore the ecological function of the San Francisco Bay coastal wetland, the wetland reconstruction project focusing on the artificial supply of sediment (dredged mud) was implemented. The design of habitat also simulates the natural intertidal zone wetland, which can be said to fully implement the concept of ecological restoration based on nature. Through the wetland reconstruction project, the wetland area of San Francisco Bay in the United States has been expanding, and the wetland ecological function has been significantly restored, which has become a model for wetland restoration around the world.

6 Conclusion

The degradation of marine ecosystems is a common problem faced by various parts of the world, and the renovation and restoration of marine and coastal zones has become a hot topic in marine ecology and oceanography research. China is a major maritime country, and the renovation and restoration of its maritime and coastal zones is an important way to alleviate and improve the degradation of China's marine ecosystem, as well as an important lever for promoting ecological civilization construction. The Chinese government attaches great importance to ecological restoration work, and in the report of the 18th National Congress of the Communist Party of China, it proposed "increasing efforts in natural ecosystem and environmental protection" and "implementing major ecological restoration projects"; The report of the 19th National Congress of the Communist Party of China clearly and reiterated the strategic policy of "implementing major projects for the protection and restoration of important ecosystems". Since 2010, projects such as the renovation, restoration, and protection of sea areas, islands, and coastal zones funded by the central government have gradually been implemented, and the number of ecological restoration projects in coastal areas has been continuously increasing. However, compared with advanced countries in marine ecological restoration, China's marine ecological restoration work started relatively late, with less practical work, and there is still insufficient research and experience summary on marine ecological restoration technology.

The renovation and restoration of the sea area and coastal zone is a complex systematic project that requires unified planning, management, and coordination. It is recommended to focus on the management and research of renovation and restoration in the future, strive to control the trend of ecological environment deterioration in the coastal zone, protect high-quality beaches and natural coastline resources, restore the service functions of some important ecosystems such as typical coastal wetlands and bays, and improve the value of the sea area and coastal zone resources.

References

1. Wu, S.S., Liu, Z.X.: Reflections and suggestions on island ecological restoration and protection projects. *Ocean Develop. Manage.* **30**(4), 9–12 (2013)
2. Zhao, L.M.: Analysis and suggestions on the current situation of island renovation and restoration project management. *Ocean Develop. Manage.* **30**(6), 47–50 (2013)
3. Guo, X.S.: Review of the reclamation land series III: sea area use funds helps the construction of marine ecological civilization. *China Ocean News*, 12–03 (2014)
4. Wong, K.T.M., Lee, J.H.W., Harrison, P.J.: Forecasting of environmental risk maps of coastal algal blooms. *Harmful Algae* **8**(3), 407–420 (2009)
5. Long, J.P., Li, P.Y., Wen, Q.: Comprehensive renovation and sustainable development of Bohai Sea. *Fortune World* **4**, 62–64 (2000)
6. Quang, Q., Ji, C.B.: Institutional arrangements for comprehensive environmental management in the Bohai Sea. *J. Ocean Univ. China (Soc. Sci.)* **2**, 1–3 (2009)
7. Manabe, K.: Environmental management in the Seto Inland Sea. National Council for the Environmental Management of the Seto Inland Sea No.69 (1999)

8. Zhang, M.H., Sun, Z.C., Liang, S.X., Sun, J.W., Suo, A.N.: Analysis of sandy coast regulation effects based on high resolution satellite remote sensing images: a case in Yueliangwan of Yingkou. *Mar. Sci. Bull.* **36**(5), 594–600 (2017)
9. Jiang, Z.P., Liu, X.B., Cao, J.L.: Causes of damage to coastal wetland ecosystems and renovation strategies. *J. Marine Inform. Technol. Appl.* **23**(3), 14–15 (2006)
10. Lam, K.C., Thomas, S.: A cooperative internet-facilitated quality management environment for construction. *Autom. Constr.* **15**(1), 1–11 (2006)
11. Patel, H., Gopal, S., Kaufman, L., et al.: A spatial decision support system for monitoring marine management mreas. *Int. Reg. Sci. Rev.* **34**(2), 191–214 (2011)
12. Suryanarayana, A., Amit, V.S.: GIS analysis for the marine environmental data off Karnataka coast. *Environ. Int.* **32**(2), 180–190 (2006)
13. Ng, S.M.Y., Wai, O.W.H., Li, Y. S., et al.: Integration of a GIS and a complex three-dimensional hydrodynamic, sediment and heavy metal transport numerical model. **40**(6), 391–401 (2009)



Building an Economic Argumentation Model for Vessel Train

Fangfang Jiao, Wendi Liu^(✉), and Jingjing Lin

China Waterborne Transport Research Institute, Beijing 100088, China
{jiaofangfang, liuwendi, lj}j@wti.ac.cn

Abstract. Vessel train has emerged as an innovative mode of transport organization and also as an intelligent ship-navigating technique. In this paper, we focus on the economic efficiency of vessel train for inland shipping and analyze the influence factors of economic efficiency. Based on the current situation of inland waterborne transport in China, we build an economic argumentation model for vessel train in inland waterways. Then, a case study is performed for the fairway along the Yangtze River trunk line that extends from Wuhan to Shanghai in the middle and lower reaches. The economic efficiency of the vessel train is estimated, and a sensitivity analysis is conducted for crew salary, identified as an important influence factor of economic efficiency. The results show that intelligent platooning cannot dramatically reduce the operating cost of vessel train under the current average crew salary in China. But as the crews' salary continues to rise, vessel train is bound to have a bright prospect in the future.

Keywords: Inland Waterways · Vessel Train · Economic Argumentation

1 Introduction

Vessel upsizing has met obstacles in recent years. In this context, to reduce the crew cost of inland vessels, the NOVIMAR project in Europe launched a large-scale coordinated vessel platooning program and proposed the concept of vessel train in 2017. This novel concept has revolutionized inland waterborne transport and ship manning practice [1].

A vessel train is composed of a fully manned lead vessel and a number of less manned or unmanned follower vessels. The lead vessel may be specifically designed for navigational purpose only or working as a container vessel itself. Equipped with navigation and control system, the lead vessel can track the status of the follower vessels, which are lowly manned or unmanned and travel along the route set by the lead vessel. The follower vessels may join or leave the vessel train near the place of departure or destination. Although the follower vessels retain their own maneuvering ability, they primarily follow the lead vessel through coupling and requires less or no manpower.

The transfer of navigational tasks from the follower vessel to the lead vessel enables crew size reduction. Especially on smaller vessels, crew cost can make up to 60% of the operating cost of a vessel [2]. Whether the vessel train can operate depends on whether it is economically superior to existing ships. The operation of vessel train requires to the

construct a network, and the economic cost is different for different operation modes and networks. Such methods have been studied by Ramaekers et al. (2017) specifically for the application of multimodal barge networks on inland waterways [3]. Colling and Hekkenberg (2020 and 2021) additionally address the waiting time created by the vessel train implementations, as well as the vessel train benefits created by exploiting different operating modes and the effects of imposing a vessel train operating speed [4, 5]. In this paper, the economic evaluation model of ships participating in the vessel train is constructed, and the conditions to be met for vessel train operation in the middle and lower reaches of the Yangtze River are calculated.

2 Analysis on the Influence Factors of Economic Efficiency of Vessel Train

The economic efficiency of vessel train for inland shipping mainly depends on whether the reduction in crew cost is equivalent to or greater than the increment of costs due to onshore management of the vessel train. The reduction in crew cost due to the concept of vessel train is mainly affected by two factors: average crew salary and number of vessels joining the vessel train. The increment of costs due to onshore management of vessel train mainly comes from shore-based control and installation and running of an onshore management and operation center for the vessel train. Besides, navigation conditions, such as waterway network density, locks, and low water period, can also affect the operational efficiency and hence the economic efficiency of the vessel train.

2.1 Manning Requirements and Salary

The manning requirements vary with the type and tonnage of vessels. The higher the number of senior officers assigned to the vessels joining the vessel train, the greater the reduction of labor costs due to unmanning or low manning level. Besides, the higher the average crew salary, the greater the reduction of the crew cost by joining the vessel train. China has experienced rapid economic and social development and a constant increase in labor costs in recent years. Crew cost has become an important influence factor of economic efficiency of inland vessels. It can be expected that the average crew salary will continue to rise in the future.

2.2 Number of Vessels Joining the Vessel Train

Vessel train represents a brand new method of organizing inland waterborne transport and cannot completely replace the existing transport mode involving a single vessel. Two preconditions to achieve an efficient operation of vessel train are described as follows: First, a sufficient number of vessels is needed to compose a vessel train with an appropriate density. It is only under this circumstance that the vessels can more easily join the platoon without waiting for too long. Second, given the increment of costs due to shore-based control of the vessel train and the installation of an onshore management and operation center, the higher the number of vessels joining the vessel train, the lower the unit cost.

2.3 Navigation Environment

The longer the operable waterway mileage, the longer the time that the vessels travel in platooning and the greater the cost reduction. With more vessels joining the vessel train, a longer operating mileage will lead to higher shift density of the vessel train and shorter time spent in waiting for the follower vessels to join.

Waterway's degree of networking and accessibility have an impact on the competitiveness and freight demand of inland shipping, which further affects the economic efficiency of transport via vessel train.

Locks are bottlenecks restricting the navigation in inland waterways. Due to the limited size of the lock chamber, only a few vessels pass through the locks at a time. The vessel train has to be disassembled temporarily to pass through the locks one by one. For this reason, vessels that have already passed the lock need to wait for those that have not yet passed through the lock. The vessels are reassembled again when all of them have passed the lock. This process increases the operating time of the vessel train and reduces the transport efficiency. The navigation environment in and out of the lock chamber is relatively complex, which makes automation difficult. In that situation, the vessels have to be navigated separately when passing through the locks.

The operating efficiency of the vessel train is also affected by suspension of navigation in dry season.

2.4 Operating Business Model

A vessel train can be assembled entirely by a single shipping enterprise and only composed of vessels controlled by this enterprise. Vessel platooning is expected to bring about a reform of transport organization within the enterprise. A third-part service platform or industry alliance provides another pathway to assemble a vessel train, which is usually composed of vessels owned by several smaller enterprises. The operating costs vary with the operating business model. If a vessel train is to be built by a single enterprise, the time of vessels' arrival and departure can be arranged more conveniently, thereby increasing the overall transport efficiency. But if a vessel train is composed of vessels owned by different enterprises, coordination of vessels entering and leaving the port poses a greater challenge. If too many vessels are moored in a port at the same time, the resulting waterway congestion will lower the operating efficiency of the vessels. Furthermore, it is more difficult to coordinate vessels entering and leaving the port if they are owned by different enterprises. This will increase the waiting time and reduce the operating efficiency of the vessel train.

3 Current Situation of Inland Shipping in China

In the new century, China has made tremendous progress in inland shipping infrastructure construction, transport vessels, and transport organization. There has been a development trend towards upsizing, standardization and professionalization in the inland shipping sector. By the end of 2020, the average net deadweight tonnage of inland motor cargo vessels was 1443 tons in China, which was 18.4 times that of the value in 2000. This

indicates a striking advance made in the safe and green ship technologies. The organizational models of inland waterborne transport, including river-sea combined transport and river-sea through transport, have been continuously optimized. Up to now, China has established a specialized transport system consisting of coal, oil, ore, and container transport and rolling transport. In 2020, China's container throughput of inland waterway ports reached 30.009 million TEU. In the same year, China's inland water freight volume reached 3.815 billion tons, making China the country with the highest demand for inland shipping in the world [6].

3.1 Manning Requirements and Crew Development

The current manning requirements for inland vessels are laid out based on the "Notice on Revising Appendix 3 of the Regulations for the Minimum Safe Manning of Ships of the People's Republic of China", issued by the Ministry of Transport in 2018. The 2018 edition of the manning requirements permits a differentiation of manning limit for inland vessels. For general navigable inland waters and general vessels traveling in such waters in China, the number of ordinary crews can be reduced as appropriate while maintaining the number of captains and senior officers constant. There has been a trend towards reduced manning in the inland shipping sector. As for the manning of "couple vessels", the minimum safe manning level is reduced to 2, according to the 2018 edition of the manning requirements. After the update, the manning requirements have come much closer to the real-world situation of inland shipping. As shown in Table 1.

China's economic and social development has caused the labor costs of ordinary employees to rise in recent years. This trend also applies to crews working on inland vessels, as shown in Fig. 1. In addition to the rising labor costs, the inland shipping sector is also faced with the problems of population aging, labor shortage, and low comprehensive quality of the crews. The attractiveness of vessel crew jobs can be improved by raising crew salary and improving their working environment. As shown in Fig. 1.

Table 1. Minimum safe manning levels in China.

Deck department of inland vessels: General specifications for general vessels					
Gross tonnage	3000 tons and above	1000 tons and above and below 3000 tons	600 tons and above and below 1000 tons	300 tons and above and below 600 tons	100 tons and above and below 300 tons
General specifications	One captain, 1 first mate, 1 second or third mate, and 1 ordinary crew	One captain, 1 first or second mate, and 1 ordinary crew	One captain and 1 driver	One captain or driver (1 captain and 1 ordinary crew for container vessel and multipurpose vessel)	One captain or driver (1 captain for container vessel and multipurpose vessel)

(continued)

Table 1. (continued)

Additional stipulation	If the uninterrupted time of voyage is longer than 16 hours, one more second or third mate and one more crew should be onboard.	If the uninterrupted time of voyage is longer than 16 hours, one more third mate should be onboard.	If the uninterrrpted time of voyage is longer than 16 hours, one more driver should be onboard. If the uninterrrpted time of voyage is no longer than 10 hours or the mileage of fixed-route navigation is no longer than 100 km, the vessel is exempted from employing one more driver onboard.	If the uninterrupted time of voyage is longer than 10 hours, one more driver should be onboard.	If the uninterrupted time of voyage is longer than 10 hours, one more driver should be onboard.
Engineering department of inland vessels: General specifications for general vessels					
Host power	500 kW and above	150 kW and above and below 500 kW	75 kW and above and below 150 kW		
General specifications	One engineer and one first, second or third engineer	One captain or engineer	One ordinary crew		
Additional stipulation	If the uninterrrpted time for navigation operation is longer than 16 hours, one more ordinary crew should be onboard.				

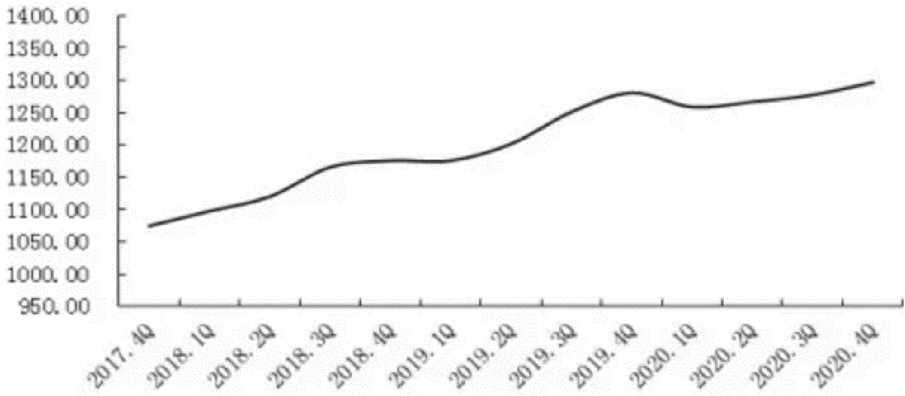


Fig. 1. Complex labor salary index for crews working in Yangtze River waterway. Source: Yangtze River Shipping Development Report

3.2 Freight Volume and Composition of the Vessel Train

In 2020, China's inland waterway freight volume was 3.815 billion tons and the inland waterway freight turnover was 1593.754 billion ton kilometers. Inland waterway freight turnover accounted for 8.1% of total freight turnover [7]. Cargoes transported by inland waterways mainly include dry bulk, break bulk, containers, and liquid bulk. Dry bulk accounts for the largest proportion of all cargoes transported by inland waterways, which is over 70%. Specifically, minerals and building materials account for about 30%, coal 20%, metallic ores 14%, non-metallic ores 5%, and cereals 2%. Iron & steel and cement collectively account for 16% of the break bulk cargo. Container transport has experienced the fastest development among all transport modes, accounting for 8.5%. Liquid bulk cargo, such as oil, natural gas, and their products, accounts for about 3%. As to geographical distribution, inland waterway freight volume is mainly concentrated in the Yangtze River system (Beijing-Hangzhou Grand Canal included). In 2020, the inland waterway freight volume of 14 provinces and municipalities located in the Yangtze River system collectively reached 3.12 billion tons, and the freight turnover was 1423.67 billion ton kilometers. They accounted for 81.9% and 89.3% of the national inland waterway freight volume and the national freight turnover, respectively [8].

By the end of 2020, China had a total of 115 thousand inland vessels with a deadweight tonnage of 137 million tons. Among them, there were 106.1 thousand motor cargo vessels with a deadweight tonnage of 130 million tons. The total deadweight tonnage of motor cargo vessels accounted for as high as 95%. Therefore, motor cargo vessels are the most important components of China's inland vessel platoon [9]. Given the types of cargoes most commonly transported, general cargo vessels (dry bulk carriers and multipurpose vessels) accounted for the largest proportion of all inland motor cargo vessels. Their total deadweight tonnage accounted for over 95%. By contrast, the total deadweight tonnage of container vessels only accounted for 1.3%. This is because inland vessels are mostly of an open type. Containers that account for a larger proportion of all cargoes are usually transported by multipurpose vessels. The total deadweight tonnage of oil tankers only accounted for 1.4%.

3.3 Navigation Environment

China's inland shipping activities are mainly concentrated in two regions, namely, Yangtze River system (Beijing-Hangzhou Grand Canal included) and Pearl River system. The main fairways in these two waters are the Yangtze River trunk line, Beijing-Hangzhou Canal, and West River trunk line. The Yangtze River trunk line extends from Shuifu, Yunnan to the Yangtze River estuary, with a navigable mileage of 2838 km. The standard-reaching rate of dredging depth is 100%. The ship lock of the Three Gorges Dam is located in Yichang in the upper reach, and there are no other ship locks on the entire route. The Beijing-Hangzhou Grand Canal extends from Liangshan, Shandong to Hangzhou, Zhejiang, with a length of 1052 km. The Canal is featured by small water level changes and has 19 locks altogether, running through several water systems, including the Yellow River, Huai River, Yangtze River, and Qiantang River. The West River trunk line extends from Nanning, Guangxi to the Pearl River estuary, with a navigable mileage of 786 km. However, the West River trunk line is facing new bottlenecks due to the large number of shoals along the fairway from the lower reach of the Changzhou water conservancy hub to Zhaoqing. It has 9 locks already built and 2 locks currently under construction.

3.4 Composition of Business Entities on the Market

The business entities in China's inland shipping sector are of various sizes and types. There are about 4800 inland shipping enterprises and more than 10 thousand self-employed entrepreneurs. Dry bulk transport organization is less centralized and the market concentration level is low due to scattered sources of goods (typically ores and building materials). Nevertheless, large cargo owners of metallic ores and coal, such as Anshan Iron and Steel Group Corporation, usually have their stable transport fleets. Containers are transported by liners, and the level of organizational centralization is higher. Besides, containers are usually transported by inner branch lines of international routes. The main enterprises organizing container transport include Shanghai International Port (Group) Co., Ltd., Shanghai Panasia Shipping Co., Ltd., and Sinotrans. The transport of liquid bulk (typical dangerous goods, such as oil) is heavily influenced by China's macro-control policies for transport capacity. The level of market concentration is higher for the transport of liquid bulk than that for dry bulk. There are 154 enterprises engaged in interprovincial transport of dangerous liquid bulk in the Yangtze River system. Most of them are private-owned enterprises. Enterprises controlling more than 20 vessels are still small in number.

4 Building an Economic Argumentation Model for Vessel Train

4.1 Purpose of Building the Economic Argumentation Model

Operating revenue and operating cost are two major influence factors of economic efficiency of waterborne transport. The former primarily depends on the unit price of transport and annual number of voyages. In the case of vessel train, it takes time to wait for follower vessels to enter and leave the port or pass through the locks. The operating

efficiency is lowered as the waiting is prolonged. The operating costs mainly consist of the following parts: investment in fixed assets, fixed costs (crew cost, lubricant and material costs, and management fee), and variable costs (fuel cost and port charges). Crew cost can be lowered by joining a vessel train, but there may be changes in fuel cost as the voyage time increases and the traveling speed changes.

For a vessel train to be economically efficient, the following conditions should be met:

- (1) The freight rate of the vessel train is lower than or equal to that of a single vessel;
- (2) The reduction of crew cost by joining the vessel train is at least equal to the sum of the increment of all costs due to joining the vessel train and the revenue reduction due to the decrease in operating efficiency.

As long as the traveling speed and the length of the operating fairway meet the actual operating demands of transport agencies, a vessel train is economically efficient if it satisfies the above conditions. The value ranges of the following indicators are estimated by sensitivity analysis, so as to determine the survival boundary of the vessel train.

- (1) Total time spent in waiting for follower vessels to enter and leave the port and pass through the locks in a single voyage;
- (2) Acceptable platform management fee paid for joining the vessel train.

4.2 Main Parameters and the Calculation Method for Financial Evaluation Indicators

When a shipping enterprise invests in vessels that joins a vessel train and performs a financial evaluation of the vessel investment project, the main parameter involved in estimation is the annual number of voyages in platooning, which is different from the situation of investing in vessels not operating in platooning. Without considering cargo supply organization, the annual number of voyages depends on the navigation environment. The main parameters involved in estimating the annual number of voyages are the traveling speed and the round voyage time of the vessel train.

$$V_{vt} = \frac{d}{\frac{d}{v_{vt}} + t_{p\&l}}$$

$$N = \frac{T}{\frac{d_{vt}}{V_{vt}} + \frac{d_o}{v_o} + t_p}$$

V_{vt} : Traveling speed of the vessel train;

v_o : Traveling speed of the vessel in self-navigation;

d : Distance covered by the vessel train along the fairway;

d_o : Distance covered by the vessel in self-navigation;

v_{vt} : Traveling speed of the vessel train;

N : Annual number of voyages;

$t_{p\&l}$: Sum of time spent in waiting for follower vessels to enter and leave the vessel train and pass through the locks;

d_{vt} : Distance covered by the vessel in platooning;

t_p : Time spent in port operation;

T : Annual number of days in operation.

4.3 Main Economic Evaluation Indicators

For economic argumentation, the main evaluation indicators include financial net present value (FNPV), financial internal rate of return (FIRR), and payback period (Pt) [5].

FNPV is defined as the summation of all present values of a series of payments and future cash flows under the specified discount rate (typically the benchmark yield *i*). The pre-tax and after-tax net present values can be calculated as follows:

$$NVP = \sum_{T=1}^n \left(\frac{P}{F}, i, t \right) \times (CI - CO) - P$$

where *P* is the initial investment, which is the ship price;

CI is the cash inflow;

CO is the cash outflow;

i is the benchmark yield;

n is the number of years in the calculation period.

Payback period (*P_t*) is the length of time it takes to recover the cost of an investment, usually in the unit of year. *P_t* is calculated as follows:

$$\sum_{t=0}^{P_t} (CI - CO)t(1 + i_c) = 0$$

FIRR is the discount rate for which the net present value (NPV) equals zero in the calculation period of the project. That is, FIRR as a discount rate makes the equation below holds true:

$$\sum_{t=1}^n (CI - CO)t(1 + FIRR)^{-t} = 0$$

Typical required freight rate (RFR) is the minimum cargo rate which the shipowner has to charge the customer just to break even. As a composite economic indicator, RFR is given below:

$$RFR = \frac{P\left(\frac{A}{P}, i, N\right) + Y}{Q}$$

or

$$RFR = (Y - S_2 + P\left(\frac{A}{P}, i, N\right) - RL\left(\frac{A}{F}, i, N\right))$$

$$Y = S_1 + S_2 + S_3 + S_4 + S_5 + S_6 + S_7 + S_8 + S_9$$

where *Y* is the annual operating cost;

RL is the salvage value of the vessel after depreciation;

S₁ – *S₉* are crew salary and other, annual depreciation expense, annual maintenance cost, annual premium, annual fuel cost, annual lubricant cost, annual material cost, annual port charge, annual management fee and other, respectively.

Since joining the vessel train requires an initial investment and increases the management fee, FNPV, *P_t* and RFR are evaluation indicators with weak comparability in this scenario. Given the above, the parameters are estimated under a constant FIRR.

5 A Case Study of Estimating the Economic Efficiency of the Vessel Train

5.1 Main Parameters Involved in the Estimation

Based on comprehensive consideration of the navigation environment of China's major inland waterway networks and the current size of inland waterborne transport market, we perform a case study of economic efficiency estimation of vessel train by choosing the fairway extending from Wuhan to Shanghai in the middle and lower reaches of the Yangtze River trunk line. That is, the route segment extending from Yangluo Port in Wuhan to Waigaoqiao Port in Shanghai to be covered by the vessel train is the route chosen for estimating the economic efficiency of the vessels joining the vessel train. The main parameters involved in the estimation are shown in Table 2 and Table 3.

Table 2. Main parameters involved in the estimation.

Container capacity	494TEU	Cost	30 million RMB
Annual number of days in operation (T)	330 days	Insurance premium	0.5% of the ship price
Traveling speed of vessel through self-navigation (v_o)	16km/h upstream 21km/h downstream	Management fee	2% of freight revenue (tax included)
Time spent in port operation (t_p)	48h	Repair cost	2% of the ship price
Average freight rate of empty containers	450 yuan/TEU	Fuel cost	4500 yuan/ton
Load rate	60% upstream 70% downstream	Lubricant and material costs	4% of fuel cost
Depreciation period	15 years	Crews	9 people (150 thousand yuan/person/year)
Salvage value	10%	Interest rate	5.5% (capital ratio of 30%)
Number of years of evaluation	15 years	Tax rate	25%/9%/13%

Table 3. Main operating parameters of the vessel train.

Traveling speed of the vessel train (v_{vt})	15km/h upstream 18km/h downstream
Sum of time spent in waiting for follower vessels to enter and leave the vessel train and pass through the locks ($t_{p\&l}$)	8h (no need to pass through the locks)

5.2 Results of Financial Evaluation

China's inland shipping enterprises are of differentiated sizes and shipping capacities, and there is barely any large-scale leading enterprise in this sector. Therefore, it is beyond the capacity of any single enterprise to build a vessel train on its own. Rather, a third-party operating platform is more suited to China's current situation of inland shipping. The operating costs of vessel train have been estimated by NOVIMAR, which shows that with the costs of office space, software upgrading, and shore-based personnel and a reasonable profit margin considered, the annual revenue from running an operating platform is about 40 million RMB. Suppose that 20 vessel trains are run, with each joined by 8 follower vessels. Then, the annual management fee paid by owners of the follower vessels is about 250 thousand RMB. Besides, each follower vessel needs to purchase a control system, which costs about 800 thousand RMB. As for the reduction of crew costs, three additional crews should be onboard apart from the initial six if the uninterrupted time of voyage is longer than 16 h, according to the manning requirements. But by joining a vessel train, a follower vessel is allowed to have only 3 crews onboard.

The results of financial evaluation for not joining the vessel train are shown in Table 4 and Table 5.

Table 4. Financial evaluation for not joining the vessel train.

Total return on investment (after-tax)	%	6.46%
Return on equity	%	24.78%
Financial internal rate of return of the project (after-tax)	%	11.30%
Financial net present value of the project (after-tax)	Ten thousand yuan	387
Payback period of the project (after-tax)	Year	7.79
Financial internal rate of return of the project	%	23.70%

Table 5. Financial evaluation for joining the vessel train.

Total return on investment (after-tax)	%	5.77%
Return on equity	%	20.81%
Financial internal rate of return of the project (after-tax)	%	10.31%
Financial net present value of the project (after-tax)	Ten thousand yuan	226
Payback period of the project (after-tax)	Year	8.26
Financial internal rate of return of the project	%	21.21%

Joining a vessel train requires an initial investment, and the shipowner has to pay the annual management fee. While the decrease in traveling speed and the time spent in waiting reduce the vessel turnover rate, the crew and fuel costs go down. The results of financial evaluation for vessel investment in the above case are presented below.

With other conditions unchanged, as the average crew salary increases to 235 thousand yuan per person per year, FIRR is the same by joining or not joining the vessel train, and it decreases to 8.47% in either situation.

5.3 Sensitivity Analysis

Crew salary and Management Fee. With FIRR unchanged and the initial investment in the control system being 800 thousand yuan, we estimate the acceptable annual management fee to be paid by shipowners under variable average crew salary.

Next, we estimate the annual management fee under a constant after-tax FIRR as the average crew salary increases from 200 to 220 and 240 and finally to 300 thousand.

We also estimate the annual management fee under a constant FIRR of 8.47% as the average crew salary increases from 200 to 300 thousand, as shown in Table 6.

Table 6. Crew salary and changes in management fee.

Crew salary Changes in crew salary		Management fee (Unit: ten thousand yuan)
-3.5	20	72.5
-1.5	22	59.5
0	23.5	50
+0.5	24	46.5
+2.5	26	33.8
+3.5	28	20.6
+5.5	30	7.8

It can be seen from the above calculations that as the average crew salary increases from 200 thousand to 300 thousand per year per person, the annual management fee decreases from 725 thousand to 78 thousand yuan per year under the constant FIRR of 8.47%.

Crew Salary and Acceptable Time Spent in Waiting for Follower Vessels to Enter and Leave the Port and Pass Through the Locks. Suppose that FIRR remains constant and the initial investment in the control system is 800 thousand yuan. We estimate the total time spent in waiting for follower vessels to enter and leave the port and pass through the locks in a single voyage under variable average crew salary.

As the average crew salary increases from 200 to 220 and 240 and finally to 300 thousand, we estimate the total time spent in waiting for follower vessels to enter and leave the port and pass through the locks in a single voyage under a constant after-tax FIRR, as shown in Table 7.

Table 7. Crew salary and changes in waiting time.

Crew salary Changes in crew salary		Total time (Unit: hour)
-3.5	20	11.75
-1.5	22	9.55
0	23.5	8
+0.5	24	7.45
+2.5	26	5.4
+3.5	28	3.35
+5.5	30	1.4

It can be seen from the above calculations that as the average crew salary increases from 200 thousand to 300 thousand per year per person, the acceptable total time spent in waiting for follower vessels to enter and leave the port and pass through the locks in a single voyage decreases from 11.75 h to 1.4 h under the constant FIRR of 8.47%.

6 Conclusion and Suggestions

China's inland shipping sector has the capacity and the potential to build a vessel train, given the current number of vessels available to join and the traffic density of inland waterways. Besides, platooning improves voyage safety, especially in waters with higher traffic density, such as the Yangtze River trunk line. But according to the estimation from the economic argumentation model, it is still hardly possible to dramatically cut down the operating cost through intelligent platooning under the current crew salary in China, compared with the case of the Rhine River. Besides, Chinese inland waterway crews usually have to work long, uninterrupted hours onboard, resulting in a higher vessel utilization rate. This situation stands in stark contrast to long hours of suspension for vessels on the Rhine River (typically 10 h per time). Another major obstacle to building a third-party shore-based control platform for vessel train in China lies in the low centralization level of business entities and cargo supply organization in the inland shipping sector. Nevertheless, vessel train is expected to have a bright prospect as the crew salary and crews' living standard continue to rise.

References

1. Novel IWT and maritime transport concepts (NOVIMAR). https://www.sohu.com/a/478982149_120056227. Accessed 22 July 2021
2. Beelen, M.: Structuring and modelling decision making in the inland navigation sector. Universiteit Antwerpen, Belgium, Faculteit Toegepaste Economische Wetenschappen (2011)

3. Ramaekers, K., Verdonck, L., Caris, A., Meers, D., Macharis, C.: Allocating collaborative costs in 21 multimodal barge networks for freight bundling. *J. Transp. Geogr.* **65**, 56–69 (2017)
4. Colling, A.P., Hekkenberg, R.G.: Waterborne platooning in the short sea shipping sector. *Transp. Res. Part C: Emerging Technol.* **120**, 102778 (2020)
5. Colling, A., Van Hassel, E., Hekkenberg, R.: Waterborne platoon on the lower Rhine. *European Journal of Transport and Infrastructure Research* (under Review) (2021)
6. Ministry of Transport. 2020 Statistical Bulletin of the Development of China's Transportation Industry. https://xxgk.mot.gov.cn/2020/jigou/zhghs/202105/t20210517_3593412.html. Accessed 09 July 2021
7. Huan, Z.P.: Analysis of reasons for decreased competence of inland waterway crews and countermeasures and suggestions. *Maritime Educ. Res.* **34**(03), 1–4 (2017)
8. Changjiang Waterway Bureau affiliated to the Ministry of Transport. 2020 Report on Changjiang River Shipping Development. China (2021)
9. Lv, J., Liang, J.: *Technological Economics*. Chemical Industrial Press, Beijing (2008)



Numerical Investigation of Turbulence Models for Swirling Nitrogen/Air

Aoshuang Ding, Nenghui Wang, Zaixing Yang, Wenqing Mei^(✉), Lin Chen, Congyang Xiao, Hai Wu, and Siyang Yi

China Shipbuilding Jiujiang Marine Equipment (Group) Company Limited, Jiujiang, China
17824832878@163.com

Abstract. In this paper, different turbulence models are researched by simulating a non-reactive swirl flow of the non-premixed cyclone burner in comparison with the experimental results. Based on the velocity analyses, obvious recirculation zone (CRZ) and jet zone (SJ) exist in the experiments and influences the swirl flow. However, the laminar flow model, SST k- ω , standard k- ω cannot simulate these two vital regions as same accurate as the RNG model, especially for the declination angles. Comparing the axial velocity curve and tangential velocity curve, axial velocity and tangential velocity peaks and trough position and velocity magnitude of the RNG k- ϵ model are the closest to the experimental results, which can fully predict the swirl characteristics. The structure of the vortex is fully represented by RNG model, and the CRZ and SJ at the burner outlet are well captured. Thus, the RNG model is most suitable for the swirl flows. Based on the simulation results of the RNG model, the CRZ and SJ are folded, corrugated, and have completely asymmetrical behavior due to Kelvin-Helmholtz instability. It may cause the turbulence models without swirl corrections to be unable to simulate the important swirl flow characteristics correctly, while the RNG model has considered the swirl influence in the turbulence viscosity correction. Therefore, a suitable swirl flow correction considering the swirl number is important in turbulence models for such simulations.

Keywords: Turbulence model · RNG · Swirl Flow

1 Introduction

In addition to axial velocity, the swirling flow also has a rotational motion or tangential velocity component, which is achieved by adding a cyclone or introducing the airflow tangentially into the combustion chamber [1]. These swirl flows find applications in various non-reacting systems [2–9]. They are also employed in reacting systems [10–17]. Swirl flows are extensively utilized and play a crucial role in combustion systems [18] due to their ability to stabilize high-intensity combustion.

Various experimental researches have been done on the swirl flows in different aspects. A M. Elbaz [18] used three-dimensional particle image velocimetry (SPIV) technology to research the turbulent field of non-premixed methane swirling flames.

Christopher O. Iyogon [19] studied on the effect of swirling intensity on the stability of swirling non-premixed methane flames by experiments, and found that increasing the intensity of swirling flow can create a flow recirculation zone. With quantitative analysis, Nazim Merlo [20] studied the effect of swirl number on flame stability through hydrogen oxygen chemiluminescence experiments, indicating that increasing the number of swirls can significantly improve flame stability. Toufik Boushaki [21] use volumetric V3V 3D3C velocity to measure turbulent flow of swirl burner.

Apart from the experimental method, the swirl flows have also been researched by the simulation methods in recent years. Based on the computational fluid dynamics, P. Wang [22] and Ying Huang [23] used large eddy simulation (LES) to analyze the isothermal turbulent swirl flow and premixed swirl combustion, respectively. Furthermore, Martin Freitag [24] studied swirling and mixing processes by using direct numerical simulation (DNS). Considering the huge calculation time of DNS, Mansouri Zakaria [25, 26] used Detached Eddy Simulation Model (DES) and Delayed detached eddy simulation (DDES) to analyze and compare the swirl combustion and non-reacting swirl flow, respectively. Beside the above turbulence model research with high calculation requests, Dr. K. Sudhakar Reddy [27] and Y Mao [28] adopted RNG $k-\epsilon$ to simulate the closed isothermal swirling flow and made improvements on this model to better catch the swirl flow characteristics. Mansouri Zakaria [29] and Sharif M [30] used other two-equation turbulence models to analyze the similar swirl flows with detailed swirl flow velocity distributions captured.

However, most of the previous simulation studies related to swirling flow deal with non-annular geometries, single turbulence model and have few considerations for the simulation influence of various turbulence models. In order to find the best turbulence model for simulating swirl flows, different turbulence models are adopted to simulate the non-reacting turbulent swirling flow in a non-premixed burner [26] and compared with experimental data [21, 26]. In comparison with other turbulence models and laminar model, the vital tangential velocity distributions of RNG model is closer to the experimental data. It is in corresponding with the characteristic swirl factor used for the turbulent viscosity correction in RNG model to capture the important details of swirl flows. Based on the flow field analyses of various turbulence models, it is found that RNG model is most suitable model to simulate swirl flow.

2 Numerical Model

2.1 Turbulence Model

As this swirl flow does not involve combustion calculation, it is assumed that the flow is isothermal and only the continuity and momentum equations are solved in turbulence models. On this basis, the continuity equation and momentum equation of the system are solved by the steady-state hypothesis. The steady-state continuity equation involved is:

$$\frac{\partial}{\partial x_j}(\rho u_j) = 0 \quad (1)$$

The steady-state momentum equation is:

$$\frac{\partial(\rho u_i u_j)}{\partial x_j} = \frac{\partial(P)}{\partial x_i} + \frac{\partial(\tau_{ij})}{\partial x_j} \quad (2)$$

where τ_{ij} is the viscous stress tensor, which is given by the following formula:

$$\tau_{ij} = \mu \left[\frac{\partial(u_i)}{\partial x_j} + \frac{\partial(u_j)}{\partial x_i} - \frac{2}{3} \frac{\partial(u_k)}{\partial x_k} \delta_{ij} \right] \quad (3)$$

where ρ , P and μ are the density, pressure and viscosity, respectively, and u is the velocity component in a certain direction.

As the swirl fluid flow is affected by swirl and rotation, the RNG model corrects the influence of swirl by modifying turbulence viscosity appropriately [31]. The modified function form is as follows:

$$\mu = \mu_{t0} f \left(\alpha_s, \Omega, \frac{k}{\varepsilon} \right) \quad (4)$$

where the swirl number α_s is constant based on the flow situations.

The below is for the averaged Reynolds stress:

$$\frac{\partial}{\partial x_j} (\rho u_i u_j) = -\frac{\partial P}{\partial x_i} - \frac{\partial \tau_{ij}}{\partial x_j} + \frac{\partial}{\partial x_i} \left(-\rho \overline{u'_i u'_j} \right) \quad (5)$$

However, additional terms for turbulence effects is called the Reynolds stresses. In order to provide closure for the momentum equation, these terms can be simulated by different turbulence models. Considering that two-way turbulence models are widely used in numerical simulation of swirling flow, the k - ε model and k - ω model are adopted in this paper, and the enhanced wall function is applied to these models.

2.2 Simulated Geometry and Conditions

The experimental apparatus and data from Boushaki et al. [21, 26] are simulated in this study. Figure 1 shows the 3D annular pipe geometry with swirler. The coordinate system is also built in Fig. 1. Table 1 shows the detailed boundary conditions with the mixture model for ideal air and ideal nitrogen. Nitrogen inlet is shown as blue fuel arrow in Fig. 1.

In view of the complex structure of cyclone blades, tetrahedral elements were used to construct the basin grid, and the basin grid was encrypted. Figure 2(a) is the global grid, and Fig. 2(b) is the partial grid of the cyclone.

2.3 Grid Independence Verification

The grid independence of three different grids is verified. The fine grid, medium grid and coarse grid consist of 10.76 million cells, 6.72 million cells and 3.60 million cells independently and are simulated by RNG k - ε model.

Table 1. Boundary conditions.

Boundary condition	Model	Parameter
Air inlet	Mass-flow	5.218 g/s
N ₂ inlet	Mass-flow	0.244 g/s, 25 °C
Wall	Adiabatic no-slip	
Outlet	Pressure	Static ambient pressure

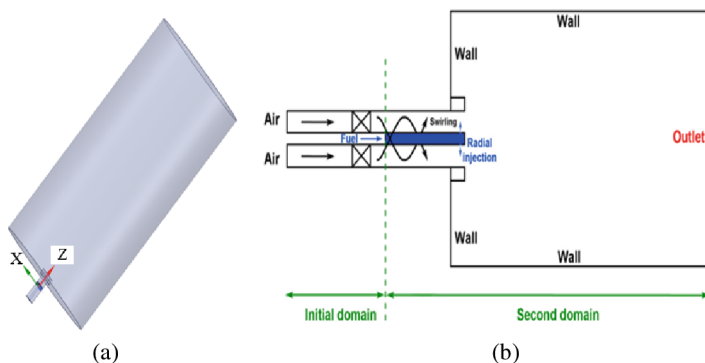


Fig. 1. (a) 3D model (b) A sketch of numerical domains.

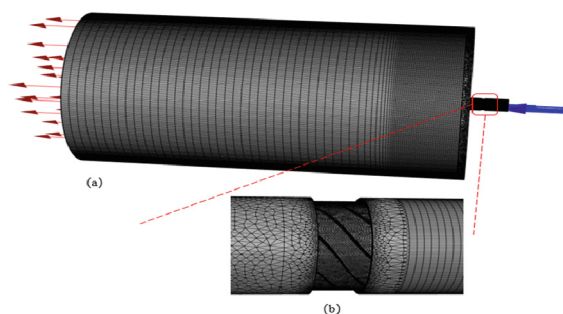


Fig. 2. (a) Mesh used for the simulation (b) Shows swirler.

As the velocity distribution is the most vital flow characteristics in swirl flows, the axial Z velocity distribution along the radial direction is averaged along the axial direction and shown in Fig. 3. The axial direction and radial direction are normalized with Z/D and X/D, and D means the diameter of Air inlet. As shown below, in the region (X/D ranges from -0.5 to 0.5), the coarse mesh results are quite different from the medium and fine mesh results. It indicates that the coarse mesh is not independent. The profiles

of the fine and the medium meshes present the same x velocity distribution in different axial Z/D directions. Thus, the medium mesh and fine mesh can be enough for the swirl flow simulations.

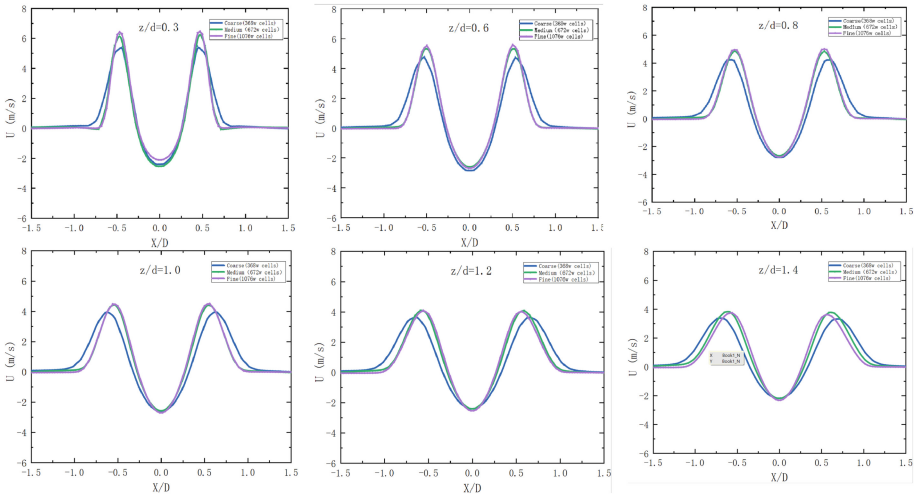


Fig. 3. Grid sensitivity solution for radial distribution of axial velocity.

In order to compare the detailed result differences between the medium and fine mesh, two peak velocity values and one trough velocity value in velocity distributions are selected to be in Table 2. Considering that the swirl flows need space to develop, the middle location $Z/D = 1.0$ is chosen to be analyzed in Table 2 with fully-developed swirl flows. As for two peaks, the peak A and C mean the peaks in negative X/D and positive X/D , respectively.

Table 2. Simulated x velocity results in $Z/D = 1.0$.

Mesh	Velocity	X/D	X velocity [m/s]
Coarse (368w cells)	Peak A	-0.56	4.25
	Trough B	-0.05	-2.78
	Peak C	0.56	4.23
Medium (672w cells)	Peak A	-0.53	4.90
	Trough B	-0.02	-2.65
	Peak C	0.53	4.88
Fine (1076w cells)	Peak A	-0.53	4.97
	Trough B	-0.02	-2.75
	Peak C	0.53	5.02

As shown above, at A, B and C, the peak and trough radial positions of the medium-sized mesh are same with the fine mesh, while the coarse mesh has different peak and trough locations. Compared with the fine mesh, the peak and trough velocity values of medium mesh have less than 4% difference, indicating that the medium mesh is good enough to capture the detailed velocity distributions in swirl flows. Therefore, the mesh density of the medium mesh is used to generate the fluid domain mesh.

3 Results and Discussions

3.1 Velocity Distributions

According to the study by Gupta, A. K [1], the axial velocity and tangential velocity of rotational motion can exhibit key characteristics of swirling flow. Therefore, in order to highlight the swirl flow simulation differences among various turbulence models, a comparative analysis is conducted on the axial velocity and tangential velocity contours as shown in Fig. 4.

Figure 4 (a) and (b) depict the experimental velocity contours [21, 26]. As the axial velocity in the radial middle center area is negative in experimental data, the gas flows back to the inlet in the radial middle center area. Thus the radial middle center area is called a central recirculation zone (CRZ), a vital area with significant swirl flow characteristics. In two sides of the CRZ, the jet flow exits with high velocity, named as swirl jet area (SJ). The SJ surrounds the CRZ with two interlayers, calling the outer shear layer (OSL) and the inner shear layer (ISL). The OSL is related to external static regions, while the ISL and the CRZ are in direct contact.

Based on Fig. 4 (c), the laminar simulation results do not exhibit the SJ and CRZ features. As for Fig. 4 (d), it is observed that vortices appear near $x = \pm 0.02$ m and moves upwards, not present in Fig. 4 (b). The transient vortices movement of laminar model shows that the swirl flow has transient characteristics. The transient analyses should be done in future simulations. However, taking the simulation time into consideration, the steady turbulent simulation is enough to simulate the important time-averaged experimental data correctly. Thus, the laminar model cannot simulate the swirl flow accurately with turbulence existing. Figure 4 (e), (f), (g), and (h) respectively show the axial velocity and tangential velocity contours simulated by the Realizable and RNG. Compared with the experimental results, the axial velocity features of these models are quite consistent in exhibiting the CRZ and SJ. However, the simulated SJ angles, shown in Fig. 4 with black lines are different. Figure 4 (a) has an angle of 15.95° , while Fig. 4 (e) and (g) have angles of 18.67° and 20.47° respectively. It indicates that the CRZ simulated by the RNG is in better agreements with experimental results than the Realizable. Therefore, the RNG is fit for simulating the swirl flows with accurate SJ results. Figure 4 (i), (j), (k), and (l) respectively show the axial velocity and tangential velocity contours simulated by the Standard and SST. Comparing Fig. 4 (i) and (k) with the experimental results, the axial velocity map features are quite consistent. Both maps exhibit the CRZ and SJ, with the main difference being the SJ angle. The SJ angles in Fig. 4 (i) and (k) are 21.52° and 20.04° respectively, higher than the RNG. Comparing Fig. 4 (j) and (l) with the experimental results, the tangential velocity map features are generally consistent. In Fig. 4 (j) and (l), the locations of the almost zero tangential velocity are at 110 mm and 135 mm,

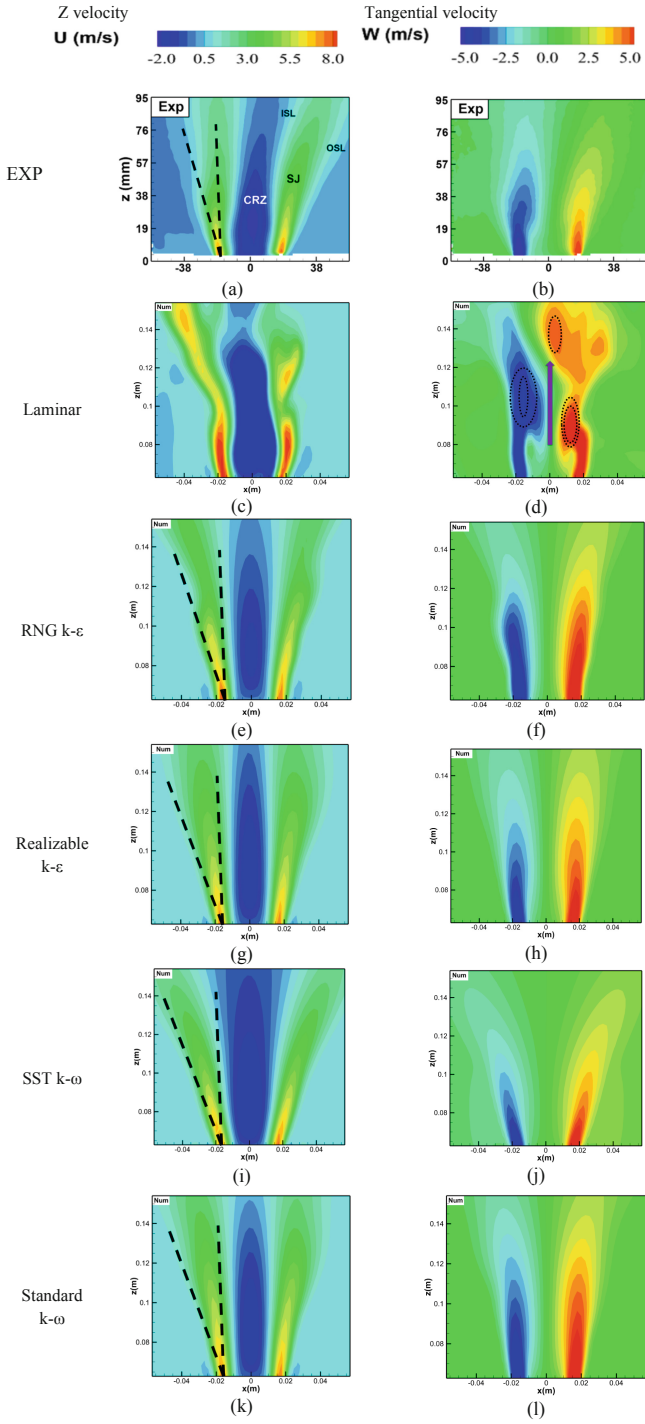


Fig. 4. Experimental and numerical axial and tangential velocities.

equaling to 50 mm and 75 mm in the experimental coordinate while the experimental data is 60 mm. Therefore, the RNG is better than other models in simulating the swirl flows with correct SJ and ORZ results.

By comparing the axial velocity distributions of various turbulence models, it is found that the laminar flow model is quite different from the experimental results, the CRZ and SJ in axial velocity contours features are not obvious, while the features of other turbulence models are close to the experimental results, but the de-flection angle of the central area of the RNG model is in the best agreement with the experiments. Comparing the tangential velocity cloud images of different turbulence models, the laminar flow model has vortices, and the vortices tend to move upwards, while the characteristics of other turbulence models are close to the experimental results, but the tangential velocity peak and valley positions of RNG are closest to the experimental results.

3.2 Analyses of Axial and Tangential Velocity

To further analyze the detailed simulation differences among the turbulence models, six axial positions are selected and the axial and tangential velocity distributions along radial direction at these axial positions are shown in Figs. 5 and 6.

Through the analyses of Fig. 5, it is found that the velocity profiles of the Standard $k-\omega$ model and the laminar flow model differ significantly from the experimental results. However, the Realizable $k-\epsilon$, RNG $k-\epsilon$, and SST $k-\omega$ models show a relatively close approximation to the experimental results in general. Compared with the experimental data, the axial velocity distributions of SST, Realizable $k-\epsilon$ and RNG $k-\epsilon$ have 0.49%, 0.79% and 0.84% root mean square error averaged with six locations, respectively. Among the six locations, the maximum root mean square error of these three turbulence models are 0.79%, 1.0% and 1.48%, respectively.

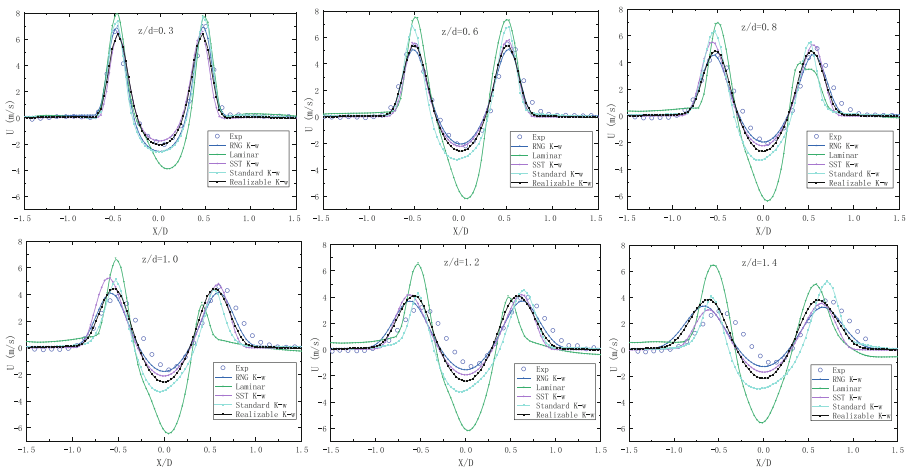


Fig. 5. Axial velocity at several position.

Compared with SST and Realizable, the biggest difference of RNG is the introduction of swirl factor in the calculation equation of turbulence viscosity μ . The three models discussed above give good predictions in the developed swirl region. But, RNG is the best as it offers more accurate results and better numerical stability than other model in undeveloped regions. As the swirl flow is developing fast in the $Z/D = 1.0$, this location should be especially analyzed. It is observed that the RNG simulates peaks and troughs that are closer to the experimental results, whose average error is less than 4.6% and maximum error is less than 6.6%. Based on the analysis of the axial velocity profiles obtained from different turbulence models, it can be concluded that the results of the RNG are closer to the experimental results.

Figure 6 shows that the velocity profiles of the SST, Standard, and laminar flow models differ significantly from the experimental curve, especially the laminar flow model. On the other side, the RNG and Realizable exhibit a relatively close agreement with the experimental curve, as already mentioned in the analysis of the velocity maps and axial velocity profiles. To further analyze this, we select the tangential velocity at the $z/d = 1$ position and compare the peaks and troughs of the tangential velocity obtained from different turbulence models with the experimental results. Through analysis, it is observed that the RNG and Realizable produce peaks and troughs that are close to the experimental data. There is a slight difference in the magnitudes of the velocities at the peaks and troughs, with average errors of 16.91% and 19.29% for the RNG and Realizable, respectively.

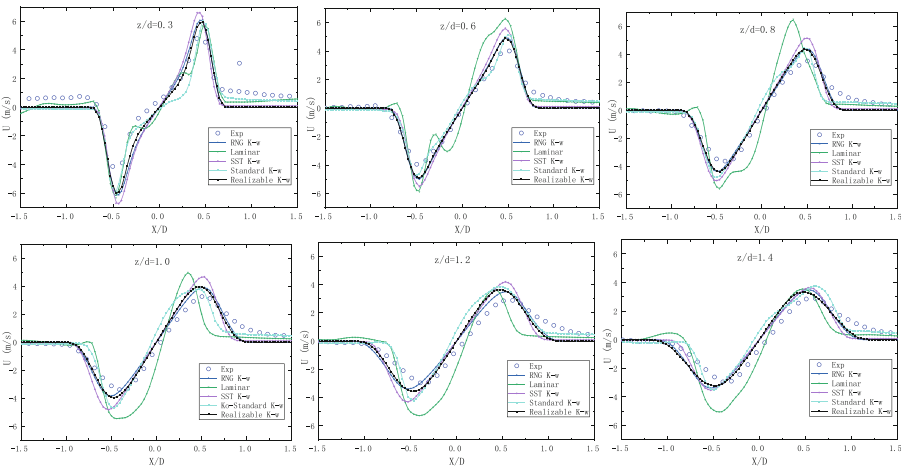


Fig. 6. Tangential velocities at several locations.

By comparing the axial velocity curves of different turbulence models at $z/d = 0.3$ etc., it is found that the error between the RNG and the experimental data is the smallest, with an average error of 0.47% and a maximum error of 0.79%. At the same time, the axial velocity peak position and velocity magnitude of RNG are the closest to the experimental results. Comparing the tangential velocity curves of different turbulence models, it is found that the error between the RNG and the experimental results is the

smallest, and the peak positions and velocities of the tangential velocity are the closest to the experimental results. Thus, it can be concluded that RNG is the most suitable turbulence model and will be used in subsequent simulations.

3.3 2D Instantaneous Flow Fields

In order to study the swirl flow characteristics, the velocity distribution in x - z plane is shown in Fig. 7, including CRZ and SJ zones.

Based on Fig. 7(a), three positions A, B and C are figured out to indicate the vital swirl flow changing process. In position A, nitrogen gas firstly flows along the axial direction and then turns to the annual combustion holes with the radial velocity because of the closed combustion top. Out of the combustion holes, the nitrogen gas mixes with the axial-moving air gas in the position B, forming the inner shear layer similar to the jet mixing flow. As the velocity directions of the nitrogen gas and the air gas are vertical, the nitrogen gas can block the air gas movement in axial direction, leading the air gas to flow back in corresponding with the recirculation region shown below the combustion holes. Apart from the recirculation, the mixture of nitrogen gas and air gas also form the annular vortex around the position C, which grows to outer shear layer. Based on the streamline shown in Fig. 7(b), the vortex (marked by red dots) formed by the layer velocity difference is influenced by the Kelvin-Helmholtz instability [32, 33]. The wavy CRZ and SJ zones are caused by the swirl flow instability with asymmetric characteristics.

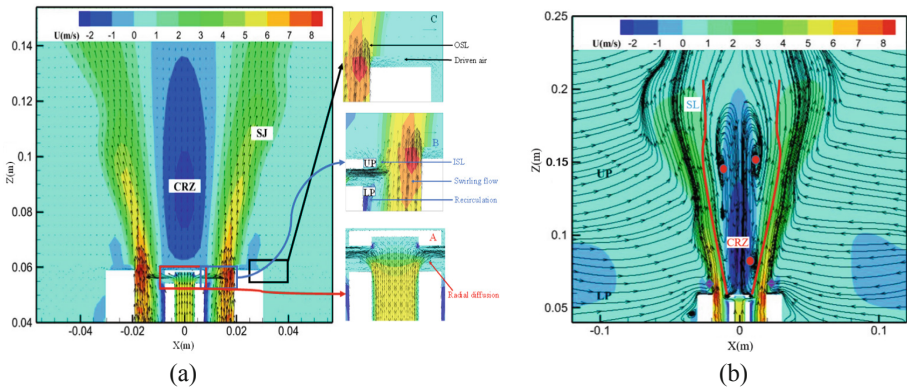


Fig. 7. (a) Flow field along the x - z plane (b) The streamline along the x - z plane.

4 Conclusions

The radial injector forms the non-reactive swirl flow in the coaxial swirl burner numerically simulated in this paper. The RNG is used to simulate turbulent swirls and conclusions can be drawn from the current investigation.

a) By comparing the axial velocity contours of different turbulence models, it is found that the laminar flow model is quite different from the experimental results, the CRZ and SJ in axial velocity contours features are not obvious, while the features of other turbulence models are close to the experimental results, the deflection angle of the central area of the RNG is the closest to the experimental results. Comparing the tangential velocity cloud images of different turbulence models, the laminar flow model has vortices, and the vortices tend to move upwards, while the characteristics of other turbulence models are close to the experimental results, but the tangential velocity peak and valley positions of RNG are closest to the experimental results.

b) By comparing the axial velocity curves of different turbulence models at $z/d = 0.3$ etc., it is found that the error between the RNG and the experimental results is the smallest, with an average error of 0.47% and a maximum error of 0.79%. At the same time, the axial velocity peak position and velocity magnitude of RNG are the closest to the experimental results. Comparing the tangential velocity curves of different turbulence models, it is found that the error between the RNG and the experimental results is the smallest, and the peak positions and velocities of the tangential velocity are the closest to the experimental results.

c) On the whole, the characteristic of the swirling flow field is fully reflected by the simulations. The high-speed gradient around the center recirculation zone (CRZ) known as the jet zone (SJ) at the burner outlet has been well captured. The vortex formed by the layer velocity difference is influenced by the Kelvin-Helmholtz instability.

References

1. Gupta, A.K., Lilley, D.G., Syred, N.: Swirl flows. Abacus Press (1984)
2. Carlos Berrio, J., Pereyra, E., Ratkovich, N.: Computational fluid dynamics modeling of gas-liquid cylindrical cyclones, geometrical analysis. *J. Energy Res. Technol.* **140**(9), 1–14 (2018)
3. Erdal, F.M., Shirazi, S.A.: Local velocity measurements and computational fluid dynamics (CFD) simulations of swirling flow in a cylindrical cyclone separator. *J. Energy Res. Technol.* **126**(4), 326–333 (2004)
4. Pang, X., et al.: Numerical simulation of a cyclone separator to recycle the active components of waste lithium batteries. *Eng. Appl. Comput. Fluid Mech.* **16**(1), 937–951 (2022)
5. Sheikholeslami, M., Gorji-Bandpy, M., Ganji, D.D.: Review of heat transfer enhancement methods: focus on passive methods using swirl flow devices. *Renew. Sustain. Energy Rev.* **49**, 444–469 (2015)
6. Guillaume, D.W., Judge, T.A.: Improving the efficiency of a jet pump using a swirling primary jet. *Rev. Sci. Instrum.* **75**(2), 553–556 (2004)
7. Zhao, H., et al.: Study on the characteristics of horn-like vortices in an axial flow pump impeller under off-design conditions. *Engineering Applications of Computational Fluid Mechanics* **15**(1), 1613–1628 (2021)
8. Alam, H.S., Redhyka, G.G., Sugiarto, A.T., Salim, T.I., Mardhiya, I.R.: Design and performance of swirl flow microbubble generator. *Int. J. Eng. Technol. (UAE)* **7**(4), 66–69 (2018)
9. Granados-Ortiz, F.J., Leon-Prieto, L., Ortega-Casanova, J.: Computational study of the application of Al_2O_3 nanoparticles to forced convection of high-Reynolds swirling jets for engineering cooling processes. *Eng. Appl. Comput. Fluid Mech.* **15**(1), 1–22 (2021)

10. Norton, D.J., Farquhar, B.W., Hoffman, J.D.: Analytical and experimental investigation of swirling flow in nozzle. *AIAA J.* **7**(10), 1992–2000 (1969)
11. Chiaverhi, M.J., Malecki, M.J., Sauer, J.A., Knuth, W.H.: Vortex combustion chamber development for future liquid rocket engine applications. American Institute of Aeronautics and Astronautics (2002)
12. Chang, C., Merkle, C., State, P., Promenade, L.E., Chang, C., Merkle, C.L.: Viscous Swirling Nozzle Flow. 27th Aerospam Sciences Meeting. American Institute of Aeronautics and Astronautics (1989)
13. Biswas, G., Som, S.K.: Coefficient of discharge and spray cone angle of a pressure nozzle with combined axial and tangential entry of power-law fluids. *Appl. Sci. Res.* **43**(1), 3–22 (1986)
14. Abo-Elfadl, S., Abd El-Sabor Mohamed, A.: The effect of the helical inlet port design and the shrouded inlet valve condition on swirl generation in diesel engine. *J. Energy Resources Technol.* **140**(3), 1–9 (2018)
15. Taylor, G.I.: The boundary layer in the converging nozzle of a swirl atomizer. *Q. J. Mech. Appl. Mech.* **3**(2), 129–139 (1950)
16. Carlanescu, R., Prisecaru, T., Prisecaru, M., Soriga, I.: Swirl injector for premixed combustion of hydrogen methane mixtures. *J. Energy Res. Technol.* **140**(7), 7 (2018)
17. Koh, H., Kim, D., Jung, K., et al.: The effects of Swirler geometry on the performance of gas turbine combustor using planar imaging technique. 37th Joint Propulsion Conference and Exhibit (2001)
18. Elbaz, A.M., Roberts, W.L.: Investigation of the effects of Quarl and initial conditions on swirling non-premixed methane flames: flow field, temperature, and species distributions. *Fuel* **169**(APR.1), 120–134 (2016)
19. Iyogun, C.O., Birouk, M., Kozinski, J.A.: Experimental investigation of the effect of fuel nozzle geometry on the stability of a swirling non-premixed methane flame. *Fuel* **90**(4), 1416–1423 (2011)
20. Merlo, N., et al.: Experimental study of oxygen enrichment effects on turbulent non-premixed swirling flames. *Energy Fuels* **27**(10), 6191–6197 (2013)
21. Boushaki, T., Koched, A., Mansouri, Z., Lespinasse, F.: Volumetric velocity measurements (V3V) on turbulent swirling flows. *Flow Meas. Instrum.* **54**, 46–55 (2017)
22. Wang, P., Bai, X.S., Wessman, M., Klingmann, J.: Large eddy simulation and experimental studies of a confined turbulent swirling flow. *Phys. Fluids*, **16**(9), 3306–24 (2004)
23. Huang, Y., Yang, V.: Effect of swirl on combustion dynamics in a lean-premixed swirl-stabilized combustor. *Proc. Combust. Inst.* **30**(2), 1775–1782 (2005)
24. Freitag, M., et al.: Mixing analysis of a swirling recirculating flow using DNS and experimental data. Begel House Inc, In Fourth International Symposium on Turbulence and Shear Flow Phenomena (2005)
25. Mansouri, Z., Aouissi, M., Boushaki, T.: Detached eddy simulation of high turbulent swirling reacting flow in a premixed model burner. *Combustion Sci. Technol.* **188**(11–12), 1777–1798 (2016)
26. Mansouri, Z., Boushaki, T.: Investigation of large-scale structures of annular swirling jet in a non-premixed burner using delayed detached eddy simulation. *Int. J. Heat Fluid Flow* **77**, 217–231 (2019)
27. Sudhakar Reddy, K., Reddy, N.D., Varaprasad, C.M.: Experimental and numerical investigations of swirling flows in a reverse flow gas turbine combustor. In: 37th AIAA Fluid Dynamics Conference and Exhibit, p. 4219 (2007)
28. Wang, J.Y., Yu, M., Meili, L., Juan, W.: Numerical simulation of strongly swirling flow in cyclone separator using an advanced RNG k- ϵ model. *Acta Petrolei Sinica* **26**(1), 8 (2010)

29. Mansouri, Z., Aouissi, M., Boushaki, T.: Numerical computations of premixed propane flame in a swirl-stabilized burner: effects of hydrogen enrichment, swirl number and equivalence ratio on flame characteristics. *Int. J. Hydrogen Energy* **41**(22), 9664–9678 (2016)
30. Islam, S.M., Khan, M.T., Ahmed, Z.U.: Effect of design parameters on flow characteristics of an aerodynamic swirl nozzle. *Progress Comput. Fluid Dyn. Int. J.* **20**(5), 249–262 (2020)
31. Yakhot, V.: Renormalization group modeling and turbulence simulations. International Conference on Near-Wall Turbulent Flows, Arizona, Tempe (1993)
32. Gargan-Shingles, C.L., Rudman, M., Ryan, K.: The formation of Kelvin-Helmholtz instabilities on swirling axisymmetric vortex rings. In Paper Presented at the Nineth Australasian Fluid Mechanics Conference (2014)
33. González-Martínez, E., Lázaro, B.J.: On the coherent modes of high Reynolds number, strongly swirling jets discharging in compact enclosures. Part B: coherent flow structure. *Aerosp. Sci. Technol.* **44**, 32–42 (2015)

Author Index

A

Ai, Xueshan 266
Alisha, Shaik Subhan 313
Altabay, Wael A. 71, 82
Andrii, Bieliatynskiy 14
Astuti, Hastining Bagyo 131

B

Bai, Yaonan 336

C

Cai, Ming 256
Cao, Xiaoxiang 102
Cao, Xueqin 296
Cao, Yingzhi 156, 372
Chen, Guowei 189
Chen, Lin 398

D

De Berardinis, Pierluigi 52
De Gregorio, Stefania 52
Deng, Hong 156, 372
Deng, Ying 201
Ding, Aoshuang 398
Ding, Jie 266
Du, Dong 336

E

Ertlmeier, Lars-Eric 278

F

Fan, Shiyue 372
Fan, Xinying 256
Fu, Jian 256

G

Gao, Guanglei 245
Gao, Wenliang 143
Gao, Xiaotao 256
Geng, Jianjun 167

Goi, Vasyl 14
Gu, Jiuli 323
Guan, Jianfei 234
Guo, Dangui 71
Guo, Jiajun 266
Guo, Lianjie 156
Guo, Xinliang 336

H

Han, Jie 363
Han, Xiaowei 245
Han, Zhiyuan 363
Hong, Weixing 71, 82
Hou, Yanlin 347
Huang, Kui 266

J

Ji, Dawei 156, 372
Jiang, Feifei 156
Jiang, Tianhao 323
Jiao, Fangfang 384

K

Khrystych, Inna 14
Kovalenko, Lyudmyla 14

L

Laurini, Eleonora 33
Le, Zhang 223
Lei, Lei 167
Li, Huaiyuan 363
Li, Jianluan 93
Li, Libiao 323
Li, Songyang 3
Li, Xi 201
Li, Xiuhong 178, 213, 223
Li, Zhengwei 256
Lin, Jingjing 384
Liu, Hongwei 336
Liu, Huan 3

Liu, Wendi 384
 Lu, Chang 189, 201
 Lu, Yanrong 178, 213, 223

M

Ma, Chuanming 336
 Ma, Hang 3
 Ma, Hao 256
 Makhdor, Rosadi 131
 Mamonov, Kostyantyn 14
 Mei, Wenqing 398
 Miao, Jinjie 336
 Montuori, Patrizia 33
 Mu, Zhenyu 266
 Murphy Jr., John D. 33

N

Nagaraju, T. V. 313

P

Peng, Cheng 102
 Peng, Jun 143

R

Refsgaard, Benjamin 278

S

Sari, Detriana Margita 131
 Setiawan, Soekhatta 131
 Shen, Yun 93, 122
 Shi, Xuanyu 266
 Shu, Rentian 296
 Sireesha, Mantena 313
 Song, Fangxin 323
 Sun, Meiyong 223
 Sunil, B. M. 313

W

Wang, Ce 323
 Wang, Jian 201
 Wang, Na 156

Wang, Nenghui 398
 Wang, Yuanjun 372
 Wu, Hai 398
 Wu, Zhigang 102

X

Xiang, Yan 347
 Xiao, Congyang 398
 Xie, Hualiang 363
 Xu, Zening 122

Y

Yan, Jing 122
 Yang, Bin 112
 Yang, Rongjin 223
 Yang, Shengwei 102
 Yang, Zaixing 398
 Yang, Zhenyu 278
 Yi, Nan 245
 Yi, Siyang 398
 Yin, Liang 102
 Yin, Yitong 178, 213
 Yu, Shuhua 143

Z

Zhang, Dongshan 112
 Zhang, Haifeng 245
 Zhang, Jian 372
 Zhang, Jianxun 189
 Zhang, Jieyu 178, 213
 Zhang, Jing 336
 Zhang, Mingfeng 201
 Zhang, Youwen 296
 Zhang, Yuying 178, 213
 Zhao, Junwei 347
 Zheng, Huaizhou 201
 Zheng, Ping 323
 Zhou, Jiayin 3
 Zhou, Liping 82
 Zhu, Xizhu 323
 Zuo, Shuhua 363